Advances in Polymer Science 268

Sebastian Seiffert *Editor*

Supramolecular Polymer Networks and Gels

Springer

268
Advances in Polymer Science

Editorial Board:

A. Abe, Yokohama, Japan
A.-C. Albertsson, Stockholm, Sweden
G.W. Coates, Ithaca, NY, USA
J. Genzer, Raleigh, NC, USA
S. Kobayashi, Kyoto, Japan
K.-S. Lee, Daejeon, South Korea
L. Leibler, Paris, France
T.E. Long, Blacksburg, VA, USA
M. Möller, Aachen, Germany
O. Okay, Istanbul, Turkey
V. Percec, Philadelphia, PA, USA
B.Z. Tang, Hong Kong, China
E.M. Terentjev, Cambridge, UK
M.J. Vicent, Valencia, Spain
B. Voit, Dresden, Germany
U. Wiesner, Ithaca, NY, USA
X. Zhang, Beijing, China

Aims and Scope

The series Advances in Polymer Science presents critical reviews of the present and future trends in polymer and biopolymer science. It covers all areas of research in polymer and biopolymer science including chemistry, physical chemistry, physics, material science.

The thematic volumes are addressed to scientists, whether at universities or in industry, who wish to keep abreast of the important advances in the covered topics.

Advances in Polymer Science enjoys a longstanding tradition and good reputation in its community. Each volume is dedicated to a current topic, and each review critically surveys one aspect of that topic, to place it within the context of the volume. The volumes typically summarize the significant developments of the last 5 to 10 years and discuss them critically, presenting selected examples, explaining and illustrating the important principles, and bringing together many important references of primary literature. On that basis, future research directions in the area can be discussed. Advances in Polymer Science volumes thus are important references for every polymer scientist, as well as for other scientists interested in polymer science - as an introduction to a neighboring field, or as a compilation of detailed information for the specialist.

Review articles for the individual volumes are invited by the volume editors. Single contributions can be specially commissioned.

Readership: Polymer scientists, or scientists in related fields interested in polymer and biopolymer science, at universities or in industry, graduate students.

Special offer:
For all clients with a standing order we offer the electronic form of Advances in Polymer Science free of charge.

More information about this series at
http://www.springer.com/series/12

Sebastian Seiffert
Editor

Supramolecular Polymer Networks and Gels

With contributions by

M. Anthamatten · M. Chau · P.Y.W. Dankers · B.W. Greenland · W. Hayes · E. Kumacheva · P. Li · R. Liu · O. Okay · A.C.H. Pape · T. Rossow · S. Seiffert · S.E. Sriskandha · H. Thérien-Aubin

Springer

Editor
Sebastian Seiffert
Freie Universität Berlin
Institute of Chemistry and Biochemistry
Berlin
Germany

ISSN 0065-3195 ISSN 1436-5030 (electronic)
Advances in Polymer Science
ISBN 978-3-319-15403-9 ISBN 978-3-319-15404-6 (eBook)
DOI 10.1007/978-3-319-15404-6

Library of Congress Control Number: 2015936665

Springer Cham Heidelberg New York Dordrecht London
© Springer International Publishing Switzerland 2015
This work is subject to copyright. All rights are reserved by the Publisher, whether the whole or part of the material is concerned, specifically the rights of translation, reprinting, reuse of illustrations, recitation, broadcasting, reproduction on microfilms or in any other physical way, and transmission or information storage and retrieval, electronic adaptation, computer software, or by similar or dissimilar methodology now known or hereafter developed.
The use of general descriptive names, registered names, trademarks, service marks, etc. in this publication does not imply, even in the absence of a specific statement, that such names are exempt from the relevant protective laws and regulations and therefore free for general use.
The publisher, the authors and the editors are safe to assume that the advice and information in this book are believed to be true and accurate at the date of publication. Neither the publisher nor the authors or the editors give a warranty, express or implied, with respect to the material contained herein or for any errors or omissions that may have been made.

Printed on acid-free paper

Springer International Publishing AG Switzerland is part of Springer Science+Business Media (www.springer.com)

Preface

Supramolecular polymer networks and gels consist of monomeric, oligomeric, or polymeric building blocks transiently and dynamically interconnected by non-covalent bonds. This mode of interconnection is responsible for the promising potential of these materials to serve as adaptive, self-healing, and stimuli-responsive coatings, elastomers, and scaffolds in both the life and materials sciences. To make this truly useful, it is necessary to achieve systematic and comprehensive understanding of the molecular-scale interactions and macromolecular-scale structures and dynamics of these networks and gels. Various efforts have been and are being made to achieve such understanding and to develop advanced functional soft materials. It is therefore a good time to review some of these activities; this volume aims to provide such a review. In the following chapters, several examples and achievements of recent and current research activities are given. Anthamatten reviews hydrogen-bonding interactions to form soft solid polymer-network structures and materials, including glasses, melts, and elastomers. Okay adds a perspective on the design, mechanics, and self-healing of hydrogels formed via hydrophobic interactions, with a particular emphasis on the role of surfactant micelles within the gels. The development of donor–acceptor – stacking interactions that serve as transient crosslinks in self-healable supramolecular polymer networks is discussed by Greenland and Hayes. Chau, Sriskandha, Thérien-Aubin, and Kumacheva highlight recent progress in the field of nanofibrillar supramolecular gels, discussing both synthetic and natural materials. Liu adds a particular view on the potential of cellulose and cellulose derivatives for the formation of chemical and physical gels and microgels, with a specific focus on supramolecular interactions within them. Finally, Pape and Dankers provide a review on supramolecular hydrogels of several kinds for use in the field of regenerative medicine.

I would like to take the chance to greatly thank all these colleagues for providing these deep and illustrative insights into their work and that of their peers. I believe

that the collection of contributions presented in this volume truly arcs from fundamental physical-chemical investigation to advanced development and use of supramolecular polymer networks and gels, which I expect to further evolve as a particularly promising and fascinating class of soft matter in the near future.

Berlin Sebastian Seiffert
April 2015

Contents

Supramolecular Polymer Networks: Preparation, Properties, and Potential

Torsten Rossow and Sebastian Seiffert

Contents

Abstract Supramolecular polymer networks consist of macromolecules interconnected by transient, noncovalent bonds such as those through hydrogen bonding, transition metal complexation, hydrophobic interaction, ionic attraction, or π–π stacking. These networks form an extraordinarily useful class of soft, stimuli-sensitive materials. Although they assemble to strong materials under

T. Rossow
Institute of Chemistry and Biochemistry, Freie Universität Berlin, Takustr. 3, 14195 Berlin, Germany

S. Seiffert (✉)
Institute of Chemistry and Biochemistry, Freie Universität Berlin, Takustr. 3, 14195 Berlin, Germany

Soft Matter and Functional Materials, Helmholtz-Zentrum Berlin, Hahn-Meitner-Platz 1, 14109 Berlin, Germany
e-mail: sebastian.seiffert@helmholtz-berlin.de

© Springer International Publishing Switzerland 2015

S. Seiffert (ed.), *Supramolecular Polymer Networks and Gels*, Advances in Polymer Science 268, DOI 10.1007/978-3-319-15404-6_1

favorable conditions, they are easily disassembled under other conditions. This ambivalent nature renders supramolecular polymer networks useful for applications in drug delivery, tissue engineering, self-healing, and shape-memory materials. These applications require a deep and comprehensive understanding of the physical chemistry of supramolecular networks, with a particular view to the complex interplay between their structure, dynamics, and properties. Approaches that have attempted to derive such knowledge are often based on investigations of supramolecular polymer networks in the melt or of supramolecular polymer networks swollen in organic media. These approaches are reviewed in the first part of this chapter. In the second part, we focus on the preparation and characterization of supramolecular hydrogels based on synthetic and natural precursors and reveal their utility and potential in life science applications.

Keywords Supramolecular polymer gels • Stimuli-responsive materials • Noncovalent interactions • Supramolecular network dynamics • Self-assembly

1 Supramolecular Interactions

"*Supramolecular chemistry may be defined as 'chemistry beyond the molecule', bearing on the organized entities of higher complexity that result from the association of two or more chemical species held together by intermolecular forces*." This definition was given by Lehn in 1987 [1] when he received the Nobel prize together with C. J. Pedersen and D. J. Cram for their work on host–guest chemistry. Since then, supramolecular chemistry has gained increasing attention and developed into an important, broad, and active field of research [2–4]. Today, research on supramolecular chemistry can be subdivided into several categories: host–guest complexes [5–7], self-assembled architectures [8, 9], supramolecular polymers [10–14], supramolecular gels [15–18], and supramolecular polymer networks [19, 20].

The term "supramolecular polymer" refers to a polymer built of monomeric units associated through directional noncovalent physical interactions. Supramolecular gels typically consist of low molecular weight precursors that self-assemble into three-dimensional networks through noncovalent interactions; these materials are often brittle and hard to customize. In contrast, supramolecular polymer networks consist of covalently joined macromolecular building blocks (polymers) that are functionalized with motifs that can bind to each other through noncovalent interactions such as hydrogen bonding [21–23], transition metal complexation [11, 24, 25], hydrophobic interaction [26], ionic attraction [10], or π–π stacking [27–29], serving to assemble the polymer chains into a network. Noncovalent interactions strongly vary in their strength, as shown in Fig. 1. As a result, supramolecular polymer materials can be tuned to exhibit different mechanical properties by custom use of these interactions for polymer cross-linking.

Supramolecular polymer networks combine the characteristics of chemical and physical networks and can be tailored to specific needs through the use of macromolecular building blocks. Although they form strong materials under favorable

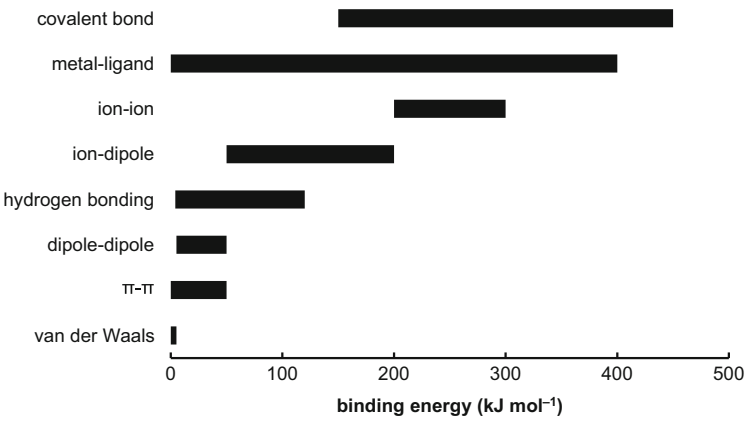

Fig. 1 The most important noncovalent interactions along with their typical range of binding strength, in comparison with covalent bonds [30]

conditions, they are easily de-cross-linked under other conditions. Physically associating motifs can be divided into those that associate with one another in a self-complementary fashion and those that require a different complementary motif to associate in a heterocomplementary fashion. The latter approach is useful for accessing more sophisticated materials because, in this approach, the strength of cross-linking is tunable by various complementary motifs. Different design principles can serve to build such supramolecular networks, as illustrated in Fig. 2. In one principle, linear chains functionalized with supramolecular linkable motifs at both chain ends are cross-linked if these motifs form associative nodes with a functionality greater than two (Fig. 2a). In a second principle, systems that form supramolecular linear chains can be cross-linked by entanglement of the polymer chains or by phase separation through lateral interactions of the transient cross-links, including stacking, clustering, or crystallization (Fig. 2b). In a third principle, the supramolecular motifs are attached as side chains to a polymer backbone, resulting in polymer cross-linking even if the supramolecular motifs assemble in a bivalent fashion. If heterocomplementary motifs are used, cross-linking is achievable by addition of low molecular weight cross-linking agents to the supramolecular cross-linkable polymers (Fig. 2c) or by using a second polymer functionalized with a complementary supramolecular motif (Fig. 2d). The supramolecular motifs can be introduced to the side chains after synthesis of the polymer backbone in a post-polymerization step. As an alternative, monomers that contain the supramolecular motifs beforehand can be polymerized in a suitable chain- or step-growth process.

Because of their transient and reversible cross-linking, supramolecular polymer networks are responsive [4] to external stimuli such as variation in temperature [31], pH [32], polarity of the solvent [33], redox reactions [34], and competitive ligation [35]. This tunability makes them useful for a plethora of applications. They can be used as drug delivery systems [36] and as matrixes in tissue engineering [37]. Drugs and cells can be encapsulated and protected within these materials and

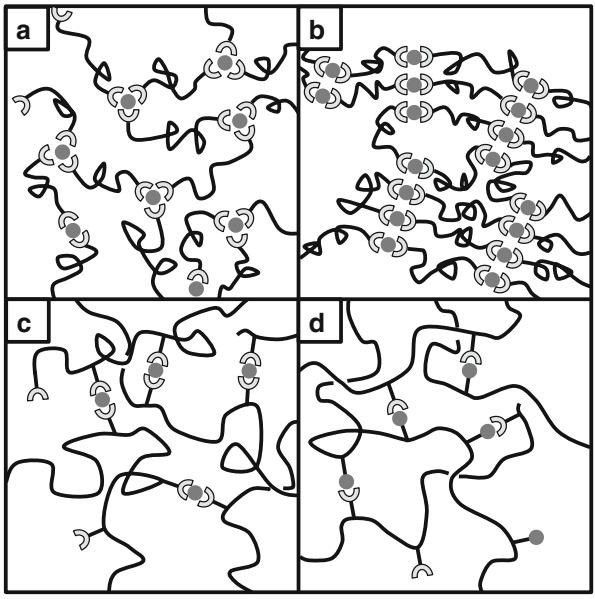

Fig. 2 Different design principles for preparation of supramolecular polymer networks by heterocomplementary interactions. Cross-linking of end-capped linear chains by (**a**) associative nodes with a functionality higher than two or (**b**) additional lateral chain interactions. As an alternative, side-chain functionalized polymer chains can associate by (**c**) low molecular weight cross-linkers or (**d**) mutual heterocomplementary polymer–polymer binding

afterward released on demand at a targeted site of action. Furthermore, supramolecular polymer networks often have self-healing properties [38, 39]; after rupture, supramolecular bonds can re-associate when brought into contact, thereby healing the material. In addition, the combination of supramolecular and covalent cross-linking gives rise to shape-memory materials [40].

Many different polymeric precursors can be used to prepare supramolecular polymer networks, including synthetic polymers, natural polymers, and hybrids of both. In approaches that serve to derive fundamental physical–chemical understanding of supramolecular polymer networks, synthetic precursors are mostly used because chemical modification allows them to be tailored as desired. When it comes to further tailoring of supramolecular polymer materials for practical applications in the biological area, a popular class of precursor polymers are those that are water soluble, including poly(ethylene glycol) (PEG) [41, 42], poly(vinyl alcohol) (PVA) [43–45], and polyglycerol [46–48]. However, several other synthetic precursors are only soluble in organic solvents. In addition, many supramolecular polymer networks are labile in water because many binding motifs do not form interactions strong enough to withstand competitive hydrogen bonding. Hence, popular alternatives to fully synthetic supramolecular polymer gels are natural polymer gels [49], such as those based on alginate [50–53], gelatin [54], or chitosan [55], which can form hydrogels even without chemical modification. These materials are biocompatible, bioavailable, biodegradable, and cheap, which makes them ideal candidates for life science applications [56]. However, natural polymers also have disadvantages [57]: they differ in their composition from batch to batch because they are harvested from living organisms [58, 59], the production of large volumes

of natural polymers is limited, and they cannot be tailored according to the demand of different applications because their properties are determined by the species that produce them [60]. As a result, the combination of synthetic and natural polymeric precursors in hybrid networks often presents an excellent compromise.

The following sections describe the preparation and characterization of supramolecular polymer networks, particularly emphasizing their physical–chemical features with regard to the type and strength of physical chain cross-linking and the resulting macroscopic material properties. Furthermore, recent work on the formation and characterization of supramolecular hydrogels based on synthetic and natural precursors is summarized with a focus on their application and potential in biomedicine.

2 Supramolecular Polymer Networks and Organogels

2.1 Hydrogen Bonding

Hydrogen bonding plays a crucial role in many biological processes such as DNA base pairing, ligand–receptor binding, enzyme catalysis, and protein folding. It has also become the most widely used noncovalent interaction for the synthesis of supramolecular polymers and reversibly cross-linked polymer networks [61–66]. This is not due to the binding strength of hydrogen bonds, which is just 4–120 kJ mol^{-1} (Fig. 1), but is a result of their strong directionality and versatility.

Nernst described weak interactions between molecules containing hydroxyl groups in 1892 [67] but the term ‘hydrogen bond’ was first introduced by Bernal and Huggins in 1935 [68, 69]. Hydrogen bonds connect atoms X and Y that have electronegativities larger than that of hydrogen. The XH group is generally referred to as the ‘proton donor’ (D), whereas Y is called the ‘proton acceptor’ (A) [61]. An increase in the dipole moment of the X–H bond and the electron lone pair on atom Y entails an increase in the hydrogen-bonding strength. For the strength of hydrogen-bonded complexes, however, the strength of a single hydrogen bond is less crucial than the number of hydrogen bonds within a hydrogen-bonding motif. When acting together in a cooperative fashion, hydrogen bonds become much stronger than their simple numerical sum. The binding constant of the DNA base pair guanine–cytosine (Fig. 3a), which contains three hydrogen bonds, is two to three orders of magnitude larger than that of the adenine–thymine complex that contains just two hydrogen bonds [63]. In the guanine–cytosine complex, not only the higher number of primary hydrogen bonds plays an important role, but also secondary interactions arising as a result of the particular arrangement of neighboring donor and acceptor sites, as shown in Fig. 3a. Complexes between the ADA–DAD motifs exhibit an association constant of around 10^2 M^{-1} in chloroform, whereas DAA–DDA complexes exhibit binding constants of 10^4 M^{-1} [70]. AAA–DDD arrays even have association constants higher than 10^5 M^{-1}. Jorgensen and

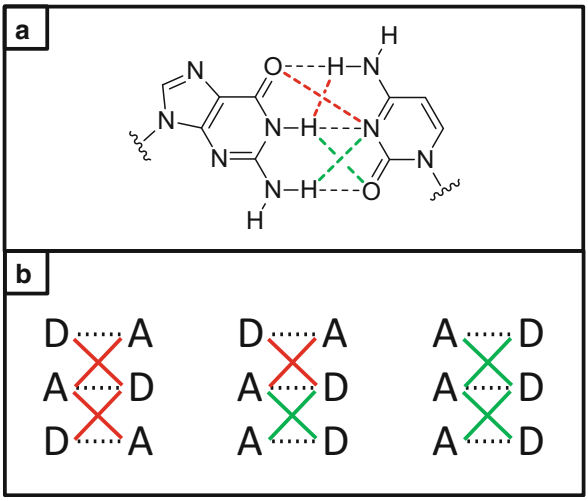

Fig. 3 Secondary hydrogen-bonding interactions. Attractive interactions are marked *green*, and repulsive interactions are marked *red*. (**a**) Guanine–cytosine complex in the DNA strand. (**b**) Possible secondary interactions in different triple hydrogen-bonding motifs

colleagues [71, 72] attributed this effect to differences in secondary interactions between these motifs. Diagonally opposed sites electrostatically repel each other when they are of the same kind, whereas contrary sites attract each other. Hence, the ADA–DAD complex has four repulsive secondary interactions, the DAA–DDA complex has two repulsive and two attractive interactions, and the AAA–DDD complex has four attracting interactions, as visualized in Fig. 3b.

Calculations by Schneider reveal that the arrangement of several hydrogen bonds can be modeled by a linear correlation, in which primary interactions contribute -8.0 kJ mol^{-1} to the complex stability, whereas secondary attractive or repulsive interactions contribute ± 2.9 kJ mol^{-1}[73]. In addition to secondary interactions, the pre-organization, intramolecular hydrogen bonding, tautomerization, and electronic substituent effects of the hydrogen-bonding motifs significantly contribute to the cooperative effect [63]. For pre-organization, a rigid aromatic framework is often used that presents multiple hydrogen-bonding sites wherein an entropy cost has to be paid only for the formation of the first hydrogen bond. In the case of amides, however, which are able to rotate and often stay in the preferred *trans*-confirmation in the uncomplexed form, the amide bond has to rotate to the *cis*-confirmation for complex formation and needs to be fixed in this position, which costs entropy. An overview of hydrogen-bonding motifs discussed in this chapter is given in Scheme 1.

In a pioneering application, the formation of thermoplastic elastomers cross-linked by hydrogen bonding was explored by Stadler and coworkers in 1986 [74–76]. In this work, nonpolar polybutadienes with narrow molecular weight distributions were modified with urazole side groups. Hydrogen bonding between the highly polar urazole groups gives rise to the formation of thermoreversible elastomeric networks. The rheological properties of these networks were investigated in the melt. No rubbery elastic equilibrium network modulus is observed due to the fragility of the transient hydrogen-bonding linkages. At low frequencies,

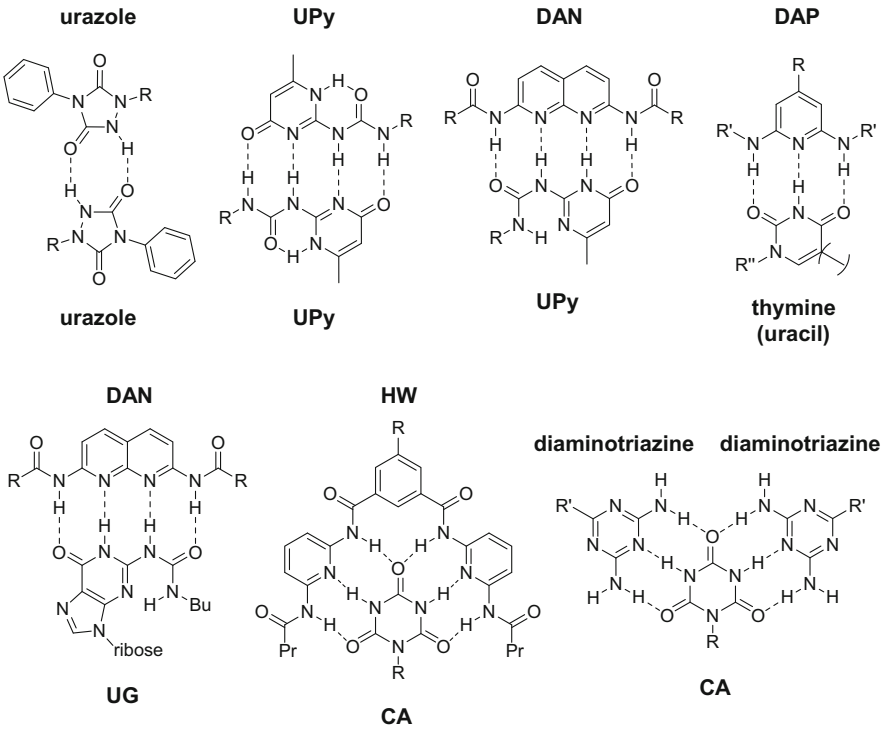

Scheme 1 Hydrogen-bonding motifs discussed in this chapter. *Upy* 2-ureido-4-pyrimidone, *DAN* 2,7-diamido-1,8-naphthyridine, *DAP* diacyldiaminopyridine, *HW* Hamilton wedge, *UG* ureidoguanosine, *CA* cyanuric acid

Newtonian flow is predominant for the same reason. Hence, although this approach showed the potential of hydrogen bonding to form supramolecular polymer networks, it remained impossible to transfer this concept to the formation of strong organogels for more than 10 years, which was because of the difficulty of preparing stronger hydrogen-bonding motifs.

In 1997, Meijer and coworkers developed easy access to derivatives of 2-ureido-4-pyrimidone (UPy) and demonstrated strong dimerization of these compounds, with $K_{eq} > 10^6\ M^{-1}$ in chloroform [77]. The strength is a result of the assembly of a self-complementary DDAA array of four hydrogen bonds [78], pre-organized by an intramolecular hydrogen bond and, therefore, markedly stabilized [77, 79]. Meijer and coworkers attached these UPy motifs to both chain ends of polyethylene polymers to form viscous solutions in chloroform [78]; the viscosity is highly dependent on concentration and temperature and can be described by the Cates model for reversibly breaking wormlike micelles [80–82], which is also adaptable to supramolecular polymers above the overlap concentration [83–87]. To exclusively ascribe the observed viscosity to the formation of linear supramolecular polymers, a monofunctional UPy motif acting as a chain stopper was added; as a

result, a dramatic decrease in viscosity was observed. To further study reversibly cross-linked networks, three UPy motifs were attached to poly(ethylene oxide-*co*-propylene oxide) polymers [78, 88]. In oscillatory shear rheology under bulk conditions at 30 °C, this compound shows a frequency-dependent transition from purely viscous to viscoelastic behavior with increasing frequency, whereupon G' exceeds G'' and a plateau modulus of 5×10^5 Pa is apparent. This plateau modulus is six times higher than that of the same copolymer when it is cross-linked covalently. This observation is attributed to the reversibility of the hydrogen bonding, which allows the polymer chains to assemble into a denser thermodynamically determined network, whereas covalent cross-links are irreversible and form a kinetically determined network. The supramolecular cross-linked networks show no additional stabilization such as crystallization or other kind of phase separation. Based on this observation, Meijer and coworkers extended their investigations of UPy-cross-linked supramolecular polymer networks in view of their solution behavior in chloroform and tetrahydrofuran [88]. The viscosity of the solutions is significantly affected by the polarity of the solvent and, again, addition of a chain stopper leads to a dramatic decrease in viscosity. These experiments demonstrate that a supramolecular cross-linked, reversible polymer network is formed in solution.

Meijer, Sijbesma, and coworkers developed new synthetic strategies capable of coupling UPy moieties to polysiloxanes [89, 90] and to a variety of hydroxy-telechelic polymers such as polyethers, polyesters, and polycarbonates [91]. OH-telechelic poly(ethylene-*co*-butylene), which is almost completely amorphous and apolar and therefore increases the strength of hydrogen bonds, was functionalized with UPy [91]. Whereas OH-telechelic poly(ethylene-*co*-butylene) is a viscous liquid (Fig. 4a), the same polymer functionalized with hydrogen-bonding units is an elastic solid (Fig. 4b). In dynamic oscillatory shear measurements, a broad rubbery elastic plateau with a storage modulus of about 10^6 Pa is observed at high frequencies. Thus, this linear supramolecular polymer exhibits mechanical properties even stronger than those of the previously discussed supramolecular UPy-based networks [78, 88]. This finding suggests that, in addition to hydrogen bonding within the polymer chains, interchain interactions such as physical cross-links are likely to be present; however, the transparent appearance of the material indicates that large clusters of hydrogen-bonded units are absent. An explanation for this finding could be the formation of urethane lateral hydrogen-bonding interactions, as shown in Fig. 4c, d. Reinvestigation of this material in a later study by atomic force microscopy (AFM) indeed confirmed the presence of fibrillar aggregates at room temperature (Fig. 4e) [92]. By using urea groups instead of urethanes as linkers to attach UPy to the polymer, the lateral interactions are increased, as evidenced through the formation of longer and more densely packed fibers (shown by AFM).The mechanical properties of the materials are further enhanced.

Other research groups have started to incorporate UPy motifs as side chains into higher molecular weight polymers via random copolymerization of UPy-functionalized alkene [93] or methacrylate monomers [94–96]. Coates and

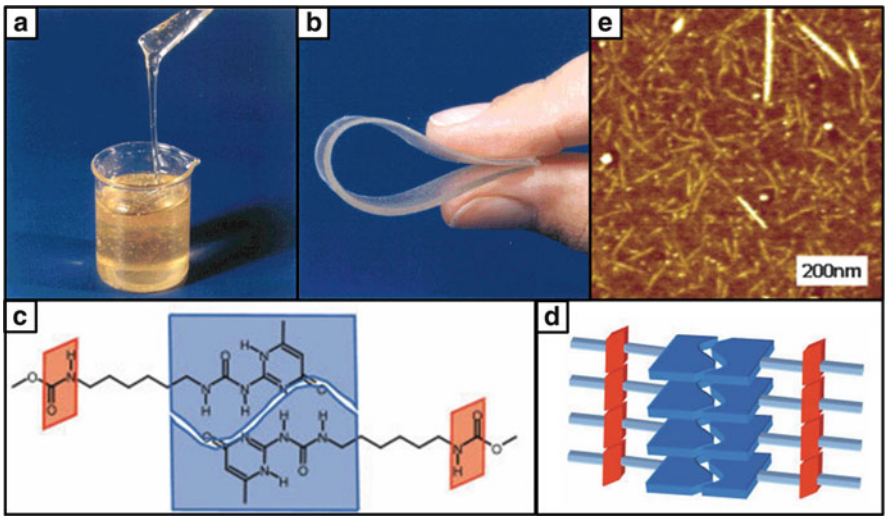

Fig. 4 Hydrogen-bonded thermoplastic elastomer based on self-complementary interactions of ureido-pyrimidinone (UPy). (**a**) Poly(ethylene-*co*-butylene) with OH end groups. (**b**) Poly(ethylene-*co*-butylene) functionalized with UPy. (**c**, **d**) Lateral interactions through π–π stacking of UPy and hydrogen bonding of urethane linkers. (**e**) AFM image of nanofibers formed through these lateral interactions. Reprinted with permission from [90–92]. Copyright 2000, 2006, 2008 Wiley-VCH Verlag GmbH, Wiley Periodicals, Inc., and American Chemical Society

colleagues prepared UPy side-chain functionalized polyolefins by copolymerizing 1-hexene and alkene-functionalized UPy derivatives using late transition metal Ziegler–Natta catalysts [93]. By this means, copolymers with molecular weights of between 33 and 104 kg mol^{-1} were obtained containing 2 mol% of UPy, along with narrow molecular weight distributions. At concentrations higher than 20 g L^{-1} these copolymers form organogels in toluene. Addition of a monofunctional UPy derivative leads to complete de-cross-linking, suggesting that individual sets of hydrogen-bonded dimers are the predominant source of network formation; stacks or clusters of UPy moieties would not be completely broken down by the presence of monofunctional UPy. Kramer and Hawker used another strategy and prepared random copolymers of poly(*n*-butyl acrylates) via controlled radical polymerization and introduced UPy moieties by post-polymerization functionalization [97]. Through this synthetic strategy, both the molecular weight and the content of the UPy monomer are excellently controllable, and very high UPy monomer contents of up to 15 mol% are achievable, along with low polydispersities. Moreover, triblock copolymers were synthesized containing a homopolymer midblock and random copolymer end blocks, effectively concentrating the hydrogen-bonding groups near the chain ends. This leads to dramatic changes in the dynamic properties of these materials in bulk: they show strongly increased effective bond lifetimes in comparison with the random copolymers, and as a result, elastomeric behavior is observed on much longer time scales.

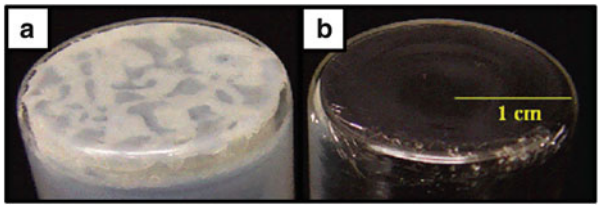

Fig. 5 Films of intrinsically immiscible polymers with and without promotion by supramolecular linking. (**a**) Heterogeneous film of plain poly(butylmethacrylate) and polystyrene functionalized with 2,7-diamido-1,8-naphthyridine (DAN). (**b**) Transparent blend of poly(butylmethacrylate) functionalized with ureidoguanosine (UG) and polystyrene functionalized with DAN, thereby enabling quadruple hydrogen bonding of DAN and UG to facilitate polymer mixing. Reprinted with permission from [101]. Copyright 2006 American Chemical Society

Besides self-complementary UPy, which is one of the most important and extensively studied hydrogen-bonding motifs, several heterocomplementary arrays of multiple hydrogen bonds serving to form supramolecular polymer networks have been developed, as also shown in Scheme 1 [63, 98]. Zimmerman and coworkers synthesized polystyrene with 2,7-diamido-1,8-naphthyridine (DAN) in the side chains, which is a ADDA hydrogen-bonding array, and also poly (butylmethacrylate) with ureidoguanosine (UG) in the side chains, which is a DAAD array [99–101]. Polystyrene and poly(butylmethacrylate) themselves are immiscible and do not form blends, as shown in Fig. 5a. Mixed solutions of the DAN- and UG-functionalized polymers, however, give transparent films upon drying as a result of strong quadruple hydrogen bonding between DAN and UG ($K_{eq} = 3 \times 10^8$ M^{-1} in chloroform), as demonstrated in Fig. 5b. Additionally, poly (butylmethacrylate) was side-chain functionalized with UPy, which is able to interact with DAN by quadruple hydrogen bonding in the form of its ADDA tautomer [77, 102]. Mixing of this polymer with the DAN-functionalized polystyrene yields viscous solutions in chloroform; however, the viscosity is lower than in the case of DAN–UG mixtures, most probably as a result of competitive UPy-self-association.

Weck and coworkers prepared polymers side-chain functionalized with cyanuric acid motifs by ring-opening metathesis polymerization of norbornene-based cyanuric acid and spacer monomers [103]. To these were added low molecular weight ditopic cross-linking agents based on 2,4-diaminotriazine, which form three-point hydrogen bonding with cyanuric acid, or a Hamilton wedge, which forms six-point hydrogen bonding with cyanuric acid, to achieve cross-linking in 1-chloronaphthalene. The extent of cross-linking is controllable by the amount of the cross-linking agent. Whereas addition of the Hamilton wedge cross-linking agent leads to highly viscous fluids, the 2,4-diaminotriazine cross-linking agent produces highly viscoelastic gels, despite weak triple hydrogen-bonding interactions, in contrast to the stronger six-point hydrogen bonding of the Hamilton wedge. The authors hypothesized that this is a result of a higher degree of network connectivity in the 2,4-diaminotriazine system, because two diaminotriazine motifs

can complex to one cyanuric acid moiety. Hence, it is not only the strength of the hydrogen bond chain linkage, but also the assembly of these cross-links and the network microstructure that determines the macroscopic mechanical network properties. Similar clustering and micellization of heterocomplementary hydrogen-bonding motifs has also been observed by Binder and coworkers, who studied telechelic polyisobutylenes with thymine and diaminotriazine end groups [104]. Clustering and stacking of supramolecular cross-links often enforces supramolecular networks rather than making them weaker [14, 88, 104–107], which stands in marked contrast to covalently cross-linked networks, wherein nanostructural network heterogeneity is assumed to entail weaker materials [108–113].

Later, Weck and coworkers extended their studies on hydrogen-bonding side-chain polymers to norbornene-based precursor polymers containing different hydrogen-bonding motifs [114]. That way, selective de- and re-cross-linking is achievable by competitive hydrogen bonding. Besides thermal responsiveness, this competitive binding allows the mechanical properties of the networks to be controlled over a broad range, from low viscous liquids to elastic gels.

The potential of hydrogen bonding for the preparation of polymersomes has been demonstrated by Rotello and coworkers, who prepared functional polystyrene copolymers and attached diacyldiaminopyridine (DAP) or thymine derivatives to their side chains [115]. By mixing equal volumes of both polymers at low concentrations (3 g L^{-1} in chloroform), formation of vesicular aggregates (3 μm in diameter) is observed as a result of complementary three-point hydrogen bonding between DAP and thymine. When polystyrene containing a higher DAP content (50 mol%) is dissolved in chloroform, discrete microspheres are created by self-complementary hydrogen bonding of DAP [116]. Addition of thymine-functionalized polystyrene leads to morphology transition into vesicles by heterocomplementary hydrogen bond formation, as visualized in Fig. 6. By the same way, mono- and multivalent guests that can undergo competitive hydrogen bonding can be specifically incorporated in this type of polymersomes [117]. In an alternative approach, DAP-functionalized polystyrenes were cross-linked by a series of linear bis-thymines, giving rise to filled spherical microspheres rather than vesicles [118]. These aggregates dissociate at 50 °C, but re-form upon cooling. When the heating–cooling cycle is repeated several times, particles with a narrower size distribution are obtained. To extend the formation of polymersomes to other polymer types, Rotello and colleagues prepared DAP and uracil side-chain functionalized polynorbornene copolymers. Again, polymersomes with diameters of several micrometers are formed through three-point hydrogen bonding in chloroform; however, these aggregates are only metastable and macroscopic organogels are obtained after 2 h of aging [119].

Hydrogen-bonding polymer networks can be even prepared in ionic liquids, as reported by Noro et al. [120]. In their work, an ABA triblock copolymer was synthesized containing end blocks that form hydrogen bonds with a specifically designed homopolymer via interactions of pyridine and hydroxystyrene. The prime role of the ionic liquid is to assure good solvent conditions over a wide range of

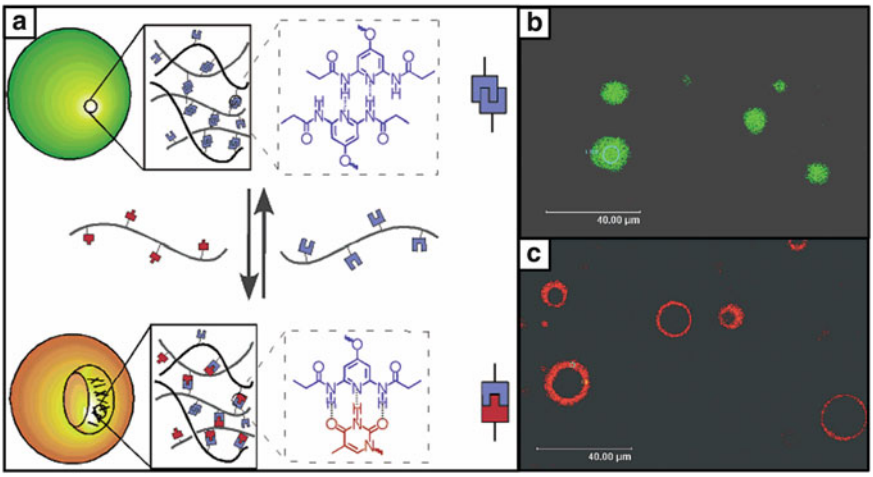

Fig. 6 Transformation of supramolecular hydrogen-bonded polymer microspheres into vesicles. (**a**) Morphology change as a result of specific hydrogen-bonding interactions. (**b**,**c**) Confocal fluorescence micrographs of labeled microspheres (**b**) and vesicles (**c**). Reprinted with permission from [116]. Copyright 2004 American Chemical Society

temperatures, allowing the network dynamics to be studied with significant variation of this parameter. Fourier transform infrared (FTIR) spectroscopy measurements serve to quantify the number of hydrogen bonds per end block as a function of temperature. This assessment shows that although the number of physical cross-links is independent of temperature below the gelation temperature, the number of active hydrogen bonds within a particular cross-linking node strongly increases upon cooling.

2.2 Metal Complexation

In addition to hydrogen bonding, metal complexation is another useful interaction for building linear supramolecular polymers [24], gels [121], and networks [122]. For this purpose, a variety of different ligands have been developed, as summarized in Scheme 2. Among them, bi- (bpy) and terpyridine (tpy) ligands are particularly popular and have been studied extensively [11, 123]. These ligands form chelate complexes with transition metal ions. Terpyridines coordinate to metal (II) ions in a bivalent fashion, whereas bipyridines coordinate to metal(II) ions in a trivalent fashion. To exploit this, Schubert and colleagues prepared poly(methyl methacrylate) copolymers with terpyridine units in the side chains by free-radical polymerization of methyl methacrylate and a terpyridine-functionalized methacrylate [124]. Then, the terpyridine units were complexed by iron(II) and zinc(II) ions in mixtures of chloroform and methanol at low polymer concentrations (17–

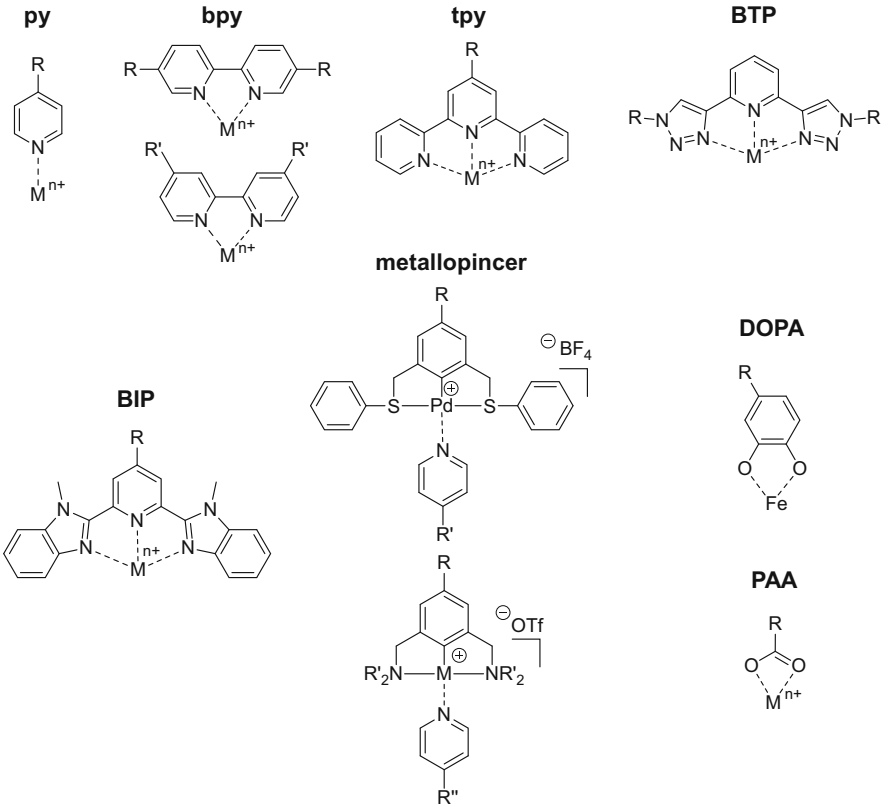

Scheme 2 Popular metal complexation motifs used for supramolecular polymer-network formation. *py* pyridine, *bpy* bipyridine, *tpy* terpyridine, *BTP* 2,6-bis(1,2,3-triazol-4-yl)pyridine, *BIP* 2,6-bis(1-methylbenzimidazolyl)pyridine, *DOPA* dihydroxy-phenylalanine, *PAA* poly(acrylic acid)

40 g L^{-1}). The complexation was studied by UV–vis and viscosity measurements. Upon metal complexation, a characteristic UV–vis absorption band is observed at 558 nm, which is attributed to the metal-to-terpyridine charge transfer, and an increase in the solution viscosity is found. Addition of zinc(II) results in lower viscosities than addition of iron(II), because zinc–terpyridine complexes are weaker than iron–terpyridine complexes. Further evidence for the weaker zinc binding is the observation that the zinc-complexed material can be redissolved after drying, whereas the iron-complexed polymer displays a gel-like appearance. To study the reversibility of complex formation, the solutions were treated with hydroxyethyl ethylenediaminetriacetic acid (HEEDTA), which is a strong chelating ligand for transition metal ions and therefore acts as a competitive ligand to the terpyridine. Upon HEEDTA addition, the purple color of the iron(II) complexes disappears and the viscosity of the solutions decreases significantly, demonstrating the reversible properties of these materials. In a similar approach, Tew and Calzia prepared

terpyridine-modified poly(methyl methacrylates) and investigated their complexation with copper ions [125].

Post-polymerization functionalization has also been applied to the synthesis of terpyridine-modified polymers [126]. In a recent approach, Schubert and colleagues employed this method to prepare poly(pentafluorostyrene) with terpyridines in the side chains [127]. First, poly(pentafluorostyrene) with a narrow polydispersity index of just 1.08 was synthesized by nitroxide-mediated polymerization. In a second step, this polymer was converted with amine-functionalized terpyridine under microwave heating, selectively substituting the *para*-fluorines. Addition of iron(II) sulfate to a solution of the terpyridine-functionalized polymer in a mixture of chloroform and methanol leads to gelation at a polymer concentration of 33 g L^{-1}. In another work, Schubert and coworkers prepared metal-cross-linked polymer networks from linear and tri-arm PEG precursors, both functionalized with terpyridine at their OH-termini [128]. Quantitative functionalization of these precursors was achieved by conversion of the hydroxy-functionalized PEG derivatives with 4-chloro-2,2′:6′,2″-terpyridine under basic conditions. However, quantitative cross-linking with iron(II) chloride was not observed in methanol solutions, neither at room temperature nor at elevated temperature, but only a small quantity of cross-linked material precipitated from the solution. This observation was attributed to a strong tendency of the tri-arm PEG to form intramolecular complexes, acting as a chain stopper rather than as a cross-linker.

The advantages of both covalent and physical polymer networks were combined in a terpolymer of poly(butyl acrylate) bearing terpyridine and oxetane units [129]. Noncovalent cross-linking of the terpyridine moieties is initiated by complexation to iron(II) ions, whereas addition of the Lewis acid $AlCl_3$ initiates covalent cross-linking by polymerizing the oxetane rings. As a result, this approach provides multiple possibilities for two-step cross-linking procedures and has the potential for the development of new materials such as smart coatings with self-healing properties.

Conjugated metallo-supramolecular polymer networks that display interesting optoelectronic properties have been reported by Weder and coworkers [130]. Their approach is based on poly(*p*-phenylene ethynylene)s (PPE) that contain bipyridines in the main chain. The authors performed complexation studies of these polymers with several different transition metals (Cu^+, Co^{2+}, Ni^{2+}, Zn^{2+}, or Cd^{2+}) and obtained three-dimensional polymer networks in mixtures of chloroform and acetonitrile, which feature bpyPPE–metal–bpyPPE cross-links. The complexes of Zn^{2+} and Cd^{2+} with d^{10} electrons are light emissive, whereas the complexes of Cu^+, Co^{2+}, and Ni^{2+} form nonradiative metal-to-ligand charge-transfer complexes with the polymers. Hecht and Meudtner used a similar approach and incorporated metal binding sites into the polymer backbone rather than into the side chains [131]. Their polymer synthesis is based on a step-growth polymerization process using multiple efficient Cu-catalyzed 1,3-dipolar cycloaddition reactions of 2,6-diethynylpyridine and 3,5-diazidobenzoate monomers. The monomers contain oligo(ethylene glycol) side chains to provide solubility in both nonpolar and polar solvents. Addition of various transition metal ions such as Zn^{2+}, Fe^{2+}, and Eu^{3+} to such polymer solutions

in acetonitrile instantaneously leads to gelation by tridentate complexation of the 2,6-bis(1,2,3-triazol-4-yl)pyridine (BTP) units to the metal ions. Whereas 1:2 complexes are formed in the case of Fe^{2+}, 1:3 complexes are created in the case of Eu^{3+} as a result of its larger atom radius [132], exhibiting binding constants of the order of 10^7 M^{-1}. Recently, in a similar approach, Weng and coworkers used polyurethane chemistry to synthesize a macromolecular ligand containing a BTP unit in the main chain [133]. Gels were prepared from this macromolecule by addition of Zn^{2+} and/or Eu^{3+} ions in mixtures of chloroform/acetonitrile or chloroform/THF. The gels containing Eu^{3+} are stronger and more elastic than the gels formed with Zn^{2+}, which is consistent with the different binding characteristics of both metals. When chloroform/methanol mixtures are used, however, no gels are obtained, despite the fact that a slight increase in the solution viscosity is observed. This observation is attributed to the chelating ability of methanol, which prevents formation of stable or long-living metal–BTP complexes. The Zn^{2+}-containing gel exhibits blue fluorescence in chloroform/acetonitrile on account of the Zn–BTP complex emission. When Zn^{2+} is replaced by Eu^{3+}, the emission is higher because of the Eu–BTP complex, resulting in a change in the gel's emission from blue to characteristic red-orange. Both the Eu^{3+}- and Zn^{2+}-containing gels are thermoresponsive and also sensitive to different chemical stimuli such as chelating agents. Moreover, both gel types show excellent self-healing properties: when freshly cut blocks of the gels are joined together and kept in contact for several hours at room temperature, the newly formed gel bar is strong enough to sustain squeezing, bending, and stretching.

Rowan and coworkers took advantage of the ability of lanthanide metals to form complexes with up to three tridentate ligands and prepared multiresponsive metallo-supramolecular polymer gels from linear ditopic macromonomers [134]. For this purpose, a 2,6-bis(1-methylbenzimidazolyl)pyridine (BIP) moiety was attached to either end of an oligo-PEG core, and either lanthanum(III) and cobalt(II) or europium(III) and zinc(II) were used to form gels in a mixture of chloroform and acetonitrile. The Co^{2+} or Zn^{2+} ions act as linear chain extension binding units, whereas the La^{3+} or Eu^{3+} ions act as cross-linking components, as illustrated in Fig. 7. By this means, four different gels were prepared containing Co/La, Zn/La, Co/Eu, and Zn/Eu. Upon removal of the solvent mixture, all four gels could be re-swollen in pure acetonitrile, in which they show thermoresponsive behavior: heating the Co/La gel to 100 °C results in a reversible gel–sol transition. At higher temperatures, the orange color of the Co-materials persists in solution, suggesting that it is the La–ligand interaction that is thermally broken. Addition of formic acid to the gels results in a loss of their mechanical stability due to strong binding of lanthanides to carboxylic acids. Furthermore, these gels were found to exhibit thixotropic (shear-thinning) behavior. Shaking the Zn/La gel, for example, results in a free-flowing liquid that reconverts into a gel state upon rest. This network reconstruction was investigated extensively by oscillatory shear rheology [135], revealing that partial reconstitution of the network takes place instantaneously within 16 s, but complete regeneration of the formerly existing gel requires

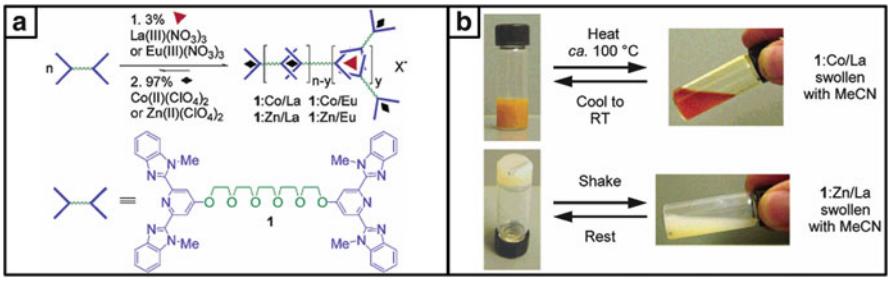

Fig. 7 Metallo-supramolecular polymer gels as introduced by Rowan and coworkers. (**a**) Organogels formed by complexation of lanthanide and transition metal ions to 2,6-bis (1-methylbenzimidazolyl)pyridine (BIP)-functionalized poly(ethylene glycol). (**b**) Thermo- and mechanoresponsiveness of these gels. Reprinted with permission from [134]. Copyright 2003 American Chemical Society

18 min. It is hypothesized that reassembly appears to be a complex three step-process.

Rowan and Beck extended their work on these gel materials and showed that the stimuli-responsiveness depends on the type of metal and counter ion as well as on the amount of the swelling agent [136]. To deeply explore the properties of these gels and the nature of the gelation mechanism, Rowan and colleagues performed a series of experimental studies, including optical and confocal microscopy, dynamic light scattering (DLS), wide-angle X-ray diffraction, and rheology [137, 138]. Morphological observation and X-ray diffraction suggest that the gelation occurs via flocculation of semicrystalline colloidal particles, which results in pronounced yielding and thixotropic mechanics of the gels. To investigate the influence of the solvent on the formation of BIP-based hydrogels, Rowan and colleagues used a mixed solvent system, consisting of a good solvent [dimethyl sulfoxide (DMSO)] with either a nonsolvent (water) or a poor solvent (ethylene glycol) [139]. For each solvent system, there is a composition window in which gels are formed. However, the gels vary drastically in turbidity, from highly opaque in the water- or ethylene glycol-rich solvent mixture to highly transparent in the DMSO-rich mixture. Morphological and DLS observations reveal that also in these materials, gelation occurs by the flocculation of semicrystalline colloidal particles: an increase in the DMSO content leads to a reduction in the particle size, accompanied by an increase in sol concentration and in gel transparency along with an increase in the shear storage modulus. Scattering analysis indicates that the degree of crystallinity of the colloidal particles is dramatically decreased compared with those formed in pure acetonitrile; however, a new lamellar organization develops when the DMSO content increases. Although Rowan and coworkers used a pentaethylene oxide core equipped with BIP moieties on either end for the previously described approaches, in 2009 the same authors explored how small changes in the length of the ethylene oxide core influence the properties of the corresponding gels [140]. For this purpose, precursors with a tetra- and hexaethylene oxide core were prepared. Investigations of the gelation kinetics indicate that the rate of gelation decreases

with the core length. In rheology under equivalent conditions of solvent quality and polymer concentration, the shear modulus of the pentaethylene core gels is substantially higher than that of the other core lengths. This finding is attributed to a lower solubility of the tetraethylene precursors, resulting in smaller, denser colloidal particles and, hence, a lower particle volume fraction. In the case of the hexaethylene cores, the lower modulus is attributed to their higher solubility, resulting in a larger sol fraction.

In analogy to their synthesis of hydrogen-bonding side-chain functionalized polynorbornenes, Weck and coworkers prepared the same polymers containing both metal coordination sites and hydrogen-bonding motifs [141]. For the metal coordination, palladated metallopincer complexes that can coordinate to pyridine (py) moieties were used, whereas cyanuric acid or diaminopyridine moieties were employed for the formation of hydrogen bonds. By this means, polymer cross-linking is achievable in an orthogonal manner via metal coordination and hydrogen bonding upon addition of suitable small-molecule cross-linking agents to the polymer solutions in chloroform. Whereas metal-complexation cross-linking results in a dramatic increase in the solution viscosities, cross-linking by hydrogen bonding only leads to minor changes in the viscosity. When just one type of supramolecular interaction is used for polymer cross-linking, the second recognition motif along the polymeric backbone can serve to add further reversible functionalization of the polymer network. In a follow-up study, Weck and coworkers prepared similarly functionalized polynorbornenes containing both hydrogen-bonding and metal-coordination sites and studied the orthogonal de-cross-linking of the resulting networks in 1-chloronaphthalene [142]. The hydrogen-bonded polymer networks are thermally reversible, whereas the metal-coordinated cross-linked networks mainly show chemoresponsive behavior. As a result, the metal coordination can be reversed by addition of suitable ligand displacement agents without affecting the hydrogen-bonded cross-links. In contrast, the hydrogen bonds can be selectively disassembled through competitive interactions with a monotopic end-capping agent without affecting the metal-coordinated cross-links.

Craig and coworkers also used metallopincer complexes to form supramolecular polymer networks [143, 144]. In their work, poly(4-vinylpyridine)s were synthesized and subsequently cross-linked by addition of small-molecule bifunctional palladium(II) or platinum(II) *N*,*C*,*N*-pincers in dimethyl sulfoxide. With this approach, the authors were able to control the dynamic mechanical properties of the gels, as discussed in detail in the Sect. 2.3.

Although some examples of thermoreversible metal coordination have been reported and discussed, very often metal complexation is too strong to be reversible within the temperature range accessible in a given experimental situation, most severely limited by the range of liquidity of the solvent or swelling agent. To extend this temperature range, Noro et al. demonstrated that ionic liquids are suitable as swelling medium for thermoreversible polymer gels via metal–ligand coordination [145]. In their work, an ABA triblock was synthesized, the end blocks of which bore pyridine side groups, which can coordinate to zinc(II) chloride. FTIR spectroscopy

reveals metal–ligand coordination in the ionic liquid, and temperature-ramp oscillatory shear measurements confirm thermoreversible viscoelastic properties between a gel-like state and a liquid-like state.

As described previously, several studies of the melt rheological properties of supramolecular polymer networks assembled through hydrogen bonds have been carried out, but much less effort has been spent on metallo-supramolecular polymers and networks. Recently, this gap was closed by Rowan et al., who prepared films of poly(tetrahydrofuran) and poly(ethylene-*co*-butylene) functionalized with BIP moieties on both chain ends [146]. Zinc(II) ions were used to induce chain elongation, whereas europium(III) ions were used to induce cross-linking. When the amount of europium is increased, more thermoresponsive films of both polymer materials are obtained, although an increase in the concentration of Eu^{3+} leads to a higher extent of supramolecular chain branching. However, in the materials with higher Eu^{3+}concentration , decomplexation of the weak Eu^{3+} complexes is easy, resulting in facile supramolecular depolymerization. Furthermore, it is observed that the polymeric core plays a significant role in the material properties. The nonpolar poly(ethylene-*co*-butylene) core displays dramatic enhancement of the storage and loss moduli as well as viscosity compared with the more polar poly (tetrahydrofuran) core.

2.3 Dynamics in Supramolecular Polymer Networks

The properties of supramolecular polymer networks display a delicate dependence on the equilibrium binding constant (thermodynamics) and the binding–unbinding dynamics (kinetics) of the constituent supramolecular cross-linking motifs, along with the accompanying physical characteristics of the polymer [20, 147]. To rationally control these properties, quantitative understanding of these relationships must be achieved. In this respect, it is necessary to control both the polymer and molecular dynamics independently of the thermodynamics of the supramolecular motifs. In a seminal work, this goal was achieved by Craig and coworkers through the use of poly(4-vinylpyridine)s (PVPs) cross-linked with bifunctional metallopincers, as shown in Fig. 8a [143, 144]. Small variations in the steric hindrance between methyl and ethyl substituents on the pincers results in large changes in the complexation–decomplexation kinetics without significantly altering the binding–unbinding thermodynamics [148]. Vice versa, the binding thermodynamics can be varied by using two different metals, palladium and platinum, while retaining the same difference in the complexation–decomplexation kinetics between the methyl- and ethyl-substituted pincers [143, 144]. This approach showed that it is not the cross-linking thermodynamics but the rate of cross-link dissociation that has a major impact on the dynamic material properties. This observation can be summarized as ‘slow dissociation means strong cross-linking.’ As a result, a master curve of the frequency-dependent viscosity is obtained when the viscosity is scaled by the ligand dissociation rate (k_d) that was measured on low

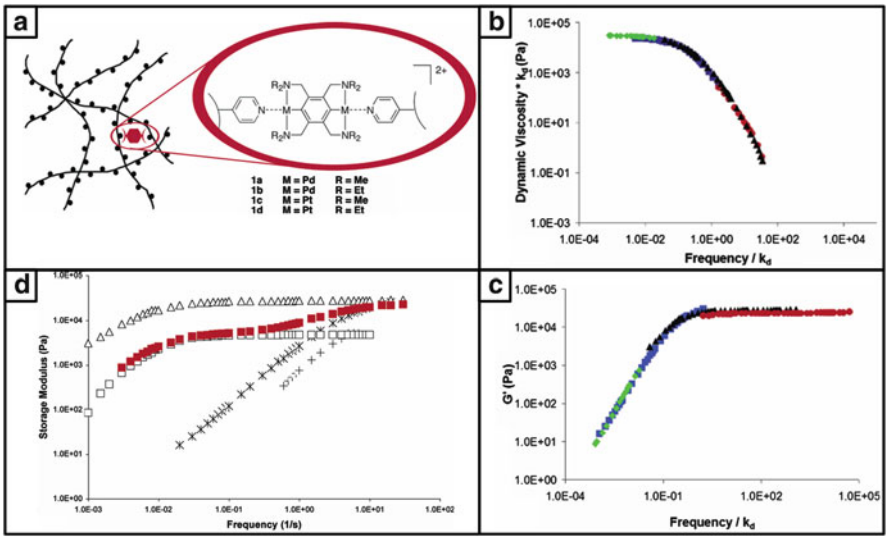

Fig. 8 Independent control of the molecular dynamics and thermodynamics of metallopincer-cross-linked poly(4-vinylpyridine) (PVP) supramolecular polymer networks in organic solvent. (**a**) Networks formed from PVP chains along with various cross-linking bimetallic compounds (*1a–1d*). (**b**) Dynamic viscosity of the resulting supramolecular organogels scaled by the dissociation rate constant of the metal–pyridine cross-linking bond, k_d, versus the frequency of oscillation, also scaled by k_d . (**c**) Storage modulus, G', versus the frequency of oscillation scaled by k_d. (**b**, **c**) Each of the networks consists of 5 % (by metal functional group per pyridine residue) of *1a* (*diamonds*), *1b* (*squares*), *1c* (*triangles*), and *1d* (*circles*) and PVP at 10 % by total weight of network in DMSO at 20 °C. (**d**) Storage modulus G' versus frequency for 2.5 % + 2.5 % (*1b* + *1c*)–PVP (*red squares*), 2.5 % *1c*–PVP (*open squares*), 5 % *1c*–PVP (*open triangles*), 2.5 % *1b*–PVP (*plus signs*), and 5 % *1b*–PVP (*asterisks*) at 10 % by total weight of network in DMSO at 20 °C. Reprinted with permission from [147, 149]. Copyright 2005, 2007 American Chemical Society

molecular weight model complexes and when the frequency of the applied strain is scaled inversely by the same value, as shown in Fig. 8b. Furthermore, a master curve of the storage modulus can be obtained if the frequency of the applied strain is scaled by the ligand dissociation rate, k_d, as shown in Fig. 8c.

Experiments on supramolecular networks formed with multiple types of cross-linkers show that the response to an applied stress occurs through discrete contributions of each type of cross-linker rather than being an average of the contributing species [149–151]. Frequency-dependent measurements of such networks exhibit multiple plateau values in $G'(\omega)$, the corresponding inverse frequencies of which can be associated with the individual time constants of dissociation of the different cross-links, as demonstrated in Fig. 8d. Because the macroscopic dynamic response is controllable at the level of molecular associations, this effect has been called the 'macromolecular analogue of the kinetic isotope effect' [147].

The observations by Craig and coworkers have been supported by other groups who studied polymer networks based on different interactions, such as hydrogen bonding and host–guest complexation. For example, Meijer and coworkers found

that the simple Maxwell model is applicable to description of the viscoelastic behavior of hydrogen-bonded UPy-functionalized polymer networks [78]. The resulting single relaxation time agrees well with the lifetime of the UPy dimer, as measured independently by NMR spectroscopy. In addition, Scherman and coworkers applied the Maxwell model to host–guest cross-linked cucurbit[8]uril (CB[8]) systems (see Sect. 3.3 for details) and were able to determine the CB [8] ternary complex kinetics [152]. Moreover, Anthamatten demonstrated that systems consisting of both covalent and supramolecular cross-links exhibit a discrete contribution from the dynamics of the supramolecular cross-linking [40]. To model both types of cross-links, the authors developed a mechanical model that consists of a parallel array of an elastic spring (covalent contribution) and a Maxwell element (supramolecular contribution). They studied the creep, stress relaxation, and strain recovery and found that it is the hydrogen bond dissociation that dominates the elastomeric creep and shape recovery. Recently, the same group investigated how the dynamic behavior of functional poly(*n*-butyl acrylate) melts and cross-linked networks is influenced by hydrogen-bonding side groups of different associative strength [153]. They observed that copolymers containing weak hydrogen-bonding side groups behave like unentangled melts and exhibit higher storage and loss moduli with increasing amounts of binding groups. In contrast, copolymers containing strong hydrogen-bonding groups behave like entanglement networks.

The influence of ligand-exchange kinetics on the material properties of supramolecular polymer networks was investigated by Sijbesma and coworkers [154], who prepared reversible coordination networks by complexing diphenylphosphinite telechelic poly(tetrahydrofuran) with rhodium(I) or iridium(I) ions in chloroform solvent. Ultrasonication of both gels causes liquefaction after 3 min; re-gelation occurs after 1 min in the case of the rhodium(I) gel, but after 1.5 h for the iridium(I) gel. NMR measurements on model complexes show that the large differences in gelation times are in agreement with the ligand-exchange kinetics of the rhodium(I) and iridium(I) complexes. It is assumed that sonication of the gels results in ligand exchange, which changes the network topology without changing the coordination chemistry. Hence, upon stopping ultrasonication, the gel fraction increases at a rate that is determined by the exchange kinetics of the metal complex.

3 Supramolecular Hydrogels

Early research on supramolecular polymer networks and gels was mostly performed in the melt state or in nonpolar organic media. This was because most of the initial supramolecular binding motifs were not strong enough to form networks in polar organic solvents or in water. Applications in the biomedical area, however, require the use of aqueous media. As a result, research on stronger supramolecular binding motifs, along with the development of supramolecular polymer hydrogels, has become a lively field. Many approaches attempt to mimic

nature, where strong directed supramolecular interactions serve to form sophisticated self-assembled structures.

3.1 Hydrogen Bonding

3.1.1 Synthetic Polymers

Approaches for the preparation of hydrogen-bonded supramolecular hydrogels based on synthetic polymers are rare because of the challenge of designing binding motifs with associative interactions strong enough to withstand competitive hydrogen bonding with water. Recently, Meijer and coworkers addressed this challenge and reported the formation of hydrogen-bonded supramolecular hydrogels formed from UPy-terminated linear PEG, with additional hydrophobic linkers between the UPy moieties and the PEG backbone [155]. To prepare these hydrogels, the UPy–PEG precursors were dissolved in an isotonic water solution at 70 °C and then cooled to room temperature. The presumed mechanism of hydrogel formation is summarized and visualized in Fig. 9a. In dilute solution, the polymers aggregate to form isolated nanofibers (Fig. 9b) as a result of the presence of an urea motif incorporated into the hydrophobic blocks, which is prone to undergo lateral hydrogen bonding [92]. With increasing polymer concentration, these nanofibers form a transient network (Fig. 9c). After approximately 16–24 h, the mechanical strength of the gel increases as a result of formation of supramolecular interchain cross-links. The equilibrium mechanical properties of these materials are tunable by variation of the ratio of hydrophilic and hydrophobic parts of the polymer chains. Erosion of the hydrogels has been studied by observation of the release of an incorporated rhodamine dye (Fig. 9d) and a fluorescent protein using fluorescence microscopy. Hydrogels formed from short PEG chains (6 kDa) release the rhodamine much more slowly than hydrogels formed from long chains (35 kDa), whereas the reverse effect is found for protein release. Furthermore, the release is much slower for aged hydrogels than for their freshly prepared counterparts. This finding can be discussed in view of an older hypothesis by Meijer and others, assuming that supramolecular polymer networks show self-repairing of network defects and reassemble into mechanically stronger structures with time [78, 88, 103].

In a follow-up study, Dankers et al. extended the UPy-precursor toolkit to linear polymers containing UPy moieties in the main chain [156]. The authors studied the rheological behavior of these materials, reported on their intrarenal behavior and tissue response, and proposed possible therapeutic applications. In another seminal work, Meijer and coworkers developed UPy-based dual-fiber networks as a synthetic analogue to fiber formation in the cytoskeleton [157]. For this purpose, mixtures of mono- and bifunctional polymers were used, which a priori form fibers in water; gelation could be achieved by decreasing the pH from 12 to 3.

Recently, Song and coworkers reported a very simple new method for fabricating tough hydrogels that are physically cross-linked by cooperative hydrogen

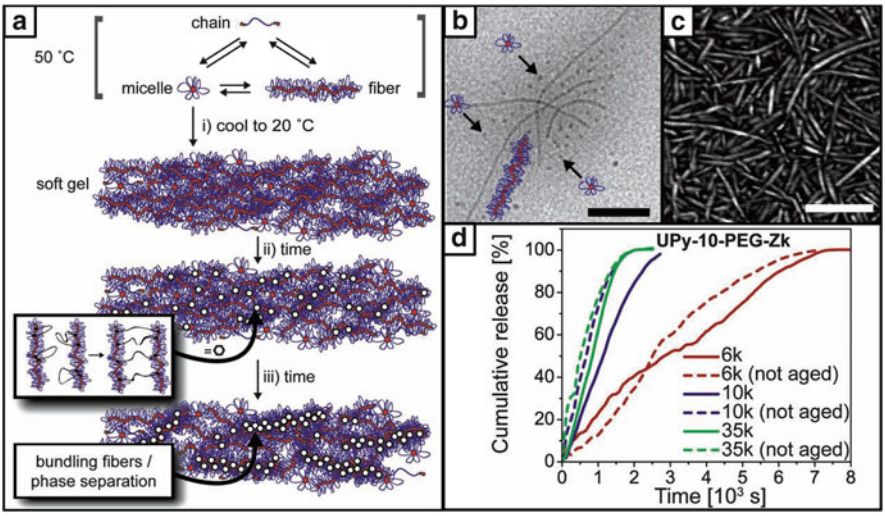

Fig. 9 Formation and characterization of supramolecular hydrogels based on poly(ethylene glycol) (PEG) chains that are end-functionalized with ureidopyrimidinone (UPy). (**a**) The process of hydrogel formation of UPy-modified PEG by hierarchical assembly of different structural units at 50 °C, comprising single chains, micelles, and fibers: *i*) Upon cooling or increasing the polymer concentration, a soft hydrogel forms. (*ii*) Formation of supramolecular cross-links after 16–24 h. (*iii*) Bundling of fibers, leading to phase-separated domains. (**b**) Cryo-transmission electron micrograph of fibers (*scale bar*: 100 nm). (**c**) Atomic force microscope (AFM) phase image of the formed fibers (*scale bar*: 100 nm). (**d**) Release of rhodamine B from hydrogels prepared from PEG precursors of different molecular weights, as well as from freshly prepared and aged hydrogels. Reprinted with permission from [155]. Copyright 2012 Wiley-VCH Verlag GmbH & Co. KGaA

bonding between a preexisting polymer and an in situ polymerized polymer [158]. These hydrogels were prepared by heating an aqueous acrylamide (AAm) solution in the presence of poly(*N*-vinylpyrrolidone) without any chemical initiators or covalent-cross-linking agents. Physical–chemical characterization, as well as molecular modeling indicates that the formation of strong cooperative hydrogen bonding between the preexisting poly(*N*-vinylpyrrolidone) and the in situ formed poly(acrylamide) (PAAm) chains contributes to the gel formation. Mechanical tests of the as-prepared and swollen hydrogels demonstrate high tensile strengths, high tensile extensibility, and high compressive strengths at low moduli.

3.1.2 Biopolymers

In contrast to the few examples of synthetic polymers that can be transiently cross-linked by hydrogen bonding, there is a huge variety of biopolymers that form supramolecular gels via hydrogen bonding. The most important representatives are polysaccharides such as cellulose [159, 160], starch [161], agarose [162, 163],

and dextran [164, 165], the physical cross-linking of which occurs via hydrogen bonding of their hydroxy groups.

The preparation of hydrogels from native cellulose is a problem because of its extended hydrogen-bonded structure, which largely limits its solubility in both aqueous and organic media at ambient temperatures [166]. Recently, new solvents such as *N*-methylmorpholine-*N*-oxide or ionic liquids have been used to dissolve cellulose, thereby providing new opportunities for the preparation of hydrogels directly from the native polymer [160]. Another strategy to increase the solubility of cellulose in water is partial alkylation by etherification of the hydroxy groups to generate methyl, hydroxypropyl, hydroxypropylmethyl, or carboxymethyl cellulose [166]. Methyl cellulose forms hydrogels when its aqueous solutions are heated above a particular temperature [167], most probably caused by hydrophobic interactions and exclusion of water between methoxylated regions of the polymer, along with hydrogen bonding between the remaining polymer hydroxy groups.

Because these cellulose derivatives are biocompatible, they have been tested in biomedical applications for the preparation of hydrogel matrixes [160]. However, these hydrogels degrade too rapidly for such applications; hence, blends of modified cellulose and other synthetic polymers or biopolymers (including PVA [168], hyaluronic acid [169], chitin [170], chitosan [171], and alginate [172]) have been investigated. Zhang and coworkers prepared cellulose/PVA hydrogels by using either chemical or physical cross-linking and compared the structure and properties of the different materials [168]. The chemical gels, which were prepared by cross-linking cellulose and PVA with epichlorohydrin, have a high swelling ratio but low mechanical strength. In contrast, the physical hydrogels, prepared by solution blending of cellulose and PVA and repeated freeze/thaw cycles, exhibit high mechanical strength as a result of the dense structure between cellulose and PVA. In another work, Shoichet and coworkers reported the development of a series of physical hydrogel blends composed of hyaluronic acid and methyl cellulose, designed for independent delivery of one or more drugs [173]. The hydrogels exhibit several useful properties such as injectability, safe swelling, satisfactory diffusivity of molecules up to 150 kg mol^{-1}, high residual particle load, and significantly slower in vitro degradation relative to earlier reports. The slow degradation rate of these hydrogels allows them to embed and release colloidal particles, rendering the composites useful for diffusion-limited and particle-mediated drug delivery for periods of 1 to 28 days. In follow-up studies, the same authors investigated this hydrogel type as a scaffold for cell transplantation [174] and drug delivery [175], focusing on the applicability of this system for treatment of injuries in the spinal cord. The authors determined the effects of polymer concentration on the hydrogel mechanical strength, gelation time, and cell viability. They found the mechanical stiffness to be tunable via manipulation of methyl cellulose and hyaluronic acid content. By this means, the mechanical properties of the hydrogels could be optimized for the encapsulation of human umbilical tissue-derived cells with viabilities of up to 90 % over a period of 3 days. As a result, these materials are promising vehicles for cell delivery and are presently being tested in ongoing in vivo studies.

3.2 Metal Complexation

3.2.1 Synthetic Polymers

Despite the high strength of metal–ligand coordination and the huge number of ligands that have been developed to form synthetic supramolecular polymer gels based on metal-complexation cross-linking in organic solvents, there are only a few examples of corresponding hydrogels.

Fraser and colleagues demonstrated that bipyridine-centered and dimethacrylate-modified PEG macroligands form hydrogels by iron (II) complexation that could be further strengthened by additional covalent cross-linking of the methacrylate moieties [176]. This approach served to form hydrogels with both supramolecular and covalent cross-links that are stimuli responsive to acid, base, peroxides, and heat, all of which lead to ligand dissociation and metal complex degradation, thereby entailing more loosely cross-linked materials.

Waite and coworkers mimicked the byssal threads of mussels, which allow mussels to physically attach to surfaces via the catechol-like amino acid dihydroxy-phenylalanine (DOPA) [177, 178], and prepared hydrogels from catechol-functionalized synthetic polymers cross-linked with iron(III) ions [179]. Tris- and bis-catechol-Fe^{3+} complexes possess some of the highest known stability constants of metal–ligand chelates (K_{eq} up to 10^{40} M^{-1}) [180]. The strength of complexation depends on the surrounding pH: whereas $pH \leq 5$ leads to formation of weak monocatechol complexes, $pH \geq 8$ promotes formation of bis- and tris-complexes. To achieve hydrogel preparation, the authors functionalized the hydroxy termini of tetra-arm PEG with DOPA moieties and mixed an aqueous solution of these precursor polymers with iron(III) ions at pH 5 to obtain a green-blue fluid. Upon increasing the pH to 8, a sticky purple gel is formed. This physically cross-linked hydrogel displays almost the same elastic shear modulus as a comparable covalently cross-linked gel. However, after applying high strain, the chemical hydrogel is irreversibly damaged, whereas the physical hydrogel regains its elastic modulus within minutes. This is attributed to its reversible cross-links, demonstrating the ability of these materials for self-healing. In a recent work, Waite and coworkers explored the utility of the DOPA derivative 3-hydroxy-4-pyridinone to form hydrogels with iron(III) [181]. When this compound is coupled to tetra-arm PEG, hydrogels can be formed with iron(III) at physiological pH. Reversible gelation can also be achieved with other biorelevant metal ions such as Al^{3+}, Ga^{3+}, and Cu^{2+}, allowing tuning of the gel dissolution profiles in controlled release applications.

Tong and coworkers reported the synthesis of a redox-responsive iron(III)-cross-linked poly(acrylic acid) (PAA)-based hydrogel [182]. Addition of iron(III) ions to a PAA solution produces a heterogeneous hydrogel as a result of fast binding of iron (III) to the carboxyl groups [183]. To prepare homogeneous gels, Tong and coworkers used citric acid to chelate the iron(III) ions and slow the binding rate. Then, the iron(III) ions were gradually released from the citrate complex by

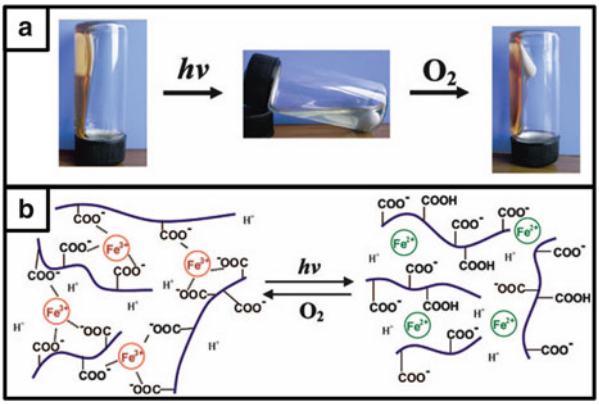

Fig. 10 Reversible gel–sol–gel transition in an iron(III)-cross-linked poly(acrylic acid)-based hydrogel. (**a**) The homogeneous hydrogel disassembles by irradiation with simulated sunlight of 80 mW cm^{-2} over a period of 12 min in the presence of citric acid. Subsequently, a homogeneous hydrogel can be re-formed by exposure to oxygen in the dark for 5 days. (**b**) Schematic of the gel–sol transition. Reprinted with permission from [182]. Copyright 2008 American Chemical Society

decreasing the pH to form a homogeneous hydrogel. The gel can be de-cross-linked by irradiation with sunlight for several minutes at room temperature through reduction of the iron(III) to iron(II). Vice versa, the hydrogel can also be re-formed by exposure to oxygen, as shown in Fig. 10.

3.2.2 Biopolymers

The most commonly used biopolymer for the preparation of metal-cross-linked hydrogels is alginate. It is obtained from brown algae and consists of mannuronic and guluronic acids that are covalently linked together in different sequences or blocks [184]. The blocks are either similar or strictly alternating, and the exact composition depends on the origin of the alginate. Alginates can be prepared with a wide range of molecular weights, from 50 to 100,000 kDa, and can be cross-linked to form hydrogels by multivalent ions such as Ca^{2+} or Ba^{2+} through complexation to their carboxy groups. The mechanical properties of these gels depend on the ratio of guluronic and mannuronic acid in the polymer and on the concentration of the cross-linking cations [185]. Alginates are highly biocompatible and nonimmunogenic [186] and are therefore widely applied in the pharmaceutical industry as excipients for drugs [187], wound dressings [188], and as synthetic extracellular matrixes for tissue engineering [189]. For these applications, the degradation of alginate-based hydrogels plays an important role. Ionically cross-linked alginates dissolve at neutral pH upon loss of the divalent cross-linking cations, which results in uncontrolled and typically slow degradation kinetics in vivo [190]. To overcome this problem, Mooney and coworkers attempted to control alginate degradation behavior by partially oxidizing the polymers and

making them susceptible to hydrolysis [191]. The biocompatibility of these modified hydrogels was investigated by culturing of myoblast cells on the surface. The cells adhered, proliferated, and differentiated at a rate comparable with that of the same cells on unmodified gels.

Alginate hydrogels are also bio-inert, because mammalian cells do not have receptors to adhere to them. As a result, it is desirable to covalently modify alginate to promote cell attachment by coupling of short peptides [189, 192–194], fibronectin [195], or collagen [196] to the alginate polymers.

3.3 Macrocyclic Inclusion Complexation

Inclusion complexation has developed to becoming another widely exploited supramolecular interaction for the formation of supramolecular polymer networks, mostly in water [197, 198]. Several classes of macrocycles have been developed, including crown ethers [199, 200], porphyrins [201, 202], cyclophanes [203], catenanes [204], cavitands [205, 206], cryptophanes [207], calix[*n*]arenes [208], and carcerands [209]. Macrocyclic-based supramolecular gels can either be formed from low molecular weight precursors or from macromolecular building blocks. The following discussion focuses on the latter.

Among the different types of macrocycles, two classes of cavitands have attracted particular attention in hydrogel chemistry [197]: cyclodextrins (CDs), which are the most extensively used macrocycles for forming supramolecular polymer gels [210–213], and cucurbit[*n*]urils (CB[*n*]s) [214–216], which are a newer promising type of binding motif. CDs consist of D-glucose repeating units coupled through α-1,4-glucosidic linkages; CB[*n*]s consist of repeating monomer units of glycoluril. Both cavitands form inclusion complexes by locking a guest molecule within the cavity of the host. Binding in CDs occurs through hydrophobic interaction between the guest and the inner cavity; in water, strong binding ($K_{eq} = 10^5\ M^{-1}$) occurs through additional solvophobic interaction [217]. CB[*n*]s exhibit even higher binding constants of around $K_{eq} = 10^{15}\ M^{-1}$ in water through additional ion–dipole interactions [218]. The exterior surface of cyclodextrins is hydrophilic due to the presence and high density of primary and secondary hydroxy groups; as a result, the commonly used α-, β-, and γ-CDs (six, seven, and eight D-glucose repeating units) are soluble in water; however, the water solubility of the β-CDs is relatively low. The solubility of CB[*n*]s varies in an odd–even fashion: CB[5] and CB[7] are highly water soluble, whereas CB[6] and CB[8] exhibit low water solubility [219]. Both CB[*n*]s and CDs are nontoxic and biocompatible and are therefore used in many life science applications and for the formation of supramolecular polymer networks. In 2000, cyclodextrins were approved by the FDA to be used in drug delivery [220].

CD-based hydrogels can be divided into several classes, as shown in Fig. 11: (a) poly(pseudo)rotaxane hydrogels that contain CDs threaded to precursor-polymer chain ends or (b) to precursor-polymer chain branches; (c) hydrogels

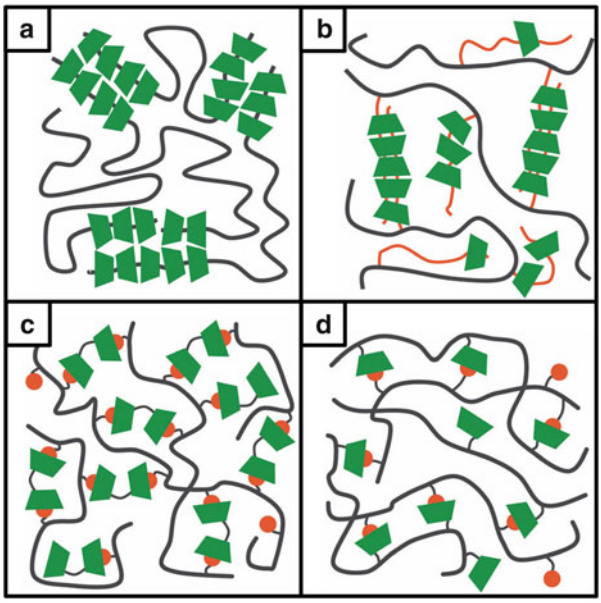

Fig. 11 Different design principles for the formation of cyclodextrin (CD)-based supramolecular polymer networks in water. (**a**) Cross-linking of hydrophilic polymer chains by threading CDs to either of their chain ends, thereby interconnecting them by hydrogen bonding between the exteriors of the CDs. (**b**) Similar cross-linking of polymer chains by threading CDs to dangling side-arm branches. (**c**) Cross-linking of precursor polymers that contain guest groups in their side chains by small-molecule CD dimers. (**d**) Cross-linking of precursor polymers that bear CD or guest moieties in their side chains. Reprinted with permission from [197]. Copyright 2012 Royal Society of Chemistry

that contain guest groups in precursor-polymer side chains, cross-linked by addition of small-molecule CD dimers; and (d) hydrogels obtained by mixing a polymer that is functionalized with CDs and another polymer that is functionalized with the corresponding guests. At least one example of each hydrogel class is presented next.

In 1994, Harada and colleagues reported the first example of hydrogels formed by the complexation of linear PEG chains with the inner cavity of α-CDs [221]. Hydrogen bonding between the exteriors of the bound cyclodextrins leads to the formation of crystalline domains and polymer-chain cross-linking. With this mechanism of cross-linking, several PEG-containing block copolymers have been developed and gelled by α-CDs [222]. The materials are biocompatible, thermoresponsive, and shear-thinning, which makes them ideal candidates for controlled release applications and drug delivery [223, 224]. If γ-CDs are used, which have a larger ring diameter, very strong networks can be formed by threading two polymer chains through the macrocycle. By this means, Yui and coworkers prepared pH-responsive networks from γ-CDs and poly(ethylene glycol)-*block*-poly (ethylenimine) [225].

Adamantyl groups are known to be strongly intercalated within β-CD. Using this principle, Ritter and coworkers prepared adamantyl-containing copolymers of *N*-isopropylacrylamide and cross-linked them using a low molecular weight CD dimer [226]. The networks exhibit a remarkable decrease in the lower critical solution temperature (LCST) of the copolymer, from 35 °C to around 15 °C, as a result of the restriction to the mobility and solubility of the polymer. In a recent approach, Ritter, Barner-Kowollik, and colleagues attempted to synthesize CD-based hydrogels by using linear double end-chain functionalized adamantyl poly(*N*,*N*-dimethylacrylamide) cross-linked by a CD trimer [227]. In this approach, however, only viscous liquids and no gel-like materials were obtained.

Instead of using CD dimers for cross-linking, several research groups attached the CDs to a second polymer; in this strategy, mixing of the host- and guest-functionalized polymers can serve for hydrogel formation [228, 229]. When the host and guest molecules are attached to the same polymer, intrachain cross-linking is observed [230]. Several different synthetic and natural backbone polymers such as polyacrylic esters, poly(allylamine)s, polymethacrylates, polyesters, poly (ethylenimine)s, and chitosan, all equipped with CD side chains, have been investigated in view of this approach [231].

In addition to their inherent thermoresponsiveness, CD-based hydrogels that respond to pH, redox-potential, and light have been designed [217, 232–234]. The first example of a light-responsive hydrogel obtained from a CD polymer and a guest polymer was reported by Harada and coworkers [235]. They used a glucan curdlan equipped with α-CDs and azobenzene-modified PAA. These materials are cross-linked by the complementary interaction of the α-CD unit and the *trans*-azo group. Upon UV-irradiation, the azo-moieties are isomerized to their *cis*-configuration, resulting in decomplexation and dissociation of the hydrogel network. This gel–sol transition is reversible, and polymer networks can be re-formed by irradiation with visible light or heating to trigger re-isomerization of the azo groups to their *trans*-configuration.

Like CD-based hydrogels, CB[*n*]-derived hydrogels can also be divided into different classes: (1) hydrogels that consist of a three-component system cross-linked by ternary CB[8] inclusion complexes and (2) hydrogels based on a two-component system of CB[6]@alkylammonium ion host–guest pairs. At least one example of each hydrogel class is described.

In 2010, Sherman and coworkers were the first to reported three-dimensional supramolecular cross-linked polymeric materials based on the CB[8] 1:1:1 ternary binding motif in water [152]. Copolymers were prepared that either contained pendant methyl viologen, which is a good first guest for CB[8], or naphthoxy derivatives, which are good second guests for CB[8], as visualized in Fig. 12a. Addition of CB[8] to a colorless solution of the two copolymers leads to transformation into a highly viscous, colored supramolecular hydrogel with a cross-linking density that can be controlled by the amount of CB[8]. The hydrogels exhibit solid-like mechanical properties at 5 wt% in water, with plateau moduli of 350–600 Pa at a cross-linking density in the range of 2.5–10 %, which is complementary to other supramolecular hydrogels that exhibit higher mechanical strength [236, 237]. In a

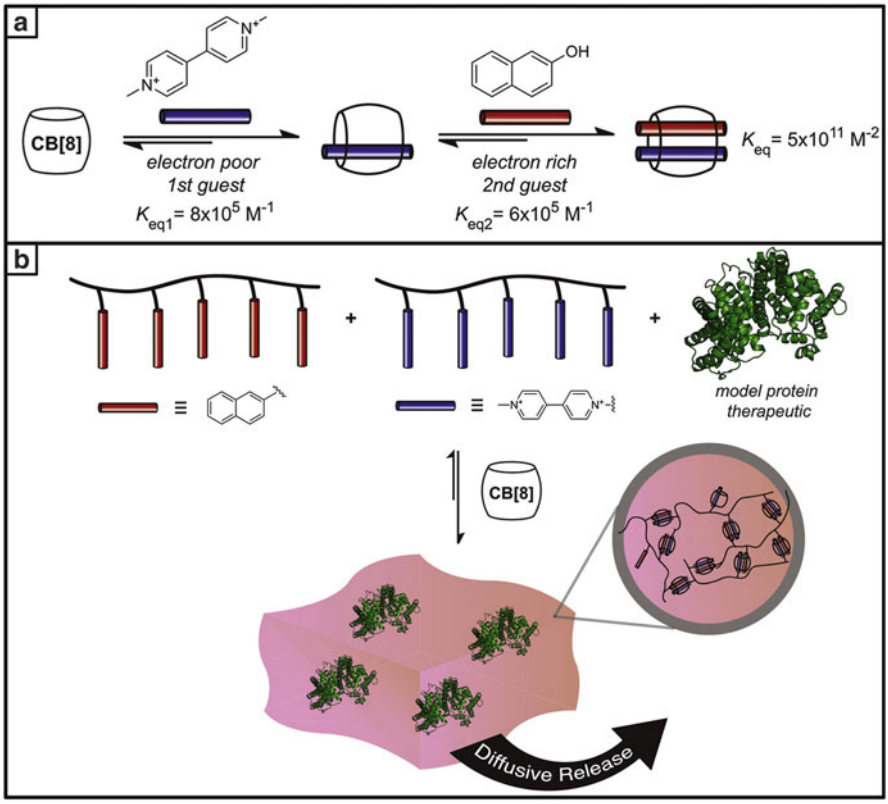

Fig. 12 Hydrogel formation by two-step, three-component binding of cucurbit[8]uril (CB[8]). (**a**) Copolymers that contain pendant methyl viologen are good first guests for CB[8], whereas copolymers that contain naphthoxy derivatives are good second guests for CB[8]. (**b**) Preparation of protein-laden high water-content CB[8] hydrogels. Reprinted with permission from [239]. Copyright 2012 Elsevier

following work, Sherman and coworkers reported on ultrahigh water content hydrogels (up to 99.75 % of water) based on the same host–guest complexation but derived from renewable cellulose derivatives [238, 239]. The authors demonstrated shear-thinning behavior as well as sustained release of model proteins from these materials (Fig. 12b) over the course of 160 days, which shows their potential for biological applications.

In another work, Kim and coworkers demonstrated the supramolecular assembly of CB[6]-conjugated hyaluronic acid and diaminohexane-conjugated hyaluronic acid to biocompatible hydrogels in the presence of living cells [240]. The authors exploited the high binding affinity and selectivity of CB[6] toward alkylammonium ions in aqueous solution ($K_{eq} = 10^{10}$–10^{12} M^{-1}). Excellent cell viabilities of more than 90 % were observed after incubation of the cell-laden hydrogels for 3 days. Moreover, the hydrogels are degradable by enzymes, which is an important

property of artificial extracellular matrixes. Favorably, the presence of free alkylammonium groups in the polymer network allows the attachment of functional tags such as dyes and adhesion peptides.

3.4 Ionic Interactions

Hydrogels based on ionic interactions are extremely robust materials and therefore provide an alternative to covalently cross-linked hydrogels [241, 242]. This is because of the extremely strong binding of the multivalent, oppositely charged precursor polymers. Nevertheless, these materials are highly responsive to and degradable by changes in the pH or salt concentration in the swelling medium. Ionic hydrogels can be obtained from both synthetic precursor polymers and from biopolymers.

3.4.1 Synthetic Polymers

Polyelectrolytes based on block copolymers are widely used for the preparation of hydrogel materials. Often, an ionic midblock serves as the water-soluble component, whereas neutral and hydrophobic end blocks lead to network formation by collapsing into local phase-separated domains [243]. In contrast, there are only a few examples of hydrogels solely based on ionic interactions. This is because mixing of oppositely charged polyelectrolytes is often impossible, favoring macroscopic phase separation; however, this can be prevented when copolyelectrolytes are used that contain neutral hydrophilic midblocks. In this case, phase separation is limited to occur microscopically, leading to micelles that consist of a core containing a polyelectrolyte complex and a corona of neutral solvophilic blocks.

Hawker and coworkers used such an approach and prepared ionic ABA triblock copolymers consisting of a central PEG block and charged end blocks, including varying numbers and types of ionic functional groups such as sulfonate, carboxylate, ammonium, and guanidinium, as shown in Fig. 13a [244]. By synthesizing triblock copolyelectrolytes that are identical in all aspects except for the ionic groups, the dependence of hydrogel formation on the effects of polyelectrolyte pK_a could be probed, as shown in Fig. 13b. When solutions of copolyelectrolytes bearing weak ionic groups such as ammonium and carboxylate or ammonium and sulfonate are mixed, transparent viscous fluids are formed. In contrast, mechanically robust hydrogels are obtained through the strong interaction of carboxylate- and guanidinium-functional triblock copolyelectrolytes. When copolyelectrolytes bearing the strongest ionic groups (sulfonate and guanidinium) are mixed, the most stable, mechanically resilient gels are formed even at low polymeric concentrations (3–5 wt%). When incubated in sodium chloride solutions, these hydrogels exhibit enhanced responsiveness with increasing salt concentration. In a subsequent work, Tirrell and coworkers investigated the effect of variations in polymer concentration,

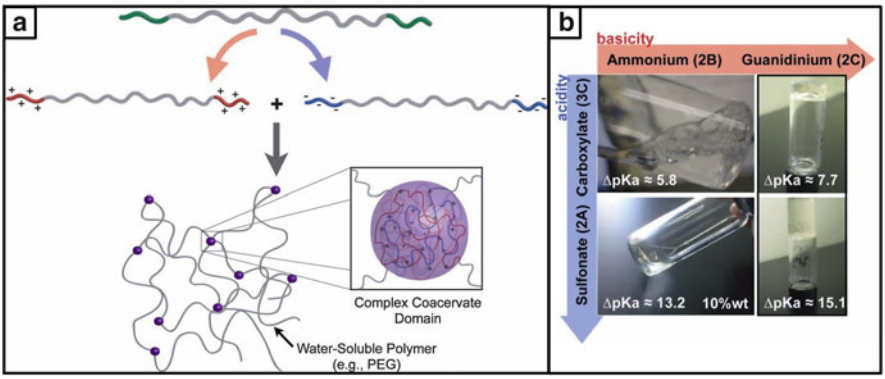

Fig. 13 Coacervate-driven hydrogel formation. (**a**) Oppositely charged ionic ABA triblock copolyelectrolytes are obtained from a triblock copolymer precursor. Mixing dilute aqueous solutions of each results in coacervate cross-linking and formation of a network structure. (**b**) Effect of polymer ionic strength on hydrogel properties. Reprinted with permission from [244]. Copyright 2011 Wiley-VCH Verlag GmbH & Co. KGaA

salt concentration, pH, and stoichiometry of the charged moieties on the structure and viscoelastic properties of these coacervate hydrogels [245].

In a similar work, Cohen Stuart and coworkers prepared ABA triblock copolymers with negatively charged end blocks and a water-soluble neutral middle block, as well as a positively charged homopolymer [32]. When aqueous solutions of the oppositely charged polymers are mixed, a highly viscous and transparent gel is formed spontaneously. In agreement with the work of Hawker and colleagues, small-angle X-ray scattering (SAXS) reveals that the gels consist of a network of interconnected polyelectrolyte-complex micelles wherein the neutral middle blocks form bridges. The network properties are tunable by the concentration, temperature, ionic strength, pH, and charge composition.

In another approach, Aida and coworkers end-capped linear PEGs with dendrimers bearing positively charged guanidinium groups [236]. When these materials are mixed with negatively charged polyacrylates and clay nanosheets, hydrogels are obtained. The mechanism of hydrogel formation is explained as follows: When the clay nanosheets, which are highly entangled with one another, come into contact with polyacrylates, they are exfoliated and dispersed homogenously as a result of the mutual repulsion caused by a possible site-specific wrapping of their positively charged edges with the anionic polyacrylates. The nanosheets, which subsequently contain highly negatively charged surfaces, are then cross-linked by the guanidinium-containing PEG dendrimers to form a 3D network in water. The hydrogels exhibit an exceptional mechanical strength (G' up to 10^6 Pa) as well as rapid self-healing. In a follow-up study, the same group was able to prepare similar hydrogels by using linear ABA triblock copolyethers carrying guanidinium groups in their end blocks [237]. These hydrogels are as tough as the dendrimer-based gels, but the linear binders can be obtained by much less elaborate syntheses from starting materials that are readily available.

Moreover, the gelling water can be freely replaced with ionic liquids and organic fluids, affording novel iono- and organogels.

3.4.2 Biopolymers

Chitosan is a well-investigated example of a polycationic biocopolymer composed of 2-acetamido-2-deoxy-D-glucopyranose and 2-amino-2-deoxy-D-glucopyranose. It is prepared industrially by hydrolysis of the aminoacetyl groups of chitin, which is a naturally available polymer [246]. Because chitosan is nontoxic, biocompatible, and biodegradable, it has attracted considerable interest in a wide range of biomedical and pharmaceutical applications, including drug delivery [247], cosmetics [248], and tissue engineering [249]. Chitosan has primary hydroxyl and cationic amino groups that can react with a number of multivalent anions to form hydrogels [249]. Various polyelectrolyte hydrogels have been prepared with natural polyanions such as xanthan [250], hyaluronic acid [251], alginate [252], collagen [253], pectin [254], and gelatin [255].

Xanthan has a cellulosic backbone and a trisaccharide side chain consisting of D-glucose, D-mannose, and D-glucuronic acid. The first report on chitosan–xanthan hydrogels was by Dumitriu and coworkers in 1994 [250]. Stable hydrogels exhibiting a fibrillar structure, as observed by electron microscopy, were formed that contained very high amounts of water (up to 95 %). Dumitriu investigated the structure–property relationship of these materials by variation of the precursor-polymer composition and found the mechanism of gelation to be based on coacervation [256]. Furthermore, electron microscopy revealed the formation of fibrillar structures, which makes this system interesting for biomedical applications such as drug delivery and cell encapsulation. As a result, numerous publications and patents have been released dealing with the applicability of these materials in areas ranging from immobilization of enzymes to dermatology [257, 258].

3.5 Hydrophobic Interactions

Hydrophobic interactions play an important role in the formation of large biological systems, but they can also be used to generate synthetic hydrogels [259]. For this purpose, hydrophobic sequences are incorporated within hydrophilic polymer-network chains. To achieve this, micellar polymerization is a commonly used technique [26]. A water-insoluble hydrophobic comonomer is solubilized within the micelles and is then copolymerized with a hydrophilic monomer in aqueous solution by free-radical addition polymerization. By this means, *n*-alkylacrylamides or *n*-alkyl methacrylates with alkyl chain lengths between 4 and 12 carbon atoms can be copolymerized with acrylamide to obtain tough hydrogels [260, 261]. Copolymerization of acrylamide with dodecyl methacrylate (C12) yields hydrogels exhibiting elastic moduli of around 1 kPa [261]. The hydrophobic associations

acting as temporary cross-links are strong enough to be retained in water during swelling of the gel network. Static light scattering reveals that these hydrogels are more homogeneous than the corresponding gels prepared by a chemical cross-linker, which is attributable to the mobility of the cross-linking nodes. Large hydrophobic monomers such as stearyl methacrylate (C18) and dococyl acrylate (C22) with very low water solubility could also be copolymerized with acrylamide in a micellar solution by the addition of salt (NaCl) [26, 262, 263]. The salt leads to micellar growth and solubilization of the hydrophobes. The hydrogels thus obtained exhibit excellent self-healing properties. When fractured, they can be repaired by joining their fractured surfaces to self-heal at room temperature, after which the materials regain their original mechanical properties. However, when swollen in water, such hydrogels lose their ability to self-heal as a result of the extraction of SDS micelles from the gel network by dilution and washing procedures. Recently, Okay and coworkers reported that complete healing of these swollen physical gels is achievable by treatment of the damaged area with an aqueous solution of wormlike SDS micelles [264].

As an alternative to alkyl side chains, fluorocarbon hydrophobes can also be used to prepare hydrogels based on hydrophobic interactions [265–267]. In water, fluorocarbon motifs display even stronger hydrophobic association than hydrogenated hydrophobes. Fluorocarbon groups possess excellent chemical and biological inertness, along with favorable high gas permeability, all of which making them useful for biomedical applications.

4 Applications

4.1 Self-Healing

Microcrack formation and crack propagation are a common cause of material failure. To overcome this problem, supramolecular polymer networks have been developed that can self-heal on the basis of the dynamic nature of their reversible cross-links [268]. The healing can either occur in an autonomous fashion or upon exposure to an external stimulus such as heat, light, pressure, or mechanical stress.

In a much-noticed approach, Leibler and coworkers prepared self-healing supramolecular polymer networks based on multiple hydrogen bonding [38]. For this purpose, commercially available fatty acids with various degrees of branching were functionalized with hydrogen-bonding ureas that are capable of self-assembly, thereby forming glassy plastic materials ($T_g = 28$ °C). These materials were transformed into elastomers by swelling in dodecane ($T_g = 8$ °C), exhibiting an elongation to break of 600 %. If ruptured, the remaining fragments are capable of self-healing within a few minutes by hand-pressing them together. Rheological studies on the repaired rubber confirmed restoration of its original mechanical properties.

In 2011, Weder and coworkers reported the first healable metallo-supramolecular polymer networks [269]. They used telechelic macromonomers based on an amorphous poly(ethylene-*co*-butylene) core with 2,6-bis(1-methylbenzimidazolyl)pyridine (BIP) ligands and cross-linked the polymers using transition or lanthanide metal salts. Mechanical defects are healable by exposure of the crack to UV light; the metal–ligand motifs are electronically excited and the absorbed energy is converted into heat, which causes temporary disengagement of the metal–ligand motifs and thereby allows quick and efficient healing of defects.

Recently, Schubert and colleagues investigated the healing properties of terpyridine-based films [270, 271]. Methacrylate copolymers containing terpyridine moieties in the side chain were prepared, and iron(II) and cadmium(II) salts were used for cross-linking. In the case of iron(II) cross-linking, superfacial scratches could be healed by modest thermal treatment at 100 °C. The use of Cd^{2+} as a cross-linker gave improved self-healing properties such as lower healing temperatures (<75 °C) and faster healing.

Colquhoun, Hayes, and coworkers demonstrated that supramolecular polymer blends cross-linked by electronically complementary aromatic π-systems exhibit self-healing properties [272, 273]. In this approach, low molecular weight polyimides that contain multiple π-electron receptor sites bind to complementary π-electron-rich pyrene termini of telechelic polysiloxanes. The obtained materials exhibit relatively poor mechanical stability, but they are healable at temperatures above 80 °C. The mechanism proposed for this thermoreversible healing involves disruption of the intermolecular π–π stacking cross-links, followed by flow and re-association of disrupted polymer chains. To improve the mechanical properties, a second generation of materials was developed by modifying the polymeric backbone while maintaining the π-systems [28]. These materials exhibit improved healing properties, because healing is possible not only directly after fracture, but also if fragments are separated for more than 24 h and then brought into contact again. Recently, the same authors developed healable materials containing two distinct types of supramolecular interaction, hydrogen bonding and π–π interactions [29].

4.2 Shape Memory

When covalent and supramolecular cross-linking is combined, shape-memory materials can be obtained. If these materials are heated to a temperature at which the supramolecular cross-links break, only the remaining permanent cross-links give rise to an elastic response upon external deformation. If such deformation is applied along with a subsequent decrease in temperature, re-association of the supramolecular cross-links locks-in the deformation. If the temperature is increased again, the supramolecular bonds are re-broken, entailing unleashing of the stored elastic response of the permanent cross-links, thereby restoring the original shape of the material.

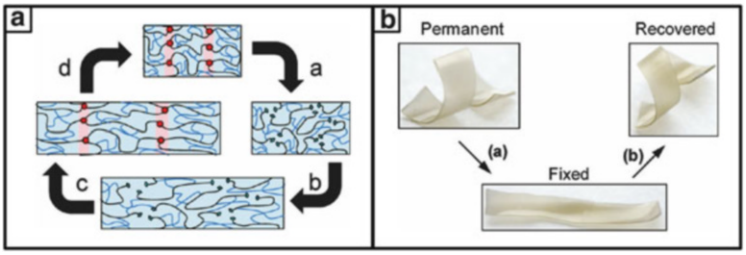

Fig. 14 Access to shape-memory materials from photocross-linked metallo-supramolecular polymers. (**a**) Formation of shape-memory materials using light as a stimulus: (*a*) UV light is absorbed by the metal–ligand complexes and is converted to localized heat, which disrupts the metal complexation; (*b*) the material can then be deformed; (*c*) removal of the light while the material is deformed allows the metal–ligand complexes to re-form and to lock-in the temporary shape; (*d*) additional exposure to UV light allows a return to the permanent shape. (**b**) Images demonstrating the shape-memory behavior. Reprinted with permission from [274]. Copyright 2011 American Chemical Society

To prepare films exhibiting multiresponsive shape-memory properties, Kumpfer and Rowan used a covalent photocross-linking process that allows the formation of complex permanent shapes and a metal–ligand hard phase serving as the reversible phase to fix an independent temporary shape [274]. For this purpose, low molecular weight polybutadiene was end-capped with BIP ligands that form high molecular weight metallo-supramolecular polymers upon addition of metal salts. In addition, the polymer solution contained a tetra-functional thiol along with a photoinitiator. Mechanically stable films obtained by solution casting comprise supramolecular metal–ligand cross-links but, so far, no covalent cross-links. Hence, the films can be brought into a variety of shapes, and exposure to UV light induces thiol-ene cross-linking, thereby fixing the shape. If the temporary metal–ligand phase is disrupted by a stimulus such as light, heat, or chemicals, an independent temporary shape can be created. Removal of the stimulus while the material is deformed allows the metal–ligand complexes to re-form and to lock-in the new shape. Applying another stimulus induces recovery back to the permanent shape, as illustrated in Fig. 14.

Besides metal-complexation, hydrogen bonding can also be applied to fix a temporary shape and to create shape-memory materials [275–277].

4.3 Drug Delivery

Because of their reversibility and stimuli responsiveness, supramolecular polymer gels have gained attention for the encapsulation of drugs and their subsequent controlled release at a targeted site [175, 278, 279]. The release can occur through autodegradation of the hydrogels by dilution of the surrounding medium, through specific stimuli at the target site (e.g., in response to decreased pH in tumor tissue [280]), or through external stimuli.

Catheter delivery of drugs to the heart is challenging, because the drugs are immediately pumped out of the heart again after injection. To overcome this problem, a carrier matrix is needed that is injectable through a long catheter in a solution state but then instantaneously gels. For this purpose, Dankers, Chamuleau and coworkers developed a UPy-based hydrogel that can be used as a carrier for catheter-injection of drugs into infarcted myocardium [281]. They prepared a supramolecular hydrogel that at pH > 8.5 is a liquid with viscosity low enough to enable passage through a catheter. Then, the natural pH of the tissue instantaneously transforms the injected solution into a drug-loaded hydrogel reservoir. Local in vivo delivery of contrast agents and growth factors by hydrogel autodegradation was demonstrated in a large animal model of ischemic heart disease.

Zhang and coworkers reported supramolecular hydrogels for dual drug release prepared by inclusion complexation [282]. Heparin was first conjugated to poly (ethylene glycol) methyl ether and then used to form a gel with α-cyclodextrin in aqueous solution. In addition, bovine serum albumin was encapsulated as a model protein drug. The resulting hydrogels show dual release behavior for the encapsulated model protein drug and conjugated heparin, along with good anticoagulant and blood-compatible properties.

Weber and coworkers developed a hydrogel for time-scheduled vaccination that consists of biohybrid materials cross-linked via multiple supramolecular interactions [283]. The hydrogel is based on two eight-arm PEG species with end groups that are either functionalized with fluorescein or with a humanized single-chain antibody fragment (scFv) that specifically binds fluorescein. Binding of the scFv to fluorescein cross-links the polymers to form a gel. The hydrogels were implanted subcutaneously into mice and could be dissolved upon oral administration of fluorescein. By this means, vaccines and pharmaceuticals can be released from the hydrogel in a remote-controlled manner.

4.4 Microgels for Cell Encapsulation

Microgels are hydrogel particles with micrometer-scale dimensions [284, 285]. They find multiple applications in drug delivery [286], biosensing [287], catalysis [288], and regenerative medicine [289]. Microgels are particularly useful for the encapsulation of living cells, because the microgel matrix can mimic the natural extracellular matrix very well and because microgel particles can be handled very easily by syringes and pipettes and are injectable [290]. If the microgels are prepared through the use of reversible chemical reactions or physical interactions, they are degradable or can be cleaved on demand, rendering them attractive for the reversible encapsulation of additives, including cells. For this purpose, several groups developed degradable microparticles on the basis of reversible cross-linking of natural polymers such as alginate [291], agarose [292, 293], or gelatin [294], all of which can serve for cell encapsulation. A versatile and powerful

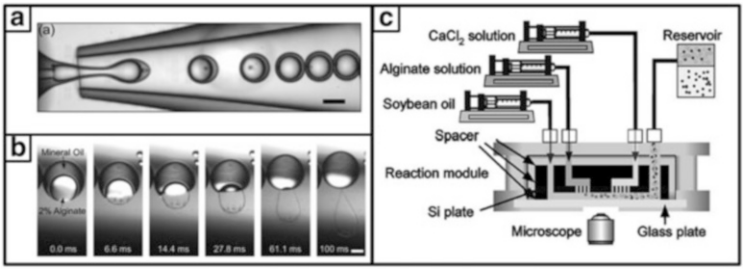

Fig. 15 Preparation of cell-laden alginate microgel particles. (**a**) Optical image of alginate/mineral oil double-emulsion drop formation. (**b**) Optical images showing the separation of the inner alginate drop from the mineral oil shell. *Scale bars*: 100 μm. (**c**) Experimental setup for preparation of alginate microgel particles using a micronozzle array. Reprinted with permission from [299, 300]. Copyright 2005, 2012 Elsevier and Wiley-VCH Verlag GmbH & Co. KGaA

technique for preparing microgel particles is droplet-based microfluidics [295–298]. In this approach, monodisperse emulsion droplets are formed and used as templates for microgel synthesis. For this purpose, a stream of an aqueous polymer or polymer-precursor solution (dispersed phase) is created in a microchannel and then periodically broken by flow focusing with an immiscible oil (continuous phase). Subsequent solidification of the droplets leads to microgel particles.

Weitz and coworkers reported a microfluidic technique for encapsulating living yeast cells in alginate hydrogel microparticles generated from monodisperse double-emulsion templates [299]. First, double emulsions were prepared that consisted of an alginate drop surrounded by a mineral oil shell, as shown in Fig. 15a. Once the alginate drop separates from the mineral oil shell and comes into contact with Ca^{2+} ions in the continuous phase, droplet gelation occurs (Fig. 15b). The viability of cells encapsulated in the resulting alginate microparticles was determined to be 65 % after 1 week.

In a related work, Nakajima and coworkers formed calcium alginate beads complexed with human kidney cells using a micronozzle array, as shown in Fig. 15c [300]. In this approach, an aqueous alginate solution containing the cells was extruded through a micronozzle and flow-focused with an oil phase to form alginate droplets. These alginate droplets were immediately reacted with $CaCl_2$ droplets downstream of the oil flow by collision and subsequent droplet coalescence, thereby forming calcium alginate gel beads with sizes between 50 and 200 μm depending on the flow rates. The viability of encapsulated cells was estimated to be around 70 %.

By using synthetic poly(*N*-isopropylacrylamide)-*block*-polystyrene precursor-polymers in combination with droplet microfluidics, Kumachev and colleagues were able to generate physically cross-linked nanofibrillar microgels [301]. The microgels can be formed under physiological conditions and rapidly dissociate upon cooling to 25–27 °C. This makes them interesting as scaffolds for temporary cell encapsulation and subsequent cell release for further cell characterization.

5 Conclusions and Outlook

The overview of supramolecular polymer networks given in this introductory chapter has shown the historical development of such materials and revealed their outstanding importance for many life science applications. Moreover, persistent challenges with respect to preparation and formulation of supramolecular networks have been addressed. In the following chapters of this volume, several examples and achievements of current research activities are given along these directions. Anthamatten reviews hydrogen-bonding interactions to form soft solid polymer materials with network architectures, including, glasses, melts, and elastomers [302]. Okay adds a perspective on the design, mechanics, and self-healing of hydrogels formed via hydrophobic interactions, with a particular emphasis on the role of surfactant micelles within the gels [303]. The development of donor–acceptor π–π stacking interactions as transient cross-links in self-healable supramolecular polymer networks is discussed by Greenland and Hayes [304]. Chau, Sriskandha, Thérien-Aubin, and Kumacheva highlight recent progress in the field of nanofibrillar supramolecular gels, discussing both synthetic and natural materials [305], whereas Li and Liu add a particular view on the potential of cellulose and cellulose derivatives for the formation of chemical and physical gels and microgels, with a specific view to supramolecular interactions within them [306]. Finally, Pape and Dankers provide a review on supramolecular hydrogels of several of the preceding kinds for use in the field of regenerative medicine [307].

References

1. Lehn J-M (1988) Angew Chem Int Ed Engl 27:89–112
2. Lehn J-M (1990) Angew Chem Int Ed Engl 29:1304–1319
3. Lehn J-M (2002) Polym Int 51:825–839
4. Wojtecki RJ, Meador MA, Rowan SJ (2011) Nat Mater 10:14–27
5. Schneider H-J, Yatsimirsky AK (2008) Chem Soc Rev 37:263–277
6. Lawrence DS, Jiang T, Levett M (1995) Chem Rev 95:2229–2260
7. Martell AE, Hancock RD, Motekaitis RJ (1994) Coord Chem Rev 133:39–65
8. Zeng F, Zimmerman SC (1997) Chem Rev 97:1681–1712
9. Moore JS (1999) Curr Opin Colloid Interface Sci 4:108–116
10. Aida T, Meijer EW, Stupp SI (2012) Science 335:813–817
11. Schubert US, Eschbaumer C (2002) Angew Chem Int Ed 41:2892–2926
12. Brunsveld L, Folmer BJB, Meijer EW, Sijbesma RP (2001) Chem Rev 101:4071–4098
13. De Greef TFA, Smulders MMJ, Wolffs M, Schenning APHJ, Sijbesma RP, Meijer EW (2009) Chem Rev 109:5687–5754
14. Fox JD, Rowan SJ (2009) Macromolecules 42:6823–6835
15. Sangeetha NM, Maitra U (2005) Chem Soc Rev 34:821–836
16. Dastidar P (2008) Chem Soc Rev 37:2699–2715
17. Piepenbrock M-OM, Lloyd GO, Clarke N, Steed JW (2009) Chem Rev 110:1960–2004
18. Smith DK (2010) Nat Chem 2:162–163
19. Noro A, Hayashi M, Matsushita Y (2012) Soft Matter 8:6416–6429
20. Seiffert S, Sprakel J (2012) Chem Soc Rev 41:909–930

21. Binder WH, Zirbs R (2007) Adv Polym Sci 207:1–78
22. Yu X, Samanta B, Xu H, Arumugam P, Ofir Y, Jordan BJ, Rotello VM (2009) Small 5:86–89
23. Boyd ASF, Carroll JB, Cooke G, Garety JF, Jordan BJ, Mabruk S, Rosair G, Rotello VM (2005) Chem Commun 2005(19):2468–2470
24. Whittell GR, Hager MD, Schubert US, Manners I (2011) Nat Mater 10:176–188
25. Lohmeijer BGG, Schubert US (2003) J Polym Sci A Polym Chem 41:1413–1427
26. Tuncaboylu DC, Sari M, Oppermann W, Okay O (2011) Macromolecules 44:4997–5005
27. Shao H, Parquette JR (2010) Chem Commun 46:4285–4287
28. Burattini S, Colquhoun HM, Fox JD, Friedmann D, Greenland BW, Harris PJF, Hayes W, Mackay ME, Rowan SJ (2009) Chem Commun 2009(44):6717–6719
29. Burattini S, Greenland BW, Merino DH, Weng W, Seppala J, Colquhoun HM, Hayes W, Mackay ME, Hamley IW, Rowan SJ (2010) J Am Chem Soc 132:12051–12058
30. Varshey DB, Sander JRG, Friščić T, MacGillivray LR (2012) Supramolecular interactions. In: Gale PA, Steed JW (eds) Supramolecular chemistry: from molecules to nanomaterials, vol 1. Wiley, New York, pp 9–24
31. Grassi G, Farra R, Caliceti P, Guarnieri G, Salmaso S, Carenza M, Grassi M (2005) Am J Drug Deliv 3:239–251
32. Lemmers M, Sprakel J, Voets IK, van der Gucht J, Cohen Stuart MA (2010) Angew Chem Int Ed 49:708–711
33. Rossow T, Hackelbusch S, van Assenbergh P, Seiffert S (2013) Polym Chem 4:2515–2527
34. Asoh T-A, Yoshitake H, Takano Y, Kikuchi A (2013) Macromol Chem Phys 214:2534–2539
35. Zhang Y, Zhang W, Li J, Dang J, Wei T (2012) Mater Lett 82:227–229
36. Qiu Y, Park K (2001) Adv Drug Del Rev 53:321–339
37. Dankers PYW, Meijer EW (2007) Bull Chem Soc Jpn 80:2047–2073
38. Cordier P, Tournilhac F, Soulie-Ziakovic C, Leibler L (2008) Nature 451:977–980
39. Murphy EB, Wudl F (2010) Prog Polym Sci 35:223–251
40. Li J, Viveros JA, Wrue MH, Anthamatten M (2007) Adv Mater 19:2851–2855
41. West JL, Hubbell JA (1995) Biomaterials 16:1153–1156
42. Osada K, Kataoka K (2006) Drug and gene delivery based on supramolecular assembly of PEG-polypeptide hybrid block copolymers. In: Klok H-A, Schlaad H (eds) Peptide hybrid polymers, vol 202. Springer, Berlin, pp 113–153
43. Alves M-H, Jensen BEB, Smith AAA, Zelikin AN (2011) Macromol Biosci 11:1293–1313
44. Abdel-Mottaleb MMA, Mortada ND, El-Shamy AA, Awad GAS (2009) Drug Dev Ind Pharm 35:311–320
45. Hassan C, Peppas N (2000) Structure and applications of poly(vinyl alcohol) hydrogels produced by conventional crosslinking or by freezing/thawing methods. In: Biopolymers · PVA hydrogels, anionic polymerisation nanocomposites. Advances in Polymer Science, vol 153. Springer, Berlin, pp 37–65
46. Radowski MR, Shukla A, von Berlepsch H, Böttcher C, Pickaert G, Rehage H, Haag R (2007) Angew Chem Int Ed 46:1265–1269
47. Zieringer M, Wyszogrodzka M, Biskup K, Haag R (2012) New J Chem 36:402–406
48. Merschky M, Wyszogrodzka M, Haag R, Schmuck C (2010) Chem Eur J 16:14242–14246
49. Lee KY, Mooney DJ (2001) Chem Rev 101:1869–1880
50. Raz N, Li JK, Fiddes LK, Tumarkin E, Walker GC, Kumacheva E (2010) Macromolecules 43:7277–7281
51. George M, Abraham TE (2006) J Control Release 114:1–14
52. Smidsrød O (1990) Trends Biotechnol 8:71–78
53. Zhang H, Tumarkin E, Peerani R, Nie Z, Sullan RMA, Walker GC, Kumacheva E (2006) J Am Chem Soc 128:12205–12210
54. Ishida K, Kuroda R, Miwa M, Tabata Y, Hokugo A, Kawamoto T, Sasaki K, Doita M, Kurosaka M (2007) Tissue Eng 13:1103–1112
55. Boucard N, Viton C, Agay D, Mari E, Roger T, Chancerelle Y, Domard A (2007) Biomaterials 28:3478–3488

56. Van Vlierberghe S, Dubruel P, Schacht E (2011) Biomacromolecules 12:1387–1408
57. Perez-Castillejos R (2010) Mater Today 13:32–41
58. Fu S, Thacker A, Sperger D, Boni R, Velankar S, Munson E, Block L (2011) AAPS Pharm Sci Tech 12:449–449
59. Paszek MJ, Zahir N, Johnson KR, Lakins JN, Rozenberg GI, Gefen A, Reinhart-King CA, Margulies SS, Dembo M, Boettiger D, Hammer DA, Weaver VM (2005) Cancer Cell 8:241–254
60. Ota T, Gilbert TW, Schwartzman D, McTiernan CF, Kitajima T, Ito Y, Sawa Y, Badylak SF, Zenati MA (2008) J Thorac Cardiovasc Surg 136:1309–1317
61. Prins LJ, Reinhoudt DN, Timmerman P (2001) Angew Chem Int Ed 40:2382–2426
62. Armstrong G, Buggy M (2005) J Mater Sci 40:547–559
63. Wilson AJ (2007) Soft Matter 3:409–425
64. Sherrington DC, Taskinen KA (2001) Chem Soc Rev 30:83–93
65. Cooke G, Rotello VM (2002) Chem Soc Rev 31:275–286
66. Binder W, Zirbs R (2007) Supramolecular polymers and networkswith hydrogen bonds in the main- and side-chain. In: Binder W (ed) Hydrogen bonded polymers, vol 207. Springer, Berlin, pp 1–78
67. Nernst W (1891) Z Phys Chem 8:110–139
68. Bernal JD, Megaw HD (1935) Proc R Soc Lond A 151:384–420
69. Huggins ML (1936) J Org Chem 01:407–456
70. Murray TJ, Zimmerman SC (1992) J Am Chem Soc 114:4010–4011
71. Jorgensen WL, Pranata J (1990) J Am Chem Soc 112:2008–2010
72. Pranata J, Wierschke SG, Jorgensen WL (1991) J Am Chem Soc 113:2810–2819
73. Sartorius J, Schneider H-J (1996) Chem Eur J 2:1446–1452
74. Stadler R, Lucca Freitas L (1986) Colloid Polym Sci 264:773–778
75. De Lucca Freitas LL, Stadler R (1987) Macromolecules 20:2478–2485
76. Lucca Freitas L, Stadler R (1988) Colloid Polym Sci 266:1095–1101
77. Beijer FH, Sijbesma RP, Kooijman H, Spek AL, Meijer EW (1998) J Am Chem Soc 120:6761–6769
78. Sijbesma RP, Beijer FH, Brunsveld L, Folmer BJB, Hirschberg JHKK, Lange RFM, Lowe JKL, Meijer EW (1997) Science 278:1601–1604
79. Beijer FH, Kooijman H, Spek AL, Sijbesma RP, Meijer EW (1998) Angew Chem Int Ed 37:75–78
80. Cates ME (1987) Macromolecules 20:2289–2296
81. Cates ME, Candau SJ (1990) J Phys Condens Matter 2:6869–6892
82. Cates ME (1988) J Phys France 49:1593–1600
83. Knoben W, Besseling NAM, Bouteiller L, Cohen Stuart MA (2005) Phys Chem Chem Phys 7:2390–2398
84. Knoben W, Besseling NAM, Cohen Stuart MA (2007) J Chem Phys 126:024907
85. Vermonden T, van Steenbergen MJ, Besseling NAM, Marcelis ATM, Hennink WE, Sudhölter EJR, Cohen Stuart MA (2004) J Am Chem Soc 126:15802–15808
86. van der Gucht J, Besseling NAM, Knoben W, Bouteiller L, Cohen Stuart MA (2003) Phys Rev E 67:051106
87. Sprakel J, van der Gucht J, Cohen Stuart MA, Besseling NAM (2008) Phys Rev E 77:061502
88. Lange RFM, Van Gurp M, Meijer EW (1999) J Polym Sci A Polym Chem 37:3657–3670
89. Hirschberg JHKK, Beijer FH, van Aert HA, Magusin PCMM, Sijbesma RP, Meijer EW (1999) Macromolecules 32:2696–2705
90. Botterhuis NE, van Beek DJM, van Gemert GML, Bosman AW, Sijbesma RP (2008) J Polym Sci A Polym Chem 46:3877–3885
91. Folmer BJB, Sijbesma RP, Versteegen RM, van der Rijt JAJ, Meijer EW (2000) Adv Mater 12:874–878
92. Kautz H, van Beek DJM, Sijbesma RP, Meijer EW (2006) Macromolecules 39:4265–4267
93. Rieth LR, Eaton RF, Coates GW (2001) Angew Chem Int Ed 40:2153–2156

94. Yamauchi K, Lizotte JR, Long TE (2003) Macromolecules 36:1083–1088
95. Elkins CL, Park T, McKee MG, Long TE (2005) J Polym Sci A Polym Chem 43:4618–4631
96. McKee MG, Elkins CL, Park T, Long TE (2005) Macromolecules 38:6015–6023
97. Feldman KE, Kade MJ, Meijer EW, Hawker CJ, Kramer EJ (2009) Macromolecules 42:9072–9081
98. Sijbesma RP, Meijer EW (2003) Chem Commun 5–16
99. Park T, Zimmerman SC, Nakashima S (2005) J Am Chem Soc 127:6520–6521
100. Park T, Zimmerman SC (2006) J Am Chem Soc 128:14236–14237
101. Park T, Zimmerman SC (2006) J Am Chem Soc 128:11582–11590
102. Wang X-Z, Li X-Q, Shao X-B, Zhao X, Deng P, Jiang X-K, Li Z-T, Chen Y-Q (2003) Chem Eur J 9:2904–2913
103. Nair KP, Breedveld V, Weck M (2008) Macromolecules 41:3429–3438
104. Herbst F, Schröter K, Gunkel I, Gröger S, Thurn-Albrecht T, Balbach J, Binder WH (2010) Macromolecules 43:10006–10016
105. Wietor J-L, van Beek DJM, Peters GW, Mendes E, Sijbesma RP (2011) Macromolecules 44:1211–1219
106. Sivakova S, Bohnsack DA, Mackay ME, Suwanmala P, Rowan SJ (2005) J Am Chem Soc 127:18202–18211
107. Colombani O, Barioz C, Bouteiller L, Chanéac C, Fompérie L, Lortie F, Montès H (2005) Macromolecules 38:1752–1759
108. Falender JR, Yeh GSY, Mark JE (1979) J Am Chem Soc 101:7353–7356
109. Falender JR, Yeh GSY, Mark JE (1979) Macromolecules 12:1207–1209
110. Mark JE, Andrady AL (1981) Rubber Chem Technol 54:366–373
111. Tang MY, Mark JE (1984) Macromolecules 17:2616–2619
112. Mark JE, Tang MY (1984) J Polym Sci Polym Phys Ed 22:1849–1855
113. Di Lorenzo F, Seiffert S (2014) Macromol Chem Phys 215:2097–2111
114. Nair KP, Breedveld V, Weck M (2011) Soft Matter 7:553–559
115. Ilhan F, Galow TH, Gray M, Clavier G, Rotello VM (2000) J Am Chem Soc 122:5895–5896
116. Uzun O, Sanyal A, Nakade H, Thibault RJ, Rotello VM (2004) J Am Chem Soc 126:14773–14777
117. Thibault RJ, Galow TH, Turnberg EJ, Gray M, Hotchkiss PJ, Rotello VM (2002) J Am Chem Soc 124:15249–15254
118. Thibault RJ, Hotchkiss PJ, Gray M, Rotello VM (2003) J Am Chem Soc 125:11249–11252
119. Drechsler U, Thibault RJ, Rotello VM (2002) Macromolecules 35:9621–9623
120. Noro A, Matsushita Y, Lodge TP (2009) Macromolecules 42:5802–5810
121. Fages F (2006) Angew Chem Int Ed 45:1680–1682
122. Brassinne J, Fustin C-A, Gohy J-F (2013) J Inorg Organomet Polym Mater 23:24–40
123. Hofmeier H, Schubert US (2004) Chem Soc Rev 33:373–399
124. Hofmeier H, Schubert US (2003) Macromol Chem Phys 204:1391–1397
125. Calzia KJ, Tew GN (2002) Macromolecules 35:6090–6093
126. Meier MAR, Schubert US (2003) J Polym Sci A Polym Chem 41:2964–2973
127. Ott C, Ulbricht C, Hoogenboom R, Schubert US (2012) Macromol Rapid Commun 33:556–561
128. Schmatloch S, Schubert US (2003) Macromol Symp 199:483–498
129. El-ghayoury A, Hofmeier H, de Ruiter B, Schubert US (2003) Macromolecules 36:3955–3959
130. Kokil A, Yao P, Weder C (2005) Macromolecules 38:3800–3807
131. Meudtner RM, Hecht S (2008) Macromol Rapid Commun 29:347–351
132. Meudtner RM, Ostermeier M, Goddard R, Limberg C, Hecht S (2007) Chem Eur J 13:9834–9840
133. Yuan J, Fang X, Zhang L, Hong G, Lin Y, Zheng Q, Xu Y, Ruan Y, Weng W, Xia H, Chen G (2012) J Mater Chem 22:11515–11522
134. Beck JB, Rowan SJ (2003) J Am Chem Soc 125:13922–13923

135. Zhao Y, Beck JB, Rowan SJ, Jamieson AM (2004) Macromolecules 37:3529–3531
136. Rowan SJ, Beck JB (2005) Faraday Discuss 128:43–53
137. Weng W, Beck JB, Jamieson AM, Rowan SJ (2006) J Am Chem Soc 128:11663–11672
138. Weng W, Jamieson AM, Rowan SJ (2007) Tetrahedron 63:7419–7431
139. Weng W, Li Z, Jamieson AM, Rowan SJ (2008) Macromolecules 42:236–246
140. Weng W, Li Z, Jamieson AM, Rowan SJ (2009) Soft Matter 5:4647–4657
141. Pollino JM, Nair KP, Stubbs LP, Adams J, Weck M (2004) Tetrahedron 60:7205–7215
142. Nair KP, Breedveld V, Weck M (2011) Macromolecules 44:3346–3357
143. Yount WC, Loveless DM, Craig SL (2005) J Am Chem Soc 127:14488–14496
144. Yount WC, Loveless DM, Craig SL (2005) Angew Chem Int Ed 44:2746–2748
145. Noro A, Matsushima S, He X, Hayashi M, Matsushita Y (2013) Macromolecules 46:8304–8310
146. Kumpfer JR, Wie JJ, Swanson JP, Beyer FL, Mackay ME, Rowan SJ (2011) Macromolecules 45:473–480
147. Serpe MJ, Craig SL (2007) Langmuir 23:1626–1634
148. Yount WC, Juwarker H, Craig SL (2003) J Am Chem Soc 125:15302–15303
149. Loveless DM, Jeon SL, Craig SL (2005) Macromolecules 38:10171–10177
150. Spruijt E, Sprakel J, Lemmers M, Stuart MAC, van der Gucht J (2010) Phys Rev Lett 105:208301
151. Hofmeier H, Hoogenboom R, Wouters MEL, Schubert US (2005) J Am Chem Soc 127:2913–2921
152. Appel EA, Biedermann F, Rauwald U, Jones ST, Zayed JM, Scherman OA (2010) J Am Chem Soc 132:14251–14260
153. Lewis CL, Stewart K, Anthamatten M (2014) Macromolecules 47:729–740
154. Paulusse JMJ, van Beek DJM, Sijbesma RP (2007) J Am Chem Soc 129:2392–2397
155. Dankers PYW, Hermans TM, Baughman TW, Kamikawa Y, Kieltyka RE, Bastings MMC, Janssen HM, Sommerdijk NAJM, Larsen A, van Luyn MJA, Bosman AW, Popa ER, Fytas G, Meijer EW (2012) Adv Mater 24:2703–2709
156. Dankers PYW, van Luyn MJA, der Huizinga-van Vlag A, van Gemert GML, Petersen AH, Meijer EW, Janssen HM, Bosman AW, Popa ER (2012) Biomaterials 33:5144–5155
157. Kieltyka RE, Pape ACH, Albertazzi L, Nakano Y, Bastings MMC, Voets IK, Dankers PYW, Meijer EW (2013) J Am Chem Soc 135:11159–11164
158. Song G, Zhang L, He C, Fang D-C, Whitten PG, Wang H (2013) Macromolecules 46:7423–7435
159. Klemm D, Heublein B, Fink HP, Bohn A (2005) Angew Chem Int Ed 44:3358–3393
160. Chang C, Zhang L (2011) Carbohydr Polym 84:40–53
161. Xiao C (2013) Starch – Stärke 65:82–88
162. Fernández E, López D, Mijangos C, Duskova-Smrckova M, Ilavsky M, Dusek K (2008) J Polym Sci B Polym Phys 46:322–328
163. Fernández E, Hernández R, Teresa Cuberes M, Mijangos C, López D (2010) J Polym Sci B Polym Phys 48:2403–2412
164. Van Tomme SR, Hennink WE (2007) Expert Rev Med Devices 4:147–164
165. de Jong SJ, van Eerdenbrugh B, van Nostrum CF, den Kettenes-van Bosch JJ, Hennink WEJ (2001) Control Release 71:261–275
166. Edgar KJ, Buchanan CM, Debenham JS, Rundquist PA, Seiler BD, Shelton MC, Tindall D (2001) Prog Polym Sci 26:1605–1688
167. Li L, Thangamathesvaran PM, Yue CY, Tam KC, Hu X, Lam YC (2001) Langmuir 17:8062–8068
168. Chang C, Lue A, Zhang L (2008) Macromol Chem Phys 209:1266–1273
169. Dave V, Tamagno M, Focher B, Marsano E (1995) Macromolecules 28:3531–3539
170. Takegawa A, Murakami M-a, Kaneko Y, Kadokawa J-i (2010) Carbohydr Polym 79:85–90
171. Liu Z, Wang H, Li B, Liu C, Jiang Y, Yu G, Mu X (2012) J Mater Chem 22:15085–15091
172. Pourjavadi A, Barzegar S, Mahdavinia GR (2006) Carbohydr Polym 66:386–395

173. Gupta D, Tator CH, Shoichet MS (2006) Biomaterials 27:2370–2379
174. Caicco MJ, Zahir T, Mothe AJ, Ballios BG, Kihm AJ, Tator CH, Shoichet MS (2013) J Biomed Mater Res A 101A:1472–1477
175. Wang Y, Lapitsky Y, Kang CE, J. Shoichet MS (2009) Control Release 140:218–223
176. Fiore GL, Klinkenberg JL, Pfister A, Fraser CL (2008) Biomacromolecules 10:128–133
177. Lee H, Dellatore SM, Miller WM, Messersmith PB (2007) Science 318:426–430
178. Lee H, Scherer NF, Messersmith PB (2006) Proc Natl Acad Sci USA 103:12999–13003
179. Holten-Andersen N, Harrington MJ, Birkedal H, Lee BP, Messersmith PB, Lee KYC, Waite JH (2011) Proc Natl Acad Sci USA 108:2651–2655
180. Avdeef A, Sofen SR, Bregante TL, Raymond KN (1978) J Am Chem Soc 100:5362–5370
181. Menyo MS, Hawker CJ, Waite JH (2013) Soft Matter 9:10314–10323
182. Peng F, Li G, Liu X, Wu S, Tong Z (2008) J Am Chem Soc 130:16166–16167
183. Spychaj T, Schmidt B (2000) Macromol Symp 152:173–189
184. Augst AD, Kong HJ, Mooney DJ (2006) Macromol Biosci 6:623–633
185. Lee KY, Rowley JA, Eiselt P, Moy EM, Bouhadir KH, Mooney DJ (2000) Macromolecules 33:4291–4294
186. Shapiro L, Cohen S (1997) Biomaterials 18:583–590
187. Liew CV, Chan LW, Ching AL, Heng PWS (2006) Int J Pharm 309:25–37
188. Hashimoto T, Suzuki Y, Tanihara M, Kakimaru Y, Suzuki K (2004) Biomaterials 25:1407–1414
189. Rowley JA, Madlambayan G, Mooney DJ (1999) Biomaterials 20:45–53
190. Nunamaker EA, Purcell EK, Kipke DR (2007) J Biomed Mater Res A 83A:1128–1137
191. Boontheekul T, Kong H-J, Mooney DJ (2005) Biomaterials 26:2455–2465
192. Shachar M, Tsur-Gang O, Dvir T, Leor J, Cohen S (2011) Acta Biomater 7:152–162
193. Kang S-W, Cha B-H, Park H, Park K-S, Lee KY, Lee S-H (2011) Macromol Biosci 11:673–679
194. Bidarra SJ, Barrias CC, Fonseca KB, Barbosa MA, Soares RA, Granja PL (2011) Biomaterials 32:7897–7904
195. Novikova LN, Mosahebi A, Wiberg M, Terenghi G, Kellerth J-O, Novikov LN (2006) J Biomed Mater Res A 77A:242–252
196. Kim G, Ahn S, Kim Y, Cho Y, Chun W (2011) J Mater Chem 21:6165–6172
197. Appel EA, del Barrio J, Loh XJ, Scherman OA (2012) Chem Soc Rev 41:6195–6214
198. Steed JW, Atwood JL (2009) Supramolecular polymers, gels and fibres. In: Supramolecular chemistry (2nd edn). Wiley, Chichester, pp 861–897.
199. Zheng B, Wang F, Dong S, Huang F (2012) Chem Soc Rev 41:1621–1636
200. Gokel GW, Leevy WM, Weber ME (2004) Chem Rev 104:2723–2750
201. Drain CM, Varotto A, Radivojevic I (2009) Chem Rev 109:1630–1658
202. Li W-S, Aida T (2009) Chem Rev 109:6047–6076
203. Ramaiah D, Neelakandan PP, Nair AK, Avirah RR (2010) Chem Soc Rev 39:4158–4168
204. Evans NH, Beer PD (2014) Chem Soc Rev 43:4658–4683
205. Sliwa W, Deska M (2002) Chem Heterocycl Compd 38:646–667
206. Hooley RJ, Rebek J Jr (2009) Chem Biol 16:255–264
207. Hardie MJ (2012) Cyclotriveratrylene and cryptophanes. In: Gale PA, Steed JW (eds) Supramolecular chemistry: from molecules to nanomaterials, vol 3. Wiley, New York, pp 895-916
208. Nimse SB, Kim T (2013) Chem Soc Rev 42:366–386
209. Warmuth R (2012) Carcerands and hemicarcerands. In: Gale PA, Steed JW (eds) Supramolecular chemistry: from molecules to nanomaterials, vol 3. Wiley, New York, pp 917-954
210. Li J (2009) Cyclodextrin inclusion polymers forming hydrogels. In: Wenz G (ed) Inclusion polymers, vol 222. Springer, Berlin, pp 175–203
211. Chen G, Jiang M (2011) Chem Soc Rev 40:2254–2266
212. Harada A, Takashima Y, Yamaguchi H (2009) Chem Soc Rev 38:875–882
213. Chen Y, Liu Y (2010) Chem Soc Rev 39:495–505

214. Kim K, Selvapalam N, Ko YH, Park KM, Kim D, Kim J (2007) Chem Soc Rev 36:267–279
215. Ni X-L, Xiao X, Cong H, Liang L-L, Cheng K, Cheng X-J, Ji N-N, Zhu Q-J, Xue S-F, Tao Z (2013) Chem Soc Rev 42:9480–9508
216. Liu Y, Yang H, Wang Z, Zhang X (2013) Chem Asian J 8:1626–1632
217. Nakahata M, Takashima Y, Yamaguchi H, Harada A (2011) Nat Commun 2:511
218. Liu S, Ruspic C, Mukhopadhyay P, Chakrabarti S, Zavalij PY, Isaacs L (2005) J Am Chem Soc 127:15959–15967
219. Lagona J, Mukhopadhyay P, Chakrabarti S, Isaacs L (2005) Angew Chem Int Ed 44:4844–4870
220. FDA (2000) GRAS Notice No. GRN 000046, gamma-cyclodextrin
221. Li J, Harada A, Kamachi M (1994) Polym J 26:1019–1026
222. Li J (2010) NPG Asia Mater 2:112–118
223. Liu KL, Zhang Z, Li J (2011) Soft Matter 7:11290–11297
224. Li J, Loh XJ (2008) Adv Drug Del Rev 60:1000–1017
225. Joung YK, Ooya T, Yamaguchi M, Yui N (2007) Adv Mater 19:396–400
226. Kretschmann O, Choi SW, Miyauchi M, Tomatsu I, Harada A, Ritter H (2006) Angew Chem Int Ed 45:4361–4365
227. Hetzer M, Schmidt BVKJ, Barner-Kowollik C, Ritter H (2014) Polym Chem 5:2142–2152
228. Charlot A, Auzély-Velty R (2007) Macromolecules 40:9555–9563
229. Koopmans C, Ritter H (2008) Macromolecules 41:7418–7422
230. Hwang J, Rodgers K, Oliver JC, Schluep T (2008) Int J Nanomed 3:359–371
231. Davis ME, Brewster ME (2004) Nat Rev Drug Discov 3:1023–1035
232. Lee MS, Kim J-C (2014) Polym Int 63:989–996
233. Tomatsu I, Hashidzume A, Harada A (2006) Macromol Rapid Commun 27:238–241
234. Peng K, Tomatsu I, Kros A (2010) Chem Commun 46:4094–4096
235. Tamesue S, Takashima Y, Yamaguchi H, Shinkai S, Harada A (2010) Angew Chem Int Ed 49:7461–7464
236. Wang Q, Mynar JL, Yoshida M, Lee E, Lee M, Okuro K, Kinbara K, Aida T (2010) Nature 463:339–343
237. Tamesue S, Ohtani M, Yamada K, Ishida Y, Spruell JM, Lynd NA, Hawker CJ, Aida T (2013) J Am Chem Soc 135:15650–15655
238. Appel EA, Loh XJ, Jones ST, Biedermann F, Dreiss CA, Scherman OA (2012) J Am Chem Soc 134:11767–11773
239. Appel EA, Loh XJ, Jones ST, Dreiss CA, Scherman OA (2012) Biomaterials 33:4646–4652
240. Park KM, Yang J-A, Jung H, Yeom J, Park JS, Park K-H, Hoffman AS, Hahn SK, Kim K (2012) ACS Nano 6:2960–2968
241. Berger J, Reist M, Mayer J, Felt O, Peppas N, Gurny R (2004) Eur J Pharm Biopharm 57:19–34
242. Berger J, Reist M, Mayer J, Felt O, Gurny R (2004) Eur J Pharm Biopharm 57:35–52
243. Cohen Stuart MA, Hofs B, Voets IK, de Keizer A (2005) Curr Opin Colloid Interface Sci 10:30–36
244. Hunt JN, Feldman KE, Lynd NA, Deek J, Campos LM, Spruell JM, Hernandez BM, Kramer EJ, Hawker CJ (2011) Adv Mater 23:2327–2331
245. Krogstad DV, Lynd NA, Choi S-H, Spruell JM, Hawker CJ, Kramer EJ, Tirrell MV (2013) Macromolecules 46:1512–1518
246. Sashiwa H, Aiba S-i (2004) Prog Polym Sci 29:887–908
247. Bhattarai N, Gunn J, Zhang M (2010) Adv Drug Del Rev 62:83–99
248. Anchisi C, Meloni MC, Maccioni AM (2007) Int J Cosmetic Sci 29:485–485
249. Giri TK, Thakur A, Alexander A, Ajazuddin, Badwaik H, Tripathi DK (2012) Acta Pharm Sin B 2:439–449
250. Dumitriu S, Magny P, Montane D, Vidal P, Chornet E (1994) J Bioact Compat Polym 9:184–209
251. Tan H, Chu CR, Payne KA, Marra KG (2009) Biomaterials 30:2499–2506

252. Dai Y-N, Li P, Zhang J-P, Wang A-Q, Wei Q (2008) Biopharm Drug Dispos 29:173–184
253. Reis LA, Chiu LLY, Liang Y, Hyunh K, Momen A, Radisic M (2012) Acta Biomater 8:1022–1036
254. Harvestine JN, Mikulski BA, Mahuta KM, Crouse JZ, Guo X, Lee JC, Midelfort KS, Chen J, Zhang W (2014) Part Part Syst Charact 31:955–959
255. Jătariu AN, Danu M, Peptu CA, Ioanid G, Ibanescu C, Popa M (2011) Soft Mater 11:45–54
256. Magnin D, Lefebvre J, Chornet E, Dumitriu S (2004) Carbohydr Polym 55:437–453
257. Dumitriu S, Chornet E (1997) Biotechnol Prog 13:539–545
258. Chellat F, Tabrizian M, Dumitriu S, Chornet E, Magny P, Rivard CH, Yahia LH (2000) J Biomed Mater Res A 51:107–116
259. Shibayama M, Tanaka T (1993) Volume phase transition and related phenomena of polymer gels. In: Dušek K (ed) Responsive gels: volume transitions I, vol 109. Springer, Berlin, pp 1–62
260. Abdurrahmanoglu S, Can V, Okay O (2009) Polymer 50:5449–5455
261. Abdurrahmanoglu S, Cilingir M, Okay O (2011) Polymer 52:694–699
262. Tuncaboylu DC, Sahin M, Argun A, Oppermann W, Okay O (2012) Macromolecules 45:1991–2000
263. Tuncaboylu DC, Argun A, Sahin M, Sari M, Okay O (2012) Polymer 53:5513–5522
264. Argun A, Algi M, Tuncaboylu D, Okay O (2014) Colloid Polym Sci 292:511–517
265. Tian J, Seery TAP, Weiss RA (2004) Macromolecules 37:9994–10000
266. Tian J, Seery TAP, Ho DL, Weiss RA (2004) Macromolecules 37:10001–10008
267. Hao J, Weiss RA (2011) Macromolecules 44:9390–9398
268. Hart LR, Harries JL, Greenland BW, Colquhoun HM, Hayes W (2013) Polym Chem 4:4860–4870
269. Burnworth M, Tang L, Kumpfer JR, Duncan AJ, Beyer FL, Fiore GL, Rowan SJ, Weder C (2011) Nature 472:334–337
270. Bode S, Zedler L, Schacher FH, Dietzek B, Schmitt M, Popp J, Hager MD, Schubert US (2013) Adv Mater 25:1634–1638
271. Bode S, Bose RK, Matthes S, Ehrhardt M, Seifert A, Schacher FH, Paulus RM, Stumpf S, Sandmann B, Vitz J, Winter A, Hoeppener S, Garcia SJ, Spange S, van der Zwaag S, Hager MD, Schubert US (2013) Polym Chem 4:4966–4973
272. Burattini S, Colquhoun HM, Greenland BW, Hayes W (2009) Faraday Discuss 143:251–264
273. Greenland BW, Burattini S, Hayes W, Colquhoun HM (2008) Tetrahedron 64:8346–8354
274. Kumpfer JR, Rowan SJ (2011) J Am Chem Soc 133:12866–12874
275. Chen S, Cao Q, Jing B, Cai Y, Liu P, Hu J (2006) J Appl Polym Sci 102:5224–5231
276. Chen S, Hu J, Liu Y, Liem H, Zhu Y, Liu Y (2007) J Polym Sci B Polym Phys 45:444–454
277. Chen S, Hu J, Zhuo H, Yuen C, Chan L (2010) Polymer 51:240–248
278. Tønnesen HH, Karlsen J (2002) Drug Dev Ind Pharm 28:621–630
279. Haag R (2004) Angew Chem Int Ed 43:278–282
280. Tao C-a, Wang J, Qin S, Lv Y, Long Y, Zhu H, Jiang Z (2012) J Mater Chem 22:24856–24861
281. Bastings MMC, Koudstaal S, Kieltyka RE, Nakano Y, Pape ACH, Feyen DAM, van Slochteren FJ, Doevendans PA, Sluijter JPG, Meijer EW, Chamuleau SAJ, Dankers PYW (2014) Adv Healthcare Mater 3:70–78
282. Ma D, Tu K, Zhang L-M (2010) Biomacromolecules 11:2204–2212
283. Gübeli RJ, Hövermann D, Seitz H, Rebmann B, Schoenmakers RG, Ehrbar M, Charpin-El Hamri G, Daoud-El Baba M, Werner M, Müller M, Weber W (2013) Adv Funct Mater 23:5355–5362
284. Seiffert S (2011) Macromol Rapid Commun 32:1600–1609
285. Seiffert S (2013) Angew Chem Int Ed 52:11462–11468
286. Malmsten M (2011) Microgels in drug delivery. In: Fernandez-Nieves A, Wyss HM, Mattsson J, Weitz DA (eds) Microgel suspensions: fundamentals and applications. Wiley-VCH, Weinheim, pp 375–405

287. Su S, Ali MM, Filipe CDM, Li Y, Pelton R (2008) Biomacromolecules 9:935–941
288. Terashima T (2002) Polymer microgels for catalysis. In: Encyclopedia of polymer science and technology. Wiley, New York
289. Jiang Y, Chen J, Deng C, Suuronen EJ, Zhong Z (2014) Biomaterials 35:4969–4985
290. Khademhosseini A, Langer R, Borenstein J, Vacanti JP (2006) Proc Natl Acad Sci USA 103:2480–2487
291. Tan WH, Takeuchi S (2007) Adv Mater 19:2696–2701
292. Tumarkin E, Tzadu L, Csaszar E, Seo M, Zhang H, Lee A, Peerani R, Purpura K, Zandstra PW, Kumacheva E (2011) Integr Biol 3:653–662
293. Kumachev A, Greener J, Tumarkin E, Eiser E, Zandstra PW, Kumacheva E (2011) Biomaterials 32:1477–1483
294. Sakai S, Ito S, Inagaki H, Hirose K, Matsuyama T, Taya M, Kawakami K (2011) Biomicrofluidics 5:013402
295. Tumarkin E, Kumacheva E (2009) Chem Soc Rev 38:2161–2168
296. Theberge AB, Courtois F, Schaerli Y, Fischlechner M, Abell C, Hollfelder F, Huck WTS (2010) Angew Chem Int Ed 49:5846–5868
297. Wang J-T, Wang J, Han J-J (2011) Small 7:1728–1754
298. Dendukuri D, Doyle PS (2009) Adv Mater 21:4071–4086
299. Martinez CJ, Kim JW, Ye C, Ortiz I, Rowat AC, Marquez M, Weitz D (2012) Macromol Biosci 12:946–951
300. Sugiura S, Oda T, Izumida Y, Aoyagi Y, Satake M, Ochiai A, Ohkohchi N, Nakajima M (2005) Biomaterials 26:3327–3331
301. Velasco D, Chau M, Therien-Aubin H, Kumachev A, Tumarkin E, Jia Z, Walker GC, Monteiro MJ, Kumacheva E (2013) Soft Matter 9:2380–2383
302. Anthamatten M (2015) Hydrogen bonding in supramolecular polymer networks: glasses, melts, and elastomers. In: Seiffert S (ed) Supramolecular polymer networks, Advances in Polymer Science. Springer, Cham
303. Okay O (2015) Self-healing hydrogels formed via hydrophobic interactions. In: Seiffert S (ed) Supramolecular polymer networks, Advances in Polymer Science. Springer, Cham
304. Greenland B, Hayes W (2015) Donor–acceptor π–π stacking interactions: from simple complexes to healable supramolecular polymer networks. In: Seiffert S (ed) Supramolecular polymer networks, Advances in Polymer Science. Springer, Cham
305. Chau M, Sriskandha SE, Thérien-Aubin H, Kumacheva E (2015) Supramolecular nanofibrillar polymer hydrogels. In: Seiffert S (ed) Supramolecular polymer networks, Advances in Polymer Science. Springer, Cham
306. Li P, Liu R (2015) Cellulose gels and microgels: synthesis, service, and supramolecular interactions. In: Seiffert S (ed) Supramolecular polymer networks, Advances in Polymer Science. Springer, Cham
307. Pape A, Dankers P (2015) Supramolecular hydrogels for regenerative medicine. In: Seiffert S (ed) Supramolecular polymer networks, Advances in Polymer Science. Springer, Cham

Hydrogen Bonding in Supramolecular Polymer Networks: Glasses, Melts, and Elastomers

Mitchell Anthamatten

Contents

Abstract Nature utilizes hydrogen bonding to guide the supramolecular assembly of lipids, proteins, and DNA, thereby imparting remarkable stimuli-responsiveness, structure-forming ability, and elasticity. Supramolecular polymers and networks

M. Anthamatten (✉)
Department of Chemical Engineering, University of Rochester, 250 Gavett Hall, Rochester, NY 14618, USA
e-mail: anthamatten@che.rochester.edu

© Springer International Publishing Switzerland 2015

S. Seiffert (ed.), *Supramolecular Polymer Networks and Gels*, Advances in Polymer Science 268, DOI 10.1007/978-3-319-15404-6_2

containing reversibly associating groups are now synthetically accessible and offer diverse properties that are highly sensitive to temperature and other stimuli. This review examines how dynamic hydrogen bonding between functional macromers influences supramolecular network formation and physical properties. The emphasis is on condensed phases, including concentrated solutions, melts, and glasses. We discuss how microscopic factors such as the polymer architecture, backbone mobility, mesoscopic ordering, and aggregation or phase segregation of binding groups influence the supramolecular structure, phase behavior, and dynamics of these materials. This understanding is crucial to advance emerging technologies such as thermoplastic elastomers, shape-memory elastomers, and self-healing materials.

Keywords Supramolecular Networks • Hydrogen Bonding • Functional Polymers • Viscoelasticity • Phase Behavior • Associating Polymers

1 Overview and Scope

Inspired by nature, the emerging field of supramolecular chemistry offers methods for dynamic assembly of small molecules, oligomers, and polymers into structures that offer an enormous range of properties [1–4]. Reversible binding allows post-synthetic molecular reorganization, and it provides additional cohesive energy to hold together supramolecular structures. Hydrogen bonding [5–7], metal–ligand interactions [8], donor–acceptor π–π stacking, and peptidic binding groups [9] have all been applied to create dynamic polymer-like chains, macromolecular networks, and phase-segregated superstructures with unique physical properties.

Hydrogen bonds (H-bonds) are a valuable type of "intermolecular glue," because they provide tunable strength, bond selectively, and bond directionality; they can also be easily integrated at specific sites of organic materials. H-bonded complexes are abundant in nature, and their ability to form ordered, functional structures is exemplified in DNA's double helix and in protein-folded β-sheets. Additionally, H-bonding is inherently reversible, providing opportunities to integrate error-correction into systems designed to robustly self-assemble into hierarchal structures. Although a single H-bond is relatively weak (~10–25 kJ mol^{-1}), motifs containing H-bonding arrays can act cooperatively to achieve higher strength. Weak H-bonds undergo fast exchange, causing superstructures to equilibrate with their surroundings, thereby offering stimuli-responsiveness. Strong H-bonds, on the other hand, retard bond exchange and impose local molecular order, resulting in more solid-like properties. The viscoelasticity of H-bonded networks is highly sensitive to temperature, allowing materials to be easily switched from low viscosity melts to solid-state elastomers. This opens up new technological concepts, including self-healing, shape-memory, and dynamic energy dissipation, as shown in Fig. 1.

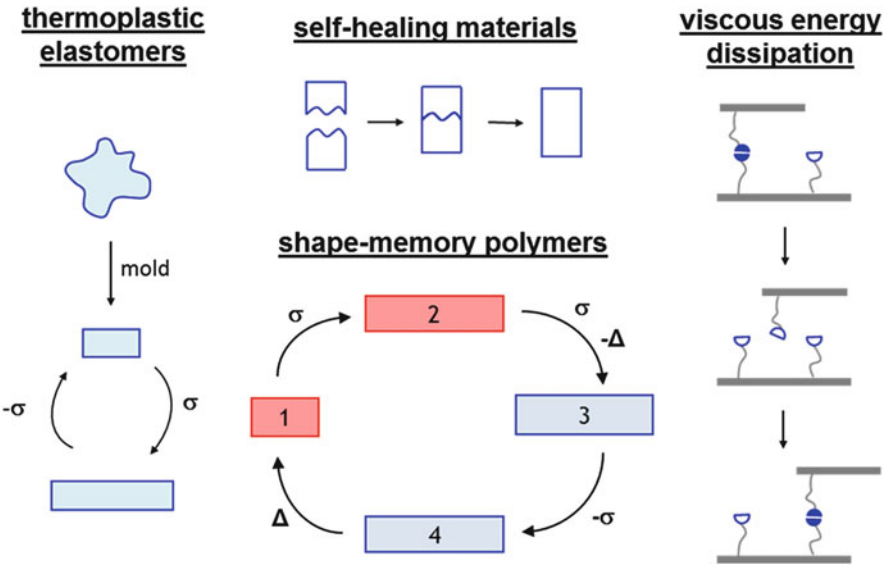

Fig. 1 Dynamic mechanical responses enabled by integrating thermoresponsive hydrogen bonds into soft materials

This review examines how the extent of bond formation and the dynamics of bond exchange can affect a supramolecular network's structural, morphological, and viscoelastic behavior. Although reversible association in solution is fairly well understood, the emphasis here is on *condensed phases*, including concentrated solutions, melts, elastomers, and glasses. Using selected examples from the literature and from our own studies, and always keeping the material end use in mind, we discuss how the polymer architecture, backbone mobility, mesoscopic ordering, phase segregation, and aggregation of binding groups can influence the extent of H-bonding and the resulting network characteristics. The emphasis is on learning how to tailor the structure, phase behavior, and dynamics of supramolecular networks.

1.1 Classification of Supramolecular Architectures and Binding Motifs

Hydrogen bonding motifs offer an array of hydrogen donor (D) and acceptor (A) sites that can reversibly form intermolecular bonds. Motifs can either form *self-complementary* or *heterocomplementary* bonds, and they can be positioned at terminal sites, such as end groups or side groups, or within the main chain of supramolecular building blocks (Fig. 2). An *open assembly* is one with free binding sites at the system's periphery, whereas in a *closed assembly* all binding sites are internally occupied. From a molecular structure perspective, the binding strength

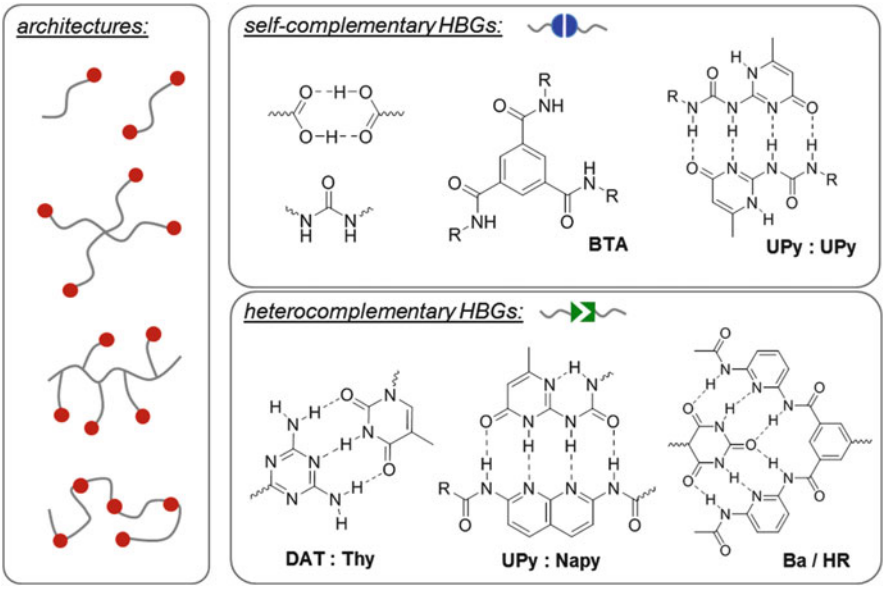

Fig. 2 Classification of supramolecular building blocks functionalized with hydrogen-bonding groups (*HBGs*) and a few examples of self-complementary and heterocomplementary binding motifs. *BTA* benzene-1,3,5-tricarboxyamide, *UPy* ureidopyrimidinone, *DAT* diamino triazine, *Thy* thymine, *Napy* 2,7-diaminonaphtyridine, *Ba* barbituric acid, *HR* hamilton receptor

and selectivity depend on the number and arrangement of donor and acceptor atoms, the presence of repulsive secondary interactions, and the overall quality of molecular fit. Pre-organization, intramolecular hydrogen bonding, tautomerization, and electronic substituents all influence the binding efficacy. Although dozens of H-bonding motifs have been synthesized and studied [10, 11], a much smaller subset is easily integrated into polymer systems while forming long-lived intermolecular bonds within condensed phases. A few exemplary motifs are briefly discussed to emphasize the important molecular features that influence binding efficacy.

1.1.1 Self-Complementary Motifs

The simplest self-complementary motif involves two-point donor–acceptor (DA) H-bonding interactions that form cyclic dimers. Carboxylic acids, for example, are ubiquitous and have been investigated for decades. Fourier transform infrared (FTIR) spectroscopy of poly(acrylic acid)s and ethylene-methacrylic acid copolymers show that dimers persist well above the glass transition temperature (T_g) of the materials [12, 13]. Furthermore, carboxylic acids can interact within polymer melts. Instead of forming dimers, they organize into clusters, providing the basis for a supramolecular network. Lillya and colleagues showed that telechelic

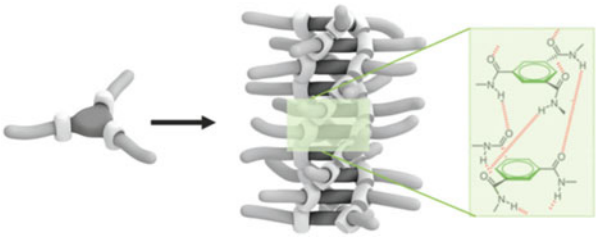

Fig. 3 Benzene-1,3,5-tricarboxamide self-assembly into helical one-dimensional aggregates. Reproduced from [21] with permission of The Royal Society of Chemistry. Copyright 2012

poly(tetrahydrofuran)s exhibit elastic behavior, which they attribute to aggregation of chain ends into crystalline domains [180]. Similarly, substituted triazolines and urazoles self-associate by forming divalent hydrogen bonds. Stadler's group first reported that poly(butadienes) substituted with phenyl urazoles organize into three-dimensional networks [14, 15]. Thus, in melt phases, even the simplest of self-complementary motifs can aggregate beyond simple dimerization to form supramolecular networks.

Amide, urethane, and urea linkages form the foundation for several families of condensation polymers on the basis of their interchain H-bonding [16]. In particular, urea linking groups form bifurcated H-bonds on opposing sides of the moiety. Small molecules containing two or more nearby urea groups undergo supramolecular polymerization, forming rigid chains in nonpolar solvents [17]. For example, 2,4-bis(2-ethylhexylureido)toluene contains two urea linkages separated by a rigid ring; its self-assembly is driven by cooperative binding of four H-bonds between two neighboring molecules. When integrated within a polymer backbone, bisurea segments give rise to physical cross-links in the form of linear aggregates, providing low temperature net-points for thermoplastic elastomers [18, 19]. Likewise, tris-urea linking groups are capable of transforming liquid siloxanes into solid materials and can be grown by condensation of carboxyhydrazide with isocyanates [20].

Benzene-1,3,5-tricarboxamide (BTA; Fig. 3) derivatives are increasingly popular self-complementary motifs containing three amide groups adjacent to a benzene core. BTAs can comprise either N-centered or C=O centered amide bonds that are capable of cooperative H-bonding to form helical one-dimensional aggregates [21]. BTAs have been utilized to induce folding, ordering, and phase segregation in oligomers, homopolymers, and block copolymers [22, 23]. They are attractive because of their simple structure, synthetic accessibility, and clear ordering tendencies.

Self-complementary ureidopyrimidinones (UPy) are perhaps the most extensively studied H-bonding motif. The UPy group, introduced by Meijer's group, contains a linear array of four H-bond sites (DDAA) and exhibits a dimerization constant, K_a, of 5.7×10^7 M^{-1} in chloroform. UPy dimerization is even relevant in hydrogels, where hydrophobic shielding enables dimerization for property improvement [24, 25], although this topic is beyond the scope of the current review. UPy groups are usually formed by a simple reaction of isocytosine with isocyanate derivatives. UPy binding and aggregation are significantly enhanced in the presence of nearby urethane or urea linkages [26], leading to formation of crystalline-like microdomains. Melamine-urea (DADA) [27] and ureidotriazine (ADAD) [28] are

related motifs with somewhat lower complex stabilities than UPy–UPy, and, comparatively, they highlight the role of secondary electrostatic interactions [29]. Ureido-functionalized cytosines (DDAA) [30] also show dimerization constants of ~9×10^6 M^{-1} in C_6D_6.

Self-aggregation or crystalline-like ordering of oligopeptide and nucleobase ends can afford supramolecular structures. Guanosine derivatives order into tetrameric arrangments, known as G-quartets; and the guanine base, capable of binding cations, is frequently employed in supramolecular self-assembly studies [31]. Single thymine chain ends can form highly ordered aggregates that impose long range order onto bulk systems [32].

1.1.2 Heterocomplementary Motifs

Reversible binding between two distinct but complementary binding motifs can lead to even more intricate supramolecular ordering as a result of bond selectivity. The double-helix of DNA and protein self-folding into α-helixes and β-sheets are wonderful and inspiring manifestations of H-bonding. Great efforts to emulate such structures with synthetic chemical systems have met limited success; however, heterocomplementary association of chemically different building blocks can result in dynamic topologies such as supramolecular pseudo block copolymers, alternating copolymers, and networks with supramolecular cross-links.

Many supramolecular polymers are derived directly from DNA's nucleobases: adenine (A), cytosine (C), guanine (G), and thymine (T) [9]. Although each nucleobase can homodimerize, as described in the previous section, heterodynamic complexation is favored to different degrees. The G–C complex involves three H-bonds, and it is two or three orders of magnitude more stable than the A–T complex, involving only two H-bonds. 2,6-Diamino triazine derivatives strongly associate with thymine, and this pair has formed the basis for many studies.

Heterocomplementary complexes involving larger H-bonding arrays generally offer higher stability. Prominent examples of multiple H-bonding arrays include guanosine complexes [33, 34], complexes involving the widely studied Hamilton receptors with barbiturates or triazines through six cooperative H-bonds [7, 35], and synthetic oligoamide strands that can be precisely engineered to have high association constants ($K_a > 10^9$ M^{-1}) [36]. The UPy motif can also transform into its 6[1H] tautomer and form a ADDA–DAAD complex with 2,7-diaminonaphtyridine (Napy), as shown in Fig. 2 [37]. At high enough concentrations, UPy–Napy is preferred over UPy–UPy. A small-molecule heterocomplementary quadruple H-bond array with minimal secondary electrostatic interactions of type AAAA–$DDDD^+$, shown in Fig. 4, was recently reported [38]. The acceptor is stabilized by two intramolecular H-bonds, and the donor is cationic, enhancing its strength. Although this complex is sensitive to light, it has a remarkably high association constant, $K_a > 3 \times 10^{12}$ M^{-1} in CH_2Cl_2. In the future, other synthetically accessible motifs are likely to be discovered, and methods to control the sequence distribution and length of H-bonding entities can potentially provide greater versatility in supramolecular network design.

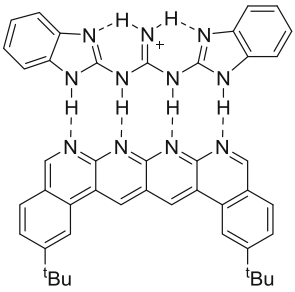

Fig. 4 A quadruple array (AAAA–DDDD$^+$) with exceptionally strong bonding

Heterocomplementary complexes can also involve complete acid–base hydrogen exchange from a donor to an acceptor, forming organic cations and anions. This concept, termed "ionic hydrogen bonding," has been widely applied to macromolecular systems, enabling the introduction of branches and cross-links and offering a clear route toward transient networks and supramolecular gels [39–41]. However, because ionic H-bonds are charged species, they lack the directionality of neutral H-bonding groups and are not considered further.

In this review, the term "macromer" is used to describe oligomer or polymer precursors that undergo reversible association to form supramolecular polymers or networks. Macromer synthesis, although a crucial aspect of supramolecular science, is also out of the scope of this review. Several comprehensive reviews of the synthesis of H-bonding polymers are available [10, 11, 42] and primarily describe the application of controlled radical polymerization techniques, including atom-transfer radical polymerization (ATRP), reversible addition-fragmentation chain transfer (RAFT) polymerization, and nitroxide-mediated polymerization (NMP). For synthesis of telechelic polymers, avoiding monofunctional impurities that can act as chain stoppers is crucially important [43].

1.2 Basic Concepts of Supramolecular Polymerization

In the simplest case, linear macromers with H-bonding end groups associate into higher molecular weight "virtual" polymers. Their assembly is frequently analyzed in the framework of classical condensation polymerization theory, which assumes that (i) end-group association is fully reversible and (ii) all reactive groups have the same propensity to associate, regardless of the chain length [44, 45]. Although both chain and ring structures can form, ring formation requires two chain ends to find each other, and, due the presence of other reactive ends in melts or solution, this becomes negligible at high concentrations [46]. With these assumptions, it is straightforward to determine the equilibrium degree of polymerization and distribution of chain lengths. Consider macromer chains with self-complementary end groups that dynamically assemble into supramolecular chains according to an

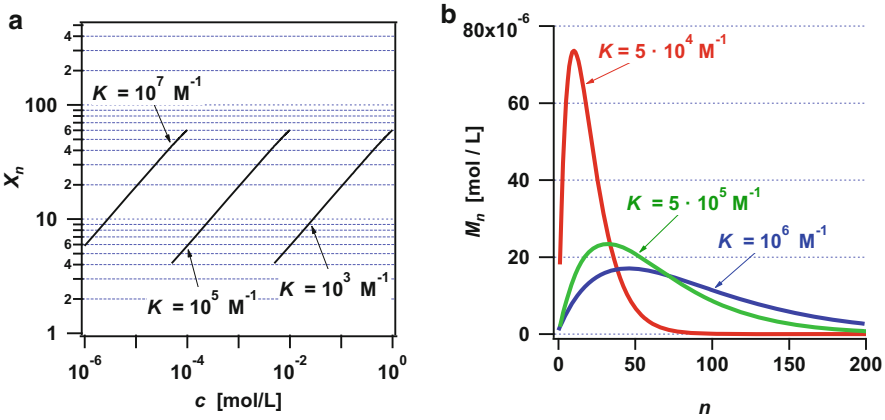

Fig. 5 Ideal chain length characteristics for end-to-end self-assembled telechelic chains for different values of K_a. (**a**) Average dynamic chain length, X_n, plotted against the total concentration of telechelic chains, c. (**b**) Distribution of chain lengths at a fixed concentration ($c = 0.002$ mol L^{-1}) of telechelic chains determined by simultaneously solving a set of $n = 200$ equations for c_i

association constant, K_a, defined by the ratio of end groups that are dimerized to those that are free:

$$K_a = \frac{[\text{H-bond dimers}]}{[\text{free H-bond motifs}]} \tag{1}$$

For bifunctional chains, the average degree of polymerization, X_n, is related to the extent of the reaction, p (i.e., the probability that an H-bonding end group is dimerized), by $X_n = 1/(1–p)$. If the total concentration of macromers is c, then, in the limit where dimerization is favored (p approaches 1):

$$p \approx 1 - \frac{1}{\sqrt{4K_a c}} \tag{2}$$

and

$$X_n \approx 2\sqrt{K_a c} \tag{3}$$

This relationship is visualized in Fig. 5a. Independently increasing either c or K_a results in higher degrees of association; however, it is not straightforward to vary either of these experimentally because they are interdependent. Assuming that all end groups have the same binding tendency, K_a becomes independent of the chain length. Denoting the free macromer as M_1, the dimer as M_2, and so forth, there are then n equilibria:

$$M_1 + M_n \leftrightarrow M_{n+1} \tag{4}$$

that can all be described by a single association constant, $K_a = [M_{n+1}]/([M_1][M_n])$. The resulting n independent equations are further constrained by $c = \Sigma[M_n]$, offering $n+1$ independent equations that can be solved simultaneously to determine each concentration, from c_0 to c_n. The resulting distribution of equilibrium chain lengths is shown in Fig. 5b. Higher equilibrium constants effectively broaden the distribution and shift its maximum to higher molecular weights.

Monofunctional "chain stoppers" can interfere with the assembly process by binding to dynamic chains and precluding further chain growth. Knoben and coworkers demonstrated that the dynamic chain length decreases significantly when the chain stopper concentration is increased to a value similar to the number of functional chains [47, 48]. They also showed that above a critical concentration of chain stoppers, the average chain length is inversely proportional to the mole fraction of chain stoppers. Hence, intentionally adding chain stoppers can control any property that is sensitive to molecular weight.

Moving from ideal dilute solution behavior to higher concentrations, chain entanglements become increasingly important. Cates theoretically examined the interplay between polymer diffusion and end-group bond exchange dynamics [47, 48]. Unlike the discrete model previously discussed, linear chains can break at any point along a chain length, L, where L is a continuous variable that can take any positive value. For the case where the average chain length $<L>$ exceeds the entanglement length, the distribution in chain length exponentially decays as $\sim\exp(L/<L>)$, where $<L>$ depends on the breakage and formation rate constants and the overall chain concentration. According to this model, if chains break on a much longer time scale (τ_{break}) than the reptation time (τ_{rep}), then stress relaxation is predicted to occur by simple reptation with Doi–Edwards stress-relaxation dynamics for a system with exponential polydispersity. On the other hand, if chain breakage is much faster than chain reptation ($\tau_{break} \leq \tau_{rep}$), then the overall relaxation time is $\tau \cong (\tau_{rep}\, \tau_{break})^{1/2}$. For a solution above its coil-overlap concentration, the model predicts the zero-shear viscosity to scale as:

$$\eta_0 = G_0\tau \approx c^{3.5} \tag{5}$$

The Cates framework has been successful in describing a variety of supramolecular systems, including hydrogels [49], transient networks [50], and H-bond assemblies of small molecules [51, 52], but it is less frequently applied to supramolecular polymers and networks involving H-bonding [43].

1.3 Transient Supramolecular Networks

If H-bonding end groups interact to create dynamic cross-links with a functionality exceeding two, then a transient network spanning macroscopic dimensions can

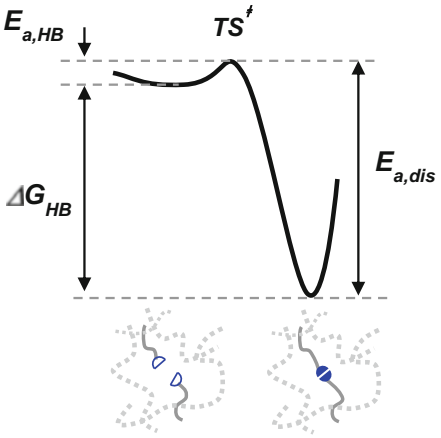

Fig. 6 Free energy profile for reversible hydrogen bond (*HB*) formation in a melt

form. Reversible cross-links, comprising isolated H-bonded dimers or end-group aggregates, can form clusters or stacks. The resulting supramolecular gel is analogous to a covalent network, except that bonds between subunits can reshuffle with time or stress. The transition from a sol (a fluid containing unbounded subunits) to a gel is an abrupt transition that has many similarities with a thermally driven phase transition [53]. According to classical gelation theory, a gel forms when the extent of bond formation, p, exceeds a critical percolation threshold, $p_c = 1/(f-1)$, where f is the functionality of the cross-link sites. For $p > p_c$, an infinite cluster spanning macroscopic dimensions is present, although not all subunits must be connected to that infinite structure. The *gel fraction* is the fraction of subunits that are part of the infinite cluster and can be experimentally determined by solvent-extracting unbound species from a swollen network. For supramolecular systems, however, the gel fraction is difficult to assess because the network bonds are dynamic.

The physical properties of supramolecular networks are sensitive to both chain thermodynamics and bond rearrangement kinetics. Chains connected by net-points within a melt or solvated state are highly mobile; yet, the resulting network exhibits a finite shear modulus, $G' \sim nk_bT$, where n is the number density of elastically effective strands, k_B is Boltzman's constant, and T is the temperature. Applied stress can influence bond dissociation kinetics, and this has been examined for cell adhesion [54, 55]. Consequently, many supramolecular networks are soft and exhibit nonlinear rheology.

To illustrate the physical picture of thermally activated bond dissociation within supramolecular networks, Fig. 6 shows the free energy profile for a reaction coordinate corresponding to supramolecular bond formation. The bond formation and dissociation rate constants, k_f and k_d, are proportional to an attempt frequency and an Arrhenius term, $\exp(-E_a/k_BT)$. The activation energy for forming a H-bond is partly a result of the entropic loss of bringing the two motifs together and partly a result of molecular rearrangement to pre-configure motifs for dimerization. In the opposite direction, the activation energy for bond dissociation is dominated by the enthalpy of H-bond formation. The equilibrium constant relates the free energy

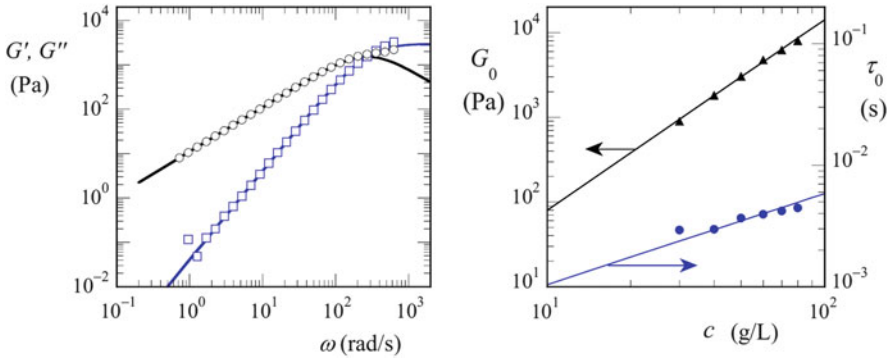

Fig. 7 *Left*: Frequency dependence of G' (*squares*) and G'' (*circles*) of a 50 g L^{-1} aqueous solution of associative polymers from [50]; *lines* are fits to the Maxwell model [Eqs. (6) and (7)]. *Right*: Plateau modulus (G_0) and relaxation time (τ_0) versus the associative-polymer concentration; *lines* are power law fits to the data. Reprinted figure with permission from [50]. Copyright 2008 by the American Physical Society

levels of the bound and unbound states by $\Delta G_{HB} = -RT \ln K_a$, and the association constant is related to kinetics by $K_a = k_f/k_d$. Although the dimerization bond exchange rate almost always strongly depends on temperature, the extent of dimerization (given by K_a) can remain nearly complete over a broad temperature range.

For systems where chain ends aggregate, a fraction of chains are elastically active, and the frequency-dependent storage (G') and loss (G'') moduli are measurable quantities from oscillatory rheology experiments. The presence of a high frequency plateau modulus and a single relaxation time, τ_0, is explained by the transient network theory of Tanaka and Edwards [56], where τ_0 corresponds to the time for a single chain to disengage from an aggregate and become a dangling end. This theory assumes unentangled networks, where each chain follows Rouse dynamics (in contrast to reptation) while being influenced by sticky traps. A single relaxation time may also correspond to a combination of reptation and chain-scission time scales. The mechanical response of such a transient network depends on the frequency, ω, as indicated in the example in Fig. 7, and can be described using a simple Maxwell (spring–dashpot) model:

$$G' = \frac{G_0 \tau_0^2 \omega^2}{1 + \omega^2 \tau_0^2} \tag{6}$$

and

$$G'' = \frac{G_0 \tau_0 \omega}{1 + \omega^2 \tau_0^2} \tag{7}$$

where τ_0 can be determined by the frequency at which G' and G'' cross over, and the plateau modulus G_0 arises from the fit at high frequency.

As the polymer concentration is increased, the plateau modulus and relaxation time both exhibit power law behavior (e.g., $G' \sim c^n$). The data in Fig. 7 illustrate this effect for a solution of hydrophobically end-functionalized poly(ethylene oxide) (PEO) chains [50]. As the concentration increases, a greater number of chains become mechanically active, and the frequency of bond exchange becomes sluggish ($\tau > 1$ s). This is a common phenomenon in solvent-free phases like polymer melts or cross-linked elastomers where entanglement and aggregation lead to heightened barriers for reorganization and diffusion. In a glassy state, supramolecular rearrangement occurs on time scales so slow that equilibrium is never achieved.

2 Dynamic Assemblies from End-Group Association

Functionalization of one or both of a polymer chain's end groups with H-bonding motifs can prompt supramolecular self-organization by end-group dimerization or aggregation. The resulting structure, whether in dynamic equilibrium or trapped in a thermodynamically frustrated state, confers new properties to the polymer and a heightened sensitivity to temperature. This section provides an overview of experimental supramolecular end-to-end polymerization and network formation and a survey of recent literature illustrating how end groups can aggregate or crystallize into structures with long range order, encourage mixing of unlike components, and form block copolymers.

2.1 End-Group Aggregation

Clustering or phase segregation of H-bonding end groups into micelles enhances intermolecular interaction and can result in network formation. This phenomenon was initially observed by Rowan and coworkers in a study of nucleobase-terminated poly(tetrahydrofuran) (PTHF) macromers [57]. Nucleobase ends self-assemble into "hard-segment" stacks connected by soft PTHF chains. The resulting network exhibits gel properties with a plateau modulus of ~4 MPa at room temperature, and rheological relaxation is controlled by the disengagement rate of chain ends from their stacks. Thus, by undergoing phase segregation, even weak interactions can promote film- and fiber-forming ability with high temperature sensitivity.

End-group association in the melt can differ tremendously from that in solution. Binder's group recently investigated mixtures of polyisobutylenes (PIBs) and poly (butyl acrylates) containing thymine (Thy) and 2,6-diaminotriazines (DAT) end groups [58–60]. Thymine and DAT both self-associate; however, they favor the formation of heterocomplementary complexes. Blends of monofunctional and telechelic polymers were systematically studied in solution and melt phases.

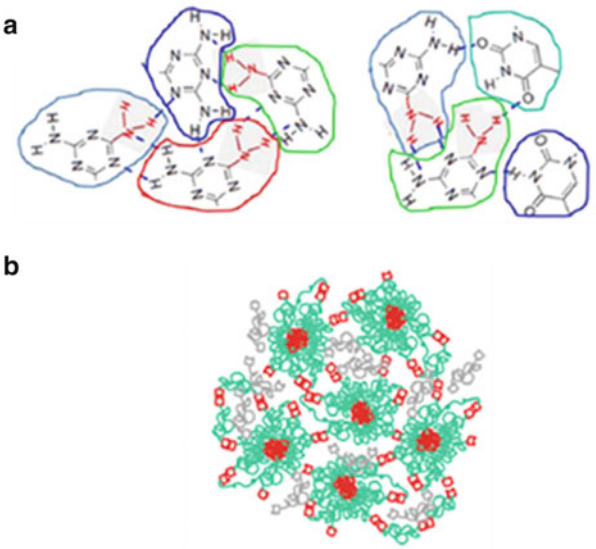

Fig. 8 Proposed aggregation of end-functional polyisobutylenes as studied by Binder and coworkers. (**a**) Hypothesized picture of unspecific H-bonding interactions between 2,6-diaminotriazine (DAT) and thymine end groups. (**b**) Cross-linked micelles of sample DAT-PIB-DAT + Th-PIB-Th. *Light gray* chains represent free matrix chains. Reprinted with permission from [58]. Copyright 2014 American Chemical Society

Their strength of association in solution, determined using ^{1}H NMR, followed the trend DAT–DAT < Thy–Thy ≪ Thy–DAT, whereas association in the melt, determined by rheology, followed a different trend: Thy–Thy < DAT–DAT ≤ Thy–DAT [60]. In solution, dimerization of monofunctional PIBs behaves nearly ideally and follows a simple association model ($K_a = 1{,}090\ M^{-1}$). However, the melt behavior is more complex. The temperature dependence of the melt viscosities is inconsistent with dimerization of chain ends, and small angle X-ray scattering (SAXS) correlation peaks were observed from samples containing only monofunctional polymers. Most likely, nonspecific aggregation of end groups leads to micellar-like structures. Remarkably, a rubbery plateau modulus of ~1 MPa was seen in rheological experiments in the case of mixtures of complementary, bifunctional chains [58]. Analysis shows that the number of bridging chains per micelle is of the same order as the number of chains within one micelle, suggesting a highly connected micellar network, as sketched in Fig. 8.

Thermoreversible clusters also form in telechelic PIBs containing Hamilton-wedge and barbituric acid end groups [61]. Although monofunctional chains were prepared, a rubbery plateau was only observed for bifunctional polymers, and this is evidence of dynamic bridges forming between clusters. The dynamics of chain pullout and re-association were studied by examining fluorescence recovery after photobleaching (FRAP) of tracer chains, which revealed that some tracer chains are highly mobile, with diffusivities of 1–10 $\mu m^2\ s^{-1}$, whereas others are completely immobilized. Understanding the distribution of chain mobility is crucial for emerging self-healing applications [62].

Guan and coworkers utilized soft domains of a block copolymer to provide terminal H-bonding motifs with sufficient dynamics for self-healing [63]. Inspired

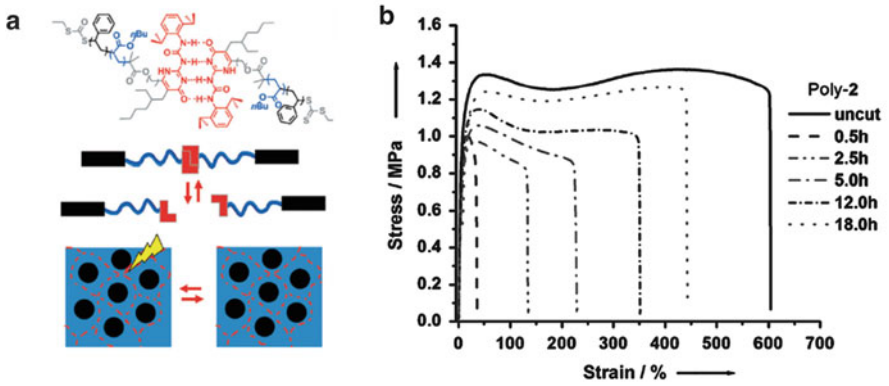

Fig. 9 Guan's supramolecular triblock copolymers with binding sites localized within soft, microphase-segregated domains. (**a**) Molecular structure and cartoon of the polymer morphology. (**b**) Self-healing of a triblock after cutting and healing at 45 °C. Adopted with permission from [63]. Copyright 2012 John Wiley & Sons, Inc.

by microphase segregation within triblocks of polystyrene and poly(butyl acrylate) (PS-*b*-PBA-*b*-PS), they prepared PBA-*b*-PS diblocks with pendant UPy groups on PBA ends (Fig. 9). The material self-assembles to form glassy, cylindrical PS domains within a soft PBA matrix. Compared with their triblock analogs, diblocks exhibit improved toughness and elongation at break of 600 % strain. After specimens were cut and healed at 45 °C, functional diblocks recovered a large fraction of their original mechanical properties, whereas triblock analogs did not. This strategy of using phase segregation to localize the binding group within a mobile environment can be applied to other material classes to encourage self-healing.

2.2 Crystal-Like Stacking of End Groups

Telechelic polymers containing 2-ureido-4-pyrimidinone (UPy) end motifs undergo linear supramolecular polymerization to resemble high molecular weight polymers [64] or form stacks, resulting in dynamic networks. The high association constant of UPy and its strong temperature dependence permits low melt viscosities and excellent processability while retaining access to the properties of high molecular weight polymers or networks at low temperatures. The UPy motif has been applied to numerous backbones including poly(ethylene butylene) [65], polyesters [66], polystyrenes [67, 68], polycarbonates [69], polysiloxanes [43], and polyethers [37] .

Nearby urethane or urea linkages provide additional lateral interactions between UPy dimers, thereby promoting stack formation as shown in Fig. 10 [26, 69–72]. In telechelic poly(ethylene butylene)s (PEBs), for example, the one-dimensional

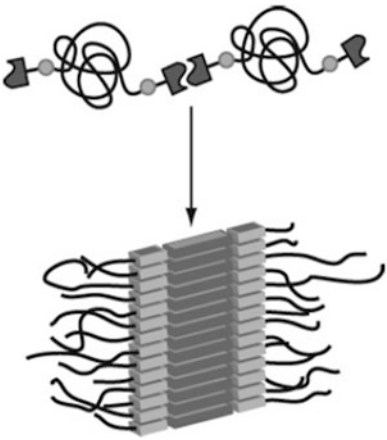

Fig. 10 Lateral UPy–UPy dimer stacking as a result of additional H-bonding between the urethane groups linking the UPy motifs to the matrix chains. Reprinted with permission from [69]. Copyright 2006 American Chemical Society

aggregation of UPy dimers, supported by nearby urea groups, results in an elastic solid with a melting point exceeding 125 °C. Drop-cast thin films show the presence of micrometer long fibers under atom force microscopy (AFM) [26]. Without the supporting linkages, PEB samples behave like simple entangled polymer melts without larger scale organization. The aggregation of dimers into stacks is remarkably sensitive to the molecular structure details near the dimerization site. Stacking can be blocked by bulky substituents that interfere with lateral π–π interactions [73]. Appel and coworkers recently showed that the size, position, and optical purity of substituents placed at the five and six positions of UPy can affect the distance between stacks and modulate crystallization kinetics [71]. Clearly, chain pullout from the dense, crystal-like fibrils is a major barrier to stress relaxation, and a complete stress-dependent characterization of this thermal barrier has not yet been accomplished.

Chen and coworkers recently studied functional macromers with stress-sensitive mechanophores to indicate when chains experience a threshold stress, while simultaneously monitoring molecular organization [72]. They examined polyurethanes with UPy end groups that were primed for lateral stacking using two urea groups and one urethane linkage. Furthermore, they added spiropyran mechanophores to the hard segment. As stress is applied, a cascade of events, shown in Fig. 11, sequentially occurs: stress-induced alignment of UPy stacks, stress-induced crystallization of PTHF soft segments, and finally, mechanochemical reaction of spiropyran groups, changing the material to a pale blue color. Looking forward, mechanophores can undoubtedly be applied to better understand molecular deformation of supramolecular elastomers.

Nearby amide and urea linking groups are not always needed to invoke UPy dimer aggregation. In fact, microphase segregation was also observed in polydimethylsiloxane (PDMS) telechelics in the absence of lateral interacting

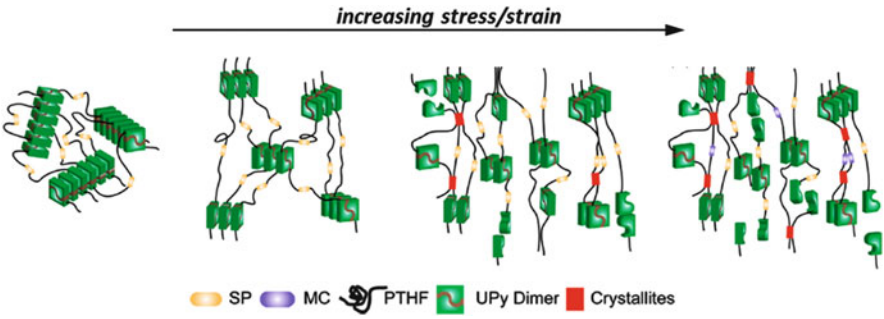

Fig. 11 Proposed mechanism of mechanical activation of polyurethane containing UPy stacking end groups and spiropyran mechanophores. *SP* spiropyran, *MC* merocyanine, *PTHF* poly(tetrahydrofuran). Reprinted with permission from [62]. Copyright 2014 American Chemical Society

linking groups [74]. Instead, long-lived physical interactions were attributed to the large incompatibility between PDMS and the UPy end groups and to π–π stacking of dimerized UPy.

Recently, Bobade and coworkers attached UPy end groups to ATRP-grown polymers, resulting in an additional triazole linkage [75]. For polybutadiene samples, the triazole linkage appears to interfere with UPy stack formation, leading to smaller clusters and a larger, more connected, network. Samples showed somewhat enhanced rubbery and glassy storage modulus values and a higher melting temperature than samples without the triazole linkages.

2.3 Supramolecular Networks with Long Range Order

Considering the tendency of single H-bonding motifs to phase segregate, dimerize, or stack within a polymer melt, one may wonder about the possibility of achieving long range order (LRO) on the nanoscale. LRO is the hallmark of well-defined systems such as low-polydispersity block copolymers and liquid crystals, and controlling LRO is technologically important. Soft interactions responsible for creating LRO (H-bonds, dispersive forces, π–π stacking) are overwhelmed by entropy at high temperatures, leading to an order–disorder transition (ODT) with an abrupt change in physical properties and a loss in anisotropy.

The first evidence of LRO from a one-component self-assembled, end-functionalized polymer was the assembly of a PIB bearing a single terminal DAT motif [59]. This material exhibited a series of SAXS diffraction peaks with relative positions at $1{:}\sqrt{2}{:}\sqrt{3}$, corresponding to a body-centered cubic (bcc) lattice with a periodicity of ~6.5 nm. The structure dissolved upon heating to 90 °C, and it reversibly re-appeared when cooled to 20 °C. The temperature dependence of the bcc structure was later assessed [58] and found to be related to the materials' rheological properties. The low-temperature elastic properties are attributed to

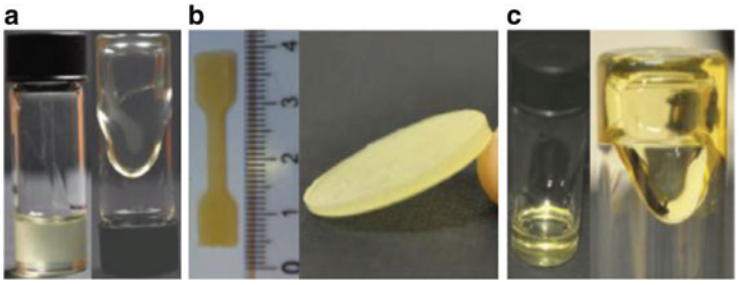

Fig. 12 Photographs of (**a**) DAT–PPO-2200–DAT, (**b**) Thy–PPO-2200–Thy, and (**c**) a stoichiometric mixture of Thy–PPO-2200–Thy and DAT–PPO-2200–DAT free matrix chains. Reprinted with permission from [32]. Copyright 2012 American Chemical Society

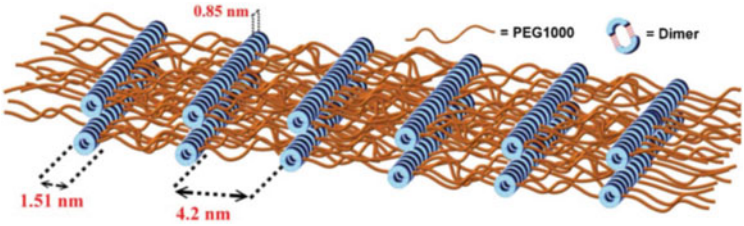

Fig. 13 Proposed lamellar structure of telechelic PEG oligomers bearing self-complementary, sextuple H-bonding end groups (D-UPy) ends. Reproduced from [79] with permission of The Royal Society of Chemistry. Copyright 2012

interaction of corona chains, and analogies are drawn to the rheology of flower-like micelles and block copolymers [76]. Notably, such ordered structures were not observed for other materials examined, including higher molecular weight DAT-terminated PIB, telechelic chains terminated with either DAT or Thy, and blends of heterocomplementary macromers. Furthermore, for systems with bifunctional chains, the ends prefer to associate and show a rubbery plateau, but interaction of chain ends in the corona disrupts the repulsion needed for LRO [58]. These studies emphasize the need for simultaneous structure and rheological studies.

Leibler's group recently demonstrated LRO and an ODT in poly(propylene oxide) (PPO) end-functionalized with a single thymine group adjacent to a urethane linkage [77]. Although thymine dimerization is quite weak ($K_{\text{Thy–Thy}} = 4.3\ \text{M}^{-1}$ in $CDCl_3$), end-group stickers crystallize into planes between layers of amorphous PPO. As shown in Fig. 12, the ordered supramolecular structure of Thy–PPO–Thy is destroyed when heterocomplementary DAT–PPO–DAT is added [32]. The blend then forms a homogeneous melt where linear association of chains prevails [78]. This is somewhat counterintuitive, because introducing a complementary interaction suppresses order. This can be understood as follows: the strong Thy–DAT interaction inhibits thymine crystallization because it is much stronger than Thy–Thy and DAT–DAT interactions. These studies highlight three main factors that influence supramolecular phase behavior: H-bonding, strong microphase segregation, and the intrinsic propensity of molecular entities to crystallize.

Chang and coworkers reported on the assembly of poly(ethylene glycol) (PEG) chains containing *N*-(6-(3-(2,4-dioxo-3,4-dihydropyrimidin-1(2H)-yl) propanamido)pyridin-2-yl)undec-10-enamide (U-DPy) [79]. Telechelic chains self-assemble in the solid state by forming periodic lamellae, as shown in Fig. 13. Higher order small angle X-ray diffraction peaks ($n = 1$–3) indicate lamellae with a long period of 5.71 nm, and the structure persists up to 150 °C, indicating impressive stability. However, when cast into thin films and studied by AFM, spherical particles are observed. The sphere size depends on the casting solution concentration, although it is independent of the annealing time. This possibly indicates that once solvent is removed, the system is out of equilibrium, that is, the time scales for morphological rearrangement exceed the laboratory time scale. The robustness and LRO of this system, as well as the superstructure's temporal and thermal stability, suggest that this is a good candidate for introducing functional supramolecular structure to other backbones.

2.4 *Modification of Macromer Phase Behavior with Associating End Groups*

The topic of polymer blends has sustained research interest for decades. Most polymer pairs are inherently immiscible because of their low entropy of mixing, but H-bonding can improve polymer–polymer miscibility [80, 81]. Blending is a simple processing step whereby a material's end properties can be easily tuned. Hydrogen bonds have been successfully employed to improve the miscibility of linear polymers with immiscible components, including other polymers [82], liquid crystals [83–86], and thermoset polymer blends [87, 88]. Predicting the phase behavior of blends of telechelic chains is important to applications such as nanocomposites, coatings, thermoplastic elastomers, and polymer–polymer bulk heterojunction organic photovoltaics [89].

Current understanding of the solution phase behavior of telechelic associating polymers is largely derived from the classical models of reversible polycondensation developed by Jacobson and Stockmayer [44] combined with Flory–Huggins lattice theory [90]. Painter and Coleman modified the classical Flory–Huggins expression for free energy of mixing (ΔG_m) of a binary polymer blend by including an additional term (ΔG_H) to account for enthalpic and entropic free energy changes as a result of H-bonding:

$$\frac{\Delta G_m}{RT} = \left(\frac{\Phi_A}{N_A}\ln\phi_A + \frac{\Phi_B}{N_B}\ln\phi_B + \chi_{AB}\Phi_A\Phi_B\right) + \frac{\Delta G_H}{RT} \tag{8}$$

where Φ_i is the volume fraction of the ith component, N_i is the number of segments of the ith polymer chain, and χ is the Flory–Huggins interaction parameter [81]. Equation (8) describes the free energy of mixing on a per-site basis using a

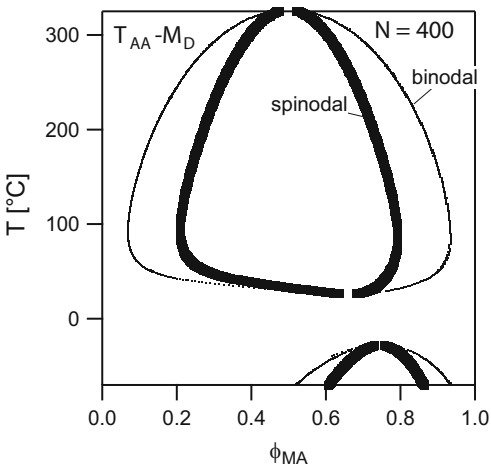

Fig. 14 Predicted phase diagram for a mixture of a telechelic polymer bearing two acceptor end groups and a monofunctional polymer containing only one complementary end group. Reprinted, with permission of John Wiley & Sons, Inc., from [91]. Copyright 2007

reference volume of a single chemical repeat unit. The final term is an excess free energy term and is determined by the number of associated and free H-bonding species. This term can be analytically evaluated by considering the stoichiometry of H-bonding and by defining and specifying an association constant. By examining how ΔG_m depends on composition, it is possible to establish regions of phase miscibility and stability.

Anthamatten applied this association model to account for equilibrium self-association of end groups [91]. Model input parameters include the polymer chain length, a temperature-dependent interaction parameter, and a temperature-dependent equilibrium constant for each associating end group. The analysis was applied to 12 possible blend combinations involving self-complementary interactions and seven combinations involving heterocomplementary interactions. Predicted phase diagrams illustrate how heterocomplementary interactions can stabilize single-phase regions. Complex phase behavior is predicted, including UCST, LCST, and re-entrant miscibility (see Fig. 14). The model is useful for understanding the delicate balance between the combinatorial entropy of mixing, the repulsive interactions between dissimilar polymers, and the additional enthalpic and entropic changes resulting from end-group association of chain ends.

Recent theoretical efforts to address the phase behavior of associating polymer blends have involved self-consistent field theory (SCFT) and lattice cluster theory (LCT). The SCFT framework was applied to enumerate all possible linear reaction products for blends of self-complementary and heterocomplementary telechelics. Mesophase regions were identified. Dudowicz and Freed reformulated the LCT to model solvent-telechelic polymer blends and identified several trends, including an enhancement of miscibility as the molar mass of the associating polymer was increased [92, 93]. This trend was explained by unbalanced entropy and enthalpy changes that occur with increasing chain length.

Experimentally, there is a need for carefully executed experiments on model end-functional materials to test theoretical capability. Our group found that self-

complementary UPy end groups stabilize the two-phase (demixed) region of the phase diagram when placed on either or both component(s) of the well-studied PS–PMMA blend pair [68]. However, Verduzco and coworkers showed that UPy end-interactions can prevent micrometer-scale phase separation conditions typically used to prepare bulk heterojunction organic photovoltaics [89]. In both of these studies, end-group association retards the kinetics of phase separation or mixing, and, when testing a prediction, it is crucial to assess whether the true thermodynamic minimum is observed. Feldman et al. studied low-T_g (meth)acrylic polymers containing monofunctional UPy and 2,7-diamido-1,8-naphthyridine (Napy) end groups [94]. Consistent with the theory, they showed that binding specificity can influence miscibility. Blends with both components containing a self-complementary UPy end showed slight compatibilization, whereas blends containing UPy–Napy (heterocomplementary) groups led to significant retardation of phase separation. If H-bond interactions completely preclude macrophase separation, microphase segregation may be relevant, resulting in "pseudo" block copolymers, which are discussed in the next section.

2.5 Supramolecular "Pseudo" Block Copolymers

Block copolymers comprise chemically distinct polymer chains bonded together to form a single macromolecule. The repulsion between chemically dissimilar blocks enables the formation of periodic microdomains and, as a result of the covalent bond between blocks, macroscopic phase segregation is avoided. The presence and type of equilibrium microstructure (e.g., lamella, cylinders, and spheres) depends on temperature, composition, the extent of repulsion between blocks, surface boundary conditions, and imposed fields.

Heterocomplementary H-bonding motifs placed exclusively at chain ends offer a route to dynamic or pseudo block copolymers [95, 96]. Advantages of dynamic block copolymers include (i) simplified synthesis because only single blocks need to be prepared, followed by blending; (ii) fast ordering and inherent reversibility for achieving aligned long range order and for error correction; (iii) tunable nanostructure and properties because the morphology and corresponding length scale depend on the volume fraction of the constituent homopolymers; and (iv) interfacial activity can stabilize blends of traditionally immiscible polymers, enabling a mix-and-match, combinatorial approach to material development.

The simplest pseudo block copolymer involves end-association of two chemically different homopolymers to form a diblock copolymer. This scenario was examined using a field theory model [97]. The energies relevant to phase behavior are (i) thermal energy kT; (ii) a bonding energy $h(kT)$, where h is the energy decrease in units of kT upon forming an associative bond; and (iii) the segment–segment interaction energy $\chi N(kT)$, where χ is the Flory–Huggins interaction parameter. The resulting phase diagram for a case where the lengths of the homopolymers are identical ($N = N_A = N_B$) is shown in Fig. 15. In this diagram, the

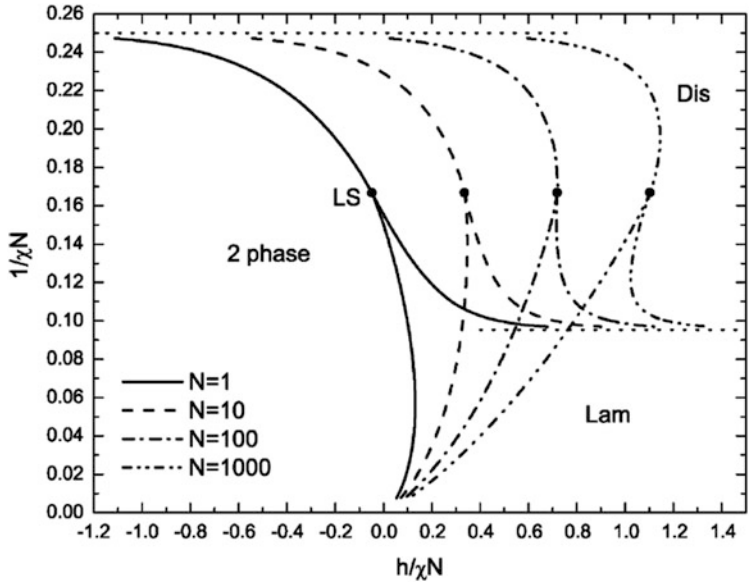

Fig. 15 Mean-field phase diagram of supramolecular diblock copolymer model with equivalent block lengths. Labeled phases are *Dis* (homogeneous disordered), *Lam* (lamellar), and *2 phase* (coexisting A-rich and B-rich homogeneous phases). The values of N indicate the diblock copolymer length. *Solid dots* denote Lifshitz points (*LS*). The *horizontal dashed line* on the *left* denotes $1/\chi N = 1/4$, the macrophase separation transition for a binary blend of polymers. The *horizontal dashed line* on the *right* signifies $1/\chi N = 0.095$, the order–disorder transition for a symmetric diblock copolymer. Reprinted with permission from [97]. Copyright 2007 American Chemical Society

ordinate is independent of temperature because h and χ are taken to be purely enthalpic, and increasing the temperature corresponds to moving upward. Three possible phases are apparent: a macroscopically phase-separated region, a single-phase disordered region, and a phase-segregated lamellar region. Figure 15 shows that to achieve lamellar morphologies requires a bond energy h that is comparable to χN. If N is too high, the system splits into two phases, and if N is too low, it becomes disordered. The phase diagram suggests that $h/\chi N$ must exceed ~0.5 for a lamellar structure. A "strong" H-bonding motif with energy of ~50 kJ mol^{-1} requires $10 < \chi N < 100$, whereas a "weak" motif with energy of ~20 kJ mol^{-1} is more constrained, $10 < \chi N < 40$.

The phase diagram in Fig. 15 is a prediction of thermodynamic equilibrium; however, the process path of a sample intuitively affects the observed phase. For example, if end-functionalized polymers are miscible in the melt, then microphase separation could occur upon cooling. However, if macroscopic phase separation occurs first, then pseudo block copolymers can only form at the interface of a phase-separated mixture, further blocking the molecular transport required for structure formation. If both free and dimerized homopolymer are present during phase separation or microphase segregation, then the length scale of phase segregation/

separation should exceed the polymer coil dimensions as a result of the presence of free homopolymers. Furthermore, because the formed block copolymers are interfacially active, they may stabilize domain growth, avoiding macrophase separation and possibly leading to new and simple methods for achieving larger length scale periodic structures (in the 100 nm range). Such structures could be useful for applications such as photonic band gap structures.

Over the past decade, a large number of pseudo block copolymers have been prepared as a result of advances in controlled radical polymerization techniques (e.g., ATRP, NMRP, RAFT) and by applying azide–alkyne click chemistry [98]. Monofunctional chains are typically grown from functionalized initiators or chain-transfer agents, guaranteeing full end-substitution. Difunctional end chains can self-assemble into multiblock $-(AB)_n$ copolymers. An exemplary case is the synthesis of supramolecular triblocks by growing poly(isoprene) from a bifunctional thymine chain-transfer agent, followed by mixing with α-DAP-functionalized chains [99].

Synthesized pseudo block copolymers are most commonly characterized in solution (suggesting end-association) through NMR and IR data [34, 37, 100]. Melt compatibilization is often reported [34, 37, 94, 99–101]; however, evidence of true nanophase segregation is rare. In Binder's early study of telechelic poly(ether ketone) and PIB polymers, solid-state NMR revealed molecular mobility differences in the melt, and TEM showed microphase segregated domains (70 nm) that were significantly larger than the extended length of the homopolymer [101]. Noro et al. observed nanophase segregation by SAXS and TEM for two different homopolymers end-functionalized with complementary oligonucleotides (thymidine phosphates and deoxyadenosine phosphates) [181]. Phase segregation has also been observed in systems involving acid–base exchange to form an ionic complex at chain ends [40, 88].

Meijer's group recently reported that PDMS bearing a single ureidoguanosine end unit associates selectively with poly(lactide) bearing a Napy unit to mimic a diblock copolymer [102]. SAXS showed higher-order diffraction peaks corresponding to lamellae, and TEM provided unambiguous evidence of phase segregation with 20 nm periodicity. The bulky H-bonding groups are believed to reinforce domain boundaries by phase-segregating into a third domain, presenting an even larger energetic penalty for melting (Fig. 16). The use of such a well-behaved system to map out phase behavior as a function of chain length, composition, and process history is needed to test theoretical predications. Additionally, as an alternative to chemical etching, it may be possible to remove one phase, noncovalently, leaving a glassy or crystalline phase to create high resolution nanoporous materials.

Polymer crystallization within supramolecular pseudo block copolymers is sensitive to many factors, including the type, length, and physical state of the complementary block. Many of the same issues are relevant to crystallization within block copolymer nanoconfinement [103]; however, pseudo block systems can experience macrophase separation [35], and end groups can act as nuclei. Unravelling how reversible bond dynamics affects nucleation as well as the type, extent, and direction of crystallization is a major step in establishing control of the

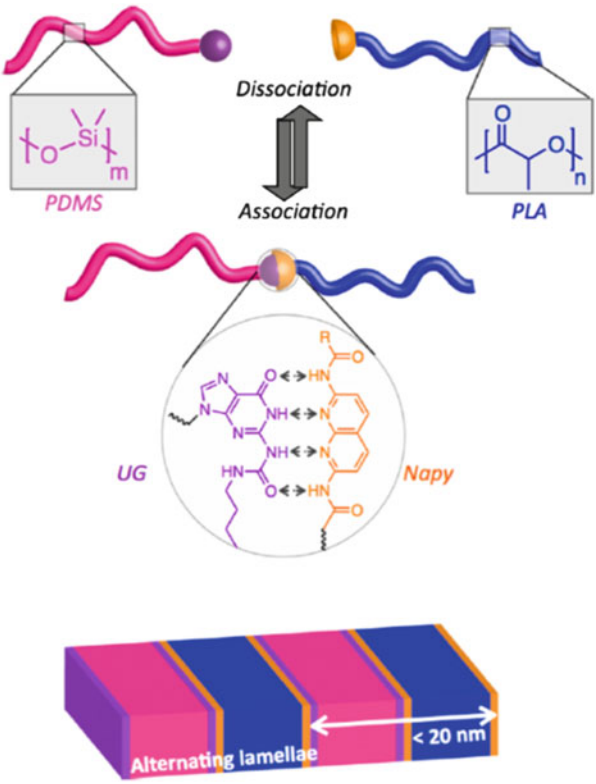

Fig. 16 Reversible association between functional homopolymers to form supramolecular diblocks with a noncovalent heterocomplementary junction. Reprinted with permission from [102]. Copyright 2013 American Chemical Society

order and physical properties of supramolecular systems. Ostas and coworkers studied crystallization of thymine end-functional poly(caprolactone)s (PCLs) blended with heterocomplementary DAT-functionalized small molecules and polymers [104, 105]. They found that the supramolecular blends exhibited Avrami exponents that were consistent with unrestricted crystal growth. Moreover, both small and large associating heteroblocks significantly lowered the crystallization temperature compared with non-associating blends, and fractionated crystallization was observed when low molecular weight functionalized PCL (~5 kDa) was employed.

More complex pseudo triblock copolymers can be created by end-functionalizing diblocks or by employing more than one orthogonal heterocomplementary binding site with sufficient selectivity [106]. Supramolecular $(ABA\text{-}C)_n$ triblocks were prepared by blending triblocks of polystyrene and poly(*n*-butyl acrylate) (PS-*b*-PnBuA-*b*-PS) containing barbiturate end groups with telechelic polyisoprenes bearing Hamilton-wedge end groups [107]. Thermal analysis (DSC) revealed two glass transition temperatures, assigned to PS and PnBuA, suggesting that microphase segregation occurs within the melt. Ambade and coworkers reported a heterotelechelic polymer with a Halmilton receptor at one end and a terminal pyridyl group capable of metal–pincer binding (Fig. 17) [108–110]. Upon blending with two complementary monofunctional chains, orthogonal

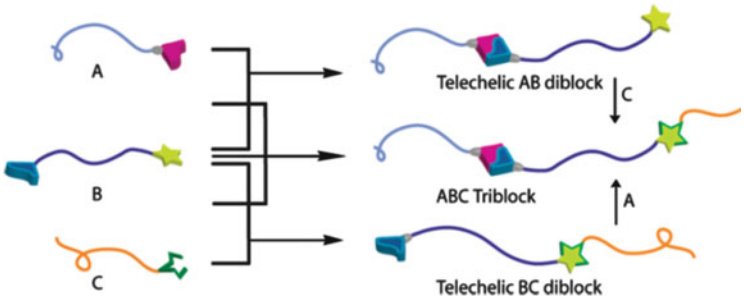

Fig. 17 Representation of a library of AB, BC, and ABC block copolymers from a pool of mono- and heterotelechelic polymers. Reprinted with permission from [110]. Copyright 2010 American Chemical Society

self-assembly into the resulting triblock could be monitored with isothermal titration calorimetry and ^{1}H NMR.

2.6 *Supramolecular Networks by End-Linking Star-Shaped Macromers*

Supramolecular networks can form by connecting primary polymer chains (cross-linking) or by connecting ends of star-shaped molecules (end-linking). End-linking results in a network with junctions having a functionality f that is determined by the architecture of network precursors. As polymerization proceeds, the growing structures eventually reach a gel point where the number of contributing substructures is limited only by the macroscopic amount of reagents. According to Flory–Stockmayer theory, for a two-component gel system comprising two components A and B with end group functionalities f_A and f_B, the gel point is defined by:

$$(f_A - 1)p_A(f_B - 1)p_B = 1 \tag{9}$$

where p_A and p_B are the fractions of A and B end groups that have reacted. Consequently, supramolecular networks made from species with high functionality have lower gel points and offer a processability advantage as a result of the temperature sensitivity of bonds, making them good candidates for thermoplastic elastomers.

Multivalent, glass-forming associating-polymers are under consideration for their energy-dissipating properties. As the temperature is reduced from the melt state, multivalent bonding intensifies the slowdown in molecular rearrangement times, leading to more fragile glasses [111, 112]. Hoy and coworkersapplied hybrid molecular dynamics to model the energy dissipation of associating trivalent glasses [113]. Their results indicate that, at large strain, strong, slow reversible bonding should improve strength and toughness, whereas weak, fast exchange should improve ductility.

Compared with linear telechelics, very few experimental studies of star-shaped molecules bearing H-bond motifs have been reported [114–119]. Meijer and coworkers initially prepared poly(ethylene oxide-*co*-propylene oxide) three-arm polymers with terminal self-complementary H-bonding groups (both UPy and urea) [116]. Their star-shaped supramolecular networks remarkably showed a higher plateau modulus than analogous, covalently connected polymer networks, and this was attributed to the ability of polymer ends to rearrange to achieve the most thermodynamically favored state. Later, Long and coworkers studied linear telechelic and star-shaped poly(ethylene-*co*-propylene)s with terminal UPy functionalities, revealing similar behavior [115, 117]. Their end-functional star polymers, each having an average of six UPy groups, exhibited a higher storage modulus than the telechelics, with a rubbery plateau that extended to lower frequencies. However, Long's star-shaped molecules showed SAXS and AFM evidence of microphase-segregated morphologies, suggesting aggregation of UPy groups beyond simple dimerization. Supramolecular networks containing chemically different polymers (trivalent PIB and bivalent PEO) were prepared using the strong heterocomplementary Halmilton receptor/barbituric acid interaction [114]. Rheological behavior upon mixing depends on the length of the PEO segment: a clear gel-point cross-over, where G' exceeds G'' upon mixing, is only observed in mixtures with oligomeric PEO segments. SAXS correlation peaks were present, indicating a microphase structure of about 5 nm.

Other researchers in this area have been motivated to develop high fidelity approaches toward discrete superstructures, initially demonstrated by Zimmerman's group [120]. Hirsch and coworkers demonstrated supramolecular assembly of discrete dendrimers by using a homotritopic core, a heterotritopic AB_2 component, and end caps [121]. They recently combined two orthogonal reversible interactions (H-bonding and metal ligand complexation), paving the way for self-assembly of more complex structures [122]. Rivera and coworkers recently studied self-assembled dendrimers, involving guanosine derivatives that form an H-bond complex around a metal cation, despite steric hindrance [123].

3 Dynamic Assemblies from Side-Group Association

The most straightforward route to forming a supramolecular network is by reversible cross-linking between macromer chains. This can be accomplished by introducing H-bonding motifs as side groups that are randomly distributed along a polymer backbone. It is usually possible to control the degree of substitution through the synthesis of random copolymers or through postfunctionalization. As the binding group content increases, systems have an increasing amount of internal cohesion while still maintaining reversible pathways for mechanical deformation. The pioneering studies by Stadler and coworkers focused on substituting pendent urazoles along nonpolar backbones such as poly(1,3-butadiene) and PIB [14, 15]. Their result, a new type of thermoplastic elastomer, demonstrated that even light substitution of a rubbery backbone could significantly broaden the storage

modulus plateau. Since then, an assortment of self-complementary H-bond motifs, including carboxylic acids, UPy [124, 125], and sulfonylurethane groups [126] have been broadly applied to modify the viscoelastic behavior of linear polymers well above their T_g. A variety of heterocomplementary interactions, mainly involving nucleobases [9, 127, 128], have also been employed to modify mechanical properties, miscibility, morphology, and crystallizability and to provide pathways for self-assembly.

3.1 The Influence of Strength and Density of Side-Group Hydrogen Bonds

When H-bond dissociation of two side groups occurs, a constraint is lifted, permitting faster chain relaxation. Several theoretical models have examined the dynamics of systems containing chains that have reversible "stickers". Leibler and coworkers extended classical reptation theory to model dynamics of entangled networks made up of linear chains with many temporary cross-links [129]. For times shorter than the H-bond lifetime, the network behaves as if the bond is permanent (i.e., like an elastic rubber). For longer time scales, bond dissociation allows chains to move along their topologically defined tubes. Chain motion in this hindered reptation model is controlled by the concentration and lifetime of tie points. Rubinstein and Semenov developed a similar theory of reversibly associating dynamics that considers correlations between bond dissociation and formation events [130]. This theory, intended for dilute and semidilute solutions, can be extended to the melt state to explain the influence of associating side groups. The model considers the possibility that H-bonds break and reform many times at the same site, not accompanied by chain motion. Accordingly, their model defines an effective, renormalized bond lifetime, τ_b*, which is the time required for associating groups to finally separate (Fig. 18). The theory also predicts a relaxation time even greater than τ_b* as a result of Rouse-like chain motion with augmented friction caused by reversible association.

Hydrogen bond strength and the density of side groups are crucial design variables that influence the formation of supramolecular networks from linear

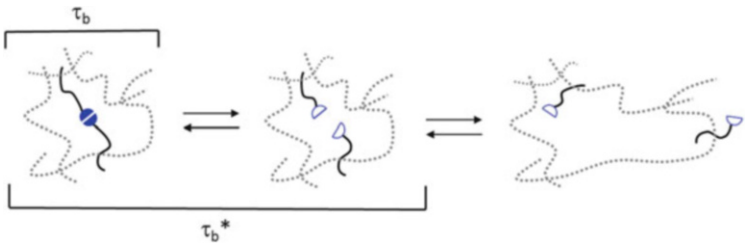

Fig. 18 The concept of renormalized bond lifetimes: $\tau_b^* > \tau_b$

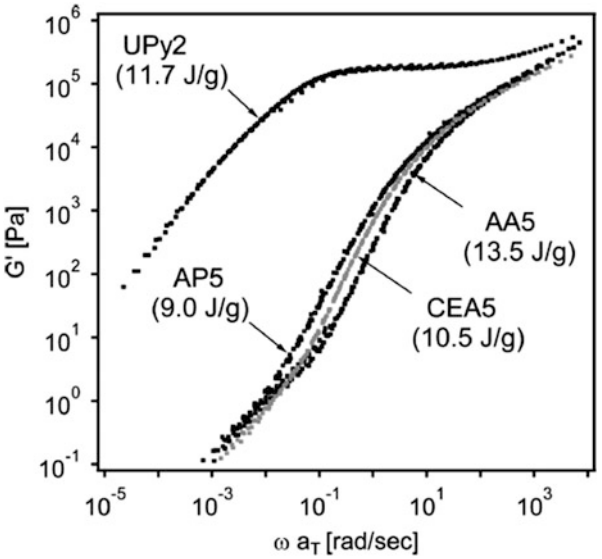

Fig. 19 Storage modulus curves of polymers with different types of H-bonding side groups but comparable H-bond energy densities, at 25 °C. *AA* acrylic acid, *CEA* carboxy ethyl acrylate, *AP* aminopyridine. Reprinted with permission from [131]. Copyright 2014 American Chemical Society

polymers. Anthamatten's group recently showed how the density of side groups, along with their strength of association, influence the viscoelastic properties of low T_g polymer melts [131]. Using PBA as a platform for all these experiments, several different copolymers were synthesized containing different binding groups: acrylic acid (AA), carboxy ethyl acrylate (CEA), and aminopyridine (AP) that form "weak" H-bonded complexes; and the UPy motif that forms "strong" complexes (~70 kJ mol^{-1}). Copolymer melts with weakly bonding side groups behaved as unentangled melts, with no rheological indication of a H-bonded network. Further, for weakly binding systems, the flow activation energy depends mainly on the departure from the glass transition temperature (T–T_g). FTIR experiments confirmed that most side groups participate in H-bonding, suggesting the physical picture that bond dynamics are simply too fast to affect rheological chain relaxation. On the other hand, copolymers with strong H-bonding groups (UPy) behave as soft, elastic solids with thermally activated rheological relaxation. The rheologically distinct behavior of UPy-containing copolymers, with a prominent plateau modulus, is attributed to dimer lifetimes exceeding the experimental time scale. Figure 19 shows that, even if the energy density of side groups is the same, a higher concentration of weakly bonding groups has a minimal impact compared with a smaller number of strongly bonding groups.

3.2 Side-Group Flexibility

Although side-group mobility is obviously needed for efficient bonding, the majority of macromers are synthesized with side groups that have short spacers and are

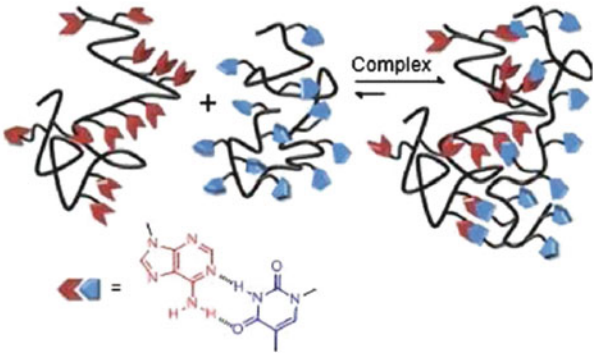

Fig. 20 Thermodynamically stable, physically cross-linked complex that forms upon blending thymine- and adenine-containing statistical copolymers. Reprinted with permission from [132]. Copyright 2012 American Chemical Society

tightly coupled to the backbone. Long's group recently reported on butyl acrylate copolymerized with a H-bonding monomer with flexible alkyl spacers between the backbone and nucleobase binding units (adenine and thymine; Fig. 20) [132]. The copolymers containing just 7 and 16 mol% of adenine units exhibited heightened T_gs, a plateau modulus extending to 50 °C, and needle-like hard structures (from AFM) that were about 100 nm in length. The samples exhibited SAXS peaks that correspond to a periodicity of 6.9 Å, which is consistent with the distance between nucleobase stacks. The strong tendency for adenine groups to aggregate and order is striking because the self-dimerization constant of adenine is less than 10 M^{-1} in $CDCl_3$. Perhaps this is a result of the highly flexible spacer employed in these studies, which could allow adenine to take advantage of its inherent π–π stacking ability. Thymine, however, did not show the same propensity to form supramolecular networks. Interestingly, the process of blending adenine and thymine copolymers together resulted in less order than found for the adenine copolymer because of preferred adenine–thymine interactions. Blended complexes also showed heightened T_gs and increased storage modulus at all frequencies for data acquired at 20 °C. Blends also showed superior adhesion and shear strength values that were three to four times higher than those of acrylic acid and vinylpyridine analogs.

3.3 Side-Group Binding with Cross-linking Agents

A two-component supramolecular network can be formed by adding small molecule "cross-link agents" to a polymer with H-bonding side groups. This scenario relies on selective and complementary binding between multiple functional groups on the small molecule and side groups on the polymer chain. In early efforts, Kato and coworkers utilized bis-pyridine and bis-imidazoyl mesogenic cross-linkers to form supramolecular liquid crystal networks [133, 134], and Rotello and coworkers showed that the diameter of self-assembled micron-sized spherical aggregates could be controlled by the spacer structure of the cross-linker [135]. These studies provide a basis for introducing dynamic cross-links into elastomers, and the selected studies in this section are only representative efforts in this area. Ideally,

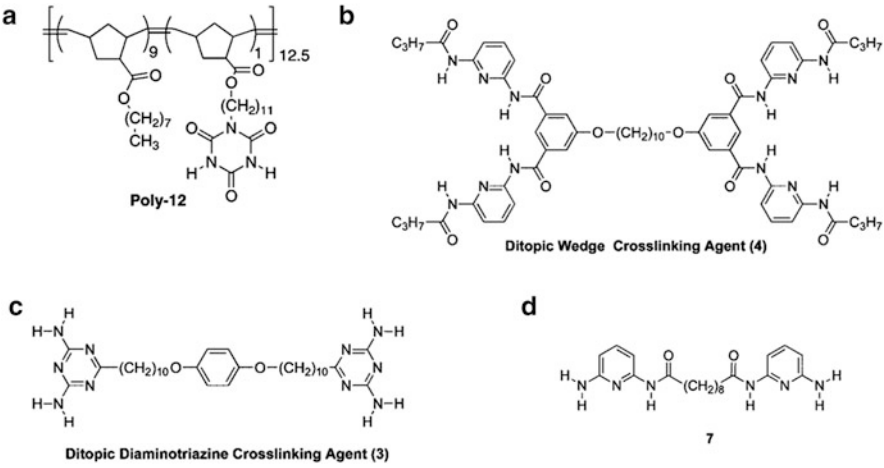

Fig. 21 Chemical structures of (**a**) poly(norbornene) copolymer containing CA side groups, (**b**) the ditopic DAT agent, (**c**) ditopic Hamilton wedge, and (**d**) modified wedge. Reprinted with permission from [136]. Copyright 2008 American Chemical Society

the polymer undergoes negligible self-association, and the degree of cross-linking can be tuned by adjusting the amount of cross-linkers present.

H-bonding between side groups and ditopic cross-linkers is extremely sensitive to bond strength, architecture, and reagent concentration. Weck's group prepared poly(norbornene)s containing cyanuric acid (CA) side group motifs (shown in Fig. 21) that are capable of forming H-bonds with two different cross-linkers by either (i) a three-point interaction between CA and 2,4-diaminotriazine or (ii) a six-point interaction between CA and the Hamilton wedge receptor [136]. A 10 % w/v solution of functional copolymer (**Poly 12**, Fig. 21) in solvent (1-chloronaphthalene) was transformed to an elastic solution upon stoichiometric addition of the ditopic diaminotriazine. However, when the ditopic wedge agent was added, a highly viscous fluid was obtained. This result is counterintuitive because the weaker, three-point H-bonding interaction resulted in the more fully percolated and stable gel. The authors hypothesized that CA residues are capable of forming H-bonds with two diaminotriazine groups from different cross-linking agents. They designed another cross-linking agent (**7**, Fig. 21) that is only capable of binding with a maximum of two CA side groups, and, consistent with their hypothesis, free-flowing liquid-like behavior was observed.

Later, Weck's group combined the concepts of orthogonality and competitive binding within a single system with the goal of demonstrating a network with precisely tunable properties [137]. They synthesized poly(norbornene)s with side groups of (i) CA motifs, (ii) thymine motifs, and (iii) both CA and thymine binding motifs. These polymers were systematically blended with ditopic and monotopic diaminotriazines and Hamilton wedges to demonstrate selective cross-linking, de-cross-linking, and re-cross-linking behavior. For example, the terpolymer

(case iii above) could be selectively cross-linked to form viscoelastic gels by adding monotopic diaminotriazine agents, which are suspected to form arrays with CA side groups. The resulting gels could be de-cross-linked by adding monotopic Hamilton wedges, which bind more strongly to CA, displacing the diaminotriazines and acting as chain stoppers. If, instead, a ditopic Hamilton wedge was added, then viscous liquids formed, indicative of some re-cross-linking. Although the study showed the ability to tune mechanical properties by adding small molecules, this strategy can only work in a solvated system where it is easy to deliver and remove reagents. Engineering melts or elastomers with similarly tunable properties remains a challenge.

The Seiffert group systematically evaluated how the associating side-group strength influences a transient network's dynamics and mechanics [138]. They employed poly(*N*-isopropylacrylamide) (PNIPAAm) polymer precursors with different side groups that selectively and reversibly associate with small molecule ditopic cross-linkers (Fig. 22). This modular toolkit allows both the type and density of cross-links to be independently tuned, enabling comparisons to be made to test theoretical predictions [139]. Network dynamics were examined by measuring the microscopic diffusivity of tracer chains in semidilute solutions, and results were compared with macroscopic rheology measurements. For weak

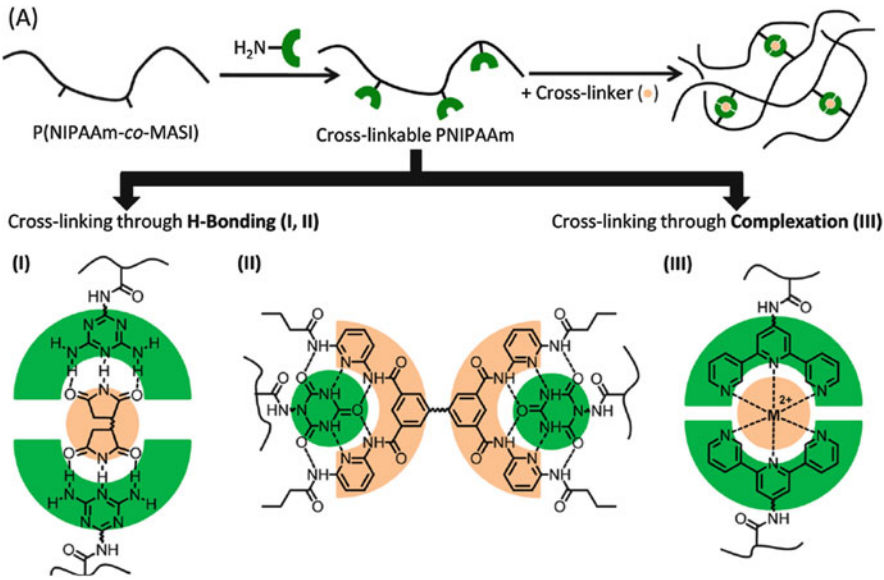

Fig. 22 Set of supramolecular PNIPAAm networks cross-linked by different types of associating groups. The starting material is an electrophilic, methacryl-succinimidyl (MASI)-modified PNIPAAm, denoted P(NIPAAm-*co*-MASI). The MASI moieties are substituted using different motifs: (*I*) diaminotriazine, (*II*) cyanuric acid, and (*III*) terpyridine, and these are cross-linked through addition of complements such as (*I*) bis-maleimide, (*II*) a Hamilton wedge, or (*III*) metal ions (here, Mn^{2+}), thereby varying the type and strength of interchain cross-linking. Reprinted with permission from [138]. Copyright 2013 American Chemical Society

H-bonded supramolecular networks (diaminotriazine side groups with bismaleimide linkers, $K_a \approx 10^2$–10^3 M^{-1}), the tracer chain diffusion scales similarly to unfunctionalized networks, in accord with the classical prediction of $D \sim c^{-1.75}$. For stronger H-bond interactions (CA side groups and Hamilton-wedge linkers, $K_a \approx 10^2$–10^3 M^{-1}), tracer diffusion scaling was slightly more pronounced ($D \sim c^{-1.8}$) and the zero-shear viscosity showed slightly enhanced scaling ($\eta \sim c^4$) compared with the unfunctionalized PNIPAAm networks. These results were compared with even stronger transient cross-links: terpyridine side groups that complex with Mn^{2+} ($K_a = 3.5 \times 10^9$ M^{-2} in chloroform–methanol [139]). The metal-containing supramolecular networks showed the most pronounced deviation from Maxwellian scaling of $G' \sim \omega^2$, which could be attributed to a combination of polydispersity, binding cooperativity, and perhaps localized phase segregation.

3.4 Block Copolymers Containing Side-Group Hydrogen-Bonding Motifs

Introducing high concentrations of H-bonds within a block copolymer structure can significantly broaden the range of accessible physical properties. For example, block copolymers can offer motifs with recognition sites that can be further "reacted" with complementary guest small molecule or polymeric species. Alternatively, microdomains containing high levels of interchain H-bonds should have enhanced cohesive energy density, thereby influencing the relationships between molecular architecture, self-assembled morphologies, and mechanical properties. Despite these exciting possibilities, very little effort has been dedicated to this area, in part because synthesis is challenging because of solubility and phase separation issues.

Feldman et al. showed that the effective bond lifetime in PBAs with UPy side groups is strongly dependent on the chain architecture [125]. They found that samples with shorter distances between UPy side groups exhibit longer effective bond lifetimes. Triblock copolymers with a UPy-free midblock and random copolymer end blocks can effectively concentrate binding groups near chain ends, enhancing their lifetime.

Weck's group synthesized copolymers containing both H-bonding and metal coordination sites using ring-opening methathesis polymerization. Four different poly(norbornene) diblocks were made, each containing one H-bonding block (substituted thymines and 2,6-diaminopyridines) and one metal-coordination block (a pallidated sulfur–carbon–sulfur pincer complex). Through solution complexation with small molecules, they showed that both noncovalent interactions act orthogonally and could form the basis for more complex macromolecular self-assembly. They also found that complexation with small molecules decreased T_g. This is consistent with the structural plasticization of noncovalent cohesive interactions previously present [140].

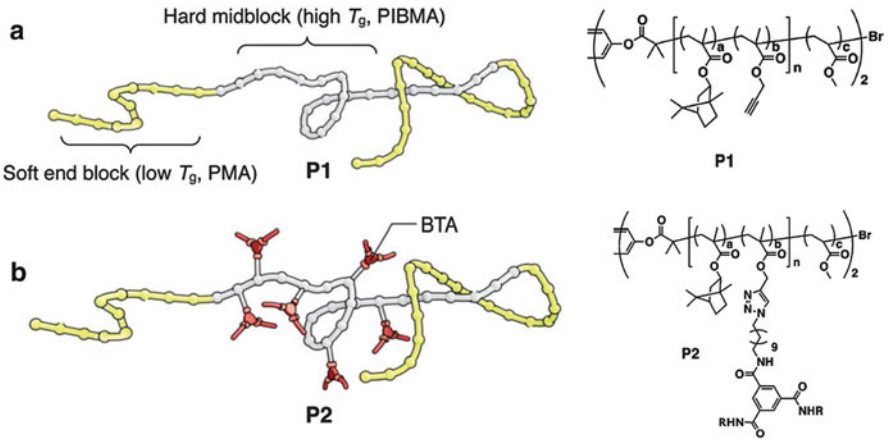

Fig. 23 "Soft–hard–soft"-type ABA triblock architectures (**a**) without and (**b**) with BTA motifs in the middle block. Molecular structures of the synthesized triblocks are shown on the *right*. Reproduced from [23] with permission of The Royal Society of Chemistry. Copyright 2014

Meijer's group recently prepared ABA triblock copolymers containing benzene-1,3,5-tricarboxamide (BTA) moieties within the central hard block, flanked by soft poly(methyl acrylate) end blocks (Fig. 23) [23]. This architecture is in contrast to the well-studied thermoplastic triblocks, poly(styrene)-*b*-poly(butadiene)-*b*-poly(styrene) (SBS), in which hard blocks are situated at the ends. Here, BTA side groups self-assemble into helical aggregates (as confirmed by CD spectroscopy) and a continuous morphological structure is observed with significantly smaller domains than in the unsubstituted triblock. This result was attributed to BTA columnar aggregates forming from several chains, which could hinder the formation of large domains. The triblock containing BTA groups exhibited a significantly higher Young's modulus (~10 MPa) than the unsubstituted control sample (~5 MPa), although BTA assembly appears to cause necking and lower strain at break (~200 % compared with 400 %). Dynamic mechanical analysis (DMA) revealed a rubbery plateau in E', extending from 20 to 100 °C, which is almost two orders of magnitude higher than that of the unsubstituted triblock.

Along similar lines, Long and coworkers recently achieved ABC triblocks that behave as exemplary thermoplastic elastomers [141]. Their triblocks contain complementary thymine and adenine nucleobases as end blocks surrounding a soft middle block (see Fig. 24). Binding groups are separated from the chain via a flexible spacer. Well-defined architectures were achieved using RAFT polymerization of acrylate monomers, and triblocks were made with different block lengths. Complementary side-group association within the end blocks provides mechanical reinforcement, leading to a plateau modulus of several 100 MPa that increases with increasing nucleobase content and extends to temperatures of nearly 90 °C (Fig. 24). SAXS profiles indicate a highly periodic lamellar structure of 23–26 nm,

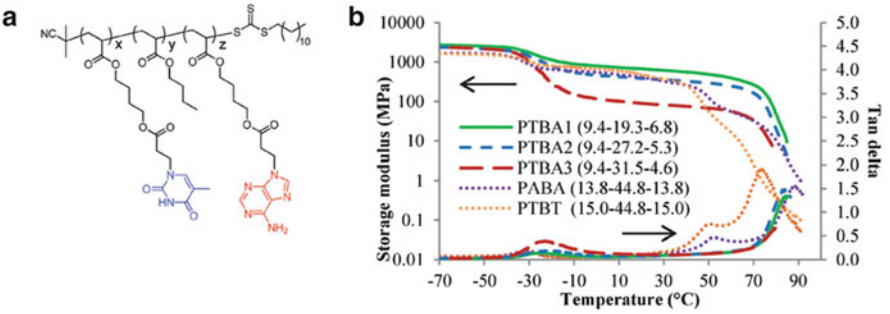

Fig. 24 (**a**) Molecular structure of poly(thymine acrylate-*b*-*n*-butyl acetate-*b*-adenine acrylate) triblock copolymers (PTBA). (**b**) Dynamic mechanical temperature ramp of PTBA and copolymer controls. Reproduced from [141] with permission of The Royal Society of Chemistry. Copyright 2014

depending on the center block length. Blends of symmetric triblocks previously studied by the Long group, consisting of adenine- and thymine-substituted styrene blocks flanking a flexible PBA block, showed well-defined domains but a significantly softer plateau modulus (~0.5 MPa) [142]. Further efforts to stoichiometrically and architecturally optimize the side group interaction between the blocks and to rigorously understand thermomechanical creep at different stress levels are needed to advance these and other block copolymers bearing H-bonding side groups into new, state-of-the-art thermoplastic elastomers.

3.5 *Effect of a Covalent Network on Viscoelastic Relaxation*

Anthamatten and coworkers showed that, just as phase segregation within a block copolymer can promote H-bonding, the presence of a covalent network significantly enhances H-bonding [143]. Elastomer networks with independently varied densities of covalent cross-links and reversible cross-links (UPy side groups) were prepared, and mechanical stress relaxation was shown to be thermally activated, with Arrhenius temperature-dependence. DMA data were time–temperature-shifted, revealing two plateaus in the storage modulus. The lower frequency plateau is a result of covalent cross-links, and the higher frequency plateau is a result of combined reversible and covalent cross-links. The Arrhenius activation energies from DMA (shown in Fig. 25) strongly depend on UPy content and can be rescaled by the UPy dissociation energy in solution to yield a cooperativity factor, z (right-hand ordinate). This factor represents the average number of cooperative dissociation events required for an incremental loss in stored elastic energy. A comparison of thermomechanical activation energies of UPy-containing networks to those prepared from random copolymers (without a covalent network) [125] indicates that mechanical relaxation is much more sensitive to the UPy content in

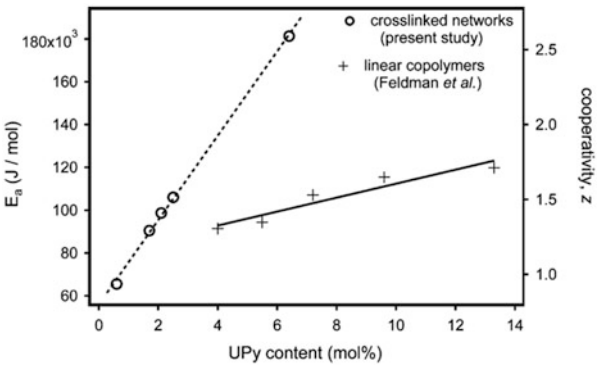

Fig. 25 Plot of activation energies calculated from storage modulus shift factors versus measured UPy content for linear random copolymers (*plus signs*) and for covalently cross-linked networks (*circles*). Reprinted with permission from [143]. Copyright 2011 American Chemical Society

cross-linked networks than in linear copolymers. Thus, covalent cross-linking supports cooperative dynamics and bonding of reversibly associating groups.

3.6 Shape-Memory Properties of Hydrogen-Bonded Networks

Anthamatten's group demonstrated that cross-linked polymers containing strong H-bonding side groups can exhibit shape-memory effects [143, 144]. At high temperatures, H-bonds rapidly exchange and the material behaves like an elastomer (states 1 and 2 in Fig. 26). If the material is strained and rapidly cooled, then deformed states are temporarily "fixed" by a newly formed interpenetrating network of H-bonds. When subsequently heated, the material transforms to its original, "remembered" shape. Because H-bonding is dynamic, strain relaxation (i.e., from states 4 to 5 in Fig. 26) does not occur instantaneously at a single "triggering" temperature. Instead, relaxation occurs over a broad temperature range, and the relaxation rate is sensitive to temperature. Shape-memory elastomers that are stabilized with H-bonds are differentiated from conventional shape-memory polymers in the following ways: (i) they remain soft and elastic well below the shape-memory transition temperature, and (ii) because H-bonding is a reversible process, the shape-recovery rate can be modulated by adjusting the strength and density of H-bonding groups.

3.7 Reversible Side-Group Bonding for Self-Healing

A supramolecular network capable of self-healing by reversible H-bond exchange was first demonstrated by Leibler and coworkers in a study of short multifunctional oligomers containing various complementary H-bonding groups [145]. Formed by condensing mixtures of fatty acids and diethylene triamine, followed by reaction

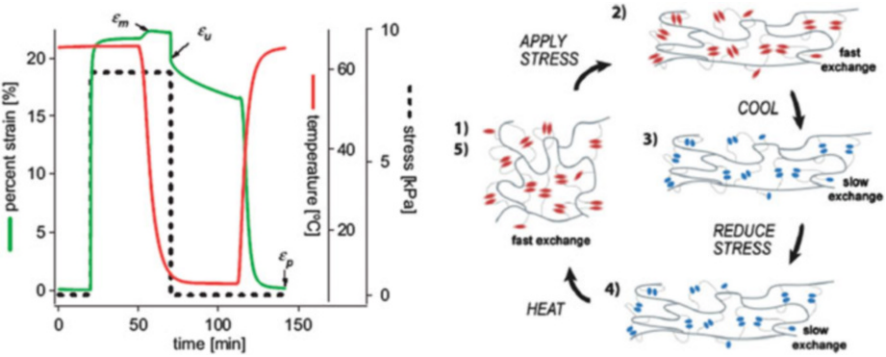

Fig. 26 *Left*: Shape-memory response curve of an elastomer containing 2 mol% of UPy pendant side groups. *Right*: Proposed shape-memory mechanism (states *1–5*) involving thermoreversible H-bonding. *Colored* side groups represent H-bonding groups in the hot (*red*) and cold (*blue*) states; *darker lines* represent the lightly cross-linked covalent network. Adopted with permission from [144]. Copyright 2007, John Wiley & Sons, Inc.

with urea, the resulting soft material is highly elastic when plasticized with a solvent. Stretched samples can maintain stress (4–20 kPa) for hours without appreciable creep. When fractured and immediately mended, the material self-heals at room temperature and recovers its original mechanical properties. Once mended, self-healing does not require heating or application of pressure. This illustration of self-healing within a soft, plasticized phase, highlights the potential of supramolecular H-bonding networks to improve the durability and lifetime of synthetic materials.

Guan and coworkers reported an elegant strategy to permit automatic self-healing while providing stiffness though a microphase-separated glassy domain [146]. Their design concept involves a PS backbone with a fraction of substituted monomers that offer short poly(amide) side chains (Fig. 27). By conducting control experiments with blocked H-bonding sites and with purely substituted chains, they deduced the following: PS backbones collapse into a glassy core, expelling and concentrating the H-bonding amide groups into a soft shell. In the soft, continuous phase, the side groups form bonds with neighboring brushes, offering cohesion and the ability to self-heal. The resulting material behaves as a true thermoplastic elastomer, combining high Young's modulus (>10 MPa) and extensibility (>300 %) at room temperature. These properties can be tuned by varying the polyamide brush length and density. Spontaneous self-healing at room temperature was demonstrated without any plasticizer, solvent, or healing agent. Nearly complete recovery of modulus, yield strength, and extensibility were achieved. Similar results were obtained by synthesizing core–shell nanoparticles and glassy triblock copolymers. Cross-linked PS nanoparticles, seeded with ATRP initiators, initiated polymerization of an acrylate monomer with an amide functional group [147]. The resulting two-phase nanocomposites form films when hot-pressed and exhibit

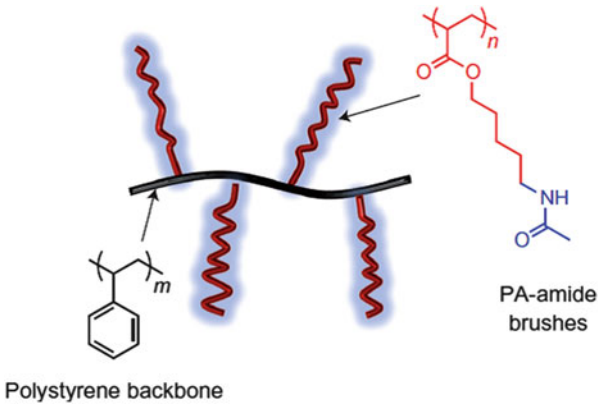

Fig. 27 Design concept for the multiphase self-healing brush polymer system. Reprinted by permission from Macmillan Publishers Ltd: Nature Chemistry, [146]. Copyright 2012

similar self-healing properties, with chain entanglement effects observed at ~200 repeat units in the soft block. Recently, ABA triblock copolymers were synthesized with PMMA as the middle, glassy block and terminal blocks containing concentrated amide linkages [148]. The material phase segregates into rigid PMMA spheres dispersed in a soft phase, exhibiting improved mechanical properties (e.g., Young's modulus of ~77 MPa). Although the efficiency of self-healing in Guan's examples can be susceptible to moisture, and surfaces must be immediately brought into contact following fracture, these studies represent a clear advance toward the engineering of robust supramolecular self-healing systems.

Self-healing requires sufficient mobility for chain ends to collocate. Recently, Rubinstein's group developed a scaling theory for self-healing of unentangled polymer systems with one end fixed in space and the other end dangling but capable of forming pairwise reversible bonds with other chains [62]. Analogous to the sticky reptation model, the renormalized bond lifetime for a bond to break and find another open sticker, τ_b*, determines stress relaxation. This lifetime is much longer than the "bare" bond lifetime, where a sticker returns to its old partner. The efficacy of self-healing depends greatly on the waiting period after two pieces are broken. The excess of open bonding sites decays with waiting time because they recombine. If the waiting period is very long, then the density of open stickers is about as low as its equilibrium value; however, new bridges can still form at a slow rate through a self-adhesion process. On the other hand, if the waiting period is short, then self-healing occurs as open sites quickly form bridges between the broken material surfaces. Although this model captures the salient features of self-healing, other physical issues, such as phase segregation and chain entanglement relevant to Guan's studies, surely also affect self-healing kinetics.

3.8 *Thermally Activated Diffusion Through Dynamic Networks*

Precise control of molecular diffusion is motivated by applications in drug delivery, biological imaging, and the ability to deploy active molecules to a surface on demand. Very few studies have examined how H-bonding affects molecular transport. Multiphoton fluorescence recovery after photobleaching (MP-FRAP) was applied to study dye transport through dynamic polymer networks [149]. Dye molecules (rhodamine) were dispersed into UPy-functionalized PBAs and fluorescence recovery studied using MP-FRAP to obtain dye diffusion coefficients at different temperatures. Figure 28 shows that UPy side-group association significantly inhibits dye diffusion. For example, relative to the unfunctionalized sample, the dye diffusivity is reduced by almost an order of magnitude in the sample containing 1.7 mol% of UPy side groups (RAC-2). Interestingly, molecular diffusion through all studied H-bonding copolymers required about the same activation energies (~50 kJ mol^{-1}). Steady-shear experiments conducted on the same polymers enabled a side-by-side comparison of diffusion versus stress relaxation dynamics. Reversibly associating polymers (RAP-1 and RAP-2) showed heightened flow activation energies, whereas the unfunctionalized samples and the control samples (CCP-1 and CCP-2, containing no H-bonding side groups) did not. Thus, reversible side-group association influences the materials' properties in two fundamentally different ways. Small-molecule diffusion through UPy-containing PBA scales with the total concentration of associating side groups. Each side group

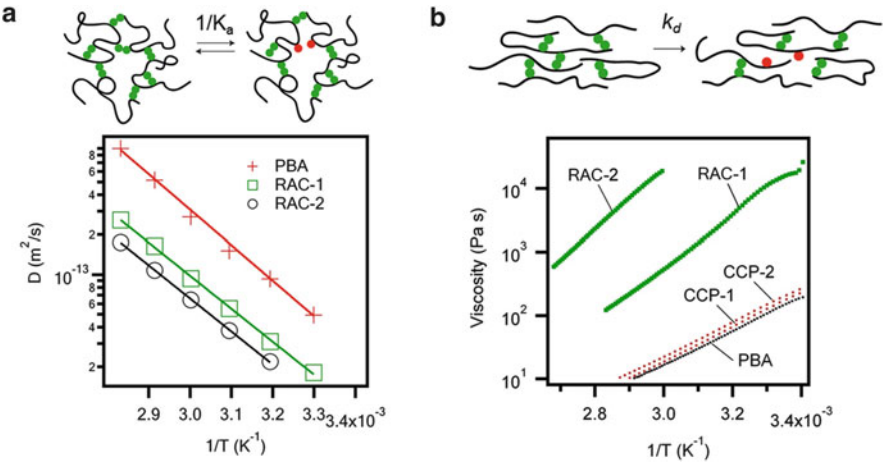

Fig. 28 Arrhenius plots of (**a**) measured dye diffusion coefficient (D) and (**b**) steady-shear viscosity for poly(butyl acrylate)s with UPy side groups. The cartoons emphasize that molecular diffusion is determined by the equilibrium association constant, whereas viscous relaxation is determined by the rate of bond dissociation. Reversibly associating copolymers (RAC) contain UPy side groups and control copolymers (CCP) do not. Adapted from [149] with permission of The Royal Society of Chemistry

behaves like a covalent cross-link, reducing the free volume and thereby incrementally decreasing the diffusivity of the dye. This could be a consequence of the fact that the overall equilibrium constant between free and associated side groups (K_a) is relatively high, even at elevated temperatures. As a result, the concentration of dimers is determined only by the concentration of side groups, and not by the kinetics of association. On the other hand, viscous relaxation, as discussed previously, is limited primarily by the bond exchange kinetics (i.e., the frequency of H-bonding dissociation events).

4 Dynamic Assemblies Involving Main-Chain Interactions

Supramolecular networks can involve intermolecular or intramolecular bonding directly between main chains. Intermolecular binding can result in phase-segregated, stack-like assemblies that serve as physical cross-links. This self-organization forms the basis of well-established segmented condensation polymers such as polyurethanes [16]. In this section, we review how new types of H-bonding groups are being integrated into segmented copolymers to promote processability, functionality, and the ability to self-heal. Then, we discuss a new class of related supramolecular polymers prepared using a H-bond motif placed in the center of a linear macromer, thereby allowing reversible assembly to form comb-like supramolecular polymers. The resulting assemblies exhibit interesting dynamic behavior and are well suited for applications in the area of pressure-sensitive adhesives. Synthetic polymers that contain main chain intramolecular H-bonds to control reversible chain folding, chain scrunching, and helix formation are also reviewed. These materials can foster new approaches to establishing hierarchal structure and precisely tuning thermomechanical properties.

4.1 Thermoplastic Elastomers by Lateral Intermolecular Hydrogen Bonding

Segmented polyurethanes and polyureas exhibit highly tunable properties (including hardness, tear strength, adhesion, and solvent resistance) that are greatly enhanced by lateral H-bonding sites along a backbone. Commercially, polyurethanes and polyureas are made by condensation of small molecule isocyanates with low-T_g polyols or polyamines in the presence of chain extenders, catalysts, cross-linkers, and other additives. In the products, polyols or polyamines form soft segments, whereas the more rigid urethane or urea linkages form hard segments. If the two segments are incompatible (i.e., with a large enough χN), then they phase-segregate into microdomains, and the hard domains act as noncovalent cross-links. At high-enough temperature, hard domains melt, allowing the material to be

melt-processed. Recently, effective methods to improve the thermal, morphological, and mechanical properties of these thermoplastic elastomers have included (i) end-capping segmented polymers with H-bonding groups [150]; (ii) controlling the length distribution of hard segments [151]; and (iii) integrating peptidic groups into soft segments [152].

Urea groups are often employed as the hard blocks of thermoplastic elastomers because they associate through bifurcated H-bonds with strengths exceeding those of amides and urethanes. Versteegen et al. systematically examined how the hard segment size and number of urea groups within the segment each influence the materials' properties [18, 19]. A balance between processability and mechanical properties was identified for hard-domain bisureas separated by different spacers. Copolymers with only one urea group per hard segment behave as viscous liquids, and those with more than two are insoluble. In thermoplastic elastomers (TPEs), bisureas microphase-segregate into fibrous hard blocks that microscopically appear like ribbons of linearly aggregated bisureas. The research has emphasized how the hard-segment architecture and H-bonding efficacy affects the materials' physical properties [153–155]. Bisurea-based TPEs can be loaded with other molecules (supramolecular fillers) that also contain bisureas to increase the hard-segment content or to modify the materials' physical properties (see Fig. 29) [156, 157]. In recent years, bisurea's molecular recognition ability has been employed in areas beyond thermoplastic elastomers, including organogelators [158], anchors for fluorescent probes [159], injectable hydrogels [160], and organized environments to promote selective reactions [161].

Supramolecular networks based on linkages containing adjacent urea groups have recently been studied. Ni and coworkers examined polyurea–urethane networks connected by H-bonding between triuret and tetrauret blocks [162].

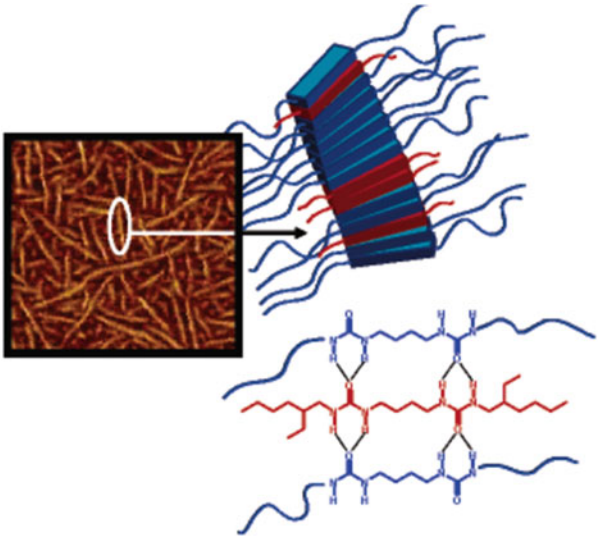

Fig. 29 Incorporation of a supramolecular filler through bisurea H-bond motifs, involving bifurcated H-bonds [157]. Copyright 2006 American Chemical Society

These networks were prepared by a single polycondensation step, resulting in a mixture of branched small molecules with expected concentrations of triuret and tetrauret linkages. DMA showed that samples with triuret linkages formed a supramolecular network with a plateau modulus of ~100 MPa extending to temperatures between 105 and 135 °C. The data suggest that the tetrauret linkages exist in a folded state at room temperature and are unable to form supramolecular bonds. Lehn's group formed tris-urea linkages in low-T_g polydimethylsiloxanes (PDMS) by polycondensation of carbohydrazide with an isocyanate-terminated PDMS chain, as shown in Fig. 30 [20]. The product is a supramolecular silicon displaying promising self-repairing properties. When cut films were brought together, they underwent self-healing within a few hours; however, if they were kept in the broken state too long, self-healing did not occur, presumably because the available H-binding sites near the surface are occupied after a long enough waiting time.

Researchers have recently utilized oxalamide groups as hard segments of segmented copolymers. The oxalamide linkage, a diamide of oxalic acid, is symmetric with two H-bond donors and two acceptors. Sijbrandi et al. prepared and characterized flexible PTHF soft segments with uniform rigid oxalamides [163]. They found that when hard segments contain at least two oxalamide groups, a broad temperature-independent rubbery plateau is observed that, depending on the number of methylenes between oxalamides, ranges from 140 to 200 °C. A combination of FTIR, AFM, and SAXS experiments indicated that the oxalamide linkage is capable of forming highly ordered nanocrystals that are dispersed within soft phases. Long's group has integrated urea oxamide motifs into segmented copolymers containing PDMS and propylene glycol soft segments [164–166]. The PDMS material exhibited a broad, temperature-insensitive rubbery plateau that, for one sample, extended above 180 °C. The morphology is microphase-separated at room temperature, and a morphological transition to a phase-mixed morphology is observed at temperatures corresponding to the onset of viscous flow.

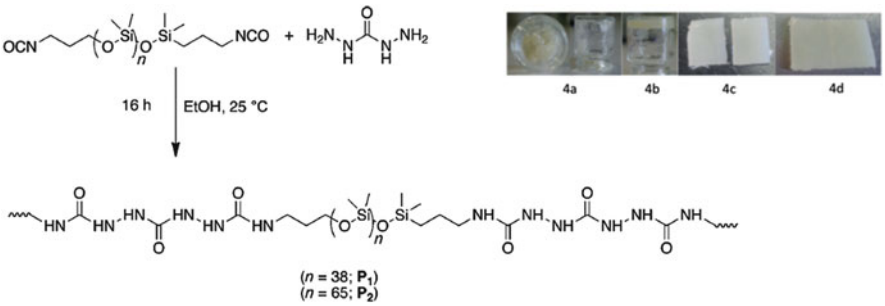

Fig. 30 Synthesis of two polydimethylsiloxane polymers containing tris-urea segments and images showing (**a**) native-damaged polymer $\mathbf{P_1}$, (**b**) self-repaired polymer $\mathbf{P_1}$, (**c**) mechanically cut polymer $\mathbf{P_2}$, and (**d**) self-healed polymer $\mathbf{P_2}$. Adopted with permission from [20]. Copyright 2013 John Wiley & Sons, Inc.

4.2 Reversible Comb Polymers

The self-assembly and physical properties of a new class of dynamic comb-shaped polymers have recently been examined [167, 168]. In these works, macromers each contained a bisurea core flanked by flexible chains such as linear poly(isobutene)s (PIBUTs) that act as side chains in the self-assembled structure. The dynamic structure of PIBUT is analogous to assemblies of the small-molecule analog, 2,4-bis(2-ethylhexylureido)-toluene, as suggested in Fig. 31 [167]. Self-assembly occurs in low-polarity solvents, and the assembled chain length depends on the solvent, concentration, and temperature. From light scattering studies in cyclohexane [169], self-assembly was found to be consistent with the physical picture presented by Wang and Safran [170]. Long aggregates form if the intermolecular H-bond strength is large enough to overcome the conformational entropic penalty of side-chain stretching. Light scattering revealed that macromers with bisurea cores, involving four H-bonds, form short, micellar-like bottle-brush structures, whereas macromers with stronger, tris-urea cores (which interact with six H-bonds) form rodlike structures with persistence lengths exceeding 300 nm [169]. If bisurea cores are used without the PIBUT tails, then the need for H-bonding strength to overcome configurational stretch is obviated and rodlike structures form [171, 172].

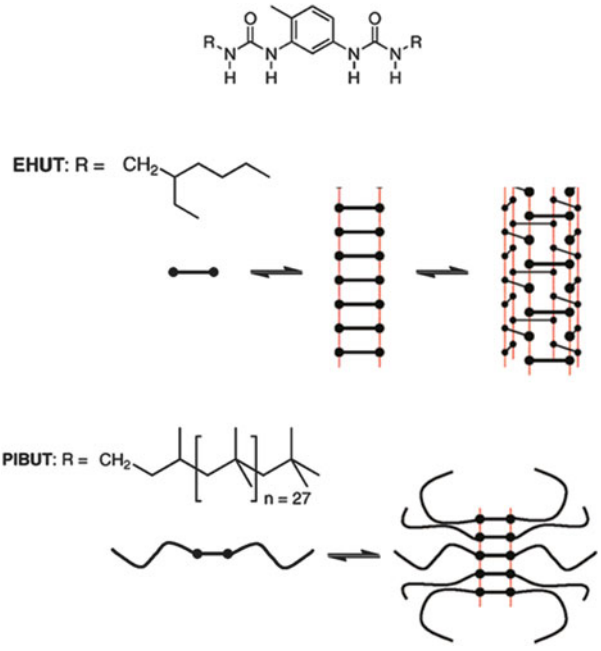

Fig. 31 Supramolecular assembly of 2,4-bis(2-ethylhexylureido)toluene (*EHUT*) to form rigid structures and poly(isobutene) (*PIBUT*) to form dynamic comb-shaped polymers. Reprinted with permission from [167]. Copyright 2010 American Chemical Society

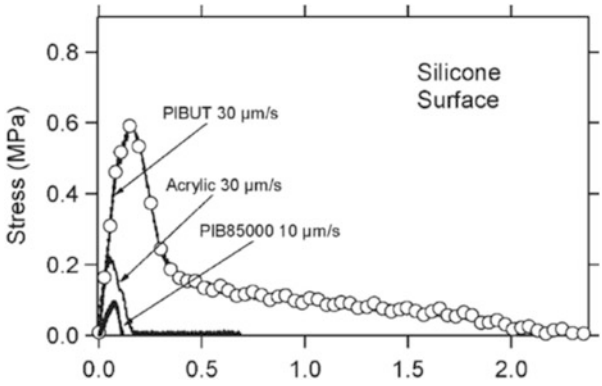

Fig. 32 Stress–strain curves for poly(isobutene) (*PIBUT*), poly(isobutylene) (*PIB85000*), and a model acrylic adhesive during adhesive testing on a silicone-coated surface. Adopted with permission from [173]. Copyright 2010 John Wiley & Sons, Inc.

In the bulk, these PIBUT dynamic comb polymers exhibit dramatically altered rheological and adhesive properties compared with PIBs [173]. Following cooling from 80 °C, the rheological properties require a long time (several thousand seconds) to equilibrate under low-strain oscillatory shear ($\gamma = 0.2$ %, $\omega = 1$ Hz), indicating that self-assembly takes on the order of an hour. When subject to large strains or high temperatures, the organization is perturbed and the material exhibits highly viscous yield stress, although H-bonding is still present up to 80 °C (based on FTIR). Adhesive studies, performed by contact and removal of a flat-ended cylinder against a silicone or glass surface, showed that a large amount of viscous energy is dissipated during a pull-off test. Figure 32 shows the stress evolution during probe removal from a silicon surface. Such surfaces are normally used as a release layer and, therefore, the energy required for removal is exceedingly high, indicating good adhesion to soft surfaces. The increase in viscosity is caused by H-bonding and does not prevent flow. The data indicate that a fibrillar structure forms on de-bonding that can sustain enough stress for the material to serve as a pressure-sensitive adhesive. Remarkably, the PIBUT material showed a much higher degree of interaction with silicone than high molecular weight PIB. A message from this is that supramolecular polymers and networks may have an important role in engineering soft adhesives or bulk shock absorbers. There is a clear need for systematic studies to help understand energy dissipation for model reversibly binding systems.

4.3 Folding and Helix Formation by Intramolecular Main-Chain Hydrogen Bonding

For certain macromer or polymer topologies, H-bond dimerization can invoke chain folding or chain scrunching. Inspired by titin, a modular protein, Guan's group investigated polymers containing multiple loops with precise and strong

H-bond units that, in the absence of stress, spontaneously fold the loop structure together [174, 175]. These studies initially employed UPy groups and peptidomimetics. AFM single-chain force extension studies showed that a large amount of energy is dissipated during unfolding because unfolding requires rupture of several H-bonding sites. The same group subsequently designed an acrylate cross-linker that has a built-in loop, with main-chain H-bonding groups. The cross-linker was polymerized with PBA, and the resulting networks showed heightened moduli and strength without sacrificing extensibility [176]. This approach was validated by using foldamer cross-links based on aromatic amide segments [177]. Alternatively, similar difunctional monomers could be polymerized using acyclic diene metathesis (ADMET) to achieve the titin-mimicking modular polymer shown in Fig. 33 [178]. The resulting material exhibits a combination of high modulus and high toughness, attributed to continuous deformation during chain unfolding. Also, the material shows self-healing and shape-memory properties.

Continuing their research on bioinspired materials, Guan's group also designed β-sheet folding into synthetic polymers, leading to hierarchal structures (Fig. 34) [179]. They integrated a simple alanyl-glycine $(AG)_3$ hexapeptide as the monomer unit into linear chains by using the copper(I)-catalyzed azide–alkyne cycloaddition "click" reaction. Upon removal of protecting groups that prevented assembly, well-defined β-sheets formed that were verified by FTIR, CD spectroscopy, and X-ray scattering.

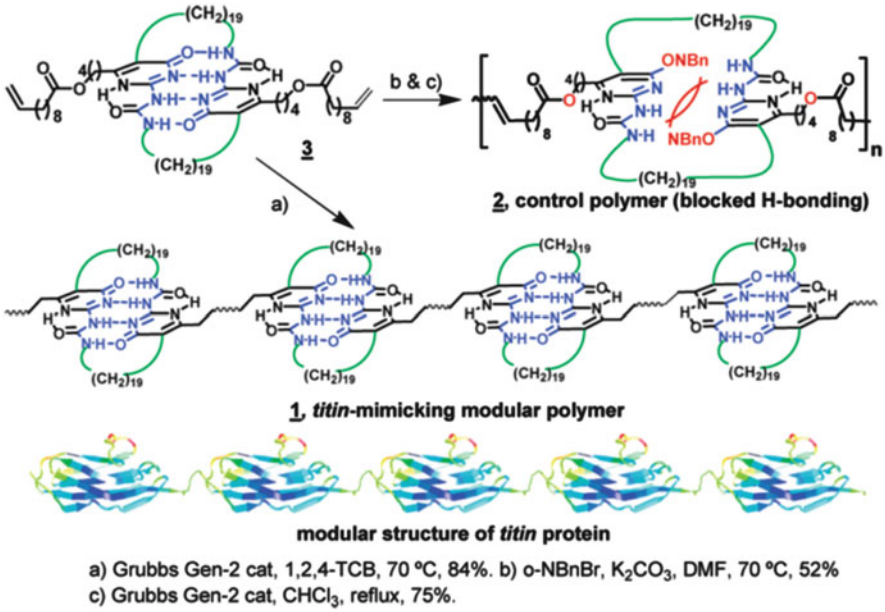

Fig. 33 Guan's synthesis of a biomimetic linear modular polymer. Reprinted with permission from [178]. Copyright 2009 American Chemical Society

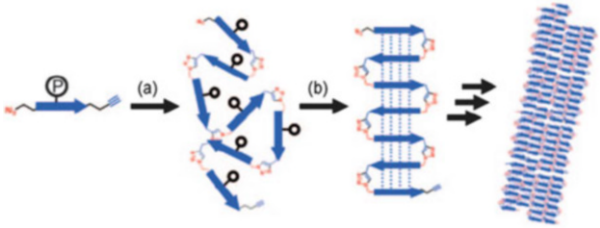

Fig. 34 Cycloaddition-induced folding and self-assembly: (*a*) polymerization of a protected monomer; (*b*) upon deprotection, polypeptides fold into antiparallel β-strands; (*c*) self-assembly of multiple β-sheets to form hierarchical nanofibrils. Adopted with permission from [179]. Copyright 2009 John Wiley & Sons, Inc.

5 Concluding Remarks

Hydrogen bonding within condensed phases can form supramolecular networks with unique physical properties and temperature sensitivities that are relevant to several emerging applications. Astonishingly, simple linear and star-like macromers bearing single H-bonding groups at their chain ends possess the ability to organize into dynamic networks. Networks can involve highly ordered aggregates or long range order that can sustain or respond to applied stress. Moreover, H-bonding at chain ends can promote mixing of unlike components or can join together immiscible macromers to form pseudo block copolymers that offer exciting possibilities for error-correction, path-dependent processing, and orthogonal assembly of complex structures. H-bonding of multiple side groups on a macromer offers a straightforward route to formation of supramolecular networks, and binding cooperativity can reinforce the network. Lateral H-bonding, through side groups or directly between backbones, can boost a material's cohesive energy density, enabling new thermoplastic elastomers. Although shape-memory and self-healing behavior have now been demonstrated in side-group systems, there are many opportunities to optimize the desired behavior on the molecular level by fine tuning, for example, backbone mobility and the length and flexibility of side-group spacers and by applying knowledge of microphase segregation and covalent cross-linking to encourage H-bonding to occur when and where it is most desired. H-binding events can also affect macromer chain configuration, triggering, for example, folding events or helix formation. Looking forward, by tailoring the concentration and molecular location of H-binding sites, it may be possible to engineer systems to sequentially and spontaneously undergo binding and configurational events, leading to complex superstructures with hierarchal ordering and functionality.

References

1. Seiffert S, Sprakel J (2012) Physical chemistry of supramolecular polymer networks. Chem Soc Rev 41(2):909–930
2. De Greef TFA, Smulders MMJ, Wolffs M, Schenning APHJ, Sijbesma RP, Meijer EW (2009) Supramolecular polymerization. Chem Rev 109(11):5687–5754
3. Serpe MJ, Craig SL (2007) Physical organic chemistry of supramolecular polymers. Langmuir 23(4):1626–1634
4. Kushner AM, Guan ZB (2011) Modular design in natural and biomimetic soft materials. Angew Chem Int Ed 50(39):9026–9057
5. Bouteiller L (2007) Assembly via hydrogen bonds of low molar mass compounds into supramolecular polymers. Adv Polym Sci 207:79–112
6. Baruah PK, Khan S (2013) Self-complementary quadruple hydrogen bonding motifs: from design to function. RSC Adv 3(44):21202–21217
7. Binder WH, Zirbs R (2007) Supramolecular polymers and networks with hydrogen bonds in the main- and side-chain. Adv Polym Sci 207:1–78
8. Rowan SJ, Burnworth M, Tang LM, Kumpfer JR, Duncan AJ, Beyer FL, Fiore GL, Weder C (2011) Optically healable supramolecular polymers. Nature 472(7343):334–U230
9. McHale R, O'Reilly RK (2012) Nucleobase containing synthetic polymers: advancing biomimicry via controlled synthesis and self-assembly. Macromolecules 45(19):7665–7675
10. Wilson AJ (2007) Non-covalent polymer assembly using arrays of hydrogen-bonds. Soft Matter 3(4):409–425
11. Bertrand A, Lortie F, Bernard J (2012) Routes to hydrogen bonding chain-end functionalized polymers. Macromol Rapid Commun 33(24):2062–2091
12. Dong J, Ozaki Y, Nakashima K (1997) Infrared, Raman, and near-infrared spectroscopic evidence for the coexistence of various hydrogen-bond forms in poly(acrylic acid). Macromolecules 30(4):1111–1117
13. Macknight WJ, Mckenna LW, Read BE, Stein RS (1968) Properties of ethylene-methacrylic acid copolymers and their sodium salts – infrared studies. J Phys Chem 72(4):1122–1126
14. Freitas LD, Burgert J, Stadler R (1987) Thermoplastic elastomers by hydrogen-bonding. 5. Thermorheologically complex behavior by hydrogen-bond clustering. Polym Bull 17 (5):431–438
15. Hilger C, Stadler R (1990) New multiphase thermoplastic elastomers by combination of covalent and association-chain structures. Makromol Chem 191(6):1347–1361
16. Rogers ME, Long TE (2003) Synthetic methods in step-growth polymers. Wiley, Hoboken
17. Boileau S, Bouteiller L, Laupretre F, Lortie F (2000) Soluble supramolecular polymers based on urea compounds. New J Chem 24(11):845–848
18. Versteegen RM, Kleppinger R, Sijbesma RP, Meijer EW (2006) Properties and morphology of segmented copoly(ether urea)s with uniform hard segments. Macromolecules 39 (2):772–783
19. Versteegen RM, Sijbesma RP, Meijer EW (2005) Synthesis and characterization of segmented copoly(ether urea)s with uniform hard segments. Macromolecules 38(8):3176–3184
20. Roy N, Buhler E, Lehn JM (2013) The tris-urea motif and its incorporation into polydimethylsiloxane-based supramolecular materials presenting self-healing features. Chem Eur J 19(27):8814–8820
21. Cantekin S, de Greef TFA, Palmans ARA (2012) Benzene-1,3,5-tricarboxamide: a versatile ordering moiety for supramolecular chemistry. Chem Soc Rev 41(18):6125–6137
22. Roosma J, Mes T, Leclere P, Palmans ARA, Meijer EW (2008) Supramolecular materials from benzene-1,3,5-tricarboxamide-based nanorods. J Am Chem Soc 130(4):1120–1121
23. Hosono N, Pitet LM, Palmans ARA, Meijer EW (2014) The effect of pendant benzene-1,3,5-tricarboxamides in the middle block of ABA triblock copolymers: synthesis and mechanical properties. Polym Chem 5(4):1463–1470

24. Lewis CL, Anthamatten M (2013) Synthesis, swelling behavior, and viscoelastic properties of functional poly(hydroxyethyl methacrylate) with ureidopyrimidinone side-groups. Soft Matter 9(15):4058–4066
25. Guo MY, Pitet LM, Wyss HM, Vos M, Dankers PYW, Meijer EW (2014) Tough stimuli-responsive supramolecular hydrogels with hydrogen-bonding network junctions. J Am Chem Soc 136(19):6969–6977
26. Kautz H, van Beek DJM, Sijbesma RP, Meijer EW (2006) Cooperative end-to-end and lateral hydrogen-bonding motifs in supramolecular thermoplastic elastomers. Macromolecules 39 (13):4265–4267
27. Ojelund K, Loontjens T, Steeman P, Palmans A, Maurer F (2003) Synthesis, structure and properties of melamine-based pTHF-urethane supramolecular compounds. Macromol Chem Phys 204(1):52–60
28. Beijer FH, Kooijman H, Spek AL, Sijbesma RP, Meijer EW (1998) Self-complementarity achieved through quadruple hydrogen bonding. Angew Chem Int Ed 37(1–2):75–78
29. Jorgensen WL, Pranata J (1990) Importance of secondary interactions in triply hydrogen-bonded complexes – guanine-cytosine vs uracil-2,6-diaminopyridine. J Am Chem Soc 112 (5):2008–2010
30. Lafitte VGH, Aliev AE, Horton PN, Hursthouse MB, Bala K, Golding P, Hailes HC (2006) Quadruply hydrogen bonded cytosine modules for supramolecular applications. J Am Chem Soc 128(20):6544–6545
31. Lena S, Masiero S, Pieraccini S, Spada GP (2009) Guanosine hydrogen-bonded scaffolds: a new way to control the bottom-up realisation of well-defined nanoarchitectures. Chem Eur J 15(32):7792–7806
32. Cortese J, Soulie-Ziakovic C, Tence-Girault S, Leibler L (2012) Suppression of mesoscopic order by complementary interactions in supramolecular polymers. J Am Chem Soc 134 (8):3671–3674
33. Park T, Todd EM, Nakashima S, Zimmerman SC (2005) A quadruply hydrogen bonded heterocomplex displaying high-fidelity recognition. J Am Chem Soc 127(51):18133–18142
34. Park T, Zimmerman SC (2006) A supramolecular multi-block copolymer with a high propensity for alternation. J Am Chem Soc 128(43):13986–13987
35. Binder WH, Bernstorff S, Kluger C, Petraru L, Kunz MJ (2005) Tunable materials from hydrogen-bonded pseudo block copolymers. Adv Mater 17(23):2824–2828
36. Gong B (2012) Molecular duplexes with encoded sequences and stabilities. Acc Chem Res 45 (12):2077–2087
37. Ligthart GBWL, Ohkawa H, Sijbesma RP, Meijer EW (2005) Complementary quadruple hydrogen bonding in supramolecular copolymers. J Am Chem Soc 127(3):810–811
38. Blight BA, Hunter CA, Leigh DA, Mcnab H, Thomson PIT (2011) An AAAA-DDDD quadruple hydrogen-bond array. Nat Chem 3(3):244–248
39. Noro A, Hayashi M, Matsushita Y (2012) Design and properties of supramolecular polymer gels. Soft Matter 8(24):6416–6429
40. Noro A, Ishihara K, Matsushita Y (2011) Nanophase-separated supramolecular assemblies of two functionalized polymers via acid–base complexation. Macromolecules 44 (16):6241–6244
41. Hayashi M, Noro A, Matsushita Y (2014) Viscoelastic properties of supramolecular soft materials with transient polymer network. J Polym Sci Pol Phys 52(11):755–764
42. Farnik D, Kluger C, Kunz MJ, Machl D, Petraru L, Binder WH (2004) Synthesis and self assembly of hydrogen-bonded supramolecular polymers. Macromol Symp 217:247–266
43. Hirschberg JHKK, Beijer FH, van Aert HA, Magusin PCMM, Sijbesma RP, Meijer EW (1999) Supramolecular polymers from linear telechelic siloxanes with quadruple-hydrogen-bonded units. Macromolecules 32(8):2696–2705
44. Jacobson H, Stockmayer WH (1950) Intramolecular reaction in polycondensations. 1. The theory of linear systems. J Chem Phys 18(12):1600–1606

45. Ciferri A (2000) Mechanism of supramolecular polymerizations. In: Ciferri A (ed) Supramolecular polymers. Marcel Dekker, Genoa, pp 1–59
46. Chen CC, Dormidontova EE (2004) Ring-chain equilibrium in reversibly associated polymer solutions: Monte Carlo simulations. Macromolecules 37(10):3905–3917
47. Cates ME (1987) Reptation of living polymers – dynamics of entangled polymers in the presence of reversible chain-scission reactions. Macromolecules 20(9):2289–2296
48. Cates ME, Candau SJ (1990) Statics and dynamics of worm-like surfactant micelles. J Phys Condens Mat 2(33):6869–6892
49. van de Manakker F, Vermonden T, el Morabit N, van Nostrum CF, Hennink WE (2008) Rheological behavior of self-assembling PEG-beta-cyclodextrin/PEG-cholesterol hydrogels. Langmuir 24(21):12559–12567
50. Sprakel J, van der Gucht J, Cohen Stuart MA, Besseling NAM (2008) Brownian particles in transient polymer networks. Phys Rev E 77(6): 061502
51. van der Gucht J, Besseling NAM, Knoben W, Bouteiller L, Cohen Stuart MA (2003) Brownian particles in supramolecular polymer solutions. Phys Rev E 67(5): 051106
52. Knoben W, Besseling NAM, Bouteiller L, Stuart AC (2005) Dynamics of reversible supramolecular polymers: independent determination of the dependence of linear viscoelasticity on concentration and chain length by using chain stoppers. Phys Chem Chem Phys 7 (11):2390–2398
53. Jones RAL (2002) Soft condensed matter. Oxford University Press, Oxford
54. Bell GI (1980) Theoretical-models for the specific adhesion of cells to cells or to surfaces. Adv Appl Probab 12(3):566–567
55. Evans EA, Calderwood DA (2007) Forces and bond dynamics in cell adhesion. Science 316 (5828):1148–1153
56. Tanaka F, Edwards SF (1992) Viscoelastic properties of physically cross-linked networks – transient network theory. Macromolecules 25(5):1516–1523
57. Sivakova S, Bohnsack DA, Mackay ME, Suwanmala P, Rowan SJ (2005) Utilization of a combination of weak hydrogen-bonding interactions and phase segregation to yield highly thermosensitive supramolecular polymers. J Am Chem Soc 127(51):18202–18211
58. Yan TZ, Schroter K, Herbst F, Binder WH, Thurn-Albrecht T (2014) Nanostructure and rheology of hydrogen-bonding telechelic polymers in the melt: from micellar liquids and solids to supramolecular gels. Macromolecules 47(6):2122–2130
59. Herbst F, Schroter K, Gunkel I, Groger S, Thurn-Albrecht T, Balbach J, Binder WH (2010) Aggregation and chain dynamics in supramolecular polymers by dynamic rheology: cluster formation and self-aggregation. Macromolecules 43(23):10006–10016
60. Herbst F, Binder WH (2013) Comparing solution and melt-state association of hydrogen bonds in supramolecular polymers. Polym Chem 4(12):3602–3609
61. Herbst F, Seiffert S, Binder WH (2012) Dynamic supramolecular poly(isobutylene)s for self-healing materials. Polym Chem 3(11):3084–3092
62. Stukalin EB, Cai LH, Kumar NA, Leibler L, Rubinstein M (2013) Self-healing of unentangled polymer networks with reversible bonds. Macromolecules 46(18):7525–7541
63. Hentschel J, Kushner AM, Ziller J, Guan ZB (2012) Self-healing supramolecular block copolymers. Angew Chem Int Ed 51(42):10561–10565
64. Sijbesma RP, Beijer FH, Brunsveld L, Folmer BJB, Hirschberg JHKK, Lange RFM, Lowe JKL, Meijer EW (1997) Reversible polymers formed from self-complementary monomers using quadruple hydrogen bonding. Science 278(5343):1601–1604
65. Folmer BJB, Sijbesma RP, Versteegen RM, van der Rijt JAJ, Meijer EW (2000) Supramolecular polymer materials: chain extension of telechelic polymers using a reactive hydrogen-bonding synthon. Adv Mater 12(12):874–878
66. Dankers PYW, van Leeuwen ENM, van Gemert GML, Spiering AJH, Harmsen MC, Brouwer LA, Janssen HM, Bosman AW, van Luyn MJA, Meijer EW (2006) Chemical and biological properties of supramolecular polymer systems based on oligocaprolactones. Biomaterials 27 (32):5490–5501

67. Yamauchi K, Lizotte JR, Hercules DM, Vergne MJ, Long TE (2002) Combinations of microphase separation and terminal multiple hydrogen bonding in novel macromolecules. J Am Chem Soc 124(29):8599–8604
68. Wrue MH, McUmber AC, Anthamatten M (2009) Atom transfer radical polymerization of end-functionalized hydrogen-bonding polymers and resulting polymer miscibility. Macromolecules 42(23):9255–9262
69. Dankers PYW, Zhang Z, Wisse E, Grijpma DW, Sijbesma RP, Feijen J, Meijer EW (2006) Oligo(trimethylene carbonate)-based supramolecular biomaterials. Macromolecules 39 (25):8763–8771
70. Li GX, Wie JJ, Nguyen NA, Chung WJ, Kim ET, Char K, Mackay ME, Pyun J (2013) Synthesis, self-assembly and reversible healing of supramolecular perfluoropolyethers. J Polym Sci Polym Chem 51(17):3598–3606
71. Appel WPJ, Portale G, Wisse E, Dankers PYW, Meijer EW (2011) Aggregation of ureidopyrimidinone supramolecular thermoplastic elastomers into nanofibers: a kinetic analysis. Macromolecules 44(17):6776–6784
72. Chen YJ, Zhang H, Fang XL, Lin YJ, Xu YZ, Weng WG (2014) Mechanical activation of mechanophore enhanced by strong hydrogen bonding interactions. ACS Macro Lett 3 (2):141–145
73. Sontjens SHM, Sijbesma RP, van Genderen MHP, Meijer EW (2001) Selective formation of cyclic dimers in solutions of reversible supramolecular polymers. Macromolecules 34 (12):3815–3818
74. Botterhuis NE, van Beek DJM, van Gemert GML, Bosman AW, Sijbesma RP (2008) Self-assembly and morphology of polydimethylsiloxane supramolecular thermoplastic elastomers. J Polym Sci Polym Chem 46(12):3877–3885
75. Bobade S, Wang YY, Mays J, Baskaran D (2014) Synthesis and characterization of ureidopyrimidone telechelics by CuAAC "click" reaction: effect of t-g and polarity. Macromolecules 47(15):5040–5050
76. Semenov AN, Joanny JF, Khokhlov AR (1995) Associating polymers – equilibrium and linear viscoelasticity. Macromolecules 28(4):1066–1075
77. Cortese J, Soulie-Ziakovic C, Cloitre M, Tence-Girault S, Leibler L (2011) Order–disorder transition in supramolecular polymers. J Am Chem Soc 133(49):19672–19675
78. Bras AR, Hovelmann CH, Antonius W, Teixeira J, Radulescu A, Allgaier J, Pyckhout-Hintzen W, Wischnewski A, Richter D (2013) Molecular approach to supramolecular polymer assembly by small angle neutron scattering. Macromolecules 46(23):9446–9454
79. Cheng CC, Lin IH, Yen YC, Chu CW, Ko FH, Wang XL, Chang FC (2012) New self-assembled supramolecular polymers formed by self-complementary sextuple hydrogen bond motifs. RSC Adv 2(26):9952–9957
80. He Y, Zhu B, Inoue Y (2004) Hydrogen bonds in polymer blends. Prog Polym Sci 29 (10):1021–1051
81. Coleman MM, Painter PC (1995) Hydrogen-bonded polymer blends. Prog Polym Sci 20 (1):1–59
82. Painter PC, Tang WL, Graf JF, Thomson B, Coleman MM (1991) Formation of molecular composites through hydrogen-bonding interactions. Macromolecules 24:3929–3936
83. Viswanathan S, Dadmun MD (2004) Miscible blends containing a liquid crystalline polymer via optimized hydrogen bonding: correlation to theory. J Polym Sci B Polym Phys 42:1010–1022
84. Viswanathan S, Dadmun MD (2003) Optimizing hydrogen-bonding in creating miscible liquid crystalline polymer blends by structural modifications of the blend components. Macromolecules 36:3196–3205
85. Viswanathan S, Dadmun MD (2002) Guidelines to creating a true molecular composite: inducing miscibility in blends by optimizing intermolecular hydrogen bonding. Macromolecules 35:5049–5060

86. Baird DC, McLeod MA (2000) Liquid crystalline polymer blends. In: Paul DR, Bucknall CB (eds) Polymer blends, vol 2. Wiley, New York, pp 429–453
87. Zheng S, Lu H (2003) Miscibility and phase behavior in thermosetting blends of polybenzoxazine and poly(ethylene oxide). Polymer 44:4689–4698
88. Hou S-S, Graf R, Spiess HW, Kuo P-L (2001) An investigation into PEO/crosslinked-silicone semi-interpenetrating polymer network using ^{1}H solid-state NMR spectroscopy under fast MAS. Macromol Rapid Commun 22:1386–1389
89. Lin YH, Darling SB, Nikiforov MO, Strzalka J, Verduzco R (2012) Supramolecular conjugated block copolymers. Macromolecules 45(16):6571–6579
90. Flory PJ (1953) Principles of polymer chemistry. Cornell University Press, Ithaca
91. Anthamatten M (2007) Phase behavior predictions for polymer blends containing reversibly associating endgroups. J Polym Sci Polym Phys 45(24):3285–3299
92. Dudowicz J, Freed KF (2012) Lattice cluster theory of associating polymers. I. Solutions of linear telechelic polymer chains. J Chem Phys 136(6): 064902
93. Dudowicz J, Freed KF, Douglas JF (2012) Lattice cluster theory of associating polymers. IV. Phase behavior of telechelic polymer solutions. J Chem Phys 136(19) :194903
94. Feldman KE, Kade MJ, de Greef TFA, Meijer EW, Kramer EJ, Hawker CJ (2008) Polymers with multiple hydrogen-bonded end groups and their blends. Macromolecules 41 (13):4694–4700
95. Yang SK, Ambade AV, Weck M (2011) Main-chain supramolecular block copolymers. Chem Soc Rev 40(1):129–137
96. Stuparu MC, Khan A, Hawker CJ (2012) Phase separation of supramolecular and dynamic block copolymers. Polym Chem 3(11):3033–3044
97. Feng EH, Lee WB, Fredrickson GH (2007) Supramolecular diblock copolymers: a field-theoretic model and mean-field solution. Macromolecules 40(3):693–702
98. Kunz MJ, Hayn G, Saf R, Binder WH (2004) Hydrogen-bonded supramolecular poly(ether ketone)s. J Polym Sci Polym Chem 42(3):661–674
99. Bertrand A, Chen SB, Souharce G, Ladaviere C, Fleury E, Bernard J (2011) Straightforward preparation of telechelic H-bonding polymers from difunctional trithiocarbonates and supramolecular block copolymers thereof. Macromolecules 44(10):3694–3704
100. Yang XW, Hua FJ, Yamato K, Ruckenstein E, Gong B, Kim W, Ryu CY (2004) Supramolecular AB diblock copolymers. Angew Chem Int Ed 43(47):6471–6474
101. Binder WH, Kunz MJ, Ingolic E (2004) Supramolecular poly(ether ketone)-polyisobutylene pseudo-block copolymers. J Polym Sci Polym Chem 42(1):162–172
102. Pitet LM, van Loon AHM, Kramer EJ, Hawker CJ, Meijer EW (2013) Nanostructured supramolecular block copolymers based on polydimethylsiloxane and polylactide. ACS Macro Lett 2(11):1006–1010
103. Jiang Q, Ward MD (2014) Crystallization under nanoscale confinement. Chem Soc Rev 43 (7):2066–2079
104. Ostas E, Schroter K, Beiner M, Yan TZ, Thurn-Albrecht T, Binder WH (2011) Poly(epsilon-caprolactone)-poly(isobutylene): a crystallizing, hydrogen-bonded pseudo-block copolymer. J Polym Sci Polym Chem 49(15):3404–3416
105. Ostas E, Yan TZ, Thurn-Albrecht T, Binder WH (2013) Crystallization of supramolecular pseudoblock copolymers. Macromolecules 46(11):4481–4490
106. Elacqua E, Lye DS, Weck M (2014) Engineering orthogonality in supramolecular polymers: from simple scaffolds to complex materials. Acc Chem Res 47:2405–2416
107. Chen SB, Deng YM, Chang XJ, Barqawi H, Schulz M, Binder WH (2014) Facile preparation of supramolecular (ABAC)(n) multiblock copolymers from Hamilton wedge and barbiturate-functionalized raft agents. Polym Chem 5(8):2891–2900
108. Ambade AV, Burd C, Higley MN, Nair KP, Weck M (2009) Orthogonally self-assembled multifunctional block copolymers. Chem Eur J 15(44):11904–11911
109. Ambade AV, Yang SK, Weck M (2009) Supramolecular ABC triblock copolymers. Angew Chem Int Ed 48(16):2894–2898

110. Yang SK, Ambade AV, Weck M (2010) Supramolecular ABC triblock copolymers via one-pot, orthogonal self-assembly. J Am Chem Soc 132(5):1637–1645
111. Angell CA (1995) Formation of glasses from liquids and biopolymers. Science 267 (5206):1924–1935
112. Huang DH, McKenna GB (2001) New insights into the fragility dilemma in liquids. J Chem Phys 114(13):5621–5630
113. Srikanth A, Hoy RS, Rinderspacher BC, Andzelm JW (2013) Nonlinear mechanics of thermoreversibly associating dendrimer glasses. Phys Rev E 88(4): 042607
114. Binder WH, Petraru L, Roth T, Groh PW, Palfi V, Keki S, Ivan B (2007) Magnetic and temperature-sensitive release gels from supramolecular polymers. Adv Funct Mater 17 (8):1317–1326
115. Elkins CL, Viswanathan K, Long TE (2006) Synthesis and characterization of star-shaped poly(ethylene-co-propylene) polymers bearing terminal self-complementary multiple hydrogen-bonding sites. Macromolecules 39(9):3132–3139
116. Lange RFM, Van Gurp M, Meijer EW (1999) Hydrogen-bonded supramolecular polymer networks. J Polym Sci Polym Chem 37(19):3657–3670
117. Mather BD, Elkins CL, Beyer FL, Long TE (2007) Morphological analysis of telechelic ureidopyrimidone functional hydrogen bonding linear and star-shaped poly(ethylene-co-propylene)s. Macromol Rapid Commun 28(16):1601–1606
118. Wang DL, Chen HY, Su Y, Qiu F, Zhu LJ, Huan XY, Zhu BS, Yan DY, Guo FL, Zhu XY (2013) Supramolecular amphiphilic multiarm hyperbranched copolymer: synthesis, self-assembly and drug delivery applications. Polym Chem 4(1):85–94
119. Karikari AS, Mather BD, Long TE (2007) Association of star-shaped poly(D,L-lactide)s containing nucleobase multiple hydrogen bonding. Biomacromolecules 8(1):302–308
120. Zimmerman SC, Zeng FW, Reichert DEC, Kolotuchin SV (1996) Self-assembling dendrimers. Science 271(5252):1095–1098
121. Franz A, Bauer W, Hirsch A (2005) Complete self-assembly of discrete supramolecular dendrimers. Angew Chem Int Ed 44(10):1564–1567
122. Grimm F, Hartnagel K, Wessendorf F, Hirsch A (2009) Supramolecular self-assembly of dendrimers containing orthogonal binding motifs. Chem Commun 2009(11):1331–1333
123. Betancourt JE, Rivera JM (2008) Hexadecameric self-assembled dendrimers built from 2′-deoxyguanosine derivatives. Org Lett 10(11):2287–2290
124. Elkins CL, Park T, McKee MG, Long TE (2005) Synthesis and characterization of poly (2-ethylhexyl methacrylate) copolymers containing pendant, self-complementary multiple-hydrogen-bonding sites. J Polym Sci Polym Chem 43(19):4618–4631
125. Feldman KE, Kade MJ, Meijer EW, Hawker CJ, Kramer EJ (2009) Model transient networks from strongly hydrogen-bonded polymers. Macromolecules 42(22):9072–9081
126. Peng CC, Abetz V (2005) A simple pathway toward quantitative modification of polybutadiene: a new approach to thermoreversible cross-linking rubber comprising supramolecular hydrogen-bonding networks. Macromolecules 38(13):5575–5580
127. Ilhan F, Gray M, Rotello VM (2001) Reversible side chain modification through noncovalent interactions. “Plug and play” polymers. Macromolecules 34(8):2597–2601
128. Ilhan F, Galow TH, Gray M, Clavier G, Rotello VM (2000) Giant vesicle formation through self-assembly of complementary random copolymers. J Am Chem Soc 122(24):5895–5896
129. Leibler L, Rubinstein M, Colby RH (1991) Dynamics of reversible networks. Macromolecules 24(16):4701–4707
130. Rubinstein M, Semenov AN (1998) Thermoreversible gelation in solutions of associating polymers. 2. Linear dynamics. Macromolecules 31(4):1386–1397
131. Lewis CL, Stewart K, Anthamatten M (2014) The influence of hydrogen bonding side-groups on viscoelastic behavior of linear and network polymers. Macromolecules 47(2):729–740
132. Cheng SJ, Zhang MQ, Dixit N, Moore RB, Long TE (2012) Nucleobase self-assembly in supramolecular adhesives. Macromolecules 45(2):805–812

133. Kato T, Hirota N, Fujishima A, Frechet JMJ (1996) Supramolecular hydrogen-bonded liquid-crystalline polymer complexes. Design of side-chain polymers and a host-guest system by noncovalent interaction. J Polym Sci Polym Chem 34(1):57–62
134. Kawakami T, Kato T (1998) Use of intermolecular hydrogen bonding between imidazolyl moieties and carboxylic acids for the supramolecular self-association of liquid-crystalline side-chain polymers and networks. Macromolecules 31(14):4475–4479
135. Thibault RJ, Hotchkiss PJ, Gray M, Rotello VM (2003) Thermally reversible formation of microspheres through non-covalent polymer cross-linking. J Am Chem Soc 125 (37):11249–11252
136. Nair KP, Breedveld V, Weck M (2008) Complementary hydrogen-bonded thermoreversible polymer networks with tunable properties. Macromolecules 41(10):3429–3438
137. Nair KP, Breedveld V, Weck M (2011) Modulating mechanical properties of self-assembled polymer networks by multi-functional complementary hydrogen bonding. Soft Matter 7 (2):553–559
138. Hackelbusch S, Rossow T, van Assenbergh P, Seiffert S (2013) Chain dynamics in supramolecular polymer networks. Macromolecules 46(15):6273–6286
139. Rossow T, Hackelbusch S, van Assenbergh P, Seiffert S (2013) A modular construction kit for supramolecular polymer gels. Polym Chem 4(8):2515–2527
140. Nair KP, Pollino JM, Weck M (2006) Noncovalently functionalized block copolymers possessing both hydrogen bonding and metal coordination centers. Macromolecules 39 (3):931–940. doi:10.1021/iiiao52222t
141. Zhang KR, Fahs GB, Aiba M, Moore RB, Long TE (2014) Nucleobase-functionalized ABC triblock copolymers: self-assembly of supramolecular architectures. Chem Commun 50 (65):9145–9148
142. Mather BD, Baker MB, Beyer FL, Berg MAG, Green MD, Long TE (2007) Supramolecular triblock copolymers containing complementary nucleobase molecular recognition. Macromolecules 40(19):6834–6845
143. Li JH, Lewis CL, Chen DL, Anthamatten M (2011) Dynamic mechanical behavior of photo-cross-linked shape-memory elastomers. Macromolecules 44(13):5336–5343
144. Li JH, Viveros JA, Wrue MH, Anthamatten M (2007) Shape-memory effects in polymer networks containing reversibly associating side-groups. Adv Mater 19(19):2851–2855
145. Cordier P, Tournilhac F, Soulie-Ziakovic C, Leibler L (2008) Self-healing and thermoreversible rubber from supramolecular assembly. Nature 451(7181):977–980
146. Chen YL, Kushner AM, Williams GA, Guan ZB (2012) Multiphase design of autonomic self-healing thermoplastic elastomers. Nat Chem 4(6):467–472
147. Chen YL, Guan ZB (2013) Self-assembly of core-shell nanoparticles for self-healing materials. Polym Chem 4(18):4885–4889
148. Chen YL, Guan ZB (2014) Multivalent hydrogen bonding block copolymers self-assemble into strong and tough self-healing materials. Chem Commun 50(74):10868–10870
149. Li JH, Sullivan KD, Brown EB, Anthamatten M (2010) Thermally activated diffusion in reversibly associating polymers. Soft Matter 6(2):235–238
150. Chen YJ, Wu W, Himmel T, Wagner MH (2013) Structure and rheological behavior of thermoreversible supramolecular polymers with weak multiple hydrogen bonds. Macromol Mater Eng 298(8):876–887
151. De D, Gaymans RJ (2009) Thermoplastic polyurethanes with TDI-based monodisperse hard segments. Macromol Mater Eng 294(6–7):405–413
152. Johnson JC, Wanasekara ND, Korley LTJ (2012) Utilizing peptidic ordering in the design of hierarchical polyurethane/ureas. Biomacromolecules 13(5):1279–1286
153. Merino DH, Slark AT, Colquhoun HM, Hayes W, Hamley IW (2010) Thermo-responsive microphase separated supramolecular polyurethanes. Polym Chem 1(8):1263–1271
154. Das S, Yilgor I, Yilgor E, Inci B, Tezgel O, Beyer FL, Wilkes GL (2007) Structure–property relationships and melt rheology of segmented, non-chain extended polyureas: effect of soft segment molecular weight. Polymer 48(1):290–301

155. Woodward PJ, Merino DH, Greenland BW, Hamley IW, Light Z, Slark AT, Hayes W (2010) Hydrogen bonded supramolecular elastomers: correlating hydrogen bonding strength with morphology and rheology. Macromolecules 43(5):2512–2517
156. Wisse E, Govaert LE, Meijer HEH, Meijer EW (2006) Unusual tuning of mechanical properties of thermoplastic elastomers using supramolecular fillers. Macromolecules 39 (21):7425–7432
157. Wisse E, Spiering AJH, Pfeifer F, Portale G, Siesler HW, Meijer EW (2009) Segmental orientation in well-defined thermoplastic elastomers containing supramolecular fillers. Macromolecules 42(2):524–530
158. van Esch J, De Feyter S, Kellogg RM, De Schryver F, Feringa BL (1997) Self-assembly of bisurea compounds in organic solvents and on solid substrates. Chem Eur J 3(8):1238–1243
159. Botterhuis NE, Karthikeyan S, Veldman D, Meskers SCJ, Sijbesma RP (2008) Molecular recognition in bisurea thermoplastic elastomers studied with pyrene-based fluorescent probes and atomic force microscopy. Chem Commun 2008(33):3915–3917
160. Pawar GM, Koenigs M, Fahimi Z, Cox M, Voets IK, Wyss HM, Sijbesma RP (2012) Injectable hydrogels from segmented PEG-bisurea copolymers. Biomacromolecules 13 (12):3966–3976
161. Yang J, Dewal MB, Shimizu LS (2006) Self-assembling bisurea macrocycles used as an organic zeolite for a highly stereoselective photodimerization of 2-cyclohexenone. J Am Chem Soc 128(25):8122–8123
162. Ni YP, Becquart F, Chen JD, Taha M (2013) Polyurea-urethane supramolecular thermoreversible networks. Macromolecules 46(3):1066–1074
163. Sijbrandi NJ, Kimenai AJ, Mes EPC, Broos R, Bar G, Rosenthal M, Odarchenko Y, Ivanov DA, Dijkstra PJ, Feijen J (2012) Synthesis, morphology, and properties of segmented poly (ether amide)s with uniform oxalamide-based hard segments. Macromolecules 45 (9):3948–3961
164. Buckwalter DJ, Hudson AG, BMoore R, Long TE (2014) Synthesis and characterization of poly(propylene glycol) polytrioxamide and poly(urea oxamide) segmented copolymers. Polym Int 63(7):1184–1191
165. Buckwalter DJ, Inglefield DL, Enokida JS, Hudson AG, Moore RB, Long TE (2013) Effects of copolymer structure on the mechanical properties of poly(dimethyl siloxane) poly (oxamide) segmented copolymers. Macromol Chem Phys 214(18):2073–2082
166. Buckwalter DJ, Zhang MQ, Inglefield DL, Moore RB, Long TE (2013) Synthesis and characterization of siloxane-containing poly(urea oxamide) segmented copolymers. Polymer 54(18):4849–4857
167. Pensec S, Nouvel N, Guilleman A, Creton C, Boue F, Bouteiller L (2010) Self-assembly in solution of a reversible comb-shaped supramolecular polymer. Macromolecules 43 (5):2529–2534
168. Fonteneau C, Pensec S, Bouteiller L (2014) Versatile synthesis of reversible comb-shaped supramolecular polymers. Polym Chem 5(7):2496–2505
169. Catrouillet S, Fonteneau C, Bouteiller L, Delorme N, Nicol E, Nicolai T, Pensec S, Colombani O (2013) Competition between steric hindrance and hydrogen bonding in the formation of supramolecular bottle brush polymers. Macromolecules 46(19):7911–7919
170. Wang ZG, Safran SA (1988) Size distribution for aggregates of associating polymers. 2. Linear packing. J Chem Phys 89(8):5323–5328
171. Knoben W, Besseling NAM, Stuart MAC (2006) Chain stoppers in reversible supramolecular polymer solutions studied by static and dynamic light scattering and osmometry. Macromolecules 39(7):2643–2653
172. Lortie F, Boileau SB, Bouteiller L, Chassenieux C, Laupretre F (2005) Chain stopper-assisted characterization of supramolecular polymers. Macromolecules 38(12):5283–5287
173. Courtois J, Baroudi I, Nouvel N, Degrandi E, Pensec S, Ducouret G, Chaneac C, Bouteiller L, Creton C (2010) Supramolecular soft adhesive materials. Adv Funct Mater 20 (11):1803–1811

174. Guan ZB, Roland JT, Bai JZ, Ma SX, McIntire TM, Nguyen M (2004) Modular domain structure: a biomimetic strategy for advanced polymeric materials. J Am Chem Soc 126 (7):2058–2065
175. Roland JT, Guan ZB (2004) Synthesis and single-molecule studies of a well-defined biomimetic modular multidomain polymer using a peptidomimetic beta-sheet module. J Am Chem Soc 126(44):14328–14329
176. Kushner AM, Gabuchian V, Johnson EG, Guan ZB (2007) Biomimetic design of reversibly unfolding cross-linker to enhance mechanical properties of 3D network polymers. J Am Chem Soc 129(46):14110–14111
177. Shi ZM, Huang J, Ma Z, Zhao X, Guan ZB, Li ZT (2010) Foldamers as cross-links for tuning the dynamic mechanical property of methacrylate copolymers. Macromolecules 43 (14):6185–6192
178. Kushner AM, Vossler JD, Williams GA, Guan ZB (2009) A biomimetic modular polymer with tough and adaptive properties. J Am Chem Soc 131(25):8766–8768
179. Yu TB, Bai JZ, Guan ZB (2009) Cycloaddition-promoted self-assembly of a polymer into well-defined beta sheets and hierarchical nanofibrils. Angew Chem Int Ed 48(6):1097–1101
180. Lillya CP, Baker RJ, Hütte S, Winter HH, Lin Y-G, Shi J, Dickinson LJ, Chien JCW (1992) Linear chain extension through associative termini. Macromolecules 25:2076–2080
181. Noro A, Nagata Y, Takano A, Matsushita Y (2006) Diblock-type supramolecule via biocomplementary hydrogen bonding. Biomacromolecules 7(6):1696–1699

Self-Healing Hydrogels Formed via Hydrophobic Interactions

Oguz Okay

Contents

Abstract Hydrogels are physically or chemically cross-linked polymers with the ability to absorb large amounts of water without dissolving. Elasticity, smartness, and high water sorption capacity make hydrogels extraordinary materials. Although synthetic hydrogels resemble biological tissue, they generally exhibit poor mechanical performance, which limits their use in stress-bearing applications. Hence, synthetic hydrogels that combine good mechanical properties with stimuli-responsiveness and self-healing ability are required for the development of several new technologies. To create such high-toughness hydrogels with self-healing abilities, hydrophobic modification of hydrophilic polymer chains has attracted great interest in recent years. Incorporation of a small amount of hydrophobic units with long alkyl side chains into hydrophilic polymers creates an energy dissipation mechanism. This mechanism appears as a result of the hydrophobic associations, i.e., reversible cross-links within the polymer network. Hydrogels formed via hydrophobic interactions in micellar solutions exhibit unique properties such as a high stretchability (up to 5,000 %), high mechanical strength (up to 1.7 MPa tensile stress), and complete autonomous self-healing ability. Mixed

O. Okay (✉)
Department of Chemistry, Istanbul Technical University, 34469 Maslak, Istanbul, Turkey
e-mail: okayo@itu.edu.tr

© Springer International Publishing Switzerland 2015

S. Seiffert (ed.), *Supramolecular Polymer Networks and Gels*, Advances in Polymer Science 268, DOI 10.1007/978-3-319-15404-6_3

micelles acting as physical cross-links in these hydrogels are formed by dynamic hydrophobic association between the hydrophobic domains of the polymer chains and grown surfactant micelles. This chapter describes some conditions for formation of hydrophobically modified hydrogels with extraordinary mechanical properties and self-healing abilities. Special emphasis is placed on the role of surfactant micelles for the dynamic and mechanical properties of these hydrophobically modified hydrogels.

Keywords Dynamics • Hydrogels • Hydrophobic associations • Mechanical properties • Self-healing

Abbreviations

AAc	Acrylic acid
AAm	Acrylamide
AIBN	2,2′-Azobis(isobutyronitrile)
APS	Ammonium persulfate
C16M	*N*-Hexadecyl methacrylate
C17.3M	Stearyl methacrylate
C18A	*N*-Octadecyl acrylate
C18M	*N*-Octadecyl methacrylate
C22A	Dococyl acrylate
C_0	Initial monomer concentration
CTAB	Cetyltrimethylammonium bromide
D	Cooperative diffusion coefficient
D_A	Apparent diffusion coefficient
DLS	Dynamic light scattering
DMA	*N*,*N*-Dimethylacrylamide
DMSO	Dimethyl sulfoxide
E	Tensile modulus
f_{HM}	Mole fraction of hydrophobic monomer in the comonomer feed
f_ν	Fraction of associations broken during the loading
G	Shear modulus
$G(t)$	Relaxation modulus
G'	Elastic modulus
G''	Viscous modulus
G_R	Rouse modulus
HM	Hydrophobically modified
$<I>_E$	Ensemble-averaged scattering intensity
$I_C(q)$	Scattered intensity as a result of the frozen structure
$<I(q)>_T$	Time-averaged scattering intensity
$<I_F(q)>_T$	Scattered intensity as a result of the liquid-like concentration fluctuations

ICF	Time average intensity correlation function
m_{rel}	Relative gel mass
$m_{rel,eq}$	Equilibrium swelling ratio
n	Refractive index
N	Polymer chain length
N_{Agg}	Aggregation number of the surfactant
N_H	Number of hydrophobes per hydrophobic block
PAAc	Poly(acrylic acid)
PAAm	Polyacrylamide
PDMA	Poly(*N*,*N*-dimethylacrylamide)
q	Scattering vector
SDS	Sodium dodecylsulfate
SMS	Sodium metabisulfite
S_n	Number of hydrophobic blocks per chain
tan δ	Loss factor (equal to G''/G')
TEMED	*N*,*N*,*N*′,*N*′-Tetramethylethylenediamine
U_{hys}	Hysteresis energy
U_{xl}	Average dissociation energy of a single association
β	Molar ratio of CTAB to the AAc units in the polymer
β_0	CTAB/AAc molar ratio in the gelation solution
γ_c	Critical shear rate for shear thickening
Γ_{fast}	Relaxation rate of the fast mode
γ_0	Strain amplitude
Γ_{slow}	Relaxation rate of the slow mode
η	Viscosity
η_{sp}	Specific viscosity
θ	Scattering angle
λ	Deformation ratio
$\lambda_{biax,max}$	Maximum biaxial extension ratio
λ_f	Stretch at failure
λ_{max}	Maximum strain
ν_e	Effective cross-linking density
ξ	Dynamic correlation length
ξ_H	Hydrodynamic correlation length
σ_f	Fracture stress
σ_{nom}	Nominal stress
σ_{true}	True stress
τ	Decay time
τ_1	Lifetime of associations
τ_c	Characteristic time (equal to ${\gamma_c}^{-1}$)
τ_R	Characteristic relaxation time (equal to ${\omega_c}^{-1}$)
ω	Angular frequency
ω_c	Cross-over frequency at which G' and G'' are equal in oscillatory shear rheology

1 Introduction

Hydrogels are similar to biological tissue in that they consist of three-dimensional networks of macromolecules and water as the main component. Elasticity, smartness, and high water sorption capacity make hydrogels extraordinary materials [1]. However, synthetic hydrogels prepared by classical chemical methods are normally brittle, which limits their use in stress-bearing applications. Therefore, design of hydrogels with good mechanical properties is crucial. Synthetic hydrogels that combine high toughness with stimuli-responsiveness and self-healing ability are promising for the development of several new technologies.

The poor mechanical performance of chemical hydrogels mainly arises from their low resistance to crack propagation because of the lack of an efficient energy dissipation mechanism in the gel network [2, 3]. As demonstrated by the cartoon in Fig. 1a, the energy accumulated close to a crack tip cannot be dissipated in chemical hydrogels, leading to fracture of the material [4]. Hence, to obtain high-toughness hydrogels, the overall viscoelastic dissipation along the hydrogel sample should be increased by introducing dissipative mechanisms at a molecular level. To improve the mechanical properties of conventional hydrogels, many studies have been conducted in recent years [5–11]. Moreover, inspired by natural healing processes, different reversible molecular interactions have been used to generate hydrogels with the ability to self-heal, autonomously or with the help of an external stimulus [12–30].

To create high-toughness hydrogels with self-healing abilities, hydrophobic modification of hydrophilic polymer chains has attracted great interest [4, 8, 31–42]. Incorporation of a small amount of hydrophobic units with long alkyl side chains in a hydrophilic polymer backbone dramatically increases the viscous modulus, G'', of aqueous polymer solutions, reflecting creation of energy dissipation mechanisms as a result of the formation of hydrophobic associations (i.e., temporary junction zones inside the gel network). The driving force for the formation of these associations is the interaction between the hydrophobic groups, which arises in order to minimize their exposure to water. The activation energy for the disengagement of hydrophobes from these associations is in the order of the thermal energy kT [43–47], so that the free and bonded hydrophobes in such physical gels are in a dynamic equilibrium. As illustrated in Fig. 1b, the crack energy along the hydrogel is dissipated by reversible disengagement of the hydrophobes from their hydrophobic associations, so that growth of a crack to a macroscopic level can be prevented. Over the past few years, intensive studies have been conducted with the aim of developing high-toughness self-healing physical hydrogels via hydrophobic interactions [32–42]. Figure 2a–c schematically depicts the strategy used for the preparation of such hydrogels. Mixed micelles acting as physical cross-links in the hydrogels are formed by dynamic hydrophobic association of the hydrophobic domains of hydrophilic polymer chains and grown surfactant micelles. Hydrogels formed via such hydrophobic interactions in micellar solutions exhibit unique

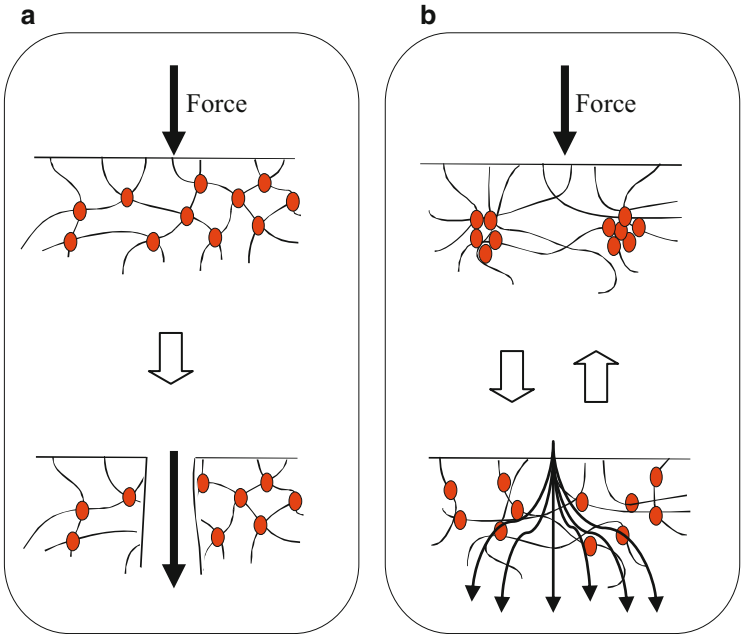

Fig. 1 (**a**) Formation of a crack in a chemical hydrogel with no viscous dissipation. (**b**) Energy dissipation in a hydrogel formed via hydrophobic interactions. From [4] with permission from Elsevier

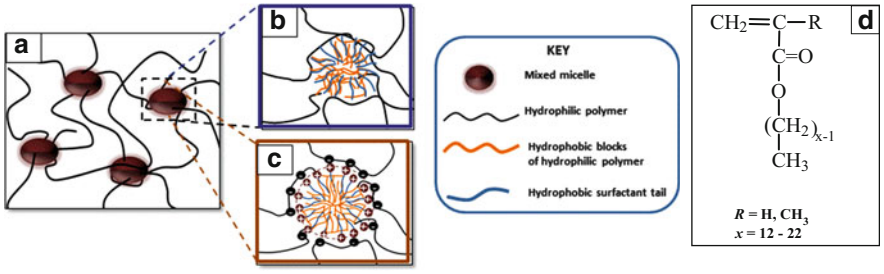

Fig. 2 (**a–c**) Physical polymer-network cross-linking provided by mixed micelles in hydrogels formed via hydrophobic interactions in surfactant solutions. Mixed micelles are formed by aggregation of hydrophobic blocks of per-se hydrophilic polymers and surfactant alkyl tails. (**b**) Nonionic polymer and ionic surfactant gel system at the state of preparation. For clarity, charges are not shown. (**c**) Ionic polymer and oppositely charged surfactant gel system after extraction of free micelles. (**d**) Structure of the hydrophobic monomers used in the micellar polymerization

properties such as a high stretchability (up to 5,000 %), high mechanical strength (up to 1.7 MPa tensile stress), and complete autonomous self-healing.

This chapter discusses formation conditions as well as rheological and mechanical properties of hydrogels formed via hydrophobic associations in micellar solutions; it also discusses why the dynamic and mechanical properties of such

hydrogels significantly differ from conventional gels formed by chemical cross-linkers. The extraordinary mechanical properties, including self-healing, are also discussed.

2 Preparation of Hydrophobically Modified Hydrogels

Hydrogels formed via hydrophobic interactions are mainly prepared by copolymerization of a hydrophilic monomer with a small amount (1–5 mol%) of a hydrophobic comonomer, most typically by a free-radical mechanism. Acrylamide (AAm), *N*,*N*-dimethylacrylamide (DMA), or acrylic acid (AAc) are mainly used as the hydrophilic monomer in the precursor-polymer preparation. Several hydrocarbon hydrophobes, including *N*-alkyl-, *N*,*N*-dialkyl-acrylamides or -(meth)acrylates of various alkyl chain length, and fluorocarbon hydrophobes such as 2-(*N*-ethylperfluorooctane sulfonamido)ethyl acrylate have been used for the preparation of physical gels from these precursor polymers [4, 31, 48, 49]. To create strong hydrophobic interactions between the hydrophilic polymer chains, hydrophobic acrylates or methacrylates with an alkyl chain length of between 12 and 22 carbon atoms are generally used (Fig. 2d). In this chapter, the hydrophobes are named C*x*R, where C represents carbon, *x* is the number of carbons in side alkyl chain, and R refers to A or M for acrylates and methacrylates, respectively. For instance, C18M and C16M stand for *n*-octadecyl methacrylate and *n*-hexadecyl methacrylate, respectively. Because stearyl methacrylate (C17.3M) consists of 65 % C18M and 35 % C16M, its average chain length, 17.3, is used in its short name.

Because hydrophilic monomers are soluble in water, whereas hydrophobes are insoluble, a common solvent or solvent mixture needs to be used for their copolymerization. Ethanol is a common solvent able to dissolve both AAc and C18A, so that their copolymerization can be conducted in this medium using free-radical initiators such as 2,2′-azobis(isobutyronitrile) (AIBN) [50]. Similarly, free-radical copolymerization of DMA with 5–22 mol% of 2-(*N*-ethylperfluorooctane sulfonamido)ethyl acrylate can be conducted in dioxane [48]. Another approach for the creation of hydrophobically modified hydrophilic polymers is polymer-analogous hydrophobic modification of preformed hydrophilic chains. For instance, hydrophobically modified poly(acrylic acid) (PAAc) can be prepared by grafting dodecyl amine onto the carboxylic acids of a PAAc backbone in the presence of dicyclohexylcarbodimide [8]. In contrast to this complicated procedure, a simple way for the synthesis of hydrophobically modified polymers is the micellar polymerization technique [51–58]. A particular advantage of this approach is the blocky structure of the resulting polymers, significantly enhancing their associative properties. In this technique, a hydrophobic monomer is first solubilized within micelles, and then it is copolymerized with a hydrophilic monomer in aqueous solution by a free-radical mechanism. Surfactants such as sodium dodecylsulfate (SDS) or cetyltrimethylammonium bromide (CTAB) serve for the solubilization of the hydrophobes in aqueous solution. Usually, redox-initiators such as ammonium

persulfate (APS) along with *N*,*N*,*N*′,*N*′-tetramethylethylenediamine (TEMED) or APS along with sodium metabisulfite (SMS) are used to initiate the reactions at ambient temperatures. Because the Krafft point for CTAB in water is around 20–25 °C [59], the reactions in CTAB solutions are carried out at elevated temperatures, 35–50 °C. As a result of the high concentration of hydrophobic monomer within the micelles, the hydrophobes are randomly distributed as blocks along the hydrophilic polymer chains. The number of hydrophobic monomeric units per hydrophobic block (N_H) and the number of blocks per chain (S_n) can be estimated from the molar concentration ratio of hydrophobic monomer (HM) to the surfactant (S) by:

$$N_H = \frac{[HM]N_{Agg}}{[S] - CMC} \tag{1a}$$

$$S_n = \frac{f_{HM}N}{N_H} \tag{1b}$$

where N_{Agg} is the aggregation number of the surfactant, CMC is its critical micelle concentration, f_{HM} is the mole fraction of HM in the comonomer feed, and N is the chain length of polymer [53]. Because incorporation of a small amount of hydrophobic groups in a hydrophilic polymer backbone results in polymers with extraordinary rheological properties in aqueous solutions, many studies have been carried out during the past two decades on the synthesis and solution properties of hydrophobically modified hydrophilic polymers [54, 55]. Candau and coworkers investigated the preparation and rheological behavior of polyacrylamides (PAAms) modified with various amounts of *N*-alkyl- or *N*,*N*-dialkylacrylamides of various alkyl-chain lengths [51–54, 56–58]. The zero-shear viscosity of semidilute solutions of hydrophobically modified polymers significantly increases as the number of hydrophobes per block (N_H) or the number of blocks per chain (S_n) is increased [52, 56, 57]. Hydrophobically modified PAAms are of great interest due to their possible application areas, including oil recovery and paints.

Physical hydrogels derived from hydrophobically modified hydrophilic polymers drew much less interest in the past, but they have recently attracted intense attention because of their extraordinary properties [4, 8, 31–42]. To produce mechanically strong hydrogels via micellar copolymerization, blocks of hydrophobes with long alkyl side chains such as *n*-octadecyl acrylate (C18A) or dococyl acrylate (C22A) should be incorporated into the hydrophilic backbone [32, 34]. However, although hydrophobes with an alkyl-chain length of up to 12 carbon atoms can easily be copolymerized with hydrophilic monomers, larger hydrophobes cannot be copolymerized in micellar solutions. This is a result of the low solubility of large hydrophobes in water (e.g., 10^{-9} mL mL^{-1} for C18M [60]), which limits their transport into the micelles [61, 62]. To solve this challenge, salts such as NaCl or NaBr were added to the micellar solution [32]; this weakened electrostatic interactions and caused the micelles to grow [63–67], which, in turn, provided solubilization of large amounts of hydrophobes in the micellar solution. Figure 3a, b demonstrates the NaCl-induced solubilization of C18A in an aqueous 22 % (w/v)

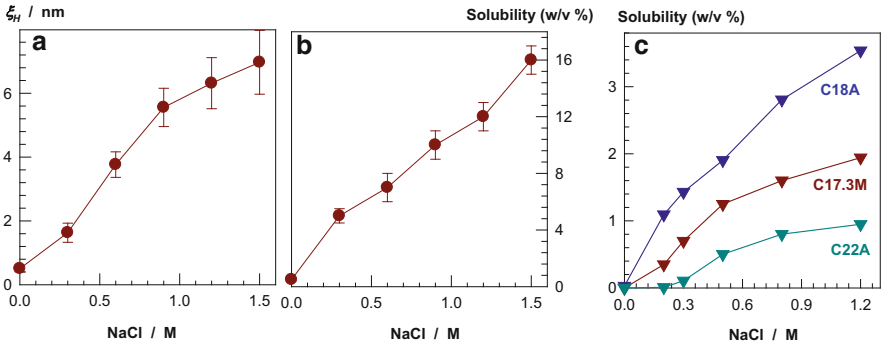

Fig. 3 (**a**) Hydrodynamic correlation length, ξ_H, of a 22 % (w/v) SDS solution and (**b**) solubility of C18A plotted against NaCl concentration; temperature = 55 °C. From [38] with permission from the American Chemical Society. (**c**) Solubilities of C17.3M, C18A, and C22A in surfactant solutions plotted against NaCl concentration; SDS = 7 % (w/v), temperature = 35 °C. From [34] with permission from Elsevier

SDS solution [34, 38]. The hydrodynamic correlation length of the solution, ξ_H (Fig. 3a), and the solubility of C18A (Fig. 3b) are plotted as a function of the NaCl concentration. As the salt concentration is increased, ξ_H also increases, indicating growth of SDS micelles. The micellar growth occurs as a result of transformation of the structure of SDS micelles from spherical to rodlike and then to flexible wormlike micelles [63–67]. Assuming a prolate ellipsoidal shape for the SDS micelles in aqueous NaCl and equating the semi-minor axis with the radius of the minimum-spherical micelle (2.5 nm) [68, 69] allows estimation of the semi-major axis of the micelles using Perrin's equations [70]. The calculations indicate that at 1.5 M NaCl, the major axis between the entanglements becomes 19 ± 4 nm, with corresponding aggregation numbers of 450 ± 100, as compared with only 60 for the minimum-spherical SDS micelle.

The growth of SDS micelles is accompanied by increased solubilization of hydrophobes. As seen in Fig. 3b, the solubility of the C18A monomer in a micellar solution increases from 0 to 16 % (w/v) as the salt concentration increases from 0 to 1.5 M [38]. Figure 3c shows the solubility of three different hydrophobes in 7 % (w/v) SDS solution plotted against the additional-NaCl concentration [34]. The increase in solubility as a result of salt addition is the largest for C18A monomer, followed by C17.3M and C22A. Although the average alkyl side chain of C17.3M is shorter than that of C18A, the methacrylate group of the former molecule seems to be responsible for its lower solubility in the micellar solution. After addition of the monomers to the solution of grown micelles, the hydrodynamic correlation length ξ_H decreases again due to the oil-induced structural change of the wormlike micelles [32, 33, 42]. Even visual inspection of the micellar solutions provides evidence that solubilization of the monomers reduces the viscosity. This change probably occurs as a result of accumulation of monomers in the surfactant palisade layer and in the core of the micelles, which increases the curvature of the micelles and leads to a rod–sphere transition of the micellar shape [71–75].

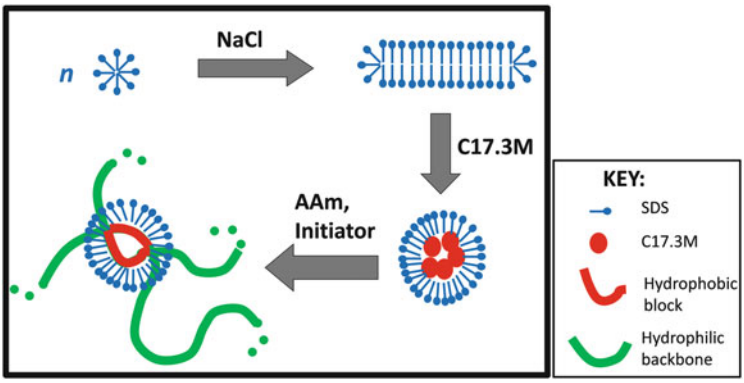

Fig. 4 Preparation of physical PAAm hydrogels in aqueous solutions of SDS–NaCl via hydrophobic C17.3M blocks. From [33] with permission from the American Chemical Society

An alternative route to promote micellar growth and, hence, to solubilize large hydrophobes is mixing of cationic and anionic surfactants. Aqueous solutions of surfactants of opposite charges, called catanionic surfactants, exhibit unique properties originating from the strong electrostatic interactions between their oppositely charged head groups. Mixtures of the anionic surfactant SDS and the cationic surfactant CTAB form mixed micelles in both SDS-rich and CTAB-rich solutions, whereas between these compositions, vesicles and formation of a 1:1 precipitate are observed [76–79]. It was shown that the correlation length of 0.24 M CTAB–SDS increases from 0.4 to 2.5 nm as the SDS content of the surfactant mixture is increased from 0 to 15 mol%, leading to increased solubility of the hydrophobic monomer C17.3M in the micellar solution [37].

After solubilization of large hydrophobes within the wormlike surfactant micelles of salt solutions, they can be copolymerized with hydrophilic monomers to obtain physical gels with tunable properties (Fig. 4). The following sections focus on the properties of hydrogels formed via micellar polymerization in the absence of any chemical cross-linker; hybrid gels formed by both covalent and noncovalent cross-links are not reviewed. If not otherwise indicated, the mole fraction of the hydrophobic monomer in the comonomer feed (f_{HM}) is 0.02; that is, the hydrophilic chains of the hydrogels discussed below contain about 2 mol% of hydrophobic units forming intermolecular hydrophobic associations. They were mainly prepared in 0.5 M NaCl solutions of 7 % (w/v) SDS, in which the aggregation number of SDS micelles is 200 [32].

3 Microstructure of the Network Chains

Polymer hydrogels formed via hydrophobic interactions of large hydrophobes such as C17.3M, C18A, or C22A are insoluble in water, with a gel fraction close to unity. This indicates the existence of strong associations between the hydrophobic blocks

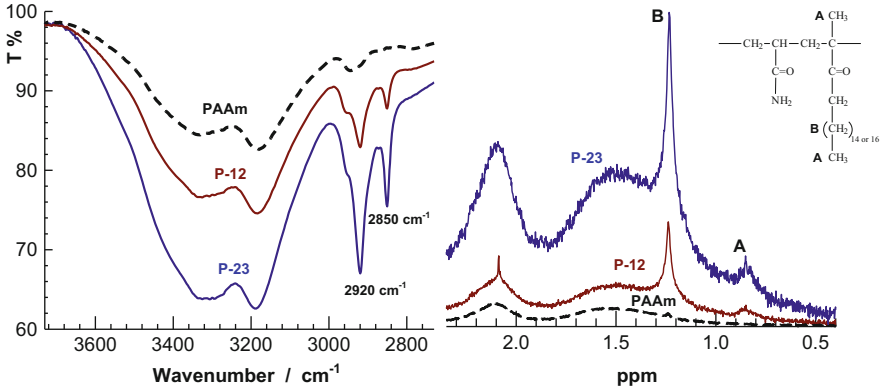

Fig. 5 FTIR (*left*) and ^{1}H NMR (*right*) spectra of HM PAAm network chains (P-12 and P-23) together with spectra of unmodified PAAm. P-12 and P-23 denote the polymers isolated from hydrogels with $N_H = 12$ and 23, respectively. The inset to the figure shows the structure of HM PAAm. The peaks denoted by A and B in NMR spectra arise due to the protons indicated in the inset. From [34] with permission from Elsevier

that cannot be destroyed during expansion of the polymer network in water. However, the networks can be dissolved in solutions of surfactant or in DMSO at high temperatures, which allows microstructural characterization of the polymers. In this section, typical results are reported for hydrophobically modified polyacrylamide (HM PAAm) hydrogels prepared using 2 mol% of C17.3M [34]. The blockiness of the polymer chains was demonstrated using physical gels synthesized at two different initial monomer concentrations (C_0),5 % and 10 % (w/v). Because the aggregation number of SDS micelles in 0.5 M NaCl solution is 200, the length of the hydrophobic blocks in the polymer chains, N_H, is 12 and 23 for hydrogels prepared at $C_0 = 5$ and 10 % (w/v), respectively [34]. Polymers isolated from hydrogels with $N_H = 12$ and 23 are designated P-12 and P-23, respectively.

FTIR and ^{1}H NMR spectra of HM and unmodified PAAm chains are shown in Fig. 5 [34]. In these FTIR spectra, HM PAAm network chains (P-12 and P-23) show characteristic peaks at 2,920 cm^{-1} and 2,850 cm^{-1} caused by the stretching vibrations of CH_2 groups of the C17.3M units. These peaks are absent in unmodified PAAm (dashed curve in Fig. 5). ^{1}H NMR spectra of HM PAAm dissolved in d_6-DMSO exhibit characteristic signals arising from the C17.3M units. In Fig. 5, peak A at 0.9 ppm corresponds to the protons of the α-methyl backbone and the terminal methyl of the alkyl chain, whereas peak B at 1.2 ppm is a result of the protons attached to carbon atoms on the alkyl side chain of the C17.3M units. Although NMR is not sensitive enough to determine the copolymer microstructure because of the low hydrophobe content (2 mol%), the increasing peak intensities with increasing N_H indicate blockiness of the polymers.

To demonstrate the associativity of the network chains, viscosity and rheological measurements were performed on HM PAAms dissolved in 0.7 % SDS solutions. These measurements also show a strong enhancement of the associativity with increasing N_H (i.e., with increasing length of the hydrophobic blocks) [34]. Figure 6a shows the dependence of the viscosity of 0.5 % (w/v) solutions of HM and

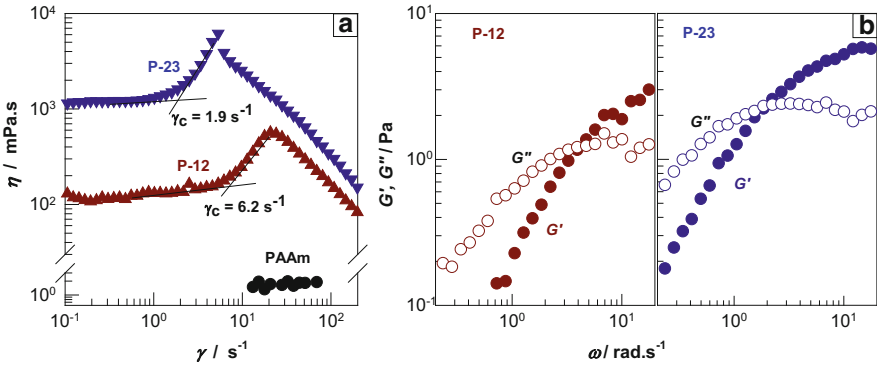

Fig. 6 (**a**) Shear-rate dependence of the viscosity and (**b**) frequency-sweeps of the elastic (G') and viscous (G'') shear moduli for solutions of P-12, P-23, and PAAm; polymer = 0.5 % (w/v), SDS = 0.7 % (w/v), NaCl = 0.5 M, temperature = 35 °C. From [34] with permission from Elsevier

unmodified PAAm on the shear rate. A significant increase in the viscosities of HM PAAm solutions (P-12 and P-23) compared with PAAm solution illustrates the existence of hydrophobic blocks in the network chains. The solutions of P-12 and P-23 exhibit a Newtonian plateau at low shear rates, followed by an abrupt shear thickening region before the onset of shear thinning. The shear thickening region is characteristic for associative flexible polymers and appears as a result of intermolecular hydrophobic associations [80–82]. Although these associations are favorable at a certain degree of coil deformation, they are disrupted at higher shear rates. The critical shear rate for the onset of shear thickening (γ_c) leads to a characteristic time, $\tau_c = 1/\gamma_c$, scaling with the zero-shear viscosity, which is verified by the data in Fig. 6. For P-23 and P-12 solutions, τ_c is 0.53 and 0.16 s, with zero-shear viscosities of 1.18 and 0.11 Pa s, respectively. Thus, despite the same hydrophobe level, solutions of P-23 ($N_H = 23$) exhibit longer τ_c and higher viscosities than solutions of P-12 ($N_H = 12$), demonstrating increasing associativity of the polymers as a result of the increasing length of their hydrophobic blocks. These results are also confirmed by frequency-sweep tests (Fig. 6b). The characteristic relaxation times (τ_R) calculated from the cross-over frequency (ω_c) at which G' and G'' are equal ($\tau_R = \omega_c^{-1}$) are 0.31 and 0.53 s for P-12 and P-23 solutions, respectively. This finding also reveals strong associativity of the network chains of the physical gels described.

4 Swelling Properties

Figure 7a shows typical swelling kinetics of HM PAAm hydrogels where the relative gel mass in water (m_{rel}) is plotted against the swelling time [33]. In Fig. 7b, the amount of SDS released from the gel is plotted as a function of the swelling time. As a result of the osmotic pressure of SDS counterions within the

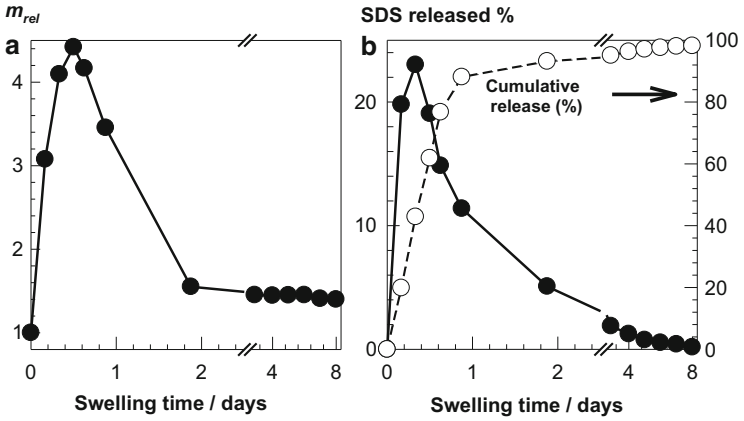

Fig. 7 (**a**) Relative weight swelling ratio (m_{rel}) of HM PAAm hydrogel formed in 7 % (w/v) SDS + 0.5 M NaCl solution and (**b**) released amount of SDS from the hydrogel, both shown as a function of the time of swelling in water; $C_0 = 10$ %, C17.3M = 2 mol%. From [33] with permission from the American Chemical Society

hydrogel, the gel initially behaves like an ionic gel and, therefore, attains a large swelling ratio m_{rel}. However, as the surfactant is gradually released from the hydrogel, the osmotic effect vanishes and the hydrogel progressively changes into a nonionic hydrogel with a distinctly reduced swelling ratio. The cumulative SDS release data in Fig. 7b reveal that all SDS was extracted from the gels after a swelling time of 8 days. Indeed, sulfur analysis of freeze-dried gel samples revealed no sulfur, indicating complete SDS extraction [33]. The swelling measurements carried out in aqueous salt solutions confirm this interpretation of the course of the swelling curves [33]. NaCl addition to the external solution reduces the swelling degrees at short times as a result of reduction of the osmotic pressure difference between the inside and outside of the hydrogel. The maximum of the swelling curves totally disappears if the salt concentration in the external solution approaches the counterion concentration in the hydrogel.

The swelling kinetics of hydrophobically modified nonionic hydrogels such as HM PAAm and HM poly(*N*,*N*-dimethylacrylamide) (PDMA) prepared in salt solutions of SDS, CTAB, or CTAB–SDS are similar to those illustrated in Fig. 7 [37, 41]. In contrast, HM PAAc hydrogels formed in SDS solutions exhibit high swelling ratios in water because of the osmotic pressure of the AAc counterions [39]. The equilibrium swelling ratio ($m_{rel,eq}$) of these hydrogels formed at $C_0 = 20$ % (w/v) is around 500, corresponding to a PAAc concentration of 0.04 % (w/v) in the swollen gel. Even at such a high degree of dilution, the hydrophobic associations acting as physical cross-links of the highly stretched PAAc network remain stable in equilibrium with water.

A completely different swelling behavior is observed for ionic hydrogels formed in solutions of oppositely charged surfactants. Figure 8a, b shows m_{rel} of HM PAAc hydrogels formed in CTAB–NaBr solutions plotted against the swelling time in

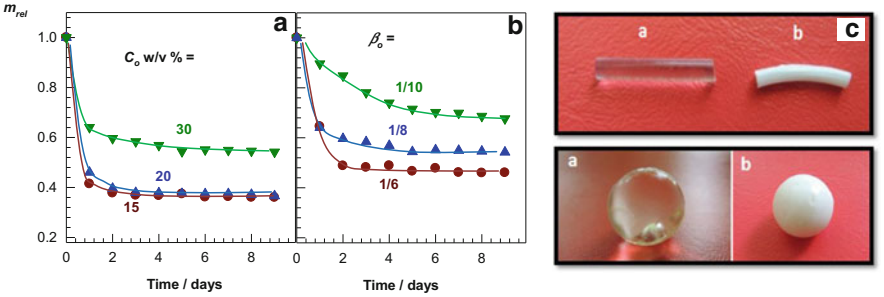

Fig. 8 (**a**, **b**) Relative mass (m_{rel}) of HM PAAc gels formed at a CTAB/AAc ratio (β_0) in the feed of 1/8 (**a**) and at C_0 of 30 % (w/v) (**b**) plotted against the swelling time in water. (**c**) Photographs of HM PAAc hydrogels after preparation (*a*) and in equilibrium with water (*b*); $C_0 = 20$ % (w/v), C17.3M = 2 mol%, $\beta_0 = 1/8$, NaBr = 0.25 M. From [42] with permission from the American Chemical Society

water [42]. The hydrogels deswell in water, with 40–60 % reduction of the gel mass as a result of the onset of complexation between PAAc and CTAB upon immersion in water. Indeed, polymers isolated from hydrogels that were in thermodynamic equilibrium with pure water contained nitrogen, indicating the presence of polymer-bound CTAB molecules. It was shown that, on average, 8–15 AAc units of the physical network carry CTA counterions that cannot be extracted with water [42]. The CTAB/AAc ratio (β) of the polymer increases as the CTAB/AAc ratio in the feed (β_0) is increased or as the initial monomer concentration (C_0) is decreased. The increase in β also leads to a more collapsed state of the gels in water, as seen in Fig. 8a, b. Because the pH inside the hydrogel after its preparation is equal to 1.5, PAAc is mostly protonated, so that no complexes form between PAAc and CTAB. However, upon immersion in water, the pH increases to 6.7, leading to ionization of the AAc units and, hence, to the onset of complexation [83, 84]. The formation of PAAc–CTAB complexes is also obvious from inspection of the gel samples (Fig. 8c): the hydrogels that are transparent after preparation become opaque in water, and the opacity increases with the β ratio [42].

5 Dynamics of Hydrogels With and Without Free Surfactant Micelles

Hydrogels formed via hydrophobic interactions in aqueous micellar solutions present two faces, depending on their state, namely:

1. The state of preparation, in which they contain surfactant micelles
2. The state of equilibrium in pure water, where free surfactant micelles have been removed

This section summarizes the dynamic properties of hydrophobically modified hydrogels in both these states. Those hydrogel systems forming no complexes with surfactants are mainly discussed, including PAAm, PDMA, or PAAc hydrogels, all formed in SDS solutions. Hydrogels capable of forming complexes with surfactants, such as polyelectrolyte hydrogels formed in solutions of oppositely charged surfactants, are discussed later in this section. Moreover, for a better understanding of the dynamics of these complex aqueous systems composed of surfactant micelles, salts, hydrophobic associations, and hydrophilic polymer chains, the dynamics of the hydrogels are also compared to those of the surfactant solutions.

Dynamic light scattering (DLS) is a powerful tool for investigating the associative and aggregation phenomena in polymer solutions and gels. DLS measurements on hydrogels formed by hydrophobic associations have been reported at various preparation steps of the gelation solutions: before and after addition of salt and monomers to the surfactant solution, after micellar copolymerization, and after removal of surfactant micelles from the hydrogels [32, 33, 37]. Figure 9a, b shows typical time-average intensity correlation functions (ICFs) obtained at a scattering angle (θ) of =90° from SDS solutions and HM PAAm hydrogels, respectively [33]. The ICF of the 7 % SDS solution shows both fast and slow relaxation modes (Fig. 9a). These relaxations merge into just one after addition of salt and the monomers C17.3M and AAm to the surfactant solution, leading to disappearance of the slow mode. After formation of physical HM PAAm hydrogels, a slow mode appears again on an even longer time scale (Fig. 9b). However, when the surfactant micelles are removed from the hydrogels, the slow mode disappears.

The scattering-vector dependencies of the relaxation rates give additional information on the dynamic properties of the physical gels [33]. In Fig. 9c, d, the relaxation rates of the fast (Γ_{fast}) and slow modes (Γ_{slow}) calculated from the peak positions in the relaxation-rate distribution functions, $G(\Gamma)$, are plotted against the square of the scattering vector, $q = (4\pi n/\lambda)\sin(\theta/2)$, with n being the refractive index of the solvent and $\lambda = 633$ nm. Both fast and slow relaxation modes for SDS solutions in water are proportional to q^2, indicating diffusive processes. The hydrodynamic correlation length (ξ_H) based on the fast mode is 0.5 nm for SDS micelles in water, but after NaCl addition, it increases to 6.1 nm due to formation of wormlike micelles [32, 33, 69, 85]. Addition of C17.3M and AAm to the SDS–NaCl solution re-decreases ξ_H to 3 nm as a result of an oil-induced structural change of the wormlike micelles [32, 33, 42]. In contrast to the slow mode of the SDS solution, the slow mode of HM PAAm hydrogels containing SDS (~30 ms) is independent of q (filled symbols in Fig. 9d). This reveals that the slow mode of the hydrogels is associated with the structural relaxation of the physical PAAm hydrogels on a time scale of milliseconds. This relaxation takes place if the surfactant micelles are present within the gel network whereas it vanishes in the absence of surfactants.

The internal dynamics of the physical hydrogels formed by hydrophobic associations was also investigated by rheological tests. In Fig. 10a–c, the elastic modulus, G' (filled symbols), the viscous modulus, G'' (open symbols), and the loss factor $\tan\delta$ (G''/G'; lines) of HM PAAm hydrogels with and without SDS are

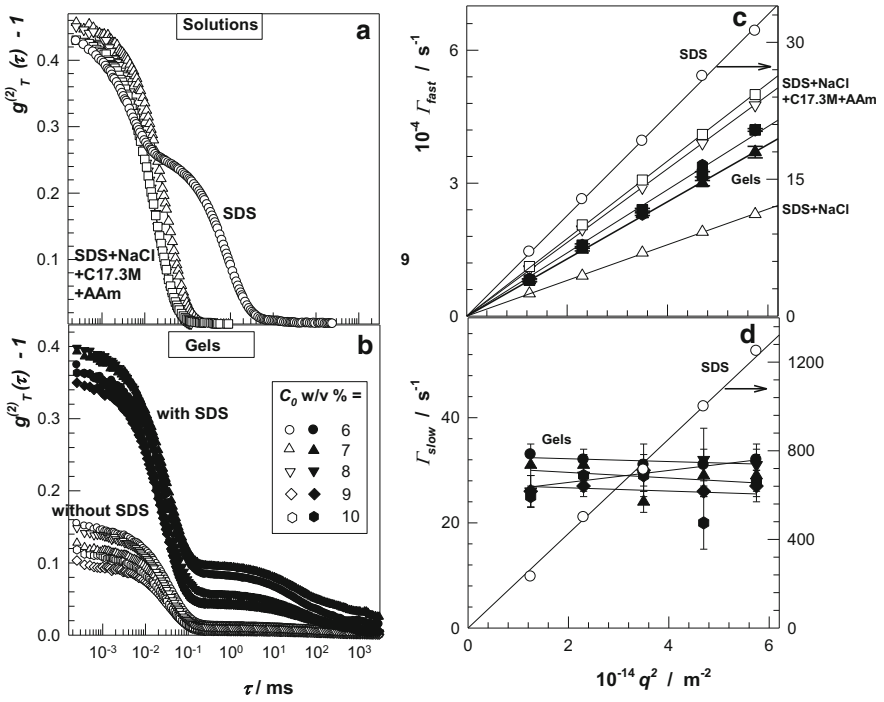

Fig. 9 (**a**, **b**) Intensity correlation functions (ICFs) of SDS solutions (**a**) and HM PAAm hydrogels (**b**), recorded at a detection angle of $\theta = 90^{\circ}$. Data are shown for solutions of SDS without (*open circles*) and with NaCl (*open up-triangles*), NaCl + C17.3M (*open down-triangles*), and NaCl + C17.3M + AAm (*open squares*). C17.3M and AAm concentrations correspond to the synthesis recipe of a hydrogel at $C_0 = 10$ % (w/v). *Filled* and *open symbols* in (**b**) show data for hydrogels with and without SDS, respectively. (**c**, **d**) Relaxation rates of the fast (Γ_{fast}) (**c**) and slow (Γ_{slow}) (**d**) modes shown as a function of q^2 for hydrogels and solutions probed by these studies. The *symbols* are the same as for (**a**, **b**). From [33] with permission from the American Chemical Society

shown as a function of the angular probe frequency ω [34]. The hydrogels were prepared using three different hydrophobes: C17.3M, C18A, and C22A [34]. The dynamic moduli of the hydrogels containing SDS are dependent on time, with a plateau region at high frequencies (10^2 rad s^{-1}), and they exhibit a loss factor, tan δ, above 0.1. This result reveals the temporary nature of the associations, with lifetimes of the order of seconds to milliseconds. Upon removal of the surfactant, the elastic moduli become nearly independent of time, and tan δ decreases below 0.1, revealing formation of a strong hydrogel with negligible viscous properties. The drastic change in the dynamics of this gel is a result of the strengthening of the hydrophobic associations in the absence of surfactant micelles, so that the dynamic behavior approaches that of conventional chemically cross-linked hydrogels.

Thus, in the presence of SDS micelles, the cross-links are reversible because of the local solubilization of the hydrophobic associations. As a consequence, the

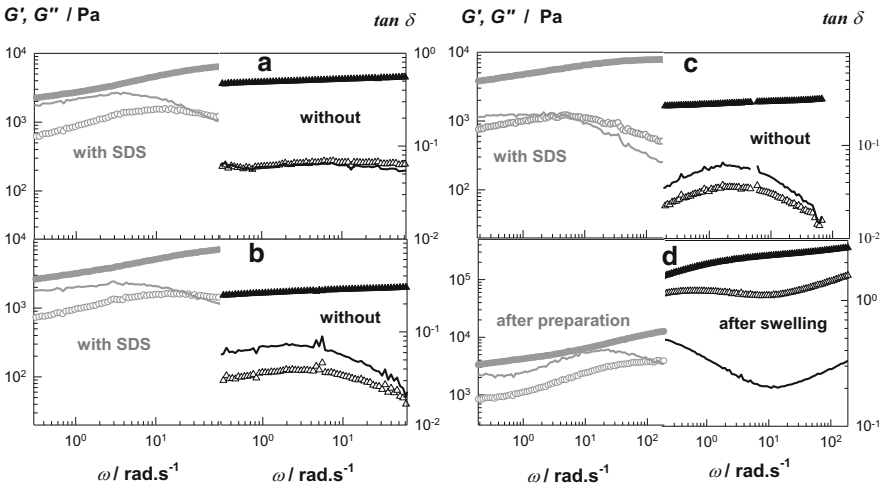

Fig. 10 (**a**–**d**) G' (*filled symbols*), G'' (*open symbols*), and tan δ (*lines*) of hydrophobically modified hydrogels shown as a function of the angular probe frequency ω; hydrophobe content = 2 mol%, $\gamma_0 = 0.01$. (**a**–**c**) HM PAAm hydrogels with 7 % (w/v) SDS and without SDS; hydrophobe = C17.3M (**a**), C18A (**b**), and C22A (**c**); $C_0 = 10$ % (w/v). From [34] with permission from Elsevier. (**d**) HM PAAc hydrogels formed in CTAB solutions after preparation and after swelling in water; $C_0 = 10$ % (w/v), hydrophobe = C17.3M, $\beta_0 = 1/8$. From [42] with permission from the American Chemical Society

hydrogels containing SDS belong to the category of weak gels. Without surfactant micelles, the lifetime of the hydrophobic associations increases as a result of their direct exposure to the aqueous environment, so that they behave like strong chemical gels, with time-independent moduli and a single relaxation mode in DLS (Fig. 9b). These findings also suggest that the existence of surfactant micelles is responsible for the slow mode of the physical gels. Previous work shows a slow relaxation mode in the micellar kinetics on a time scale of milliseconds to seconds, which corresponds to the dissolution of a micelle into individual surfactant molecules [86]. Because the disintegration of a micelle around the hydrophobic blocks increases the extent of hydrophobic interactions at this site, whereas its re-formation reduces these interactions again, one may expect that the micellar kinetics and resulting transient strong associations are responsible for the slow relaxation mode in physical gels containing surfactant micelles.

The water insolubility of the physical gels formed via hydrophobic interactions, even in a critical gel state [32], is in accord with the above findings. During the swelling process, removal of surfactants from the hydrogels increases the lifetime of the associations, so that the gels become increasingly stable as the surfactant is gradually extracted. By contrast, if swelling is carried out without extraction of the surfactants, the hydrogels should dissolve because of the weak hydrophobic associations. As mentioned in Sect. 3, this was indeed observed. At or above 5 % SDS concentration, HM PAAm hydrogels formed in 7 % SDS solution totally dissolve within 7–21 days. As a result of weakening of the hydrophobic associations with

rising surfactant concentration, physical gels dissolve faster as the SDS amount in the external solution increases.

The rheological behavior of HM PAAc hydrogels formed in CTAB solutions is similar to that of the nonionic hydrogels summarized above, as long as they are probed at a state of preparation (Fig. 10d) [42]. Both moduli of the hydrogels are dependent on frequency, and the loss factor tan δ remains above 0.1 in a range of frequencies between 0.08 and 400 rad s^{-1}. However, upon immersion in water and after extraction of free CTAB micelles, a different behavior is observed. As seen in Fig. 10d, the dynamic moduli of HM PAAc hydrogels increase by one order of magnitude, suggesting the effect of complex formation between PAAc with CTA counterions (Fig. 8). Nevertheless, both moduli of the gel are still dependent on frequency, and tan δ remains above 0.1 in equilibrium with water (i.e., after extraction of free CTAB micelles). This finding emphasizes the viscous character of the HM PAAc hydrogels in aqueous environment as a result of the presence of polymer-bound CTA counterions.

The size of the micelles also affects the dynamics of the hydrogels. This effect was investigated in HM PAAm hydrogels formed in aqueous solutions of CTAB containing 0–15 mol% of SDS [37]. Similarly to the addition of NaCl, addition of SDS–CTAB solution increases the size of the micelles (see Sect. 2). Because an increasing micellar size also increases the number of hydrophobic molecules solubilized in a given micelle (Eq. 1a), the length of the hydrophobic blocks of the hydrophilic network chains can be changed by varying the SDS content of the cationic surfactant solution. Figure 11a shows the frequency dependencies of G' (filled symbols) and G'' (open symbols) for HM PAAm hydrogels formed in 0.24 M CTAB–SDS solutions with varying SDS content [37]. Figure 11b shows the relaxation moduli, $G(t)$, of the same gels in the linear regime as a function of time (t) at different strains (γ_0). The hydrogels show frequency- or time-dependent dynamic moduli, with $G'(\omega)$ being a mirror image of $G(t)$. At time scales spanning two decades (1–100 s), they exhibit a power-law behavior, $G(t) \sim t^{0.31 \pm 0.08}$, as indicated in Fig. 11b by the solid red lines. At times shorter than 1 s, Rouse-type relaxation is seen, which is fitted using a stretched-exponential function, $G(t) = G_R \exp[-(t/\tau_1)^{\beta}]$, with an exponent $\beta = 0.46 \pm 0.04$, where G_R is the Rouse modulus and τ_1 is the lifetime of associations (i.e., the average residence time of a hydrophobic block in a given association, shown by dashed red curves in Fig. 11b) [49, 87–89].

The Rouse modulus, G_R, and the lifetime τ_1 derived from the fits are plotted against the SDS content in Fig. 12 [37]. The elastic moduli of the gels, G'_{ω} at $\omega = 250$ rad s^{-1}, corresponding to an experimental time scale of 4 ms, are also shown in Fig. 12. As the SDS content of the hydrogels is increased (i.e., as the micelles grow), the lifetime of the hydrophobic associations also increases, whereas the modulus G_R or G'_{ω} decreases at short times. These results highlight the effect of the size of the micelles on the length of the hydrophobic blocks. Because the hydrophobe level is fixed (2 mol%, except for the gels formed in CTAB solutions, where it is 1.4 mol%), increasing micellar size also increases the number of C17.3M

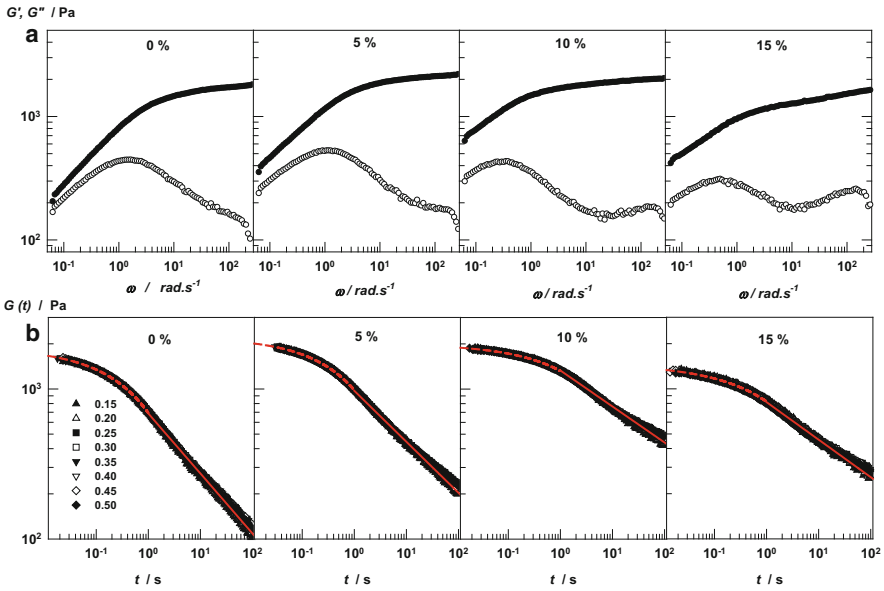

Fig. 11 (**a**) G' (*filled circles*) and G'' (*open circles*) of HM PAAm hydrogels plotted against the angular probe frequency (ω); $\gamma_0 = 0.01$. SDS amounts (mol%) in the gel-formation media, which are CTAB–SDS mixtures, are indicated in the panels; temperature = 35 °C, $C_0 = 5$ % (w/v), C17.3M = 2 mol%, CTAB + SDS = 0.24 M. (**b**) Relaxation modulus, $G(t)$, of the hydrogels plotted against time (t) for strains (γ_0) ranging from 0.15 to 0.50. SDS amounts (mol%) in the gel-formation media are indicated in the panels. From [37] with permission from the Royal Society of Chemistry

molecules solubilized in a given micelle, so that longer hydrophobic blocks form after polymerization, but the number of blocks per primary polymer chain decreases. This increases the lifetime of the associations but decreases their concentration, as evidenced by the Rouse modulus of the physical gels. The lower modulus of the gels formed in the absence of SDS is attributed to the incomplete solubility of C17.3M in the reaction solution, leading to less hydrophobic associations in the final gels.

An experimental proof of this mechanism requires microstructural characterization of the network chains isolated from the physical gels. The hydrogels can be dissolved in CTAB–SDS solutions to prepare a polymer solution [0.5 % (w/v)] having the same concentration and composition of the surfactant mixture as that used for gel preparation [37]. This way, although the gels are solubilized, the surfactant environment of the disintegrated network chains remains unchanged. Figure 13a presents flow curves for 0.5 % (w/v) polymer solutions obtained by this approach from gels made with SDS contents between 0 % and 15 % [37]. The solutions of polymers with 0 % and 5 % SDS show low viscosities, whereas those with 10 % and 15 % SDS exhibit higher viscosities at low shear rates, along with marked shear thinning. Because the increase in the viscosity with rising SDS

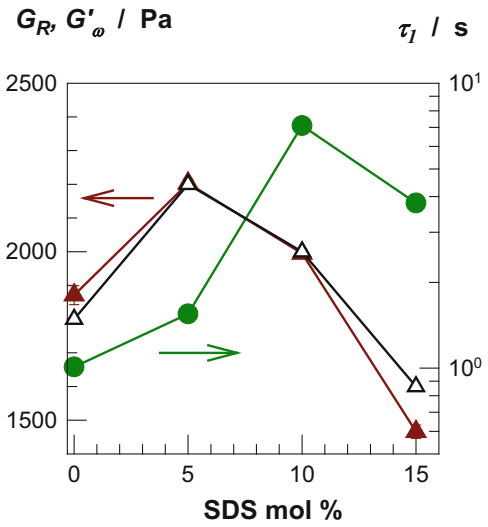

Fig. 12 Rouse modulus, G_R (*filled triangles*), elastic modulus, G'_ω at $\omega = 250$ rad s^{-1} (*open triangles*), and the lifetime τ_1 of hydrophobic associations in HM PAAm hydrogels formed in 0.24 M CTAB–SDS solutions (*filled circles*), plotted against the SDS content. From [37] with permission from the Royal Society of Chemistry

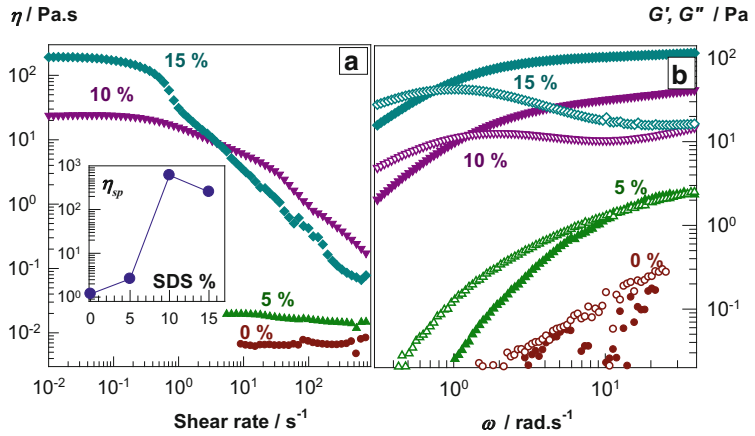

Fig. 13 (**a**) Viscosity versus shear rate and (**b**) frequency sweeps for 0.5 % (w/v) HM PAAm solution in 0.24 M CTAB–SDS solutions. The SDS amounts (in mol%) of CTAB–SDS mixtures are indicated. In (**b**), the elastic modulus G' and viscous modulus G'' are shown by *filled* and *open symbols*, respectively. *Inset* to (**a**) shows the specific viscosity, η_{sp}, of polymer solutions plotted against their SDS content; temperature = 35 °C. From [37] with permission from the Royal Society of Chemistry

content can be attributed to micellar growth rather than to the increasing associativity of polymers, the viscosities of the surfactant solutions without polymers were also measured. The relative viscosity increase as a result of the polymer is represented as the specific viscosity, η_{sp}, defined as $\eta_{sp} = \eta_{0,polymer}/\eta_{0,solvent} - 1$, where $\eta_{0,polymer}$ and $\eta_{0,solvent}$ are the zero-shear viscosities of CTAB–SDS solutions with and without polymers. The inset to Fig. 13a shows the specific viscosity η_{sp} of polymer solutions plotted against their SDS content. The value of η_{sp} sharply increases with rising SDS content, indicating increasing associativity of the network chains as the amount of SDS present during gel preparation is increased.

In Fig. 13b, the dynamic moduli G' and G'' of HM PAAm solutions are plotted against the angular probe frequency. The characteristic relaxation times (τ_R) calculated from the cross-over frequencies at which the G' and G'' curves intersect (ω_c) are 0.09, 0.83, and 1.3 s for SDS contents of 5, 10, and 15 mol%, respectively. This finding indicates increasing associativity of the polymer chains with increasing content of SDS in the gel system. Figure 13b also shows that at 5 % SDS, a distinct plateau appears in G' at high frequencies. The height of this plateau increases and its width enlarges with increasing amounts of SDS. For HM PAAm solution containing 15 % of SDS, the elastic modulus at the plateau is two orders of magnitude higher than that for the polymer solution with just 5 %. Thus, the polymers prepared in CTAB–SDS solutions with 10 % and 15 % of SDS show remarkable associativity. This effect can be attributed to the noticeable blockiness of the polymer chains and to the increasing size of the wormlike CTAB micelles around the hydrophobic blocks.

6 Structural Inhomogeneity

Polymer gels are known to exhibit pronounced scattering of light, neutrons, and X-rays at low scattering vectors, corresponding to concentration fluctuations at length scales between 10^0 and 10^2 nm [90, 91]. Such large-scale concentration fluctuations, which are absent in polymer solutions, are a result of the mesoscopic static structures in gels, called the spatial gel inhomogeneity [90–94]. This inhomogeneity can be visualized as strongly cross-linked nanogel clusters embedded in a less densely cross-linked environment. Because the gel inhomogeneity results in a drastic reduction in the mechanical performance of hydrogels and is thus undesirable in many gel applications, preparation of homogeneous gels is a challenging task. As the gel inhomogeneity is connected to the spatial concentration fluctuations, it is widely investigated using scattering methods such as DLS. This technique provides the time-average intensity correlation function, $g_T^{(2)}(q,\tau)$, whose short-time limit is related to an apparent diffusion coefficient, D_A, via [95, 96]:

$$D_A = -\frac{1}{2q^2}\lim_{\tau\to 0}\ln\left(g_T^{(2)}(q,\tau) - 1\right) \tag{2}$$

where τ is a decay time. For a nonergodic system containing an infinite network such as polymer gels, D_A and the time-averaged scattering intensity $<I(q)>_T$ fluctuate randomly with the sample position. $<I(q)>_T$ has two contributions: one from static inhomogeneities (frozen structure) and another from dynamic fluctuations, as represented by the following equation [95–97]:

$$\langle I(q)\rangle_T = I_C(q) + \langle I_F(q)\rangle_T \tag{3}$$

where $I_C(q)$ and $<I_F(q)>_T$ represent the scattered intensity as a result of static inhomogeneity and dynamic fluctuations, respectively. By applying the partial heterodyne approach [95], $<I(q)>_T$ can be separated into its two parts:

$$\frac{\langle I(q)\rangle_T}{D_A} = \frac{2\langle I(q)\rangle_T}{D} - \frac{\langle I_F(q)\rangle_T}{D} \tag{4}$$

where D is a cooperative diffusion coefficient related to the dynamic correlation length by $\xi = kT/(6\pi\eta D)$, with η the viscosity of the medium and kT the Boltzmann thermal energy. Equation (4) applies to each sample position. Thus, for different sample positions, different D_A and $<I(q)>_T$ are obtained. Using DLS measurements conducted at different sample positions together with Eq. (4), one may calculate the cooperative diffusion coefficient D and the dynamic part of the scattering intensity $<I_F(q)>_T$.

Figure 9b shows a significant decrease in the initial amplitude of the ICF upon removal of the surfactant from HM PAAm hydrogels, indicating an increasing extent of frozen concentration fluctuations. Figure 14a shows the time-averaged

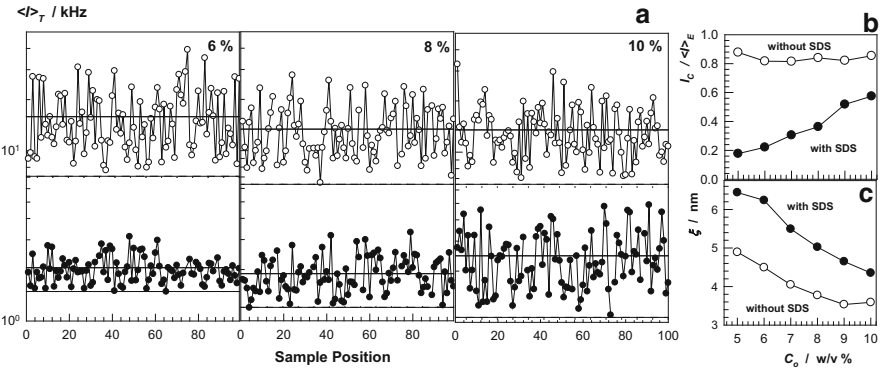

Fig. 14 (**a**) $<I>_T$ at various sample positions for HM PAAm hydrogels formed using 2 mol% of C17.3M with 7 % (w/v) of SDS (*filled circles*) and without SDS (*open circles*). C_0 is indicated in the panels. (**b**, **c**) C_0 dependences of $I_C/<I>_E$ (**b**) and ξ (**c**). From [33] with permission from the American Chemical Society

scattering intensity $<I>_T$ at $\theta = 90^\circ$ for randomly chosen sample positions within HM PAAm gels with 7 % (w/v) of SDS (filled symbols) and without SDS (open symbols) [33]. The solid lines in Fig. 9b represent the ensemble-averaged scattering intensity, $<I>_E$, obtained by averaging $<I>_T$ over many sample positions. The dashed lines represent that part of the scattering intensities $<I_F>_T$ that is due to liquid-like concentration fluctuations. It is seen that the removal of surfactant from the hydrogels results in an almost one order of magnitude increase in the spatial fluctuations in $<I>_T$. To capture the spatial gel inhomogeneity, the relative contribution of the static component (frozen structure) of the scattered intensity, $I_C/<I>_E$, is plotted against C_0 in Fig. 14b. A considerable portion of the thermal scattering from the surfactant-containing gels is due to the presence of large SDS micelles; $I_C/<I>_E$ monotonically increases from 20 % to 60 % with rising C_0 as a result of suppression of the fluctuations by the polymer chains. Without surfactant, $I_C/<I>_E$ of the hydrogels is independent of C_0 and equals 83 ± 3 %. Thus, the degree of spatial gel inhomogeneity considerably increases after extraction of the surfactant molecules. This increase is possibly related to a loss of reversibility of the cross-linkages and a resulting increase in the apparent cross-linking density of the gels at long experimental time scales. In Fig. 14c, the correlation length ξ of the gels based on their fast modes is plotted against C_0. The value of ξ of the surfactant-containing gels decreases slightly from 6 to 4 nm, indicating a decreasing gel-network mesh size with rising C_0; it further decreases after extraction of the SDS micelles.

7 Mechanical Properties

Uniaxial compression and tensile measurements on hydrophobically modified hydrogels serve to evaluate their elastic properties such as moduli, fracture stresses, and deformation ratios at break [33–35, 39–42]. The stress is presented by its nominal, σ_{nom}, or true values, σ_{true} (equal to $\lambda\sigma_{nom}$), defined as the forces per unit undeformed and deformed area, respectively; λ is the deformation ratio. Cyclic mechanical tests are powerful tools for investigating the large-strain properties and the reversible nature of cross-links of physical gels. These tests are carried out by stretching or compressing hydrogel samples at a constant cross-head speed to a predetermined maximum load below failure, followed by immediate retraction to zero displacement. After a fixed wait time, the cycles are repeated several times. As no standard method exists to evaluate the self-healing abilities of hydrogels, healing of cylindrical samples after being cut in half is monitored as a function of the healing time in closed containers to prevent water evaporation [33]. The healing efficiency is calculated from the mechanical properties of the virgin and healed gel samples.

Typical compressive stress–strain curves of surfactant-containing hydrophobically modified hydrogels are shown in Fig. 15a, where σ_{nom} and σ_{true} are plotted against the deformation ratio λ [41]. The results obtained from 15 separate HM PDMA hydrogel samples at a state of preparation are presented. The

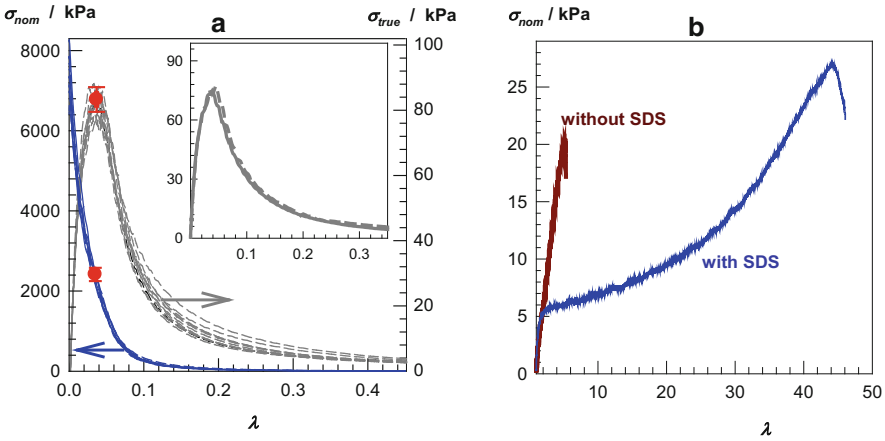

Fig. 15 (**a**) Typical stress–strain curves of a surfactant-containing HM PDMA hydrogel formed using 2 mol% of C17.3M under compression, represented as the dependences of nominal σ_{nom} (*blue solid curves*) and true stresses σ_{true} (*gray dashed curves*) on the deformation ratio λ; SDS = 7 % (w/v). Results of 15 separate tests are shown. *Red circles* represent the points of failure of the gel samples. The *inset* shows σ_{true} versus λ curves of two successive tests conducted on the same gel sample for up to 99.99 % compression. (**b**) Stress–strain curve of the same HM PDMA hydrogel with 7 % (w/v) of SDS (*solid blue curve*) and without SDS (*solid dark red curve*); C_0 = 15 % (w/v), C17.3M = 2 mol%, NaCl = 0.5 M. From [41] with permission from Elsevier

samples do not break, even at a strain of about 100 % compression and, therefore, the nominal stress σ_{nom} increases continuously with increasing strain (solid curves in Fig. 15a). However, the corresponding σ_{true} versus λ plots pass through maxima, indicating the onset of failure in the gel specimen (gray dashed curves in Fig. 15a). The fracture nominal stress and stretch at failure (λ_f), calculated from the maxima in the σ_{true} versus λ plots, are 2.4 ± 0.2 MPa and 0.04 (96 % compression), respectively [41]. However, successive compression tests conducted on the same gel sample show that this failure is recoverable in nature. This is illustrated in the inset to Fig. 15a, where two successive test results are given. Good superposition of the stress–strain curves indicates that the damage in the hydrogel is self-healed upon unloading. The results reveal that the gel can be compressed up to about 100 % strain without any permanent failure. This is a typical behavior of surfactant-containing hydrogels formed via hydrophobic associations. Next, the fracture nominal stress and stretch at failure are reported from the maxima in σ_{true} versus λ plots.

Figure 16a represents stress–strain data of surfactant-containing HM PAAm hydrogels; seven different hydrophobes with linear alkyl side chains of 12–22 carbon atoms were used in their synthesis [34]. In compression tests ($\lambda < 1$), λ at fracture is 0.04, indicating that all these hydrogels are mechanically stable up to 96 % compression. In elongation tests ($\lambda > 1$), λ at break is larger than 16, meaning that the elongation at break is above 1,500 % for these HM PAAm hydrogels. The tensile strength of the hydrogels prepared using hydrophobic acrylates is larger (30–

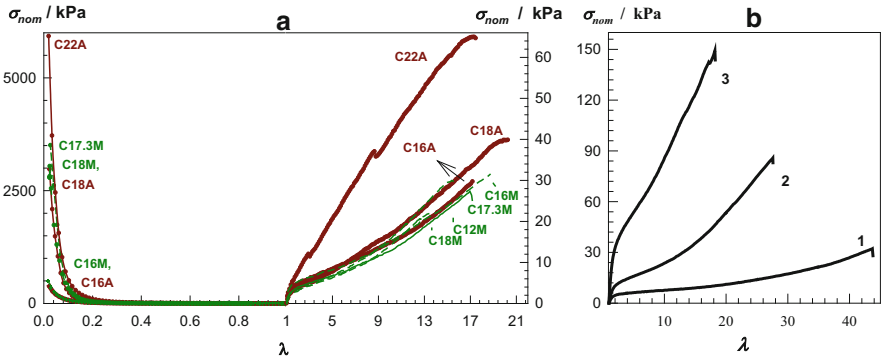

Fig. 16 (**a**, **b**) Stress–strain curves of HM PAAm (**a**) and HM PAAc hydrogels (**b**) after preparation in 7 % SDS + 0.5 M NaCl solutions; hydrophobe content = 2 mol%. (**a**) $C_0 = 10$ % (w/v). From [34] with permission from Elsevier. (**b**) Hydrophobe C17.3M; $C_0 = 15$ % (*1*), 20 % (*2*), and 30 % (*3*). From [39] with permission from the Royal Society of Chemistry

65 kPa) than that of those formed using methacrylates (20–30 kPa). This is a result of the restricted mobility of the methacrylate backbones, reducing the number of hydrophobic associations acting as physical cross-links [34].

In addition to the alkyl side chain length of the hydrophobes, the type of hydrophilic chains also affects the mechanical performance of hydrogels formed via hydrophobic interactions. For instance, replacing PAAm by a PAAc backbone leads to mechanically stronger hydrogels as a result of stabilization of the hydrophobic associations by cooperative hydrogen bonding between the PAAc carboxyl groups [39]. Figure 16b represents tensile stress–strain data of surfactant-containing HM PAAc hydrogels formed at three different concentrations (C_0). At $C_0 = 15$ % (curve 1 in Fig. 16b), the gel withstands 41 ± 11 kPa stresses, and the fracture stress further increases up to 173 ± 33 kPa if C_0 is increased [39]. The stretch at break (λ_f) of the hydrogels is between 19 and 51 (1,800–5,000 % elongation), which is a decreasing function of C_0. Similar improvement of the mechanical performance was observed by replacement of PAAm with a PDMA backbone (solid curve in Fig. 15b). A HM PDMA hydrogel with 7 % (w/v) of SDS ruptures when stretched to 43 ± 4 times its original length, corresponding to $4{,}200 \pm 400$ % elongation [41]. By contrast, PAAm hydrogels formed under identical conditions exhibit elongation at break of only about 2,000 % [33, 34]. This suggests that the hydrogen bonding and hydrophobic interactions between the DMA units additionally contribute to the mechanical properties of these gels.

The results of the mechanical tests presented so far were obtained from hydrogels just after preparation (i.e., from surfactant-containing hydrogels). Because the dynamic features of the hydrogels formed via hydrophobic interactions drastically change after removal of surfactant micelles, similar changes were observed in their mechanical properties. In Fig. 17a, the stress relaxation data of HM PAAm hydrogels with and without SDS are shown in form of the variation of the relaxation modulus of the gels, $G(t)$, with increasing strain at fixed times

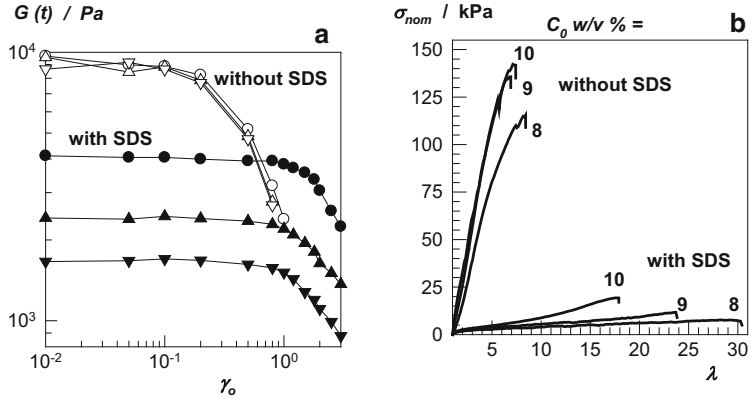

Fig. 17 (**a**) Relaxation modulus $G(t)$ plotted against strain (γ_0) for various times (t) for HM PAAm hydrogels with 7 % (w/v) of SDS (*filled symbols*) and without SDS (*open symbols*); $t = 0.1$ (*circles*), 1.0 (*triangles up*), and 10 s (*triangles down*); $C_0 = 10$ % (w/v), C17.3M = 2 mol%, NaCl = 0.5 M. (**b**) Stress–strain curves of HM PAAm gels with 7 % (w/v) of SDS and without SDS formed at $C_0 = 8$–10 % (w/v), as indicated on the curves; C17.3M = 2 mol%, NaCl = 0.5 M. From [33] with permission from the American Chemical Society

[33]. For surfactant-containing hydrogels, the linear viscoelastic regime extends up to approximately 100 % strain, whereas it is restricted to strains up to ~10 % for surfactant-free hydrogels. This difference shows a significant decrease in the stretchability of these hydrogels upon removal of surfactant [33, 40]. Figure 17b represents tensile stress–strain data of HM PAAm hydrogels prepared at three different concentrations (C_0). With SDS, the elongation at break exceeds 1,700 %, and it increases further as C_0 is decreased. Without SDS, however, the hydrogels break at about 700 % strain and exhibit an order of magnitude larger ultimate strength than the SDS-containing gels. Highly stretchable HM PDMA hydrogels also become brittle after extraction of SDS micelles, and the elongation ratio at break decreases from 43 ± 4 to 5 ± 1 (dark red curve in Fig. 15b) [41].

The amount of surfactant within the hydrogels also affects their mechanical properties [34]. This is illustrated in Fig. 18 for HM PAAm hydrogels where the tensile moduli, the ultimate strength, the elongation at break, and toughness are summarized for samples containing various amounts of SDS. Enhancement of the mechanical strength is seen when the SDS content is decreased, becoming dramatic between 1 % and 0 % of SDS. Hydrogels without SDS exhibit high moduli (~50 kPa), high ultimate strength (~200 kPa), and high toughness (~1 MJ m^{-3}) because of the increased lifetime of hydrophobic associations in the absence of SDS (Fig. 10). The elongation at break decreases from 1,600 % to 800 % as the amount of SDS in the hydrogels is decreased. These results demonstrate that the mechanical properties of the physical hydrogels can be tuned by varying their SDS content.

Ionic hydrogels formed in oppositely charged surfactant solutions exhibit a significant enhancement of their mechanical properties when they are immersed in water [42]. For instance, Fig. 19 shows the stress–strain data of HM PAAc gels

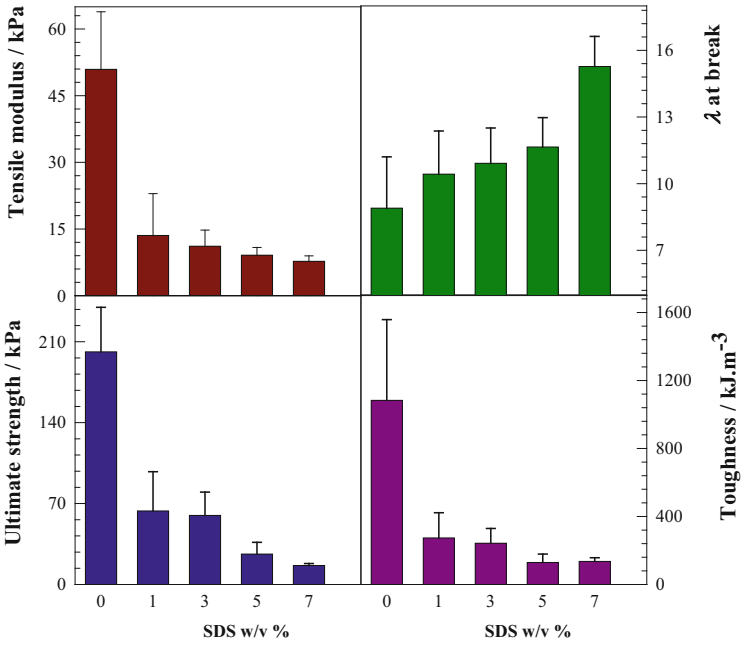

Fig. 18 Tensile modulus, elongation ratio λ at break, ultimate strength, and toughness of HM PAAm hydrogels prepared using 2 mol% of C17.3M plotted against their SDS contents; $C_0 = 10$ % (w/v). From [34] with permission from Elsevier

formed in CTAB–NaBr solutions. Dashed and solid curves show the data obtained from gels after preparation and in equilibrium with water, respectively. Extraction of free CTAB micelles from the physical gels results in a drastic increase in their Young's moduli (from 8–30 to 180–600 kPa) and tensile strengths (from 0.1–0.2 to 0.7–1.7 MPa) as a result of complex formation between PAAc and CTAB [42]. The largest modulus and fracture stress are 605 ± 20 kPa and 1.66 ± 0.24 MPa, respectively, obtained at the highest β ratio of 1/8.3. Such a drastic change in the mechanical properties of the gels upon immersion in water is a result of extraction of CTA counterions from the micelles by AAc anions and simultaneous formation of ionic bonds at neutral pH [42].

7.1 Large-Strain Properties

For a deeper understanding of the nature of physical cross-links in HM PAAm hydrogels, the gels were subjected to loading and unloading experiments [34]. Figure 20a, b shows the typical stress–strain curves of HM PAAm hydrogels from tensile tests composed of three repeated cycles [34]. The tests were conducted on

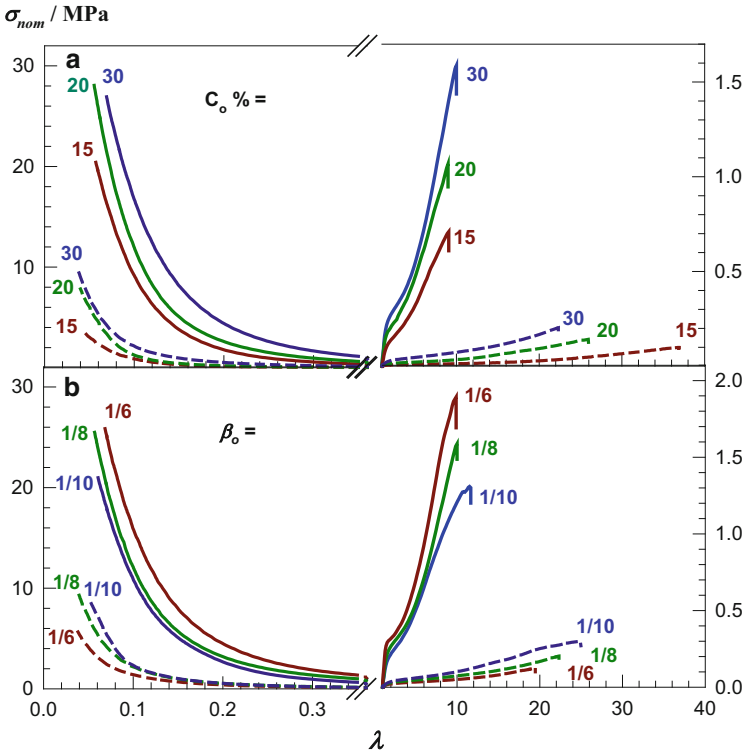

Fig. 19 Stress–strain curves of HM PAAc gels after preparation in CTAB solutions (*dashed curves*) and in equilibrium with water (*solid curves*) under compression ($\lambda < 1$) and elongation ($\lambda > 1$); C17.3M = 2 mol%, NaBr = 0.25 M. (**a**) $\beta_0 = 1/8$; percentage concentrations C_0 (w/v) as indicated. (**b**) $C_0 = 30$ % (w/v); β_0 values as indicated. From [42] with permission from the American Chemical Society

hydrogels with (Fig. 20a) and without surfactant (Fig. 20b) up to a stretch (λ_{max}) of 5, with a relaxation time of 7 min until the next tensile cycle started. The surfactant-containing hydrogel sample undergoes reversible cycles with a substantial hysteresis, revealing that the original microstructure can be restored by allowing the damaged hydrogel to rest for 7 min. Visually, it was observed that the residual stretch after each cycle decreases with increasing wait time between cycles and disappears after 7 min, so that the next loading curve follows the path of the first loading. In accord with DLS and rheological measurements, these cyclic tensile tests also indicate the existence of reversible cross-links in surfactant-containing hydrogels.

In contrast, the hydrogel sample without SDS behaves differently (Fig. 20b). Although the loading curve of the first tensile cycle is different from the unloading curve, and although a substantial hysteresis occurs (similar to that seen for the SDS-containing hydrogel), the subsequent cycles are nearly elastic with just a small amount of hysteresis; they also closely follow the path of the first unloading. This

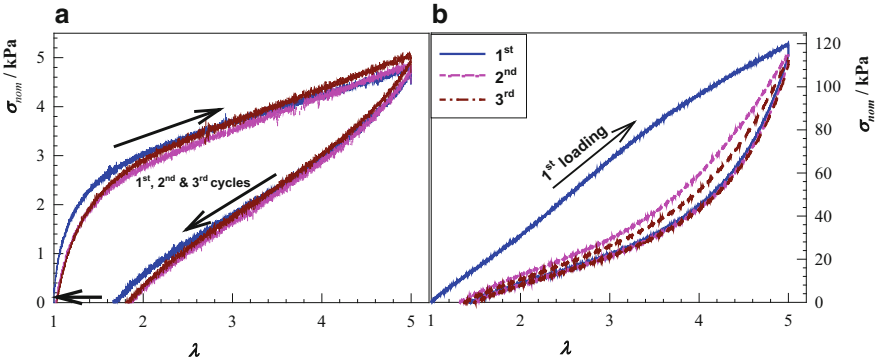

Fig. 20 (**a**, **b**) Loading–unloading curves of HM PAAm hydrogels with 7 % of SDS (**a**) and without SDS (**b**); $\lambda_{max} = 5$, C17.3M = 2 mol%. Waiting time between the cycles was 7 min. Cross-head speed was 50 mm min^{-1}. From [34] with permission from Elsevier

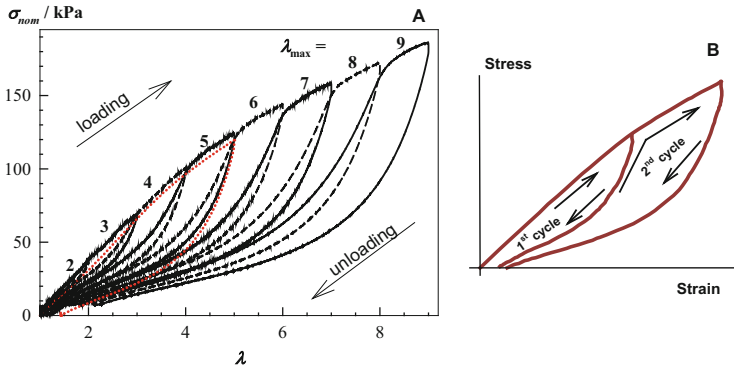

Fig. 21 (**a**) Eight successive loading–unloading cycles for different maximum strains (λ_{max}) as indicated on the curves. The *dotted red curve* represents the cycle conducted on a virgin gel sample ($\lambda_{max} = 5$). The tests were conducted using HM PAAm hydrogel samples without SDS; C17.3M = 2 mol%. (**b**) Idealized view of two successive cycles. From [34] with permission from Elsevier

finding indicates occurrence of an irrecoverable damage to the hydrogel sample during the first cycle, leading to a permanent residual elongation. In Fig. 21a, eight successive loading–unloading cycles are shown where the maximum strain, λ_{max}, increases from 2 to 9, corresponding to increasing elongation from 100 % to 800 % [34]. Successive cycles in Fig. 21a are represented by solid and dashed curves. Figure 21b shows an idealized view of two successive cycles. Each loading curve after the first cycle consists of two regions [34]:

1. Elastic region that closely follows the path of the unloading curve of the previous cycle
2. Damage region continuing the loading curve of the previous cycle

The passage from the elastic to the damage region takes place at the λ_{max} of the previous cycle. For instance, the loading curve of cycle 5 with $\lambda_{max} = 5$ follows the unloading and loading curves of cycle 4 between $\lambda = 1$–4 and $\lambda = 4$–5, respectively. This means that, because of the irreversible damage during the previous cycle, additional damage only occurs at a higher maximum strain. The dotted red curve in Fig. 21a shows the cycle conducted on a virgin hydrogel sample up to $\lambda_{max} = 5$. Because there was no previous damage to the gel sample, the loading curve follows the second region of the loading curves of cycles with $\lambda_{max} \leq 5$. Thus, the hysteresis of the first cycle is related to irreversible fracture of a part of the hydrophobic associations, whose extent increases with increasing λ_{max} during the loading step. This behavior is similar to that of double-network (DN) hydrogels [3, 98], where the first-cycle hysteresis occurs as a result of the irreversible fracture of covalent bonds in the highly cross-linked primary network.

Similar to the results of cyclic tensile tests, cyclic compression measurements also confirm the presence of reversibly breakable cross-links in hydrogels containing surfactant micelles. Figure 22a shows successive loading–unloading compression ($\lambda < 1$) and tensile cycles ($\lambda > 1$) of HM PDMA hydrogels containing 7 % of SDS [41]. The tests were carried out with increasing λ_{max} and with a waiting time of 7 min between cycles. In all cases, the loading curve of the compressive or tensile cycle is different from the unloading curve, indicating damage in the gel samples and dissipation of energy during the cycle. The good superposition of the successive loading curves demonstrates that the damage done to the gel samples during the loading cycle is recoverable. However, after swelling in water, these HM PDMA gels exhibit irreversible cycles with less significant hysteresis.

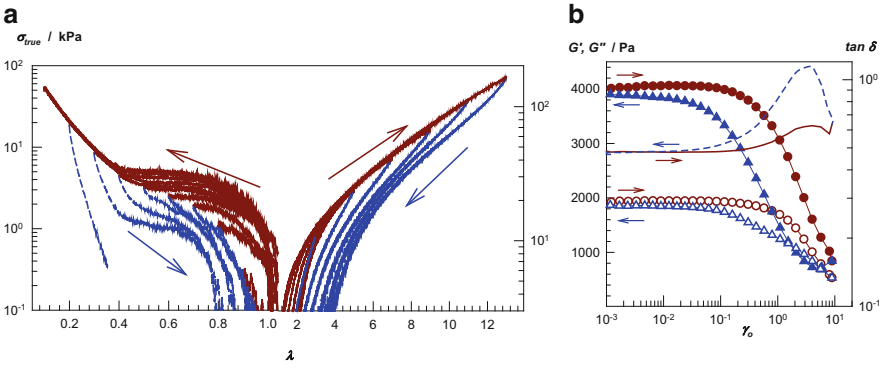

Fig. 22 (**a**) True stress (σ_{true}) versus deformation ratio (λ) of a surfactant-containing HM PDMA hydrogel from cyclic compression ($\lambda < 1$) and elongation ($\lambda > 1$) tests. The tests were conducted with increasing strain, with a waiting time of 7 min between cycles. (**b**) G' (*filled symbols*), G'' (*open symbols*), and tan δ (*curves*) of a HM PDMA hydrogel shown as a function of the strain (γ_0) at $\omega = 6.3$ rad s^{-1}. Sweep tests were conducted in up (*dark red circles*) and down directions (*blue triangles*), as indicated by the *arrows*; $C_0 = 15$ % (w/v), C17.3M = 2 mol%, SDS = 7 % (w/v), NaCl = 0.5 M. From [41] with permission from Elsevier

Strain-sweep tests conducted on HM PDMA hydrogels with 7 % (w/v) of SDS also demonstrate recoverability of the damage in the gel samples. Figure 22b shows up and down strain-sweep experiments, where the dynamic moduli G' and G'' together with the loss factor tan δ are plotted as a function of strain γ_0 [41]. The upward curves show a linear viscoelastic region at low strains ($\gamma_0 < 0.1$), beyond which the dynamic moduli decrease while the loss factor increases. Comparison of the up and down curves indicates that the gel exhibits an almost reversible strain-sweep spectrum; the breakdown of the microstructure caused by the strain is recovered at low strain amplitudes. Thus, this surfactant-containing HM PDMA hydrogel softens with increasing deformation and exhibits a liquid-like response (tan $\delta > 1$) at high strains, but reversibly; if the force is removed, the solution turns back to the same gel state.

The reversibility of the mechanical cycles of surfactant-containing gels indicates that the energy associated with the hysteresis is a result of the hydrophobic associations that break and reform dynamically, preventing fracture of the polymer backbone. The energy dissipated during the cycles, U_{hys}, is calculated from the area between the loading and unloading curves. Because uniaxial compression is equivalent to biaxial stretching [98], the maximum strain during compression (λ_{max}) is converted to the maximum biaxial extension ratio ($\lambda_{biax,max}$) by $\lambda_{biax,max} = \lambda_{max}^{-0.5}$. In Fig. 23a, the hysteresis energies (U_{hys}) calculated from the cycles in Fig. 22a are plotted against the maximum strain in terms of uniaxial (λ_{max}) and biaxial ($\lambda_{biax,max}$) extension ratios. All U_{hys} data collapse onto a single curve; hence, the hysteresis energy only depends on the maximum extension of the polymer chains.

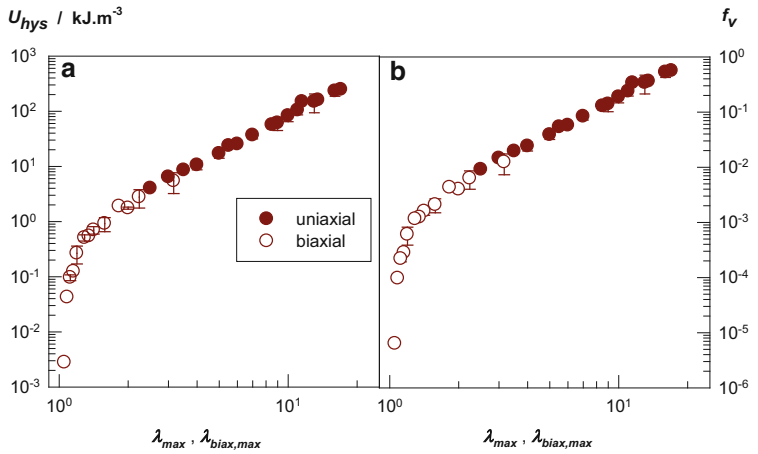

Fig. 23 (**a**) Hysteresis energy U_{hys} and (**b**) fraction f_v of dissociated cross-links during loading–unloading compression (*open symbols*) and elongation cycles (*filled symbols*) of a surfactant-containing HM PDMA hydrogel, shown as a function of the maximum strain λ_{max} or $\lambda_{biax,\ max}$; $C_0 = 15$ % (w/v), C17.3M = 2 mol%, SDS = 7 % (w/v), NaCl = 0.5 M. From [41] with permission from Elsevier

The energy dissipated during the reversible cycles (U_{hys}) can be interpreted as the sum of the dissociation energies of hydrophobic associations broken down reversibly during the cyclic tests [98, 99]:

$$U_{hys} = U_{xl}\,\nu_e\,f_\nu \tag{5a}$$

where U_{xl} is the average dissociation energy of a single association (~10^2 kJ mol^{-1} [44, 100]), ν_e is the cross-linking density of the gel (i.e., the concentration of elastically effective hydrophobic associations), and f_ν is the fraction of associations broken during the loading. The cross-linking density of the hydrogels, ν_e, can be estimated from their shear moduli, G [101, 102]:

$$G = \nu_e RT \tag{5b}$$

where R and T represent their usual meanings. Equation (5b) assumes affine deformation of the network chains, which is a reasonable assumption for physical gels formed by hydrophobic associations [33]. Using the values of U_{hys} and ν_e together with Eq. (5a), one can estimate the fraction of physical cross-links reversibly broken during the mechanical cycles (f_ν). In Fig. 23b, f_ν is plotted against the maximum strain (λ_{max} or $\lambda_{biax,max}$) achieved during the tensile and compression cycles in Fig. 22a [41]. Like the hysteresis energy (Fig. 23a), f_ν only depends on the maximum strain, indicating that the maximum extension ratio of the chains is the only parameter controlling the fraction of physical cross-links broken during loading. Thus, both compression and elongation have the same effect on the physical cross-links of hydrogels formed by hydrophobic associations. Figure 23b also shows that f_ν varies between 10^{-6} and 10^0, indicating that all of the physical cross-links can dissociate under force, but they reversibly reform if the force is removed.

The cyclic mechanical test results presented above demonstrate the existence of reversibly breakable cross-links in surfactant-containing hydrogels. In such hydrogels, a large portion of the physical cross-links dissociate under force, but they do so reversibly: if the force is removed, they reform again. However, swelling in water (i.e., extraction of surfactant micelles from the physical network) results in loss of the reversible nature of the cross-linking as a result of an increase in the lifetime of the hydrophobic associations. Thus, one may propose that when the surfactant alkyl chains are trapped electrostatically in an ionic hydrogel formed via hydrophobic interactions, the cross-links in the resulting gel system exhibit reversible behavior both after preparation and after swelling in water. This was indeed observed [42]. HM PAAc hydrogels formed in CTAB solutions exhibit reversible cycles, both at the state of preparation and in equilibrium in water. The hysteresis energy (U_{hys}) of these gels in equilibrium with water is about one order of magnitude larger than that of the gels after preparation, indicating formation of a larger number of reversibly breakable cross-links upon gel swelling [42].

8 Self-Healing

The reversible manner of disengagement of the hydrophobic units of surfactant-containing physical gels under an external force forms a basis for their self-healing. Figure 24 shows photographs of typical healing processes of HM PAAm hydrogels [32, 33]. First, hydrogel samples were cut into two separate parts using a blade. Then the two parts were put into contact and allowed to stand at 24 °C. After a few minutes, it was not possible to separate the two parts by stretching manually. However, in accord with the cyclic test results, such autonomous self-healing did not occur in surfactant-free hydrogels [33].

The self-healing efficiency of HM PAAm hydrogels was quantified by uniaxial tensile tests conducted on virgin and healed gel samples [33]. The healing efficiency of surfactant-containing hydrogels depends on several factors, including the healing time, the polymer and surfactant contents of the hydrogels, and the type and amount of the hydrophobes. Figure 25 shows the elongation at break of healed hydrogels, denoted by λ_b, as a function of the healing time [33]. The value of λ_b rapidly increases with the healing time and, after 20 min, it approaches that of the virgin gel sample $\lambda_{b,0}$, as represented by the horizontal solid line in Fig. 25. As the inset to Fig. 25 demonstrates, the healing efficiency markedly decreases with increasing polymer concentration of the gels. The efficiency also crucially depends on the comonomer feed composition; efficiency decreases as the amount of hydrophobe in the feed increases (i.e., as the fraction of dissociable cross-links decreases) [33].

As mentioned in the previous section, surfactant-containing HM PDMA hydrogels exhibit a high stretchability $4{,}200 \pm 400$ % as a result of additional hydrogen bonding and hydrophobic interactions between the DMA units. It was shown that this high stretchability can be recovered autonomously after sample damage after just a short healing time. In Fig. 26a, stress–strain curves of virgin and healed HM PDMA hydrogel samples are shown for different healing times [41]. In Fig. 26b, the tensile modulus (E), the fracture stress (σ_f), and the elongation ratio at

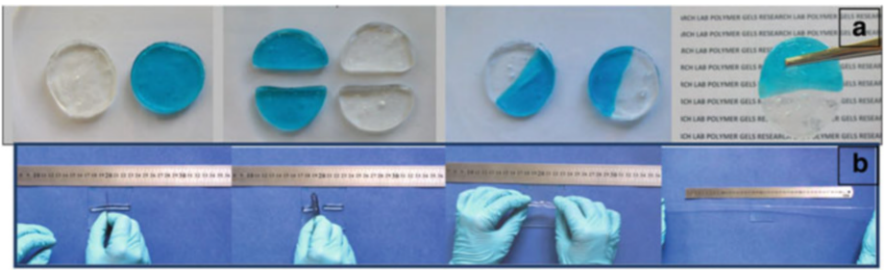

Fig. 24 (**a**, **b**) Autonomous self-healing of HM PAAm hydrogels formed using 2 mol% of C17.3M hydrophobe in 7 % SDS + 0.5 M NaCl solution; $C_0 = 5$ % (**a**) and 10 % (**b**). In (**a**), one of the hydrogel samples is colored for clarity. From [32, 33] with permission from the American Chemical Society

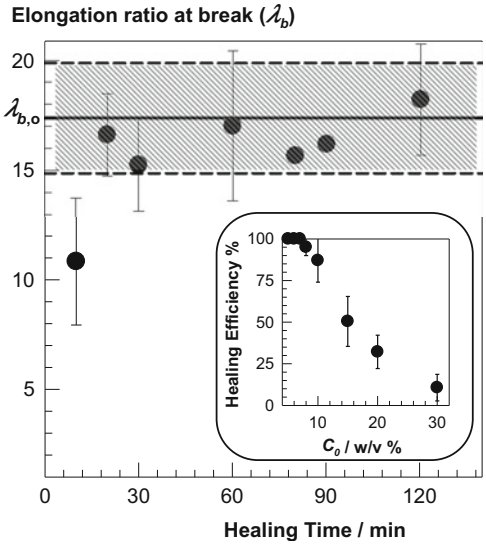

Fig. 25 Elongation at break of healed HM PAAm gels (λ_b) plotted against the healing time; $C_0 = 10$ %, C17.3M = 2 mol%, SDS = 7 %, NaCl = 0.5 M. The *horizontal line* represents λ_b of the virgin sample, denoted by $\lambda_{b,0}$. The *dashed area* represents its standard deviation. The *inset* illustrates the healing efficiency of the hydrogels as a function of C_0; healing time = 30 min. From [33] with permission from the American Chemical Society

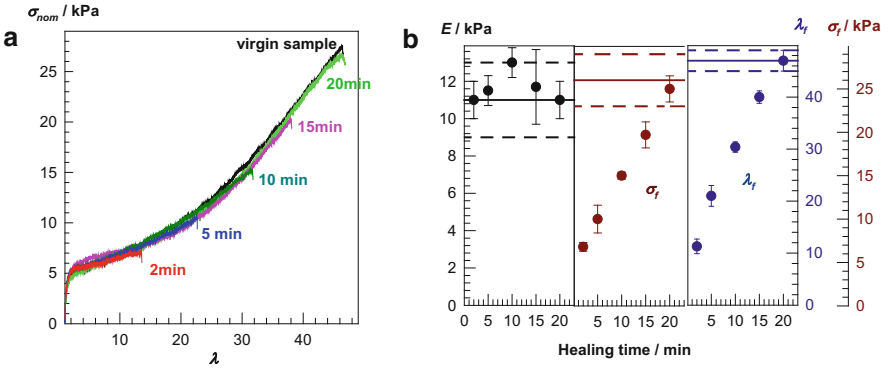

Fig. 26 (**a**) Stress–strain curves of virgin and healed HM PDMA hydrogel samples after preparation; $C_0 = 15$ % (w/v), C17.3M = 2 mol%, SDS = 7 % (w/v), NaCl = 0.5 M. Healing times are indicated next to the curves; temperature = 24 °C. (**b**) Tensile modulus E, tensile fracture stress σ_f, and elongation ratio λ_f at break of healed HM PDMA gels plotted against the healing time. The behavior of the original gel sample is represented by the *solid lines*. The *dashed lines* indicate the corresponding standard deviations. From [41] with permission from Elsevier

break (λ_f), of the healed gel samples are plotted as a function of the healing time. The modulus E is recovered within 2 min, indicating a very rapid and autonomous self-healing process in the PDMA hydrogel. After 10 min, the fracture stress of the

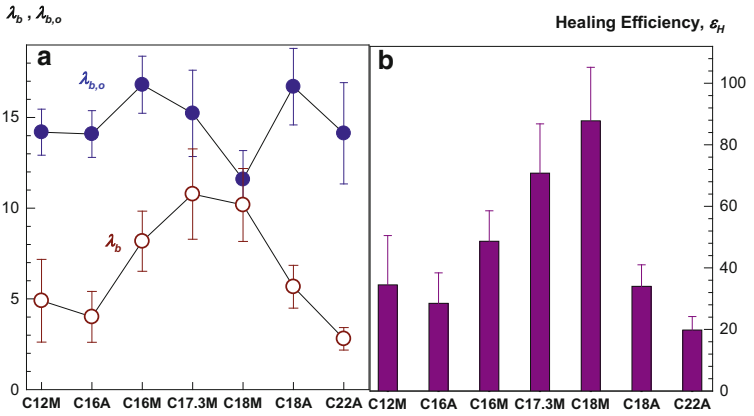

Fig. 27 (**a**) Elongation at break of healed (λ_b) and original ($\lambda_{b,0}$) HM PAAm gel samples. (**b**) Healing efficiency ε_H for gels prepared using seven different hydrophobes in 7 % SDS + 0.5 M NaCl solution; hydrophobe content = 2 mol%. From [34] with permission from Elsevier

healed gel is 15 kPa, which is 60 % of the fracture stress of the virgin sample. A healing time of 20 min suffices to recover all the initial mechanical properties of the physical hydrogel.

The side chain length of the hydrophobic monomers is another structural parameter that is crucially important for obtaining self-healing hydrogels with a high autonomic healing efficiency [34]. Figure 27a shows the elongation at break of HM PAAm hydrogel samples prepared using 2 mol% hydrophobic monomer of various alkyl side chain length. The data denoted by λ_b and $\lambda_{b,0}$ in Fig. 27a are obtained from the healed and virgin gels, respectively. The healing efficiencies of the hydrogels (ε_H), calculated as $\varepsilon_H = (\lambda_b/\lambda_{b,0}) \times 10^2$, are shown in Fig. 27b. The value of λ_b approaches $\lambda_{b,0}$, that is, ε_H increases as the length of the alkyl side chain increases. A maximum healing efficiency is found in the physical hydrogel prepared with C18M hydrophobe [34]. At longer side chain lengths, the healing efficiency decreases again. This indicates that the self-healing ability of the hydrogels depends critically on the length of alkyl side chains. Hydrophobes with an alkyl side chain of 18 carbons produce the strongest self-healing in these physical hydrogels.

Figure 27 also shows that hydrophobic monomers with methacrylate groups produce physical hydrogels with a higher healing efficiency than those with acrylate groups. For example, at an alkyl side chain length of 18 carbons, the efficiency of healing rises from 34 % to 88 % if acrylate (C18A) is replaced by methacrylate (C18M). A similar tendency is seen for hydrogels prepared with either C16A or C16M hydrophobic monomers (29 % versus 49 %). The restricted mobility of the methacrylate backbones as compared to acrylates is probably responsible for this behavior. Previous studies on side-chain crystalline polymers indeed show that hydrophobic methacrylates produce polymers with a lesser degree of crystallinity than the corresponding acrylates [103]. This indicates that the methacrylate

backbone restricts molecular mobility and the ability of alkyl side chains to align. Thus, the number of hydrophobic associations decreases while the fraction of free hydrophobic blocks increases in hydrogels formed by hydrophobic methacrylates. Lower tensile strength and a higher tan δ of gels prepared using hydrophobes with methacrylate groups indicate a larger number of free associative groups and also confirm this picture (Fig. 16a). Thus, as the number of free hydrophobic blocks at the cut surfaces increases, they find their partners much faster so that hydrogels prepared by methacrylates exhibit higher self-healing efficiencies than acrylate-based gels that have lower numbers of nonassociated blocks.

The autonomous self-healing efficiency of hydrophobically modified hydrogels decreases as their mechanical strength is increased. This is a result of the antagonistic feature of the self-healing ability to the mechanical strength of these hydrogels. For instance, the efficiency of self-healing increases with decreasing lifetime of dynamic cross-links in the gel because of favorable chain diffusion across fractured gel surfaces [34]. However, hydrogels with short-living cross-links necessarily become mechanically weak on experimental time scales. It was shown that self-healing in mechanically strong hydrogels can be induced by an external stimulus such as temperature or addition of a healing agent. Figure 28a illustrates stress–strain data of virgin HM PAAc gel samples (solid curves) together with those of healed samples at various temperatures (dashed curves) [39]. In Fig. 28b, the efficiency of healing based on the recovered fracture stress is plotted as a function of the healing temperature. Without any external stimulus, healed gels formed at $C_0 = 15$ % (w/v) withstand 10 kPa stress, that is, autonomous self-healing takes place with an efficiency of 60 %. Increasing C_0 from 15 % to 30 % also increases the fracture stress of self-healed gels up to 40 kPa while the healing efficiency

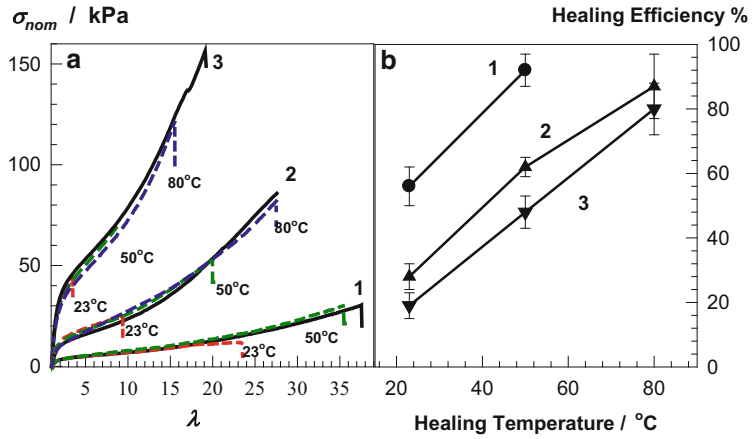

Fig. 28 (**a**) Stress–strain curves of virgin (*solid curves*) and healed surfactant-containing HM PAAc gel samples (*dashed curves*). Healing temperatures are indicated next to the curves; C17.3M = 2 mol%. (**b**) Efficiency of healing of hydrogel samples plotted against the healing temperature; healing time = 30 min. (**a**, **b**) $C_0 = 15$ % (*1*), 20 % (*2*), and 30 % (w/v) (*3*). From [39] with permission from the Royal Society of Chemistry

decreases to 20 %. This is a result of the simultaneous increase in the cross-linking density of the hydrogels, reducing the chain mobility [39]. Figure 28 also shows that the efficiency of healing increases remarkably as the temperature is increased. For instance, at $C_0 = 30$ % (w/v), gels healed at 23 °C fail upon application of 42 ± 5 kPa stress, whereas those healed at 80 °C withstand more than 120 kPa of stress. All the hydrogel samples self-heal with at least 80 % efficiency at 80 °C. The primary mechanism of temperature-induced healing in HM PAAc hydrogels is attributed to increased solubility of hydrophobic moieties in aqueous solutions, leading to a decrease in the association degree of the polymers [52]. Thus, increasing ability of the hydrogels to self-heal at a high temperature is a result of a decrease in the lifetime of hydrophobic associations, as already observed in semidilute solutions of HM PAAms [52, 104]. This simultaneously increases the chain mobility, so that the polymer chains on the two cut surfaces can easily diffuse from one side to the other, and the hydrophobes across the ruptured interface become more accessible to each other. Indeed, the dynamic moduli of HM PAAc gels sharply decrease with increasing temperature, indicating that the gels become weak with rising temperature [39, 42].

Another stimulus to trigger self-healing in hydrogels formed via hydrophobic interactions is the treatment of the damaged area of the gels with an aqueous solution of wormlike surfactant micelles [40]. In Fig. 29a, stress–strain curves of a virgin HM PAAm gel sample without SDS (dashed curve) and gel samples healed by addition of an SDS solution (solid curves) are shown. The fracture stress after 1 h of healing is 25 ± 5 kPa, which is almost twice the fracture stress of the virgin gel sample containing SDS [40]. For healing times ranging from 30 min to 9 h, the healed region of the gels is more swollen than the gel bulk region. This is due to

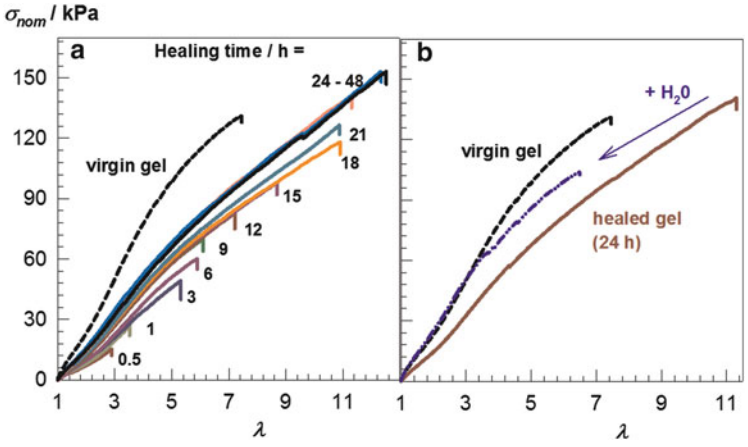

Fig. 29 (**a**, **b**) Stress–strain curves of a virgin HM PAAm gel sample without SDS (*dashed curve*) and healed gel samples (*solid curves*). Healing times are indicated next to the curves. The *blue* (*dash-dot*) *curve* in (**b**) represents the stress–strain data of a gel sample healed for 24 h and then immersed in an excess of water for 2 weeks to extract SDS prior to the mechanical tests. From [40] with permission from Springer

absorption of SDS by the polymer at the welded interface, producing an excess of counterion concentration inside the gel and leading to increased gel swelling [40]. This interface also acts as a weak point in the healed gels, so that they always rupture at this region. However, for longer healing times (>9 h), the welded interface deswells again and becomes identical to the bulk region. Simultaneously, the healed gel samples rupture in the bulk region, while the welded interface remains unbroken. For all healing times indicated in Fig. 29a, the surfactant-mediated healing is irreversible: when immersed in water to extract the healing agent, the healed gel samples remain as stable as the virgin gels [40].

Figure 29a also shows that both the fracture stress and the elongation at break of the gel samples rapidly increase with increasing healing time, and after 20 h they reach the values of the virgin gel sample. For longer healing times, the gel samples become stronger and tougher than the original gel, while the moduli of the healed gels partially recover their original values. This was attributed to the presence of SDS in the healed gel samples, weakening their hydrophobic interactions [40]. Indeed, when the healed samples are immersed in an excess of water to extract SDS micelles, their stress–strain curves approach the curve of the virgin sample. This is illustrated by the blue (dash-dot) curve in Fig. 29b, representing the stress–strain data of a gel sample healed for 24 h and then immersed in an excess of water for 2 weeks to extract SDS prior to the mechanical tests. Both the fracture stress and the elongation at break are 80 % of the original values. In conclusion, because the surfactant-induced healing technique is applicable to physical gels formed by hydrophobic associations, it overcomes the requirement of the presence of surfactants in the gels for their healing, thereby allowing applications in aqueous environment.

High-strength PAAc hydrogels formed in oppositely charged surfactant solutions can also be healed by treatment of cut surfaces with surfactant solutions [42]. In Fig. 30, the stress–strain curves of virgin and healed PAAc gel samples

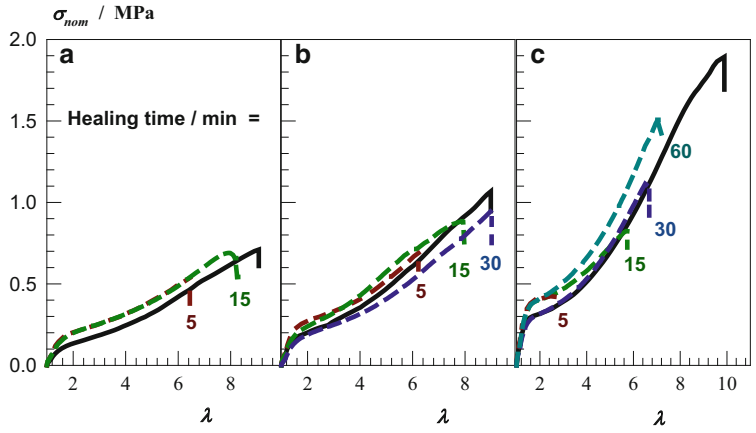

Fig. 30 (**a**–**c**) Stress–strain curves of virgin (*solid curves*) and healed HM PAAc gel samples in equilibrium with water (*dashed curves*): (**a**) $C_0 = 15$ %, $\beta_0 = 1/8$; (**b**) $C_0 = 20$ %, $\beta_0 = 1/8$; (**c**) $C_0 = 30$ %, $\beta_0 = 1/6$. From [42] with permission from the American Chemical Society

in equilibrium with water are shown for various healing times in surfactant solutions. The fracture stress of the healed gels increases with increasing healing time or with increasing PAAc concentration. After a healing time of 60 min, the hydrogel sample formed at $C_0 = 30$ % and $\beta_0 = 1/6$ sustains 1.5 ± 0.2 MPa stresses and ruptures at a stretch of 7 ± 1 (Fig. 30c) [42]. To our knowledge, this fracture stress is the highest value reported in the literature.

The hydrophobe content of the self-healing hydrogels described above is 2 mol % (relative to the amount of monomers in total). It was shown that at a high hydrophobe level, hydrogels containing crystalline domains and exhibiting shape memory properties can be obtained [38]. These hydrogels can also be healed by treatment of a potentially damaged area with surfactant solutions. Such self-healing hydrogels with shape memory behavior were prepared by copolymerization of AAc with 20–50 mol% of C18A in aqueous SDS–NaCl solutions [38]. After extraction of the surfactant micelles, these HM PAAc hydrogels possess 60–70 % of water and exhibit three orders of magnitude change in their elastic moduli when the temperature changes between below and above the melting temperature of the crystalline domains (~50 °C). In addition, these hydrogels exhibit complete shape recovery to the permanent shape at 60 °C, together with surfactant-triggered self-healing. The blocky structure of the HM PAAc chains formed by micellar polymerization is responsible for the drastic change in their mechanical properties and for their significant shape memory effect.

9 Concluding Remarks

In this chapter, recent developments in the design of hydrogels formed via hydrophobic interactions are reviewed, with a special emphasis on the function of surfactant in their dynamic and mechanical properties. Micellar copolymerization is a simple technique for the synthesis of such hydrogels. A particular advantage of this technique is the blocky structure of the resulting hydrophobically modified polymers, significantly enhancing their associative properties.

Because preparation of mechanically strong hydrogels via micellar copolymerization requires blocks of large hydrophobes, salts such as NaCl or NaBr should be included in the micellar solution. These salts screen electrostatic interactions, causing the micelles to grow. In turn, the growth of the micelles provides solubilization of substantial amounts of hydrophobic monomers in the aqueous solution. After solubilization of large hydrophobes within wormlike surfactant micelles of salt solutions, they can be copolymerized with hydrophilic monomers to obtain hydrophobically modified hydrogels with tunable properties.

Hydrogels formed via hydrophobic interactions in aqueous micellar solutions present two faces, depending on which state they are in. These states are (i) the preparation state, when the gels contain surfactant micelles, and (ii) the state in equilibrium with pure water, when the free surfactant micelles have been removed after preparation.

At the state of preparation, the hydrogels exhibit a slow mode in DLS, independent of the scattering vector, that is related to structural relaxation of their physical polymer network. This relaxation only occurs in the presence of surfactant micelles and disappears when SDS is removed. A gel containing surfactant micelles exhibits time-dependent dynamic moduli with a plateau modulus at high frequencies and a loss factor above 0.1. After removal of the surfactants, the dynamic moduli become nearly independent of time, and the loss factor decreases to below 0.1, corresponding to solid-like behavior. Simultaneously, the degree of spatial gel inhomogeneity increases considerably after extraction of surfactant molecules, also demonstrating a loss of reversibility of the cross-linkages.

Thus, with surfactants, the cross-links are reversible as a result of local solubilization of the hydrophobic associations, so that the hydrogels are weak. After removal of surfactant, however, direct exposure of the hydrophobic associations to the aqueous environment increases their lifetimes so that the hydrogels behave mostly like chemical gels with time-independent dynamic moduli and a single relaxation mode in DLS. These findings also demonstrate that the presence of surfactant micelles is responsible for the slow mode of the physical hydrogels. Because breakup of a micelle around the hydrophobic blocks enhances the hydrophobic interactions at this location, while its re-formation re-decreases these interactions, the micellar kinetics and resulting temporary strong associations are responsible for the slow network relaxation in surfactant-containing physical gels.

Hydrophobically modified ionic hydrogels formed in oppositely charged surfactant solutions exhibit frequency-dependent dynamic moduli if they are in equilibrium in water after extraction of free surfactant micelles. This is a result of complex formation between the ionic polymer and the oppositely charged surfactant, leading to polymer-bound surfactant counterions in the hydrogels.

The mechanical strength of hydrogels formed using hydrophobic acrylates is higher than that of those formed using methacrylates. This is due to the limited flexibility of the methacrylate backbones, reducing the number of hydrophobic associations acting as physical cross-links. Similarly, the length of the alkyl side chain of the hydrophobes as well as the type of hydrophilic chains also affect the mechanical performance of hydrogels formed via hydrophobic interactions. For instance, replacing PAAm by PAAc leads to mechanically stronger hydrogels because of stabilization of the cross-linking hydrophobic associations by cooperative hydrogen bonding between carboxyl groups. A similar improvement of the mechanical performance is observed by replacement of PAAm by PDMA as a result of additional hydrophobic interactions between the DMA units. Moreover, because the dynamic features of the hydrogels drastically change after removal of surfactant micelles, similar changes are also observed in their mechanical properties. Most importantly, a remarkable decrease in the stretchability of such hydrogels is observed upon extraction of surfactant micelles. Ionic hydrogels formed in oppositely charged surfactant solutions exhibit a significant enhancement in their mechanical properties when they are immersed in water. This is a result of extraction of surfactant counterions from the micelles and simultaneous formation of ionic bonds. By tuning the preparation conditions, hydrogels formed via

hydrophobic interactions in micellar solutions exhibit a high stretchability (up to 5,000 %), high mechanical strength (up to 1.7 MPa tensile stress), and complete autonomous self-healing ability.

Current research in the field of self-healing hydrogels is focused on improving the mechanical performance of self-healing gels formed via reversible molecular interactions. Because self-healing of a hydrogel is opposite to its mechanical strength, the magnitude of the tensile strength recovered after repair for most healable hydrogels is below 0.4 MPa. As discussed in this chapter, hydrophobically modified hydrogels that are self-healed via heating and surfactant treatment of the damaged areas withstand up to 1.5 MPa stresses and rupture at a stretch of 600 %. Thus, hydrogels formed via hydrophobic interactions combine good mechanical properties with a high self-healing efficiency and are promising materials for new technologies.

Acknowledgement Work was supported by the Scientific and Technical Research Council of Turkey (TUBITAK, KBAG–114Z312). The author thanks the Turkish Academy of Sciences (TUBA) for partial support.

References

1. Okay O (2009) General properties of hydrogels. In: Gerlach G, Arndt K-F (eds) Hydrogel sensors and actuators, Springer series on chemical sensors and biosensors, vol 6. Springer, Berlin, pp 1–14
2. Ahagon A, Gent AN (1975) J Polym Sci Polym Phys Ed 13:1903
3. Brown HR (2007) Macromolecules 40:3815
4. Abdurrahmanoglu S, Can V, Okay O (2009) Polymer 50:5449
5. Gong JP, Katsuyama Y, Kurokawa T, Osada Y (2003) Adv Mater 15:1155
6. Tanaka Y, Gong JP, Osada Y (2005) Prog Polym Sci 30:1
7. Okumura Y, Ito K (2001) Adv Mater 13:485
8. Miquelard-Garnier G, Demoures S, Creton C, Hourdet D (2006) Macromolecules 39:8128
9. Haraguchi K, Takehisa T (2002) Adv Mater 14:1120
10. Huang T, Xu H, Jiao K, Zhu L, Brown HR, Wang H (2007) Adv Mater 19:1622
11. Deng G, Tang C, Li F, Jiang H, Chen Y (2010) Macromolecules 43:1191
12. Phadke A, Zhang C, Arman B, Hsu C-C, Mashelkar A, Lele AK, Tauber MJ, Arya G, Varghese S (2012) Proc Natl Acad Sci USA 109:4383
13. Zhang H, Xia H, Zhao Y (2012) ACS Macro Lett 1:1233
14. Cui J, del Campo A (2012) Chem Commun 48:9302
15. Liu J, Song G, He C, Wang H (2013) Macromol Rapid Commun 34:1002
16. Haraguchi K, Uyama K, Tanimoto H (2011) Macromol Rapid Commun 32:1253
17. South AB, Lyon LA (2010) Angew Chem Int Ed 49:767
18. Wang Q, Mynar JL, Yoshida M, Lee E, Lee M, Okura K, Kinbara K, Aida T (2010) Nature 463:339
19. Sun J-Y, Zhao X, Illeperuma WRK, Chaudhuri O, Oh KH, Money DJ, Vlassak JJ, Suo Z (2012) Nature 489:133
20. Foo CTSWP, Lee JS, Mulyasasmita W, Parisi-Amon A, Heilshorn SC (2009) Proc Natl Acad Sci USA 106:22067
21. Appel EA, Biedermann F, Rauwald U, Jones ST, Zayed JM, Scherman OA (2010) J Am Chem Soc 132:14251

22. Skrzeszewska PJ, Sprakel J, Wolf FA, Fokkink R, Stuart MAC, van de Gucht J (2010) Macromolecules 43:3542
23. Holten-Andersen N, Harrington MJ, Birkedal H, Lee BP, Messersmith PB, Lee KYC, Waite JH (2011) Proc Natl Acad Sci USA 108:2651
24. Shafiq Z, Cui J, Pastor-Perez L, San Miguel V, Gropeanu RA, Serrano C, del Campo A (2012) Angew Chem Int Ed 124:4408
25. Xu Y, Wu Q, Sun Y, Bai H, Shi G (2010) ACS Nano 4:7358
26. Liu F, Li F, Deng G, Chen Y, Zhang B, Zhang J, Liu C-Y (2012) Macromolecules 45:1636
27. Zhang Y, Tao L, Li S, Wei Y (2011) Biomacromolecules 12:2894
28. He L, Fullenkamp DE, Rivera JG, Messersmith PB (2011) Chem Commun 47:7497
29. Froimowicz P, Klinger D, Landfester K (2011) Chem Eur J 17:12465
30. Quint SB, Pacholski C (2011) Soft Matter 7:3735
31. Abdurrahmanoglu S, Cilingir M, Okay O (2011) Polymer 52:694
32. Tuncaboylu DC, Sari M, Oppermann W, Okay O (2011) Macromolecules 44:4997
33. Tuncaboylu DC, Sahin M, Argun A, Oppermann W, Okay O (2012) Macromolecules 45: 1991
34. Tuncaboylu DC, Argun A, Sahin M, Sari M, Okay O (2012) Polymer 53:5513
35. Tuncaboylu DC, Argun A, Algi MP, Okay O (2013) Polymer 54:6381
36. Baskan T, Tuncaboylu DC, Okay O (2013) Polymer 54:2979
37. Akay G, Hassan-Raeisi A, Tuncaboylu DC, Orakdogen N, Abdurrahmanoglu S, Oppermann W, Okay O (2013) Soft Matter 9:2254
38. Bilici C, Okay O (2013) Macromolecules 46:3125
39. Gulyuz U, Okay O (2013) Soft Matter 9:10287
40. Argun A, Algi MP, Tuncaboylu DC, Okay O (2014) Colloid Polym Sci 292:511
41. Algi MP, Okay O (2014) Eur Polym J 59:113
42. Gulyuz U, Okay O (2014) Macromolecules 47:6889
43. Tanaka F, Edwards SF (1992) Macromolecules 25:1516
44. Annable T, Buscall R, Ettelaie R, Whittlestone D (1993) J Rheol 37:695
45. Bell GI (1978) Science 178:618
46. Pham QT, Russel WB, Thibeault JC, Lau W (1999) Macromolecules 32:5139
47. Tripathi A, Tam KC, McKinley GH (2006) Macromolecules 39:1981
48. Tian J, Seery TAP, Weiss RA (2004) Macromolecules 37:10001
49. Hao J, Weiss RA (2011) Macromolecules 44:9390
50. Matsuda A, Sato J, Yasunaga H, Osada Y (1994) Macromolecules 27:7695
51. Hill A, Candau F, Selb J (1993) Macromolecules 26:4521
52. Volpert E, Selb J, Candau F (1998) Polymer 39:1025
53. Regalado EJ, Selb J, Candau F (1999) Macromolecules 32:8580
54. Candau F, Selb J (1999) Adv Colloid Interface Sci 79:149
55. Gao B, Guo H, Wang J, Zhang Y (2008) Macromolecules 41:2890
56. Candau F, Regalado EJ, Selb J (1998) Macromolecules 31:5550
57. Kujawa P, Audibert-Hayet A, Selb J, Candau F (2004) J Polym Sci B Polym Phys 42:1640
58. Kujawa P, Audibert-Hayet A, Selb J, Candau F (2006) Macromolecules 39:384
59. Beyer K, Leine D, Blume A (2006) Colloids Surf B Biointerfaces 49:31
60. Chern CS, Chen TJ (1998) Colloids Surf A Physicochem Eng Aspects 138:65
61. Leyrer RJ, Machtle W (2000) Macromol Chem Phys 201:1235
62. Lau W (2002) Macromol Symp 182:283
63. Rehage H, Hoffman H (1991) Mol Phys 74:933
64. Magid LJ (1998) J Phys Chem B 102:4064
65. Hassan PA, Raghauan SR, Kaler EW (2002) Langmuir 18:2543
66. Missel PJ, Mazer NA, Benedek GB, Young CY (1980) J Phys Chem 84:1044
67. Sutherland E, Mercer SM, Everist M, Leaist D (2009) J Chem Eng Data 54:272
68. Mazer NA, Benedek GB, Carey MC (1976) J Phys Chem 80:1075
69. Young CY, Missel PJ, Mazer NA, Benedek GB, Carey MC (1978) J Phys Chem 82:1375

70. Pecora R (1985) Dynamic light scattering: application of photon correlation spectroscopy. Plenum, New York
71. Molchanov VS, Philippova OE, Khokhlov AR, Kovalev YA, Kuklin AI (2007) Langmuir 23:105
72. Kumar S, Bansal D, Din K (1999) Langmuir 15:4960
73. Kunieda H, Ozawa K, Huang K-L (1998) J Phys Chem B 102:831
74. Siriwatwechakul W, LaFleur T, Prud'homme RK, Sullivan P (2004) Langmuir 20:8970
75. Sato T, Acharya DP, Kaneko M, Aramaki K, Singh Y, Ishitobi M, Kunieda HJ (2006) J Dispers Sci Technol 27:611
76. Törnblom M, Henriksson U, Ginley M (1994) J Phys Chem 98:7041
77. Wang F, Chen T, Shang Y, Liu H (2011) Korean J Chem Eng 28:923
78. Zhang S, Teng HN (2008) Colloid J 70:105
79. Tah B, Pal P, Mahato M, Talapatra GB (2011) J Phys Chem B 115:8493
80. Marrucci G, Bhargava S, Cooper SL (1993) Macromolecules 26:6483
81. Patruyo LG, Muller AJ, Saez AE (2002) Polymer 43:6481
82. Penott-Chang EK, Gouveia L, Fernandez IJ, Muller AJ, Diaz-Barrios AD, Saez AE (2007) Colloids Surf A Physicochem Eng Aspects 295:99
83. Magny B, Iliopoulos I, Zana R, Audebert R (1994) Langmuir 10:3180
84. Philippova OE, Hourdet D, Audebert R, Khokhlov AR (1996) Macromolecules 29:2822
85. Hayashi S, Ikeda S (1980) J Phys Chem 84:744
86. Patist A, Oh SG, Leung R, Shah DO (2001) Colloids Surf A Physicochem Eng Aspects 176:3
87. Williams G, Watts DC (1970) Trans Faraday Soc 66:80
88. Gurtovenko AA, Gotlib YY (2001) J Chem Phys 115:6785
89. Ng TSK, McKinley GH (2008) J Rheol 52:417
90. Bastide J, Candau SJ (1996) Structure of gels as investigated by means of static scattering techniques. In: Cohen Addad JP (ed) Physical properties of polymeric gels. Wiley, New York, p 143
91. Shibayama M (1998) Macromol Chem Phys 199:1
92. Shibayama M, Ikkai F, Nomura S (1994) Macromolecules 27:6383
93. Lindemann B, Schröder UP, Oppermann W (1997) Macromolecules 30:4073
94. Kizilay MY, Okay O (2003) Macromolecules 36:6856
95. Joosten JGH, Mccarthy JL, Pusey PN (1991) Macromolecules 24:6690
96. Pusey PN, van Megen W (1989) Phys A 157:705
97. Ikkai F, Shibayama M (1999) Phys Rev Lett 82:4946
98. Webber RE, Creton C, Brown HR, Gong JP (2007) Macromolecules 40:2919
99. Lake GJ, Thomas AG (1967) Proc R Soc Lond A 300:108
100. Ng WK, Tam KC, Jenkins RD (2000) J Rheol 44:137
101. Flory PJ (1953) Principles of polymer chemistry. Cornell University Press, Ithaca, NY
102. Treloar LRG (1975) The physics of rubber elasticity. University Press, Oxford
103. Livshin S, Silverstein MS (2007) Macromolecules 40:6349
104. Biggs S, Selb J, Candau F (1993) Polymer 34:580

Donor–Acceptor π–π Stacking Interactions: From Small Molecule Complexes to Healable Supramolecular Polymer Networks

Wayne Hayes and Barnaby W. Greenland

Contents

Abstract This chapter presents selected literature examples to review the development of the use of donor–acceptor π–π stacking interactions as transient cross-links in supramolecular polymer networks. The chapter examines notable examples of these highly specific and directional interactions and illustrates how they can be

W. Hayes (✉)
Department of Chemistry, University of Reading, Whiteknights, Reading, Berkshire RG6 6AD, UK
e-mail: w.c.hayes@reading.ac.uk

B.W. Greenland (✉)
Reading School of Pharmacy, University of Reading, Whiteknights, Reading, Berkshire RG6 6AU, UK
e-mail: b.w.greenland@reading.ac.uk

© Springer International Publishing Switzerland 2015

S. Seiffert (ed.), *Supramolecular Polymer Networks and Gels*, Advances in Polymer Science 268, DOI 10.1007/978-3-319-15404-6_4

utilised to reliably produce functional supramolecular, self-assembled systems. Knowledge gained from these fundamental studies has enabled the design, synthesis and application of donor–acceptor stacked supramolecular motifs in non-covalent polymer networks, which is exemplified through detailing the production, physical properties and optimisation of healable materials.

1 Introduction to Supramolecular Materials

Supramolecular chemistry has become one of the major growth areas in the chemical and materials sciences over the past 30 years [1–5]. Initial studies focused on understanding the fundamental supramolecular interactions between molecules to build up an understanding of their strength, directionality and limitations. Inspired by nature, hydrogen bonding interactions have found the most widespread use. However, multiple applications have also been demonstrated for structures that harness halogen bonding [6], metal–ligand [7] and donor–acceptor (D–A) π–π stacking interactions [8]. In each case, it is the fidelity and predictable nature of supra-structures assembled by supramolecular interactions that enables their use in complex functional and responsive materials.

With precise design criteria established, supramolecular interactions have been exploited to design and synthesise new and functional mechanically interlocked molecules in high yields [9]. Over a relatively short period of time, mastery of controlled synthesis of mechanically interlocked molecules has led to an extraordinary array of functional materials and molecular machines [10]. Examples of these include logic gates, sensors for explosives, anions and cations, in addition to exquisite molecules with complex topologies (such as molecular knots) that have yet to be thoroughly exploited.

In more recent times, the possibilities enabled by utilising the reversible nature [11] of supramolecular interactions has resulted in their introduction into materials chemistry [12, 13]. The driving force for such studies is that the strength of supramolecular interactions can be reversibly altered by application of external stimuli. In the case of materials chemistry, this means that a physical property of the material (for example, its tensile strength) can be changed in real time and in situ. This feature has transformative potential in numerous applications, including those as healable materials [14–24] and shape-memory polymers [25–28].

With the field of supramolecular chemistry expanding at an increasing rate, the remainder of this article focuses on donor–acceptor (D–A) π–π stacking interactions. The chapter begins by looking at D–A stacking interactions from an historical perspective and how these initial structure–property studies of infinite stacks of D–A pairs enabled the construction of mechanically interlocked materials and linear polymers in the solid and solution states (Fig. 1a–c, respectively). The later sections of this chapter focus of the introduction of D–A stacking interactions into

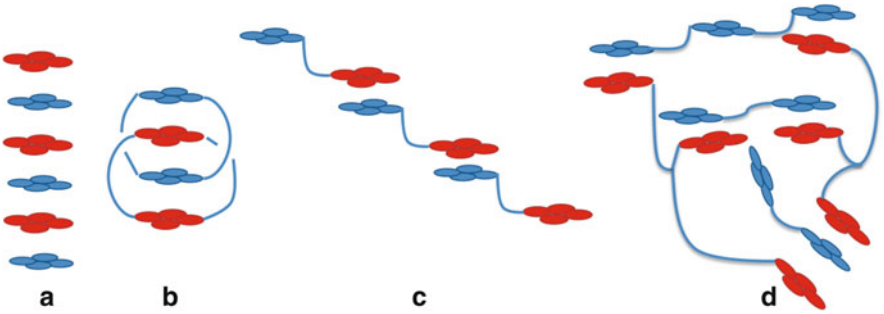

Fig. 1 Supramolecular donor (*red*) and acceptor (*blue*) self-assembled systems: (**a**) infinite stack of donor and acceptor species; (**b**) mechanically interlocked structure; (**c**) linear supramolecular polymer; and (**d**) cross-linked supramolecular polymer network

transiently cross-linked polymer networks (Fig. 1d), with emphasis in producing healable and thermally responsive materials. (For insights into the molecular scale dynamics of transiently cross-linked systems see [29–31].)

In view of the extensive literature, this chapter does not aim to be comprehensive, but uses selected notable examples from the field to demonstrate the concepts and applications of these fascinating species. For example, there are numerous examples of linear supramolecular polymers in solution [32], solvated nanotubes [33], vesicles [34] and gel networks [35–38] that rely on donor–acceptor interactions; however, this review focuses on unsolvated, cross-linked supramolecular polymers and their bulk properties.

2 Donor–Acceptor π–π Stacking

2.1 Historical Context

Donor–acceptor π–π stacking has been recognised as a valuable interaction for many years, with several detailed monographs produced on these systems over 50 years ago [39, 40]. Over the intervening years, the number of structural motifs that can form charge-transfer (CT) complexes has expanded to such an extent that a comprehensive list is not practical to compile; for illustrative purposes, four of the most commonly used donor and acceptor motifs are shown in Fig. 2.

Inspection of these structures highlights common chemical motifs that are required to generate the required donor or acceptor properties in a given molecule. Most donor and acceptor residues are planar, with extensive π-surfaces frequently incorporating multiple, often fused, aromatic rings. Acceptor species typically have strong electron-withdrawing groups in conjugation with their π-system, whereas the electronically complementary donor species contain electron-donating residues at their periphery.

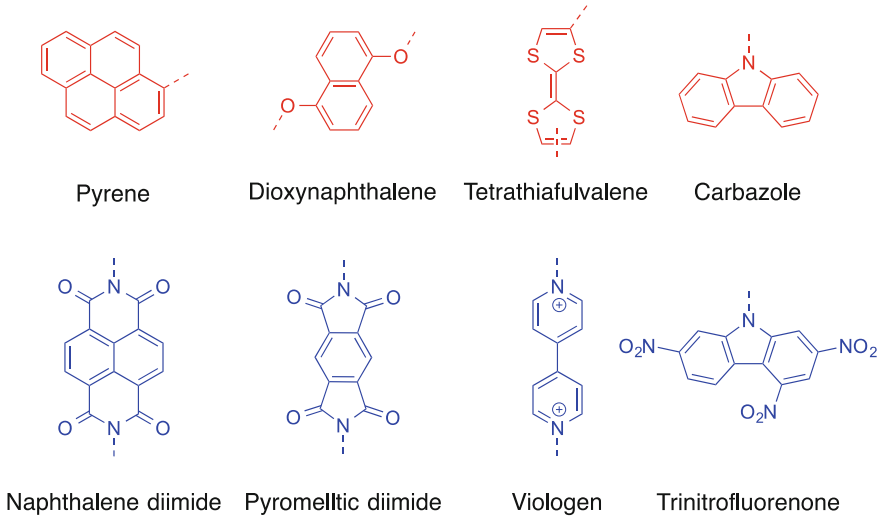

Fig. 2 Structures of common donor (*red*) and acceptor (*blue*) compounds

As might be expected from an interaction that can occur between molecules with such a diversity of structures, the strength of the interaction depends on many factors, including the size and geometry of the aromatic core, the nature of the substituents and also the solvent. Despite these variables, the separation between the D–A residues in the solid state is extremely consistent at approximately 3.5 Å [41].

2.2 *Binding Constant and Stoichiometry Determination for D–A Complexes*

D–A complexes are formed by electronic transition from the highest occupied molecular orbital (HOMO) of the donor to the lowest unoccupied molecular orbital (LUMO) of the acceptor. Although λ_{max} of this transition is not always intense or observed in the visible region, many CT complexes are strongly coloured. This property allows significant structural data to be extracted through comparatively simple techniques including UV/vis spectroscopy, which is one of the factors that facilitated early identification and structural studies on these complexes.

For systems that exhibit a relatively intense charge-transfer band, binding constants can be routinely quantified by UV/vis spectroscopy. This is achieved by measuring the intensity of the absorption band associated with the complex over a range of concentrations. This methodology was first used to assess the complexation constants of D–A complexes by Stoddart, Colquhoun and co-workers [42]

using a methodology developed by Ray [43] for studying ion-pair formation. Colquhoun and Stoddart derived the following equation [Eq. (1)]:

$$\frac{c}{A} = \left(\frac{1}{K\varepsilon l}\right)^{1/2} \frac{1}{A^{1/2}} + \frac{1}{\varepsilon l} \tag{1}$$

c concentration
A measured absorbance
K association constant
ε extinction coefficient
l path length

The association constant can be calculated from a plot of c/A versus $1/A^{1/2}$, which yields a straight line with a slope $\alpha = \left(\frac{1}{K\varepsilon l}\right)^{1/2}$ and intercept $y = \frac{1}{\varepsilon l}$ [Eq. (2)]:

$$K = y/\alpha^2 \tag{2}$$

K association constant
y intercept
α slope

The binding-constant calculation with Eq. (2) is restricted to 1:1 complexes of D–A residues. The binding stoichiometry can be verified independently by a Job's plot, which can also be conveniently produced by UV/vis spectrometry [44]. In this experiment, the absorbance is recorded for a series of solutions where the total concentration of D and A species remains constant, but their molar fractions are varied. For 1:1 complexes, the maximum intensity of the charge-transfer band is observed at equimolar concentrations of D and A.

Over recent years, a range of techniques including ^{1}H NMR spectroscopy [45, 46] and isothermal titration calorimetry (ITC) [47, 48] have been shown to provide excellent methods for the determination of binding constants for these systems. In addition, more advanced two-dimensional NMR techniques (e.g. NOESY) have been employed to ascertain the three-dimensional structure of the multicomponent complexes in solution [49], and generally show good agreement with data obtained in the solid state [50].

2.3 Donor–Acceptor Interactions in Supramolecular Polymer Chemistry: Strength of Binding

Examining the structures of simple D–A stacks is informative (Fig. 1a); however, to harness D–A interactions in more complex structures, it is imperative to use functionalised donor and acceptor residues and to be able to manipulate the association constants of these systems systematically. Many hydrogen-bonded systems that form linear supramolecular polymers in solution exhibit a degree of polymerisation (DP) related to the binding constant (K) and the molar concentration ([M]) of mono- or oligomeric building blocks according to the following relationship [Eq. (3)] [51, 52]:

$$\mathrm{DP} = (K[\mathrm{M}])^{1/2} \tag{3}$$

This simple relationship can be complicated by many factors, especially solvent effects and the formation of inclusion complexes [53]. Generally, in dilute solution (e.g. 0.1 M), significant DP (>100) can only be achieved using supramolecular interactions with high binding constants (e.g. 100,000 M^{-1}). Typical D–A interactions have low binding constants (1–20 M^{-1}). Therefore, significant effort has been focused on producing systems that harness multiple complimentary D–A interactions.

For materials chemistry applications, where the concentration term in Eq. (3) is not applicable, the effect of increasing K is harder to predict. The physical properties of the materials are also dependent on phase separation, glass transition temperature (T_g) and crystallinity [54]. However, it has been demonstrated that the modulus of toughness and thermal responsiveness of supramolecular materials that incorporate either hydrogen bonded [55] or D–A interactions [56] are still dependent on the strength of the supramolecular interactions.

2.4 Co-operative Effects in the Design of Supramolecular Motifs

Conceptually, increasing the strength of the binding interactions between components that form D–A complexes can be achieved by changing the chemical structure and electronic nature of the D and A components (Fig. 2) or by increasing the number of co-operative, complementary binding interactions within a single complex (Fig. 3).

Seminal effort toward these goals was made by Colquhoun and Stoddart in a series of papers beginning in the early 1980s [57]. During these studies, these groups synthesised a macrocyclic dibenzo-30-crown-10 (DB30C10, Fig. 4) that contained two π-electron-rich aromatic residues [42]. Solution-mixing of this macrocycle with the acceptor Diquat (Fig. 4) resulted in a slight but observable

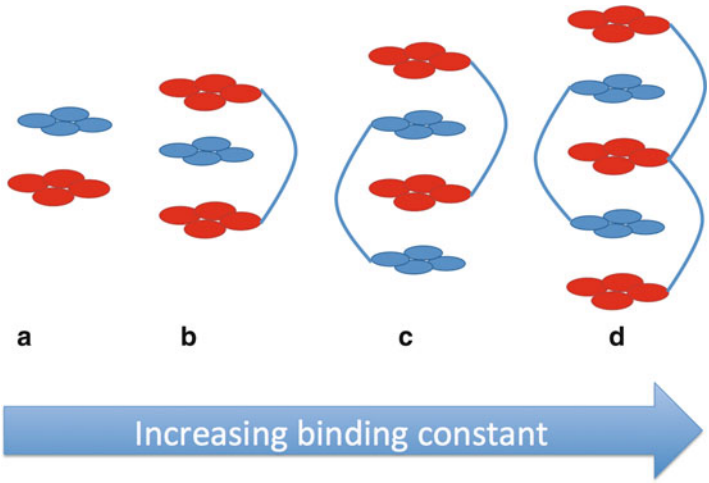

Fig. 3 Design of ditopic complexes (**a**–**d**) with increasing number of donor–acceptor interactions

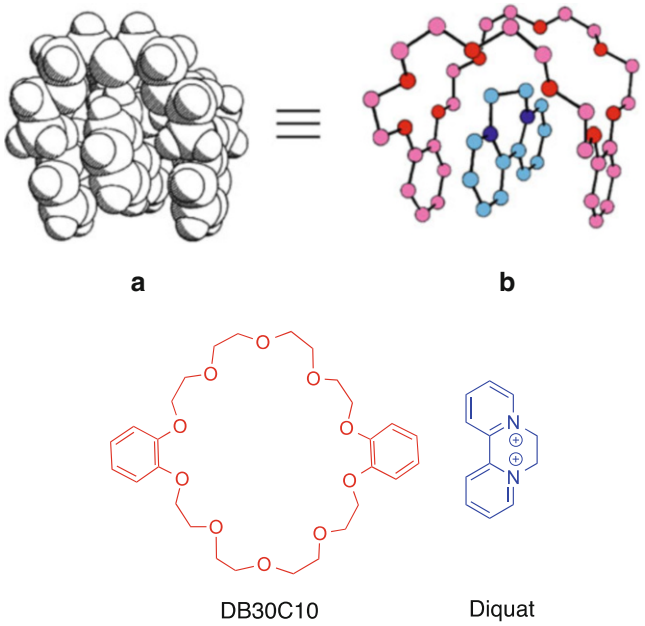

Fig. 4 Solid-state suprastructures of the complex formed between DB30C10 and Diquat: (**a**) space-filling representation and (**b**) ball-and-stick representation. (Adapted with permission from [42], copyright 2008 Elsevier)

change of colour. The crystal structure of the resulting complexes revealed that the conformational flexibility of the ether units enables the two aromatic residues in the macrocycle DB30C10 to 'chain fold' around the electron-deficient acceptor

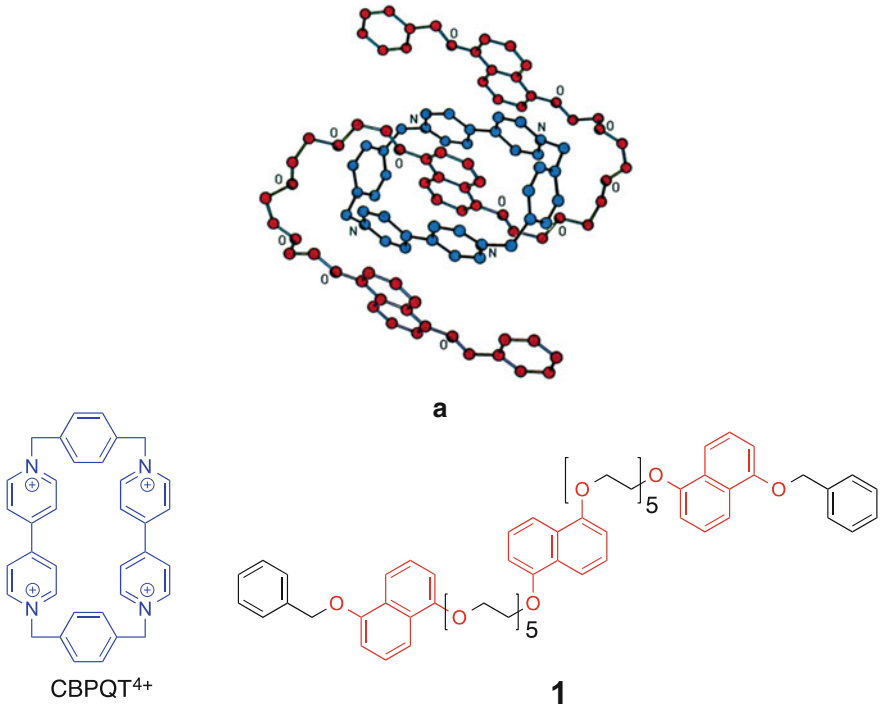

Fig. 5 (**a**) Ball-and-stick solid-state structure of the complex between **1** and $CBPQT^{4+}$. (**b**) Chemical structure of $CBPQT^{4+}$ and an oligoether containing three electron-rich dioxynaphthalene residues (**1**). (Used with permission from [61], copyright 1994 RSC)

species. This folding results in a highly defined D–A–D π-stack with interplanar distances of about 3.4 Å (Fig. 4a, b), exactly as observed for simple D–A infinite lattices (Fig. 1a). Closely related structures are still receiving significant interest in the literature, even 20 years after these initial disclosures [58–60].

The Stoddart group proceeded to exploit these D–A complexes and reported the synthesis of a family of macrocycles containing multiple donor and acceptor residues. The most recognisable of these cyclophanes is the tetracationic species cyclobis(paraquat-*p*-phenylene) ($CBPQT^{4+}$, Fig. 5) [62, 63]. This acceptor has been found to form strong complexes with a wide range of donor species (such as **1**, see Fig. 5), thereby providing a versatile basis of molecular shuttles, logic gates and other nanoscale devices.

Gabriel and Iverson investigated the production of duplexes from oligomers containing suitably spaced donor or acceptor residues (**2** and **3**, respectively, Fig. 6) [65]. Co-assembly of these components results in duplexes as identified by UV/vis, ITC and ^{1}H NMR spectroscopy. These duplexes exhibit binding constants dependent on the number of naphthalene diimide (NDI) and 1,5-dialkoxynaphthalene (DAN) residues in the complex, highlighting co-operativity as a potential major

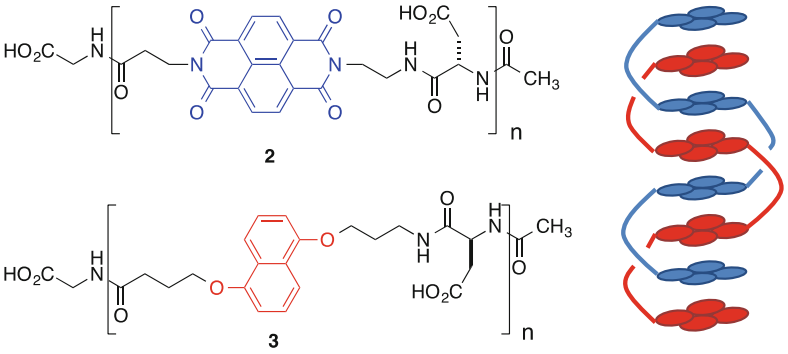

Fig. 6 *Left*: Structures of the oligomeric species containing NDI (*blue*) and DAN (*red*), as produced by Gabriel and Iverson ($n = 1$–4). *Right*: Proposed solution-state structure of the ditopic complex formed between **2** and **3** when $n = 4$ [64]

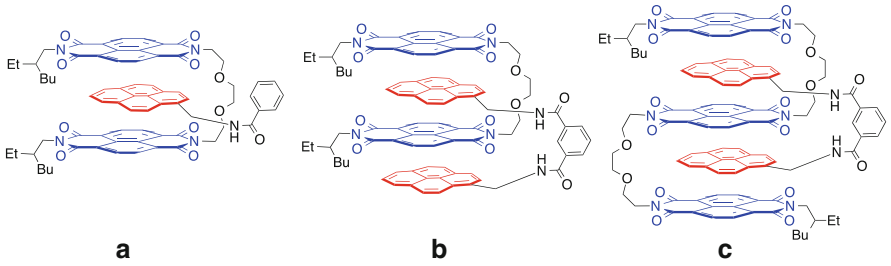

Fig. 7 (**a**–**c**) Structures of the supramolecular complexes studied by Colquhoun, Hayes and co-workers. The association constants of the complexes are 130, 3,500 and 11,000 M^{-1} for **a**, **b** and **c**, respectively [66]

design consideration to tune the properties of supramolecular materials based on these weak non-covalent interactions.

More recently, Colquhoun, Hayes and co-workers designed and synthesised a series of two-component D–A complexes that also differed in the number of face-to-face stacking interactions [64]. It was demonstrated that, in solution, the complexes all form with a 1:1 stoichiometry, as exemplified in Fig. 7a–c. The binding constant of the three complexes increases by two orders of magnitude (from approximately 130 to 11,000 M^{-1}) as the number of D–A interactions increases from two to three to four (Fig. 7).

In more recent work, Greenland, Colquhoun, Cardin and co-workers produced a supramolecular receptor that contains both D and A components: two pyrenyl residues and a single NDI residue (**4**, Fig. 8) [50]. The receptor was designed such that the separation of the pyrenyl resides is 7 Å, which allows formation of a 'tweezer'-like complex with the π-electron-deficient NDI residue of a second component. The solid-state structure of this system reveals that a dimeric complex is formed with a suprastructure reminiscent of a 'Roman handshake' (Fig. 4a). One-

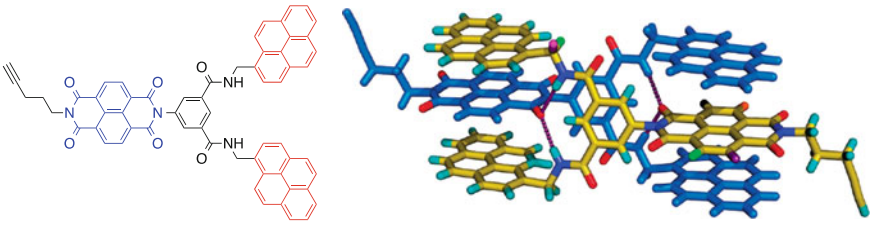

4 A

Fig. 8 *Left*: Chemical structure of the supramolecular motif (**4**) synthesized by Greenland et al. containing one acceptor and two donor residues. *Right*: Solid-state structure of this motif showing the interactions between two discrete molecules (*yellow* and *blue*) resulting in a highly stable ditopic structure **A** supported by four face-to-face π–π stacking interactions. (Image of **A** reprinted with permission from [50], Copyright 2013 RSC)

and two-dimensional ^{1}H NMR spectroscopic studies demonstrated that this highly ordered structure is maintained in solution. This complex, which is maintained by four complementary D–A interactions, exhibits a binding constant of around 10^{5} M^{-1}, showing the positive effect of an increasing the number of interactions on the associativity of these systems.

3 Supramolecular Polymers Maintained by D–A Interactions

Although the remainder of this review focuses on cross-linked polymers, there is a range of linear systems with complex topologies that have been produced from D–A based receptors. For example, there are several examples of 'polycatenane'-type materials, in which the monomeric components of a linear polymer are connected through mechanical rather than covalent bonds [66]. Several groups have produced high molecular weight linear polymers containing donor or acceptor residues in pendent side groups [67, 68] or in the main chain [69–73] that can change their conformations in solution in response to addition of an electronically complementary small molecule. However, these complex structures have yet to find application as high-strength responsive solid-state materials.

3.1 Chain-Folding, Healable Materials Containing D–A Interactions

Colquhoun, Hayes and co-workers designed a two-component responsive polymer blend harnessing the chain folding interactions that the group had investigated

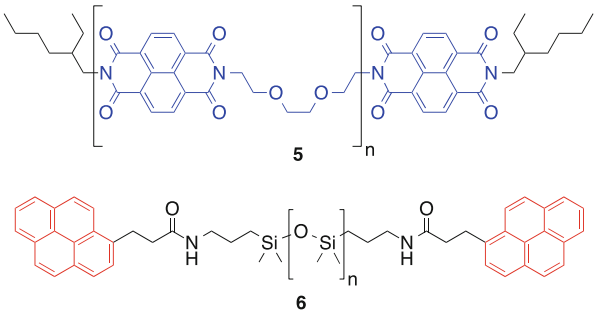

Fig. 9 Structures of the chain-folding polydiimide (**5**) and pyrenyl-terminated PDMS (**6**) synthesized by Colquhoun, Hayes and co-workers

previously (Fig. 7a–c) [74]. One of the components in the polymer blend was designed to contain multiple NDI residues, each separated by an ethylenedioxy-bisethylamine spacer unit. This spacer unit allows the diimide units to chain-fold around and encapsulate π-electron-rich pyrenyl residues, as observed in small-molecule studies. The targeted oligomer (**5**) was readily synthesised by condensation of 2,2′-(ethylenedioxy)-bis(ethylamine) and 1,4,5,8-naphthalenetetracarboxylic dianhydride. The molecular weight of **5** was limited by an end-capping monoamine residue, resulting in a powder-like, brittle polymer with number-average molecular weight (M_n) of 3,200 g mol^{-1} and polydispersity ($Đ$) of 2.30. A polymer containing electronically complementary donor end groups was synthesised by addition of pyrenyl, resulting in a commercially available amine-terminated poly(dimethyl siloxane) (PDMS, **6**) (Fig. 9).

Despite the low molecular weight of the diimide-containing oligomer (**5**), it could be calculated to contain approximately five chain-folding residues in the backbone. Thus, addition of the ditopic PDMS results in a supramolecularly cross-linked (rather than linear) material, because multiple pyrenyl residues can bind to each acceptor within a single oligomer of **5**. Attempts to cast films from just polydiimide **5** or PDSM **6** resulted in a tan powder and waxy solid, respectively. In contrast, peelable films could be cast from solution blends of these components, demonstrating the positive effect of creating supramolecular cross-linked systems on the mechanical properties.

The film produced from a blend of **5** and **6** was cut with a scalpel; the separated edges were then placed in close proximity and heated to approximately 90 °C. Visual observation of the material over this temperature ramp showed that the surface remained homogeneous. After cooling back to room temperature, the broken edges had re-engaged, and the material could again be peeled like a continuous polymer film (Fig. 10).

It was postulated that the observed healing occurred as a consequence of thermal energy disrupting the D–A stacking interactions. This results in a dramatic yet reversible change in the viscosity of the blend. The uncomplexed oligomers diffuse rapidly, bridging a fracture void, prior to re-establishing the complementary D–A interactions on cooling, thereby restoring the mechanical properties of the original, pristine material (Fig. 11).

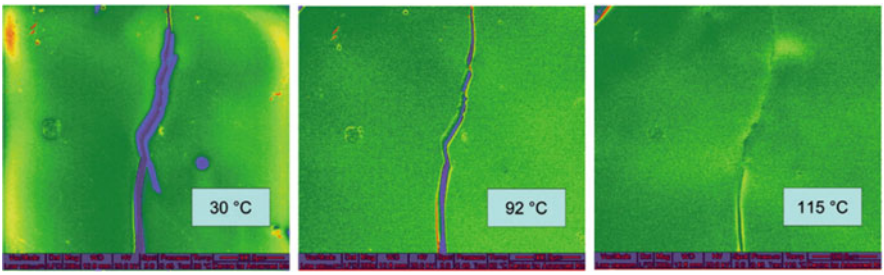

Fig. 10 Environmental scanning electron microscopic (ESEM) images of a film cast from **5** + **6** at various temperatures (magnification ×200). (Image reprinted with permission from [74], copyright 2009 RSC)

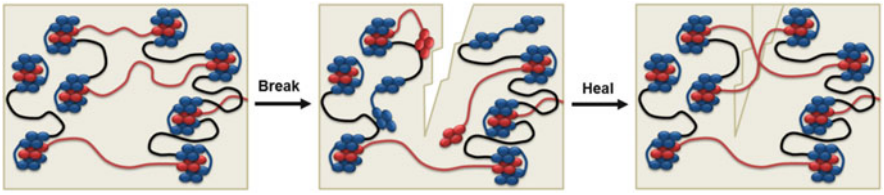

Fig. 11 Proposed healing mechanism for D–A supported blends of oligomers. (Adapted with permission from [78], copyright 2014 RSC)

3.2 Structural Optimisation of Chain-Folding, Healable Materials Containing D–A Interactions

A major design benefit of supramolecular materials is that the polymeric components of the material (e.g. the PMDS in **6**) can be changed to improve the mechanical performance of the materials. Provided that the D and A motifs of the supramolecular receptor are retained, the thermoresponsive nature of the materials (exhibited by healing in this case) are retained. This was realised in practice by introducing amine-terminated co-oligomers, termed 'Jeffamines™', into each of the polymers bearing the D and A residues. The result of this optimisation work was the generation of two new polymers (**7** and **8**, see Fig. 12) [75] that, when mixed, retain the ability to form a stable cross-linked network supported by D–A stacking interactions. The resulting material exhibits substantially better material properties than the materials containing the PDMS-derived oligomers (Fig. 9) (i.e., the tensile modulus of the pristine sample is 1 MPa at 30 °C).

Healing experiments were conducted on this structurally optimised film by cutting the sample with a scalpel, overlapping the cut edges and heating for varying periods of time at 50 °C. After heating for only 50 s, the overlapped region had fused and the tensile moduli of the healed material could be re-measured.

The ratio of a physical property of a pristine material to that of a corresponding healed sample gives an indication of the success of healing. When expressed in percentage terms, this ratio is termed the healing efficiency (η_{eff}) [18]. An η_{eff} value

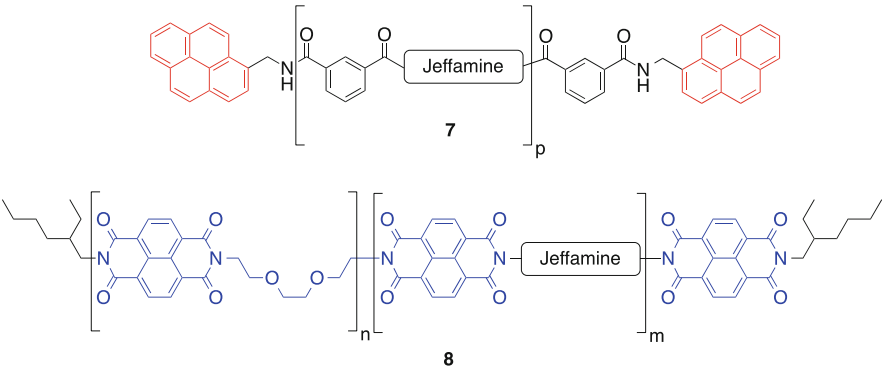

Fig. 12 Structures of the D- (**7**) and A- (**8**) containing components of a supramolecular polymer blend containing Jeffamine oligomers in the main chain produced by Colquhoun, Hayes and co-workers [75]

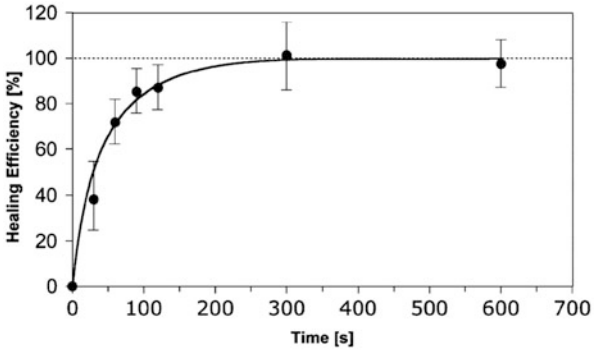

Fig. 13 Healing efficiency of the tensile modulus as a function of healing time at 50 °C for a supramolecular blend comprising **7** and **8.** (Reprinted with permission from [75], copyright 2009 RSC)

of 100 % indicates that the healed and pristine sample exhibit exactly the same physical property. For the polymer blend (**7** + **8**), η_{eff} of the tensile modulus increased from less than 40 % to 100 % over a period of approximately 5 min (Fig. 13). Additional experiments revealed that the material could be broken and re-healed multiple times, essentially without loss of its healing efficiency even if the broken edges of the sample were separated for 24 h before healing; this result is in stark contrast to healing polymers that employ hydrogen bonding as the self-assembly vehicle [76].

The supramolecular blend (**7** + **8**) was analysed by rheometry. A plot of the rheometric time–temperature shift factor, a_{T}, as a function of temperature shows a dramatic reduction of more that five orders of magnitude between 35 and 60 °C (Fig. 14). This can be compared with a typical thermoplastic (e.g. polystyrene [75]), which exhibits a reduction of a_{T} of only one order of magnitude over the same temperature range.

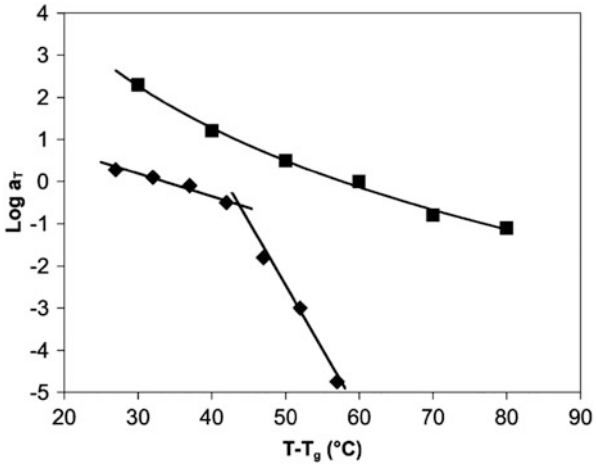

Fig. 14 Time–temperature superposition shift factor in rheology, a_T, as a function of temperature, normalised to T_g, for the supramolecular polymer blend **7** and **8** (*diamonds*) and linear polystyrene (*squares*). (Reprinted with permission from [75], copyright 2009 RSC)

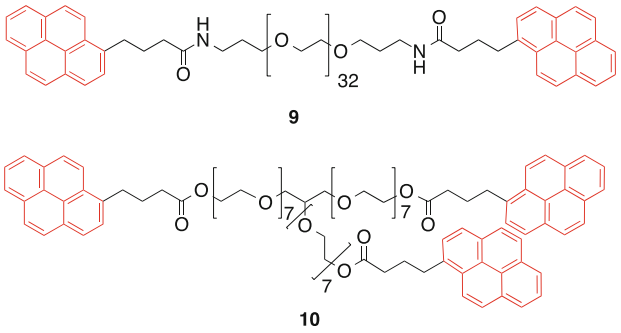

Fig. 15 Structures of PEG oligomers functionalised with either two (**9**) or three pyrenyl (**10**) residues, synthesised to assess the impact of cross-linking density on the thermoresponsive nature of D–A cross-linked materials

To investigate the effect of cross-linking density on the materials properties of supramolecular materials, two new polymer blends were produced containing PEG oligomers functionalised with either two (**9**) or three pyrenyl (**10**) residues (Fig. 15) [78].

The higher valency of **10** as compared with that of **9** acts to increase the potential density of cross-links within the network (Fig. 16). Blends of either of these new polymers with the diimide polymer **8** (Fig. 12) resulted in deep red elastomeric materials.

The effect of this increase in cross-linking density between blends containing either **9** or **10** with **8** was readily seen in the mechanical performance of the materials. The blend containing ditopic PEG **9** exhibited an extension at break of only 80 % and moduli of toughness of approximately just 1.5 MPa, whereas the

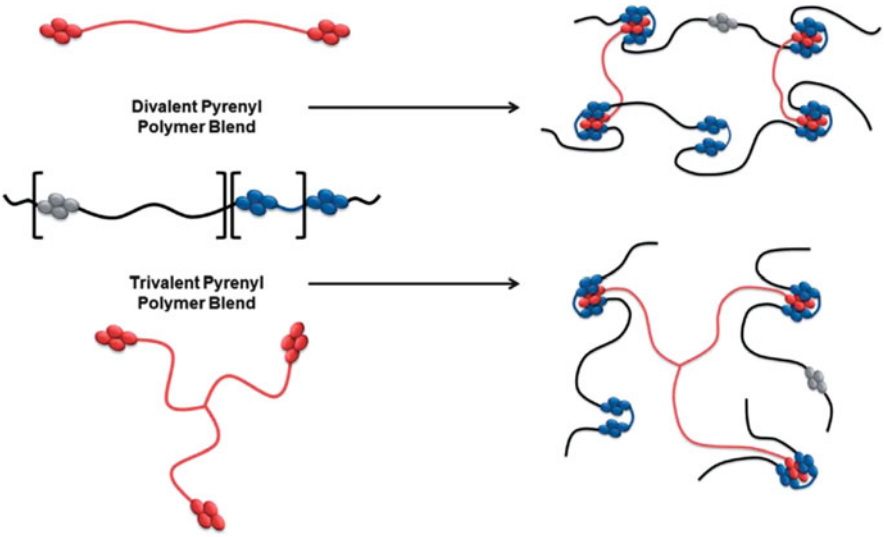

Fig. 16 Proposed cross-linked networks produced from mixing di- and tri-pyrenyl PEGs with chain-folding polymeric diimide **8**. (Reprinted with permission from [78], copyright 2014 RSC)

blend containing tritopic PEG **10** was extremely elastomeric, extending to over five times its original length prior to breaking, with a modulus of toughness of more than 22 MPa. Healing efficiencies were at least 90 % for both materials, although the materials possessing the higher cross-linking density required more forcing conditions (i.e. a higher temperature) to achieve satisfactory healing efficiencies.

3.3 Increasing the Strength of D–A Interactions within Supramolecular Materials: Effect on Materials Properties

The structure of the polymer main chains and supramolecular D–A motifs can be optimised independently. To demonstrate this feature, a pyrenyl-containing polymer was synthesised that contained tweezer-type dipyrenyl end groups (**11**, Fig. 17) [56]. Solution-state studies (Fig. 7b) predicted that these tweezer-type donor residues can interact with NDI-containing polymers through a highly organised interchelating complex that contains four face-to-face D–A interactions (Fig. 17). The successful synthesis of **11** permitted study of the impact of changing the supramolecular D–A interactions supporting the transiently cross-linked [29–31] network.

A blend of the tweezer-end-capped polymer with **8** exhibited essentially the same tensile modulus (1.8 MPa) as the analogous healable blend (1.2 MPa) supported by weaker interactions (**7** and **8**, Fig. 12). This finding confirms that the major contributing factor to the tensile modulus of the material is the nature of the

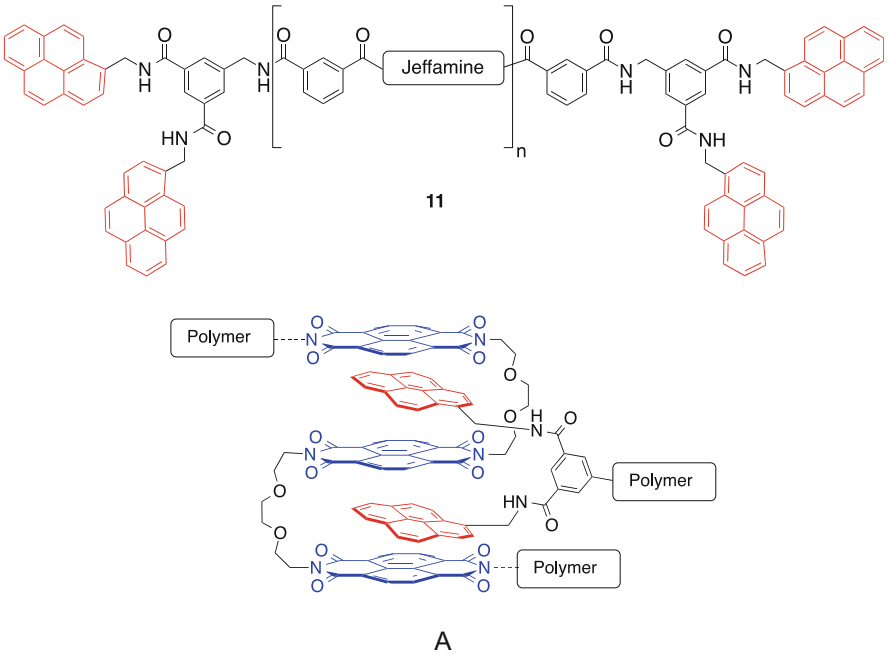

Fig. 17 *Top*: Structure of a Jeffamine-based polymer with pyrenyl-tweezer-type end groups (**11**). *Bottom*: Proposed interactions between polymers **11** and **8**, forming interchelating complex **A**

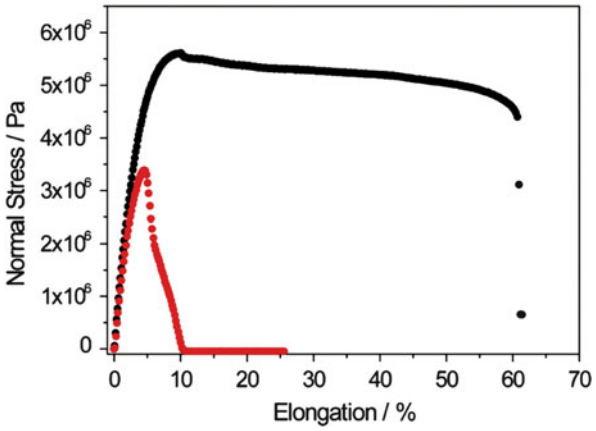

Fig. 18 Stress versus elongation plots for supramolecualr polymer blends containing polydiimide **8** (Fig. 12) and polymers containing either a single pyrenyl residue (**7**) (*red circles*), or dipyrenyl tweezer-type end groups (**11**, *black circles*). (Reprinted with permission from [56], copyright 2011 ACS)

covalent polymer's main chains. However, the material (**11** + **8**) with stronger supramolecular D–A interactions exhibited an elongation to break and an ultimate tensile strength that were approximately five and three times greater, respectively, than that of blend **7** + **8** (Fig. 18).

Increasing the strength of the supramolecular interactions between the components in the polymer blend increases the energy required to weaken the association between the polymers to facilitate healing. Significant healing of the film formed from **8** and **11** required longer heating times at higher temperatures (160 min at 140 °C) than the film comprising **7** and **8** (5 min at 50 °C).

3.4 *Healable Materials Containing D–A Interactions and Hydrogen Bonding*

Materials containing two distinct classes of supramolecular interactions, both D–A interactions and hydrogen bonding, have also been studied [81]. Such a material was produced by solution-casting of a pyrenyl-end-capped polyurethane, **12** (Fig. 19), with the chain-folding polydiimide **8** (Fig. 12). This approach produced a tough and elastic material that exhibited an elongation to break of up to 170 %. Over multiple healing experiments (240 min at 100 °C), the hydrogen-bonded material containing D–A interactions exhibited a healing efficiency of 95 % for its tensile modulus and 77 % for the modulus of toughness.

A plot of a_T as a function of temperature for the polymers **8** + **12** exhibits a drop in the shift factor of 14 orders of magnitude over a readily accessible temperature range (−10 to 110 °C), as expected for a system that changes its effective molecular weight with temperature (Fig. 20a). The supramolecular nature of the material was

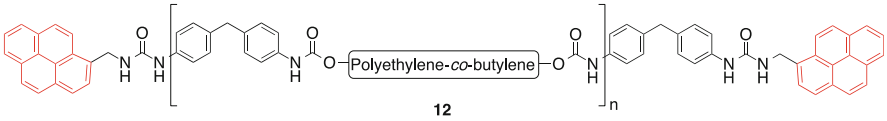

Fig. 19 Structure of a pyrenyl-end-capped polyureathane capable of forming D–A complexes with polydiimide **8**, along with hydrogen-bonded stacks in the solid state

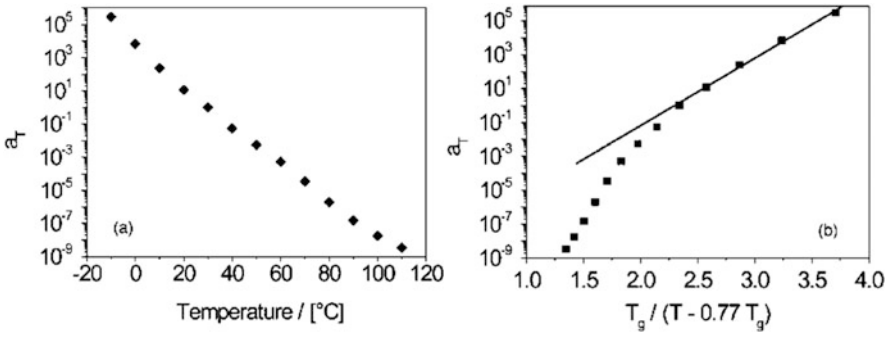

Fig. 20 Plots of the rheometric time–temperature shift factor a_T for the polymer **8** + **12** as a function of (**a**) temperature and (**b**) temperature normalised to T_g. (Reprinted with permission from [81], copyright 2010 ACS)

further confirmed by plotting a_T normalised to T_g, which greatly deviates from linearity (Fig. 20b) [82]. This is in stark contrast to linear amorphous polymers, which exhibit strictly linear relationships between these variables [79, 80].

This section has demonstrated the design and synthesis of supramolecular materials containing D–A interactions in which the molecular composition of the polymer blends has been iteratively optimised toward the end goal of producing tough healable materials. Rheological studies demonstrated the highly thermosensitive nature of the supramolecular cross-links, resulting in dramatic viscosity changes over small temperature ranges. This property of this type of supramolecular polymer blends opens up new applications that cannot be achieved by the current generation of covalent polymers. However, the systems reported to date are generally elastomeric, with T_g below room temperature. This renders these materials largely unsuitable for many high-value applications, for example, in complex structural assemblies for use in either the aerospace or automotive industries. Nevertheless, there is significant potential for their use in reversible adhesives or surface coatings.

3.5 Healable Supramolecular Polymer Nanocomposites with D–A Interactions in the Matrix Polymer

A frequently used methodology for improving the mechanical properties of polymeric materials is to produce composite systems by introducing a 'filler' component to the bulk matrix. The filler is typically a high-modulus material that forms a percolating network spanning the polymeric matrix, thereby greatly enhancing its properties.

Healable supramolecular polymer nanocomposites [83] were first reported by Fox and co-workers [84]. This material harnessed the supramolecular polymer containing **7** and **8** (Fig. 12). The filler component was cellulose nanocrystals (CNCs) extracted from small sea creatures known as turnicates. The CNCs from this bioresource are known to be extremely stiff, with a tensile strength of 140 GPa, and they possess a high aspect ratio (length/diameter ≈ 80). CNCs are widely used as a filler to improve the stiffness of a range of matrix polymers. During processing, the CNCs are dispersed in sulfuric acid, resulting in a high concentration of anionic sulfate groups on the surface. The success of CNCs in reinforcing a diverse range of polymers is a consequence of the strong hydrogen-bonding interactions between the nanocrystals (as detailed by Li and Liu in another chapter of this volume [85]). Maximising the number of hydrogen-bonding interactions drives the formation of a coherent percolating network of the filler, which carries stress through the material, thereby protecting the weaker matrix polymer.

Nanocomposites containing CNC filler loading levels of up to 20 wt% were prepared by film-casting **7** + **8** from a DMF suspension of CNCs. The tensile modulus was found to increase with increasing CNCs loading levels, ranging

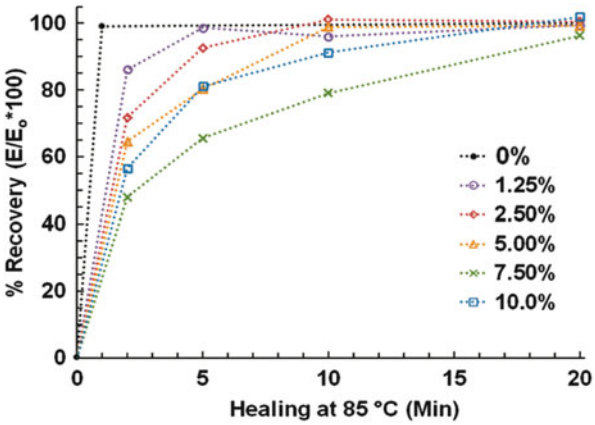

Fig. 21 Healing efficiency η_{eff} as a function of healing time for a series of D–A containing supramolecular materials with increasing loading levels of CNCs. (Reprinted with permission from [84], copyright 2012 ACS)

from 8 MPa to 261 MPa at 10 wt% of CNCs. For nanocomposites containing more than 10 % of CNCs, the materials properties were observed to become less favourable, suggesting phase separation of the CNCs from the matrix polymer. Phase separation results in regions with low CNC concentrations, where the weak polymer is exposed to stresses exerted on the material without any re-enforcing properties of the filler.

Healing experiments were conducted through established procedures: the sample was cut, edges overlapped and the sample heated to 80 °C for varying periods of time. All samples exhibited more than 90 % healing efficiency (η_{eff}) for their tensile moduli (Fig. 21), although the time required to reach this value increased from about 5 min (at 1.25 wt% of CNCs) to about 20 min (at 10 wt% of CNCs).

3.6 Supramolecular Molecular Nanocomposites with D–A Stacking Interactions Between the Filler and Matrix Polymer

For the supramolecular material containing CNCs outlined above, the interactions between the filler and polymer matrix were maintained through non-specific hydrogen bonding rather than designed D–A interactions. Hayes and co-workers designed a series of a nanocomposites containing gold nanoparticle (AuNP) fillers. AuNPs were selected because they can be readily functionalised with a range of thiol derivatives [86]. In these nanocomposites, the AuNPs were functionalised with donor pyrenyl residues (P-AuNPs, Fig. 22). Addition of a colloidal suspension of P-AuNPs to a solution of the chain-folding polydiimide **5** (Fig. 9) resulted in precipitation of a red solid, as the P-AuNPs formed nodes within a supramolecular network cross-linked through D–A interactions. Films cast from these components were extremely brittle, and tensile properties were not reported as a consequence.

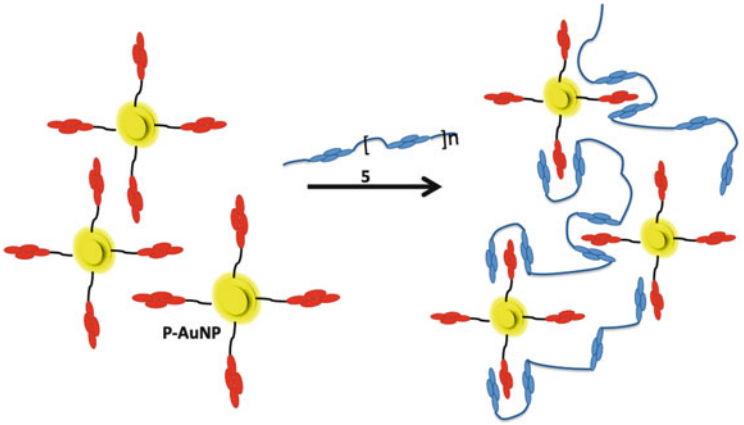

Fig. 22 Proposed cross-linked network produced through D–A interactions resulting from addition of P-AuNPs to the chain-folding polydiimide **5**

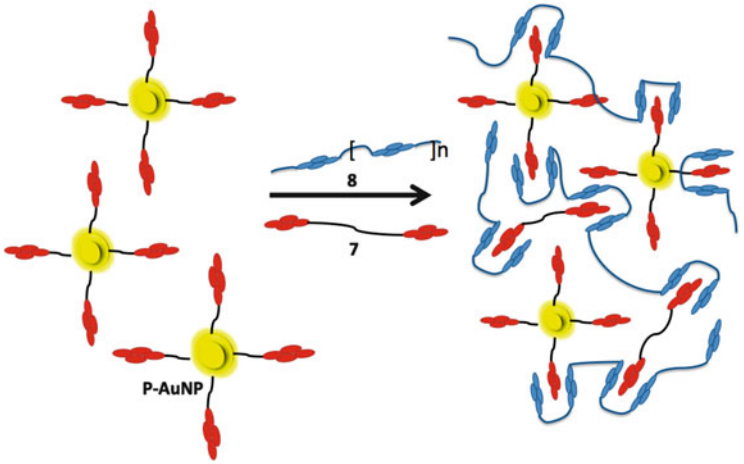

Fig. 23 Proposed network formed by addition of P-AuNPs to polymers **7** and **8** (see Fig. 12 for the structures of **7** and **8**)

To improve the mechanical properties of the nanoparticle-containing nanocomposite, a novel three-component blend was designed (Fig. 23) [87]. These materials contained P-AuNPs, a pyrenyl-containing polymer **7** (Fig. 12) and the chain-folding polydiimide **8**.

Nanocomposites containing P-AuNPs **7** and **8** exhibited increasing tensile moduli with increasing nanoparticle loading level (up to 15 wt% of P-AuNPs) (Fig. 24). Break-and-heal tests carried out on these samples showed that for all loading levels up to 10 wt% of P-AuNPs, highly efficient restoration of the tensile modulus was observed. The lack of healing exhibited by the samples with the highest loading

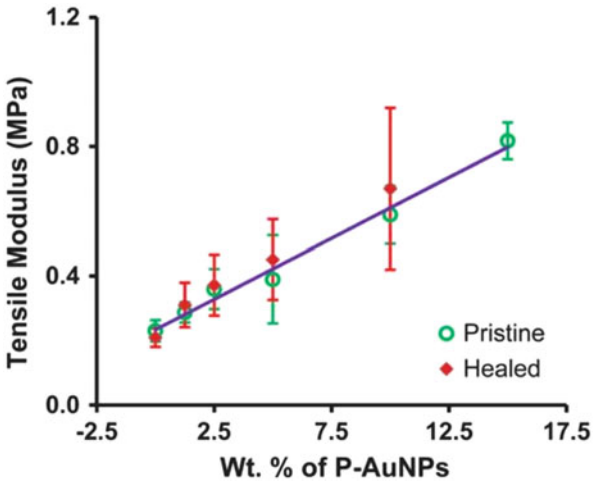

Fig. 24 Tensile moduli of pristine and healed samples of nanocomposites produced from P-AuNPs and polymers **7** and **8** with increasing levels of P-AuNP filler. (Reprinted with permission from [87], copyright 2013 RSC)

levels of P-AuNPs (15 wt%) implies that the polymer mobility might be decreased at higher filler loading levels.

To verify that the contribution of the additional D–A interactions between the pyrenyl residues on the P-AuNPs and the polymer were vital to achieving the observed increase in the mechanical performance of the materials, a nanocomposite containing Au-NPs that did not feature pyrenyl residues was produced. The tensile strength of this material was approximately half that of the analogous P-AuNP-containing material, thus confirming that the P-AuNP fillers do play a key role in network assembly.

4 Conclusions and Future Perspectives

Donor–acceptor interactions have become a powerful motif in supramolecular chemistry. Through understanding the fundamental interactions between highly characterised small-molecule systems, including infinite stacks of D–A residues, catenanes and rotaxanes, it became possible to build these supramolecular complexes into functional materials. The materials exhibit mechanical properties that can be varied in real time by external stimuli. This chapter has demonstrated how the reversible nature of D–A interactions has been used to construct healable materials with predictable properties that can be designed using a 'bottom-up' approach. Manipulation of the strength and cross-linking density of the D–A interactions at a molecular level results in predictable and measurable improvements in the tensile strength and modulus at a macroscopic level. We envisage that the use of D–A interactions will continue to find applications in various areas of materials chemistry, especially those that harness their electronic and photophysical properties.

References

1. Seiffert S, Sprakel J (2012) Chem Soc Rev 41:909
2. De Greef TFA, Smulders MMJ, Wolffs M, Schenning APHJ, Sijbesma RP, Meijer EW (2009) Chem Rev 109:5687
3. Brunsveld L, Folmer BJB, Meijer EW, Sijbesma RP (2001) Chem Rev 101:4071
4. Huang F, Scherman OA (2012) Chem Soc Rev 41:5879
5. Li S-Y, Xiao T, Lin C, Wang L (2012) Chem Soc Rev 41:5950
6. Beale TM, Chudzinski MG, Sarwar MG, Taylor MS (2013) Chem Soc Rev 42:1667
7. Kaliappan T, Kannan P (2000) Prog Polym Sci 25:343
8. Das A, Ghosh S (2014) Angew Chem Int Ed Engl 53:2038
9. Raymo FM, Stoddart JF (1999) Chem Rev 99:1643
10. Coskun A, Banaszak M, Astumian RD, Stoddart JF, Grzybowski BA (2012) Chem Soc Rev 41:19
11. Fox JD, Rowan SJ (2009) Macromolecules 42:6823
12. Yerushalmi R, Scherz A, van der Boom ME, Kraatz HB (2005) J Mater Chem 15:4480
13. Ariga K, Ito H, Hill JP, Tsukube H (2012) Chem Soc Rev 41:5800
14. van der Zwaag S (2007) Self healing materials: an alternative approach to 20 centuries of materials science. Springer, Dordrecht
15. Ghosh SK (2009) Self healing materials: fundamentals, design strategies and applications. Wiley-VCH, Weinheim
16. Wagg D, Bond I, Weaver P, Friswell M (2007) Adaptive structures: engineering applications. Wiley, Chichester
17. Hayes W, Greenland BW (2013) Healable polymer systems. Royal Society of Chemistry, Cambridge
18. Burattini S, Greenland BW, Chappell D, Colquhoun HM, Hayes W (2010) Chem Soc Rev 39:1973
19. Wu DY, Meure S, Solomon D (2008) Prog Polym Sci 33:479
20. Bergman SD, Wudl F (2008) J Mater Chem 18:41
21. Urban MW (2009) Prog Polym Sci 34:679
22. Wool RP (2008) Soft Matter 4:400
23. Syrett JA, Becer CR, Haddleton DM (2010) Polym Chem 1:978
24. Yang Y, Urban MW (2013) Chem Soc Rev 42:7446
25. Behl M, Lendlein A (2007) Mater Today 10:20
26. Liu C, Qin H, Mather PT (2007) J Mater Chem 17:1543
27. Ratna D, Karger-Kocsis J (2008) J Mater Sci 43:254
28. Meng H, Li G (2013) Polymer 54:2199
29. Rossow T, Habicht A, Seiffert S (2014) Macromolecules 47:6473
30. Rossow T, Seiffert S (2014) Polym Chem 5:3018
31. Hackelbusch S, Rossow T, van Assenbergh P, Seiffert S (2013) Macromolecules 46:6273
32. Park JS, Yoon KY, Kim DS, Lynch VM, Bielawski CW, Johnston KP, Sessler JL (2011) Proc Natl Acad Sci USA 108:20913
33. Wang C, Yin S, Chen S, Xu H, Wang Z, Zhang X (2008) Angew Chem Int Ed 47:9049
34. Molla MR, Ghosh S (2012) Chem Eur J 18:9860
35. Maitra U, Kumar PV, Chandra N, D'Souza LJ, Prasanna MD, Raju AR (1999) Chem Commun 1999(7):595
36. Moffat JR, Smith DK (2008) Chem Commun 2008(19):2248
37. Das A, Molla MR, Banerjee A, Paul A, Ghosh S (2011) Chem Eur J 17:6061
38. Das A, Molla MR, Maity B, Koley D, Ghosh S (2012) Chem Eur J 18:9849
39. Foster R (1969) Organic charge transfer complexes. Academic, London, pp 33–93
40. Briegleb G (1961) Elektronen-Donor-Acceptor-Komplexe. Springer, Berlin
41. Hunter CA, Sanders JKM (1990) J Am Chem Soc 112:5525

42. Colquhoun HM, Goodings EP, Maud JM, Stoddart JF, Wolstenholme JB, Williams DJ (1985) J Chem Soc Perkin Trans 2 5:607
43. Ray A (1971) J Am Chem Soc 93:7146
44. Bruneau E, Lavabre D, Levy G, Micheau JC (1992) J Chem Educ 69:833
45. Zych AJ, Iverson BL (2000) J Am Chem Soc 122:8898
46. Colquhoun HM, Zhu Z (2002) J Am Chem Soc 124:13346
47. Biedermann F, Scherman OA (2012) J Phys Chem B 116:2842
48. Biedermann F, Uzunova VD, Scherman OA, Nau WM, De Simone A (2012) J Am Chem Soc 134:15318
49. Gabriel GJ, Sorey S, Iverson BL (2005) J Am Chem Soc 127:2637
50. Greenland BW, Bird MB, Burattini S, Cramer R, O'Reilly RK, Patterson JP, Hayes W, Cardin CJ, Colquhoun HM (2013) Chem Commun 49:454
51. Ciferri A (2000) Supramolecular polymers. Marcel Dekker, New York
52. Sijbesma RP, Beijer FH, Brunsveld L, Folmer BJB, Hirschberg JHKK, Lange RFM, Lowe JKL, Meijer EW (1997) Science 278:1601
53. Biedermann F, Vendruscolo M, Sherman OA, De Simone A, Mau WM (2013) J Am Chem Soc 135:14879
54. Sivakova S, Bohnsack DA, Mackay ME, Suwanmala P, Rowan SJ (2005) J Am Chem Soc 127:18202
55. Woodward PJ, Hermida Marino D, Greenland BW, Hamley IW, Light Z, Slark AT, Hayes W (2010) Macromolecules 43:2512
56. Burattini S, Greenland BW, Hayes W, Mackay ME, Rowan SJ, Colquhoun HM (2011) Chem Mater 23:6
57. Stoddart JF, Colquhoun HM (2008) Tetrahedron 64:8231
58. Niu Z, Huang F, Gibson HW (2011) J Am Chem Soc 133:2836
59. Huang F, Fronczek FR, Gibson HW (2003) Chem Commun 2003(13):1480
60. Huang F, Lam M, Mahan EJ, Rheingold AL, Gibson HW (2005) Chem Commun 2005 (26):3268
61. Ashton PR, Philp D, Spencer N, Stoddart JF, Williams DJ (1994) Chem Commun 1994(2):181
62. Ashton PR, Odell B, Reddington MV, Slawin AMZ, Stoddart JF, Williams DJ (1988) Angew Chem Int Ed Engl 27:1550
63. Odell B, Reddington MV, Slawin AMZ, Spencer N, Stoddart JF, Williams DJ (1988) Angew Chem Int Ed Engl 27:1547
64. Greenland BW, Burattini S, Hayes W, Colquhoun HM (2008) Tetrahedron 64:8346
65. Gabriel GJ, Iverson BL (2002) J Am Chem Soc 124:15174
66. Fang L, Olson MA, Benitez D, Tkatchouk E, Goddard WA III, Stoddart JF (2010) Chem Soc Rev 39:17
67. Ilhan F, Gray M, Blanchette K, Rotello VM (1999) Macromolecules 32:6159
68. Burattini S, Colquhoun HM, Greenland BW, Hayes W, Wade M (2009) Macromol Rapid Commun 30:459
69. Colquhoun HM, Zhu Z (2004) Angew Chem Int Ed 43:5040
70. Colquhoun HM, Zhu Z, Cardin CJ, Gan Y (2004) Chem Commun 2004(23):2650
71. Colquhoun HM, Zhu Z, Cardin CJ, Gan Y, Drew MGB (2007) J Am Chem Soc 129:16163
72. Colquhoun HM, Zhu Z, Cardin CJ, Drew MGB, Gan Y (2009) Faraday Discuss 143:205
73. Zhu Z, Cardin CJ, Gan Y, Colquhoun HM (2010) Nat Chem 2:653
74. Burattini S, Colquhoun HM, Greenland BW, Hayes W (2009) Faraday Discuss 143:251
75. Burattini S, Colquhoun HM, Fox JD, Friedmann D, Greenland BW, Harris PJF, Hayes W, Mackay ME, Rowan SJ (2009) Chem Commun 2009(44):6717
76. Cordier P, Tournilhac F, Soulié-Ziakovic C, Leibler L, Soulie C (2008) Nature 451:977
77. Onogi S, Masuda T, Keishi K (1970) Macromolecules 3:109
78. Hart LR, Hunter JH, Nguyen NA, Harries JL, Greenland BW, Mackay ME, Colquhoun HM, Hayes W (2014) Polym Chem 5:3680
79. Liu C-Y, He J, Keunings R, Bailly C (2006) Macromolecules 39:8867

80. Liu C-Y, Halasa AF, Keunings R, Bailly C (2006) Macromolecules 39:7415
81. Burattini S, Greenland BW, Merino DH, Weng W, Seppala J, Colquhoun HM, Hayes W, Mackay ME, Hamley IW, Rowan SJ (2010) J Am Chem Soc 132:12051
82. Stadler FJ, Pyckhout-Hintzen W, Schumers JM, Fustin CA, Gohy JF, Bailly C (2009) Macromolecules 42:6181
83. Vaiyapuri R, Greenland BW, Colquhoun HM, Elliott JM, Hayes W (2014) Polym Int 63:933
84. Fox JD, Wei JJ, Greenland BW, Burattini S, Hayes W, Colquhoun HM, Mackay ME, Rowan SJ (2012) J Am Chem Soc 134:5362
85. Li P, Liu R (2015) Cellulose gels and microgels – synthesis, service, and supramolecular interactions. In: Seiffert S (ed) Supramolecular polymer networks, Advances in Polymer Science. Springer, Cham
86. Vaiyapuri R, Greenland BW, Rowan SJ, Colquhoun HM, Elliott JM, Hayes W (2012) Macromolecules 45:5567
87. Vaiyapuri R, Greenland BW, Rowan SJ, Colquhoun HM, Elliott JM, Hayes W (2013) Polym Chem 4:4902

Supramolecular Nanofibrillar Polymer Hydrogels

Mokit Chau, Shivanthi Easwari Sriskandha, Héloïse Thérien-Aubin, and Eugenia Kumacheva

Contents

Abstract Nanofibrillar supramolecular hydrogels are hierarchical structures formed by physical association of high-aspect-ratio nanoscale building blocks, each containing many molecules held together via supramolecular interactions. Nanofibrils have diameters in the range of tens to hundreds of nanometers, and their lengths can exceed micrometers. The driving forces involved in the formation

M. Chau • S.E. Sriskandha • H. Thérien-Aubin
Department of Chemistry, University of Toronto, Toronto, ON, Canada, M5S 3H6

E. Kumacheva (✉)
Department of Chemistry, University of Toronto, Toronto, ON, Canada, M5S 3H6

Institute of Biomaterials and Biomedical Engineering, University of Toronto, 164 College Street, Toronto, ON, Canada, M5S 3G9
e-mail: ekumache@chem.utoronto.ca

© Springer International Publishing Switzerland 2015

S. Seiffert (ed.), *Supramolecular Polymer Networks and Gels*, Advances in Polymer Science 268, DOI 10.1007/978-3-319-15404-6_5

of nanofibrillar structures include hydrogen bonding, hydrophobic forces, forces of electrostatic origin, and guest–host interactions. Nanofibrillar hydrogels are formed by biopolymers such as proteins and polysaccharides, and by synthetic supramolecular units such as cylindrical micelles of block copolymers and peptide amphiphiles. In the present review, we discuss the hierarchical assembly of nanofibrillar hydrogels, give examples of hydrogels formed by the most important groups of polymers, discuss structure–property relationships of these nanofibrillar hydrogels, and review their current and potential applications in the fields of bioengineering, cell biology, medicine, and cosmetics.

Keywords Supramolecular hydrogels • Nanofibers • One-dimensional objects • Self-assembly • Biopolymers • Biomaterials

1 Introduction

Hydrogels are networks e.g., polymer networks, swollen with water [1, 2]. A polymer network can be formed by irreversible covalent cross-linking or by reversible physical cross-linking [3] via hydrogen bonding, hydrophobic forces, electrostatic interactions, or host–guest interactions [4]. The "building blocks" of hydrogels can be individual molecules or supramolecular objects comprising many molecules. In the latter case, gelation can occur by association of shape-isotropic molecular aggregates such as spherical micelles [5] or shape-anisotropic supramolecular species such as high-aspect-ratio nanofibrils [6, 7]. A great number of hydrogels composed of biological polymers, including proteins and polysaccharides, are formed by reversible physical association of nanofibrillar building blocks, also called strands or filaments [8]. The nanofibrillar nature of these hydrogels is crucial to their mechanical properties, structure, and biological activity, as in the case of extracellular matrices, the cellular cytoskeleton, axons, and dendrites [9]. The unique properties and broad range of applications of naturally derived supramolecular nanofibrillar hydrogels have motivated the design of their synthetic analogues, that is, hydrogels formed by wormlike block copolymer micelles [10] and amphiphilic peptides [11].

Nanofibrillar dimensions depend on the type of constituent polymer, but typically their diameter is in the order of tens of nanometers. The length of nanofibrils can vary from hundreds of nanometers to micrometers. Generally, hydrogel formation is a hierarchical multistep process that begins with the association of individual molecules into discrete high-aspect-ratio supramolecular structures that then associate to form larger nanofibrils and subsequently develop into a three-dimensional (3D) network (Fig. 1). All these steps can be controlled thermodynamically and kinetically, yielding hydrogels with a broad range of structures. Association of nanofibrils into a 3D network can be triggered by changes in temperature, increase in polymer concentration, increase in ionic strength, or by the addition of ions charged oppositely to the nanofibrils. Hydrogels can also be formed by

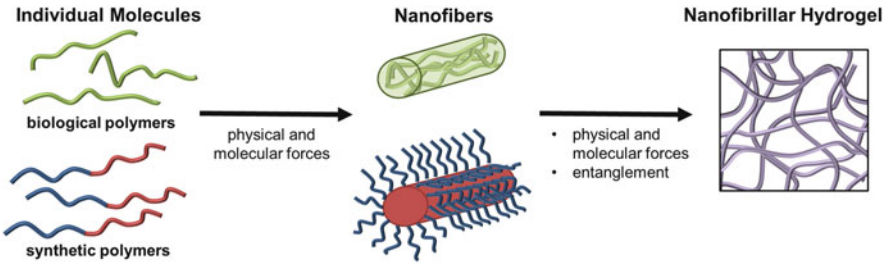

Fig. 1 Hierarchical assembly of nanofibrillar hydrogels. Individual molecules organize into nanofibrils, which subsequently associate and/or entangle to form a 3D water-swollen network. Biopolymer molecules are often oriented parallel to the long axis of the nanofibril, whereas synthetic polymer chains are oriented perpendicularly to the main axis. Gelation can be triggered by changes in temperature and pH, an increase in polymer concentration, or an increase in ionic strength of the polymer solution, to name a few

entanglement of nanofibrils. This mechanism is especially important for synthetic nanofibrillar hydrogels formed by wormlike micelles of block copolymers.

First and foremost, studies of on nanofibrillar hydrogels are greatly motivated by their biological relevance [9, 12]. For example, the biophysical properties of filamentous collagenous hydrogels affect interactions between cells and their extracellular matrix [13, 14], while the mechanical properties of fibrin gels influence the obstruction of blood vessels with blood clots [15]. Fundamental and applied studies of nanofibrillar hydrogels are needed to further develop existing and potential novel applications of man-made nanofibrillar gels such as scaffolds in tissue engineering [16], artificial extracellular matrices for cell encapsulation [17, 18], and cargo carriers in pharmaceutics and cosmetics [19–23]. Second, current interest in intelligent soft materials also embraces the field of nanofibrillar hydrogels. Due to the hierarchical nature of such gels, they demonstrate an interesting stimulus-responsive behavior, that is, a reversible, stimulus-mediated sol–gel transition [10]. Third, natural resources such as algae [24–26], wood [27, 28], and chitin [29] offer vast, cost-efficient and green materials for producing gel-forming nanofibrils (e.g., cellulose nanofibrils, alginate, and agarose). Alternatively, recent progress in the design and self-assembly of synthetic supramolecular structures [30, 31] can greatly benefit the field of synthetic nanofibrillar hydrogels. Fourth, there are a variety of methods to shape nanofibrillar gels into useful morphologies. In the past decade, microfluidic generation of micrometer-size hydrogel modules was used to make vast combinatorial libraries of instructive extracellular matrixes or as building blocks in tissue engineering and drug delivery [32].

This article provides an overview of the recent progress in fundamental studies, preparation, characterization, and application of nanofibrillar hydrogels formed by physical (noncovalent) cross-linking of one-dimensional (1D) supramolecular building blocks of synthetic and biological polymers. High-aspect-ratio nanofibrils, as focused on in the present review, are formed by autonomous association (self-assembly) of individual molecules and not by their forced fabrication (directed

assembly) such as achieved by electrospinning [33, 34]. Hydrogels formed by the assembly of individual polymer molecules as opposed to nanofibrillar building blocks [35] or by association of supramolecular species of nonpolymeric origin [36, 37] are not included in this review. We focus on hydrogels formed by nanoscopic supramolecular building blocks. Thus, hydrogels formed from microfibers [2, 38–41] are not discussed.

The present review has the following structure. Following this introductory section, we concisely discuss the forces involved in the formation of nanofibrillar gels in Sect. 2. In Sect. 3, we review some recent progress in the fundamental studies and applications of nanofibrillar hydrogels formed by the most important biological, synthetic, and composite polymers. Section 4 discusses some structure–property relationships of nanofibrillar hydrogels. Applications of nanofibrillar hydrogels are reviewed in Sect. 5. Section 6 summarizes current trends and future directions in fundamental studies and applications of nanofibrillar gels.

2 Driving Forces for the Formation of Nanofibrillar Hydrogel Networks

The assembly of nanofibrillar hydrogels involves the formation of fibers by association of individual polymer chains into nanofibrils, which are physically crosslinked and/or entangled into a water-swollen network (Fig. 1). The process of network formation is polymer-specific, can involve different mechanisms, and can be governed by different forces that depend on the chemical composition of the building blocks and the gelation conditions.

2.1 Formation of Nanofibrils from Polymer Molecules

The driving force for the molecular assembly of polymeric molecules into 1D fiber-like objects stems from a fine balance between the entropic cost of forming ordered supramolecular structures with reduced flexibility and the enthalpic gain resulting from intermolecular interactions [8]. Inter- and intrachain hydrogen bonding is by far the most important driving force for the association of biopolymer chains and the stabilization of fibrils in aqueous media.

In natural systems, biopolymers are the building blocks of nanofibrillar materials. Proteins and polysaccharides often form double and triple helices that are the origin of the fibrillar structure. The inclusion of rigid repeating units in the polymer backbone dictates the helical structure. These rigid units control the torsion angles within the helical structures. For instance, in collagen, these repeat units are proline and hydroxyproline residues [42], whereas anhydrogalactose cages are the monomeric units in agarose and κ- and ι-carrageenans [43].

In the case of synthetic hydrogels formed by long wormlike micelles of block copolymers [44] or fiber-like structures of short amphiphilic peptides [45], hydrophobic forces govern the association of hydrophobic blocks in an aqueous environment, in order to minimize the surface energy of the system. The segregated hydrophobic blocks form the core of the wormlike micelle, resulting in 1D supramolecular aggregates that have enhanced stability in water in comparison with the original molecules [46]. The self-assembly of fiber-like structures can be fine-tuned by varying, for example, the copolymer composition and concentration [46]. During the assembly of peptide amphiphiles, the formation of β-sheets in the peptide region of the molecule is crucial to the creation of fiber-like supramolecular structures [47].

Formation of nanofibrils may be a several-step process, in which smaller fibrils associate into larger gel-forming nanofibers. Sometimes, the fibril elongation step is referred to as 'polymerization', analogous to the polymerization of monomer molecules in polymer chemistry. For example, fibrils of type 1 collagen elongate when triple helices assemble side-by-side in a staggered fashion, thereby leading to the formation of nanofibrils with a width of ~500 nm and a length of up to several micrometers [48]. In a similar process, fibrin lengthens to form 200–300 nm-thick nanofibers via lateral aggregation of protofibrils [49]. The formation of longer nanofibrils may be crucial for gelation if the network is formed by entanglement.

2.2 Formation of a Nanofibrillar Network

Nanofibrils assemble into supramolecular gels by association, branching, or entanglement. During assembly, the enthalpic gain associated with the formation of a network should exceed the entropic loss that takes place due to gelation. Noncovalent bonds responsible for the formation of a network structure are formed due to hydrogen bonding, electrostatic attraction, hydrophobic interactions, or guest–host interactions. In certain cases, the type of functional groups on the surface of individual nanofibrils determines whether a nanofibrillar network is formed, as observed for different types of carrageenan. Nanofibrillar networks can also be created by bundling and twisting of individual nanofibrils [26]. For example, agarose helices form kinks due to interruption of the helical structure by irregularities in the agarose molecule [50]. At a sufficiently high concentration of nanofibrils, gelation can also occur by entanglement of nanofibrillar building blocks [51].

To achieve gelation instead of uncontrolled aggregation and precipitation, a balance needs to be maintained between attractive forces that lead to network formation and hydrophilic forces that solvate the nanofibrils. To generate a hydrated, non-collapsed nanofibrillar network, the nanofibrils should either be stabilized by sufficient swelling and electrostatic repulsion or they must contain interconnected regions with conformational disorder that increase the entropy of the system. The coexistence of 'soluble' and 'insoluble' regions within the nanofibrils makes the nanofibrillar network stable and swollen.

3 Examples of Nanofibrillar Hydrogels Formed by Biopolymers and Synthetic Polymers

3.1 Biopolymer Hydrogels

3.1.1 Proteinaceous Hydrogels

Collagen Collagen is the most abundant protein in the mammalian extracellular matrix [42]. It provides mechanical function to tissues, as well as structural support and biochemical instruction to cells within connective, epithelial, skin, cardiac, and muscular tissues [52]. There are 27 different types of collagen, seven of which are classified as "fibrillar" [53]. For brevity, the present review focuses on fibril-forming type I collagen found in dermis, bones, tendons, and ligaments [42]. The nanofibrillar structure of collagen imparts to tissues viscoelasticity and resistance to tensile load at large strains [54, 55].

As shown in Fig. 2a, gel-forming collagen nanofibrils are hierarchically assembled. The primary building blocks are collagen molecules containing repeating units of XaaYaaGly, where Xaa and Yaa are commonly proline (Pro) and hydroxyproline (Hyp) [42]. Under appropriate conditions, collagen molecules organize into a right-handed triple-helix (tropocollagens) that is composed of three left-handed polyproline II helices [42]. Tropocollagens are stabilized by interstrand hydrogen bonding between the amides along the backbone of the three protein strands, where N–H(Gly). . .O=C(Xaa). Tropocollagens in type 1 collagen are $<$2 nm in diameter and ~300 nm in length. They further assemble laterally in a staggered fashion into nanofibrils of up to 500 nm in diameter and up to 1 cm in length, with a 64 nm D-periodicity (Fig. 2a) [59]. Tropocollagen are held to each other by interhelical water bridges with no direct contact between the triple helices [60]. Gelation of nanofibrillar collagen gels in vitro can be formed by adjusting the pH, temperature, and ionic strength of the solution [55]. Generally, an acid-soluble collagen solution is neutralized and warmed to 30–34 °C to induce fibrillogenesis and gelation [55, 61]. The gel network is formed by entanglement of nanofibrils, as well as by hydrophobic and electrostatic attraction forces [62].

Nanofibrillar collagen gels show a complex response to deformation. Figure 2b shows a representative stress–strain curve for collagen type 1 hydrogel matrices under tensile deformation in physiological conditions [56]. The toe region (defined as the region between zero strain and the intersection of linear fit and strain axis) corresponds to the straightening of crimps in the fibrils due to the flexibility of the fibers and the presence of nonhelical telomeric regions on the molecular level [63]. In the linear region, an increase in the Young's modulus of the gel is associated with stretching the collagen triple helices and with sliding of the collagen molecules past each other [54, 64]. At even higher strain, disruption of the fibrillar structure results in failure of the gel.

Variation of the mechanical properties of nanofibrillar collagen type 1 gels, in conjunction with changes in their structure, can be achieved by varying the

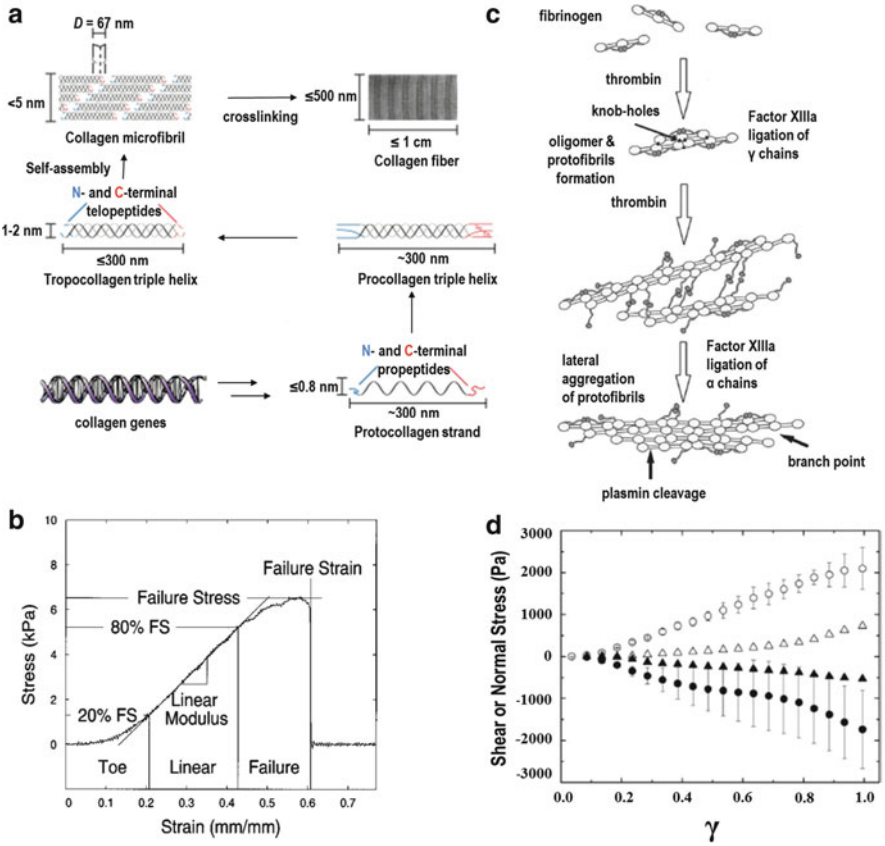

Fig. 2 Nanofiber composition and properties of proteinaceous hydrogels. (**a**) The biosynthetic route to collagen fibers. Reproduced, with permission, from [42]. Copyright 2009 Annual Reviews. (**b**) Representative stress–strain curve of the collagen matrix hydrogel (polymer content 2 g L^{-1}, pH 7.4) tested at a strain rate of 38.5 % per minute. The stress–strain curve is separated into three distinct regions designated *toe*, *linear*, and *failure*. Adapted, with permission, from [56]. Copyright 2002 American Society of Mechanical Engineers. (**c**) Fibrin polymerization from fibrinogen monomers. Reproduced, with permission, from [57]. Copyright 2005 Elsevier. (**d**) Shear (open symbols) and normal (closed symbols) stresses plotted against increasing strain for a 2.5 g L^{-1} fibrin gel at pH 7.4 (*circles*) and pH 8.5 (*triangles*). Reproduced, with permission, from [58]. Copyright 2009 American Chemical Society

concentration of collagen in the precursor solution. An increase in collagen concentration affects the fibril density and results in a higher linear elastic modulus and increase in failure stress, while the diameter of the nanofibrils remains similar to the fibril diameters of intact tissue [56].

As a result of the transient nature of entanglements in nanofibrillar collagen gels, they exhibit a reversible shear thinning effect. However, for controlled drug release applications, nonfibrillar rather than fibrillar collagen gels may be preferred, due a smaller mesh size in nonfibrillar gels [62]. Fibrillar collagen gels have mesh sizes in

the order of microns [65], whereas nonfibrillar gels may have mesh sizes of 4–30 nm [62]. Drug molecules with dimensions of 0.5–1.5 nm do not experience hindered diffusion in the large pores of nanofibrillar collagen. Nanofibrillated collagen gels have also been used as scaffolds for tissue engineering [12, 16, 66–68].

Actin Muscle proteins comprise 15–22 % of the total muscle weight in humans [69]. They are categorized into three groups: sarcoplasmic or water-soluble proteins, myofibrillar or salt-soluble proteins, and insoluble stromal proteins [69]. Apart from its presence in myofibrillar muscle proteins, actin is also a major structural component of the cytoskeleton, which is an interconnected network of polymerized protein filaments. Structural units of myofibrils are F-actins, 6–8 nm diameter filaments composed of polymerized actin proteins [69, 70]. Monomeric globular actin, or G-actin, self-assembles into double helical filaments of F-actin that are 7–8 nm in diameter and up to several microns in length [71]. The G-actin monomer is flat, with two similar major domains (outer and inner) with an adenosine triphosphate or adenosine diphosphate unit located between them [72]. The self-assembly of F-actin occurs through nucleation, polymerization, and depolymerization [73]. It is thought that a minimum of three G-actin monomers are required for nucleation, which is followed by elongation at the barbed end of the filaments and shorting at the pointed end of the filaments through its disassembly into G-actin monomers [71]. The barbed and pointed ends are so named due to the shape of the filament ends. The helical structure of F-actin was found to have 13 actin molecules per six left-handed turns and a helical pitch of ~38 nm [74, 75]. Recently, it was proposed that the transition from G- to F-actin involves a 20° rotation of the outer domain with respect to the inner domain about a rotation axis approximately perpendicular to the helix axis [72, 76].

The assembly of F-actin filaments into stable networks and dynamic bundles (essential for myosin-based motility) is mediated by cross-linking agents such as α-actinin or actin-binding proteins such as fascin, fimbrin, and filamin [71, 77]. Even in the absence of any cross-linking proteins, nanofibrils of F-actin can associate with each other to form gels [78, 79].

Purified F-actin assembles into long filaments that overlap at random angles in the range from 0° to 90° [80]. In the presence of actin-binding proteins, F-actin forms an isotropic network of short, straight filaments that branch at 90° angles to one another [80]. High magnification electron micrographs reveal two types of filament intersections, either X- or T-shaped [81]. The distance between the branching points is inversely related to the molar ratio of actin-binding protein to actin. Thus, the rigidity of the gel increases when actin-binding protein is added [80].

Filamentous F-actin gels show viscoelastic properties with an average elastic shear modulus in the range of 20–420 Pa [78]. The modulus depends strongly on the length of the filaments and the history of sample preparation, such as the mechanical disruption of actin nanofibrils prior to or during the deformation. Fluorescence microscopy experiments confirmed that applying small shear stresses to F-actin can

orient and rupture the filaments [78]. With the addition of actin-binding protein, the gel becomes more resistant to stress deformation. In addition, higher concentrations of actin ($\geq$4 g L^{-1}) are needed to form networks that cease flow under stress [80]. These findings confirm that networks of isotropic F-actin filaments are strong enough to stabilize cells [78].

Actin gels have applications as scaffolds for cell encapsulation or 3D tissue growth. In one example, an isotropic gel was formed through bundling and subsequent aggregation of F-actin and α-actinin. A structured protein skin layer formed at the interface between the gel and the surrounding buffer [82]. In another application, an adenosine 5′-triphosphate-fueled gel machine was prepared from an actin–poly(L-lysine) complex cross-linked with the enzyme transglutaminase. The resulting actin gel moved with an average velocity of 1 μm s^{-1} (almost equivalent to native F-actins) over an oriented and covalently cross-linked myosin gel. Potential applications involving the use of gels with autonomous motion include artificial muscles or biomimetic robots [83].

Fibrin Fibrinogen is a centrosymmetric high molecular weight protein with length of ~46 nm and diameter of 3–5 nm [49]. The fibrinogen molecule is composed of a central globular E-region that is connected by coiled-coil chains (α-helices wound around each other) to two globular D-regions at each end. An enzyme thrombin cleaves a pair of small peptides (called fibrinopeptides A) from the central E-region, thereby uncovering two A-sites, thereby producing fibrin molecules, which bind to a complementary exposed A-site in the D-region of another fibrin molecule, as shown in Fig. 2c [84]. In essence, the A-sites form positively charged "knobs" that electrostatically interact with the negatively charged "holes" (exposed Gly-Pro-Arg peptide units) that are located near the ends of another fibrin molecule, although hydrogen bonding is also involved [85]. This process leads to the formation of protofibrils with a staggered structure, which are reinforced by a transglutaminate blood clotting factor (factor XIII) and cross-linked before their lateral association (Fig. 2c) [86]. These protofibrils repeat axially every 22.5 nm, or about half the molecular length of fibrinogen, thereby yielding a half-staggered structure [57, 87]. Once the protofibrils reach the length of 600–800 nm, they undergo lateral aggregation to form 200–300 nm-thick nanofibers [49, 57]. Further lateral growth of the fibers is restricted because the protofibrils in the nanofibers are twisted. As the fiber diameter increases, protofibrils near the surface must be stretched relative to those near the center, in order to maintain the 22.5 nm axial repeat [87]. Thus, nanofiber growth stops when the energy required to stretch added protofibrils exceeds the energy of their bonding [87].

Association and branching of nanofibers leads to the formation of a 3D gel (illustrated as the final step of Fig. 2c). Branching can be initiated by a fibrin monomer or fiber that binds to the end of another monomer or fiber and then diverges to interact with the second monomer, thereby producing a trimolecular branch point. Alternatively, a bimolecular branch point can be formed when two parallel strands diverge from each other. Conditions that favor lateral nanofiber aggregation tend to produce fibrin gels built from thick fibers with few branching

points. In addition, gels with a larger number of branching points, shorter fiber segments, and a smaller pore size are formed at a higher concentration of thrombin. The resulting gel is stabilized by cross-linking the fibers with factor XIIIa, which makes the fibrin gel resistant to mechanical and proteolytic damage [57]. It also prevents the protofibrils from sliding past one another, thus eliminating persistent creep.

The formation of a fibrin gel is central to homeostasis and the formation of blood clots in thrombosis and cancer metathesis, which results from the imbalance of procoagulant, anticoagulant, and fibrinolytic factors [49, 88]. Although fibrin constitutes only 0.25 % of the volume in blood clots, it determines the biophysical properties of the clot [89]. Upon stretching, the gel exhibits nonlinear viscoelasticity and strain-hardening behavior, which is explained by the coil–rod conformational transformations of fibrin(ogen) and deformation of nanofibrils. Figure 2d shows the response of a soft and compliant fibrin gel to strain. The gel exhibits strain stiffening and negative normal stress under shear deformation [58]. In addition, upon stretching, fibrin gels exhibit a large decrease in volume due to expulsion of water, which is explained by unfolding and association of protein molecules as a result of exposure of hydrophobic groups to the aqueous medium and stretching of fibrinogen molecules and fibers [90]. This behavior is essential for the ability of fibrin gels to act as efficient hemostatic plugs and wound-healing matrices.

Fibrin hydrogels have many clinical and bioengineering applications, especially because of their gelation at a relatively low polymer volume fraction and the ability to control gelation time. Furthermore, the mechanical properties of the gels can be modified by tuning the concentration of thrombin. Fibrin glue is used to stem bleeding and replace sutures for mesh fixation in hernia repair, severed sciatic nerve reattachment, stabilization of microsurgical anastomoses, and skin graft adhesion [91]. Fibrin gels are also useful in the controllable local delivery of tissue-specific growth factors through modulation of the interaction between the gel and the signaling protein. These growth factors and gel components include fibronectin, hyaluronic acid, and von Willebrand factor. Fibrin hydrogels are also used for cell culture. For example, myoblasts or endothelial cells cultured within a fibrin gel became aligned and divided along the fibrin bundles when a tensile strain of 25 % or greater was applied. Aligned fibrin gels have also shown evidence of enhancing neurite alignment and could be a useful filler for nerve guidance channels [91, 92].

3.1.2 Polysaccharide Gels

Agarose Agarose is a linear polysaccharide extracted from red algae composed of alternating 1,3-linked β-D-galactopyranosyl and 1,4-linked 3,6-anhydro-α-L-galactopyranosyl residues; a fraction of these residues (~2 %) contains sulfate groups [93, 94]. Agarose solutions can form thermoresponsive gels. Temperatures as high as 95 °C are required for agarose molecules in solution to completely adopt

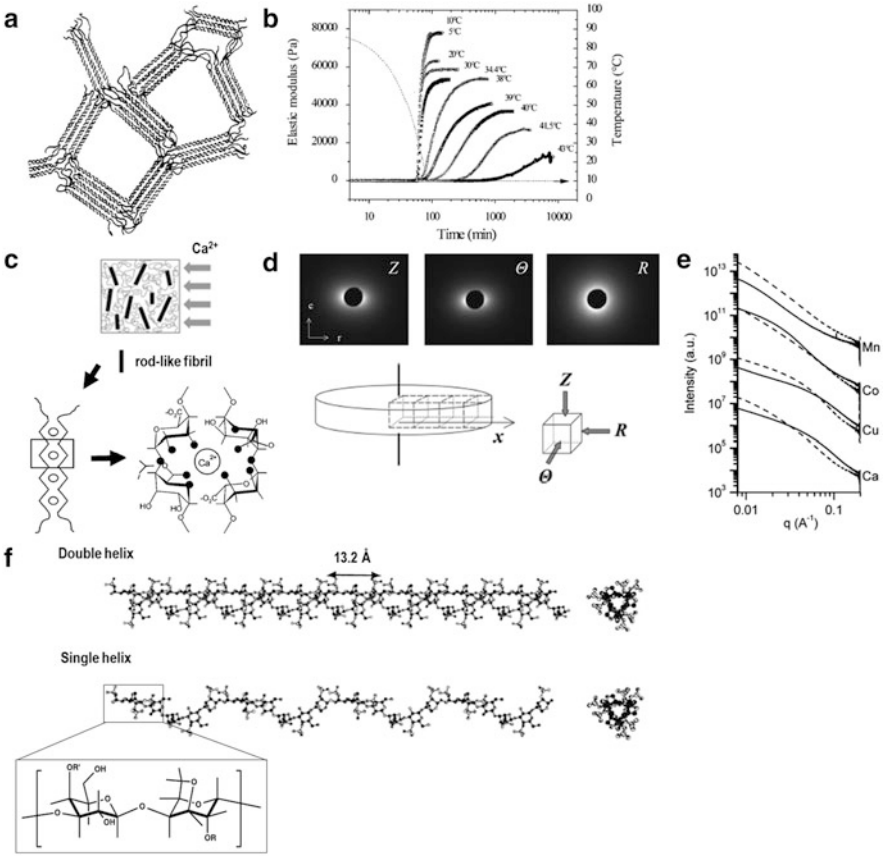

Fig. 3 Structure of nanofibrils and properties of polysaccharide hydrogels. (**a**) Agarose gel network made by association of double helices and amorphous domains. Adapted, with permission, from [97]. Copyright 1989 American Chemical Society. (**b**) Variation in the elastic modulus over time of 2 % (w/w) aqueous agarose gels that were cured isothermally at temperatures T_f, as indicated. Samples were cooled from 90 to 10 °C at a rate of 1 °C min^{-1}. Reproduced, with permission, from [95]. Copyright 2001 Wiley-VCH. (**c**) The "egg-box" model. The *top-most* image illustrates the direction of Ca^{2+} flow and the orientation of the rodlike fibrils formed within the gel. *Dark circles* represent the oxygen atoms involved in coordination of the Ca^{2+} cation. Reproduced, with permission, from [98] and [99]. Copyright 2011 and 2001 American Chemical Society. (**d**) SAXS patterns for a 2 % (w/w) Ca-alginate gel obtained from the incident X-ray beams of three different directions, *Z*, *Θ*, and *R*. Reproduced, with permission, from [98]. Copyright 2011 American Chemical Society. (**e**) SAXS patterns of hydrogel samples of low guluronic (*dashed line*) and high guluronic (*solid line*) content, with varying cations. Reproduced, with permission, from [100]. Copyright 2012 American Chemical Society. (**f**) Models of the double and single helices of ι-carrageenan. Adapted, with permission, from [101]. Copyright 2002 Elsevier

a random coil conformation [26, 95]. Upon cooling the solution below the temperature of complete melting (95 °C), typically to 10–40 °C, agarose coils assemble into left-handed double helices. The presence of a 3,6-anhydro bridge in the covalent structure and numerous hydrogen bonds contribute to the formation of left-handed helices [26].

The formation of agarose networks occurs on both the supramolecular and molecular levels. On the supramolecular level, agarose double helices aggregate to form bundles [96]. At temperatures of ~20–40 °C, depending on the agarose concentration in solution, 7–11 double helices assemble into these bundles, or nanofibrils (Fig. 3a) [26, 97]. On the molecular level, some of the agarose repeat units lack the regular 3,6-anhydro residues, which leads to disruption of the double helix and formation of "soluble kinks" [43]. The kinks result in branching, which contributes to formation of the 3D gel network.

Agarose sol–gel transitions exhibit strong hysteresis in response to changes in temperature. Depending on the agarose concentration and type, the gelling temperature of agarose solutions is between 10 and 40 °C, which is significantly lower than the melting temperature of the gel (approximately 90 °C) [95]. The hysteresis and thermal stability of agarose gels originate from cooperative hydrogen bonding in both the double helices and their bundles [96]. The "memory" of intermolecular associations can be erased upon heating agarose solutions to ~90 °C, at which agarose molecules adopt a random coil conformation.

The mechanical and structural properties of agarose gels are sensitive to their thermal history [95]. For example, when the cooling temperature was held below 35 °C, fast agarose gelation resulted in strong, homogenous and elastic gels with a pore size of ~100 nm. When the gelation temperature was held above 35 °C, phase separation competed with the gelation process to form heterogeneous, turbid gels with poor mechanical properties. The elastic modulus of 2 % (w/w) agarose gels increased from 12 to 78 kPa as the curing temperature ranged from 43 to 5 °C, respectively (Fig. 3b).

Agarose gels have a broad range of applications as a result of their thermal stability, non-adhesive nature, and controllable average pore size. Agarose hydrogels have been extensively used as molecular sieves in gel electrophoresis for the separation of macromolecules such as nucleic acids and proteins [50]. The pore size in agarose hydrogels can be varied from <100 to ~1,200 nm by decreasing the concentration of agarose from 3 % to 0.5 % (w/w), respectively [102]. In the food industry, agarose is the gelling component in agar and is used to gel canned meat, fish, and poultry products [93]. High melting temperature and resistance to degradation make agarose gels suitable for autoclaving. In addition, agarose gels are being explored as artificial 3D extracellular matrices because of their biocompatibility, lack of cell-adhesion, and tunable mechanical properties (Young's and shear moduli), which are achieved by varying the concentration of agarose [103–105].

Alginate Alginate is a linear unbranched polysaccharide primarily extracted from brown algae. Within the intracellular matrix of algae, alginate exists as a mixed salt

of various cations such as Mg^{2+}, Ca^{2+}, Sr^{2+}, Ba^{2+}, and Na^{+}, with Ca^{2+}-ions being the most abundant [106]. To isolate alginate, the dried algae is treated with a dilute mineral acid such as HCl to degrade laminarin and fucoidin. Simultaneously, the cations are exchanged for a H^{+} ion. Alginate is then converted to the soluble salt by adding Na_2CO_3 to the insoluble alginic acid [107, 108].

Alginates contain varying amounts of 1,4′-β-D-mannuronic acid (M-units) and α-L-guluronic acid (G-units) residues. Within the alginate chains, they are arranged in homopolymer blocks of M-units and G-units, concurrently with blocks of alternating sequence of M- and G-units. Aqueous solutions of alginate undergo gelation in the presence of divalent cations (e.g., Ca^{2+}, Cu^{2+} and Ba^{2+}) [98]. The mechanism of alginate gelation was proposed in the 1970s; however, this mechanism was continuously revised on the basis of more recent experimental evidence. In the initially proposed "egg-box" model shown in Fig. 3c, cationic ions (e.g., Ca^{2+} cations) induce chain–chain association of guluronic acid residues in a zig-zag manner, which places the Ca^{2+} cations in junction or intersection zones. The egg-box model can explain how divalent metal cations bound in the interchain cavities of alginate molecules produce rodlike cross-linked complexes [109]. Gel formation is driven mainly by the interactions of cations with G blocks, although mannuronic acid–guluronic acid blocks can also contribute to chain association [106].

Although alginate gels have been considered to be molecular rather than nanofibrillar, small angle X-ray scattering (SAXS) characterization of the structure of alginate gels has revealed an asymptotic behavior at low scattering vector (q) values, which is indicative of rodlike scattering objects with random orientation (Fig. 3d and e) [98]. These rodlike objects were composed of tens of alginate molecules and had a cross-sectional radius of 5.1–7.1 nm. The cross-sectional radius of these rodlike alginate structures increased with an increasing concentration of Ca^{2+}-cations in the gel [98]. Thus, alginate gelation mediated by the addition of Ca^{2+} cations can be explained by the formation of rodlike nanofibrils due to interchain association induced by Ca^{2+} within the framework of the egg-box model [110].

Alginate gels are generally prepared by the diffusion setting method or the internal setting method [108]. In the diffusion setting method, cross-linking ions diffuse from a large outer reservoir into an alginate solution. This method is typically used for the formation of alginate beads by dripping a solution of sodium alginate into a bath containing a solution of divalent cross-linking cations. Figure 3e depicts SAXS patterns of alginate hydrogels prepared with different cations. The internal setting method utilizes an inactivated form of calcium (e.g., $CaCO_3$ or Ca-ethylenediametetraacetic acid), which is introduced into the alginate solution. The Ca^{2+} ions, liberated by a decrease in pH bind to the alginate molecules, thereby causing cross-linking. The diffusion method yields gels with a Ca^{2+} ion concentration gradient across the thickness of the gel, whereas the internal setting method produces gels with a homogeneous Ca^{2+} ion concentration and thus more uniform gel structure.

Alginate gels have been prepared as large beads (>1 mm diameter) , microbeads (<0.2 mm in diameter), films, and fibers [107]. They are used in the food,

pharmaceutical, and biomedical industries because of the biocompatibility of alginate and its mild gelation conditions. In situ alginate gelation has applications in wound healing, in which Na^+ ions exuded from the wound are exchanged with Ca^{2+} ions in the alginate molecules, resulting in gel formation [107, 111]. Alginate gels can also be used for cell immobilization and encapsulation. After alginate gelation, water molecules trapped within the alginate matrix are free to migrate [20].

Alginate gels possess bioadhesive properties that are advantageous in mucosal drug delivery. A mucoadhesive drug delivery system increases the interaction time at the site of activity or resorption, thereby localizing the drug and increasing its effectiveness. Alginate molecules contain carboxylate groups and can thus be identified as an anionic mucoadhesive polymer acting as a potential drug-delivery vehicle to mucosal tissues (e.g., in the gastrointestinal tract or the nasopharynx) [107]. Derivatization of the alginate backbone includes acetylation, phosphorylation, sulfation, hydrophobic modification, attachment of cell-signaling molecules, covalent cross-linking, and graft copolymerization [108]. The functionalization of alginate hydrogels yields biomaterials with enhanced properties. For example, covalent modification of alginate with peptides containing arginylglycylaspartic acid (RGD) via aqueous carbodiimide coupling increased the cellular interaction of alginate hydrogel with mouse skeletal myoblasts [108]. The partial oxidation of alginates may also be desirable in biomedical applications, because oxidized alginate degrades in aqueous media, whereas unmodified alginates do not.

Carrageenan Gel forming κ- and ι-carrageenans are linear polysaccharides, largely with alternating repeat units of 1,3-linked β-D-galactopyranose and 1,4-linked 3,6-anhydro-α-D-galactopyranose. These polysaccharides can be collected from red algae [94, 112]. κ- and ι-carrageenans contain one and two sulfate groups per disaccharide unit, respectively. Unlike agarose, the 3,6-anhydro residue of carrageenan is in the D-configuration instead of the L-configuration. At high temperatures, κ- and ι-carrageenans exist in random coil conformations. Low temperatures induce κ- and ι-carrageenans to arrange into right-handed double helices (Fig. 3f) [113].

Formation of a gel network from the double helices of κ- and ι-carrageenans can be achieved by temperature- or salt-setting [101, 114]. Gel formation of κ-carrageenan follows a hierarchical assembly of double helices into superhelical rods, which then assemble latterly into bundles [101]. On the other hand, ι-carrageenan double helices do not further associate into bundles due to the electrostatic repulsion caused by the additional sulfate group in each disaccharide unit. Gel formation in ι-carrageenans relies on a branching mechanism [113]. Similar to agarose, double helices of ι-carrageenans are terminated by kinks due to irregularities in the covalent structure of the polymer chain, in which some disaccharide units are missing the 3,6-anhydro ring. These kinks allow each chain to participate in ordered associations with several different carrageenan molecules.

Gelation of carrageenans is promoted by the presence of appropriate cations. The influence of different types of cations on the gelation of carrageenans is not

straightforward. For κ-carrageenan, cations are categorized as having either specific or nonspecific interactions with the polysaccharide. Examples of specific cations for κ-carrageenan are K^+, NH_4^+, Rb^+, and Cs^+ [115]. Both specific and nonspecific cations screen the electrostatic repulsion of sulfate groups on the helices favoring their association [116]. Specific cations induce the intermolecular association of κ-carrageenan by binding both the sulfate group of D-galactose and the anhydro-bridge oxygen atom of the adjacent galactose residue [117]. This results in more effective screening of surface charges. On the other hand, no specific cations promote the gelation of ι-carrageenan in the same manner as κ-carrageenan [118].

The rheological properties of carrageenan gels depend on the concentration of carrageenan and its ionic environment. In general, κ-carrageenan gels are stronger, but are more brittle and exhibit strong hysteresis and syneresis relative to ι-carrageenan gels as a result of interhelical aggregation [117, 119]. κ-Carrageenan gels prepared by the addition of specific cations are stronger than those prepared by the addition of nonspecific cations, even at comparable ionic strengths [118]. The effect of the cation specificity on the shear modulus of κ-carrageenan is $K^+ > Ca^{2+} = Cu^{2+} \gg Na^+$, in a low salt concentration range [116]. Salt addition in ι-carrageenan solutions yields soft, clear, elastic gels [116]. For ι-carrageenan gels, shear modulus increases with the valency of the cation used. In contrast to κ-carrageenan, where there is specific binding between the cation and the polymer, ι-carrageenan gelation is only caused by screening of the surface charge. The addition of cations with higher charge is more effective at screening the electrostatic repulsion of sulfate groups, thereby inducing a coil-to-helix transition.

As a result of their ability to bind proteins, carrageenan gels have been used in the food and pharmaceutical sectors. Carrageenans are heavily used as gelling agents in the food industry [93] to gel milk and meat products [120]. Electrostatic interactions are formed between carrageenans and casein micelles found in milk. Carrageenans also display antimicrobial and antitumor activities [121]. In particular, carrageenan gels are potent infection inhibitors for a range of genital human papillomaviruses [122]. Carrageenan blocks papillomavirus infectivity (the ability of a pathogen to establish infection) by directly binding to the viral capsid. Carrageenan gels are potential candidates for vaginal microbicides in sexual lubricant products.

Chitin Chitin is the second-most abundant natural polymer on earth after cellulose, and it is the most abundant nitrogen-containing organic compound [123]. Raw chitin is collected from cephalopods, crustacean cuticles, arthropod exoskeletons, mollusk shells, and the cell walls of algae and fungi. Commercially, chitin is obtained from waste products of the fishing industry. Chitin is a linear, water-insoluble, semicrystalline polymer of β-1,4-*N*-acetylglucosamine residues. The insolubility of chitin in water is caused by its high crystallinity [124]. The partial deacetylation of chitin yields chitosan, a derivative of chitin, which is composed of *N*-acetyl D-glucosamine and D-glucosamine units. Chitosan is readily soluble in acidic, neutral and basic media allowing for greater processability, unlike its insoluble chitin precursor [125]. Non-modified chitosan molecules do not

self-assemble into nanofibrils. For the purposes of this review, only hydrogels formed from chitin nanofibrils will be discussed.

Two types of chitin crystals, α-chitin and β-chitin, result in three polymorphic forms, all of which can be found within the same organism. Chitin has a hierarchical organization, starting from long-chain chitin molecules that assemble in an antiparallel manner to form an α-chitin crystalline structure. The assembly of 18–25 of these molecular chains yields fibrils that are 2–5 nm in diameter and 300 nm in length [123]. The fibrils are wrapped in protein layers, which cluster into chitin–protein nanofibers of 50–300 nm diameter [126]. The chitin–protein nanofibers further assemble into bundles that arrange themselves in a parallel fashion to form horizontal planes. The spacing between the fibers is filled with a variety of proteins and clusters of minerals such as calcite and calcium carbonate. The planes stack in a helicoidal fashion. To isolate individual nanofibrils without the addition of proteins and minerals, the network of chitin nanofibers can be treated with aqueous sodium hydroxide and hydrochloric acid [127]. Following chitin purification to remove proteins and minerals, the aggregates of chitin nanofibers are disintegrated. The resulting nanofibrils have a width of 10–20 nm and an aspect ratio that exceeds 100. The structure of chitin nanofibrils also has the same antiparallel crystal pattern as the original molecular structure of α-chitin. Alternatively, individual chitin nanofibers of 3–4 nm in diameter and aspect ratios greater than 500 have been prepared using ultrasonication of β-chitin dispersed in water at pH 3–4 [128].

Nanofibrillar chitin hydrogels are obtained by dispersing squid pen in Triton X-100 (to remove lipoproteins), suspending the nanofibers in aqueous NaOH to remove remaining proteins [129], and ultrasonicating the transparent suspension of chitin nanofibers at low pH. The suspension forms a hydrogel at elevated temperatures. The hydrogel contains thin entangled nanofibrils with an average diameter significantly smaller than that in the suspension. The mechanical strength of the gels (evaluated as the force that is needed to break the gel) increases with increasing chitin nanofiber concentration.

Nanofibrillar chitin hydrogels are biodegradable, biocompatible, and nontoxic, and thus show promise for biomedical applications. The protonation of amino groups on the surface of chitin allows its application in wound dressings due to the antimicrobial properties of cationic gels [130]. Polymeric fibers that mimic the structure and function of the extracellular matrix are also of interest in tissue engineering and cell culture. Chitin nanofibers can promote cell attachment and show potential as extracellular matrix mimics [29, 125].

Cellulose

Cellulose, the most abundant renewable organic material produced in the biosphere, is extracted from plants, bacteria, algae, fungi, and tunicates [28]. The structure of nature-derived cellulosic materials is hierarchical. The primary building unit of cellulose is β-1,4,-linked-anhydro-D-glucose. A discrete number of cellulose molecules pack in a parallel fashion to form elementary fibrils, also known as

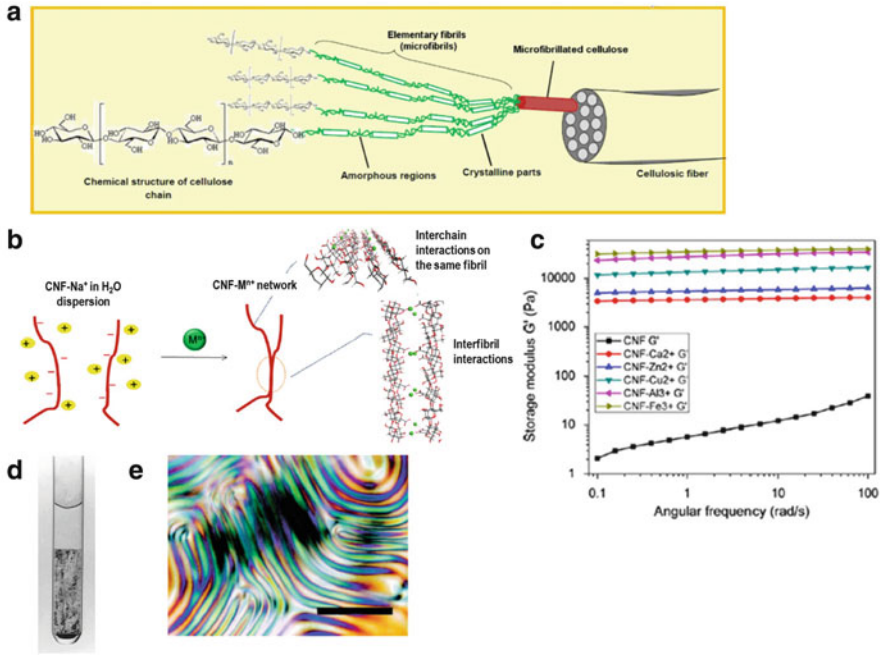

Fig. 4 Structure and properties of nanocellulose. (**a**) Hierarchical assembly of cellulose molecules into cellulosic fibers. Adapted, with permission, from [131]. Copyright 2012 Elsevier. (**b**) Proposed mechanism of formation of CNF cross-linked with metal cations. Reproduced, with permission, from [132]. Copyright 2013 American Chemical Society. (**c**) Effect of the type of metal cation on the frequency-dependent storage modulus of CNF hydrogels, probed by dynamic frequency sweeps (25 °C) at a strain rate of 0.5 %. Adapted, with permission, from [132]. Copyright 2013 American Chemical Society. (**d**) Polarization optical microscopy photograph of a biphasic 8.78 % (w/w) CNC suspension. Adapted, with permission, from [133]. Copyright 1996 American Chemical Society. (**e**) Polarization optical microscopy photograph of a CNC suspension. S*cale bar*: 200 μm. Reproduced, with permission, from [134]. Copyright 2000 American Chemical Society

microfibrils (Fig. 4a) [135]. Depending on the source, elementary fibrils have widths of 3–50 nm [135] and lengths that can exceed 10 μm [136]. Elementary fibrils are composed of alternating regions of crystalline and amorphous cellulose. The crystalline regions of elementary fibrils can be isolated by selectively degrading the amorphous regions by acid hydrolysis. These isolated highly crystalline regions are called cellulose nanocrystals, also known as nanocrystalline cellulose or cellulose nanowhiskers. Wood fibers and other plant fibers can be used to produce cellulose nanofibrils, which have dimensions similar to that of elementary fibrils [135]. The following sections describe nanofibrillar hydrogels formed by cellulose nanofibrils and cellulose nanocrystals. Further details on cellulose-based supramolecular networks and hydrogels can also be found in the chapter by Li and Lui in this volume [137].

Cellulose Nanofibrils Cellulose fibers are composed of aggregates of elementary fibrils held together by numerous hydrogen bonds [135, 138]. Chemical or enzymatic treatment coupled with mechanical treatment of cellulose fibers is used to produce individual cellulose nanofibrils (CNFs), which have high aspect ratios and widths similar to those of the elementary fibrils [131]. Surface chemical functionalization helps to reduce the energy required to produce CNFs. Surface modification can be performed by 2,2,6,6-tetramethylpiperidine-1-oxyl radical (TEMPO)-mediated oxidation of wood pulp [139]. The TEMPO-functionalized CNFs are 3–4 nm in diameter and have carboxylic surface groups. Similarly, carboxymethylation of wood fibers used in conjunction with high-pressure homogenization and ultrasonication leads to the formation of functionalized CNFs [140]. In this case, the CNFs are 4 nm in diameter and 300–1,000 nm long and have carboxymethyl groups on the surface. Another method is to combine enzymatic hydrolysis and mechanical shearing, which yields CNFs that are mostly ~5 nm thick [141]. The presence of anionic surface functionalities leads to electrostatic repulsion between the CNFs and allows their separation from each other.

For suspensions of CNFs that carry charged surface groups, gelation can be induced by adding salt [132] or reducing the pH of the suspension [140]. Suspensions of CNFs with carboxylic surface groups are gelled by adding divalent and trivalent metal cations [132]. Gelation is attributed to screening of the electrostatic interactions between CNFs by strong metal–carboxylate bonding. In addition, the metal cations can bridge multiple CNFs through formation of ionic cross-links (Fig. 4b). The storage modulus, G', of the resulting CNF gel decreases from 32 to 3.4 kPa with decreasing binding energy between the cations and the carboxylic groups in the order $Fe^{3+} > Al^{3+} > Cu^{2+} > Zn^{2+} > Ca^{2+}$ (Fig. 4c). Gels formed using inorganic cations as cross-linkers can be disintegrated by adding a chelator such as tetrasodium ethylenediaminetetraacetate (Na_4EDTA). Similarly, CNF gels can be prepared by adjusting the pH [140]. Suspensions of carboxymethylated CNFs in the semiconcentrated regime have been gelled by reducing the pH, thus decreasing the electrostatic repulsion between fibrils, thereby driving gel formation.

In addition to physical cross-linking and interfibrillar association, CNFs can form networks by entanglement [141]. The mechanical properties of the gels can be changed by varying the CNF concentration in the precursor suspension. Gels with a storage modulus, G', of 10^5 and 10^2 Pa were obtained at CNF concentrations of ~6 and 1 % (w/w), respectively. These gels showed almost no dependence on temperature in the range 20–80 °C. Entanglement of CNFs in the gels leads to a high value of the storage modulus G'. For example, $G' = 10^3$ Pa was measured for 2 % (w/w) CNF gels. In the absence of entanglements, cellulose nanocrystal gels have a G' of only 10 Pa at 2 % (w/w).

Fibrils in CNF gels can be shear-aligned to enhance the mechanical properties of the gel in the shear direction [140]. The network is oriented in a particular direction by applying shear strain during or after gelation. Aligned CNF networks are stronger in the direction of shear than unaligned isotropic gels. Elastic deformation of the network is observed at small strain and is due to fibril bending. At high strain,

plastic deformation is observed as a result of the rotation and sliding of fibril–fibril joints in the shear direction.

Aligned CNF hydrogels can also be used as intermediates for nanocomposites with significantly higher stiffness and strength in the direction of shear compared with isotropic samples [142]. CNF hydrogels are used as precursors for the preparation of deformable aerogels [143]. As a result of the entanglement of long nanofibers, these CNF aerogels have uncommonly high compressive strain, with linear elastic behavior up to ~40 % strain. Moreover, CNF hydrogels can be used as 3D scaffolds for cell culture, because their nanofibrillar structure mimics the structure of the extracellular matrix and they have tunable mechanical properties [18, 144]. The plant-derived CNF hydrogels were explored as xeno-free 3D culture systems that promote functional 3D spheroid formation of human liver cells [144] and support the pluripotency of human pluripotent stem cells (hPSC) [18]. The viscoelastic properties of CNF hydrogels used for cell culture were tuned by varying the concentration of CNF in the suspension. For hPSC, spheroids were formed at 0.5 % (w/w) CNF hydrogels but not at 1 % (w/w). Poor cell adhesion to the CNF gel was key to promoting the cell–cell interactions required to form 3D spheroids. To retrieve the embedded 3D cells, CNFs could be enzymatically degraded by adding cellulase. The cellulase did not affect the animal cells, and the products of CNF degradation were nontoxic sugars. The resulting intact hPSC spheroids were transferred to other platforms for differentiation.

Cellulose Nanocrystals Acid hydrolysis of cellulose fibers degrades the amorphous regions of the microfibers and yields cellulose nanocrystals (CNCs) with an average diameter of 5–70 nm and length of 100–250 nm (Fig. 4a) [28, 145]. Different cellulose sources such as wood or algae yield CNCs with different dimensions, even under similar preparation conditions [146]. For example, cotton and wood yield highly crystalline CNCs with narrow size distribution, whereas tunicin and algae generate CNCs with larger dispersities and lengths that range from 100 nm to several micrometers [147]. During hydrolysis, sulfuric acid reacts with surface hydroxyl groups on CNCs leading to the functionalization of the surface of the CNC with sulfate ester groups. Stability of aqueous CNC suspensions results from an electrostatic repulsion between individual CNCs that counteracts their attraction due to van der Waals forces and hydrogen bonding [27, 148].

Low-concentration CNC suspensions are clear isotropic fluids, whereas beyond a critical concentration the solution phase separates into a birefringent chiral nematic liquid crystalline phase and an isotropic phase (Fig. 4d) [149]. As the CNC content is further increased, a critical concentration is reached where the entire suspension forms a chiral nematic liquid crystalline phase with a characteristic fingerprint pattern, as shown in Fig. 4e [150]. The origin of this chirality is not entirely clear and was proposed to be a result of the helicoidal structure of CNCs [28]. At a higher CNC content, a gel is formed. The aspect ratio of the CNCs is a key variable in determining CNC gelation and phase separation during the formation of a liquid crystalline phase [28, 151, 152]. Suspensions of long CNCs tend to gel before attaining the liquid crystalline structure [149]. The degree of sulfation of

CNCs determines the surface charge density and also significantly affects the critical concentration at which the transition isotropic → liquid crystal → gel takes place. It was shown that at lower degrees of sulfation the electrostatic repulsion between CNCs decreases, which leads to gel formation at lower CNC concentrations than for CNCs with a higher degree of sulfation [153, 154]. An early work in the field revealed the formation of a birefringent gel when a suspension of CNC was heated on a steam bath [155]. This gelation was likely due to desulfation of CNC surfaces under heating.

Gelation of CNC suspensions is also induced by suppressing electrostatic repulsion between CNCs, either by decreasing the surface density of charged sulfate ester groups or by increasing the ionic strength of the aqueous medium. For example, shear thinning (thixotropic) CNC hydrogels were obtained by desulfation of CNCs with glycerol [147]. Alternatively, the addition of NaCl can be used to control the rheological behavior of CNC suspensions in the isotropic, chiral nematic and gel states over a range of CNC and NaCl concentrations [156]. For biphasic samples (above the threshold of isotropic-to-chiral nematic transition), the addition of NaCl up to 5 mM concentration decreased the size of chiral nematic domains and increased the sample viscosity at low shear rates, while for gel samples, the addition of NaCl decreased CNC gel viscosity [156].

Surface modification of CNCs results in a decrease in surface negative charge and enables the formation of gels by changes in temperature, pH, or ionic strength [157, 158]. For example, cationic surface functionalization of CNCs resulted in the formation of thixotropic gels at CNC concentrations of 3.5 % (w/w) or greater [159]. In addition, functionalization of the CNC surface with carboxylic acid or amine groups rendered the CNCs responsive to pH [160]. Sol–gel transitions occurred at pH values corresponding to neutral or weakly charged CNCs, thereby allowing hydrogen bonding to dominate.

Hydrogels of CNCs have many desirable properties, including low cost, nontoxicity, hydrophilicity, biocompatibility, and biodegradability, all of which contribute to their potential applications in bioengineering and biomedicine. For example, CNC dispersed in a solution of cellulose, sodium hydroxide, and urea formed a gel that steadily released bovine serum albumin into a simulated body fluid [161]. Nanocomposites of CNC and poly(vinyl alcohol), a hydrophilic biocompatible polymer, exhibited a broad range of mechanical properties that could be tuned to mimic those of cardiovascular tissues and, therefore, have potential applications as cardiovascular implants [162].

3.2 Synthetic Nanofibrillar Hydrogels

Block Copolymers In solutions, amphiphilic block copolymers self-assemble into a variety of supramolecular micellar nanostructures [163–165]. Micelles form when one block is insoluble or only sparingly soluble in the solvent, whereas the other block is soluble and swollen in the solvent. In order to reduce the interfacial energy of the system, the insoluble block segregates in the core of the micelle. When the

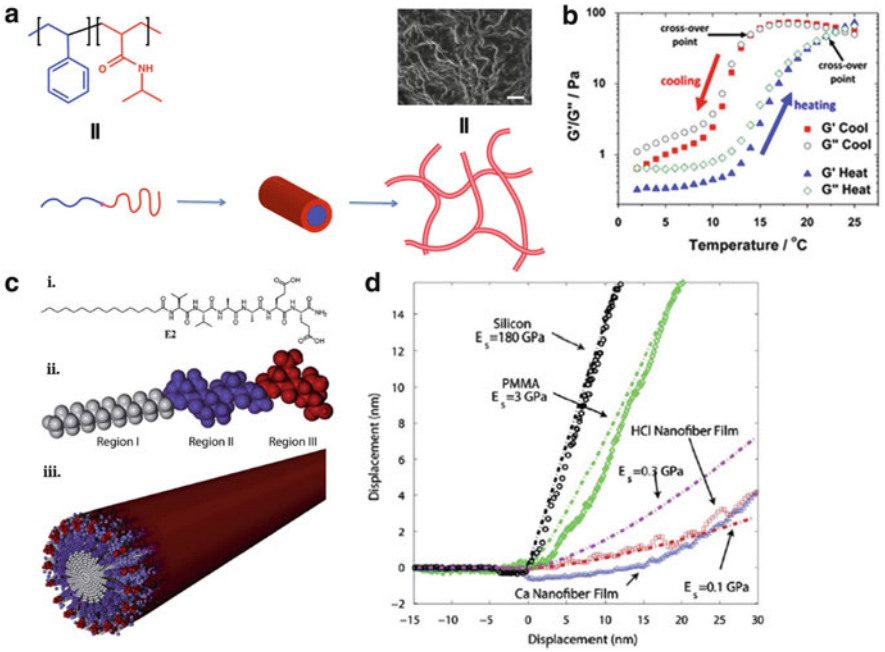

Fig. 5 Nanofiber composition and properties of synthetic hydrogels. (**a**) Stepwise formation of a poly(styrene)-*block*-poly(*N*-isopropyl acrylamide) gel. The inset shows scanning electron microscopy image of the structure of hydrogels formed by the block-copolymer micelles. *Scale bar*: 5 μm. Adapted, with permission, from [167]. Copyright 2013 The Royal Society of Chemistry. (**b**) Effect of temperature on the storage and loss moduli of poly(glycerol-monomethacrylate)-*block*-poly(2-hydroxypropyl-methacrylate) solution undergoing gelation ($G' > G''$) above 20 °C and liquification ($G'' > G'$) upon cooling below 20 °C. Reproduced, with permission, from [10]. Copyright 2012 American Chemical Society. (**c**) Chemical structure (*i*) and corresponding space-filling model (*ii*) of a peptide amphiphile (PA). (*iii*) Illustration of the self-assembled supramolecular nanofibrillar structure formed by PA molecules. Reproduced, with permission, from [21]. Copyright 2012 The Royal Society of Chemistry. (**d**) Variation in elastic moduli versus displacement measured for thin PA films of a PA solution mixed with HCl (*red diamonds*), and a PA solution mixed with Ca^{2+} ions (*blue triangles*). Thin films of silicon (*black circles*) and poly(methyl methacrylate) (*green squares*) are shown for comparison. Reproduced, with permission, from [168]. Copyright 2011 The Royal Society of Chemistry

volume fraction of the solvophilic block is approximately equal to or slightly larger than the solvophobic block [46, 166], block copolymers assemble into wormlike micelles (Fig. 5a). The diameter of these nanofibrillar-like structures is in the range of 5–20 nm and the lengths range from 100 nm up to several micrometers. Crystallization-driven self-assembly [30, 169] and polymerization-induced self-assembly [44, 170] have been used to extend the range of compositions of block copolymers forming wormlike micelles. Examples of polymers forming cylindrical micelles in water include poly(styrene)-*block*-poly(acrylic acid), in which poly (styrene) is the hydrophobic block forming the core of the micelle and poly(acrylic acid) forms the outer water-swollen block, thereby making the micelle colloidally stable in water [46].

Initially, hydrogels formed by the self-assembly of wormlike micelles were obtained from a poly(ethylene oxide)-*block*-poly(butadiene) copolymer [171]. This gel was probably formed by entanglement of the micelles; however, the mechanism of gelation was not studied. Cylindrical micelles of the triblock copolymer poly(ethylene oxide)-*block*-poly(propylene oxide)-*block*-poly(ethylene oxide) have also shown gel-like behavior in highly concentrated [>20 % (w/w)] solutions [172, 173]. Recently, wormlike micelles have been pre-designed to act as nanofibrillar building blocks for the synthesis of hierarchically structured hydrogels. The exact mechanism leading to gel formation is still under debate [44]; however, wormlike micelles made by small molecules are known to form gels by entanglement of the micelles [174–176]. The same mechanism could dominate in gel formation in the case of polymer wormlike micelles.

The formation of nanofibrillar gels was observed for poly(styrene)-*block*-poly (*N*-isopropyl acrylamide) synthesized by reversible addition–fragmentation chain transfer (RAFT) emulsion polymerization of styrene using a macroinitiator of poly (*N*-isopropyl acrylamide) [167, 177]. Polymerization-induced self-assembly and sonication of the solution led to the formation of wormlike micelles of 15–17 nm diameter and 2–5 μm length. Upon heating the aqueous micellar solution to 32–34 °C, the poly(*N*-isopropyl acrylamide) block lost its solubility in water and the micelles assembled into a nanofibrillar network, with fibrils of 90–130 nm diameter (Fig. 4a) [167]. The gel disassembled into individual micelles upon reducing the temperature below 32–34 °C. Polymerization-induced self-assembly of poly(glycerol monomethacrylate)-*block*-poly(2-hydroxypropyl methacrylate) leads to the formation of wormlike micelles of 25–30 nm diameter [10, 178, 179]. Gelation of the solution of these wormlike micelles occurred at room temperature (Fig. 5b) [10]. The gel network was sensitive to temperature; when the temperature was decreased to 4 °C [10], the wormlike micelles broke down into smaller spherical micelles and gel–sol transition took place. The transition from wormlike to spherical micelles was ascribed to the higher hydration of the hydrophobic poly(2-propyl methacrylate) block when the temperature decreased [10]. The volume ratio of hydrophobic core-to-hydrophilic block influenced the storage and loss moduli of the nanofibrillar gel. A larger volume fraction of the hydrophobic block in the copolymer led to the formation of a more rigid gel [178].

Recently, hydrogels were obtained from wormlike micelles of a copolypeptoid, poly(*N*-methyl glycine)-*block*-poly(*N*-decyl glycine). Assembly of these molecules was governed by the crystallization-driven segregation of the short crystalline poly (*N*-decyl glycine) blocks into the micellar core [180]. The diameter of the individual micelles was 31 nm; however, their bundling yielded fibrillar structures of 56–120 nm diameter, indicating the tendency for side-by-side aggregation of the micelles.

The applications of hydrogels formed by wormlike micelles are still in development; however, it may be expected, after extensive testing of their cytotoxicity, that they could be used as artificial extracellular matrices [167]. Stimuli-responsive gels that can assemble and disassemble on demand when an external trigger is applied (e.g., change in temperature) are particularly interesting because

disassembly obviates the need for degradation of the matrix to release the cells or tissue grown in the artificial extracellular matrix. Furthermore, the reversible gelation observed for the wormlike micelles described above allows easy sterilization of the extracellular matrix before cell culture by simple filtration of the micellar solution prior to gelation [10].

Synthetic Peptides Molecules of peptide amphiphiles (PAs) that form nanofibrillar gels contain three structural regions: an unbranched hydrophobic tail, a region of amino acids, and a peripheral region of charged hydrophilic residues that impart water solubility (Fig. 5c) [21, 181]. A subset of these molecules have a wedge shape that progresses from a narrow aliphatic tail to a voluminous peptide head. The self-assembly of PAs into cylindrical supramolecular structures is triggered by counterion screening and is influenced by other factors, including hydrogen bonding and molecular geometry. The resulting nanofibers are approximately 6–7 nm in diameter and can reach micrometers in length [45, 168]. The unbranched hydrophobic tail comprises the core of the cylindrical structure or nanofibril, as shown in Fig. 5c [21]. The self-assembly of PAs is a result of hydrophobic interactions between the aliphatic tails, causing them to associate in aqueous solutions. The bulkiness of the hydrophilic peptide head prevents the PAs from adopting a lamellar structure. The formation of β-sheets by the peptide region plays a crucial role in PA self-assembly into nanofibrils, and is a result of hydrogen bonding occurring along the long axis of the nanofibril [45]. Thus, PAs form nanofibrils with hydrophobic tails packed in the core of the fiber and hydrophilic peptides situated on the periphery [47].

Peptide amphiphile nanofibrils form a gel under appropriate pH and osmolality conditions, that is, when the repulsive forces between the surface hydrophilic residues are suppressed. For example, further addition of $CaCl_2$ or HCl reduces the charge of the ionizable residues on the peripheral peptide sequences and results in the formation of a hydrogen-bonded 3D network of nanofibrils [168]. No significant difference was observed in the nanofiber diameter or length for PA hydrogels prepared with the addition of HCl (HCl-PA gel) or $CaCl_2$ (Ca^{2+}-PA gel); yet, in studies of the rheological properties of these gels it was found that Ca^{2+}-PA gels withstand larger strains before plastic deformation than the HCl-PA gels. This result suggests that ionic bridges formed in Ca^{2+}-PA gels form stronger intra- and interfiber cross-links than the hydrogen bonds in HCl-PA gels [182]. The implication of this effect is that Ca^{2+} ions bridging glutamic acid residues between and within PA fibers provide stronger interactions than the hydrogen bonds between water molecules and acidic side chains in the PA molecules of HCl-PA gels. For similar reasons, the thermal stability of the gels was affected by the charge-screening mechanism. At 30–40 °C, the HCl-PA gels started to lose their mechanical integrity, whereas the Ca^{2+}-PA gels only degraded at 60–70 °C [168]. Yet, after sustained deformation at 100 % strain, hydrogen-bonded gels (HCl-PA) recovered most of their stiffness, whereas ionically cross-linked networks (Ca^{2+}-PA) were unable to recover [182]. It was hypothesized that the reason for this effect was the slow diffusion of Ca^{2+} ions into the deformed PA gel. The gelation of these PA

nanofibrillar gels was reversed by introducing a metal chelator (ethylenediaminetetraacetic acid), whereas gels prepared with HCl dissolved upon addition of NaOH [45]. Disruption of the hydrogen bonds suppressed the formation of elongated cylindrical nanostructures.

In atomic force microscopy (AFM) indentation measurements, thin films of Ca^{2+}-PA gels displayed an apparent elastic modulus of ~200 MPa, whereas HCl-PA gels had an elastic modulus of ~100 MPa (Fig. 5d) [168]. The mesh size of Ca^{2+}-PA gels was calculated according to the MacKintosh model for sterically entangled semiflexible networks. The persistence length and the mesh size were estimated to be ~102 and ~20 nm, respectively [182].

The structure of nanofibrillar PA gels resembles the structure of the extracellular matrix. Peptide amphiphile gels have potential applications in tissue engineering and nanotechnology [21, 183, 184]. The mechanical properties of these gels can be tuned by modifying their amino acid sequences, a feature that is desirable in view of increasing evidence of a cellular response to the mechanical properties of the extracellular matrix [168]. In addition, hydrogels formed by PA nanofibrils have great chemical variability and can be customized to specific cell responses [11]. These hydrogels can also be used in drug delivery by tethering drugs to a peptide-based scaffold using pH-sensitive bonds such as acetals, orthoesters, or hydrazones [21, 185, 186]. The controlled release of the drug through hydrolysis of the hydrazone can be tuned by varying the packing density and β-sheet character of the peptide [21]. There is also growing interest in artificial 3D scaffolds for regenerative medicine that can direct cell proliferation and differentiation [11].

3.3 Composite Gels

Nanofibrillar hydrogels closely mimic the microstructure and porosity of extracellular matrices, which should diffuse growth factors, drugs, or nutrients to embedded cells [187]. Many of the hydrogels discussed in this review are used to mimic extracellular matrix properties in cell delivery and tissue reconstruction. In addition, a broad range of applications depend on hydrogel friction, lubrication, wetting, and adhesive properties [188]. However, hydrogels often lack certain characteristics such as mechanical strength, stiffness, or cell-adhesion properties that would be advantageous for specific applications [189]. Nanofibrillar gels with desired properties can be achieved by preparation of composite gels. For example, reinforcement of nanofibrillar hydrogels with biological or synthetic polymers increases their effectiveness over a wider range of applications. Moreover, the ability to control hydrogel characteristics in a reversible manner (through variations in environmental temperature, pH, and ionic strength) gives composite gels their allure.

For instance, fibrin can form a nanofibrillar gel; however, as a cell-delivery vehicle it lacks mechanical strength and exhibits low hydration capacity. Therefore, hyaluronic acid was attached to a fibrinogen molecule (a precursor of fibrin) to

create a hybrid molecule [190]. The new composite gel exhibited a greater hydration capacity and a thinner fibrillar structure than the original fibrin gel. As a second example, the mechanical strength of Ca^{2+}-cross-linked alginate hydrogels is susceptible to biodegradation and swelling. By incorporating polyurethane, a semicrystalline, non-swelling, and high-strength polymer, the stability of the polyurethane/alginate composite gel can be greatly improved. Suggested applications of this composite material include tissue engineering, drug delivery, and heavy metal ion adsorption [191]. In addition, composite hydrogels can be used for bone regeneration, whereby an injectable scaffold with surface properties similar to bone surfaces can aid in the formation of bone tissue. Bone is mainly composed of nanohydroxyapatite and collagen fibers. A composite material prepared from chitosan, nanohydroxyapatite, and collagen rapidly formed a stable gel at physiological temperature. TEM images of the composite microstructure showed the mineralized collagen fibrils entrapped in a chitosan matrix [192].

4 Structure–Property Relationships of Nanofibrillar Gels

4.1 Rheological Properties

Light scattering, SAXS, electron microscopy, and spectroscopic examinations of nanofibrillar gels provide information on the organization of gels on the molecular level, whereas measurements of rheological properties probe gel networks on a macroscopic or supramolecular level. For example, the transition from viscous liquid → viscoelastic liquid → viscoelastic solid can be examined using rheology which provides insight on the structure of the polymer network. For the liquid state, the loss modulus G'' (characterizing the viscous response of the system) exceeds the storage modulus G' (characterizing the elastic response of the system). In the gel state, $G' > G''$ and tan δ (equal to G''/G') < 1. Note that the values of G' and G'' depend on the frequency of the oscillatory shear. Experiments are generally performed at low strains and frequencies to avoid significantly disturbing the gelation process and gel structure. In the course of gelation, the values of G' and G'' vary and, according to the generally accepted Winter–Chambon criterion [193], the gel point is reached when tan δ becomes independent of the oscillatory frequency [194].

After gel formation, the rheological properties of gels are used to characterize the structure and dynamics of the gel. Most nanofibrillar gels show non-Newtonian behavior, characterized by a variation in their elastic and loss moduli, when either the frequency of the oscillations or the strain (deformation) applied to the system is varied [8]. For example, at large deformations, disentanglement of fibrils leads to a decrease in the both elastic and loss moduli. At very large deformation, a liquid-like behavior is observed, wherein $G'' > G'$. Nanofibrillar gels formed by wormlike micelles, exhibit higher elastic and loss moduli with increasing length of the micelle

core-forming block but are more brittle; that is, a lower minimum strain is needed to break the network because the fracture mechanism changes with the extent of worm bundling [178]. In other systems such as fibrin gels, an increase in both elastic and loss moduli under shear, known as shear hardening was observed under sufficiently large strains [195]. This effect was caused by partial alignment of the fibers and reorientation and uncoiling of fibrin molecules, thereby promoting interactions between fibrin chains and expulsion of water [196, 197].

4.2 Mechanical Properties

Similar to molecular gels, the mechanical properties of nanofibrillar hydrogels (Young's modulus, tensile strength, rigidity, stiffness, relaxation time, etc.) [104, 198, 199] are affected by a variety of factors such as the properties of the building blocks, gel porosity, temperature, ionic strength, and degree of gel swelling [200, 201]. For example, as the porosity of the gel increases, the stiffness of the gel decreases [200]. Generally, increasing the cross-linking density and, hence, the mesh size leads to an increase in the gel strength [200]. Nanofibrillar gels are more permeable and resist compressive stress less efficiently than their nonfibrillar counterparts [202].

The striking differences between physically cross-linked nanofibrillar gels and chemically cross-linked molecular gels stem from the transient nature of the nanofibrillar gel network and the difference in the time scale on which the motion of the building blocks takes place. The finite lifetime of junctions in nanofibrillar gels provides "fluidity" to the network. The dynamics of this reconfiguration control the mechanical properties of the network [203]. Under oscillatory shear, at short time scales or high frequencies, the storage modulus G' of the transient network is higher than the loss modulus G''. However, on a larger time scale (larger than the relaxation time of the network τ_r), or at low frequency ω of the oscillatory shear ($\omega < 1/\tau_r$), the gel behaves like a liquid and $G'' > G'$. This solid-like to liquid-like transition is controlled by the dynamics of fibril motion. A weak gel shows a solid-to-liquid transition at lower frequency than a strong gel. Pioneering work on transient networks showed that, at high frequency, a network with n fibers per unit volume has a storage modulus $G'_\infty = nk_bT$, where G'_∞ is the storage modulus independent of the shear rate, k_b is the Boltzmann constant, and T is the temperature. The network has a zero-shear viscosity $\eta = \tau\, G'_\infty$ [204–206], where τ is the relaxation time [207]. The relaxation time τ varied with the stiffness and dimensions of the fibrils as $\propto 1/Er^4$, where E is the Young's modulus of the fiber and r its radius [208–210]. This dependence was caused by the combined effect of the variations in persistence length, friction coefficient, and moment of inertia of the fiber.

4.3 Stability and Responsiveness

Similar to molecular gels formed by physical bonding, nanofibrillar gels can dissociate into individual building blocks when intermolecular interactions are disrupted by changing ambient conditions. When the energy of the bonds is on the order of k_bT, gels can disassemble and re-form reversibly by heating and cooling, and by changing the pH or ionic strength of the medium.

Nanofibrillar gels formed by thermosetting can be disrupted by heat. For example, transmission and differential scanning calorimetry experiments showed that the sol–gel transition of nanofibrilar κ-carrageenan gels occurred at a temperature of 29 °C [211, 212]. However, the gel–sol temperature at which the network was disrupted was ~47 °C. A large hysteresis between the temperature of network formation and network defragmentation was observed for nanofibrillar hydrogels formed by other biopolymers (e.g., fibrin and agarose) [194, 213, 214]. Such behavior is expected because the formation of the network is usually limited by its kinetics [95], whereas the formation of nanofibrils has a thermodynamic origin.

In contrast to nanofibrillar gels made of biopolymers that disassemble upon heating, nanofibrillar gels made of wormlike micelles exhibit a unique thermoresponsive behavior [10, 44]. As described above in Sect. 3.2, cooling of the gel formed by wormlike micelles of poly(glycerol monomethacrylate)-*block*-poly(2-hydroxypropyl methacrylate) yielded small spherical micelles [10]. Transformation of the nanofibrils into spherical micelles led to disassembly of the transient network. Consequently, at a low temperature of 4 °C, the system exhibited a liquid-like behavior with $G'' > G'$, whereas at 25 °C the system had a solid-like behavior with $G' > G''$.

Temperature-responsive behavior was also observed for gels formed by wormlike micelles of poly(styrene)-*block*-poly(*N*-isopropyl acrylamide). Poly(*N*-isopropyl acrylamide) molecules are known to associate when the ambient temperature is increased above their lower critical solubility temperature (LCST) of ~32 °C [215]. When the gel was heated to a temperature above the LCST of the poly(*N*-isopropyl acrylamide) block, a nanofibrillar network was formed [167, 177]. The association of poly(*N*-isopropyl acrylamide) was reversible [215]; cooling of the nanofibrillar gel led to dissociation of the polymer network.

5 Applications of Nanofibrillar Hydrogels

Current and potential applications of nanofibrillar hydrogels are mostly targeted toward bioengineering, cell culture, drug delivery, and cosmetics [216]. This is partly explained by the fact that most nanofibrillar hydrogels are formed by biopolymers. Great effort in polymer synthesis and supramolecular chemistry is focused on mimicking nature-derived nanofibrillar hydrogels. In addition, reversible "on-demand" sol–gel transitions of nanofibrillar gels that would enable their

programmed response to external stimuli are useful for cell encapsulation, drug delivery, and drug clearance from the body [217].

5.1 Cell Encapsulation and Tissue Engineering

The basic function of the extracellular matrix (ECM) is to provide a structural scaffold for cells that will differentiate, proliferate, migrate, apoptose, or perform other functions in response to interactions with the ECM. Natural ECMs are gels formed by protein fibrils (filaments) that are interwoven within a hydrated network of glycosaminoglycan molecules [218]. Nanofibrillar hydrogels can mimic the filamentous nature of biological ECMs if their structure, composition, and properties are carefully designed. The stiffness, biodegradability, and porosity of nanofibrillar hydrogels must be considered during their construction as artificial ECMs.

A large number of nanofibrillar gels have been used for cell encapsulation [9]. For example, fibrin gels are good 3D scaffolds for cell studies because fibrin contains cell-binding sites and possesses tunable mechanical properties [218]. Fibrin has been used to control the differentiation and proliferation rates of tumor cell subsets [9]. Much research has been conducted on agarose hydrogels to seed chondrocytes for fabricating tissue constructs or to study chondrogenic differentiation of adult human stem cells [9, 104]. Figure 6a shows optical microscopy images of murine embryonic stem cells encapsulated within agarose microgels.

Utilizing composite gels enables the rational design of nanofibrillar hydrogels with desired properties. For example, bone marrow stromal cells were encapsulated in a fibrin–alginate gel, in which the fibrin enhanced the bioactivity of the composite and the alginate provided a long encapsulation period [219]. Human mesenchymal stem cells were encapsulated within a spherical hydrogel consisting of collagen type I and agarose, with the goal of inducing osteoblastic differentiation. Cell viability post-encapsulation was 75–90 % over 8 days in culture [220].

Tissue engineering aims to repair, regenerate, or replace damaged tissue or defunct organs [221]. Scaffolds that mimic the natural ECM should provide structural integrity for cell differentiation and proliferation, and biodegradability for removal after tissue is grown [221]. The advantage of self-assembled nanofibrillar hydrogels over cross-linked molecular gels in tissue engineering applications is that they possess mechanical properties similar to the replaced tissues [135]. Biological fiber-forming polymers such as collagen, fibrin, agarose, alginate, and chitosan have been used to regenerate or repair damaged tissues and organs [4]. Studies of collagen hydrogels placed between the stumps of a transected spinal cord demonstrate axons emerging from the spinal tissue interface and growing into the collagen bioimplant after only one month [222, 223]. The surface of an alginate polysaccharide was modified with RGD-containing peptides and was then seeded with mouse skeletal myoblasts. The myoblasts adhered to the GRGDY-modified

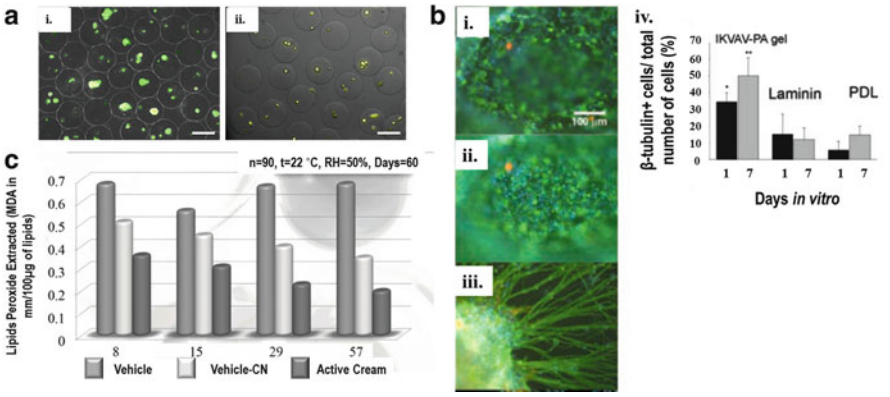

Fig. 6 Applications of nanofibrillar hydrogels. (**a**) Fluorescent optical microscopy images of agarose microgels encapsulating murine embryonic stem cell lines *i*) R1 and (*ii*) YC5–YFP–NEO in HBSS buffer. *Green* fluorescence indicates cell viability. *Scale bar*: 100 µm. Reproduced, with permission, from [104]. Copyright 2011 Elsevier. (**b**) In vitro differentiation of neural progenitor cells encapsulated within a pentapeptide amphiphile hydrogel after 1 day (*i* and *ii*) and 7 days of culture (*iii*). β-Tubulin is labeled *green* and astrocytes *orange*. *Scale bar*: 100 µm. (*iv*) Percentage of total cells that differentiated into neurons (β-tubulin^{+}); $^{*}P < 0.05$, $^{**}P < 0.01$. Reproduced, with permission, from [11]. Copyright 2004 The American Association for the Advancement of Science. (**c**) Variation in the activity of chitin nanofibers complexed with antioxidants/immunomodulant ingredients (*active cream*), chitin nanofibers supported by a matrix (*vehicle-CN*), and the matrix itself (*vehicle*), plotted as a function of the amount of lipid peroxides extracted from the skin of photoaged women. Reproduced, with permission, from [22]. Copyright 2011 Scientific Research Publishing

alginate surface and proliferated into nucleated myofibrils that exhibited heavy-chain myosin, a differentiation marker for skeletal muscle [224].

On the other hand, significant progress has been achieved in the usage of synthetic nanofibrillar gels, for example, gels formed by peptide amphiphiles [225]. The antimicrobial properties of PAs make them ideal candidates for scaffolds in tissue engineering and regenerative medicine [225]. A 3D nanofibrillar hydrogel of PAs (containing a pentapeptide that is found within laminin) induced the selective in vitro differentiation of murine neural progenitor cells into neurons (Fig. 6b) [11]. As Fig. 6b shows, differentiated neurons were labeled for β-tubulin (in green) and differentiated astrocytes (a subclass of the central nervous system glia) were labeled for GFAP (in orange). The graph in Fig. 6b-iv shows that gels formed by PAs had significantly more neurons than laminin and poly-D-lysine controls after both 1 and 7 days of culture [11]. In many cases, short peptide sequences such as RGD were attached to the peptide backbone of an amphiphilic peptide polymer to imbue passive hydrogels with biological activity [226].

5.2 Drug Delivery

Nanofibrillar hydrogels can be used as intelligent drug carriers in controlled drug delivery. The physical and chemical properties of such hydrogels can be engineered at the molecular level to optimize permeability, environmental-responsive nature, surface functionality, biodegradability, and surface biorecognition sites [221].

An example of nanofibrillar gels in drug delivery is a pH-sensitive microsphere-based controlled release system [227]. It utilizes CNCs, chitin nanowhiskers, and starch nanocrystals embedded within alginate microspheres, and illustrates the sustained release of the drug theophylline [228]. Gels formed by PAs are also good candidates for drug delivery as a result of their ability to traverse the phospholipid bilayer. The amphiphilic nature of PAs and their nanofibrillar structure facilitates the internalization of encapsulated drugs [225], while the increase in hydrophobicity of the peptide tails helps to deliver hydrophobic anticancer drugs such as doxorubicin and paclitaxel [229].

5.3 Stimuli-Responsive Nanofibrillar Hydrogels

The reversible nature of nanofibrillar gels allows the preparation of intelligent materials that respond to external triggers (e.g., changes in pH, temperature, or light) [216]. Micellar gels formed by block copolymers are particularly interesting because their self-assembly is governed by the hydrophobicity of the segregated block. Gelation can be reversible if the system's hydrophobicity is changed in response to an external stimulus. Due to the temperature-responsive nature of poly(*N*-isopropyl acrylamide)-*block*-poly(styrene) gels they have applications in the encapsulation and release of cells for subsequent characterization [167]. In addition, poly(glycerol momomethacrylate)-*block*-poly(2-hydroxypropyl methacrylate) copolymer, self-assembles into wormlike particles at 21 °C in aqueous solutions and forms a free-standing hydrogel above ambient temperature (21–25 °C). This block copolymer liquefies upon cooling to 4 °C, forming spherical micelles [10]. This behavior is beneficial for the sterilization of hydrogels, which is required for their biomedical applications. Ultrafiltration of these micelles leads to the complete removal of micrometer-sized bacteria.

5.4 Cosmetics and Skin Care

The inherent biocompatibility and relevant biological properties of nanofibrillar biopolymers render them useful for cosmetic and skin care applications. Current products largely utilize synthetic materials that are abrasive to the skin and are foreign to the protein-enriched epidermis [230]. Commercially available shampoos

and cosmetics employ low molecular weight surfactants for cleaning purposes. In contrast, self-assembled PA gels can act as antiwrinkle and antimicrobial products due to their inherent biological functions. Certain peptide sequences can stimulate the synthesis of skin constituents such as collagen, elastin, and glucosaminoglycans, which can aid in replenishing skin texture and reducing wrinkles without skin irritation [225].

Gels prepared from chitin nanofibers have the ability to sequester drugs and active cosmetic ingredients, subsequently releasing them by diffusion. Chitin nanofiber complexes may be used for skin and mucous membrane hydration, bone regeneration, and anti-aging or anti-acne cosmetic therapy. As seen in Fig. 6c, chitin nanofibers complexed with antioxidant or immunomodulant ingredients have great efficacy as anti-aging agents [22].

6 Outlook

The growing interest in nanofibrillar hydrogels is largely a testament to the realization that the extracellular matrix (ECM) has a profound influence on cell fate. In the present review, we have attempted to describe supramolecular nanofibrillar hydrogels derived from synthetic and natural polymers as instructive ECMs that mimic the composition, mechanical properties, and structure of natural ECMs. This aspect of nanofibrillar gels is currently a very active area of research in tissue engineering and therapeutics, as well as in basic cell biology research [218]. Future studies will continue to decouple the chemical, biophysical, and structural properties of gels in order to tune and explore the role of each property independently [9]. A greater emphasis will be placed on studies of cells in 3D hydrogel environments, which would complement conventional cell studies on 2D substrates.

The self-assembly of intelligent, responsive, and programmable hydrogels is a very active area of research in soft matter materials and nanofibrillar hydrogels in view of their biological importance. This work is especially important for cell-laden nanofibrillar hydrogels as these gels strongly scatter visible light, which interferes with the optical characterization of the encapsulated cells. An attractive concept is the reversible gelation of cell-laden nanofibrillar gels by applying a biological stimulus. After cell culture, the nanofibrillar hydrogel can be disintegrated "on demand" to release cells for further analysis.

In addition to cell culture and tissue engineering, nanofibrillar hydrogels can also be used in therapeutic applications, such as drug delivery. As an example, PA hydrogels have been used as injectable delivery agents of human embryonic stem cell secretome within a therapeutic setting [231]. In addition, these self-assembling nanofibrillar hydrogels can be designed to bind proteins and cells, and can be degraded in a predictable manner with respect to time and location.

Fundamental understanding has to be developed on the relationship between the structure of individual building blocks (including molecules and nanofibrils), their self-assembly mechanism into gels, and the resulting mechanical, optical, and

physical properties of the gel. The characteristics of nanofibrillar gels made from synthetic polymers also require further investigation. This is exemplified in the work of polymer wormlike micelles, whose gelation mechanism is disputed [44]. Furthermore, greater effort has to be directed toward enhancing the biocompatibility of man-made polymers. Each new hydrogel should be profoundly characterized and tested for its cytotoxicity. Although natural and synthetic polymers can be chemically modified, no single material can suit all potential applications. Consequently, interest is generated in composite systems that could build upon the lack of diverse properties in purely natural or synthetic polymers.

Fibrin gels are particularly important because their properties determine the behavior of occlusive thrombi. Recent reports describe the unique behavior of fibrin gels upon deformation, shear, and stretching [90, 196, 197, 232, 233]. Yet, fundamental understanding of the behavior of fibrin gels under strong confinement in blood vessels should shed light on the reasons for failed lysis with plasminogen activators, which is frequently observed in therapeutic treatment of occlusive thrombi.

Recently, microscale technologies offer a series of high-throughput combinatorial methods for exploring the properties of hydrogels. In particular, microfluidic methods have been used to generate vast libraries of cell-laden microgel particles acting as 3D cellular microenvironments with controllable dimensions and compositions [234–236]. Currently, microfluidic methods have been used to produce microgels from agarose [104], alginate [237], collagen [238], κ-carrageenan [239], and wormlike micelles [167], as well as from mixtures of polymers [105, 240]. Yet, the potential of microfluidics has not yet been fully realized with respect to fundamental and applied research on nanofibrillar gels.

The ability to form 3D hydrogels with anisotropic properties unlocks a new system for the exploration of the effect of ECM structure on cell fate, as cells may benefit from the directional cues provided by the anisotropic scaffolds. This effect was reported for neurons encapsulated within a PA gel that guided the growth of oriented neurites and the direction of cell migration [241]. The enticing field of cellulose nanofibrils offers the ability to form nematic and chiral nematic hydrogels with tunable structural characteristics [159, 242, 243]. Further work in this field could lead to the development of therapies that require directed cell migration or growth, or make use of the interconnections between cells in tissues such as heart, brain, and spinal cord [244].

In summary, in recent years, intense research has focused on the synthesis and assembly of nanofibrillar supramolecular polymer hydrogels. The nanofibrillar structure of these gels offers many potential benefits to their application; however, future development of this field will largely depend on the results of fundamental studies and applications of nanofibrillar hydrogels.

References

1. Hoffman AS (2002) Hydrogels for biomedical applications. Adv Drug Deliv Rev 54:3–12
2. Langer R, Tirrell DA (2004) Designing materials for biology and medicine. Nature 428:487–492
3. Djabourov M, Nishinari K, Ross-Murphy SB (2013) Physical gels from biological and synthetic polymers. Cambridge University Press, Cambridge
4. Lee KY, Mooney DJ (2001) Hydrogels for tissue engineering. Chem Rev 101:1869–1880
5. Vasudevan M, Buse E, Lu D et al (2010) Irreversible nanogel formation in surfactant solutions by microporous flow. Nat Mater 9:436–441
6. Jung JP, Gasiorowski JZ, Collier JH (2010) Fibrillar peptide gels in biotechnology and biomedicine. Pept Sci 94:49–59
7. Palmer LC, Leung C-Y, Kewalramani S et al (2014) Long-range ordering of highly charged self-assembled nanofilaments. J Am Chem Soc 136:14377–14380
8. Thomas S, Durand D, Chassenieux C, Jyotishkumar P (2013) Handbook of biopolymer-based materials: from blends and composites to gels and complex networks. Wiley, New York, 988p
9. Thiele J, Ma Y, Bruekers SMC et al (2014) Designer hydrogels for cell cultures: a materials selection guide. Adv Mater 26:125–147
10. Blanazs A, Verber R, Mykhaylyk OO et al (2012) Sterilizable gels from thermoresponsive block copolymer worms. J Am Chem Soc 134:9741–9748
11. Silva GA, Czeisler C, Niece KL et al (2004) Selective differentiation of neural progenitor cells by high-epitope density nanofibers. Science 303:1352–1355
12. Beachley V, Wen X (2010) Polymer nanofibrous structures: fabrication, biofunctionalization, and cell interactions. Prog Polym Sci 35:868–892
13. Cukierman E, Pankov R, Yamada KM (2002) Cell interactions with three-dimensional matrices. Curr Opin Cell Biol 14:633–639
14. Besseau L, Coulomb B, Lebreton-Decoster C, Giraud-Guille M-M (2002) Production of ordered collagen matrices for three-dimensional cell culture. Biomaterials 23:27–36
15. Mosesson MW (2005) Fibrinogen and fibrin structure and functions. J Thromb Haemost 3:1894–1904
16. Gentleman E, Lay AN, Dickerson D et al (2003) Mechanical characterization of collagen fibers and scaffolds for tissue engineering. Biomaterials 24:3805–3813
17. Lutolf MP (2009) Integration column: artificial ECM: expanding the cell biology toolbox in 3D. Integr Biol 1:235–241
18. Lou Y-R, Kanninen L, Kuisma T et al (2014) The use of nanofibrillar cellulose hydrogel as a flexible three-dimensional model to culture human pluripotent stem cells. Stem Cells Dev 23:380–392
19. Goldberg M, Langer R, Jia X (2007) Nanostructured materials for applications in drug delivery and tissue engineering. J Biomater Sci 18:241–268
20. Tønnesen HH, Karlsen J (2002) Alginate in drug delivery systems. Drug Dev Ind Pharm 28:621–630
21. Matson JB, Newcomb CJ, Bitton R, Stupp SI (2012) Nanostructure-templated control of drug release from peptide amphiphile nanofiber gels. Soft Matter 8:3586–3595
22. Morganti P (2011) From waste materials skin-friendly nanostructured products to save humans and the environment. J Cosmet Dermatol Sci Appl 01:99–105
23. Valenta C, Schultz K (2004) Influence of carrageenan on the rheology and skin permeation of microemulsion formulations. J Control Release 95:257–265
24. Augst AD, Kong HJ, Mooney DJ (2006) Alginate hydrogels as biomaterials. Macromol Biosci 6:623–633
25. De Ruiter GA, Rudolph B (1997) Carrageenan biotechnology. Trends Food Sci Technol 8:389–395

26. Arnott S, Fulmer A, Scott WE et al (1974) The agarose double helix and its function in agarose gel structure. J Mol Biol 90:269–284
27. Dufresne A (2012) Nanocellulose: from nature to high performance tailored materials. Walter de Gruyter, Berlin, 460p
28. Habibi Y, Lucia L, Rojas OJ (2010) Cellulose nanocrystals: chemistry, self-assembly, and applications. Chem Rev 110:3479–3500
29. Dutta PK, Dutta J, Tripathi VS (2004) Chitin and chitosan: chemistry, properties and applications. J Sci Ind Res 63:20–31
30. Qian J, Zhang M, Manners I, Winnik MA (2010) Nanofiber micelles from the self-assembly of block copolymers. Trends Biotechnol 28:84–92
31. Stupp SI, LeBonheur V, Walker K et al (1997) Supramolecular materials: self-organized nanostructures. Science 276:384–389
32. Kumacheva E, Garstecki P (2011) Microfluidic reactors for polymer particles. Wiley, New York, 236p
33. Matthews JA, Wnek GE, Simpson DG, Bowlin GL (2002) Electrospinning of collagen nanofibers. Biomacromolecules 3:232–238
34. Huang Z-M, Zhang Y-Z, Kotaki M, Ramakrishna S (2003) A review on polymer nanofibers by electrospinning and their applications in nanocomposites. Compos Sci Technol 63:2223–2253
35. Appel EA, del Barrio J, Loh XJ, Scherman OA (2012) Supramolecular polymeric hydrogels. Chem Soc Rev 41:6195–6214
36. De Loos M, Feringa BL, van Esch JH (2005) Design and application of self-assembled low molecular weight hydrogels. Eur J Org Chem 2005:3615–3631
37. Buerkle LE, Rowan SJ (2012) Supramolecular gels formed from multi-component low molecular weight species. Chem Soc Rev 41:6089–6102
38. Ekaputra AK, Prestwich GD, Cool SM, Hutmacher DW (2008) Combining electrospun scaffolds with electrosprayed hydrogels leads to three-dimensional cellularization of hybrid constructs. Biomacromolecules 9:2097–2103
39. Huang L, McMillan RA, Apkarian RP et al (2000) Generation of synthetic elastin-mimetic small diameter fibers and fiber networks. Macromolecules 33:2989–2997
40. Daniele MA, North SH, Naciri J et al (2013) Rapid and continuous hydrodynamically controlled fabrication of biohybrid microfibers. Adv Funct Mater 23:698–704
41. Lee J, Macosko CW, Urry DW (2001) Elastomeric polypentapeptides cross-linked into matrixes and fibers. Biomacromolecules 2:170–179
42. Shoulders MD, Raines RT (2009) Collagen structure and stability. Annu Rev Biochem 78:929–958
43. Morris ER, Rees DA, Thorn D, Welsh EJ (1977) Conformation and intermolecular interactions of carbohydrate chains. J Supramol Struct 6:259–274
44. Warren NJ, Armes SP (2014) Polymerization-induced self-assembly of block copolymer nano-objects via RAFT aqueous dispersion polymerization. J Am Chem Soc 136:10174–10185
45. Stendahl JC, Rao MS, Guler MO, Stupp SI (2006) Intermolecular forces in the self-assembly of peptide amphiphile nanofibers. Adv Funct Mater 16:499–508
46. Mai Y, Eisenberg A (2012) Self-assembly of block copolymers. Chem Soc Rev 41:5969–5985
47. Paramonov SE, Jun H, Hartgerink JD (2006) Self-assembly of peptide – amphiphile nanofibers: the roles of hydrogen bonding and amphiphilic packing. J Am Chem Soc 128:7291–7298
48. Craig AS, Birtles MJ, Conway JF, Parry DAD (2009) An estimate of the mean length of collagen fibrils in rat tail-tendon as a function of age. Connect Tissue Res 19:51–62
49. Koutsioubas A, Profumo A, Trevarin D et al (2014) A comprehensive mechanism of fibrin network formation involving early branching and delayed single-to double-strand transition from coupled time-resolved X. J Am Chem Soc 136:5376–5384

50. Serwer P (1983) Agarose gels: properties and use for electrophoresis. Electrophoresis 4:375–382
51. Raghavan SR, Douglas JF (2012) The conundrum of gel formation by molecular nanofibers, wormlike micelles, and filamentous proteins: gelation without cross-links? Soft Matter 8:8539–8546
52. Chiquet M (1999) Regulation of extracellular matrix gene expression by mechanical stress. Matrix Biol 18:417–426
53. Kadler KE, Baldock C, Bella J, Boot-Handford RP (2007) Collagens at a glance. J Cell Sci 120:1955–1958
54. Fratzl P, Misof K, Zizak I et al (1998) Fibrillar structure and mechanical properties of collagen. J Struct Biol 122:119–122
55. Vader D, Kabla A, Weitz D, Mahadevan L (2009) Strain-induced alignment in collagen gels. PLoS One 4:e5902
56. Roeder BA, Kokini K, Sturgis JE et al (2002) Tensile mechanical properties of three-dimensional type I collagen extracellular matrices with varied microstructure. J Biomech Eng 124:214–222
57. Weisel JW (2005) Fibrinogen and fibrin. Adv Protein Chem 70:247–299
58. Kang H, Wen Q, Janmey PA et al (2009) Nonlinear elasticity of stiff filament networks: strain stiffening, negative normal stress, and filament alignment in fibrin gels. J Phys Chem B 113:3799–3805
59. Kadler KE, Holmes DF, Trotter JA, Chapman JA (1996) Collagen fibril formation. Biochem J 316:1–11
60. Kuznetsova N, Rau DC, Parsegian VA, Leikin S (1997) Solvent hydrogen-bond network in protein self-assembly: solvation of collagen triple helices in nonaqueous solvents. Biophys J 72:353–362
61. Shayegan M, Forde NR (2013) Microrheological characterization of collagen systems: from molecular solutions to fibrillar gels. PLoS One 8:e70590
62. Wallace D (2003) Collagen gel systems for sustained delivery and tissue engineering. Adv Drug Deliv Rev 55:1631–1649
63. Diamant J, Keller A, Baer E et al (1972) Collagen; ultrastructure and its relation to mechanical properties as a function of ageing. Proc R Soc B 180:293–315
64. Folkhard W, Mosler E, Geercken W et al (1987) Quantitative analysis of the molecular sliding mechanisms in native tendon collagen—time-resolved dynamic studies using synchrotron radiation. Int J Biol Macromol 9:169–175
65. Yang Y, Motte S, Kaufman LJ (2010) Pore size variable type I collagen gels and their interaction with glioma cells. Biomaterials 31:5678–5688
66. Achilli M, Mantovani D (2010) Tailoring mechanical properties of collagen-based scaffolds for vascular tissue engineering: the effects of pH, temperature and ionic strength on gelation. Polymer 2:664–680
67. Laco F, Grant MH, Black RA (2013) Collagen-nanofiber hydrogel composites promote contact guidance of human lymphatic microvascular endothelial cells and directed capillary tube formation. J Biomed Mater Res A 101:1787–1799
68. Beier JP, Klumpp D, Rudisile M et al (2009) Collagen matrices from sponge to nano: new perspectives for tissue engineering of skeletal muscle. BMC Biotechnol 9:34
69. Xiong YL (1997) Structure-function relationships of muscle proteins. In: Damodaran S (ed) Food proteins and their application. CRC, Boca Raton, pp. 341–342
70. Sun XD, Holley RA (2011) Factors influencing gel formation by myofibrillar proteins in muscle foods. Compr Rev Food Sci Food Saf 10:33–51
71. Kim T, Hwang W, Kamm RD (2007) Computational analysis of a cross-linked actin-like network. Exp Mech 49:91–104
72. Holmes KC (2009) Structural biology: actin in a twist. Nature 457:389–390
73. Plastino J, Lelidis I, Prost J, Sykes C (2004) The effect of diffusion, depolymerization and nucleation promoting factors on actin gel growth. Eur Biophys J 33:310–320

74. Holmes KC, Popp D, Gebhard W, Kabsch W (1990) Atomic model of the actin filament. Nature 347:44–49
75. Shao Z, Shi D, Somlyo AV (2000) Cryoatomic force microscopy of filamentous actin. Biophys J 78:950–958
76. Oda T, Iwasa M, Aihara T et al (2009) The nature of the globular- to fibrous-actin transition. Nature 457:441–445
77. Maciver SK, Wachsstock DH, Schwarz WH, Pfollard TD (1991) The actin filament severing protein actophorin promotes the formation of rigid bundles of actin filaments crosslinked with α-actinin. J Cell Biol 115:1621–1628
78. Janmey PA, Hvidt S, Kas J et al (1994) The mechanical properties of actin gels. J Biol Chem 269:32503–32513
79. Zaner KS (1995) Physics of actin networks. 1. Rheology of semi-dilute F-actin. Biophys J 68:1019–1026
80. Niederman R, Amrein PC, Hartwig J (1983) Three-dimensional structure of actin filaments and of an actin gel made with actin-binding protein. J Cell Biol 96:1400–1413
81. Hartwig JH, Shevlin P (1986) The architecture of actin filaments and the ultrastructural location of actin-binding protein in the periphery of lung macrophages. J Cell Biol 103:1007–1020
82. Hirst LS, Pynn R, Bruinsma RF, Safinya CR (2005) Hierarchical self-assembly of actin bundle networks: gels with surface protein skin layers. J Chem Phys 123:104902
83. Kakugo A, Sugimoto S (2002) Gel machines constructed from chemically cross-linked actins and myosins. Adv Mater 14:1124–1126
84. Fogelson AL, Keener JP (2010) Toward an understanding of fibrin branching structure. Phys Rev E 81:51922
85. Yang Z, Mochalkin I, Doolittle RF (2000) A model of fibrin formation based on crystal structures of fibrinogen and fibrin fragments complexed with synthetic peptides. Proc Natl Acad Sci USA 97:14156–14161
86. Bale MD, Janmey PA, Ferry JD (1982) Kinetics of formation of fibrin oligomers. II. Size distributions of ligated oligomers. Biopolymers 21:2265–2277
87. Nagaswami C, Weisel JW, Makowski L (1987) Twisting of fibrin fibers limits their radial growth. Proc Natl Acad Sci USA 84:8991–8995
88. Magatti D, Molteni M, Cardinali B et al (2013) Modeling of fibrin gels based on confocal microscopy and light-scattering data. Biophys J 104:1151–1159
89. Weisel JW (2004) The mechanical properties of fibrin for basic scientists and clinicians. Biophys Chem 112:267–276
90. Brown AEX, Litvinov RI, Discher DE et al (2009) Multiscale mechanics of fibrin polymer: gel stretching with protein unfolding and loss of water. Science 325:741–744
91. Janmey PA, Winer JP, Weisel JW (2009) Fibrin gels and their clinical and bioengineering applications. J R Soc Interface 6:1–10
92. Ahmed TAE, Dare EV, Hincke M (2008) Fibrin: a versatile scaffold for tissue engineering applications. Tissue Eng B 14:199–215
93. Stanley FN (2006) Agars in food polysaccharides their applications. CRC, Boca Raton, pp 217–238
94. Domozych DS (2011) Algal cell walls in eLS. Wiley, London, pp 1–11
95. Aymard P, Martin DR, Plucknett K et al (2001) Influence of thermal history on the structural and mechanical properties of agarose gels. Biopolymers 59:131–144
96. Indovina PL, Tettamanti E, Micciancio-Giammarinaro MS, Palma MU (1979) Thermal hysteresis and reversibility of gel–sol transition in agarose–water systems. J Chem Phys 70:2841
97. Djabourov M, Clark AH, Rowlands DW, Ross-Murphy SB (1989) Small-angle x-ray scattering characterization of agarose sols and gels. Macromolecules 22:180–188

98. Maki Y, Ito K, Hosoya N et al (2011) Anisotropic structure of calcium-induced alginate gels by optical and small-angle X-ray scattering measurements. Biomacromolecules 12:2145–2152
99. Braccini I, Perez S (2001) Molecular basis of Ca 2+-induced gelation in alginates and pectins: the egg-box model revisited. Biomacromolecules 2:1089–1096
100. Agulhon P, Robitzer M, David L, Quignard F (2012) Structural regime identification in ionotropic alginate gels: influence of the cation nature and alginate structure. Biomacromolecules 13:215–220
101. Yuguchi Y, Thu Thuy TT, Urakawa H, Kajiwara K (2002) Structural characteristics of carrageenan gels: temperature and concentration dependence. Food Hydrocoll 16:515–522
102. Narayanan J, Xiong J-Y, Liu X-Y (2006) Determination of agarose gel pore size: absorbance measurements vis a vis other techniques. J Phys Conf Ser 28:83–86
103. Kumachev A, Tumarkin E, Walker GC, Kumacheva E (2013) Characterization of the mechanical properties of microgels acting as cellular microenvironments. Soft Matter 9:2959–2965
104. Kumachev A, Greener J, Tumarkin E et al (2011) High-throughput generation of hydrogel microbeads with varying elasticity for cell encapsulation. Biomaterials 32:1477–1483
105. Chau M, Abolhasani M, Li Y et al (2014) Microfluidic generation of composite biopolymer microgels with tunable compositions and mechanical properties. Biomacromolecules 15:2419–2425
106. Smidsrod O (1974) Molecular basis for some physical properties of alginates in the gel state. Faraday Discuss 57:263–274
107. Gombotz WR, Wee SF (2012) Protein release from alginate matrices. Adv Drug Deliv Rev 64:194–205
108. Pawar SN, Edgar KJ (2012) Alginate derivatization: a review of chemistry, properties and applications. Biomaterials 33:3279–3305
109. Pathak TS, Kim JS, Lee S-J et al (2008) Preparation of alginic acid and metal alginate from algae and their comparative study. J Polym Environ 16:198–204
110. Maki Y, Furusawa K, Yasuraoka S et al (2014) Universality and specificity in molecular orientation in anisotropic gels prepared by diffusion method. Carbohydr Polym 108:118–126
111. Qin Y (2004) Gel swelling properties of alginate fibers. J Appl Polym Sci 91:1641–1645
112. Campo VL, Kawano DF, Da Silva DB, Carvalho I (2009) Carrageenans: biological properties, chemical modifications and structural analysis – a review. Carbohydr Polym 77:167–180
113. Morris ER, Rees DA, Robinson G (1980) Cation-specific aggregation of carrageenan hekes: domain model of polymer gel structure. J Mol Biol 138:349–362
114. Piculell L, Borgström J, Chronakis I et al (1997) Organisation and association of κ-carrageenan helices under different salt conditions. Int J Biol Macromol 21:141–153
115. Chronakis IS, Doublier J-L, Piculell L (2000) Viscoelastic properties for kappa- and iota-carrageenan in aqueous NaI from the liquid-like to the solid-like behaviour. Int J Biol Macromol 28:1–14
116. Michel A-S, Mestdagh MM, Axelos MAV (1997) Physico-chemical properties of carrageenan gels in presence of various cations. Int J Biol Macromol 21:195–200
117. Thrimawithana TR, Young S, Dunstan DE, Alany RG (2010) Texture and rheological characterization kappa and iota carrageenan in the presence of counter ions. Carbohydr Polym 82:69–77
118. Picullel L, Håkansson C, Nilsson S (1987) Cation specificity of the order—disorder transition in iota carrageenan: effects of kappa carrageenan impurities. Int J Biol Macromol 9:297–301
119. Kara S, Tamerler C, Bermek H, Pekcan Ö (2003) Cation effects on sol–gel and gel–sol phase transitions of κ-carrageenan–water system. Int J Biol Macromol 31:177–185
120. Langendorff V, Cuvelier G, Michon C et al (2000) Effects of carrageenan type on the behaviour of carrageenan/milk mixtures. Food Hydrocoll 14:273–280
121. Prajapati VD, Maheriya PM, Jani GK, Solanki HK (2014) Carrageenan: a natural seaweed polysaccharide and its applications. Carbohydr Polym 105:97–112

122. Buck CB, Thompson CD, Roberts JN et al (2006) Carrageenan is a potent inhibitor of papillomavirus infection. PLoS Pathog 2:e69
123. Raabe D, Romano P, Sachs C et al (2006) Microstructure and crystallographic texture of the chitin–protein network in the biological composite material of the exoskeleton of the lobster Homarus americanus. Mater Sci Eng A 421:143–153
124. Tamura H, Nagahama H, Tokura S (2006) Preparation of chitin hydrogel under mild conditions. Cellulose 13:357–364
125. Jayakumar R, Prabaharan M, Nair SV, Tamura H (2010) Novel chitin and chitosan nanofibers in biomedical applications. Biotechnol Adv 28:142–150
126. Ifuku S, Nogi M, Abe K et al (2009) Preparation of chitin nanofibers with a uniform width as α-chitin from crab shells. Biomacromolecules 10:1584–1588
127. Ifuku S, Saimoto H (2012) Chitin nanofibers: preparations, modifications, and applications. Nanoscale 4:3308–3318
128. Fan Y, Saito T, Isogai A (2008) Preparation of chitin nanofibers from squid pen β-chitin by simple mechanical treatment under acid conditions. Biomacromolecules 9:1919–1923
129. Nata IF, Wang SS-S, Wu T-M, Lee C-K (2012) β-Chitin nanofibrils for self-sustaining hydrogels preparation via hydrothermal treatment. Carbohydr Polym 90:1509–1514
130. Araki J, Yamanaka Y, Ohkawa K (2012) Chitin-chitosan nanocomposite gels: reinforcement of chitosan hydrogels with rod-like chitin nanowhiskers. Polym J 44:713–717
131. Lavoine N, Desloges I, Dufresne A, Bras J (2012) Microfibrillated cellulose – its barrier properties and applications in cellulosic materials: a review. Carbohydr Polym 90:735–764
132. Dong H, Snyder JF, Williams KS, Andzelm JW (2013) Cation-induced hydrogels of cellulose nanofibrils with tunable moduli. Biomacromolecules 14:3338–3345
133. Dong XM, Kimura T, Gray DG (1996) Effects of ionic strength on the isotropic – chiral nematic phase transition of suspensions of cellulose crystallites. Langmuir 12:2076–2082
134. Araki J, Wada M, Kuga S, Okano T (2000) Birefringent glassy phase of a cellulose microcrystal suspension. Langmuir 16:2413–2415
135. Moon RJ, Martini A, Nairn J et al (2011) Cellulose nanomaterials review: structure, properties and nanocomposites. Chem Soc Rev 40:3941–3994
136. Abdul Khalil HPS, Bhat AH, Ireana Yusra AF (2012) Green composites from sustainable cellulose nanofibrils: a review. Carbohydr Polym 87:963–979
137. Li P, Liu R (2015) Cellulose gels and microgels – synthesis, service, and supramolecular interactions. In: Seiffert S (ed) Supramolecular polymer networks, Advances in Polymer Science. Springer, Cham
138. Isogai A, Saito T, Fukuzumi H (2011) TEMPO-oxidized cellulose nanofibers. Nanoscale 3:71–85
139. Saito T, Kimura S, Nishiyama Y, Isogai A (2007) Cellulose nanofibers prepared by TEMPO-mediated oxidation of native cellulose. Biomacromolecules 8:2485–2491
140. Fall AB, Lindström SB, Sprakel J, Wågberg L (2013) A physical cross-linking process of cellulose nanofibril gels with shear-controlled fibril orientation. Soft Matter 9:1852–1863
141. Pääkkö M, Ankerfors M, Kosonen H et al (2007) Enzymatic hydrolysis combined with mechanical shearing and high-pressure homogenization for nanoscale cellulose fibrils and strong gels. Biomacromolecules 8:1934–1941
142. Sehaqui H, Ezekiel Mushi N, Morimune S et al (2012) Cellulose nanofiber orientation in nanopaper and nanocomposites by cold drawing. ACS Appl Mater Interfaces 4:1043–1049
143. Pääkkö M, Vapaavuori J, Silvennoinen R et al (2008) Long and entangled native cellulose I nanofibers allow flexible aerogels and hierarchically porous templates for functionalities. Soft Matter 4:2492–2499
144. Bhattacharya M, Malinen MM, Lauren P et al (2012) Nanofibrillar cellulose hydrogel promotes three-dimensional liver cell culture. J Control Release 164:291–298
145. Ranby BG (1951) Fibrous macromolecular systems. Cellulose and muscle. The colloidal properties of cellulose micelles. Faraday Discuss 11:158–164

146. Marchessault RH, Morehead FF, Koch MJ (1961) Some hydrodynamic properties of neutral suspensions of cellulose crystallites as related to size and shape. J Colloid Sci 344:327–344
147. Dorris A, Gray DG (2012) Gelation of cellulose nanocrystal suspensions in glycerol. Cellulose 19:687–694
148. Lin N, Dufresne A (2014) Surface chemistry, morphological analysis and properties of cellulose nanocrystals with gradiented sulfation degrees. Nanoscale 6:5384–5393
149. Klemm D, Kramer F, Moritz S et al (2011) Nanocelluloses: a new family of nature-based materials. Angew Chem 50:5438–5466
150. Dong XM, Revol J-F, Gray DG (1998) Effect of microcrystallite preparation conditions on the formation of colloid crystals of cellulose. Cellulose 5:19–32
151. Liu D, Chen X, Yue Y et al (2011) Structure and rheology of nanocrystalline cellulose. Carbohydr Polym 84:316–322
152. Urena-Benavides EE, Ao G, Davis VA, Kitchens CL (2011) Rheology and phase behavior of lyotropic cellulose nanocrystal suspensions. Macromolecules 44:8990–8998
153. Shafiei-Sabet S, Hamad WY, Hatzikiriakos SG (2013) Influence of degree of sulfation on the rheology of cellulose nanocrystal suspensions. Rheol Acta 52:741–751
154. Derakhshandeh B, Petekidis G, Shafiei-Sabet S et al (2013) Ageing, yielding, and rheology of nanocrystalline cellulose suspensions. J Rheol 57:131–148
155. Marchessault RH, Morehead FF, Walter NM (1959) Liquid crystal systems from fibrillar polysaccharides. Nature 184:632–633
156. Shafiei-Sabet S, Hamad WY, Hatzikiriakos SG (2014) Ionic strength effects on the microstructure and shear rheology of cellulose nanocrystal suspensions. Cellulose 21:3347–3359
157. Habibi Y (2014) Key advances in the chemical modification of nanocelluloses. Chem Soc Rev 43:1519–1542
158. Eyley S, Thielemans W (2014) Surface modification of cellulose nanocrystals. Nanoscale 6:7764–7779
159. Hasani M, Cranston ED, Westman G, Gray DG (2008) Cationic surface functionalization of cellulose nanocrystals. Soft Matter 4:2238–2244
160. Way AE, Hsu L, Shanmuganathan K et al (2012) pH-Responsive cellulose nanocrystal gels and nanocomposites. ACS Macro Lett 1:1001–1006
161. Wang Y, Chen L (2011) Impacts of nanowhisker on formation kinetics and properties of all-cellulose composite gels. Carbohydr Polym 83:1937–1946
162. Kalia S, Dufresne A, Cherian BM et al (2011) Cellulose-based bio- and nanocomposites: a review. Int J Polym Sci 2011:1–35
163. Bates FS, Fredrickson GH (1999) Block copolymers-designer soft materials. Phys Today 52:32–38
164. Zhang L, Eisenberg A (1999) Thermodynamic vs kinetic aspects in the formation and morphological transitions of crew-cut aggregates produced by self-assembly of polystyrene-b-poly(acrylic acid) block copolymers in dilute solution. Macromolecules 32:2239–2249
165. Jain S, Bates FS (2003) On the origins of morphological complexity in block copolymer surfactants. Science 300:460–464
166. Discher DE, Ahmed F (2006) Polymersomes. Annu Rev Biomed Eng 8:323–341
167. Velasco D, Chau M, Therien-Aubin H et al (2013) Nanofibrillar thermoreversible micellar microgels. Soft Matter 9:2380–2383
168. Dagdas YS, Tombuloglu A, Tekinay AB et al (2011) Interfiber interactions alter the stiffness of gels formed by supramolecular self-assembled nanofibers. Soft Matter 7:3524–3532
169. Gilroy JB, Gädt T, Whittell GR et al (2010) Monodisperse cylindrical micelles by crystallization-driven living self-assembly. Nat Chem 2:566–570
170. Charleux B, Delaittre G, Rieger J, D'Agosto F (2012) Polymerization-induced self-assembly: from soluble macromolecules to block copolymer nano-objects in one step. Macromolecules 45:6753–6765
171. Won Y-Y, Davis HT, Bates FS (1999) Giant wormlike rubber micelles. Science 283:960–963

172. Fernández VVA, Tepale N, Álvarez JG et al (2009) Rheology of the Pluronic P103/water system in a semidilute regime: evidence of nonequilibrium critical behavior. J Colloid Interface Sci 336:842–849
173. Duval M, Waton G, Schosseler F (2005) Temperature-induced growth of wormlike copolymer micelles. Langmuir 21:4904–4911
174. Cates ME (1996) Flow behaviour of entangled surfactant micelles. J Phys Condens Matter 8:9167
175. Clausen TM, Vinson PK, Minter JR et al (1992) Viscoelastic micellar solutions: microscopy and rheology. J Phys Chem 96:474–484
176. Dreiss CA (2007) Wormlike micelles: where do we stand? Recent developments, linear rheology and scattering techniques. Soft Matter 3:956–970
177. Kessel S, Urbani CN, Monteiro MJ (2011) Mechanically driven reorganization of thermoresponsive diblock copolymer assemblies in water. Angew Chem 50:8082–8085
178. Verber R, Blanazs A, Armes SP (2012) Rheological studies of thermo-responsive diblock copolymer worm gels. Soft Matter 8:9915–9922
179. Blanazs A, Ryan AJ, Armes SP (2012) Predictive phase diagrams for RAFT aqueous dispersion polymerization: effect of block copolymer composition, molecular weight, and copolymer concentration. Macromolecules 45:5099–5107
180. Lee C-U, Lu L, Chen J et al (2013) Crystallization-driven thermoreversible gelation of coil-crystalline cyclic and linear diblock copolypeptoids. ACS Macro Lett 2:436–440
181. Hartgerink JD, Beniash E, Stupp SI (2001) Self-assembly and mineralization of peptide-amphiphile nanofibers. Science 294:1684–1688
182. Greenfield MA, Hoffman JR, de la Cruz MO, Stupp SI (2010) Tunable mechanics of peptide nanofiber gels. Langmuir 26:3641–3647
183. Kisiday J, Jin M, Kurz B et al (2002) Self-assembling peptide hydrogel fosters chondrocyte extracellular matrix production and cell division: implications for cartilage tissue repair. Proc Natl Acad Sci USA 99:9996–10001
184. Holmes TC, de Lacalle S, Su X et al (2000) Extensive neurite outgrowth and active synapse formation on self-assembling peptide scaffolds. Proc Natl Acad Sci USA 97:6728–6733
185. Nanda J, Banerjee A (2012) β-Amino acid containing proteolitically stable dipeptide based hydrogels: encapsulation and sustained release of some important biomolecules at physiological pH and temperature. Soft Matter 8:3380
186. Kim J, Anderson J, Jun H et al (2009) Self-assembling peptide amphiphile-based nanofiber gel for bioresponsive cisplatin delivery. Mol Pharm 6:978–985
187. Chen J, Chen X, Yang X et al (2013) Bioactive glasses-incorporated, core-shell-structured polypeptide/polysaccharide nanofibrous hydrogels. Carbohydr Polym 92:612–620
188. Acciaro R, Aulin C, Wågberg L et al (2011) Investigation of the formation, structure and release characteristics of self-assembled composite films of cellulose nanofibrils and temperature responsive microgels. Soft Matter 7:1369–1377
189. Jang J, Oh H, Lee J et al (2013) A cell-laden nanofiber/hydrogel composite structure with tough-soft mechanical property. Appl Phys Lett 102:211914
190. Acciaro R, Aulin C, Lars W et al (2011) A novel fibrin gel derived from hyaluronic acid-grafted fibrinogen. Biomed Mater 6:25009
191. Wang J, Ying X, Li X, Zhang W (2014) Preparation, characterization and swelling behaviors of polyurethane-grafted calcium alginate hydrogels. Mater Lett 126:263–266
192. Huang Z, Feng Q, Yu B, Li S (2011) Biomimetic properties of an injectable chitosan/nano-hydroxyapatite/collagen composite. Mater Sci Eng C 31:683–687
193. Chambon F, Winter HH (1987) Linear viscoelasticity at the gel point of a crosslinking PDMS with imbalanced stoichiometry. J Rheol 31:683–697
194. Fernández E, López D, Mijangos C et al (2008) Rheological and thermal properties of agarose aqueous solutions and hydrogels. J Polym Sci B 46:322–328
195. Shah J, Janmey P (1997) Strain hardening of fibrin gels and plasma clots. Rheol Acta 36:262–268

196. Liu W, Carlisle CR, Sparks EA, Guthold M (2010) The mechanical properties of single fibrin fibers. J Thromb Haemost 8:1030–1036
197. Münster S, Jawerth LM, Leslie BA et al (2013) Strain history dependence of the nonlinear stress response of fibrin and collagen networks. Proc Natl Acad Sci USA 110:12197–12202
198. Li Y, Kumacheva E, Ramachandran A (2013) The motion of a microgel in an axisymmetric constriction with a tapered entrance. Soft Matter 9:10391–10403
199. Zamora-Mora V, Velasco D, Hernández R et al (2014) Chitosan/agarose hydrogels: cooperative properties and microfluidic preparation. Carbohydr Polym 111:348–355
200. Anseth KS, Bowman CN, Brannon-Peppas L (1996) Mechanical properties of hydrogels and their experimental determination. Biomaterials 17:1647–1657
201. Parry DAD (1988) The molecular fibrillar structure of collagen and its relationship to the mechanical properties of connective tissue. Biophys Chem 29:195–209
202. Lake SP, Hald ES, Barocas VH (2011) Collagen-agarose co-gels as a model for collagen–matrix interaction in soft tissues subjected to indentation. J Biomed Mater Res A 99A:507–515
203. Carrillo J-MY, MacKintosh FC, Dobrynin AV (2013) Nonlinear elasticity: from single chain to networks and gels. Macromolecules 46:3679–3692
204. Tanaka F, Edwards SF (1992) Viscoelastic properties of physically crosslinked networks: Part 3. Time-dependent phenomena. J Nonnewton Fluid Mech 43:289–309
205. Tanaka F, Edwards SF (1992) Viscoelastic properties of physically crosslinked networks: Part 2. Dynamic mechanical moduli. J Nonnewton Fluid Mech 43:273–288
206. Tanaka F, Edwards SF (1992) Viscoelastic properties of physically crosslinked networks: Part 1. Non-linear stationary viscoelasticity. J Nonnewton Fluid Mech 43:247–271
207. Green MS, Tobolsky AV (1946) A new approach to the theory of relaxing polymeric media. J Chem Phys 14:80–92
208. Gittes F, MacKintosh FC (1998) Dynamic shear modulus of a semiflexible polymer network. Phys Rev E 58:R1241–R1244
209. Shankar V, Pasquali M, Morse DC (2002) Theory of linear viscoelasticity of semiflexible rods in dilute solution. J Rheol 46:1111
210. Fakhri N, Tsyboulski DA, Cognet L et al (2009) Diameter-dependent bending dynamics of single-walled carbon nanotubes in liquids. Proc Natl Acad Sci USA 106:14219–14223
211. Kara S, Tamerler C, Bermek H, Pekcan Ö (2003) Hysteresis during sol-gel and gel-sol phase transitions of κ-carrageenan: a photon transmission study. J Bioact Compat Polym 18:33–44
212. Iijima M, Takahashi M, Hatakeyama T, Hatakeyama H (2013) Detailed investigation of gel-sol transition temperature of κ-carrageenan studied by DSC, TMA and FBM. J Therm Anal Calorim 114:895–901
213. Lahaye M, Rochas C (1991) Chemical structure and physico-chemical properties of agar. Hydrobiologia 221:137–148
214. Forget A, Christensen J, Lüdeke S et al (2013) Polysaccharide hydrogels with tunable stiffness and provasculogenic properties via α-helix to β-sheet switch in secondary structure. Proc Natl Acad Sci USA 110:12887–12892
215. Schild HG (1992) Poly(N-isopropylacrylamide): experiment, theory and application. Prog Polym Sci 17:163–249
216. Xu B (2009) Gels as functional nanomaterials for biology and medicine. Langmuir 25:8375–8377
217. Patil SP, Jeong HS, Kim BH (2012) A low-molecular-weight supramolecular hydrogel of riboflavin bolaamphiphile for VEGF-siRNA delivery. Chem Commun 48:8901–8903
218. Lutolf MP, Hubbell JA (2005) Synthetic biomaterials as instructive extracellular microenvironments for morphogenesis in tissue engineering. Nat Biotechnol 23:47–55
219. Ho STB, Cool SM, Hui JH, Hutmacher DW (2010) The influence of fibrin based hydrogels on the chondrogenic differentiation of human bone marrow stromal cells. Biomaterials 31:38–47
220. Batorsky A, Liao J, Lund AW et al (2005) Encapsulation of adult human mesenchymal stem cells within collagen-agarose microenvironments. Biotechnol Bioeng 92:492–500

221. Peppas NA, Hilt JZ, Khademhosseini A, Langer R (2006) Hydrogels in biology and medicine: from molecular principles to bionanotechnology. Adv Mater 18:1345–1360
222. Friess W (1998) Collagen–biomaterial for drug delivery. Eur J Pharm Biopharm 45:113–136
223. Valdes N, Bertrand L, Woerly S, Marchand R (1993) Evaluation of two cross-linked collagen gels implanted in the transected spinal cord. Brain Res Bull 30:415–422
224. Rowley JA, Madlambayan G, Mooney DJ (1999) Alginate hydrogels as synthetic extracellular matrix materials. Biomaterials 20:45–53
225. Zhao X, Pan F, Xu H et al (2010) Molecular self-assembly and applications of designer peptide amphiphiles. Chem Soc Rev 39:3480–3498
226. Shroff K, Rexeisen EL, Arunagirinathan MA, Kokkoli E (2010) Fibronectin-mimetic peptide-amphiphile nanofiber gels support increased cell adhesion and promote ECM production. Soft Matter 6:5064–5072
227. Lin N, Huang J, Chang PR et al (2011) Effect of polysaccharide nanocrystals on structure, properties, and drug release kinetics of alginate-based microspheres. Colloids Surf B 85:270–279
228. Lin N, Huang J, Dufresne A (2012) Preparation, properties and applications of polysaccharide nanocrystals in advanced functional nanomaterials: a review. Nanoscale 4:3274–3294
229. Wiradharma N, Tong YW, Yang Y-Y (2009) Self-assembled oligopeptide nanostructures for co-delivery of drug and gene with synergistic therapeutic effect. Biomaterials 30:3100–3109
230. Proksch E, Brandner JM, Jensen J-M (2008) The skin: an indispensable barrier. Exp Dermatol 17:1063–1072
231. Bakota E, Wang Y (2011) Injectable multidomain peptide nanofiber hydrogel as a delivery agent for stem cell secretome. Biomacromolecules 12:1651–1657
232. Kim OV, Litvinov RI, Weisel JW, Alber MS (2014) Structural basis for the nonlinear mechanics of fibrin networks under compression. Biomaterials 35:6739–6749
233. Liu W, Jawerth L, Sparks E et al (2006) Fibrin fibers have extraordinary extensibility and elasticity. Science 313:634
234. Velasco D, Tumarkin E, Kumacheva E (2012) Microfluidic encapsulation of cells in polymer microgels. Small 8:1633–1642
235. Tumarkin E, Tzadu L, Csaszar E et al (2011) High-throughput combinatorial cell co-culture using microfluidics. Integr Biol 3:653–662
236. Khademhosseini A, Langer R, Borenstein J, Vacanti JP (2006) Microscale technologies for tissue engineering and biology. Proc Natl Acad Sci USA 103:2480–2487
237. Liu K, Ding H, Liu J et al (2006) Shape-controlled production of biodegradable calcium alginate gel microparticles using a novel microfluidic device. Langmuir 22:9453–9457
238. Hong S, Hsu H-J, Kaunas R, Kameoka J (2012) Collagen microsphere production on a chip. Lab Chip 12:3277–3280
239. Zhang H, Tumarkin E, Peerani R et al (2006) Microfluidic production of biopolymer microcapsules with controlled morphology. J Am Chem Soc 128:12205–12210
240. Ma S, Thiele J, Liu X et al (2012) Fabrication of microgel particles with complex shape via selective polymerization of aqueous two-phase systems. Small 8:2356–2360
241. Berns EJ, Sur S, Pan L et al (2014) Aligned neurite outgrowth and directed cell migration in self-assembled monodomain gels. Biomaterials 35:185–195
242. Kelly JA, Shukaliak AM, Cheung CCY et al (2013) Responsive photonic hydrogels based on nanocrystalline cellulose. Angew Chem 52:8912–8916
243. Hu Z, Cranston ED, Ng R, Pelton R (2014) Tuning cellulose nanocrystal gelation with polysaccharides and surfactants. Langmuir 30:2684–2692
244. Zhang S, Greenfield MA, Mata A et al (2010) A self-assembly pathway to aligned monodomain gels. Nat Mater 9:594–601

Cellulose Gels and Microgels: Synthesis, Service, and Supramolecular Interactions

Pingping Li and Ruigang Liu

Contents

Abstract This chapter provides an overview of recent research on cellulose-based gels and microgels cross-linked by and/or subject to supramolecular interactions, in which native cellulose, regenerated cellulose, cellulose derivatives, and cellulose graft copolymers are used as the building blocks. Supramolecular interactions such as hydrophobic interactions, hydrogen bonding, and ionic interactions act as a physical means of cross-linking within these cellulose-based gels and microgels. The resulting "smart" supramolecular gels and microgels have many advantages,

P. Li
State Key Laboratory of Polymer Physics and Chemistry, Beijing National Laboratory of Molecular Sciences, Institute of Chemistry, Chinese Academy of Sciences, Beijing 100190, China

University of Chinese Academy of Science, Beijing 100049, China

R. Liu (✉)
State Key Laboratory of Polymer Physics and Chemistry, Beijing National Laboratory of Molecular Sciences, Institute of Chemistry, Chinese Academy of Sciences, Beijing 100190, China
e-mail: rgliu@iccas.ac.cn

© Springer International Publishing Switzerland 2015

S. Seiffert (ed.), *Supramolecular Polymer Networks and Gels*, Advances in Polymer Science 268, DOI 10.1007/978-3-319-15404-6_6

with a particular view to their intelligent behavior in reaction to environmental stimuli such as pH, temperature, light, electricity, magnetic fields, and mechanical forces, all mediated by specific supramolecular polymer–polymer and polymer–solvent interactions. Cellulose-based supramolecular gels and microgels have been applied or have promising potential for applications in tissue engineering, drug delivery, blood purification, sensors, agriculture, water purification, chromatographic supports, and catalyst supports. This review provides information on using celluloses as building blocks for the fabrication of functional supramolecular materials that are not limited to just gels and microgels.

Keywords Aerogels • Cellulose • Derivatives • Graft copolymers • Hydrogels • Physical cross-linking • Supramolecular interactions

Abbreviations

AMIMCl	1-Allyl-3-methylimidazolium chloride
ATRP	Atom transfer radical polymerization
AuNP	Gold nanoparticle
BC	Bacterial cellulose
BMIMCl	1-Butyl-3-methylimidazolium chloride
CA	Cellulose acetate
CDA	Cellulose diacetate
CMC	Carboxymethyl cellulose (sodium)
CNC	Cellulose nanocrystal
CNF	Cellulose nanofibril
CRP	Controlled/living radical polymerization
DMAc	*N*,*N*-Dimethyacetamide
DMSO	Dimethylsulfoxide
EC	Ethyl cellulose
HA	Hyaluronic acid
HEC	Hydroxyethyl cellulose
HPC	Hydroxypropyl cellulose
HPMC	Hydroxypropylmethyl cellulose
IL	Ionic liquid
IPN	Interpenetrating polymer network
LCST	Lower critical solution temperature
MBA	*N*,*N*′-methylene bisacrylamide
MC	Methyl cellulose
MNP	Magnetic nanoparticle
NMMO	*N*-Methylmorpholine-*N*-oxide
NMP	Nitroxide-mediated polymerization
P4VP	Poly(4-vinyl pyridine)
PAA	Poly(acrylic acid)

PAAm	Polyacrylamide
PANI	Polyanaline
PCL	Poly(ε-caprolactone)
PNIPAm	Poly(*N*-isopropylacrylamide)
PVA	Poly(vinyl alcohol)
QD	Quantum dot
RAFT	Reversible addition-fragmentation chain transfer
ROP	Ring-opening polymerization
TEM	Transmission electron microscopy
TEMPO	2,2,6,6-Tetramethypiperidine-1-oxyl

1 Introduction

As a typical type of soft material, gels and microgels have the properties of both liquids and solids, pervading our daily life in a variety of forms such as stabilizing agents and suspending agents in cosmetics and pharmaceutical formulations [1], contact lenses [2], purification [3] and agriculture [4], as well as the food industry [5]. In general, gels and microgels are viscoelastic solid-like materials comprising an elastic, cross-linked polymer network and a solvent [6]. They have two distinct features: continuity of their macrostructure and of rheological properties, similar to that of solid-like materials [7–9]. Gels can be classified in different ways according to their cross-linking type, source, medium, and size [8]. According to the cross-linkages, gels are sorted into chemical gels [10, 11] and physical gels [12–15] that can also be generally called supramolecular gels [8]. Chemical gels and microgels are cross-linked by covalent bonds and are nonreversible. In physical gels, the networks are held together by weak noncovalent interactions like hydrogen bonding, π–π stacking, donor–acceptor interactions, metal coordination, host–guest interaction, solvophobic forces (hydrophobic forces for gels in water), and van der Waals interactions. These weak noncovalent interactions are easy to break; hence, such physical gels are reversible and can be readily transformed to a fluid (sol) on changing environmental conditions such as temperature, pH, ionic strength, light, redox agents, and electric and magnetic fields. In an additional scheme of classification, gels can be divided into natural macromolecular gels and synthetic gels on the basis of the origin of their source. Over the last decades, synthetic gels with controllable compositions and architectures as well as adjustable mechanical properties have been developed and applied; a popular example is that of poly (ethylene glycol)-based hydrogels [16]. However, these synthetic gels often lack unique biological properties such as nontoxicity, biocompatibility, and biodegradability, which are preferred or even required design criteria for use in biomedical fields [17]. As an alternative to synthetic polymers like poly(ethylene glycol), polysaccharides such as chitosan [18], dextran [19], hyaluronate [20], alginate [21], cellulose [22], and their derivatives have been used to fabricate gels. Of

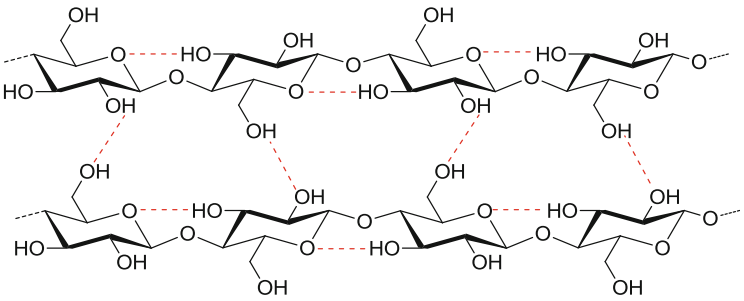

Fig. 1 Molecular structure and inter- and intramolecular hydrogen bonds of cellulose (Reproduced by referring to [24])

these polysaccharides, cellulose is the most abundant renewable natural polymer, and it is a strong candidate for the fabrication of gels and microgels [23].

Cellulose is a polysaccharide consisting of D-anhydrogluco-pyranose units linked by β-(1-4)-glycosidic bonds. The high content of hydroxyl groups enables cellulose-based networks to be formed and strengthened by hydrogen bonding (Fig. 1) [25]. The design and use of cellulose-based gels and microgels, which usually combine safety, biocompatibility, hydrophilicity, and biodegradability, together with the vast availability of cellulose in nature and the low cost of cellulose derivatives, make them particularly attractive [22]. These properties enable cellulose-based gels and microgels to be used in a vast array of fields such as drug delivery [26], blood purification [27], waste treatment [28], and reinforcement of materials [29].

This chapter presents the recent progress in cellulose-based supramolecular gels and microgels, including gels and microgels prepared from natural cellulose and its derivatives, cellulose graft copolymers, and composite gels and microgels based on cellulose, with a particular emphasis on physical cross-linking of cellulose-based gels. In addition, the properties, supramolecular interactions, and some resulting potential applications of cellulose-based gels and microgels are discussed. With this scope, this chapter offers an overview of cellulose-based gels and microgels, which may assist in the design of novel, effective, and functional supramolecular materials.

2 Gels and Microgels Prepared from Cellulose

Cellulose is insoluble in water and common organic solvents, and cannot melt because of strong inter- and intra-molecular hydrogen bonds caused by the abundant content of hydroxyl groups and the stereoregularity of the cellulose chains (Fig. 1). Therefore, it is difficult to produce cellulose articles by solution or melting processes [23]. Recently, Lindman and coworkers pointed out that cellulose is significantly amphiphilic and hydrophobic interactions may be important in

understanding its solubility pattern [30]; this is generally debated in the society of cellulose researchers [31]. Nevertheless, in principle, the strong inter- and intramolecular hydrogen bonds, together with the hydrophobic interactions between cellulose chains, play key roles in the formation of hydrogels or microgels from cellulose, especially for supramolecular cellulose hydrogels prepared from native celluloses such as nanocellulose (including cellulose nanocrystals, nanofibrils and bacterial cellulose) and regenerated cellulose from cellulose solutions. Cellulose gels, for example, are utilized for chromatographic columns [32], as modified membranes for waste cleaning [4], as substitutes in fermented sausages [33], and as superabsorbent materials applied for body water elimination in the treatment of edemas [34].

2.1 Supramolecular Gels Prepared from Cellulose Solutions

As a result of the strong hydrogen bonding networks in cellulose, the so-named viscose process dominates for the preparation of regenerated-cellulose products. However, this process has the drawbacks of environmental pollution and long tedious processing procedures. Over the past decades, direct and environmental friendly solvent systems, such as *N*-methylmorpholine-*N*-oxide (NMMO) monohydrate [35, 36], *N*,*N*-dimethyacetamide (DMAc)/LiCl [37–39], ionic liquids (ILs) [40, 41], and NaOH (or LiOH)/(thio)urea aqueous systems [42–45], have been developed to dissolve cellulose, providing great opportunities for the preparation of cellulose-based materials, including gels. On the other hand, it is possible to take advantage of the exceptional rigidity of the cellulose backbone, which is the primary basis for the strength of cellulose-based gels [17, 46].

Cellulose gels prepared from the above-mentioned solvent systems are stabilized by physical cross-linking via strong intra- and intermolecular hydrogen bonds, as shown in Fig. 1, leading to extended networks. Therefore, even if these gels are fabricated by physical cross-linking, they are mostly irreversible and hard to disrupt. Generally, physical cellulose gels are prepared by two approaches, as shown schematically in Fig. 2. One is the coagulation approach, in which cellulose solutions are first precipitated in coagulation media, followed by washing out of the coagulation media and cellulose solvents with water to obtain cellulose hydrogels. The other is the gelation approach, in which cellulose solutions form gels through thermal gelation, and then the solvents are washed out with water. The resulting cellulose hydrogels can be dried to obtain cellulose aerogels.

2.1.1 Cellulose Hydrogels via Coagulation

The preparation of cellulose hydrogels via coagulation depends on the properties of the pre-gel cellulose solutions. In this approach, cellulose solutions are generally stable. The solutions for preparing cellulose hydrogels include cellulose in DMAc/

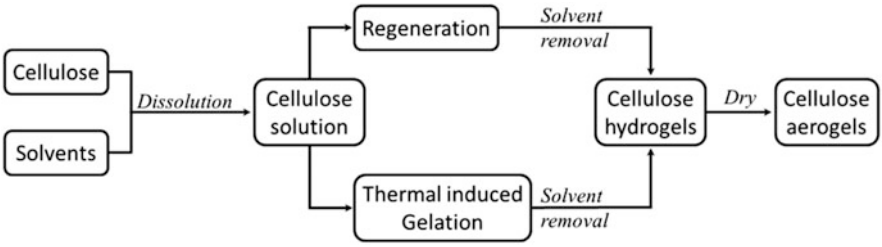

Fig. 2 Methods for preparing cellulose hydrogels and aerogels from cellulose solutions

LiCl, ILs, and NMMO. DMAc/LiCl has been chosen for the analysis of high molecular weight cellulose, which contributes to the exploration of cellulose gels and microgels. Cellulose hydrogels in bead form have been prepared by dropwise addition of cellulose/DMAc/LiCl solutions into methanol or isopropanol as the nonsolvent. Results show that the resulting bead properties greatly depend on the cellulose concentration in the solution; they also depend on the viscosity and the molecular weight of the precursor cellulose [47]. Following this work, highly transparent cellulose hydrogels were prepared by coagulation and regeneration of cellulose from various cellulose solutions by using water-miscible organic solvents as the coagulation/regeneration bath. The solvent systems used for preparing cellulose solutions were DMAc/LiCl (9:1, v/v), paraformaldeyde/dimethylsulfoxide (DMSO) (1:15, v/v), and triethylammonium chloride/DMSO (7:13, v/v). The physical properties of the resulting hydrogels were found to mainly depend on the composition of the regeneration bath. Cellulose hydrogels with a maximum transparency of 97 % were prepared using nonaqueous organic solutions as the regeneration bath [48, 49]. The parameters for the preparation of cellulose hydrogels from cellulose/DMAc/LiCl solutions, such as the activation of cellulose, dissolution time, gelation humidity, and cellulose concentration, were also optimized, and their correlations with the optical transparency and/or tensile/tear strength of the resulting hydrogels were investigated in detail. The presence of water has a great influence on the physical properties of cellulose solutions. Even a small amount of water gives rise to a strong increase in viscosity, resulting in gelation [50]. Similar behavior was observed in a tetrabutylammonium fluoride (TBAF)/DMSO system, and the influence of water was attributed to competitive hydrogen bonding. Östlund and coworkers found that cellulose hydrogels can be regenerated from a mixture of TBAF/DMSO solutions by varying the water content or the cellulose concentration [51].

Cellulose can be directly dissolved in some hydrophilic ionic liquids, such as 1-butyl-3-methylimidazolium chloride (BMIMCl) and 1-allyl-3-methylimidazolium chloride (AMIMCl) [52]. Cellulose can be easily regenerated from its IL solutions by addition of water, ethanol, or acetone, showing the same degree of polymerization as the initial cellulose, thereby indicating that no degradation occurred during the procedure. By different regeneration processes, regenerated cellulose materials can be obtained in powder, tube, beard, fiber, and film forms [40,

41, 52–54]. Novel transparent cellulose hydrogels with good chemical stabilities and acceptable mechanical properties have been prepared by regenerating cellulose from cellulose/AMIMCl solution in deionized water [55]. Kaneko and coworkers reported a facile approach for preparation of a flexible cellulose hydrogel material from cellulose/BMIMCl (15 wt%) solution by keeping the solution at room temperature for 7 days [56]. Low humidity is required for the gelation, because water interferes by coordinating to the anions [57]. Zaumseil and coworkers prepared a new class of biofriendly ionogels by gelation of microcellulose thin films with tailored 1-ethyl-3-methylimidazolium methylphosphonate ILs. These cellulose ionogels show properties such as transparency, flexibility, transferability, and high specific capacitances of 5–15 μF cm^{-2} that make them promising for applications in flexible electronics [58].

Many studies have shown the NMMO aqueous system to be a simple physical technology that can be used as a substitute for the viscose technology for preparing regenerated-cellulose materials [36]. The NMMO monohydrate is able to dissolve cellulose of high molecular weight at high temperature to give a transparent solution. Innerlohinger et al. prepared gels from cellulose/NMMO solutions by regenerating with water, NMMO, alcohol, or acetone and then drying under supercritical conditions, which will be discussed in Sect. 6 [59]. However, only a few other reports have focused on hydrogels prepared using the NMMO system.

2.1.2 Cellulose Hydrogels via Gelation

The thermally induced gelation approach for preparing cellulose gels is based on the finding of fast dissolution of cellulose in precooled alkali/(thio)urea aqueous solutions by Zhang's research group at Wuhan University (China). The specific cellulose direct solvent system is based on alkali/(thio)urea aqueous solutions, such as NaOH/urea, NaOH/thiourea, and LiOH/urea aqueous systems. After the solvents are pre-cooled to a temperature of −12 to −5 °C, cellulose powder can be completely dissolved in them in about 2 min [42, 44]. These solvent systems have a great capacity for dissolving cellulose. Regenerated-cellulose materials in different forms (fibers, membranes, microspheres, and hydrogels) have been successfully prepared from cellulose solutions of the new solvents [60–62].

Cellulose solutions in alkali/(thio)urea aqueous systems tend to gel with rising temperature [63–65] or even during storage at low temperature [66], which is a result of reconstruction of the intermolecular hydrogen bonding networks of cellulose in the system. The gelation point of the cellulose solutions depends on temperature, storage time, concentration, and molecular weight of the cellulose. The gelation procedure is irreversible. Cellulose hydrogels can be obtained after washing out NaOH and urea from the resultant gels [63]. Based on this pioneering work, cellulose gels with various swelling ratios and compressive strengths have been prepared. The morphology, swelling ratio, and compressive strength of the resultant cellulose hydrogels depend on the acid concentration in the washing bath, the time that the primary gels were immersed in the washing bath, and the

molecular weight of the cellulose [67]. The NaOH/thiourea aqueous system has better dissolution ability and needs less energy to dissolve cellulose than a NaOH/urea aqueous system [43]. The gelation of cellulose/6 wt% NaOH/5 wt% thiourea aqueous solutions was investigated in detail [64]. It was found that gelation occurred at either a relatively high temperature for a short time (e.g., 60 °C for 30 s) or at a low temperature for a longer time (e.g., 30 °C for 157 s). The gels were composed of relatively stable network units, with an average diameter of about 47 nm [64]. In the case of dissolving cellulose in a NaOH/thiourea aqueous system with higher NaOH content, the resultant cellulose solutions were more stable. Physical gelation occurred during storage of the cellulose solution at either high temperature or low temperature. At a temperature of 10–30 °C, the sol–gel transition of the cellulose solution is partially reversible. However, cellulose gels formed at a higher temperature (above 60 °C) are irreversible [66]. An aqueous solution of 5 wt% LiOH/12 wt% urea pre-cooled to −12 °C has higher solubility for cellulose compared with that of NaOH/urea and NaOH/thiourea systems. The LiOH hydrate combines more easily with cellulose hydroxyl groups to form new hydrogen-bonding networks at low temperature, resulting in the destruction of the cellulose original hydrogen bonds, and thereby bringing cellulose into aqueous solution [65]. This solvent system has been used to prepare highly porous and strong aerogels by gelation of cellulose/LiOH/urea aqueous solutions [61, 68].

Besides the popular alkali/(thio)urea aqueous system, a new all-aqueous process of dissolution and regeneration of cellulose by using lithium bromide (LiBr) aqueous solution at high temperature has been reported [69]. In this novel aqueous solution system, cellulose can be completely dissolved in a LiBr (54–60 wt%) aqueous solution at a temperature of 110–130 °C within just 1 h. Cellulose in the solution can be directly regenerated from the solution by cooling to approximately 70 °C and removing the salts with water, yielding a translucent gel. No significant chemical decomposition of the cellulose occurs during dissolution and regeneration in this solvent system. Cellulose gels prepared by this approach had highly porous three-dimensional networks composed of fairly long cellulose fibrils interconnected with one another [69]. The dissolution and regeneration of cellulose in this LiBr aqueous system therefore offers a new and important option for preparing new cellulose-based materials.

The irreversible supramolecular hydrogels prepared from cellulose solutions by physical cross-linking via strong intra- and intermolecular hydrogen bonds mentioned in the previous section are attractive. However, their mechanical and swelling properties are somewhat poor and, hence, their applications are limited. The introduction of chemical cross-linking to the networks can improve the mechanical strength and the swelling properties of native cellulose gels without destroying their inner structures, thereby broadening their application range. There are abundant hydroxyl groups on the cellulose chains that can be used for introducing chemical cross-links. Other methods that can produce free radicals (e.g., irradiation) or other reactive functional groups can also be used for introducing cross-links to cellulose gels.

2.2 *Supramolecular Cellulose Hydrogels Prepared from Nanocellulose*

Nanocelluloses, including long and entangled cellulose nanofibrils (CNFs) with an aspect ratio of over 250 and short rodlike cellulose nanocrystals (CNCs) with an aspect ratio of 10–100 [29, 70], have gained much attention because of their inherent renewability and sustainability, their abundance, and also because of their unsurpassed quintessential physical and chemical properties [71–73]. Nanocelluloses have diameters of a few nanometers and excellent mechanical properties, with a modulus of about 140 GPa and a tensile strength in the gigapascal range as a result of the strong hydrogen-bonded assembly of parallel cellulose chains in their native cellulose I crystalline domains [74]. One of the attractive features of nanocelluloses is the possibility of tailoring their surface properties through functionalization of the surface hydroxyl groups [75]. Nanocelluloses have been used as reinforcing fillers in plastic materials and as synthetic supports for functional materials [76–78]. Furthermore, fundamental studies have recently proven that the CNFs can adapt diverse bulk forms, such as films [79–81], hydrogels [17, 82, 83], and aerogels [70, 84–86]. Capadona et al. [87–89] reported a versatile processing approach based on the formation of a three-dimensional template through self-assembly of well-individualized CNCs, and then filling of the template with a polymer of choice. This process is broadly applicable and allows the fabrication of otherwise inaccessible nanocomposites of immiscible components. In their work, a CNC gel template was first prepared from homogeneous aqueous dispersions of CNC through solvent exchange using a water-miscible solvent (routinely acetone). The CNC gel template was then filled with a matrix polymer by immersing the gel in a polymer solution. In this approach, the polymer solvent must be miscible with the gel solvent and must not re-disperse the CNCs. The reported materials show significantly improved mechanical properties and are of interest in their own right [71, 88].

CNCs were first carboxylated by 2,2,6,6-tetramethypiperidine-1-oxyl (TEMPO) oxidation, followed by grafting of amine-terminated Jeffamine through peptidic coupling. Based on CNCs functionalized with carboxylic acid (CNC–COOH) or with amine moieties (CNC–NH_2), pH-responsive supramolecular gels and nanocomposites were fabricated [29]. In an aqueous environment of high pH, the CNC–COOH blocks are deprotonated and negatively charged, which leads to significant attenuation of the attractive interactions between the CNCs. Conversely, at low pH, the CNC–COOH blocks are protonated, and attractive interactions should occur through hydrogen bonding of the carboxylic acid and hydroxyl moieties. The CNC–NH_2 blocks can be expected to behave in an opposite manner. It was found that neutral or weakly charged CNCs show better mechanical reinforcement than their highly charged counterparts. It is possible to alter the surface chemistry of the CNCs. Therefore, a change in the stimulus that is used to alter the CNC interactions allows tailoring of the mechanical properties of the corresponding CNC suspensions, gels, and nanocomposites. Thus, the stimuli-sensitivity of the

dynamic nanocomposites can be reprogrammed by simple surface functionalization of the CNCs, which offers exciting opportunities for designing mechanically adaptable materials that are responsive to desired stimuli [29, 89]. Following this pioneering work, physically cross-linked aqueous CNF supramolecular gels were fabricated by reducing the pH or adding salt to diminish the electrostatic repulsion between the CNFs, thus preserving the uniform spatial distribution of CNFs in the dispersed state. By applying shear during or after this gelation process, the CNFs can be oriented in a preferred direction within the gel. In this state, the high stiffness and strength of the CNFs can be fully utilized as the reinforcement component, which can optimize the potentially large reinforcement capacity of the CNFs [70, 90]. A facile concept, in which enzymatic hydrolysis is used in combination with mechanical shearing and high-pressure homogenization, has been proposed to control the CNFs down to the nanoscale network of long and highly entangled cellulose I elements. The resulting strong aqueous gels exhibit excellent mechanical properties [82]. Abe and Yano prepared hydrogels from an aqueous suspension of CNFs simply by alkaline treatment followed by neutralization, by which two types of hydrogels with different crystal forms (cellulose I and highly crystalline II) were formed below and above NaOH concentrations of approximately 12 wt%, respectively. The cellulose I-type hydrogel was formed by entanglement of original nanofibers, and the cellulose II-type hydrogel had a network formed by coalescence of CNFs via mercerization, caused by longitudinal shrinkage of the CNFs in aqueous alkaline solutions [83]. Both of the hydrogels exhibited excellent tensile properties because of the crystalline network in the gels, especially the nanofiber hydrogel with a cellulose II crystal structure [91].

Pelton and coworkers found that the gelation of dilute CNC suspensions is induced by introduction of the nonionic polysaccharides hydroxyethyl cellulose (HEC), hydroxypropyl guar, and locust bean gum, whereas dextran has no influence on gelation. The ability of a polysaccharide to induce gelation directly correlates with the tendency of adsorption of the polymer onto the CNC surfaces and leads to a dramatic increase in the effective volume fraction of CNC dispersions, by which the CNCs are driven into a completely anisotropic phase with a sufficient yield stress to not flow when inverted. Addition of surfactants to HEC–CNC invertible gels gives a range of behaviors depending on the nature of the surfactant. Anionic sodium dodecyl sulfate and nonionic Triton X-100 decompose the gels by inducing HEC desorption from CNC surfaces, whereas gels are preserved in the presence of cationic hexadecyltrimethylammonium bromide. The CNCs gels were found to be very sensitive to the presence of water-soluble polymers and surfactants in the system [92]. Ikkala and coworkers reported a particularly facile and scalable method for preparing tunable all-cellulose thermosensitive gels by incorporating a mixture of colloidal rodlike CNCs physically bound together with methyl cellulose (MC) chains. By changing the CNC loading and temperature, the storage modulus of the nanocomposite hydrogels could be tuned over a broad window of three orders of magnitude, from 1 Pa (20 °C) to 2,200 Pa (75 °C) with a fixed amount of MC (1.0 wt%). This facile method allows homogeneous dispersions of

CNCs within a biopolymer matrix to be prepared and provides a versatile approach for preparing new types of CNC-based hydrogels [93].

2.3 *Supramolecular Cellulose Hydrogels Prepared from Bacterial Cellulose*

Microbial or bacterial cellulose (BC) produced by *Acetobacter xylinuma* is formed by a hierarchical cell-directed self-assembly process and is chemically identical to plant cellulose [93]. Compared with cellulose from plants, however, BC has a higher crystallinity (above 60 %), a higher degree of polymerization (between 2,000 and 6,000), and more favorable tensile strength; it is also totally pure [94]. BC exhibits remarkable mechanical properties as a result of its uniform ultrafine-fiber network structure, highly planar orientation of the ribbon-like fibers when compressed into sheets, good chemical stability, and high water holding capacity [25].

On static cultivation, BC displays a gel-like fibril network with inappropriate orientation at the air–liquid interface. With regard to the structure of this BC gel, a simple technique was developed to prepare tubular BC gels with proper fibril orientation via culturing *A. xylinuma* in oxygen-permeable silicone tubes with inner diameters of less than 8 mm. The tubular BC gels have the desired length, inner diameter, and thickness, with uniaxially oriented cellulose fibrils, which is beneficial for the stiffness and strength of these BC gels [95]. The water content in BC gels produced by *A. xylinuma* is about 99 wt%. However, only about 10 % of the water present in BC gels behaves like free bulk water, while the majority of the water molecules in the gels are bound to the cellulose [96]. These gels have been used in headphone diaphragms, electroacoustic transducers, high strength paper, and components for precision optical devices [97, 98]. Applications in the biomaterials field [99] including wound dressing [100], meniscus implants [101], and dental implants [102]; scaffolds for tissue engineering [50, 103] have also been investigated.

Despite their favorable characteristics, BC gels in the nascent state lack certain properties, which limits their applications. Thus, composite hydrogels with improved functional properties have been designed to address these limitations [104]. A variety of BC composite synthetic strategies have been developed based on combined materials, including xyloglucan, pectin, gelatin, and other synthetic polymers such as poly(vinyl alcohol) (PVA) or polyanaline (PANI) [98, 105, 106], or inorganic nanoparticles of silver, gold, palladium, iron oxide, platinum, and titanium oxide [103]. BC composites are primarily synthesized through in situ addition of reinforcement materials to BC synthetic media or ex situ penetration of such materials into BC microfibrils [106].

3 Supramolecular (Micro)Gels Based on Cellulose Derivatives

There are a huge number of hydroxyl groups on cellulose chains, offering various possibilities for preparing cellulose derivatives via esterification and etherification (Fig. 3). Most water-soluble cellulose derivatives are obtained via etherification of cellulose, which involves reaction of the hydroxyl groups of cellulose with organic species such as methyl and ethyl units. The degree of substitution, defined as the average number of etherified hydroxyl groups in a glucose unit, can be controlled to a certain extent to obtain cellulose derivatives with given solubility and viscosity in water. Most of the cellulose derivatives are biocompatible polymers used in a wide range of applications, especially as thickeners, binding agents, emulsifiers, film formers, suspension aids, surfactants, lubricants, and stabilizers in the food, cosmetics, and pharmaceutical industries [107, 108]. The most common cellulose derivatives, including MC [109], hydroxypropyl cellulose (HPC) [110], carboxymethyl cellulose (CMC) [111], and hydroxypropylmethyl cellulose (HPMC) [107], can be used to prepare gels by using both physical and chemical cross-linking.

It has been reported that cellulose derivatives such as MC [109], cellulose diacetate (CDA) [112], HPC [110], and HPMC [107] can form thermoreversible supramolecular gels in aqueous solution upon heating [113]. In principle, gelation

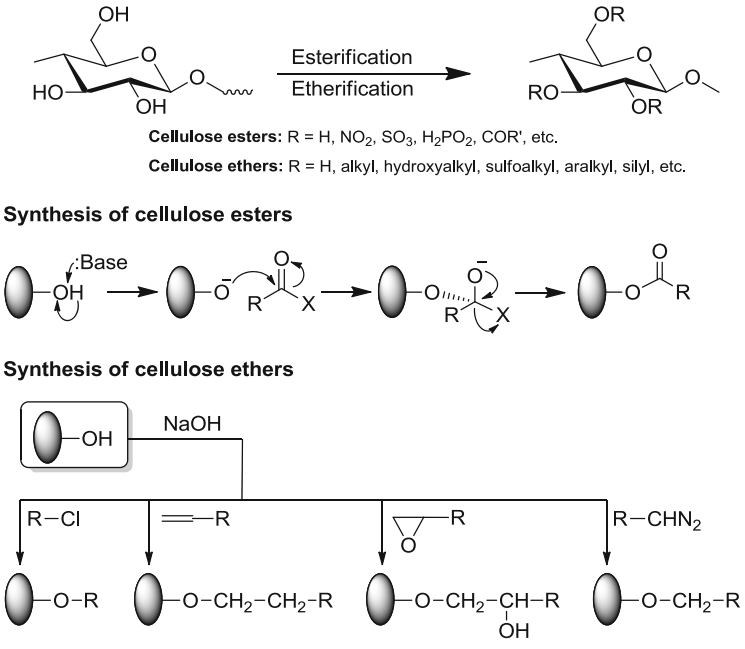

Fig. 3 Synthetic approaches for cellulose derivatives

of such cellulose derivatives in aqueous solution occurs as a result of dehydration of the chains along with hydrophobic association of the chain segments, by which physical cross-links are formed, leading to three-dimensional polymer-network structures. The gelation of different cellulose derivatives occurs with different efficiency and kinetics, depending on parameters such as the degree of substitution of the functional groups, the molar mass of the polymer, temperature, etc.

In MC aqueous systems, thermally induced gelation is reversible. MC aqueous solutions undergo gelation upon heating but revert to a liquid phase upon cooling [114]. MC can be considered as an alternative block copolymer that consists of densely substituted hydrophobic and less-substituted hydrophilic block sequences. The hydrophobic parts are considered to form a structure of water around them in aqueous solution. Experimental results suggest that there are two stages during the thermally induced gelation of MC in an aqueous environment [109, 115–119]: slow coalescence and aggregation of hydrophobic chain segments, followed by optimization of hydrophobic contacts that act as effective cross-links, which is opposed by network stresses due to chain stretching [109, 115–119]. On raising the temperature, the structure of water molecules around the densely substituted hydrophobic block sequences is disrupted. The densely substituted parts of MC form droplets, while the hydrophilic parts prefer to remain in water, thereby preventing coalescence of the droplets. Therefore, the droplets are actually described as "micelles" and act as "cross-linking loci" to form MC supramolecular gels [114]. The resultant MC hydrogel networks consist of hydrophobically associating domains as the junctions, with a mean chain length of 2.75×10^4 g mol^{-1} as bridges connecting them [118–120]. For isothermally stabilized samples, 42.5 °C was found to be the critical temperature differentiating weak gels from strong gels [119, 120]. Reported data indicate that the gelation of MC aqueous solutions depends on the chain length, degree of substitution and/or positions of substituents, salt, surfactant, and the polymer concentration [117, 121, 122].

Sekiguchi et al. discussed the hydrophobic interactions and hydrogen bonds contributing to thermally reversible gelation of aqueous solutions for *O*-methylcellulose. It was found that the gelation behavior of the regioselectively substituted 2,3-di-*O*-methylcellulose differed from that of randomly substituted *O*-methylcellulose. The difference could be a result of cooperation of the hydrophobic interaction between methyl substituents with intermolecular hydrogen bonds between hydroxyl groups at the C(6) position, which are dependent on the distribution of methyl groups [123].

In the case of HPMC, the hydroxyl groups are replaced by hydroxypropyl and methyl groups. Compared with MC of equivalent substitution and molecular weight, HPMC has a higher gelation temperature and forms a looser gel structure, suggesting that hydroxypropyl substituents make the gelation process more difficult [107, 123, 124]. Investigation of the thermal behavior of HPMC aqueous solutions depicts the gelation procedure of the system upon heating: First, polymer reptation becomes faster as a result of thermal motion, which leads to a weaker network. Second, above 55 °C, the polymer chains become more hydrophobic, and polymer clusters start to form. Finally, the number of physical cross-links between polymer

clusters and the respective lifetimes increase, and a three-dimensional supramolecular network is formed [107].

In contrast, HPC, which does not contain methoxyl substituents, precipitates on heating but does not form a gel. This has been seen as evidence that gelation of cellulose derivatives results from exclusion of water (syneresis) from richly methoxylated regions of the polymer [107, 123, 124]. However, in dilute aqueous solutions of HPC, dynamically stable nano-aggregates can be formed by heating the solution to a temperature of a few degrees higher than the lower critical solution temperature (LCST) (41–44 °C). The nano-aggregates are formed via chain association and can last for a few days without changing their sizes and molar masses. Increasing temperature in this range and increasing HPC concentration resulted in larger and denser nano-aggregates. The self-associated HPC chain nanoparticles can be cross-linked to obtain narrowly distributed surfactant-free HPC microgels [110]. By further introduction of other functional group on the HPC chains, such as thiolate [125] and azobenzene groups [126], it is possible to fabricate HPC microgels responsive to physiological, environmental, or photo stimuli.

Besides the above-mentioned common cellulose derivatives, amphiphilic self-associating cellulose derivatives, that is, hydrophobically modified HEC (HM-HEC), have been synthesized by introducing hydrophobic moieties (long-chain alkyl groups) onto the HEC backbones. The amphiphilic HM-HEC can self-assemble into nano-aggregates with hydrophobic alkyl-segment cores and hydrophilic shells. The core can act as a reservoir for accommodating hydrophobic fluorescent conjugated polymers (CPs). As a result of the maximized interaction between the analyte (e.g., nitroaromatics) and fluorescent sensing material in the cellulose-based nano-aggregates, the sensitivity of the resulting fluorescent nanoaggregate aqueous solution to trace amounts of hydrophobic nitroaromatics is 50-fold higher than that of the chromophores in organic solvent [127].

Host–guest interactions have also been applied for the fabrication of cellulose supramolecular hydrogels. β-Cyclodextrin (β-CD) amphiphiles, substituted with hydrophobic *n*-dodecyl chains on the primary side and hydrophilic oligo(ethylene glycol) groups on the secondary side of the macrocycle, and adamantane-functionalized HEC can assemble into supramolecular hydrogels. The HEC/β-CD supramolecular hydrogels are responsive as they can be readily destroyed by addition of a competitive host and guest. Most striking, these hydrogels show shear-thinning and self-healing properties and have been demonstrated to be injectable, with a fast recovery of the gel bulk structure [128]. Moreover, Huang and coworkers developed a cellulose supramolecular gel based on β-CD-cellulose/ferrocene (Fc)-cellulose under mild conditions. Results show that the sol–gel transition can be controlled by altering the oxidation and reduction state of Fc using NaClO as the oxidant and glutathione as the reductant. The compressive strength of the Fc-cellulose/β-CD-cellulose gel increases with the cellulose concentration, while the host–guest interactions between the side chains of cellulose strengthen the gel [129].

In principle, any host–guest pair that is known from supramolecular chemistry can be used for preparing cellulose-based gels through host–guest interactions. The

key issue is to link functional groups onto the cellulose backbones. More details about such supramolecular gels can be found in recent reviews [130–135].

Recently, much effort has been spent on preparing physically cross-linked cellulose-based gels and microgels to circumvent the use of cross-linking agents, which can affect the integrity of a substance to be entrapped within the gel in an application (e.g., proteins, cells) and which are often toxic and need to be removed/extracted from the gel before its use. However, physically cross-linked supramolecular hydrogels are reversible [136]; thus, they can flow under given conditions (e.g., under perceptible mechanical loading) and might degrade in an uncontrollable manner. Because of such drawbacks, physical hydrogels based on MC and HPMC are not recommended for use in vivo. By contrast, in vitro, MC hydrogels have been recently proposed as novel sheet harvest systems [137].

4 Supramolecular (Micro)Gels Based on Cellulose Graft Copolymers

In the past decades, chemical modifications of cellulose or its derivatives has been investigated extensively for the preparation of cellulose-based materials with desired properties, such as resistance to heat or abrasion, mechanical strength, water or oil repellence, and antibacterial activity [138]. Modification of cellulose via graft copolymerization is an attractive approach, by which the chemical and physical properties of the cellulose can be combined with those of the synthetic side chains. Three approaches for the synthesis of graft copolymers, "grafting to," "grafting from," and "grafting through" [139], can be applied for synthesizing cellulose graft copolymers [140–143]. Of these, "grafting from" is the most popular technique.

The graft copolymerization of many monomers onto cellulose or its derivatives has been investigated extensively. Typical methods include conventional free-radical polymerization, controlled/living radical polymerization (CRP), and ring-opening polymerization (ROP) [144]. In the conventional free-radical graft copolymerization of cellulose, radicals can be conveniently generated along the cellulose backbone by chemical initiators such as potassium persulfate, Fenton's reagent (Fe^{2+}–H_2O_2), and Ce(IV) ions or by applying irradiation such as γ-radiation, ultraviolet radiation, and plasma radiation [144]. Typical CRPs, including nitroxide-mediated polymerization (NMP) [145], atom transfer radical polymerization (ATRP) [146], and reversible addition-fragmentation chain transfer (RAFT) [147], have also received great attention for the design of cellulose-based graft copolymers with well-defined architectures. The synthesis of cellulose graft copolymers using free radical graft copolymerization is summarized in Table 1. The properties of the resulting graft copolymers are various, depending on the chemical structure of both the cellulosic backbones and the grafted side chains (e.g., thermal, pH, or dually stimuli-responsive properties) [197], and contribute to the physical

Table 1 Selection of cellulose graft copolymers

	Monomers	Grafting methods	Properties	References
Cellulose	MMA, MA, St, GMA	(ARGET) ATRP, RAFT	Hydrophobic	[148–152]
	HEMA, AA, DEGMA, EDMA	Ozone	pH sensitive	[153–157]
	NIPAAm, 4-VP	Ce(IV), ATRP, RAFT	Thermosensitive	[158–160]
	DMAEMA	ATRP, RAFT	Thermo/pH sensitive	[161–163]
	Lactide	ROP	Spherical nanomicelles	[164]
	SBMA	ATRP	Ziwitterionic	[165]
CNC	4-VP	Ce(IV)	pH sensitive	[166]
	DMAEMA	APS	Thermo/pH sensitive	[167]
	DMAEMA, NpMA	ATRP		[168]
BC	AbA	Irradiation	pH sensitive	[169]
MC	NIPAAm	APS/TEMED	Thermosensitive	[170]
EC	2-HEMA	ATRP		[171]
	DMAEMA, CL	ATRP and ROP	pH sensitive	[172]
	CL, with folate (FA)	ROP	Targeted drug release	[173]
	EGMA	ATRP	Thermosensitive	[174]
	MMAZO	ATRP	Photosensitive	[175]
	MMA	ATRP	Rodlike	[176]
	t-BA	ATRP	Hydrolyzes to EC-*g*-PAA	[177, 178]
	St	ATRP	Core–shell structure	[179, 180]
	DEAEMA	ATRP	pH sensitive	[181]
	PEGMA, NIPAAm	ATRP	Thermosensitive	[140, 182]
HPC	AA, 2-HEMA, AN	Benzoyl peroxide	Comb	[183]
	MMA, *t*-BA, HDMA	ATRP	Thermo/pH sensitive	[184]
	DMAEMA	ATRP	Thermo/pH sensitive	[185, 186]
	NIPAAm	ATRP	Thermosensitive	[187, 188]
	AA	APS/TEMED	Thermo/pH sensitive	[189]
	4-VP	ATRP	Thermo/pH sensitive	[146]
HEC	AA	Ce(IV)		[190]
	PPDO	ROP and "grafting to"		[191]

(continued)

Table 1 (continued)

	Monomers	Grafting methods	Properties	References
CDA	MMA St, MMA, BuA	ATRP		[192, 193]
	St, BuA, MMA, CL	ROP and ATRP		[194]
CMC	PEPO	Graft to	Thermosensitive	[195]
	AAm	APS/TEMED	pH sensitive	[196]

AbA acrylated abietic acid, *APS* $(NH_4)_2S_2O_8$, *ARGET* activators regenerated by electron transfer, *t-BA tert*-Butyl acrylate, *CL* ε-caprolactone, *DEAEMA* 2-(diethylamino)ethyl methacrylate, *DMAEMA N,N*-dimethyl aminoethyl methacrylate, *PEGMA* poly(ethylene glycol) methyl ether methacrylate, *PMMAZO* 6-[4-(4-methoxyphenyl azo)phenoxy]hexyl methacrylate, *SBMA* sulfobetaine methacrylate, *St* styrene, *TEMED N,N,N′,N′*-tetramethyl ethylene diamine

cross-linking to form (micro)gels. The architectures of the supramolecular (micro) gels can be tailored through the architecture of the cellulose graft copolymers and the environmental conditions [143, 198]. These gels have promising applications as carriers for controlled-released delivery of drugs [181, 199].

Cellulose graft copolymers can self-assemble into coacervates with different structures and morphologies in suitable media. Unlike micelles formed by surfactants or block copolymers with well-defined molecular weight, coacervate micelles are tiny spherical droplets held together by hydrophobic forces from the surrounding liquid. They can be considered as microgels or nanogels, depending on their size. Such supramolecular microgels have potential applications in various fields by choosing different types of side chains [200, 201]. Because of their relatively long side chains, supramolecular microgels prepared from cellulose graft copolymers can have core–shell structures, in which the core is rich in the cellulose backbone and the shell rich in the side chains, or vice versa, depending on the properties of the graft copolymers and the medium [191].

The formation of coacervate micelles of cellulose graft copolymers can be induced by changing the temperature, pH, or ionic strength, or by adding nonsolvent or incompatible polymers to the solutions, depending on the properties of the copolymers. One typical example is HPC with poly(2-dimethylamino-ethylmethacrylate) (PDMAEMA) side chains (HPC-*g*-PDMAEMA). The HPC backbone is thermally sensitive in aqueous solution. The PDMAEMA side chains are weak polyelectrolytes ($pK_a \approx 8.0$) and can be protonated in acidic solution, which leads to an increase in electrostatic repulsion and prevents phase separation [202, 203]. Therefore, HPC-*g*-PDMAEMA copolymers are dually sensitive, and the structure of the coacervate micelles formed by these copolymers can be controlled by the temperature and pH of the solution [186]. Figure 4 shows the formation of coacervate micelles of HPC-*g*-PDMAEMA under different conditions. The ^1H NMR spectra clarify the structures of the coacervate micelles obtained. The LCST of HPC-*g*-PDMAEMA shifts to lower temperatures with increasing pH. At pH 3.0, the HPC backbone becomes hydrophobic upon heating to above 42 °C, during which coacervate micelles with a HPC-rich core are formed and stabilized by a protonated PDMAEMA-rich shell. At pH 8.0, the HPC backbone and the PDMAEMA side chains collapse simultaneously upon heating. At pH 11.0, the

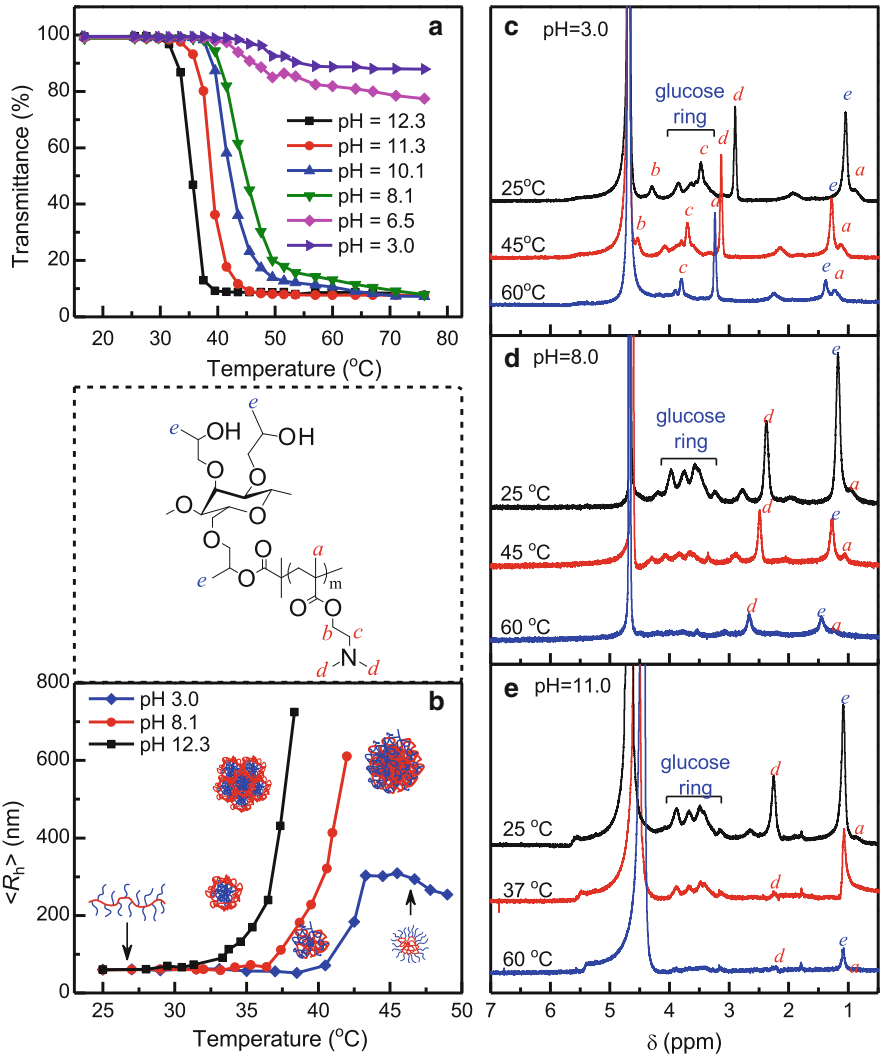

Fig. 4 Formation of coacervate micelles of HPC-*g*-PDMAEMA. (**a**) Transmittance of the copolymer aqueous solutions as a function of temperature at different pH values. (**b**) Temperature dependence of $<R_h>$ of the copolymers in aqueous solution at different pH values.(**c**–**d**) ^{1}H NMR spectra of the copolymer solutions in D_2O at pH values of 3.0 (**c**), 8.0 (**d**), and 11.0 (**e**) at the denoted temperatures. Peaks *a*–*e* correspond to the positions shown in the copolymer structure on the *left* (Reproduced, with permission, from [186], Copyright 2010, American Chemical Society)

PDMAEMA side chains first collapse to form the core of oppositely structured coacervate micelles stabilized with HPC chains upon heating. Further heating at this pH leads to aggregation of the micelles as a result of collapse of the shell HPC chains [186].

HPC-*g*-P4VP, with thermally sensitive HPC backbones and pH-sensitive poly (4-vinyl pyridine) (P4VP) side chains, can form coacervate micelles by changing the temperature and pH of the solutions (Fig. 5). At pH < 4, coacervate micelles with HPC-rich cores stabilized by P4VP-rich shells are formed. Moreover, as a result of deprotonation of the P4VP side chains at pH > 4, coacervate micelles with P4VP-rich cores stabilized by HPC-rich shells are formed at room temperature [146]. The self-assembled micelles can be used as carriers for drugs [181] and genes [185] and also for their controlled release. Moreover, cellulose graft copolymers can be used as biosensors: HPC-*g*-P4VP graft copolymers have been further conjugated with Os(bipyridine) [Os(bpy)] to yield HPC-*g*-P4VP-Os(bpy) with pH-dependent redox properties and a wide working window, making it possible to be used for the decoration of electrodes in biosensor applications. The electrochemical properties of the graft polymer-modified electrode are responsive to the pH of the electrolyte solution. At high pH (e.g., above the pK_a of P4VP), the

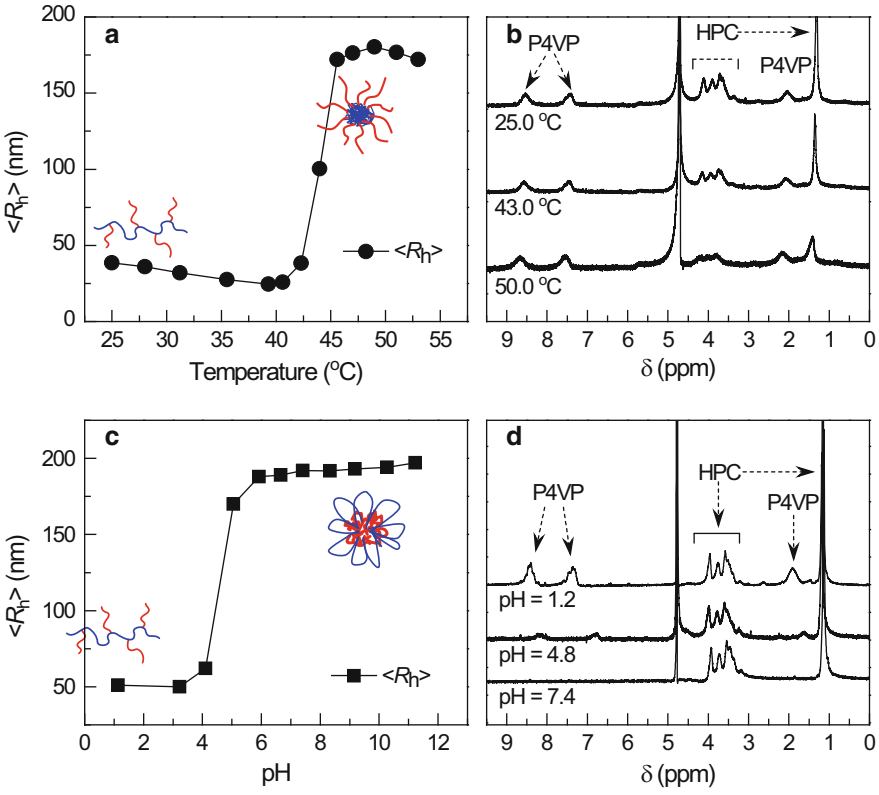

Fig. 5 Formation of coacervate micelles of HPC-*g*-P4VP. (**a**) <R_h> of $HPC_{0.05}$-*g*-$P4VP_{35}$ as a function of temperature in aqueous solution at pH 1.2. (**b**) Corresponding ^1H NMR spectra in D_2O at the indicated temperatures; (**c**) <R_h> of $HPC_{0.05}$-*g*-$P4VP_{35}$ as a function of pH. (**d**) Corresponding ^1H NMR spectra in D_2O solution at different pH values, as denoted in the figure (Reproduced, with permission, from [146], Copyright 2010, American Chemical Society)

electrochemical activity of the electrode is reduced as result of collapse of the P4VP chains. However, the hydrophilic property of the backbone still maintains the electrochemical process. With further immobilization of glucose oxidase on the graft copolymer-decorated electrode, the obtained biosensor can be used to detect glucose [204].

Cellulose-based graft-polymer gels can also be fabricated through supramolecular interactions. Based on the host–guest interaction of β-CD and the *trans*-isomer of azo-benzene (Azo), a UV–visible light-controlled supramolecular system has been fabricated based on ethyl cellulose (EC). EC-*g*-PCL copolymers were synthesized via ROP, and the free ends of the poly(ε-caprolactone) (PCL) side chains were functionalized by β-CD via click chemistry. The obtained graft copolymer, EC-*g*-PCL–β-CD, can form complex supramolecular micelles in aqueous solution. The complex micelles have photoresponsive properties according to the *trans*- and *cis*-conformation transition of the azo groups upon UV–vis irradiation [205].

Ikkala et al. introduced naphthyl moieties on the surface of CNC via surface-initiated ATRP of dimethylaminoethyl methacrylate and naphthyl-functionalized methacrylate, denoted as CNC-*g*-P(DMAEMA-*r*-NpMA). The brush-modified "hard" CNC and methyl-viologen-functionalized PVA can be bounded together by cucurbit[8]uril (CB[8]) via supramolecular cross-links established by dynamic host–guest interactions as well as through selective and simultaneous binding of naphthyl and methyl-viologen moieties (Fig. 6). The obtained nanocomposite hydrogels have three important criteria: rapid sol–gel transition (<6 s), high storage modulus ($G' > 10$ kPa), and rapid self-healing even upon aging for several months, which arises from the balancing colloidal reinforcement as well as the selectivity

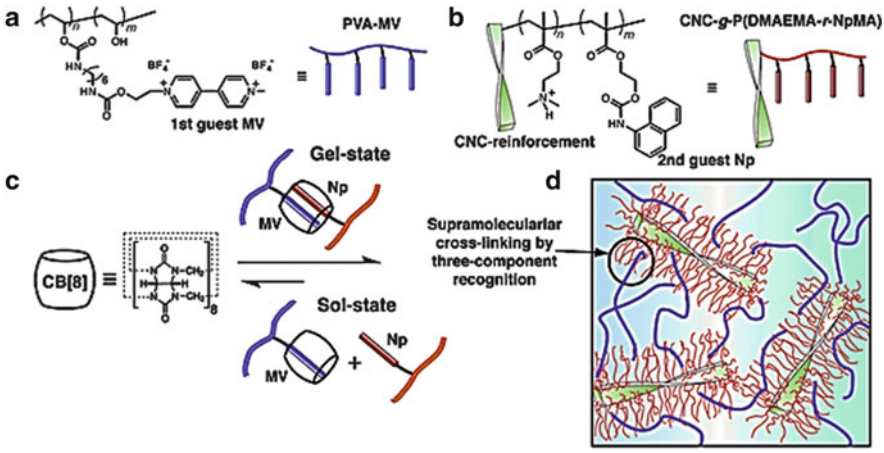

Fig. 6 Schematics and architecture of highly specific, dynamic and stiff three-component recognition-driven supramolecular hydrogels based on CNC and CB[8] host–guest chemistry. (**a**) PVA-MV with methyl-viologen (MV) guest moieties; (**b**) CNC-*g*-P(DMAEMA-*r*-NpMA) with naphthyl (Np) guest moieties. (**c**) CB[8] as the host motif. (**d**) Selective supramolecular cross-links based on three-component recognition (Reproduced, by permission, from [168], Copyright 2014, Wiley)

and dynamics of the CB[8] three-component supramolecular interactions [168]. Such approaches can be applied in the preparation of advanced dynamic materials from renewable sources.

5 Composite Gels and Microgels with Cellulose Blocks

For the purpose of obtaining polymer gels with desired properties, composite gels are generally prepared by mixing polymers with different properties. Either chemical or physical cross-linking, or both, are used in the preparation of such gels. In the case of using cellulose or its derivatives, and a graft copolymer as one component, the other component could be a natural or synthetic polymer or an inorganic material. Typical natural polymers used in cellulose-based composite gels are chitin [206–208], chitosan [28, 78, 209, 210], starch [211], alginate [212–215], dextran [7], carrageenans [216], and hyaluronic acid (HA) [217–219]. Synthetic polymers, especially those that are water soluble and functional, such as PVA [220–222], PANI [223, 224], and polyacrylamide (PAAm) [225, 226], are also used in cellulose-based composite gels. Alternatively, inorganic materials of nanoscopic size, including quantum dots (QDs) [227], TiO_2 [77], gold nanoparticles (AuNPs) [228], and magnetic nanoparticles (MNPs) [229], are often combined with cellulose to obtain composite hydrogels with specific properties.

5.1 Supramolecular Gels Prepared by Blending

Solvents for cellulose can often also dissolve other natural polymers, which can therefore be used for preparation of cellulose-based composite gels. A typical example is cellulose/chitin composite gel prepared from cellulose/chitin/NaOH/thiourea aqueous solution. Cellulose/chitin beads prepared by coagulating cellulose/chitin-blended solutions in a NaOH/thiourea aqueous system have homogeneous and microporous structures in the surfaces and cross-sections [3, 206]. Cellulose/chitin hybrid gels were also prepared from IL solutions for application as an electric double layer capacitor. The hybrid gel electrolyte exhibits excellent high-rate discharge capacity for a wide range of current densities. The discharge capacitance of the test cell can retain 80 % of its initial value in 10^5 cycles, even at a high current density of 5,000 mA g^{-1} [207].

Physical composite hydrogels composed of HA and MC can meet the design criteria of injectability, safe and fast swelling, satisfactory permeability for molecules with molecular weights of up to 150 kg mol^{-1}, high residual particle load, non-cell-adhesiveness, degradability, and biocompatibility (from 1 to 28 days) for an injectable intrathecal drug delivery system for application in spinal-cord injury repair [230]. To achieve a diversity of release profiles, poly(lactide-*co*-glycolide) particles were dispersed within the HA/MC gels. With this strategy, fast diffusion-

controlled release of dissolved solutes from the HA/MC itself and slow drug release from poly(lactide-*co*-glycolide) particles dispersed within the HA/MC gels were both achieved [218]. Novel physically cross-linked hydrogels by hydrogen bonding of component polymers have been obtained by mixing aqueous solutions of carboxymethyl chitosan (CMCS) with cellulose ethers, including HEC or MC. It was found that the intermolecular hydrogen bonding in CMCS/HEC is stronger than that in CMCS/MC. The swelling ratio and drug release rate of these hydrogels both decrease with increase in the interaction of the component polymers in the system [231]. MC/alginate blend hydrogels were prepared in the presence of distinct salts such as $CaCl_2$, Na_2HPO_4, or NaCl. The obtained physical MC/alginate hydrogels have thermal and pH dual-sensitive properties, enabling potential applications as protein drug carriers for site-specific release in the intestine [212].

The properties of natural polymers are limited for preparing cellulose-based gels with desired properties. Hence, synthetic polymers are often more suitably introduced for the fabrication of cellulose-based gels because the structure of synthetic polymers can be tailored to obtain materials with desired properties. For example, poly(*N*-isopropylacrylamide-*co*-butylmethacrylate) (PNB) nanogels with reversible thermosensitive phase behavior have been synthesized via soap-free emulsion polymerization. Complex hydrogels can be prepared by mixing the PNB nanogels with bacterial cellulose whiskers, in which the BC whiskers act as a backbone to string the PNB nanogel particles together. The resultant hydrogels have temperature-dependent properties due to the poly(*N*-isopropylacrylamide) (PNIPAm) component [232].

Acidic phosphate-ester-doped PANI can be dissolved in cellulose/NaOH/urea aqueous solutions through formation of new complexes, in which the water-soluble cellulose inclusion complexes surrounded by urea are entangled by PANI through hydrogen bonds, leading to dissolution of the PANI [223]. The phosphate-ester-doped PANI is therefore miscible with cellulose in these complex solutions, and the solutions are processable. Physical gelation occurs upon heating to high temperature, which is a result of reconstruction of an intermolecular hydrogen-bonding network between the cellulose chains. The gelation is irreversible and dominated by the cellulose concentration in the system [224]. The obtained PANI/cellulose complex gels can be used as precursors for the preparation of conductive materials.

Physically cross-linked cellulose-based gels and composites are generally weak. Hence, further chemical cross-linking is usually needed. For example, PVA, which can be cross-linked by physical thermocycling [220], chemical agents [233], or irradiation [221], is a good candidate for the preparation of hydrogels. By blending nanofibrillated cellulose (NFC), PVA, and borax, a hybrid hydrogel was obtained with enhanced material stability [233]. Both PVA–borax complexes (cross-linking) and hydrogen bonding contribute to the mechanical performance of the hydrogels. Moreover, the hydrogels exhibit self-healing ability as a result of reversible breakdown and reformation of the PVA–borax complexes and hydrogen bonds in the hydrogels [233].

Cellulose and its derivatives have also been used to prepare interpenetrating polymer network (IPN) hydrogels. In the case of using cellulose, both regenerated

cellulose and nanocellulose (including CNCs and BC) are generally used as the reinforced counterpart for the hydrogels. In one example, poly(*N*,*N*-dimethylacrylamide) (DMAm)/cellulose semi-IPN hydrogels were prepared in LiCl/DMAc. The hydrogels with 25 % cellulose have a sixfold higher storage modulus and lower equilibrium water content than a plain DMAm control system [234].

Combining the concept of double-network and nanocomposite gels by coupling a covalent network with reversible interactions using CNCs as physical cross-links allows tough and stretchable cellulose nanocrystal-poly(acrylamide) (CNC-PAM) composite hydrogels to be prepared. The attractive physical interactions in the network are considered to increase the fracture strength of the hydrogels via reversible adsorption–desorption on the CNC surface. It is found that the polymer chains desorb from the CNC surface under periodic strains and entangle with the free chains after a resting time via conformational rearrangement, consequently triggering a recovering mechanism during multiple crazing and shear relaxation. This concept can be extended to functionalized CNC assemblies and polymer interfaces to prepare tough hydrogels at multiple scales [235].

Using inorganic clay as a multifunctional supramolecular cross-linker, pH- and temperature-responsive CMC/PNIPAm/clay hydrogels were fabricated. These hydrogels have excellent toughness and higher swelling ratios than conventional chemically cross-linked CMC/PNIPAm hydrogels [236]. The CMC/PNIPAm/clay hydrogels exhibit a volume-phase transition temperature at around 32 °C, and the swelling behavior depends on the content of clay and pH. Moreover, the CMC/PNIPAm/clay hydrogels have excellent mechanical properties with high tensile stress, and elongation at break of up to 1,200 % [237, 238]. pH- and temperature-sensitive CNC/PNIPAm hydrogels were also fabricated via the free-radical polymerization of NIPAAm with carboxylated CNC [239].

5.2 *Supramolecular Gels Prepared via Polyelectrolyte Complex*

Polyelectrolyte complexes (PECs) possessing both positive and negative charges are formed by electrostatic interactions of polyelectrolytes with oppositely charged polyelectrolytes in an aqueous solution [240]. Films, fibers, and hydrogels have been prepared via PECs and have potential applications as antistatic coatings, environmental sensors, chemical detectors [241], and medical prosthetic materials [242–247]. A series of complex supramolecular hydrogels based on CMC with negative charge have been prepared by introducing positively charged polyelectrolytes, such as the common cationic polymers chitosan (CS) and poly(vinyl amine) (PVAm). Commercially available PVAm and a range of copolymers of poly(*N*-vinylformamide) (PNVF) can be used to prepare complex hydrogels with CMC. PVAm/CMC, PNVF/CMC, and PVAm-*co*-PNVF/CMC complex hydrogels have been prepared by casting from 50 % formic acid solutions. The hydrogels are macroscopically uniform and transparent. The tensile strength and tensile modulus

of the complex hydrogels depend on polymer ratio, molecular weight, functional group content, and water content. It was proposed that hydrogen bonding is the predominant intermolecular force responsible for the strength of dry film blends, whereas ionic bonds between CMC-carboxyl and PVAm ammonium ions are responsible for the integrity of water-swollen PEC films [248]. The swelling behavior of the PEC films depends on the polymer composition, pH, and salt concentration. Films containing excess ammonium groups gave the greatest swelling at low pH, whereas excess carboxyl groups enhanced swelling at high pH [249].

Similar to other supramolecular physical gels prepared using cellulose as the building blocks, the PEC gels are somewhat weak and lack stability. Therefore, further chemical cross-linking may be needed. For example, CS/CMC hydrogels cross-linked with glutaraldehyde can bend toward either an anode or cathode with an equilibrium bending angle that depends on pH, ionic strength, and electric voltage. The materials can be used for microsensors and actuators, especially in the biomedical field [250].

5.3 Hybrid Cellulose Hydrogels

Recently, polymeric–inorganic hybrid materials have received increasing attention because of their potential applications in electric, optical, magnetic, and biological fields. The properties of these materials depend on the preparation method, the microstructure of the materials (e.g., their crystalline structure), and the type of bonding interactions between the polymeric and inorganic components [77, 251–253]. Following this idea, introduction of inorganic materials such as AuNPs [228], MNPs [229], carbon nanotubes [254], TiO_2 nanoparticles [255], tungsten carbide [256], palladium nanoparticles [257], and QDs [227] into cellulose hydrogels is an effective way to fabricate cellulose-based functional materials.

AuNPs have attracted great interest in recent years because of their unique physicochemical properties and potential applications in catalysis, optoelectronics, sensors, biotechnology, and medicine. Modification of AuNPs with smart polymers can introduce stimuli-responsive properties. Figure 7 shows a pH-responsive AuNPs/CMC hybrid system prepared using a simple approach. In this approach, AuNPs were prepared by a hydrothermal method using CMC as the reducing agent and stabilizer. Then, the AuNPs were decorated by an electrostatic compound of cysteamine hydrochloride (CAH) and CMC through ligand exchange. The resulting Au–CAH/CMC dispersion exhibits strongly reversible pH-responsiveness, with triggered aggregation of the AuNPs caused by the combined actions of chain-conformation changes of the CMC and electrostatic interactions between CAH and CMC at pH < 2.6 [228]. These Au–CAH/CMC hybrid nanogels can be used for calorimetric detection of cysteine [258].

A novel off–on colorimetric sensor has been established for selective detection of cysteine and Hg^{2+} based on similar AuNPs stabilized by carboxyethyl-quaternized cellulose (CEQC). This assay is based on the thiophilicity of Hg^{2+} and AuNPs as well as on the unique optical properties of CEQC-stabilized AuNPs.

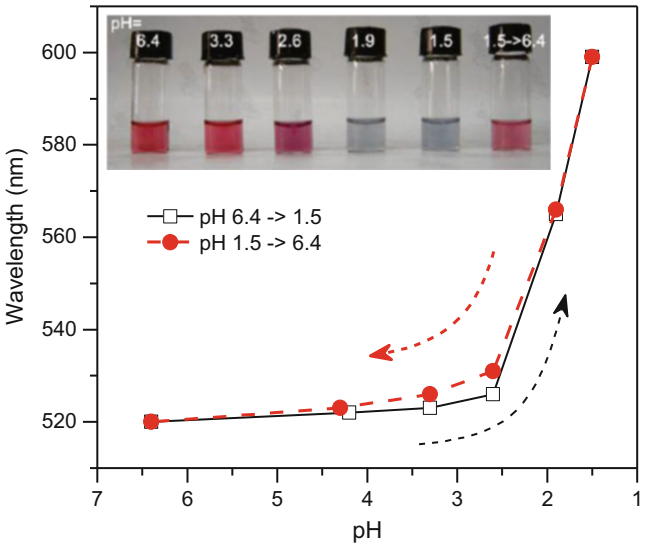

Fig. 7 Effect of pH on the surface plasma resonance absorbance on UV–vis spectra of Au–CAH/CMC aqueous solution. *Inset* photos show the color of the Au–CAH/CMC dispersions at different pH (Reprinted, with permission, from [228], Copyright (2010) American Chemical Society)

The detection limits for cysteine and Hg^{2+} are as low as 20 and 40 nM, respectively, in aqueous solution [241]. However, the stability of the above-mentioned AuNPs is limited, especially at extreme pH (e.g., $pH < 1$ or $pH > 13$), so that additional stabilizers such as cysteamine hydrochloride are needed. In our recent work, a new cellulose derivative, amidoxime-functionalized cellulose (AOFC), was synthesized. It was found that AOFC can be used as both reducing agent and stabilizer for the preparation of AuNPs by a hydrothermal approach, such that AuNPs can be obtained even at room temperature. The AOFC-stabilized AuNPs are stable at a pH range of 0.4–13.5 without any additional stabilizer [259], which renders them attractive for applications at conditions of extreme pH and pH range.

MNPs, which are powerful markers and carriers for diverse applications, have attracted great interest in recent decades. As a result of their response to external magnetic fields and convenient separation from complex multiphase systems, MNPs with tailed surface functionalities have been widely used in life sciences for biolabeling, drug delivery, contrast enhancement of magnetic resonance imaging, and purification [229]. For example, magnetic cores decorated with EC via an emulsion solvent evaporation process have improved biocompatibility, such that 5-fluorouracil loaded in the nanoparticles could be released in a controlled fashion for cancer targeting [252]. Magnetic Fe_3O_4/cellulose microspheres, fabricated by in situ synthesis of Fe_3O_4 nanoparticles in the pores of regenerated-cellulose microspheres, can be used as a solid-template microreactor and have excellent adsorption properties. They have been used, for example, for magnetic-induced delivery of bovine serum albumin [260]. Bromoesterified EC (EC-Br) was used to decorate

amino-functionalized magnetite (Fe_3O_4) nanoparticles. The EC-grafted Fe_3O_4 nanoparticles are interfacially active and highly ordered at an oil–water interface. This means that they can be used for rapid separation of water droplets from emulsions by an external magnetic field [261].

Nanofibrillar hybrid materials consisting of bacterial nanocellulose (BNC) and photo-catalytically active anatase nanoparticles (TiO_2-NPs) have been prepared by an in situ biosynthesis process. The nanofibrillar BNC network with high specific surface area and an interconnected pore system acts as a carrier for the catalysts. The prepared photo-catalytically active and stable BNC–TiO_2 hybrid might be of specific interest for environmental applications like purification of drinking water and cleaning of polluted air [255]. This method can be extended to prepare BNC hybrid functional materials using other nanoparticles.

QDs are fluorescent semiconductors applied in the fields of molecular imprinting, nanophotonics, fluorescence probes, nonlinear optical devices, and UV-protective materials. By simply blending water-soluble QDs with cellulose/NaOH/urea aqueous solutions, it is possible to prepare cellulose-QD (CdSe/ZnS) hybrid hydrogels with strong fluorescence. Then, the ligands of the QDs can be removed by hydrolyzing to obtain hydrophobic QDs that are embedded in cellulose matrixes via hydrophobic interactions. The cellulose-QD hydrogels emit strong fluorescence of different colors, depending on the size of the CdSe/ZnS nanoparticles [253]. QDs have also been encapsulated in cellulose-derivative microgels. Sun and coworkers prepared HPC/AA microgels with Ce(IV), initiating graft copolymerization in the presence of the cross-linker *N,N′*-methylene bisacrylamide (MBA). Then, cysteamine-capped CdTe QDs were adsorbed in the microgels and covalently bonded to the polymer chains via amidation. The QDs were dispersed throughout the microgel. The microgels possess an abrupt volume variation at a certain volume-phase transition temperature (TVPT), and the fluorescence intensity of hybrid microgels is reversible when cycling the temperature from below to above the TVPT [227].

6 Cellulose Aerogels

Aerogels are highly porous materials prepared by replacing a liquid solvent in a gel by air, without substantially altering the network structure or the volume of the gel [262], with no or limited shrinkage during this replacement process, and the volume of the solid phase being only a small percentage of the total volume (0.2–20 %) [263]. Because aerogels often exhibit a unique topological porous structure with porosity of up to 99 %, they have many exciting properties, including low density (0.004–0.5 g cm^{-3}), high specific surface area, low dielectric permittivity, and extraordinarily low thermal conductivity, holding 15 entries in *Guinness World Records* for material properties [262, 264, 265]. The characteristics of aerogels make them interesting for applications in gas or liquid permeation and adsorption, thermal and acoustic insulation, optical applications, and as carriers for catalysts or

drugs. Aerogels may also function as low-density cores in sandwich structures or as templates for precipitation of inorganic nanoparticles [266].

As a new generation of materials, cellulose aerogels possess all the features of a traditional aerogels [267–269] and, at the same time, have their own excellent specificity. Cellulose aerogels have the advantages of comparatively high strength, renewability, biodegradability, and ductility compared with other typical aerogels [85, 266, 269]. Specifically, the structure of cellulose in solutions can be retained during the transition from a gel state to a solid state, resulting in a material with density as little as 0.05 g cm^{-3} and specific surface area of up to 280 m^2 g^{-1} [269]. Therefore, cellulose aerogels have attracted increasing attention in recent years [59–61]. As shown schematically in Fig. 2, cellulose aerogels can be prepared by regeneration of cellulose solutions such as in NMMO monohydrate [59], alkali aqueous systems [60, 68, 270], ILs [271, 272], LiCl/DMAc [273], and calcium thiocyanate [274]. The cellulose solutions are generally regenerated or coagulated in a nonsolvent (e.g., water, alcohols) and then dried in a special way that prevents pore collapse, either via freezing or under supercritical conditions, resulting in highly porous materials. The properties of cellulose aerogels greatly depend on the source [271, 275], solvents, regeneration conditions, exchanging solvent, temperature, drying methods, parameters, etc.

Both native and regenerated cellulose can be used for the preparation of cellulose aerogels. Cellulose in native form, generally nanofibrillar such as bacterial cellulose and microfibrillated cellulose, has been proposed for the preparation of aerocellulose [77, 266]. Aerogels based on NFC can offer advantages from an environmental point of view, because NFC is obtained from renewable resources and no harmful solvents are required during the processing.

Paakko et al. pioneered cellulose I nanofiber aerogels by freeze-drying of an NFC dispersion [85]. Then, Sehaqui et al. then prepared a series of low density (0.005–0.069 kg L^{-1}) foams with porosity in the range of 93.1–99.5 %. The foams were based on NFC using freeze-drying with a low degree of undercooling during the freezing stage. A limitation of the NFC materials is that the highest specific surface area reported is limited to 66 m^2 g^{-1}, which is probably a result of NFC agglomeration during the freezing and sublimation stages of the freeze-drying process [276]. Therefore, a simple one-step procedure was developed to fabricate NFC aerogels of ultrahigh porosity (93–99 %) by *tert*-butanol freeze-drying of NFC hydrocolloidal dispersions. This method was used to prepare a wood-based NFC nanopaper with high surface area of up to 480 m^2 g^{-1} [86]. In this procedure, NFC hydrogels were first solvent-exchanged into ethanol and subsequently into supercritical CO_2, liquid CO_2, or *tert*-butanol, followed by evaporation, supercritical drying, or sublimation, respectively. The porosity range was 40–86 %. The specific surface area, porosity, and mechanical properties in tension greatly depended on the drying procedures and type of NFC (e.g., enzymatically pretreated native NFC or TEMPO-oxidized NFC). Compared with water-dried nanopaper, the material was softer, with substantially different deformation behavior. The range of nanopaper densities was extended, and the mechanical behavior was substantially different to that of water-dried nanopaper [277]. Recently, ultralight pure natural aerogel

microspheres were prepared using natural CNF by a facile spraying-freezing-drying method [264]. In this work, softwood pulp cellulose fibers with diameters of 20–50 μm were first defibrillated via high-speed homogenizer mechanical shearing, resulting in a highly viscous gel-like nanofibril cellulose suspension in water. Then, native-cellulose nanofibril aqueous gels were prepared by cross-linking between the CNF and epichlorohydrin resin, followed by spraying and atomizing at constant pressure (40 MPa) through a steel nozzle directly into liquid nitrogen for instant freezing. The frozen droplets were subsequently freeze-dried to obtain aerogel microspheres with high porosity and bulk density as low as 0.0018 g cm^{-3}. The pore size of the cellulose aerogel microspheres ranged from nano- to micrometers. The unique ultralight and highly porous structure ensured high moisture (∼90 g g^{-1}) and water uptake capacity (∼100 g g^{-1}) of the aerogel microspheres. Covalent cross-linking between the native nanofibrils and cross-linkers made the aerogel microspheres very stable, even in a harsh environment [264].

In the above-mentioned works, native cellulose with cellulose I crystals were used for the preparation of aerogels. As an alternative, cellulose aerogels with cellulose II crystals obtained through dissolution and coagulation have been prepared with relatively low modulus. By optimization of the preparation method, aerogels with remarkable mechanical strength and light transmittance can be prepared. The resultant cellulose aerogels have high porosity with open structures and thus provide an effective substrate for the synthesis of metallic nanoparticles [278]. Moreover, using regenerated-cellulose gels from cellulose/NMMO monohydrate solution, in situ synthesis of silica in cellulose gels has been attempted, using tetraethyl orthosilicate as the SiO_2 precursor. The resulting composite gels were dried with supercritical CO_2 to give cellulose–silica aerogels with low density, moderate light transmittance, large surface area, high mechanical integrity, and excellent heat insulation [279]. Cellulose aerogels prepared in aqueous alkali-based solvents have a surface area of 356 m^2 g^{-1}. A silica loading of more than 60 % (w/w) resulted in a surface area even greater than 600 m^2 g^{-1}. These cellulose aerogels were also used for the preparation of silica-only aerogels through removal of the cellulose by calcination [265].

In the case of using cellulose derivatives for preparing aerogels, pioneering work has focused on preparation of aerogels with high impact strength from chemically cross-linked gels of cellulose acetate (CA) and cellulose acetate butyrate in acetone solutions, followed by drying under supercritical CO_2 [267, 280]. CA aerogels were further loaded with silver nanoparticles for various biomedical applications, such as antimicrobial membranes [281]. Furthermore, CA aerogels can be used as precursors for the preparation of carbon aerogels: supercritical CO_2-dried CA aerogels were carbonized and activated by CO_2 at 800 °C. The carbon aerogels were impregnated in $PtCl_6^{2-}$, and the platinum salt was then chemically or electrochemically reduced to result in platinized carbon aerogels (Pt/CA). These Pt/CA aerogels can be used as electrocatalyst supports for proton-exchange membrane fuel cells [282]. Cellulose diacetate (CDA) gels were prepared by first mixing CDA acetone solution with $Ca(SCN)_2$ aqueous solution at room temperature and mildly heating to result in a transparent solution, followed by cooling the solution to room

temperature to form a gel. The $Ca(SCN)_2$ was washed out and the sample was freeze-dried to obtain CDA aerogel. Then, Pt was loaded onto the CDA aerogel and carbonized to mesoporous Pt-carbon nanorods, which have potential applications in various catalytic and electrochemical systems [283].

7 Conclusions and Perspectives

Cellulose gels, microgels, and aerogels can be prepared in various forms and from various precursors, including native cellulose (such as bacterial cellulose, cellulose nanocrystals, and cellulose nanofibrils), regenerated cellulose, cellulose derivatives, and cellulose graft copolymers. A particularly useful means of cross-linking these polymers is based on supramolecular interactions, including hydrophobic interactions, hydrogen bonding, and ionic interactions. The properties of the obtained cellulose gels and microgels depend on the properties and contents of the counterparts in the system, the cross-linking densities, and the methods and parameters of the cross-linking. Cellulose-based gels and microgels have favorable properties such as biocompatibility, biodegradability, renewability, hydrophilicity, environmental friendliness, transparency, low cost, and nontoxicity, all allowing promising applications in controlled drug delivery, tissue engineering, waste treatment, blood purification, and the agriculture and food industry.

Cellulose, the most important skeletal component in plant cells, is an abundant and renewable naturally occurring polymer with fascinating structures and properties, which can meet the increasing demands for environmental friendly and biocompatible products. Raw cellulose materials, such as cotton and wood, have been widely used in human society for thousands of years, not only in our everyday life but also in the cultural inheritance of human beings. Cellulose is the origin of the first man-made fiber (rayon) and the first synthetic polymer material (celluloid), which has played a key role in the founding and developing of polymer science. However, it should be remembered that cellulose, the gift of nature, still remains mysterious to us. Cellulose is synthesized in aqueous media in nature. However, the interactions that hold cellulose chains together to form high-performance materials and the interactions of cellulose with other molecules such as lignin, hemicellulose, and other components in the natural state are still not fully understood. These fundamental issues could offer us the basic concepts for using cellulose in more environmental friendly ways and the principles for the design and fabrication of composite materials with desired properties. Our ideal is to replace the chemicals and materials from limited fossil resources with cellulose and other natural polymers.

References

1. Zhao GH, Kapur N, Carlin B, Selinger E, Guthrie JT (2011) Characterisation of the interactive properties of microcrystalline cellulose-carboxymethyl cellulose hydrogels. Int J Pharm 415:95–101
2. Kuriaki M, Nakamura K, Mizutani J (1989) Application of transparent poly(vinyl alcohol) (PVA) gel to contact lens. Kobunshi Ronbunshu 46:739–743
3. Zhou D, Zhang LN, Zhou JP, Guo SL (2004) Cellulose/chitin beads for adsorption of heavy metals in aqueous solution. Water Res 38:2643–2650
4. Chauhan GS, Lal H (2003) Novel grafted cellulose-based hydrogels for water technologies. Desalination 159:131–138
5. Shi ZJ, Zhang Y, Phillips GO, Yang G (2014) Utilization of bacterial cellulose in food. Food Hydrocoll 35:539–545
6. Aleman J, Chadwick AV, He J, Hess M, Horie K, Jones RG, Kratochvil P, Meisel I, Mita I, Moad G, Penczek S, Stepto RFT (2007) Definitions of terms relating to the structure and processing of sols, gels, networks, and inorganic-organic hybrid materials (IUPAC Recommendations 2007). Pure Appl Chem 79:1801–1827
7. Yang X, Bakaic E, Hoare T, Cranston ED (2013) Injectable polysaccharide hydrogels reinforced with cellulose nanocrystals: morphology, rheology, degradation, and cytotoxicity. Biomacromolecules 14:4447–4455
8. Sangeetha NM, Maitra U (2005) Supramolecular gels: functions and uses. Chem Soc Rev 34:821–836
9. Flory PJ (1953) Principles of polymers chemistry. Cornell University Press, Ithaca, NY
10. Li M, Feng S, Fang S, Xiao X, Li X, Zhou X, Lin Y (2007) Quasi-solid state dye-sensitized solar cells based on pyridine or imidazole containing copolymer chemically crosslinked gel electrolytes. Chin Sci Bull 52:2320–2325
11. Otsuka E, Kudo S, Sugiyama M, Suzuki A (2011) Effects of microcrystallites on swelling behavior in chemically crosslinked poly(vinyl alcohol) gels. J Polym Sci Polym Phys 49:96–102
12. Jannasch P (2002) Physically crosslinked gel electrolytes based on a self-assembling ABA triblock copolymer. Polymer 43:6449–6453
13. Sakasegawa D, Goto M, Suzuki A (2009) Adhesion properties of physically crosslinked elastic gels of poly(sodium acrylate)-poly(acrylic acid) mixtures evaluated by a point contact method. Colloid Polym Sci 287:1281–1293
14. Liu G, Xiong YL, Butterfield DA (2000) Chemical, physical, and gel-forming properties of oxidized myofibrils and whey- and soy-protein isolates. J Food Sci 65:811–818
15. Yang Z, Ding J (2008) A thermosensitive and biodegradable physical gel with chemically crosslinked nanogels as the building block. Macromol Rapid Commun 29:751–756
16. Zhu J (2010) Bioactive modification of poly(ethylene glycol) hydrogels for tissue engineering. Biomaterials 31:4639–4656
17. Chang CY, Zhang LN (2011) Cellulose-based hydrogels: present status and application prospects. Carbohydr Polym 84:40–53
18. Liu C, Thormann E, Claesson PM, Tyrode E (2014) Surface grafted chitosan gels. Part II. Gel formation and characterization. Langmuir 30:8878–8888
19. Naumov S, Knolle W, Becher J, Schnabelrauch M, Reichelt S (2014) Electron-beam generated porous dextran gels: experimental and quantum chemical studies. Int J Radiat Biol 90:503–511
20. Liu H, Li HF, Wang JY (2014) Prevention effect of medical self-crosslinking sodium hyaluronate gel on epidural scar adhesion after laminectomy. Asian Pac J Trop Med 7:501–504
21. Agulhon P, Robitzer M, Habas JP, Quignard F (2014) Influence of both cation and alginate nature on the rheological behavior of transition metal alginate gels. Carbohydr Polym 112:525–531

22. Qiu XY, Hu SW (2013) "Smart" materials based on cellulose: a review of the preparations, properties, and applications. Materials 6:738–781
23. Klemm D, Philipp B, Heinze T, Heinze U, Wagenknecht W (1998) Comprehensive cellulose chemistry, vol 1, Fundamentals and analytical methods. Wiley-VCH, Weinheim
24. Krässig HA (1993) Cellulose: structure, accessibility, and reactivity. Gordon and Breach Science, South Africa
25. Klemm D, Heublein B, Fink HP, Bohn A (2005) Cellulose: fascinating biopolymer and sustainable raw material. Angew Chem Int Ed 44:3358–3393
26. Bajpai AK, Mishra A (2008) Carboxymethyl cellulose (CMC) based semi-IPNs as carriers for controlled release of ciprofloxacine: an *in-vitro* dynamic study. J Mater Sci Mater Med 19:2121–2130
27. Ye SH, Watanabe J, Iwasaki Y, Ishihara K (2003) Antifouling blood purification membrane composed of cellulose acetate and phospholipid polymer. Biomaterials 24:4143–4152
28. Li N, Bai R (2005) Copper adsorption on chitosan-cellulose hydrogel beads: behaviors and mechanisms. Sep Purif Technol 42:237–247
29. Way AE, Hsu L, Shanmuganathan K, Weder C, Rowan SJ (2012) pH-responsive cellulose nanocrystal gels and nanocomposites. ACS Macro Lett 1:1001–1006
30. Medronho B, Romano A, Miguel MG, Stigsson L, Lindman B (2012) Rationalizing cellulose (in)solubility: reviewing basic physicochemical aspects and role of hydrophobic interactions. Cellulose 19:581–587
31. Glasser WG, Atalla RH, Blackwell J, Brown RM, Burchard W, French AD, Klemm DO, Nishiyama Y (2012) About the structure of cellulose: debating the Lindman hypothesis. Cellulose 19:589–598
32. Kim UJ, Kuga S (2000) Reactive interaction of aromatic amines with dialdehyde cellulose gel. Cellulose 7:287–297
33. Campagnol PC, dos Santos BA, Wagner R, Terra NN, Rodrigues Pollonio MA (2012) Amorphous cellulose gel as a fat substitute in fermented sausages. Meat Sci 90:36–42
34. Sannino A, Esposito A, De Rosa A, Cozzolino A, Ambrosio L, Nicolais L (2003) Biomedical application of a superabsorbent hydrogel for body water elimination in the treatment of edemas. J Biomed Mater Res A 67A:1016–1024
35. Liu RG, Shen YY, Shao HL, Wu CX, Hu XC (2001) An analysis of Lyocell fiber formation as a melt-spinning process. Cellulose 8:13–21
36. Fink HP, Weigel P, Purz HJ, Ganster J (2001) Structure formation of regenerated cellulose materials from NMMO-solutions. Prog Polym Sci 26:1473–1524
37. Zhang C, Liu RG, Xiang JF, Kang HL, Liu ZJ, Huang Y (2014) Dissolution mechanism of cellulose in N,N-dimethylacetamide/lithium chloride: revisiting through molecular interactions. J Phys Chem B 118:9507–9514
38. Striegel AM (2003) Advances in the understanding of the dissolution mechanism of cellulose in DMAc/LiCl. J Chil Chem Soc 48:73–77
39. Henniges U, Schiehser S, Rosenau T, Potthast A (2009) Cellulose solubility: dissolution and analysis of "problematic" cellulose pulps in the solvent system DMAc/LiCl. In: Liebert TF, Heinze TJ, Edgar KJ (eds) Cellulose solvents: for analysis, shaping and chemical modification. ACS symposium series, vol 1033. American Chemical Society, Washington, pp 165–177
40. Swatloski RP, Spear SK, Holbrey JD, Rogers RD (2002) Dissolution of cellulose with ionic liquids. J Am Chem Soc 124:4974–4975
41. Zhang H, Wu J, Zhang J, He JS (2005) 1-Allyl-3-methylimidazolium chloride room temperature ionic liquid: a new and powerful nonderivatizing solvent for cellulose. Macromolecules 38:8272–8277
42. Cai J, Zhang LN (2005) Rapid dissolution of cellulose in LiOH/urea and NaOH/urea aqueous solutions. Macromol Biosci 5:539–548
43. Zhang LN, Ruan D, Gao SJ (2002) Dissolution and regeneration of cellulose in NaOH/thiourea aqueous solution. J Polym Sci Polym Phys 40:1521–1529

44. Luo XG, Zhang LN (2013) New solvents and functional materials prepared from cellulose solutions in alkali/urea aqueous system. Food Res Int 52:387–400
45. Jiang ZW, Fang Y, Xiang JF, Ma YP, Lu A, Kang HL, Huang Y, Guo HX, Liu RG, Zhang LN (2014) Intermolecular interactions and 3D structure in cellulose-NaOH-urea aqueous system. J Phys Chem B 118:10250–10257
46. Klemm DP B, Heinze T, Heinze U, Wagenknecht W (1998) Comprehensive cellulose chemistry, vol 2, Functionalization of cellulose. Wiley-VCH, Weinheim
47. Turbak AF, Synder FW, Sandberg KR (1982) Microfibrillated cellulose. US Patent US4483743, 20 Nov 1984
48. Saito H, Sakurai A, Sakakibara M, Saga H (2003) Preparation and properties of transparent cellulose hydrogels. J Appl Polym Sci 90:3020–3025
49. Xia Z, Patchan M, Maranchi J, Elisseeff J, Trexler M (2013) Determination of crosslinking density of hydrogels prepared from microcrystalline cellulose. J Appl Polym Sci 127:4537–4541
50. Patchan M, Graham JL, Xia Z, Maranchi JP, McCally R, Schein O, Elisseeff JH, Trexler MM (2013) Synthesis and properties of regenerated cellulose-based hydrogels with high strength and transparency for potential use as an ocular bandage. Mater Sci Eng C Mater Biol Appl 33:3069–3076
51. Ostlund A, Lundberg D, Nordstierna L, Holmberg K, Nyden M (2009) Dissolution and gelation of cellulose in TBAF/DMSO solutions: the roles of fluoride ions and water. Biomacromolecules 10:2401–2407
52. Zhu SD, Wu YX, Chen QM, Yu ZN, Wang CW, Jin SW, Ding YG, Wu G (2006) Dissolution of cellulose with ionic liquids and its application: a mini-review. Green Chem 8:325–327
53. Suzuki T, Kono K, Shimomura K, Minami H (2014) Preparation of cellulose particles using an ionic liquid. J Colloid Interface Sci 418:126–131
54. Kunchornsup W, Sirivat A (2014) Thermo-electromechanical responses of 1-butyl-3-methylimidazolium chloride ionic liquid-cellulose gel. J Polym Res 21:369
55. Li L, Lin Z, Yang X, Wan Z, Cui S (2009) A novel cellulose hydrogel prepared from its ionic liquid solution. Chin Sci Bull 54:1622–1625
56. Kadokawa J, Murakami MA, Kaneko Y (2008) A facile preparation of gel materials from a solution of cellulose in ionic liquid. Carbohydr Res 343:769–772
57. Mazza M, Catana DA, Vaca-Garcia C, Cecutti C (2009) Influence of water on the dissolution of cellulose in selected ionic liquids. Cellulose 16:207–215
58. Thiemann S, Sachnov SJ, Pettersson F, Bollstrom R, Osterbacka R, Wasserscheid P, Zaumseil J (2014) Cellulose-based ionogels for paper electronics. Adv Funct Mater 24:625–634
59. Innerlohinger J, Weber HK, Kraft G (2006) Aerocellulose: aerogels and aerogel-like materials made from cellulose. Macromol Symp 244:126–135
60. Gavillon R, Budtova T (2008) Aerocellulose: new highly porous cellulose prepared from cellulose-NaOH aqueous solutions. Biomacromolecules 9:269–277
61. Cai J, Kimura S, Wada M, Kuga S, Zhang LN (2008) Cellulose aerogels from aqueous alkali hydroxide-urea solution. ChemSusChem 1:149–154
62. Cai J, Zhang LN, Zhou JP, Qi HS, Chen H, Kondo T, Chen XM, Chu B (2007) Multifilament fibers based on dissolution of cellulose in NaOH/urea aqueous solution: structure and properties. Adv Mater 19:821–825
63. Cai J, Zhang LN (2006) Unique gelation behavior of cellulose in NaOH/Urea aqueous solution. Biomacromolecules 7:183–189
64. Weng LH, Zhang LN, Ruan D, Shi LH, Xu J (2004) Thermal gelation of cellulose in a NaOH/thiourea aqueous solution. Langmuir 20:2086–2093
65. Cai J, Liu YT, Zhang LN (2006) Dilute solution properties of cellulose in LiOH/urea aqueous system. J Polym Sci Polym Phys 44:3093–3101
66. Ruan D, Lue A, Zhang LN (2008) Gelation behaviors of cellulose solution dissolved in aqueous NaOH/thiourea at low temperature. Polymer 49:1027–1036

67. Gong X, Wang Y, Tian Z, Zheng X, Chen L (2014) Controlled production of spruce cellulose gels using an environmentally "green" system. Cellulose 21:1667–1678
68. Isobe N, Kim UJ, Kimura S, Wada M, Kuga S (2011) Internal surface polarity of regenerated cellulose gel depends on the species used as coagulant. J Colloid Interface Sci 359:194–201
69. Yang YJ, Shin JM, Kang TH, Kimura S, Wada M, Kim UJ (2014) Cellulose dissolution in aqueous lithium bromide solutions. Cellulose 21:1175–1181
70. Saito T, Uematsu T, Kimura S, Enomae T, Isogai A (2011) Self-aligned integration of native cellulose nanofibrils towards producing diverse bulk materials. Soft Matter 7:8804–8809
71. Habibi Y, Lucia LA, Rojas OJ (2010) Cellulose nanocrystals: chemistry, self-assembly, and applications. Chem Rev 110:3479–3500
72. Klemm D, Kramer F, Moritz S, Lindstrom T, Ankerfors M, Gray D, Dorris A (2011) Nanocelluloses: a new family of nature-based materials. Angew Chem Int Ed 50:5438–5466
73. Moon RJ, Martini A, Nairn J, Simonsen J, Youngblood J (2011) Cellulose nanomaterials review: structure, properties and nanocomposites. Chem Soc Rev 40:3941–3994
74. Saito T, Kimura S, Nishiyama Y, Isogai A (2007) Cellulose nanofibers prepared by TEMPO-mediated oxidation of native cellulose. Biomacromolecules 8:2485–2491
75. Hasani M, Cranston ED, Westman G, Gray DG (2008) Cationic surface functionalization of cellulose nanocrystals. Soft Matter 4:2238–2244
76. Eichhorn SJ, Dufresne A, Aranguren M, Marcovich NE, Capadona JR, Rowan SJ, Weder C, Thielemans W, Roman M, Renneckar S, Gindl W, Veigel S, Keckes J, Yano H, Abe K, Nogi M, Nakagaito AN, Mangalam A, Simonsen J, Benight AS, Bismarck A, Berglund LA, Peijs T (2009) Review: current international research into cellulose nanofibres and nanocomposites. J Mater Sci 45:1–33
77. Kettunen M, Silvennoinen RJ, Houbenov N, Nykanen A, Ruokolainen J, Sainio J, Pore V, Kemell M, Ankerfors M, Lindstrom T, Ritala M, Ras RHA, Ikkala O (2011) Photoswitchable superabsorbency based on nanocellulose aerogels. Adv Funct Mater 21:510–517
78. Spagnol C, Rodrigues FHA, Pereira AGB, Fajardo AR, Rubira AF, Muniz EC (2012) Superabsorbent hydrogel composite made of cellulose nanofibrils and chitosan-*graft*-poly (acrylic acid). Carbohydr Polym 87:2038–2045
79. Aulin C, Gallstedt M, Lindstrom T (2010) Oxygen and oil barrier properties of microfibrillated cellulose films and coatings. Cellulose 17:559–574
80. Fukuzumi H, Saito T, Wata T, Kumamoto Y, Isogai A (2009) Transparent and high gas barrier films of cellulose nanofibers prepared by TEMPO-mediated oxidation. Biomacromolecules 10:162–165
81. Henriksson M, Berglund LA, Isaksson P, Lindstrom T, Nishino T (2008) Cellulose nanopaper structures of high toughness. Biomacromolecules 9:1579–1585
82. Paakko M, Ankerfors M, Kosonen H, Nykanen A, Ahola S, Osterberg M, Ruokolainen J, Laine J, Larsson PT, Ikkala O, Lindstrom T (2007) Enzymatic hydrolysis combined with mechanical shearing and high-pressure homogenization for nanoscale cellulose fibrils and strong gels. Biomacromolecules 8:1934–1941
83. Abe K, Yano H (2011) Formation of hydrogels from cellulose nanofibers. Carbohydr Polym 85:733–737
84. Aulin C, Netrval J, Wagberg L, Lindstrom T (2010) Aerogels from nanofibrillated cellulose with tunable oleophobicity. Soft Matter 6:3298–3305
85. Paakko M, Vapaavuori J, Silvennoinen R, Kosonen H, Ankerfors M, Lindstrom T, Berglund LA, Ikkala O (2008) Long and entangled native cellulose I nanofibers allow flexible aerogels and hierarchically porous templates for functionalities. Soft Matter 4:2492–2499
86. Sehaqui H, Zhou Q, Berglund LA (2011) High-porosity aerogels of high specific surface area prepared from nanofibrillated cellulose (NFC). Compos Sci Technol 71:1593–1599
87. Capadona JR, Shanmuganathan K, Trittschuh S, Seidel S, Rowan SJ, Weder C (2009) Polymer nanocomposites with nanowhiskers isolated from microcrystalline cellulose. Biomacromolecules 10:712–716

88. Capadona JR, Van Den Berg O, Capadona LA, Schroeter M, Rowan SJ, Tyler DJ, Weder C (2007) A versatile approach for the processing of polymer nanocomposites with self-assembled nanofibre templates. Nat Nanotechnol 2:765–769
89. Capadona JR, Shanmuganathan K, Tyler DJ, Rowan SJ, Weder C (2008) Stimuli-responsive polymer nanocomposites inspired by the sea cucumber dermis. Science 319:1370–1374
90. Fall AB, Lindström SB, Sprakel J, Wågberg L (2013) A physical cross-linking process of cellulose nanofibril gels with shear-controlled fibril orientation. Soft Matter 9:1852–1863
91. Abe K, Yano H (2012) Cellulose nanofiber-based hydrogels with high mechanical strength. Cellulose 19:1907–1912
92. Hu Z, Cranston ED, Ng R, Pelton R (2014) Tuning cellulose nanocrystal gelation with polysaccharides and surfactants. Langmuir 30:2684–2692
93. Mckee JR, Hietala S, Seitsonen J, Laine J, Kontturi E, Ikkala O (2014) Thermoresponsive nanocellulose hydrogels with tunable mechanical properties. ACS Macro Lett 3:266–270
94. Nakagaito AN, Iwamoto S, Yano H (2005) Bacterial cellulose: the ultimate nano-scalar cellulose morphology for the production of high-strength composites. Appl Phys A Mater Sci Process 80:93–97
95. Putra A, Kakugo A, Furukawa H, Gong JP, Osada Y (2008) Tubular bacterial cellulose gel with oriented fibrils on the curved surface. Polymer 49:1885–1891
96. Gelin K, Bodin A, Gatenholm P, Mihranyan A, Edwards K, Strømme M (2007) Characterization of water in bacterial cellulose using dielectric spectroscopy and electron microscopy. Polymer 48:7623–7631
97. Iguchi M, Yamanaka S, Budhiono A (2000) Bacterial cellulose – a masterpiece of nature's arts. J Mater Sci 35:261–270
98. Yano H, Sugiyama J, Nakagaito AN, Nogi M, Matsuura T, Hikita M, Handa K (2005) Optically transparent composites reinforced with networks of bacterial nanofibers. Adv Mater 17:153–155
99. Backdahl H, Helenius G, Bodin A, Nannmark U, Johansson BR, Risberg B, Gatenholm P (2006) Mechanical properties of bacterial cellulose and interactions with smooth muscle cells. Biomaterials 27:2141–2149
100. Chen SW, Ma X, Wang RM (2008) Application of bacterial cellulose as the wound dressing in rats. J Biotechnol 136:S419
101. Bodin A, Concaro S, Brittberg M, Gatenholm P (2007) Bacterial cellulose as a potential meniscus implant. J Tissue Eng Regen Med 1:406–408
102. Svensson A, Nicklasson E, Harrah T, Panilaitis B, Kaplan DL, Brittberg M, Gatenholm P (2005) Bacterial cellulose as a potential scaffold for tissue engineering of cartilage. Biomaterials 26:419–431
103. Shah N, Ul-Islam M, Khattak WA, Park JK (2013) Overview of bacterial cellulose composites: a multipurpose advanced material. Carbohydr Polym 98:1585–1598
104. Grande CJ, Torres FG, Gomez CM, Troncoso OP, Canet-Ferrer J, Martinez-Pastor J (2009) Development of self-assembled bacterial cellulose-starch nanocomposites. Mater Sci Eng C Biomim Supramol Syst 29:1098–1104
105. Buyanov AL, Gofman IV, Revel'skaya LG, Khripunov AK, Tkachenko AA (2010) Anisotropic swelling and mechanical behavior of composite bacterial cellulose-poly(acrylamide or acrylamide-sodium acrylate) hydrogels. J Mech Behav Biomed Mater 3:102–111
106. Gea S, Bilotti E, Reynolds CT, Soykeabkeaw N, Peijs T (2010) Bacterial cellulose-poly(vinyl alcohol) nanocomposites prepared by an in-situ process. Mater Lett 64:901–904
107. Silva SM, Pinto FV, Antunes FE, Miguel MG, Sousa JJ, Pais AA (2008) Aggregation and gelation in hydroxypropylmethyl cellulose aqueous solutions. J Colloid Interface Sci 327:333–340
108. Talasaz AHH, Ghahremankhani AA, Moghadam SH, Malekshahi MR, Atyabi F, Dinarvand R (2008) In situ gel forming systems of poloxamer 407 and hydroxypropyl cellulose or hydroxypropyl methyl cellulose mixtures for controlled delivery of vancomycin. J Appl Polym Sci 109:2369–2374

109. Desbrieres J, Hirrien M, Rinaudo M (1998) A calorimetric study of methylcellulose gelation. Carbohydr Polym 37:145–152
110. Gao J, Haidar G, Lu XH, Hu ZB (2001) Self-association of hydroxypropylcellulose in water. Macromolecules 34:2242–2247
111. Dolz M, Bugaj J, Pellicer J, Hernandez MJ, Gorecki M (1997) Thixotropy of highly viscous sodium (carboxymethyl)cellulose hydrogels. J Pharm Sci 86:1283–1287
112. Tsunashima Y, Ikuno M, Onodera G, Horii F (2006) Low-temperature dynamic light scattering. I. Structural reorganization and physical gel formation in cellulose triacetate/methyl acetate dilute solution at −99–45 °C. Biopolymers 82:222–233
113. Sannino A, Demitri C, Madaghiele M (2009) Biodegradable cellulose-based hydrogels: design and applications. Materials 2:353–373
114. Joshi SC, Liang CM, Lam YC (2008) Effect of solvent state and isothermal conditions on gelation of methylcellulose hydrogels. J Biomater Sci Polym Ed 19:1611–1623
115. Li L (2002) Thermal gelation of methylcellulose in water: scaling and thermoreversibility. Macromolecules 35:5990–5998
116. Schupper N, Rabin Y, Rosenbluh M (2008) Multiple stages in the aging of a physical polymer gel. Macromolecules 41:3983–3994
117. Kundu PP, Kundu M (2001) Effect of salts and surfactant and their doses on the gelation of extremely dilute solutions of methyl cellulose. Polymer 42:2015–2020
118. Li L, Shan H, Yue CY, Lam YC, Tam KC, Hu X (2002) Thermally induced association and dissociation of methylcellulose in aqueous solutions. Langmuir 18:7291–7298
119. Li L, Thangamathesvaran PM, Yue CY, Tam KC, Hu X, Lam YC (2001) Gel network structure of methylcellulose in water. Langmuir 17:8062–8068
120. Arvidson SA, Lott JR, McAllister JW, Zhang J, Bates FS, Lodge TP, Sammler RL, Li Y, Brackhagen M (2013) Interplay of phase separation and thermoreversible gelation in aqueous methylcellulose solutions. Macromolecules 46:300–309
121. Joshi SC, Lam YC (2006) Modeling cellulose heat and degree of gelation for methyl hydrogels with NaCl additives. J Appl Polym Sci 101:1620–1629
122. Nishinari K, Takahashi R (2003) Interaction in polysaccharide solutions and gels. Curr Opin Colloid Interface Sci 8:396–400
123. Sekiguchi Y, Sawatari C, Kondo T (2003) A gelation mechanism depending on hydrogen bond formation in regioselectively substituted *O*-methylcelluloses. Carbohydr Polym 53:145–153
124. Sammon C, Bajwa G, Timmins P, Melia CD (2006) The application of attenuated total reflectance Fourier transform infrared spectroscopy to monitor the concentration and state of water in solutions of a thermally responsive cellulose ether during gelation. Polymer 47:577–584
125. Tan JJ, Kang HL, Liu RG, Wang DQ, Jin X, Li QM, Huang Y (2011) Dual-stimuli sensitive nanogels fabricated by self-association of thiolated hydroxypropyl cellulose. Polym Chem 2:672–678
126. Huang YZ, Kang HL, Li GH, Wang CY, Huang Y, Liu RG (2013) Synthesis and photosensitivity of azobenzene functionalized hydroxypropylcellulose. RSC Adv 3:15909–15916
127. Wang XH, Guo YZ, Li D, Chen H, Sun RC (2012) Fluorescent amphiphilic cellulose nanoaggregates for sensing trace explosives in aqueous solution. Chem Commun 48:5569–5571
128. Himmelein S, Lewe V, Stuart MCA, Ravoo BJ (2014) A carbohydrate-based hydrogel containing vesicles as responsive non-covalent cross-linkers. Chem Sci 5:1054–1058
129. Duan JF, Zhang XJ, Jiang JX, Han CR, Yang J, Liu LJ, Lan HY, Huang DZ (2014) The synthesis of a novel cellulose physical gel. J Nanomater 2014:1–7
130. Appel EA, del Barrio J, Loh XJ, Scherman OA (2012) Supramolecular polymeric hydrogels. Chem Soc Rev 41:6195–6214
131. Dong SY, Zheng B, Wang F, Huang FH (2014) Supramolecular polymers constructed from macrocycle-based host-guest molecular recognition motifs. Acc Chem Res 47:1982–1994

132. Harada A, Takashima Y, Nakahata M (2014) Supramolecular polymeric materials via cyclodextrin-guest interactions. Acc Chem Res 47:2128–2140
133. Hu JM, Liu SY (2014) Engineering responsive polymer building blocks with host-guest molecular recognition for functional applications. Acc Chem Res 47:2084–2095
134. Seiffert S, Sprakel J (2012) Physical chemistry of supramolecular polymer networks. Chem Soc Rev 41:909–930
135. Tan S, Ladewig K, Fu Q, Blencowe A, Qiao GG (2014) Cyclodextrin-based supramolecular assemblies and hydrogels: recent advances and future perspectives. Macromol Rapid Commun 35:1166–1184
136. Te Nijenhuis K (2007) On the nature of crosslinks in thermoreversible gels. Polym Bull 58:27–42
137. Chen CH, Tsai CC, Chen WS, Mo FL, Liang HF, Chen SC, Sung HW (2006) Novel living cell sheet harvest system composed of thermoreversible methylcellulose hydrogels. Biomacromolecules 7:736–743
138. Tizzotti M, Charlot A, Fleury E, Stenzel M, Bernard J (2010) Modification of polysaccharides through controlled/living radical polymerization grafting – towards the generation of high performance hybrids. Macromol Rapid Commun 31:1751–1772
139. Odian G (2004) Principles of polymerization, 4th edn. Wiley, Hoboken
140. Li YX, Liu RG, Liu WY, Kang HL, Wu M, Huang Y (2008) Synthesis, self-assembly, and thermosensitive properties of ethyl cellulose-*g*-P(PEGMA) amphiphilic copolymers. J Polym Sci Polym Chem 46:6907–6915
141. Li YX, Liu RG, Huang Y (2008) Synthesis and phase transition of cellulose-*graft*-poly (ethylene glycol) copolymers. J Appl Polym Sci 110:1797–1803
142. Li QM, Kang HL, Liu RG, Huang Y (2012) Block and hetero ethyl cellulose graft copolymers synthesized via sequent and one-pot ATRP and "click" reactions. Chin J Chem 30:2169–2175
143. Kang HL, Liu RG, Huang Y (2013) Cellulose derivatives and graft copolymers as blocks for functional materials. Polym Int 62:338–344
144. Roy D, Semsarilar M, Guthrie JT, Perrier S (2009) Cellulose modification by polymer grafting: a review. Chem Soc Rev 38:2046–2064
145. Daly WH, Evenson TS, Iacono ST, Jones RW (2001) Recent developments in cellulose grafting chemistry utilizing barton ester intermediates and nitroxide mediation. Macromol Symp 174:155–163
146. Ma L, Kang HL, Liu RG, Huang Y (2010) Smart assembly behaviors of hydroxypropyl-cellulose-*graft*-poly(4-vinyl pyridine) copolymers in aqueous solution by thermo and pH stimuli. Langmuir 26:18519–18525
147. Lin CX, Zhan HY, Liu MH, Habibi Y, Fu SY, Lucia LA (2013) RAFT synthesis of cellulose-*g*-polymethylmethacrylate copolymer in an ionic liquid. J Appl Polym Sci 127:4840–4849
148. Meng T, Gao X, Zhang J, Yuan JY, Zhang YZ, He JS (2009) Graft copolymers prepared by atom transfer radical polymerization (ATRP) from cellulose. Polymer 50:447–454
149. Carlmark A, Malmstrom E (2002) Atom transfer radical polymerization from cellulose fibers at ambient temperature. J Am Chem Soc 124:900–901
150. Hansson S, Ostmark E, Carlmark A, Malmstrom E (2009) ARGET ATRP for versatile grafting of cellulose using various monomers. ACS Appl Mater Interfaces 1:2651–2659
151. Hernandez-Guerrero M, Davis TP, Barner-Kowollik C, Stenzel MH (2005) Polystyrene comb polymers built on cellulose or poly(styrene-*co*-2-hydroxyethylmethacrylate) backbones as substrates for the preparation of structured honeycomb films. Eur Polym J 41:2264–2277
152. Lin CX, Zhan HY, Liu MH, Fu SY, Zhang JJ (2009) Preparation of cellulose graft poly (methyl methacrylate) copolymers by atom transfer radical polymerization in an ionic liquid. Carbohydr Polym 78:432–438
153. Karlsson JO, Andersson N, Berntsson P, Chihani T, Gatenholm P (1998) Swelling behavior of stimuli-responsive cellulose fibers. Polymer 39:3589–3595
154. Karlsson JO, Gatenholm P (1996) Solid-supported wettable hydrogels prepared by ozone induced grafting. Polymer 37:4251–4256

155. Karlsson JO, Gatenholm P (1997) Preparation and characterization of cellulose-supported HEMA hydrogels. Polymer 38:4727–4731
156. Karlsson JO, Gatenholm P (1999) Surface mobility of grafted hydrogels. Macromolecules 32:7594–7598
157. Karlsson JO, Gatenholm P (1999) Cellulose fibre-supported pH-sensitive hydrogels. Polymer 40:379–387
158. Hufendiek A, Trouillet V, Meier MA, Barner-Kowollik C (2014) Temperature responsive cellulose-*graft*-copolymers via cellulose functionalization in an ionic liquid and RAFT polymerization. Biomacromolecules 15:2563–2572
159. Xie JB, Hsieh YL (2003) Thermosensitive poly(*N*-isopropylacrylamide) hydrogels bonded on cellulose supports. J Appl Polym Sci 89:999–1006
160. Lindqvist J, Nystrom D, Ostmark E, Antoni P, Carlmark A, Johansson M, Hult A, Malmstrom E (2008) Intelligent dual-responsive cellulose surfaces via surface-initiated ATRP. Biomacromolecules 9:2139–2145
161. Sui XF, Yuan JY, Zhou M, Zhang J, Yang HJ, Yuan WZ, Wei Y, Pan CY (2008) Synthesis of cellulose-graft-poly(N, N-dimethylamino-2-ethyl methacrylate) copolymers via homogeneous ATRP and their aggregates in aqueous media. Biomacromolecules 9:2615–2620
162. Roy D, Guthrie JT, Perrier S (2008) Synthesis of natural-synthetic hybrid materials from cellulose via the RAFT process. Soft Matter 4:145–155
163. Roy D, Knapp JS, Guthrie JT, Perrier S (2008) Antibacterial cellulose fiber via RAFT surface graft polymerization. Biomacromolecules 9:91–99
164. Guo Y, Wang X, Shu X, Shen Z, Sun RC (2012) Self-assembly and paclitaxel loading capacity of cellulose-*graft*-poly(lactide) nanomicelles. J Agric Food Chem 60:3900–3908
165. Zhao YH, Wee KH, Bai R (2010) A novel electrolyte-responsive membrane with tunable permeation selectivity for protein purification. ACS Appl Mater Interfaces 2:203–211
166. Kan KH, Li J, Wijesekera K, Cranston ED (2013) Polymer-grafted cellulose nanocrystals as pH-responsive reversible flocculants. Biomacromolecules 14:3130–3139
167. Tang J, Lee MF, Zhang W, Zhao B, Berry RM, Tam KC (2014) Dual responsive pickering emulsion stabilized by poly[2-(dimethylamino)ethyl methacrylate] grafted cellulose nanocrystals. Biomacromolecules 15:3052–3060
168. McKee JR, Appel EA, Seitsonen J, Kontturi E, Scherman OA, Ikkala O (2014) Healable, stable and stiff hydrogels: combining conflicting properties using dynamic and selective three-component recognition with reinforcing cellulose nanorods. Adv Funct Mater 24:2706–2713
169. Abeer MM, Amin MC, Lazim AM, Pandey M, Martin C (2014) Synthesis of a novel acrylated abietic acid-*g*-bacterial cellulose hydrogel by gamma irradiation. Carbohydr Polym 110:505–512
170. Liu WG, Zhang BQ, Lu WW, Li XW, Zhu DW, De Yao K, Wang Q, Zhao CR, Wang CD (2004) A rapid temperature-responsive sol-gel reversible poly(*N*-isopropylacrylamide)-*g*-methylcellulose copolymer hydrogel. Biomaterials 25:3005–3012
171. Kang HL, Liu WY, Liu RG, Huang Y (2008) A novel, amphiphilic ethyl cellulose grafting copolymer with poly(2-hydroxyethyl methacrylate) side chains and its micellization. Macromol Chem Phys 209:424–430
172. Yan Q, Yuan JY, Zhang FB, Sui XF, Xie XM, Yin YW, Wang SF, Wei Y (2009) Cellulose-based dual graft molecular brushes as potential drug nanocarriers: stimulus-responsive micelles, self-assembled phase transition behavior, and tunable crystalline morphologies. Biomacromolecules 10:2033–2042
173. Jian CM, Gong C, Wang SQ, Wang SF, Xie XM, Wei Y, Yuan JY (2014) Multifunctional comb copolymer ethyl cellulose-*g*-poly(ε-caprolactone)-rhodamine B/folate: synthesis, characterization and targeted bonding application. Eur Polym J 55:235–244
174. Leone G, Fini M, Torricelli P, Giardino R, Barbucci R (2008) An amidated carboxymethylcellulose hydrogel for cartilage regeneration. J Mater Sci Mater Med 19:2873–2880

175. Tang XD, Gao LC, Fan XH, Zhou QF (2007) Controlled grafting of ethyl cellulose with azobenzene-containing polymethacrylates via atom transfer radical polymerization. J Polym Sci Polym Chem 45:1653–1660
176. Shen D, Yu H, Huang Y (2005) Densely grafting copolymers of ethyl cellulose through atom transfer radical polymerization. J Polym Sci Polym Chem 43:4099–4108
177. Kang HL, Liu WY, He BQ, Shen D, Ma L, Huang Y (2006) Synthesis of amphiphilic ethyl cellulose grafting poly(acrylic acid) copolymers and their self-assembly morphologies in water. Polymer 47:7927–7934
178. Liu WY, Liu YJ, Hao XH, Zeng GS, Wang W, Liu RG, Huang Y (2012) Backbone-collapsed intra- and inter-molecular self-assembly of cellulose-based dense graft copolymer. Carbohydr Polym 88:290–298
179. Liu WY, Liu RG, Li YX, Kang HL, Shen D, Wu M, Huang Y (2009) Self-assembly of ethyl cellulose-*graft*-polystyrene copolymers in acetone. Polymer 50:211–217
180. Shen D, Yu H, Huang Y (2006) Synthesis of graft copolymer of ethyl cellulose through living polymerization and its self-assembly. Cellulose 13:235–244
181. Wang DQ, Tan JJ, Kang HL, Ma L, Jin X, Liu RG, Huang Y (2011) Synthesis, self-assembly and drug release behaviors of pH-responsive copolymers ethyl cellulose-*graft*-PDEAEMA through ATRP. Carbohydr Polym 84:195–202
182. Kang HL, Liu RG, Huang Y (2013) Synthesis of ethyl cellulose grafted poly(*N*-isopropylacrylamide) copolymer and its micellization. Acta Chim Sin 71:114–120
183. Chauhan GS, Sharma R, Lal H (2004) Synthesis and characterization of graft copolymers of hydroxypropyl cellulose with acrylamide and some comonomers. J Appl Polym Sci 91:545–555
184. Ostmark E, Harrisson S, Wooley KL, Malmstrom EE (2007) Comb polymers prepared by ATRP from hydroxypropyl cellulose. Biomacromolecules 8:1138–1148
185. Xu FJ, Ping Y, Ma J, Tang GP, Yang WT, Li J, Kang ET, Neoh KG (2009) Comb-shaped copolymers composed of hydroxypropyl cellulose backbones and cationic poly((2-dimethyl amino)ethyl methacrylate) side chains for gene delivery. Bioconjug Chem 20:1449–1458
186. Ma L, Liu RG, Tan JJ, Wang DQ, Jin X, Kang HL, Wu M, Huang Y (2010) Self-assembly and dual-stimuli sensitivities of hydroxypropylcellulose-graft-poly(N, N-dimethyl aminoethyl methacrylate) copolymers in aqueous solution. Langmuir 26:8697–8703
187. Xu FJ, Zhu Y, Liu FS, Nie J, Ma J, Yang WT (2010) Comb-shaped conjugates comprising hydroxypropyl cellulose backbones and low-molecular-weight poly(*N*-isopropylacryamide) side chains for smart hydrogels: synthesis, characterization, and biomedical applications. Bioconjug Chem 21:456–464
188. Jin X, Kang HL, Liu RG, Huang Y (2013) Regulation of the thermal sensitivity of hydroxypropyl cellulose by poly(*N*-isopropylacryamide) side chains. Carbohydr Polym 95:155–160
189. Zhang Z, Chen L, Zhao CW, Bai YY, Deng MX, Shan HL, Zhuang XL, Chen XS, Jing XB (2011) Thermo- and pH-responsive HPC-*g*-AA/AA hydrogels for controlled drug delivery applications. Polymer 52:676–682
190. Dou HJ, Jiang M, Peng HS, Chen DY, Hong Y (2003) pH-dependent self-assembly: micellization and micelle-hollow-sphere transition of cellulose-based copolymers. Angew Chem Int Ed 42:1516–1519
191. Dong XT, Shi WT, Dang HC, Bao WY, Wang XL, Wang YZ (2012) Thermal, crystallization properties, and micellization behavior of HEC-*g*-PPDO copolymer: microstructure parameters effect. Ind Eng Chem Res 51:14037–14046
192. Shen D, Huang Y (2004) The synthesis of CDA-*g*-PMMA copolymers through atom transfer radical polymerization. Polymer 45:7091–7097
193. Vlcek P, Janata M, Latalova P, Kriz J, Cadova E, Toman L (2006) Controlled grafting of cellulose diacetate. Polymer 47:2587–2595

194. Vlcek P, Janata M, Latalova P, Dybal J, Spirkova M, Toman L (2008) Bottlebrush-shaped copolymers with cellulose diacetate backbone by a combination of ring opening polymerization and ATRP. J Polym Sci Polym Chem 46:564–573
195. Karakasyan C, Lack S, Brunel F, Maingault P, Hourdet D (2008) Synthesis and rheological properties of responsive thickeners based on polysaccharide architectures. Biomacromolecules 9:2419–2429
196. Eldin MSM, El-Sherif HM, Soliman EA, Elzatahry AA, Omer AM (2011) Polyacrylamide-grafted carboxymethyl cellulose: smart pH-sensitive hydrogel for protein concentration. J Appl Polym Sci 122:469–479
197. Motornov M, Roiter Y, Tokarev I, Minko S (2010) Stimuli-responsive nanoparticles, nanogels and capsules for integrated multifunctional intelligent systems. Prog Polym Sci 35:174–211
198. Kang HL, Gao X, Liu RG, Huang Y (2012) Synthesis and properties of cellulose graft copolymers with well-defined architecture. In: Liebner F, Rosenau T (eds) Functional materials from renewable sources. ACS symposium series, vol 1107. American Chemical Society, Washington, pp 109–131
199. Tan JJ, Li YX, Liu RG, Kang HL, Wang DQ, Ma L, Liu WY, Wu M, Huang Y (2010) Micellization and sustained drug release behavior of EC-*g*-PPEGMA amphiphilic copolymers. Carbohydr Polym 81:213–218
200. Prabaharan M, Mano JF (2006) Stimuli-responsive hydrogels based on polysaccharides incorporated with thermo-responsive polymers as novel biomaterials. Macromol Biosci 6:991–1008
201. Hennink WE, van Nostrum CF (2012) Novel crosslinking methods to design hydrogels. Adv Drug Deliv Rev 64:223–236
202. Mahltig B, Jerome R, Stamm M (2003) The influence of an acid–base-equilibrium on the adsorption behaviour of a weak polyampholyte. J Polym Res 10:219–223
203. Plamper FA, Ruppel M, Schmalz A, Borisov O, Ballauff M, Mueller AHE (2007) Tuning the thermoresponsive properties of weak polyelectrolytes: aqueous solutions of star-shaped and linear poly(N, N-dimethylaminoethyl methacrylate). Macromolecules 40:8361–8366
204. Kang HL, Liu RG, Sun HF, Zhen JM, Li QM, Huang Y (2012) Osmium bipyridine-containing redox polymers based on cellulose and their reversible redox activity. J Phys Chem B 116:55–62
205. Jian CM, Liu BW, Chen X, Zhou ST, Fang T, Yuan JY (2014) Construction of photoresponsive supramolecular micelles based on ethyl cellulose graft copolymer. Chin J Polym Sci 32:690–702
206. Zhou D, Zhang L, Guo SL (2005) Mechanisms of lead biosorption on cellulose/chitin beads. Water Res 39:3755–3762
207. Takegawa A, Murakami M, Kaneko Y, Kadokawa J (2010) Preparation of chitin/cellulose composite gels and films with ionic liquids. Carbohydr Polym 79:85–90
208. Yamazaki S, Takegawa A, Kaneko Y, Kadokawa J, Yamagata M, Ishikawa M (2009) An acidic cellulose-chitin hybrid gel as novel electrolyte for an electric double layer capacitor. Electrochem Commun 11:68–70
209. Shih CM, Shieh YT, Twu YK (2009) Preparation and characterization of cellulose/chitosan blend films. Carbohydr Polym 78:169–174
210. Hoemann CD, Chenite A, Sun J, Hurtig M, Serreqi A, Lu Z, Rossomacha E, Buschmann MD (2007) Cytocompatible gel formation of chitosan-glycerol phosphate solutions supplemented with hydroxyl ethyl cellulose is due to the presence of glyoxal. J Biomed Mater Res A 83:521–529
211. Kadokawa J, Murakami M, Takegawa A, Kaneko Y (2009) Preparation of cellulose-starch composite gel and fibrous material from a mixture of the polysaccharides in ionic liquid. Carbohydr Polym 75:180–183

212. Liang HF, Hong MH, Ho RM, Chung CK, Lin YH, Chen CH, Sung HW (2004) Novel method using a temperature-sensitive polymer (methylcellulose) to thermally gel aqueous alginate as a pH-sensitive hydrogel. Biomacromolecules 5:1917–1925
213. Krishna Rao KSV, Subha MCS, Vijaya Kumar Naidu B, Sairam M, Mallikarjuna NN, Aminabhavi TM (2006) Controlled release of diclofenac sodium and ibuprofen through beads of sodium alginate and hydroxy ethyl cellulose blends. J Appl Polym Sci 102:5708–5718
214. Karewicz A, Zasada K, Szczubialka K, Zapotoczny S, Lach R, Nowakowska M (2010) "Smart" alginate-hydroxypropylcellulose microbeads for controlled release of heparin. Int J Pharm 385:163–169
215. Chang CY, Duan B, Zhang LN (2009) Fabrication and characterization of novel macroporous cellulose-alginate hydrogels. Polymer 50:5467–5473
216. Prasad K, Kaneko Y, Kadokawa J (2009) Novel gelling systems of κ-, ι- and λ-carrageenans and their composite gels with cellulose using ionic liquid. Macromol Biosci 9:376–382
217. Sannino A, Madaghiele M, Conversano F, Mele G, Maffezzoli A, Netti PA, Ambrosio L, Nicolais L (2004) Cellulose derivative-hyaluronic acid-based microporous hydrogels cross-linked through divinyl sulfone (DVS) to modulate equilibrium sorption capacity and network stability. Biomacromolecules 5:92–96
218. Baumann MD, Kang CE, Stanwick JC, Wang YF, Kim H, Lapitsky Y, Shoichet MS (2009) An injectable drug delivery platform for sustained combination therapy. J Control Release 138:205–213
219. Sannino A, Pappada S, Madaghiele M, Maffezzoli A, Ambrosio L, Nicolais L (2005) Crosslinking of cellulose derivatives and hyaluronic acid with water-soluble carbodiimide. Polymer 46:11206–11212
220. Wang JH, Gao C, Zhang YS, Wan YZ (2010) Preparation and in vitro characterization of BC/PVA hydrogel composite for its potential use as artificial cornea biomaterial. Mater Sci Eng C Mater Biol Appl 30:214–218
221. Abou Taleb MF, Abd El-Mohdy HL, Abd El-Rehim HA (2009) Radiation preparation of PVA/CMC copolymers and their application in removal of dyes. J Hazard Mater 168:68–75
222. Millon LE, Wan WK (2006) The polyvinyl alcohol-bacterial cellulose system as a new nanocomposite for biomedical applications. J Biomed Mater Res B Appl Biomater 79B:245–253
223. Shi XW, Zhang LN, Cai J, Cheng GZ, Zhang HM, Li J, Wang X (2011) A facile construction of supramolecular complex from polyaniline and cellulose in aqueous system. Macromolecules 44:4565–4568
224. Shi XW, Lu A, Cai J, Zhang LN, Zhang HM, Li J, Wang XH (2012) Rheological behaviors and miscibility of mixture solution of polyaniline and cellulose dissolved in an aqueous system. Biomacromolecules 13:2370–2378
225. Zhou C, Wu Q, Yue Y, Zhang Q (2011) Application of rod-shaped cellulose nanocrystals in polyacrylamide hydrogels. J Colloid Interface Sci 353:116–123
226. Zhou C, Lee S, Dooley K, Wu Q (2013) A facile approach to fabricate porous nanocomposite gels based on partially hydrolyzed polyacrylamide and cellulose nanocrystals for adsorbing methylene blue at low concentrations. J Hazard Mater 263:334–341
227. Dou HJ, Yang WH, Tao K, Li WW, Sun K (2010) Thermal sensitive microgels with stable and reversible photoluminescence based on covalently bonded quantum dots. Langmuir 26:5022–5027
228. Tan JJ, Liu RG, Wang W, Liu WY, Tian Y, Wu M, Huang Y (2010) Controllable aggregation and reversible pH sensitivity of AuNPs regulated by carboxymethyl cellulose. Langmuir 26:2093–2098
229. Luo XG, Zhang LN (2009) High effective adsorption of organic dyes on magnetic cellulose beads entrapping activated carbon. J Hazard Mater 171:340–347

230. Gupta D, Tator CH, Shoichet MS (2006) Fast-gelling injectable blend of hyaluronan and methylcellulose for intrathecal, localized delivery to the injured spinal cord. Biomaterials 27:2370–2379
231. Yan SF, Yin JB, Tang L, Chen XS (2011) Novel physically crosslinked hydrogels of carboxymethyl chitosan and cellulose ethers: structure and controlled drug release behavior. J Appl Polym Sci 119:2350–2358
232. Wu L, Zhou H, Sun HJ, Zhao Y, Yang X, Cheng SZ, Yang G (2013) Thermoresponsive bacterial cellulose whisker/poly(NIPAM-*co*-BMA) nanogel complexes: synthesis, characterization, and biological evaluation. Biomacromolecules 14:1078–1084
233. Spoljaric S, Salminen A, Luong ND, Seppälä J (2014) Stable, self-healing hydrogels from nanofibrillated cellulose, poly(vinyl alcohol) and borax via reversible crosslinking. Eur Polym J 56:105–117
234. Williamson SL, Armentrout RS, Porter RS, McCormick CL (1998) Microstructural examination of semi-interpenetrating networks of poly(N, N-dimethylacrylamide) with cellulose or chitin synthesized in lithium chloride N, N-dimethylacetamide. Macromolecules 31:8134–8141
235. Yang J, Han CR, Zhang XM, Xu F, Sun RG (2014) Cellulose nanocrystals mechanical reinforcement in composite hydrogels with multiple cross-links: correlations between dissipation properties and deformation mechanisms. Macromolecules 47:4077–4086
236. Ekici S (2011) Intelligent poly(*N*-isopropylacrylamide)-carboxymethyl cellulose full interpenetrating polymeric networks for protein adsorption studies. J Mater Sci 46:2843–2850
237. Ma JH, Xu YJ, Fan B, Liang BR (2007) Preparation and characterization of sodium carboxymethylcellulose/poly(*N*-isopropylacrylamide)/clay semi-IPN nanocomposite hydrogels. Eur Polym J 43:2221–2228
238. Ma JH, Zhang L, Fan B, Xu YJ, Liang BR (2008) A novel sodium carboxymethylcellulose/poly(*N*-isopropylacrylamide)/clay semi-IPN nanocomposite hydrogel with improved response rate and mechanical properties. J Polym Sci Polym Phys 46:1546–1555
239. Cha RT, He ZB, Ni YH (2012) Preparation and characterization of thermal/pH-sensitive hydrogel from carboxylated nanocrystalline cellulose. Carbohydr Polym 88:713–718
240. Neyret S, Vincent B (1997) The properties of polyampholyte microgel particles prepared by microemulsion polymerization. Polymer 38:6129–6134
241. You J, Hu HZ, Zhou JP, Zhang LN, Zhang YP, Kondo T (2013) Novel cellulose polyampholyte-gold nanoparticle-based colorimetric competition assay for the detection of cysteine and mercury(II). Langmuir 29:5085–5092
242. Etienne O, Gasnier C, Taddei C, Voegel JC, Aunis D, Schaaf P, Metz-Boutigue MH, Bolcato-Bellemin AL, Egles C (2005) Antifungal coating by biofunctionalized polyelectrolyte multilayered films. Biomaterials 26:6704–6712
243. Zhao Q, Qian J, An Q, Gao C, Gui Z, Jin H (2009) Synthesis and characterization of soluble chitosan/sodium carboxymethyl cellulose polyelectrolyte complexes and the pervaporation dehydration of their homogeneous membranes. J Membr Sci 333:68–78
244. Casalbore-Miceli G, Zanelli A, Girotto EM, Rinaldi AW, Rubira AF, Berlin A (2006) Interactions between humidity and ferrocene-functionalised polythiophene. Electrochim Acta 51:5268–5273
245. Yao KD, Tu HL, Cheng F, Zhang JW, Liu J (1997) pH-sensitivity of the swelling of a chitosan-pectin polyelectrolyte complex. Angew Makromol Chem 245:63–72
246. Lee KY, Park WH, Ha WS (1997) Polyelectrolyte complexes of sodium alginate with chitosan or its derivatives for microcapsules. J Appl Polym Sci 63:425–432
247. Vasiliu S, Popa M, Rinaudo M (2005) Polyelectrolyte capsules made of two biocompatible natural polymers. Eur Polym J 41:923–932
248. Feng XH, Pelton R, Leduc M (2006) Mechanical properties of polyelectrolyte complex films based on polyvinylamine and carboxymethyl cellulose. Ind Eng Chem Res 45:6665–6671

249. Feng XH, Pelton R (2007) Carboxymethyl cellulose: polyvinylamine complex hydrogel swelling. Macromolecules 40:1624–1630
250. Shang J, Shao Z, Chen X (2008) Electrical behavior of a natural polyelectrolyte hydrogel: chitosan/carboxymethylcellulose hydrogel. Biomacromolecules 9:1208–1213
251. Nie K, Pang W, Wang Y, Lu F, Zhu Q (2005) Effects of specific bonding interactions in poly (ε-caprolactone)/silica hybrid materials on optical transparency and melting behavior. Mater Lett 59:1325–1328
252. Arias JL, Lopez-Viota M, Delgado AV, Ruiz MA (2010) Iron/ethylcellulose (core/shell) nanoplatform loaded with 5-fluorouracil for cancer targeting. Colloid Surf B Biointerfaces 77:111–116
253. Chang CY, Peng J, Zhang LN, Pang DW (2009) Strongly fluorescent hydrogels with quantum dots embedded in cellulose matrices. J Mater Chem 19:7771–7776
254. Li L, Meng LJ, Zhang XK, Fu CL, Lu QH (2009) The ionic liquid-associated synthesis of a cellulose/SWCNT complex and its remarkable biocompatibility. J Mater Chem 19:3612–3617
255. Wesarg F, Schlott F, Grabow J, Kurland HD, Hessler N, Kralisch D, Muller FA (2012) In situ synthesis of photocatalytically active hybrids consisting of bacterial nanocellulose and anatase nanoparticles. Langmuir 28:13518–13525
256. Phottraithip W, Lin DQ, Shi F, Yao SJ (2011) A novel method for the preparation of spherical cellulose-tungsten carbide composite matrix with NMMO as nonderivatizing solvent. J Appl Polym Sci 121:2985–2992
257. Chen FR, Huang MM, Li YQ (2014) Synthesis of a novel cellulose microencapsulated palladium nanoparticle and its catalytic activities in Suzuki-Miyaura and Mizoroki-Heck reactions. Ind Eng Chem Res 53:8339–8345
258. Wei XY, Qi L, Tan JJ, Liu RG, Wang FY (2010) A colorimetric sensor for determination of cysteine by carboxymethyl cellulose-functionalized gold nanoparticles. Anal Chim Acta 671:80–84
259. Li WW, Liu RG, Kang HL, Sun YM, Dong FY, Huang Y (2013) Synthesis of amidoxime functionalized cellulose derivatives as a reducing agent and stabilizer for preparing gold nanoparticles. Polym Chem 4:2556–2563
260. Luo XG, Liu SL, Zhou JP, Zhang LN (2009) In situ synthesis of Fe_3O_4/cellulose microspheres with magnetic-induced protein delivery. J Mater Chem 19:3538–3545
261. Peng BL, Han X, Liu HL, Berry RC, Tam KC (2013) Interactions between surfactants and polymer-grafted nanocrystalline cellulose. Colloid Surf A Physicochem Eng Asp 421:142–149
262. Kistler SS (1932) Coherent expanded aerogels. J Phys Chem 36:52–64
263. Husing N, Schubert U (1998) Aerogels airy materials: chemistry, structure, and properties. Angew Chem Int Ed 37:23–45
264. Cai HL, Sharma S, Liu WY, Mu W, Liu W, Zhang XD, Deng YL (2014) Aerogel microspheres from natural cellulose nanofibrils and their application as cell culture scaffold. Biomacromolecules 15:2540–2547
265. Cai J, Liu SL, Feng J, Kimura S, Wada M, Kuga S, Zhang LN (2012) Cellulose-silica nanocomposite aerogels by in situ formation of silica in cellulose gel. Angew Chem Int Ed 51:2076–2079
266. Olsson RT, Samir MASA, Salazar-Alvarez G, Belova L, Strom V, Berglund LA, Ikkala O, Nogues J, Gedde UW (2010) Making flexible magnetic aerogels and stiff magnetic nanopaper using cellulose nanofibrils as templates. Nat Nanotechnol 5:584–588
267. Fischer F, Rigacci A, Pirard R, Berthon-Fabry S, Achard P (2006) Cellulose-based aerogels. Polymer 47:7636–7645
268. Hoepfner S, Ratke L, Milow B (2008) Synthesis and characterisation of nanofibrillar cellulose aerogels. Cellulose 15:121–129
269. Liebner F, Potthast A, Rosenau T, Haimer E, Wendland M (2008) Cellulose aerogels: highly porous, ultra-lightweight materials. Holzforschung 62:129–135

270. Sescousse R, Smacchia A, Budtova T (2010) Influence of lignin on cellulose-NaOH-water mixtures properties and on aerocellulose morphology. Cellulose 17:1137–1146
271. Aaltonen O, Jauhiainen O (2009) The preparation of lignocellulosic aerogels from ionic liquid solutions. Carbohydr Polym 75:125–129
272. Sescousse R, Gavillon R, Budtova T (2011) Aerocellulose from cellulose–ionic liquid solutions: preparation, properties and comparison with cellulose–NaOH and cellulose–NMMO routes. Carbohydr Polym 83:1766–1774
273. Duchemin BJC, Staiger MP, Tucker N, Newman RH (2010) Aerocellulose based on all-cellulose composites. J Appl Polym Sci 115:216–221
274. Jin H, Nishiyama Y, Wada M, Kuga S (2004) Nanofibrillar cellulose aerogels. Colloid Surf A Physicochem Eng Asp 240:63–67
275. Surapolchai W, Schiraldi DA (2010) The effects of physical and chemical interactions in the formation of cellulose aerogels. Polym Bull 65:951–960
276. Sehaqui H, Salajkova M, Zhou Q, Berglund LA (2010) Mechanical performance tailoring of tough ultra-high porosity foams prepared from cellulose I nanofiber suspensions. Soft Matter 6:1824–1832
277. Sehaqui H, Zhou Q, Ikkala O, Berglund LA (2011) Strong and tough cellulose nanopaper with high specific surface area and porosity. Biomacromolecules 12:3638–3644
278. Cai J, Kimura S, Wada M, Kuga S (2009) Nanoporous cellulose as metal nanoparticles support. Biomacromolecules 10:87–94
279. Litschauer M, Neouze MA, Haimer E, Henniges U, Potthast A, Rosenau T, Liebner F (2010) Silica modified cellulosic aerogels. Cellulose 18:143–149
280. Tan CB, Fung BM, Newman JK, Vu C (2001) Organic aerogels with very high impact strength. Adv Mater 13:644–646
281. Luong ND, Lee YK, Nam JD (2008) Highly-loaded silver nanoparticles in ultrafine cellulose acetate nanofibrillar aerogel. Eur Polym J 44:3116–3121
282. Guilminot E, Fischer F, Chatenet M, Rigacci A, Berthon-Fabry S, Achard P, Chainet E (2007) Use of cellulose-based carbon aerogels as catalyst support for PEM fuel cell electrodes: electrochemical characterization. J Power Sources 166:104–111
283. Luong ND, Lee Y, Nam JD (2008) Facile transformation of nanofibrillar polymer aerogel to carbon nanorods catalyzed by platinum nanoparticles. J Mater Chem 18:4254–4259

Supramolecular Hydrogels for Regenerative Medicine

A.C.H. Pape and Patricia Y.W. Dankers

Contents

Abstract Regenerative medicine is the science of re-creating or repairing living functional tissue, often inside the body. Biomaterials for regenerative medicine are inspired by the extracellular matrix (ECM), which provides the natural scaffold for cells inside the body. The use of supramolecular hydrogels as man-made tunable replacements for the ECM is being investigated because hydrogels offer an aqueous environment. In addition, supramolecular systems offer modularity and dynamics, also found in the ECM. This chapter gives an overview of translational research on different supramolecular hydrogels, showing systems that have been used in vivo in the field of regenerative medicine. We discuss the chemical structures and biomedical applications of various natural compounds, biosynthetic compounds, biohybrid systems, and fully synthetic materials. Furthermore, we discuss tuning of the mechanical properties and functionalization of these hydrogels with bioactive compounds. Both characteristics are essential for their function in contact with cells and for the creation of a regenerative niche, thereby controlling cellular adherence, proliferation, homing, and differentiation.

A.C.H. Pape • P.Y.W. Dankers (✉)
Laboratory of Chemical Biology, Institute for Complex Molecular Systems, Eindhoven University of Technology, Eindhoven, The Netherlands

Laboratory of Chemical Biology, Department of Biomedical Engineering, Eindhoven University of Technology, Eindhoven, The Netherlands
e-mail: p.y.w.dankers@tue.nl

© Springer International Publishing Switzerland 2015

S. Seiffert (ed.), *Supramolecular Polymer Networks and Gels*, Advances in Polymer Science 268, DOI 10.1007/978-3-319-15404-6_7

Keywords Biomedical applications • Regenerative medicine • Supramolecular hydrogels • Translational research

1 Introduction

In the field of regenerative medicine, scientists aim to re-create or repair living, functional tissue up to the size of complete organs. Complete organs are one of the greatest promises of regenerative medicine, as these organs could potentially replace donor organs and provide a solution for the shortage of available organs for transplantation [1]. Regenerative medicine and other biomedical applications are naturally only concerned with aqueous systems and, therefore, hydrogels are widely investigated, for example, as scaffolds for tissue engineering and as drug delivery vehicles [2–7]. Although polymeric hydrogels have already proven their application in medicine (e.g., as contact lenses), supramolecular hydrogels are still emerging as biomaterials, mainly because of a lack of design rules [8, 9].

Supramolecular hydrogels consist of supramolecular polymers that are able to form freestanding three-dimensional (3D) networks when swollen in water. Supramolecular polymers consist of monomers or oligomers linked together by noncovalent, well-defined, directional interactions such as hydrogen bonding arrays, steric interactions, metal–ligand complexes, hydrophobic interactions, van der Waals forces, π–π stacking, and other electrostatic effects [10]. Via these supramolecular interactions, both long polymers and physically cross-linked networks can be formed [11]. Supramolecular polymers have found use in many other polymer applications such as adhesives, cosmetics, and coatings [12].

Supramolecular systems offer distinct advantages as biomaterials over chemically cross-linked gels. First, because of their noncovalent nature, supramolecular systems are inherently responsive to stimuli such as variations in temperature and pH. Second, the noncovalent bonding allows a unique mix-and-match principle to be used for tuning properties. Third, supramolecular materials biodegrade faster than chemically cross-linked gels as a result of the small molecular precursors that these materials are made of. Furthermore, these supramolecular systems are proposed to be able to display dynamic reciprocal behavior, as found in the natural environment of cells [13]. Supramolecular biomaterials are proposed to be able to spatiotemporally adapt to changes exerted by cells and their natural environment. To fulfill this promise, important features of supramolecular systems are their hierarchical structure/assembly, their dynamic and nonlinear behavior, and their biochemical properties.

The use of supramolecular hydrogels in regenerative medicine is inspired by the extracellular matrix (ECM), which provides the natural scaffolding for cells inside the body [14]. Mimicking the ECM is a major objective for tissue engineering, in order to create a regenerating niche for cells [15]. The natural ECM is inherently

dynamic, and the structural support is given by macromolecules such as proteoglycans and fibrous proteins; therefore, supramolecular hydrogels might be an ideal replacement [16]. Furthermore, the ECM provides cells with handles for attachment and signaling, and it regulates the transport and presentation of soluble components such as growth factors. These three roles of the ECM – mechanical support, cell signaling, and soluble factor transport/presentation – need to be fulfilled by an ideal ECM mimic.

The mechanical properties of the ECM in natural tissue show a highly variable stiffness, ranging from hundreds of pascals in the mammary gland to megapascals for articular cartilage [17] (Fig. 1). These tissues resist tensile forces using fibrillar proteins such as collagens, whereas hydrated proteins and glycosaminoglycans resist compressive forces [15]. Cells can sense this mechanical microenvironment and respond to the ECM by changing their own mechanical properties via the cytoskeletal network [18]. Therefore, for adherence, proliferation, and differentiation of cells, the mechanical components of designed cell matrices are essential [19–21]. However, hydrogels generally possess inferior mechanical properties, such as mechanical toughness and resistance to friction, compared with natural tissues [5]. Therefore, it is important to improve the mechanical properties of hydrogels and tailor them for their specific application.

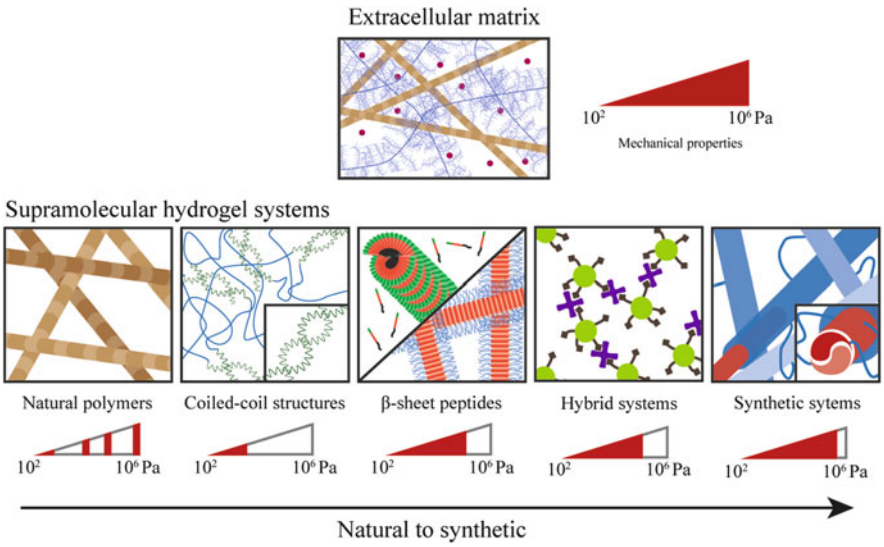

Fig. 1 Supramolecular systems described in this chapter. *Top*: The extracellular matrix inspires most of the work and consists of fibers to resist tensile stresses such as collagens, fibers to resist compressive stresses such as the glycosaminoglycans, and soluble factors for cell signalling. *Bottom*: Natural systems such as collagen, coiled-coil structures, β-sheet peptides such as peptide amphiphiles and multidomain peptides, hybrid systems such as streptavadin–biotin cross-linked microparticles, and synthetic systems such as the UPy-based hydrogelators

Besides the physical factors, cell–matrix interactions are also regulated by biological factors. Thus, hydrogels should contain bioactive signals to facilitate and enhance these cell–matrix interactions. Furthermore, they also need to fulfill special functions such as the attraction of specific cells and controlled release of bioactives to regulate cell behavior. In the development of supramolecular hydrogels for biomedical applications, it is necessary to take into account the tuning and optimization of the mechanical properties of these hydrogels as well as their functionalization with bioactive components.

Numerous reviews describe supramolecular hydrogels in detail [22–28]; therefore, this article is focused on those supramolecular hydrogel systems designed for applications in regenerative medicine and tested in vivo, as translational research is essential to show the applicability of these materials. We discuss the chemical structures of the systems, their mechanical properties, and the introduction of bioactivity. Additionally, we show examples of various applications in regenerative medicine. Components derived from the ECM have been used extensively as hydrogelators, and we first discuss some of these natural components together with other natural supramolecular polymers that have been used in vivo (Sect. 2) (Fig. 1). Next, we discuss biosynthetic compounds, where man-made peptides are used to mimic the fibrous proteins found in the ECM (Sects. 3 and 4). Then, we discuss hybrid hydrogels, which combine natural structures with synthetic compounds (Sect. 5). In Sect. 6, fully synthetic compounds, inspired by the ECM but showing no resemblance in the chemical structure, are discussed.

2 Supramolecular Hydrogels Based on Natural Polymers

The use of natural polymers for the preparation of hydrogels is inspired by the ECM, which consists of many small and large natural polymers such as collagens and polysaccharides. The use of these hydrogelators and other natural polymers for tissue engineering has been reviewed extensively, for example, the use of elastins, glycosaminoglycans, hyaluronic acids, collagens, gelatins, and keratins [24, 29–33]. Often, chemical cross-linking is essential to obtain stable gels. Here, we describe natural polymers that form 3D networks via supramolecular interactions.

Collagen is the main structural component of the interstitial ECM and basement membrane. Different types of collagens exist, but all collagens share the repeated –Gly–Xaa–Yaa– sequence and have a high proline and hydroxyproline content [34]. Three peptides containing this repeating sequence form a triple helical chain that subsequently bundles together with other chains. These bundles align to form long collagen fibrils (Fig. 2a). Self-supporting gels can be formed via end cross-linking of these fibers. They show shear moduli of tens of pascals under physiological conditions, compressive moduli of tens of kilopascals, and tensile moduli of hundreds of kilopascals. This shows the importance of collagens in resisting tensile forces in the ECM [15, 35, 36]. The properties of collagen depend heavily on temperature and pH, and they can be altered by simply changing the pH during

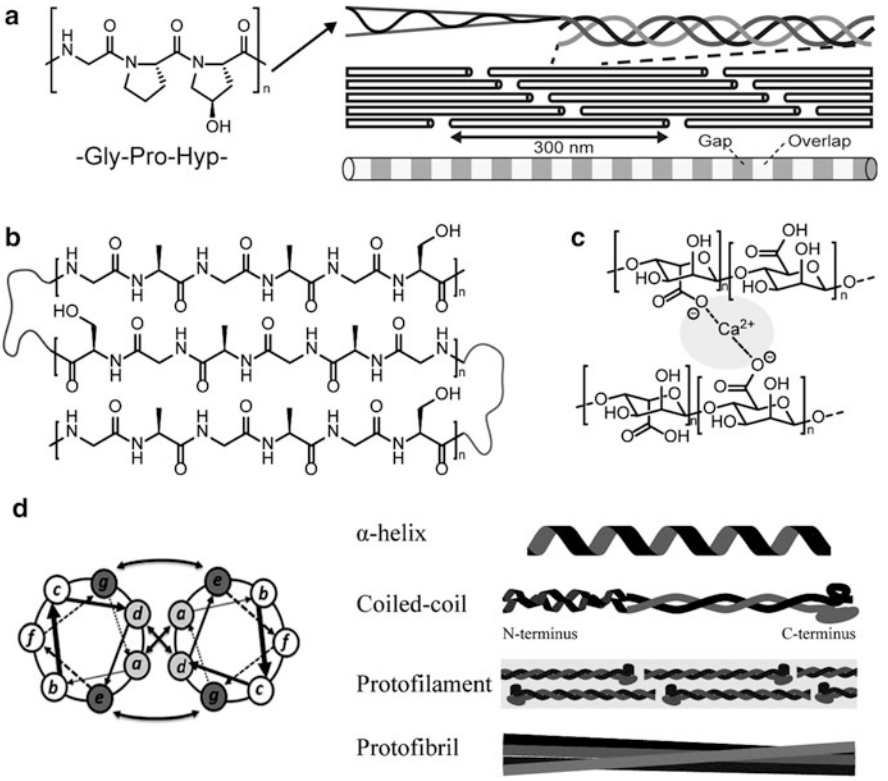

Fig. 2 Supramolecular natural polymeric hydrogels discussed in this chapter. (**a**) Chemical structure of the most-repeated sequence in collagen, forming the α-chain that folds in a three-stranded superhelix [135]. These superhelices bundle to form the collagen fiber. (**b**) Representative chemical structure of fibroin and the antiparallel β-sheet formation connected by hydrophilic linkers. (**c**) Chemical structure of alginic acid, cross-linked by calcium ions (*highlighted*). (**d**) *Left*: Top view of two α-helixes of keratin forming a coiled coil by hydrophobic interactions. *Right*: Overview of subsequent formation of the fibril. The *left part* is adapted from [57] with permission of The Royal Society of Chemistry

polymerization [37, 38]. By increasing the pH, fibrils of collagen become longer and thinner, leading to increased moduli and failure stresses. However, under physiological conditions, no orders of magnitude difference in moduli can be obtained. Collagens contain cellular binding epitopes, for instance the CNYYSNSYSFWLASLNPER sequence in collagen type IV [39]. Cell binding can also be mediated by mixing glycoproteins with the collagen substrate [40] or by mixing in drugs. Collagenous scaffolds have been used extensively for biomedical applications because of their inherent biocompatibility. They have often been applied as skin grafts or together with other cells and biopolymers as disks, meshes, or foams in tissue such as cartilage and bone [41, 42]. As early as 1990, aliquots of collagenous hydrogels were used as a drug delivery system for sustained delivery of an anticancer drug in the mouse brain [43].

Natural polymers not present inside the body have also been tested for regenerative medicine. Silks are structural proteins, and the fibers from the *Bombyx mori* silkworm are the most-used silks for biomedical applications [44]. Silk mainly consists of fibroin, a protein rich in glycine and alanine that forms β-sheets and becomes insoluble in water, forming cross-links for the gel (Fig. 2b) [45]. Several techniques have been used to prepare silk scaffolds, such as freeze-drying, salt leaching, and gas foaming, which influence the mechanical properties of the silk fibroin gels [46]. Sonication and vortexing have also been used to aid gelation. The properties of silk fibroin hydrogels depend on the processing conditions. Gel formation is irreversible, and compressive moduli are largely determined by the pore sizes in the gel, which can be influenced by silk fibroin concentration, gelation temperature, and calcium ion concentration [47, 48]. In general, compressive moduli of 30–3,000 kPa are obtained. Increasing the concentration or temperature leads to accelerated formation of the physical cross-links. Without the presence of ions, this leads to increasing compressive strength and moduli. Bioactivity can be obtained by mixing in growth factors or other types of bioactive natural polymers, such as collagen, gelatin, and glycosaminoglycans [31]. Several examples of the use of these silk fibroin hydrogels in regenerative medicine exist. Silk fibroin hydrogels aided bone remodeling and maturation in a critical size defect in rabbits, but degraded within 12 weeks [49]. By encapsulation of vascular endothelial growth factor (VEGF) and bone morphogenetic protein 7 (BMP-7) in a sonication-induced silk fibroin hydrogel, bone regeneration was promoted in rabbits [50].

Alginate is a polysaccharide derived from algae that has many carboxylic acid groups and therefore can be cross-linked by calcium ions (Fig. 2c). The mechanical properties of hydrogels formed by alginates are determined by molecular weight when there is a low cross-linking density and by the guluronic acid content; hence, at high cross-linking density the properties depend on the amount of cross-links on the alginate [51]. By varying the polymer and salt concentration, compressive moduli of 5–200 kPa can be obtained. Often, alginate hydrogels are combined with other natural polymers such as collagens to influence cell attachment, or with bioactive signaling proteins such as growth factors to influence cell signaling. In one example, alginate gels were loaded with angiogenic growth factors and placed subcutaneously in the dorsal area of rats [52]. Sequential delivery of three growth factors [VEGF, platelet-derived growth factor, and transforming growth factor beta (TGF-β)] led to enhanced formation of stable and mature blood vessels after 3 months.

The use of human-hair-based keratin has also been explored, but only in a limited number of regenerative-medicine applications [53]. Keratin consists of a family of structural proteins, of which we have already discussed one member, fibroin. In the examples below, we discuss keratin from the human hair, α-keratin, which consists of two α-helices that form a coiled coil as a result of hydrophobic interactions (Fig. 2d). The process of converting hair into a hydrogel consists of oxidizing the keratin and subsequent breaking of the disulfide linkages. After cooling to room temperature, the remaining disulfide and hydrogen bonds form

the gel [30]. Temperature, concentration, and vortexing can be used to tune the shear moduli of the gel between 1 Pa and 1 MPa [54]. About 78 % of human hair keratins contain the cell-binding sequence RGD and, therefore, cells easily attach to keratin [55]. Keratin hydrogels have been used in a mouse tibia nerve injury model, where the hydrogel caused improved axon regeneration and functional recovery [55]. In another study, keratin gels were used to stop bleeding in a lethal liver injury in rabbits [56]. Enhanced 24-h survival rates were shown for rabbits treated with keratin hydrogels, and the keratin gels performed better than commercial hemostatic agents used to stop bleeding.

Natural materials offer many advantages, such as inherent biocompatibility and the natural presence of bioactive sequences. However, problems can arise with batch-to-batch variability, contamination by pathogens (when derived from animal origin, for example, collagen I), and contamination by other non-compatible components. For example, silk contains, in addition to the structural protein fibroin, a glue between the fibers, sericin, which needs to be removed because it can lead to problems with biocompatibility and hypersensitivity [44]. Furthermore, tuning the mechanical properties of natural hydrogels is only possible in a limited range. To be able to adapt materials for different applications with the full range of mechanical properties found in natural tissue, the mechanical tailoring possibilities of synthetic materials can be beneficial.

3 Biosynthetic Supramolecular Hydrogels Based on Coiled Coils

Biosynthetic hydrogels are synthetic systems with binding motifs copied from nature and allow exact control over the chemical structure. Therefore, designed supramolecular hydrogelators can be chemically modified to alter the mechanical properties and to include bioactive sequences.

A large body of literature concentrates on the use of coiled coils as cross-linkers for the development of biomaterials [57, 58]. Coiled coils are formed by two interacting α-helices, where, once folded, the subsequent orientation of hydrophobic amino acids leads to the formation of dimers in a superhelical fashion. These coiled coils are some of the most abundant oligomer folding motifs in nature. Tirrell and coworkers developed a large artificial protein consisting of a water-soluble $[(AG)_3PEG]_{10}$ random coil block flanked by two leonine-zipper blocks, all prepared by bacterial expression [59]. These end blocks can be selectively folded into an α-helix, forming coiled coils and subsequent gel networks with shear moduli of 200 Pa (Fig. 3a).

These leucine-zippers require the use of a trigger such as pH or temperature, for example, to encapsulate cells. Therefore, a two-component system was developed using recombinant protein engineering [60]. The first component consists of a small peptide spacer extended with WW domains (with conserved tryptophan residues,

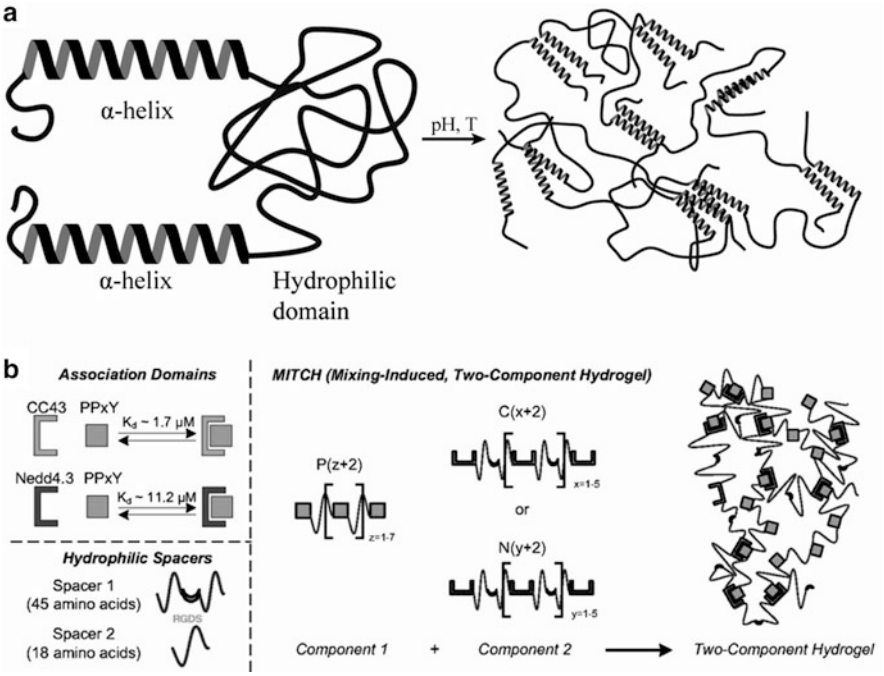

Fig. 3 Coiled-coil hydrogelators. (**a**) Secondary structure of a coiled coil with soluble linkers (*left*), ultimately leading to a 3D network (*right*). (**b**) Engineered two-component hydrogel, where bioactivity is introduced in the hydrophilic spacer via the RGDS sequence. Adapted with permission from [60]

abbreviated by the single-letter amino acid symbol W), which binds to proline-rich peptides incorporated in the second component (Fig. 3b). Protein engineering gives full control over the sequence and, hence, over binding affinity and subsequent bulk properties. This two-component material forms a weak gel with shear moduli of 10–50 Pa, depending on the type of proline-rich sequence used. The binding affinity of the complex can be increased by an order of magnitude by changing the WW component or by changing the amount of repeating units of both binding domains and, thereby, changing the gel point and modulating the plateau modulus slightly [60]. These two-component gels show shear-thinning and self-healing behavior and are therefore suitable as injectable material. Because the material only forms a gel after mixing, simultaneous addition of cells allows mild incorporation of these cells into the material.

Because these peptides are made via protein engineering, cell-adhesion RGD peptide sequences can be encoded in the spacer between the binding motifs, thereby adding bioactivity to the hydrogels. By incorporation of the RGD-motif, PC-12 cells, human umbilical vein endothelial cells (HUVECs), and neural stem cells can be conveniently cultured in 3D. Implanted subcutaneously in mice, this material

shows improved retention of adipose-derived stem cells and is therefore promising as a cell carrier in stem cell injection therapies [61].

Poly(ethylene glycol) (PEG) has also been end-functionalized with these α-helical coiled-coil structures to form hydrogels with storage moduli of 1 kPa [62]. Additionally, it was shown that the self-assembly can only induce an immunogenic response in mice as a result of formation of oligomeric aggregates. The individual components do not induce a response, showing that the effect of the self-assembly can be different from the effect of its individual components and should be taken into account when studying supramolecular biomaterials [63].

Coiled coils are interesting as designable cross-linkers because of the well-understood relation between the peptide sequence, the folded and dimerized structure, and the binding affinity. However, as described above, hydrogels based on coiled coils are generally weak, with shear moduli only up to 1 kPa. Furthermore, the use of recombinant protein expression or solid-phase peptide synthesis limits the scale on which these materials can be prepared. However, this approach allows tuning both the cross-links as well as the backbone to regulate the mechanical properties and incorporate bioactivity.

4 Biosynthetic Supramolecular Hydrogels Based on β-Sheets

Peptide-based hydrogelators are a special class of small molecular building blocks in which short peptide sequences are not only used to induce bioactivity, but also to induce self-assembly into a hydrogel. Several groups have investigated this class of hydrogels for application in tissue engineering, inspired by the self-assembly found in nature and because of the inherent biocompatibility and biodegradability of peptides. Several β-sheet-forming peptides have been developed for use in regenerative medicine and have shown promising potential in vitro; nevertheless, to the best of our knowledge, they have not yet been applied in vivo. For example, Schneider, Pochan, and coworkers developed the MAX8 sequence, an amphiphilic β-hairpin peptide of 20 amino acids of alternating hydrophobic valine and hydrophilic lysine or glutamic acid, folded by prolines in the center, yielding gels with shear moduli of a few hundred pascals [64]. The laboratory of Collier has developed a β-sheet-forming peptide, Ac-QQKFQFQFEQQ-Am (Q11), which slowly assembles into gels via long single fibrils in aqueous environments, resulting in gels with moduli of around 10 Pa [65–67].

Peptide amphiphiles (PAs) are well known to form functional supramolecular materials [68]. PAs consists of (i) a short hydrophobic domain, often an alkyl chain, linked to (ii) an oligopeptide that induces and guides self-assembly by the formation of β-sheets, and (iii) an oligopeptide containing a bioactive domain [69]. In water, these molecules assemble into high-aspect-ratio nanofibers, which entangle and

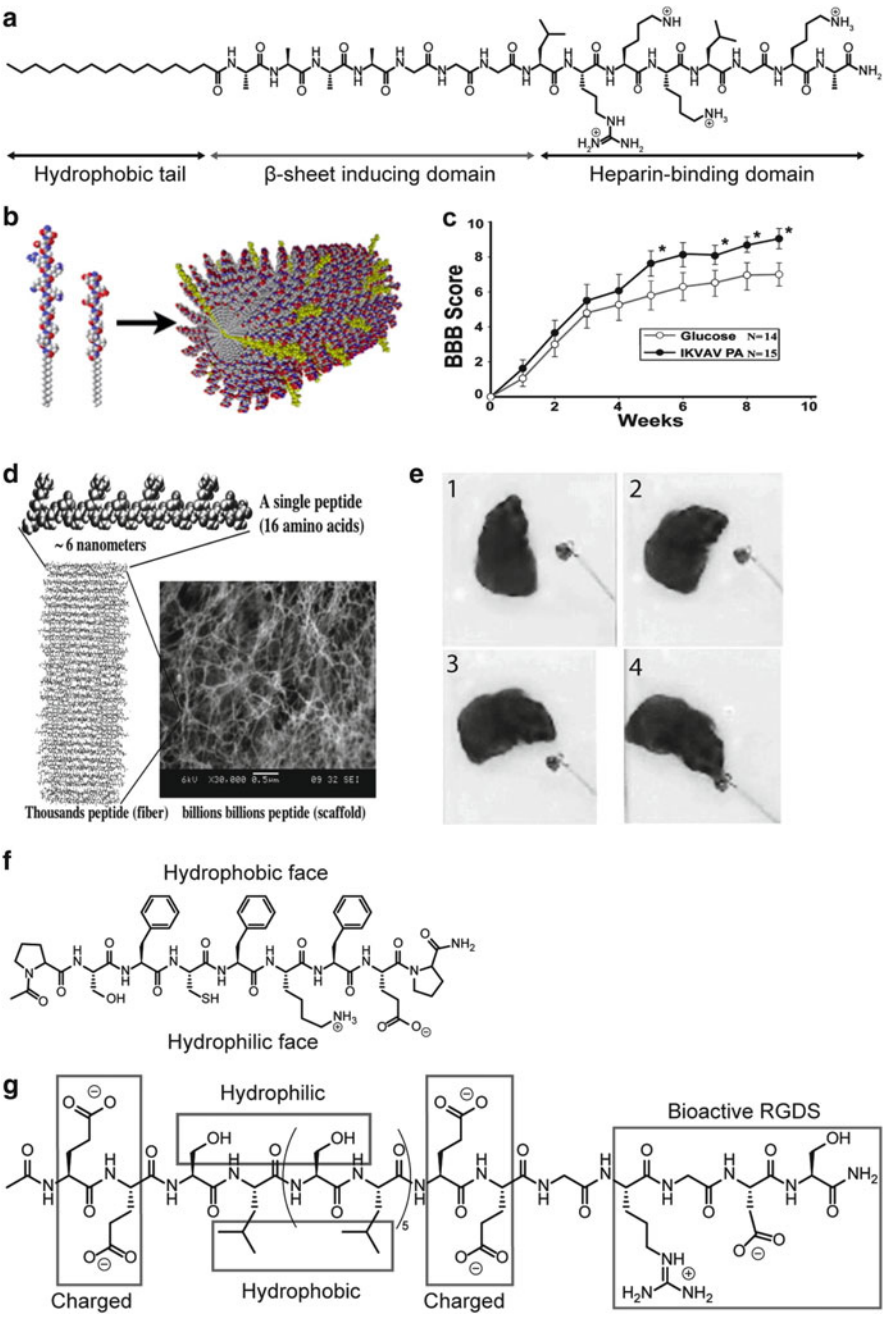

Fig. 4 Self-assembling hydrogelators based on β-sheets. (**a**) Representative chemical structure of a peptide amphiphile, here without charged residues and with a heparin binding domain. (**b**) Peptide amphiphile with bioactive epitopes (*left*) and its assembly leading to formation of 1D fibers (*right*). Reprinted from [136], Copyright 2010, with permission from Elsevier. (**c**) Graph showing the enhanced functional recovery for animals treated with the peptide amphiphile, as assessed via the BBB score. Adapted with permission from [78]. Copyright 2008 Society for

form self-supporting hydrogels. This fibrillar structure mimics the ECM components, including the signaling peptides at the periphery.

The chemical structure of the PAs guides self-assembly into nanofibers and ultimately determines the mechanical properties of the hydrogel (Fig. 4a). The self-assembly of these amphiphiles is triggered by screening of the charges on the epitope by counter-ions or changes in pH [70]. These counter-ions also induce a change in the molecular geometry, which, together with the van der Waals forces, hydrogen bonding, and hydrophobic forces, induces self-assembly into cylindrical micelles. Within these nanofibers, parts of the peptide form β-sheets, leading to high-aspect-ratio objects (Fig. 4b). Mechanical properties originate from the strength and stiffness of these nanofibers and the density and strength of cross-links. Counter-ions have an effect on the fiber stiffness, through which the moduli can be modulated, leading to gels with shear moduli of 100 Pa to 10 kPa. The incorporation of carboxylic acids at the periphery of the PA allows cross-linking of fibers with divalent cations such as calcium, giving rise to different gelation kinetics and networks that can withstand more strain, although the moduli are not influenced [71].

Gels made from PAs have been used in several regenerative-medicine applications such as the induction of angiogenesis [72], bone regeneration [73], cartilage regeneration [74], enamel regeneration [75], and artery engineering [76]. We discuss three examples here, showing the different ways of introducing bioactivity into these PA systems.

Neural progenitor cells (NPCs) can be encapsulated inside PA gels [77]. By incorporating the laminin-mimicking IKVAV sequence, which promotes neurite sprouting and growth, cells were rapidly differentiated into neurons. Bioactivity was obtained by displaying a peptide-mimicking sequence on the periphery of the nanofibers. Furthermore, PAs in solution gel upon contact with tissue. In vivo experiments using a mouse spinal cord injury model showed promising results in the regeneration of the central nervous system [78]. Mice treated with IKVAV-PA showed enhanced regeneration of both descending motor axons and ascending sensory axons and showed functional recovery (Fig. 4c). This IKVAV-PA gel was used to deliver embryonic stem cells into the auditory nerves of rats [79].

Incorporation of a TGF-binding domain on the epitope of PA leads to capture and display of TGF-β1 in the hydrogels [74]. These materials were used to treat a full thickness chondral defect in a rabbit model. They promote the regeneration of articular cartilage by capturing growth factors from the host animal.

Fig. 4 (continued) Neuroscience. (**d**) RADA16 peptide, the formation of a β-sheet, and SEM image of fibers in a gel. Adapted from [84]. (**e**) (*1–4*) Functional recovery of the vision of animals treated with a RADA16 hydrogel, as shown by the response to a light trigger. Adapted from [89]. Copyright (2006) National Academy of Sciences, USA. (**f**) Chemical structure of an amphiphilic PSFCFLFEP peptide. (**g**) Chemical structure of an ABA multidomain peptide, here with an additional bioactive sequence attached

As a third example, inclusion of a heparin-binding domain on the periphery of PAs leads to self-assembled nanofibers, where heparin can be displayed on the nanofiber surface (Fig. 4a) [80]. Subsequently, this bound heparin can be used to capture angiogenic growth factors such as VEGF and fibroblast growth factor 2 (FGF-2) [81]. Implanted in the rat cornea, these materials induced significant blood vessel growth compared with the growth factors alone, showing the added value of a structured delivery system.

Another class of peptide hydrogel formed by β-sheets are hydrogels that consist of ionic alternating hydrophobic and hydrophilic residues, such as the materials based on a β-sheet-forming segment found in a yeast protein developed by Zhang and coworkers [82]. This EAK16 (AEAEAKAKAEAEAKAK) peptide forms β-sheets distinct polar and hydrophobic surfaces, enabling further self-assembly into 20-nm fibers, leading to stable hydrogels in water. In these types of systems, the length of the peptide can be used to tune the mechanical properties, as demonstrated by increasing KFE8 to KFE12 with an accompanying change in the shear moduli from 400 Pa to 2 kPa. This effect can be used together with changing the concentration to obtain gels with shear moduli of 400 Pa to 15 kPa [83].

The RAD self-assembling peptide (Fig. 4d) has been used to locally deliver growth factors such as EGF to accelerate wound-healing in an in vitro model [84]. Both the EAK and RAD systems have been further developed to increase cell adhesion [85], and functional motifs such as laminin and collagen-mimicking sequences have been attached and optimized to culture cells in a 3D environment [86, 87]. These peptides have been used for the delivery of genes to cells [88], and they have proven their feasibility in regenerative medicine by enabling reconnection of brain tissue in hamsters [89]. The peptide scaffold was used to knit together tissue after an acute injury and resulted in increased recovery of the central nervous system and recovery of functional behavioral (Fig. 4e).

Ruan et al. designed peptide-forming nanofibers via β-turn secondary folding [90]. The sequence of the peptide consists of the ionic amino acids lysine and glutamic acid on one end and two phenyl groups and a cysteine on the other end, creating an amphiphile (Fig. 4f). This amphiphilic PSFCFLFEP peptide also includes a proline to increase the formation of fibrils and to induce the β-turn. Hydrogels prepared with this peptide showed shear moduli of around 20 Pa, and addition of sodium chloride increased the moduli approximately tenfold [91]. The fibrils were able to gradually release hydrophobic model compounds such as pyrenes. The peptide hydrogel functioned as a hemostat, stopping bleeding of an injured surface on the rat liver faster than other hemostats.

Another example of a hydrogel based on β-sheet-forming peptides consists of a multidomain peptide (MDP) with an ABA structure [92]. The A-block consists of charged residues to keep the aggregates in solution, attached on both sides to a B-block consisting of alternating glutamine and leucine residues to create a facial amphiphile. Subsequent self-assembly of the B-block leads to poorly soluble aggregates in aqueous environments. This allows formation of a hydrogel. Both blocks of these MDPs can be changed to tune the mechanical properties of these gels, giving moduli ranging from 10 to 500 Pa [93]. Chemical cross-linking via

disulfides even leads to gels with moduli of 6 kPa. The gels undergo rapid shear thinning and recovery, and have therefore been used as injectable drug carriers [94]. Bioactive sequences such as the RGD sequence can be incorporated into the material during the solid-phase peptide synthesis of the MDPs (Fig. 4g). Gels were pre-loaded with the secretome from stem cells, which contains more than 36 secreted proteins, and subsequently used to study the effect on a lipopolysaccharide model of acute kidney injury in mice and an ischemia-reperfusion model of kidney injury in mice [95]. The preconditioned nanofibers protect the kidney against injury by delivery of the secretome of stem cells, which is proposed to be the cause of the improvement resulting from stem cell treatment of acute kidney injury.

Many excellent examples of the biomedical application of peptide-based hydrogelators demonstrate their promise in regenerative medicine. The relation between the design of the peptide and the secondary structure is well understood and helps in designing these types of materials. Furthermore, bioactive sequences are attached to these materials in the same way as the self-assembling domain is synthesized. However, the scale on which the solid-phase peptide synthesis used for the preparation of these systems can be performed is limited. The mechanical properties of these materials can be tuned to obtain moduli between 10 Pa and 10 kPa, giving a larger working range than natural hydrogels and hydrogels based on natural motifs. The maximally obtainable moduli are only one order of magnitude lower than those of tissues found in the body.

5 Hybrid Supramolecular Hydrogel Systems

Systems have been developed that combine both natural and naturally derived compounds with synthetic structures. Many groups have adapted peptide-based structures or have used natural cross-linkers to develop hydrogels. Inspired by the collagens in the ECM, collagen mimetic peptides (CMPs) have been developed [96]. The development of solid-phase peptide synthesis has enabled synthesis of more stable collagen-like peptides such as (proline–hydroxyproline–glycine)$_{10}$, (POG_{10}), which forms stable short helixes. To obtain hydrogels, the focus has been on the self-assembly of these structures into nanofibers and 3D structures. The POG_{10} structure has been modified with three different metal-binding groups: histidine, nitrolotriacetic acid, and a bipyridyl moiety [97]. Subsequently, these structures were cross-linked using nickel ions. However, the mechanical properties of the resulting gels have not been determined. Bioactive sequences can be coupled covalently to promote cell adhesion [98]. By functionalization of growth factors with a His tag, these growth factors can also be supramolecularly complexed to the matrix using nickel ions.

Another interesting approach is the use of tubulin, which by itself forms long cylinders [99]. Forming a stable 3D gel using these cylindrical fibers requires cross-linking of the tubulin fibers with PEG polymers, yielding gels with shear moduli of

1.8 kPa. This cross-linking can only be performed when the tubulins are assembled into fibers to prevent blocking the supramolecular polymerization site of the tubulins. The gel still shows reversible gelation after cross-linking, demonstrating the supramolecular nature of this system. Furthermore, Wieduwild et al. prepared star-shaped PEGs end-functionalized with heparin-binding peptides, creating physical cross-links and subsequent gel formation upon addition of heparin; the obtained materials had shear moduli of around 2 kPa [100].

A different approach involves functionalization of chitosan with α-cyclodextrins and use of PEG as a thread through the α-cyclodextrins to form polypseudorotaxanes [101]. Cells can be encapsulated inside these gels, which showed fast degradation as a result of dethreading of the PEG. However, although these approaches show the promise of hybrid systems, the materials have not yet been tested in vivo.

Yang and coworkers developed a hydrogel based on two amino acid derivatives and bisphosphonate, which self-assemble into hydrogels with shear moduli of 20 Pa to 20 kPa via nanofibers [102]. The amino acid derivative contained the *N*-(fluorenyl-9-methoxycarbonyl) (Fmoc) group, which induces self-assembly via π–π stacking (Fig. 5a). A more systematic study of the use of aromatic–aromatic interactions in the formation of supramolecular peptide hydrogels has been performed, showing the universality of this approach [103]. Incorporation of a terminal carboxylic acid group allows tuning and cross-linking of fibers using different types of salts, and subsequent tuning of the gel moduli with salt and concentration to give moduli between 25 Pa and 75 kPa [104]. The method of preparation of the hydrogels also has an influence on their mechanical properties [21]. Slowly adjusting the pH to form homogenous gels elevates the storage moduli of the gels from 5 to 184 kPa. Simple functionalization of RGD peptides with an aromatic Fmoc group leads to direct cell adhesion to these 3D scaffolds [105]. Besides functioning as a 3D support for the gel, these small molecules can also reduce inflammation [102]: The biphosphonate component of the hydrogel developed by Yang and colleagues lowers into uranyl oxide toxicity. Topical application of the hydrogel to wound sites on skin of mice, previously administered with uranyl oxide, showed effective recovery of the skin to normal, showing the therapeutic effect of these gels.

Yang et al. also showed that glucosamine (a naturally occurring precursor for glycosaminoglycans, proteoglycans, and glycolipids) modified with naphthalene can form a hydrogel (Fig. 5b) [106]. After cooling a solution of the modified glucosamine to room temperature, ribbons are formed. These subsequently form large bundles and tangle to make a 3D hydrogel with a storage modulus of 1 kPa. This hydrogel assisted in wound healing and prevented scar formation, as shown in a mouse animal model.

Gels were also shown to form when biotinylated poly(lactic acid) (PLA)–PEG microparticles were cross-linked using avidin (Fig. 5c) [107]. Gels can be formed that can encapsulate cells, although in rheology the gels do not behave as viscoelastic solids and show a large frequency dependence of their shear moduli. The microparticles can be used as conventional carriers for drugs or signaling

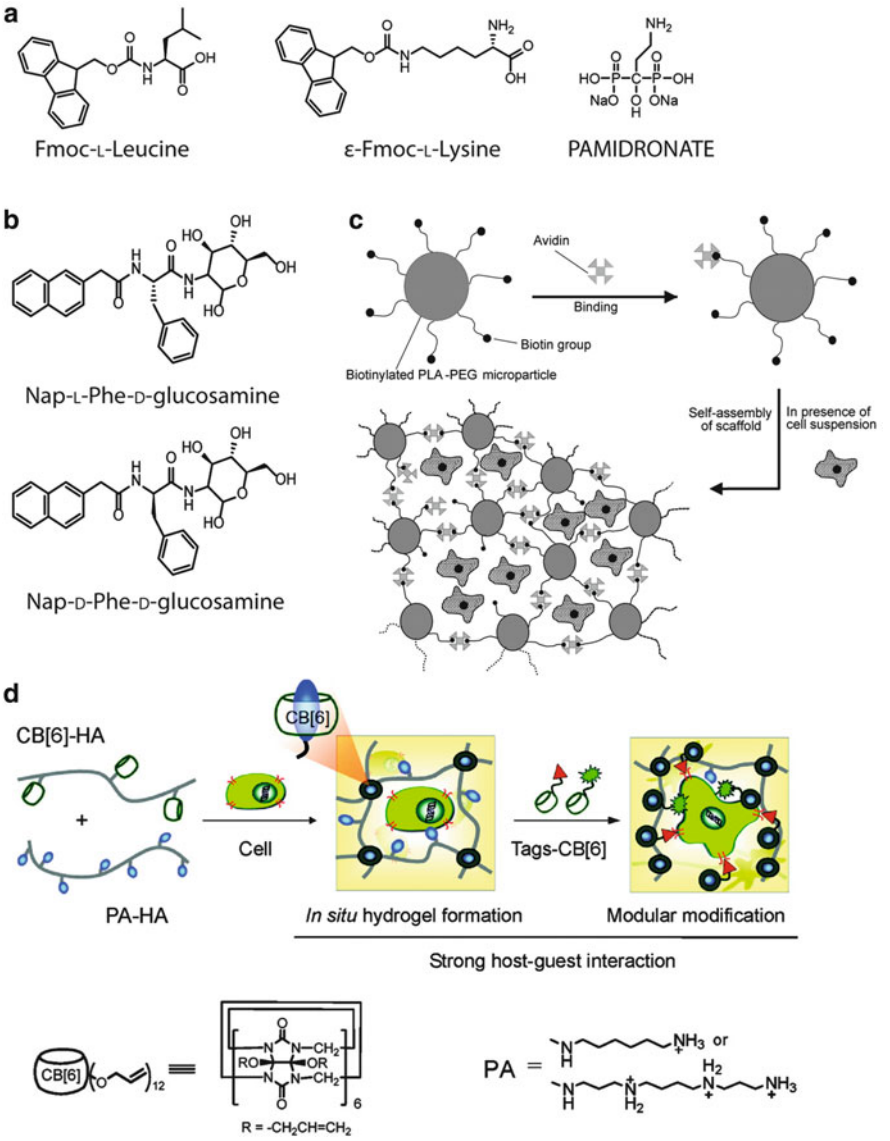

Fig. 5 Hybrid supramolecular hydrogel systems. (**a**) Chemical structures of the three components of Fmoc-gels that assemble via π–π stacking. (**b**) Chemical structures of hydrophobically modified glucosamines. (**c**) Self-assembly of a hydrogel in the presence of cells [107]. Copyright 2003 Wiley-VCH Verlag GmbH&Co. KGaA, Weinheim. (**d**) Hyaluronic acid cross-linking by host–guest interaction of cucurbituril and amines, and the incorporation of cells and dyes. Reprinted with permission from [108]. Copyright 2012 American Chemical Society

molecules, providing a well-understood sustained release. Bone defect in femurs of chicken embryos were filled with these materials and the viability of the bone could be shown, proving applicability in regenerative medicine.

Hyaluronic acid has been modified with cucurbit[6]uril (CB[6]) and polyamines to form stable hydrogels with shear moduli of around 3 kPa when mixed [108]. The CB[6] can then also be used to include functional molecules in the hydrogel in a supramolecular fashion (as demonstrated with dyes to allow in vivo imaging) without influencing the mechanical properties of the hydrogel (Fig. 5d). Subsequently, RGD was incorporated by conjugation to CB[6] to promote cell adhesion of encapsulated cells in these gels, showing that this gel is a promising candidate for in vivo cell delivery. The gel can be formed under the skin of mice and functionalized in a supramolecular fashion inside the body.

The hybrid materials discussed here are still in their infancy and only initial experiments in regenerative medicine have been performed using them. Furthermore, not much knowledge has been gained yet on the mechanical tuning of these materials, except for their small peptide fragments. So far, the use of aromatic–aromatic interactions with small peptide fragments has shown promising properties for regenerative medicine, but more work is needed to demonstrate the applicability of these materials.

6 Synthetic Supramolecular Hydrogels

Besides functionalization of synthetic polymers with peptides or functionalization of peptides with synthetic cross-linkers, fully synthetic supramolecular systems have also been developed for use in regenerative medicine, although they have hardly been tested in vivo. Nature provides good inspiration for new synthetic biomaterials. We envision that many benefits can be gained by using completely synthetic systems, because such systems are infection-free, cheap, fully tunable, and scalable [5]. Before discussing the ureido-pyrimidinone (Upy) hydrogelators developed in our group, we discuss two classes of synthetic systems that are presently being developed for application in regenerative medicine but have not yet been tested in vivo. The first class consists of low molecular weight hydrogelators; the second class consists of hydrogels made from macromolecular monomers that are cross-linked via supramolecular interactions.

Low molecular weight hydrogelators form one-dimensional (1D) stacks and, subsequently, gel networks in water. The behavior of these molecules in organic solvents is well known, and the ability to tune these materials lies in the power of the chemistry to be scalable. Therefore, we consider these materials promising for application in regenerative medicine and give a few examples.

van Esch and coworkers developed hydrogelators based on 1,3,5-triamide cyclohexane with amino acid derivatives and water-soluble chains in the periphery [109]. These molecules interact via hydrophobic interactions and hydrogen bonds to form long 1D stacks, which at low concentration form hydrogels. A similar

C3-symmetric molecule, benzene-tricarboxamide, has been developed that forms a hydrogel via a similar mechanism [110]. Lee and coworkers synthesized coordination polymers by functionalization of pyridine ligands with dendritic tri(ethylene glycol) chains, which lead to helical chains after the addition of silver ions, forming a 3D network [111].

The second class consists of polymers that are cross-linked by different moieties. Cyclodextrin (CD) has been widely studied as a supramolecular cross-linker for hydrogels [112]. The cavity of β-CD can include hydrophobic molecules as guests. For example, adamantane can be grafted onto poly(acrylic acid), which can form a complex with poly(acrylic acid) functionalized with β-CD to yield a supramolecular hydrogel [113]. This versatile approach allows the use of different polymers and different guests. Some polymers that have been cross-linked to form hydrogels using this complex are chitosan [114], poly(acrylamide)s [115], and polyacrylates [116]. Other guests that have been used include cholesterol [117], alkyl chains [118], azobenzenes [119], and ferrocenes [120], to name a few. However, not many systems containing CD have been used in vivo because of toxicity and reduced performance [112].

Another popular supramolecular host used to form supramolecular hydrogels is cucurbituril (CB), as described above. The big CB[8] molecule allows encapsulation of two hydrophobic guests. For instance, naphthol and methyl-viologen attached to PEG can be complexed inside CB[8] to form cross-links via a ternary complex, leading to gels with plateau modulus of around 10–1,000 Pa [121]. Also a short butane linker has been used to connect napthol and methyl-viologen to prepare supramolecular hydrogels [122]. Although the CB[8] and the guest show limited water solubility, encapsulation of the guests leads to enhanced water solubility and, subsequently, to formation of a hydrogel.

The synthetic systems described above have not been tested in vivo and their mechanical properties have not been determined. In our group, bifunctional telechelic hydrogelators were developed based on PEG cross-linked with UPy groups at both ends of the polymer (Fig. 6a) [123]. In dilute solution, stacking of UPy dimers results in the formation of nanofibrous structures, aided by additional urea hydrogen bonds in a hydrophobic pocket formed by long alkyl spacers. Above a critical concentration, bundling causes formation of a transient network (Fig. 6b).

Analysis of the telechelic hydrogel with rheology and small angle X-ray scattering (SAXS) has shown that gel formation coincides with the formation of hydrophobic domains, where the fibers formed by the UPy stacks probably bundle to form cross-links [124]. The storage modulus and the relaxation time depend on concentration, temperature, and pH. By increasing the concentration, higher moduli and slower relaxation times are obtained, whereas increasing the temperature induces a switch from a hydrogel to a viscous liquid. The change from a viscous liquid to a hydrogel by increasing the pH allows the use of this system as an injectable delivery system with shear moduli of 100 Pa to 10 kPa. Interestingly, the addition of small monofunctional oligo(ethylene glycol) chains (modified only on one side with a UPy group) to the bifunctional UPy-hydrogelator gives a stronger gel than that formed from the individual components (Fig. 6c). In this

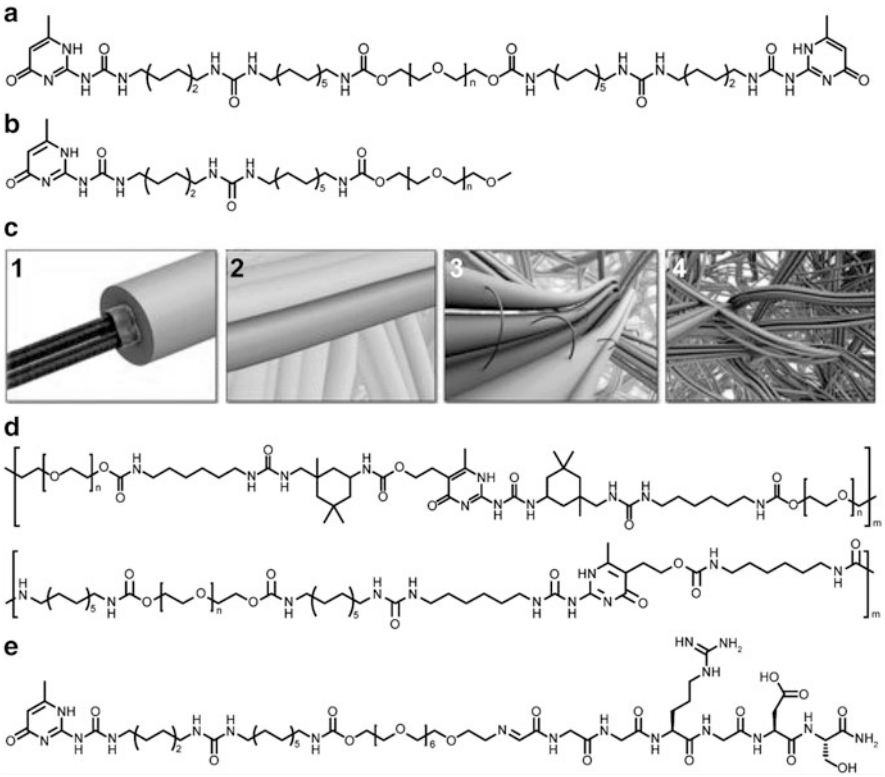

Fig. 6 Ureido-pyrimidinone (UPy)-based hydrogelators. (**a**) Chemical structure of telechelic UPy-functionalized PEG. (**b**) Chemical structure of monofunctional UPy-functional PEG monomethylether. (**c**) (*1–4*) Formation of fibers and subsequent bundling, leading to a 3D hydrogel [131]. Copyright (c) Wiley-VCH Verlag GmbH & Co. KGaA, Weinheim. (**d**) Chemical structures of chain-extended UPy- modified PEGs [127]. (**e**) Chemical structure of RGD-peptide functionalized with the UPy moiety [128]

mixture, the transient network is vitrified [125]. The synergetic network formed shows a storage modulus of 20 kPa, corresponding to a tenfold increase over that of the bifunctional hydrogelators at the same concentration. After mixing, the gel loses its responsiveness to temperature but is still responsive to pH. By incorporating UPy groups in the main chain of a PEG polymer, the hydrogels can be extended further while retaining the storage moduli (Fig. 6d) [126, 127]. These hydrogels show tensile moduli of 480–920 kPa, reaching almost the modulus of articular cartilage. This opens the opportunity for carefully designed gels by mixing-and-matching of the components for specific applications.

Although not yet applied in hydrogel materials, several UPy-modified peptides have been synthesized, such as UPy–RGD and a UPy–collagen I binding peptide, which in principle can be used for bioactivation of these hydrogels (Fig. 6e) [128]. These UPy–peptide conjugates have already proven their value in activating

solid supramolecular polycaprolactone–UPy-based materials for regenerative medicine [129, 130].

Bifunctional UPy–PEG hydrogels have been applied to deliver the growth factor BMP7 under the kidney capsule in rats, and are able to promote fibrous tissue formation by diminishing the amount of infiltrating inflammatory cells and myofibroblasts. The bifunctional hydrogels have also been used for minimally invasive delivery of growth-factor proteins IGF and HGF in the infarcted myocardium in a porcine model using a long thin catheter. This was possible as a result of the pH responsiveness of the hydrogelators. At basic conditions with a pH of approximately 8.5–9, the UPy-hydrogelator formed a solution, whereas at the site of injection, the hydrogelator solution was neutralized to form a hydrogel drug delivery depot in situ [131]. Delivery of the growth-factor proteins stimulated endogeneous cardiac regeneration, that is, diminished collagen deposition, improved cardiac function, reduced hypertrophy, improved cell proliferation, and promoted formation of more capillaries [131, 132].

Although synthetic supramolecular hydrogelators offer several advantages over biomimetic systems and could be an interesting addition to the field, not many fully synthetic systems have been tested in vivo. This might be partially due to the easy availability of non-supramolecular conventional synthetic hydrogels, which have a proven track-record in medicine. However, as new systems are being developed, cheaper and scalable hydrogelators that more closely mimic the ECM can become available. We have shown that, with supramolecular hydrogels, it is possible to obtain good control over the mechanical properties (both strength and dynamics). Furthermore, bioactivity can be conveniently introduced into supramolecular hydrogels by using a mix-and-match approach.

7 Perspective

This chapter demonstrates that supramolecular hydrogels are promising materials for use in regenerative medicine. The examples show how a modular approach allows convenient tuning of mechanical properties and controlled addition of bioactive compounds. The use of the resulting soft dynamic and bioactive materials can provide a more natural-like environment for cells interacting with the biomaterial. Mimicking the native environment, and more specifically the ECM, has inspired a large body of the work performed in this field. However, the ECM is much more complex than the currently used biomaterials. There is not a single supramolecular biomaterial yet that is able to perform in a similar way as the complex set of components in the ECM. For example, the ECM consists of different components that are involved in resisting tensile, compressive, and shear forces, whereas in general only one of these is measured and considered for the hydrogels discussed in this chapter. Furthermore, many biological tissues show strain stiffening, which is essential for their physiological function [133], but nonlinear behavior is observed and studied only in a limited number of synthetic systems, such as

polyisocyanopeptides hydrogels [134]. In addition, although short peptide sequences such as cell-adhesive RGD peptides offer an easy way to incorporate cell-attachment sites in biomaterials, these peptides are not very specific for inducing cell signaling. Fortunately, the use of supramolecular systems allows mixing of different (bioactive) components, both naturally derived and synthetically produced. This can lead to more complex systems offering all the structural and bioactive components required for specific functions. Although many systems are in the developmental phase, more translational research is required to show the true applicability of these systems in vivo.

Acknowledgments Our work is funded by the Ministry of Education, Culture and Science (Gravity program 024.001.035), the Netherlands Organisation for Scientific Research (NWO), the European Research Council (FP7/2007–2013) ERC Grant Agreement 308045, and conducted within the LSH TKI framework. The authors thank E.W. Meijer for many useful discussions.

References

1. NIH (2010) NIH fact sheet – regenerative medicine. National Institutes of Health, Bethesda, http://report.nih.gov/nihfactsheets/Pdfs/RegenerativeMedicine(NIBIB).pdf. Accessed 9 Oct 2014
2. Peppas NA, Hilt JZ, Khademhosseini A, Langer R (2006) Hydrogels in biology and medicine: from molecular principles to bionanotechnology. Adv Mater 18:1345–1360. doi:10.1002/adma.200501612
3. Thiele J, Ma Y, Bruekers SMC, Ma S, Huck WTS (2013) 25th Anniversary article: designer hydrogels for cell cultures: a materials selection guide. Adv Mater 26:125–148. doi:10.1002/adma.201302958
4. Seliktar D (2012) Designing cell-compatible hydrogels for biomedical applications. Science 336:1124–1128. doi:10.1126/science.1214804
5. Gong J, Osada Y (2010) Soft and wet materials: from hydrogels to biotissues. High Solid Dispers 236:203–246
6. Skardal A (2014) Extracellular matrix-like hydrogels for applications in regenerative medicine. In: Connon CJ, Hamley IW (eds) Hydrogels in cell-based therapies. Royal Society of Chemistry, Cambridge, doi: 10.1039/9781782622055-00191
7. Ulijn RV (2006) Enzyme-responsive materials: a new class of smart biomaterials. J Mater Chem 16:2217. doi:10.1039/b601776m
8. Abul-Haija YM, Ulijn RV (2014) Enzyme-responsive hydrogels for biomedical applications. In: Connon CJ, Hamley IW (eds) Hydrogels in cell-based therapies. Royal Society of Chemistry, Cambridge, doi: 10.1039/9781782622055-00112
9. Hirst AR, Escuder B, Miravet JF, Smith DK (2008) High-tech applications of self-assembling supramolecular nanostructured gel-phase materials: from regenerative medicine to electronic devices. Angew Chem Int Ed Engl 47:8002–8018. doi:10.1002/anie.200800022
10. Jones RG, Ober CK (2012) Terminology for aggregation and self-assembly in polymer science (IUPAC Recommendations 2013). Pure Appl Chem 85:463. doi:10.1351/PAC-REC-12-03-12
11. Yui N (ed) (2002) Supramolecular design for biological applications. CRC, Boca Raton
12. Bosman AW, Sijbesma RP, Meijer EW (2004) Supramolecular polymers at work. Mater Today 7:34–39. doi:10.1016/S1369-7021(04)00187-7

13. Xu R, Boudreau A, Bissell M (2009) Tissue architecture and function: dynamic reciprocity via extra- and intra-cellular matrices. Cancer Metastasis Rev 28:167–176. doi:10.1007/s10555-008-9178-z
14. Frantz C, Stewart KM, Weaver VM (2010) The extracellular matrix at a glance. J Cell Sci 123:4195–4200
15. Collier JH, Rudra JS, Gasiorowski JZ, Jung JP (2010) Multi-component extracellular matrices based on peptide self-assembly. Chem Soc Rev 39:3413–3424. doi:10.1039/B914337H
16. Rehmann MS, Kloxin AM (2013) Tunable and dynamic soft materials for three-dimensional cell culture. Soft Matter 9:6737–6746. doi:10.1039/C3SM50217A
17. Levental I, Georges PC, Janmey PA (2007) Soft biological materials and their impact on cell function. Soft Matter 3:299–306. doi:10.1039/B610522J
18. Guilak F, Cohen DM, Estes BT, Gimble JM, Liedtke W, Chen CS (2009) Control of stem cell fate by physical interactions with the extracellular matrix. Cell Stem Cell 5:17–26. doi:10.1016/j.stem.2009.06.016
19. Trappmann B, Gautrot JE, Connelly JT, Strange DGT, Li Y, Oyen ML, Cohen Stuart MA, Boehm H, Li B, Vogel V, Spatz JP, Watt FM, Huck WTS (2012) Extracellular-matrix tethering regulates stem-cell fate. Nat Mater 11:642–649. doi:10.1038/nmat3339
20. Choquet D, Felsenfeld DP, Sheetz MP (1997) Extracellular matrix rigidity causes strengthening of integrin-cytoskeleton linkages. Cell 88:39–48. doi:10.1016/S0092-8674(00)81856-5
21. Wang H, Yang Z, Adams DJ (2012) Controlling peptide-based hydrogelation. Mater Today 15:500–507. doi:10.1016/S1369-7021(12)70219-5
22. Tsitsilianis C (2010) Responsive reversible hydrogels from associative "smart" macromolecules. Soft Matter 6:2372. doi:10.1039/b923947b
23. Kopecek J (2007) Hydrogel biomaterials: a smart future? Biomaterials 28:5185–5192. doi:10.1016/j.biomaterials.2007.07.044
24. Jonker AM, Löwik DWPM, van Hest JCM (2012) Peptide- and protein-based hydrogels. Chem Mater 24:759–773. doi:10.1021/cm202640w
25. Kopeček J, Yang J (2012) Smart self-assembled hybrid hydrogel biomaterials. Angew Chem Int Ed Engl 51:7396–7417. doi:10.1002/anie.201201040
26. Seiffert S, Sprakel J (2012) Physical chemistry of supramolecular polymer networks. Chem Soc Rev 41:909–930. doi:10.1039/C1CS15191F
27. Krieg E, Rybtchinski B (2011) Noncovalent water-based materials: robust yet adaptive. Chem A Eur J 17:9016–9026. doi:10.1002/chem.201100809
28. Weiss R, Terech P (eds) (2006) Molecular gels: materials with self-assembled fibrillar networks. Springer, Dordrecht
29. Whittaker J, Balu R, Choudhury NR, Dutta NK (2014) Biomimetic protein-based elastomeric hydrogels for biomedical applications. Polym Int 63:1545–1557. doi:10.1002/pi.4670
30. Silva R, Fabry B, Boccaccini AR (2014) Fibrous protein-based hydrogels for cell encapsulation. Biomaterials 35:6727–6738. doi:10.1016/j.biomaterials.2014.04.078
31. Van Vlierberghe S, Dubruel P, Schacht E (2011) Biopolymer-based hydrogels as scaffolds for tissue engineering applications: a review. Biomacromolecules 12:1387–1408. doi:10.1021/bm200083n
32. Patterson J, Martino MM, Hubbell JA (2010) Biomimetic materials in tissue engineering. Mater Today 13:14–22. doi:10.1016/S1369-7021(10)70013-4
33. Kim TG, Shin H, Lim DW (2012) Biomimetic scaffolds for tissue engineering. Adv Funct Mater 22:2446–2468. doi:10.1002/adfm.201103083
34. Engel J, Bächinger H (2005) Structure, stability and folding of the collagen triple helix. In: Brinckmann J, Notbohm H, Müller PK (eds) Collagen SE-2. Springer, Berlin, pp 7–33
35. Yang Y, Leone LM, Kaufman LJ (2014) Elastic moduli of collagen gels can be predicted from two-dimensional confocal microscopy. Biophys J 97:2051–2060. doi:10.1016/j.bpj.2009.07.035

36. Achilli M, Mantovani D (2010) Tailoring mechanical properties of collagen-based scaffolds for vascular tissue engineering: the effects of pH, temperature and ionic strength on gelation. Polymers (Basel) 2:664–680. doi:10.3390/polym2040664
37. Yamamura N, Sudo R, Ikeda M, Tanishita K (2007) Effects of the mechanical properties of collagen gel on the in vitro formation of microvessel networks by endothelial cells. Tissue Eng 13:1443–1453. doi:10.1089/ten.2006.0333
38. Roeder BA, Kokini K, Sturgis JE, Robinson JP, Voytik-Harbin SL (2002) Tensile mechanical properties of three-dimensional type I collagen extracellular matrices with varied microstructure. J Biomech Eng 124:214. doi:10.1115/1.1449904
39. Han J, Ohno N, Pasco S, Monboisse J-C, Borel JP, Kefalides NA (1997) A cell binding domain from the α3 chain of type IV collagen inhibits proliferation of melanoma cells. J Biol Chem 272:20395–20401. doi:10.1074/jbc.272.33.20395
40. Kleinman HK, Murray JC, McGoodwin EB, Martin GR (1978) Connective tissue structure: cell binding to collagen. J Invest Dermatol 71:9–11
41. Lee CH, Singla A, Lee Y (2001) Biomedical applications of collagen. Int J Pharm 221:1–22. doi:10.1016/S0378-5173(01)00691-3
42. Place ES, Evans ND, Stevens MM (2009) Complexity in biomaterials for tissue engineering. Nat Mater 8:457–470
43. Sutton R, Yu N, Luck E, Brown D, Conley F (1990) Reduction of vinblastine neurotoxicity in mice utilizing a collagen matrix carrier. Sel Cancer Ther 6:35–49. doi:10.1089/sct.1990.6.35
44. Altman GH, Diaz F, Jakuba C, Calabro T, Horan RL, Chen J, Lu H, Richmond J, Kaplan DL (2003) Silk-based biomaterials. Biomaterials 24:401–416. doi:10.1016/S0142-9612(02)00353-8
45. Jin H-J, Kaplan DL (2003) Mechanism of silk processing in insects and spiders. Nature 424:1057–1061
46. Nazarov R, Jin H-J, Kaplan DL (2004) Porous 3-D scaffolds from regenerated silk fibroin. Biomacromolecules 5:718–726. doi:10.1021/bm034327e
47. Kim U-J, Park J, Kim HJ, Wada M, Kaplan DL (2005) Three-dimensional aqueous-derived biomaterial scaffolds from silk fibroin. Biomaterials 26:2775–2785. doi:10.1016/j.biomaterials.2004.07.044
48. Kim U-J, Park J, Li C, Jin H-J, Valluzzi R, Kaplan DL (2004) Structure and properties of silk hydrogels. Biomacromolecules 5:786–792. doi:10.1021/bm0345460
49. Fini M, Motta A, Torricelli P, Giavaresi G, Nicoli Aldini N, Tschon M, Giardino R, Migliaresi C (2005) The healing of confined critical size cancellous defects in the presence of silk fibroin hydrogel. Biomaterials 26:3527–3536. doi:10.1016/j.biomaterials.2004.09.040
50. Zhang W, Wang X, Wang S, Zhao J, Xu L, Zhu C, Zeng D, Chen J, Zhang Z, Kaplan DL, Jiang X (2011) The use of injectable sonication-induced silk hydrogel for VEGF(165) and BMP-2 delivery for elevation of the maxillary sinus floor. Biomaterials 32:9415–9424. doi:10.1016/j.biomaterials.2011.08.047
51. Kuo CK, Ma PX (2001) Ionically crosslinked alginate hydrogels as scaffolds for tissue engineering: Part 1. Structure, gelation rate and mechanical properties. Biomaterials 22:511–521. doi:10.1016/S0142-9612(00)00201-5
52. Freeman I, Cohen S (2009) The influence of the sequential delivery of angiogenic factors from affinity-binding alginate scaffolds on vascularization. Biomaterials 30:2122–2131. doi:10.1016/j.biomaterials.2008.12.057
53. Rouse JG, Van Dyke ME (2010) A review of keratin-based biomaterials for biomedical applications. Materials (Basel) 3:999–1014. doi:10.3390/ma3020999
54. Yucel T, Cebe P, Kaplan DL (2009) Vortex-induced injectable silk fibroin hydrogels. Biophys J 97:2044–2050
55. Sierpinski P, Garrett J, Ma J, Apel P, Klorig D, Smith T, Koman LA, Atala A, Van Dyke M (2008) The use of keratin biomaterials derived from human hair for the promotion of rapid regeneration of peripheral nerves. Biomaterials 29:118–128. doi:10.1016/j.biomaterials.2007.08.023

56. Aboushwareb T, Eberli D, Ward C, Broda C, Holcomb J, Atala A, Van Dyke M (2009) A keratin biomaterial gel hemostat derived from human hair: evaluation in a rabbit model of lethal liver injury. J Biomed Mater Res B Appl Biomater 90:45–54. doi:10.1002/jbm.b.31251
57. Apostolovic B, Danial M, Klok H-A (2010) Coiled coils: attractive protein folding motifs for the fabrication of self-assembled, responsive and bioactive materials. Chem Soc Rev 39:3541–3575. doi:10.1039/b914339b
58. Wang C, Stewart RJ, Kopecek J (1999) Hybrid hydrogels assembled from synthetic polymers and coiled-coil protein domains. Nature 397:417–420. doi:10.1038/17092
59. Petka W, Harden J, McGrath K, Wirtz D, Tirrell D (1998) Reversible hydrogels from self-assembling artificial proteins. Science 281:389–392. doi:10.1126/science.281.5375.389
60. Wong Po Foo CTS, Lee JS, Mulyasasmita W, Parisi-Amon A, Heilshorn SC (2009) Two-component protein-engineered physical hydrogels for cell encapsulation. Proc Natl Acad Sci USA 106:22067–22072. doi:10.1073/pnas.0904851106
61. Parisi-Amon A, Mulyasasmita W, Chung C, Heilshorn SC (2013) Protein-engineered injectable hydrogel to improve retention of transplanted adipose-derived stem cells. Adv Healthcare Mater 2:428–432. doi:10.1002/adhm.201200293
62. Jing P, Rudra JS, Herr AB, Collier JH (2008) Self-assembling peptide-polymer hydrogels designed from the coiled coil region of fibrin. Biomacromolecules 9:2438–2446. doi:10.1021/bm800459v
63. Rudra JS, Tripathi PK, Hildeman DA, Jung JP, Collier JH (2010) Immune responses to coiled coil supramolecular biomaterials. Biomaterials 31:8475–8483. doi:10.1016/j.biomaterials.2010.07.068
64. Haines-Butterick L, Rajagopal K, Branco M, Salick D, Rughani R, Pilarz M, Lamm MS, Pochan DJ, Schneider JP (2007) Controlling hydrogelation kinetics by peptide design for three-dimensional encapsulation and injectable delivery of cells. Proc Natl Acad Sci USA 104:7791–7796. doi:10.1073/pnas.0701980104
65. Collier JH, Messersmith PB (2003) Enzymatic modification of self-assembled peptide structures with tissue transglutaminase. Bioconjug Chem 14:748–755. doi:10.1021/bc034017t
66. Rudra JS, Tian YF, Jung JP, Collier JH (2010) A self-assembling peptide acting as an immune adjuvant. Proc Natl Acad Sci USA 107:622–627. doi:10.1073/pnas.0912124107
67. Jung JP, Nagaraj AK, Fox EK, Rudra JS, Devgun JM, Collier JH (2009) Co-assembling peptides as defined matrices for endothelial cells. Biomaterials 30:2400–2410. doi:10.1016/j.biomaterials.2009.01.033
68. Aida T, Meijer E, Stupp S (2012) Functional supramolecular polymers. Science 335:813–817. doi:10.1126/science.1205962
69. Webber MJ, Kessler JA, Stupp SI (2010) Emerging peptide nanomedicine to regenerate tissues and organs. J Intern Med 267:71–88. doi:10.1111/j.1365-2796.2009.02184.x
70. Stendahl JC, Rao MS, Guler MO, Stupp SI (2006) Intermolecular forces in the self-assembly of peptide amphiphile nanofibers. Adv Funct Mater 16:499–508. doi:10.1002/adfm.200500161
71. Greenfield MA, Hoffman JR, Olvera de la Cruz M, Stupp SI (2009) Tunable mechanics of peptide nanofiber gels. Langmuir 26:3641–3647. doi:10.1021/la9030969
72. Webber MJ, Tongers J, Newcomb CJ, Marquardt K-T, Bauersachs J, Losordo DW, Stupp SI (2011) Supramolecular nanostructures that mimic VEGF as a strategy for ischemic tissue repair. Proc Natl Acad Sci USA 108:13438–13443. doi:10.1073/pnas.1016546108
73. Mata A, Geng Y, Henrikson KJ, Aparicio C, Stock SR, Satcher RL, Stupp SI (2010) Bone regeneration mediated by biomimetic mineralization of a nanofiber matrix. Biomaterials 31:6004–6012. doi:10.1016/j.biomaterials.2010.04.013
74. Shah RN, Shah NA, Del Rosario Lim MM, Hsieh C, Nuber G, Stupp SI (2010) Supramolecular design of self-assembling nanofibers for cartilage regeneration. Proc Natl Acad Sci USA 107:3293–3298. doi:10.1073/pnas.0906501107

75. Huang Z, Newcomb CJ, Zhou Y, Lei YP, Bringas P Jr, Stupp SI, Snead ML (2013) The role of bioactive nanofibers in enamel regeneration mediated through integrin signals acting upon C/EBPα and c-Jun. Biomaterials 34:3303–3314. doi:10.1016/j.biomaterials.2013.01.054
76. McClendon MT, Stupp SI (2012) Tubular hydrogels of circumferentially aligned nanofibers to encapsulate and orient vascular cells. Biomaterials 33:5713–5722. doi:10.1016/j.biomaterials.2012.04.040
77. Silva GA, Czeisler C, Niece KL, Beniash E, Harrington DA, Kessler H, Stupp SI (2004) Selective differentiation of neural progenitor cells by high-epitope density nanofibers. Science 303:1352–1355. doi:10.1126/science.1093783
78. Tysseling-Mattiace VM, Sahni V, Niece KL, Birch D, Czeisler C, Fehlings MG, Stupp SI, Kessler JA (2008) Self-assembling nanofibers inhibit glial scar formation and promote axon elongation after spinal cord injury. J Neurosci 28:3814–3823. doi:10.1523/JNEUROSCI.0143-08.2008
79. Palmgren B, Jiao Y, Novozhilova E, Stupp SI, Olivius P (2012) Survival, migration and differentiation of mouse tau-GFP embryonic stem cells transplanted into the rat auditory nerve. Exp Neurol 235:599–609. doi:10.1016/j.expneurol.2012.03.014
80. Behanna HA, Rajangam K, Stupp SI (2007) Modulation of fluorescence through coassembly of molecules in organic nanostructures. J Am Chem Soc 129:321–327. doi:10.1021/ja062415b
81. Rajangam K, Behanna HA, Hui MJ, Han X, Hulvat JF, Lomasney JW, Stupp SI (2006) Heparin binding nanostructures to promote growth of blood vessels. Nano Lett 6:2086–2090. doi:10.1021/nl0613555
82. Zhang S, Holmes T, Lockshin C, Rich A (1993) Spontaneous assembly of a self-complementary oligopeptide to form a stable macroscopic membrane. Proc Natl Acad Sci USA 90:3334–3338. doi:10.1073/pnas.90.8.3334
83. Caplan MR, Schwartzfarb EM, Zhang S, Kamm RD, Lauffenburger DA (2002) Effects of systematic variation of amino acid sequence on the mechanical properties of a self-assembling, oligopeptide biomaterial. J Biomater Sci Polym Ed 13:225–236. doi:10.1163/156856202320176493
84. Schneider A, Garlick JA, Egles C (2008) Self-assembling peptide nanofiber scaffolds accelerate wound healing. PLoS One 3:e1410. doi:10.1371/journal.pone.0001410
85. Zhang S, Holmes TC, DiPersio CM, Hynes RO, Su X, Rich A (1995) Self-complementary oligopeptide matrices support mammalian cell attachment. Biomaterials 16:1385–1393. doi:10.1016/0142-9612(95)96874-Y
86. Gelain F, Bottai D, Vescovi A, Zhang S (2006) Designer self-assembling peptide nanofiber scaffolds for adult mouse neural stem cell 3-dimensional cultures. PLoS One 1:e119. doi:10.1371/journal.pone.0000119
87. Genové E, Shen C, Zhang S, Semino CE (2005) The effect of functionalized self-assembling peptide scaffolds on human aortic endothelial cell function. Biomaterials 26:3341–3351. doi:10.1016/j.biomaterials.2004.08.012
88. Zhao X, Pan F, Xu H, Yaseen M, Shan H, Hauser CAE, Zhang S, Lu JR (2010) Molecular self-assembly and applications of designer peptide amphiphiles. Chem Soc Rev 39:3480–3498. doi:10.1039/b915923c
89. Ellis-Behnke RG, Liang Y-X, You S-W, Tay DKC, Zhang S, So K-F, Schneider GE (2006) Nano neuro knitting: peptide nanofiber scaffold for brain repair and axon regeneration with functional return of vision. Proc Natl Acad Sci USA 103:5054–5059. doi:10.1073/pnas.0600559103
90. Ruan L, Zhang H, Luo H, Liu J, Tang F, Shi Y-K, Zhao X (2009) Designed amphiphilic peptide forms stable nanoweb, slowly releases encapsulated hydrophobic drug, and accelerates animal hemostasis. Proc Natl Acad Sci USA 106:5105–5110. doi:10.1073/pnas.0900026106
91. Ruan L-P, Luo H-L, Zhang H-Y, Zhao X (2009) Investigation on structure and properties of a novel designed peptide. Macromol Res 17:597–602. doi:10.1007/BF03218915

92. Dong H, Paramonov SE, Aulisa L, Bakota EL, Hartgerink JD (2007) Self-assembly of multidomain peptides: balancing molecular frustration controls conformation and nanostructure. J Am Chem Soc 129:12468–12472. doi:10.1021/ja072536r
93. Aulisa L, Dong H, Hartgerink JD (2009) Self-assembly of multidomain peptides: sequence variation allows control over cross-linking and viscoelasticity. Biomacromolecules 10:2694–2698. doi:10.1021/bm900634x
94. Bakota EL, Wang Y, Danesh FR, Hartgerink JD (2011) Injectable multidomain peptide nanofiber hydrogel as a delivery agent for stem cell secretome. Biomacromolecules 12:1651–1657. doi:10.1021/bm200035r
95. Wang Y, Bakota E, Chang BHJ, Entman M, Hartgerink JD, Danesh FR (2011) Peptide nanofibers preconditioned with stem cell secretome are renoprotective. J Am Soc Nephrol 22:704–717. doi:10.1681/ASN.2010040403
96. He L, Theato P (2013) Collagen and collagen mimetic peptide conjugates in polymer science. Eur Polym J 49:2986–2997. doi:10.1016/j.eurpolymj.2013.05.033
97. Pires MM, Przybyla DE, Chmielewski J (2009) A metal-collagen peptide framework for three-dimensional cell culture. Angew Chem Int Ed Engl 48:7813–7817. doi:10.1002/anie.200902375
98. Hernandez-Gordillo V, Chmielewski J (2014) Mimicking the extracellular matrix with functionalized, metal-assembled collagen peptide scaffolds. Biomaterials 35:7363–7373. doi:10.1016/j.biomaterials.2014.05.019
99. Sano K-I, Kawamura R, Tominaga T, Nakagawa H, Oda N, Ijiro K, Osada Y (2011) Thermoresponsive microtubule hydrogel with high hierarchical structure. Biomacromolecules 12:1409–1413. doi:10.1021/bm101578x
100. Wieduwild R, Tsurkan M, Chwalek K, Murawala P, Nowak M, Freudenberg U, Neinhuis C, Werner C, Zhang Y (2013) Minimal peptide motif for non-covalent peptide–heparin hydrogels. J Am Chem Soc 135:2919–2922. doi:10.1021/ja312022u
101. Tran NQ, Joung YK, Lih E, Park KM, Park KD (2010) Supramolecular hydrogels exhibiting fast in situ gel forming and adjustable degradation properties. Biomacromolecules 11:617–625. doi:10.1021/bm100047y
102. Yang Z, Xu K, Wang L, Gu H, Wei H, Zhang M, Xu B (2005) Self-assembly of small molecules affords multifunctional supramolecular hydrogels for topically treating simulated uranium wounds. Chem Commun 2005(35):4414–4416. doi: 10.1039/b507314f
103. Ma M, Kuang Y, Gao Y, Zhang Y, Gao P, Xu B (2010) Aromatic–aromatic interactions induce the self-assembly of pentapeptidic derivatives in water to form nanofibers and supramolecular hydrogels. J Am Chem Soc 132:2719–2728. doi:10.1021/ja9088764
104. Chen L, Pont G, Morris K, Lotze G, Squires A, Serpell LC, Adams DJ (2011) Salt-induced hydrogelation of functionalised-dipeptides at high pH. Chem Commun 47:12071–12073. doi:10.1039/C1CC15474E
105. Zhou M, Smith AM, Das AK, Hodson NW, Collins RF, Ulijn RV, Gough JE (2009) Self-assembled peptide-based hydrogels as scaffolds for anchorage-dependent cells. Biomaterials 30:2523–2530. doi:10.1016/j.biomaterials.2009.01.010
106. Yang Z, Liang G, Ma M, Abbah AS, Lu WW, Xu B (2007) D-Glucosamine-based supramolecular hydrogels to improve wound healing. Chem Commun 2007(8):843–845. doi: 10.1039/b616563j
107. Salem AK, Rose FRAJ, Oreffo ROC, Yang X, Davies MC, Mitchell JR, Roberts CJ, Stolnik-Trenkic S, Tendler SJB, Williams PM, Shakesheff KM (2003) Porous polymer and cell composites that self-assemble in situ. Adv Mater 15:210–213. doi:10.1002/adma.200390047
108. Park KM, Yang J-A, Jung H, Yeom J, Park JS, Park K-H, Hoffman AS, Hahn SK, Kim K (2012) In situ supramolecular assembly and modular modification of hyaluronic acid hydrogels for 3D cellular engineering. ACS Nano 6:2960–2968. doi:10.1021/nn204123p
109. Van Bommel KJC, van der Pol C, Muizebelt I, Friggeri A, Heeres A, Meetsma A, Feringa BL, van Esch J (2004) Responsive cyclohexane-based low-molecular-weight hydrogelators with modular architecture. Angew Chem Int Ed 43:1663–1667. doi:10.1002/anie.200352396

110. Leenders CMA, Albertazzi L, Mes T, Koenigs MME, Palmans ARA, Meijer EW (2013) Supramolecular polymerization in water harnessing both hydrophobic effects and hydrogen bond formation. Chem Commun 49:1963–1965. doi:10.1039/C3CC38949A
111. Kim H-J, Lee J-H, Lee M (2005) Stimuli-responsive gels from reversible coordination polymers. Angew Chem Int Ed 44:5810–5814. doi:10.1002/anie.200501270
112. Van de Manakker F, Vermonden T, van Nostrum CF, Hennink WE (2009) Cyclodextrin-based polymeric materials: synthesis, properties, and pharmaceutical/biomedical applications. Biomacromolecules 10:3157–3175. doi:10.1021/bm901065f
113. Li L, Guo X, Wang J, Liu P, Prud'homme RK, May BL, Lincoln SF (2008) Polymer networks assembled by host–guest inclusion between adamantyl and β-cyclodextrin substituents on poly(acrylic acid) in aqueous solution. Macromolecules 41:8677–8681. doi:10.1021/ma8020147
114. Auzély-Velty R, Rinaudo M (2002) New supramolecular assemblies of a cyclodextrin-grafted chitosan through specific complexation. Macromolecules 35:7955–7962. doi:10.1021/ma020664o
115. Koopmans C, Ritter H (2008) Formation of physical hydrogels via host–guest interactions of β-cyclodextrin polymers and copolymers bearing adamantyl groups. Macromolecules 41:7418–7422. doi:10.1021/ma801202f
116. Gosselet NM, Beucler F, Renard E, Amiel C, Sebille B (1999) Association of hydrophobically modified poly (N,N-dimethylacrylamide hydroxyethylmethacrylate) with water soluble β-cyclodextrin polymers. Colloids Surf A Physicochem Eng Asp 155:177–188. doi:10.1016/S0927-7757(99)00026-6
117. Van de Manakker F, van der Pot M, Vermonden T, van Nostrum CF, Hennink WE (2008) Self-assembling hydrogels based on β-cyclodextrin/cholesterol inclusion complexes. Macromolecules 41:1766–1773. doi:10.1021/ma702607r
118. Hashidzume A, Tomatsu I, Harada A (2006) Interaction of cyclodextrins with side chains of water soluble polymers: a simple model for biological molecular recognition and its utilization for stimuli-responsive systems. Polymer 47:6011–6027. doi:10.1016/j.polymer.2006.06.021
119. Tomatsu I, Hashidzume A, Harada A (2006) Contrast viscosity changes upon photoirradiation for mixtures of poly(acrylic acid)-based α-cyclodextrin and azobenzene polymers. J Am Chem Soc 128:2226–2227. doi:10.1021/ja058345a
120. Nakahata M, Takashima Y, Yamaguchi H, Harada A (2011) Redox-responsive self-healing materials formed from host–guest polymers. Nat Commun 2:511
121. Appel EA, Biedermann F, Rauwald U, Jones ST, Zayed JM, Scherman OA (2010) Supramolecular cross-linked networks via host-guest complexation with cucurbit[8]uril. J Am Chem Soc 132:14251–14260. doi:10.1021/ja106362w
122. Liu Y, Yu Y, Gao J, Wang Z, Zhang X (2010) Water-soluble supramolecular polymerization driven by multiple host-stabilized charge-transfer interactions. Angew Chem Int Ed 49:6576–6579. doi:10.1002/anie.201002415
123. Dankers PYW, Hermans TM, Baughman TW, Kamikawa Y, Kieltyka RE, Bastings MMC, Janssen HM, Sommerdijk NAJM, Larsen A, Bosman AW, Popa R, Fytas G, Meijer EW, van Luyn MJA, Popa ER (2012) Hierarchical formation of supramolecular transient networks in water: a modular injectable delivery system. Adv Mater 24:2703–2709. doi:10.1002/adma.201104072
124. Pape ACH, Bastings MMC, Kieltyka RE, Wyss HM, Voets IK, Meijer EW, Dankers PYW (2014) Mesoscale characterization of supramolecular transient networks using SAXS and rheology. Int J Mol Sci 15:1096–1111. doi:10.3390/ijms15011096
125. Kieltyka RE, Pape ACH, Albertazzi L, Nakano Y, Bastings MMC, Voets IK, Dankers PYW, Meijer EW (2013) Mesoscale modulation of supramolecular ureidopyrimidinone-based poly (ethylene glycol) transient networks in water. J Am Chem Soc 135:11159–11164. doi:10.1021/ja403745w

126. Guo M, Pitet LM, Wyss HM, Vos M, Dankers PYW, Meijer EW (2014) Tough stimuli-responsive supramolecular hydrogels with hydrogen-bonding network junctions. J Am Chem Soc 136:6969–6977. doi:10.1021/ja500205v
127. Dankers PYW, van Luyn MJA, Huizinga-van der Vlag A, van Gemert GML, Petersen AH, Meijer EW, Janssen HM, Bosman AW, Popa ER (2012) Development and in-vivo characterization of supramolecular hydrogels for intrarenal drug delivery. Biomaterials 33:5144–5155. doi:10.1016/j.biomaterials.2012.03.052
128. Kieltyka RE, Bastings MMC, van Almen GC, Besenius P, Kemps EWL, Dankers PYW (2012) Modular synthesis of supramolecular ureidopyrimidinone-peptide conjugates using an oxime ligation strategy. Chem Commun 48:1452–1454. doi:10.1039/c1cc14728e
129. Mollet BB, Comellas-Aragones M, Spiering AJH, Sontjens SHM, Meijer EW, Dankers PYW (2014) A modular approach to easily processable supramolecular bilayered scaffolds with tailorable properties. J Mater Chem B 2:2483–2493. doi:10.1039/C3TB21516D
130. Dankers PYW, Harmsen MC, Brouwer LA, van Luyn MJA, Meijer EW (2005) A modular and supramolecular approach to bioactive scaffolds for tissue engineering. Nat Mater 4:568–574. doi:10.1038/nmat1418
131. Bastings MMC, Koudstaal S, Kieltyka RE, Nakano Y, Pape ACH, Feyen DAM, van Slochteren FJ, Doevendans PA, Sluijter JPG, Meijer EW, Chamuleau SAJ, Dankers PYW (2014) A fast pH-switchable and self-healing supramolecular hydrogel carrier for guided, local catheter injection in the infarcted myocardium. Adv Healthcare Mater 3:70–78. doi:10.1002/adhm.201300076
132. Koudstaal S, Bastings MC, Feyen DM, Waring C, van Slochteren F, Dankers PW, Torella D, Sluijter JG, Nadal-Ginard B, Doevendans P, Ellison G, Chamuleau SJ (2014) Sustained delivery of insulin-like growth factor-1/hepatocyte growth factor stimulates endogenous cardiac repair in the chronic infarcted pig heart. J Cardiovasc Transl Res 7:232–241. doi:10.1007/s12265-013-9518-4
133. Storm C, Pastore JJ, MacKintosh FC, Lubensky TC, Janmey PA (2005) Nonlinear elasticity in biological gels. Nature 435:191–194
134. Kouwer PHJ, Koepf M, Le Sage VAA, Jaspers M, van Buul AM, Eksteen-Akeroyd ZH, Woltinge T, Schwartz E, Kitto HJ, Hoogenboom R, Picken SJ, Nolte RJM, Mendes E, Rowan AE (2013) Responsive biomimetic networks from polyisocyanopeptide hydrogels. Nature. doi:10.1038/nature11839
135. Birk DE, Bruckner P (2005) Collagen suprastructures. In: Brinckmann J, Notbohm H, Müller PK (eds) Collagen SE-7. Springer, Berlin, pp 185–205
136. Webber MJ, Tongers J, Renault M-A, Roncalli JG, Losordo DW, Stupp SI (2010) Development of bioactive peptide amphiphiles for therapeutic cell delivery. Acta Biomater 6:3–11. doi:10.1016/j.actbio.2009.07.031

Index

© Springer International Publishing Switzerland 2015

S. Seiffert (ed.), *Supramolecular Polymer Networks and Gels*, Advances in Polymer Science 268, DOI 10.1007/978-3-319-15404-6